

AGARD

ADVISORY GROUP FOR AEROSPACE RESEARCH & DEVELOPMENT

7 RUE ANCELLE, 92200 NEUILLY-SUR-SEINE, FRANCE

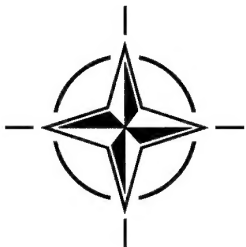
AGARD CONFERENCE PROCEEDINGS 591

Subsystem Integration for Tactical Missiles (SITM) and Design and Operation of Unmanned Air Vehicles (DOUAV)

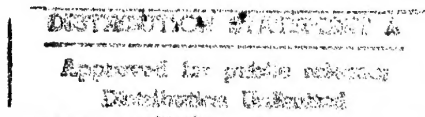
(l'Intégration des sous-systèmes dans les missiles tactiques et
la Conception et l'exploitation des véhicules sans pilote)

*Copies of papers presented at the Flight Vehicle Integration Panel Specialists' Meetings held in
Ankara, Turkey, from 9-12 October 1995.*

19970210 178



NORTH ATLANTIC TREATY ORGANIZATION



Published November 1996

Distribution and Availability on Back Cover

AGARD

ADVISORY GROUP FOR AEROSPACE RESEARCH & DEVELOPMENT

7 RUE ANCELLE, 92200 NEUILLY-SUR-SEINE, FRANCE

AGARD CONFERENCE PROCEEDINGS 591

**Subsystem Integration for Tactical Missiles
(SITM) and Design and Operation of
Unmanned Air Vehicles (DOUAV)**

(l'Intégration des sous-systèmes dans les missiles tactiques et
la Conception et l'exploitation des véhicules sans pilote)

Copies of papers presented at the Flight Vehicle Integration Panel Specialists' Meetings held in
Ankara, Turkey, from 9-12 October 1995.



North Atlantic Treaty Organization
Organisation du Traité de l'Atlantique Nord

The Mission of AGARD

According to its Charter, the mission of AGARD is to bring together the leading personalities of the NATO nations in the fields of science and technology relating to aerospace for the following purposes:

- Recommending effective ways for the member nations to use their research and development capabilities for the common benefit of the NATO community;
- Providing scientific and technical advice and assistance to the Military Committee in the field of aerospace research and development (with particular regard to its military application);
- Continuously stimulating advances in the aerospace sciences relevant to strengthening the common defence posture;
- Improving the co-operation among member nations in aerospace research and development;
- Exchange of scientific and technical information;
- Providing assistance to member nations for the purpose of increasing their scientific and technical potential;
- Rendering scientific and technical assistance, as requested, to other NATO bodies and to member nations in connection with research and development problems in the aerospace field.

The highest authority within AGARD is the National Delegates Board consisting of officially appointed senior representatives from each member nation. The mission of AGARD is carried out through the Panels which are composed of experts appointed by the National Delegates, the Consultant and Exchange Programme and the Aerospace Applications Studies Programme. The results of AGARD work are reported to the member nations and the NATO Authorities through the AGARD series of publications of which this is one.

Participation in AGARD activities is by invitation only and is normally limited to citizens of the NATO nations.

The content of this publication has been reproduced
directly from material supplied by AGARD or the authors.

Published November 1996

Copyright © AGARD 1996
All Rights Reserved

ISBN 92-836-0033-9



*Printed by Canada Communication Group
45 Sacré-Cœur Blvd., Hull (Québec), Canada K1A 0S7*

Subsystem Integration for Tactical Missiles (SITM) and Design and Operation of Unmanned Air Vehicles (DOUAV)

(AGARD CP-591)

Executive Summary

Both Tactical Missiles and Unmanned Air Vehicles (UAV) are important defence capabilities for NATO nations, and they will become more important in the future. The 21st century will be a turning point for tactical missiles and UAVs with regard to their affordability. Tactical missile suppliers are moving now toward efficiency which will greatly reduce the per unit costs. With dramatic improvements foreseen in multi-spectral sensors and secure, wide-band data links, UAVs will come into their own as reconnaissance assets able to provide high quality, real-time target imagery. The objective of these two meetings was to capture the current situation in these rapidly changing technical arenas.

These Specialists' Meetings met their objective. Different parts of this Conference Proceedings should be valuable to anyone currently:

- considering the procurement and tactical application of UAVs and Tactical Missiles;
- designing or developing UAVs and Tactical Missiles;
- doing basic research in UAV.

In the field of subsystem integration for tactical missiles, papers focused on successful examples of integrating advanced sensors, guidance control systems, and navigation systems. An additional session focused on methods for testing missiles, including lessons learned from Norway's testing of the Penguin Mk2.

The meeting on UAVs focused on design issues, payloads and their associated technologies, and operational issues. Specific systems described included: the French Self Contained Early Warning System against anti-ship missiles; the Phoenix; Boeing's heliwing; the Crecelle, and the US Navy's Tilt Rotor UAV demonstrator.

L'intégration des sous-systèmes dans les missiles tactiques et la Conception et l'exploitation des véhicules sans pilote

(AGARD CP-591)

Synthèse

Les missiles tactiques, comme les véhicules aériens sans pilote (UAV) représentent des moyens de défense importants pour les pays membres de l'OTAN et cette tendance doit s'accroître à l'avenir. Le vingt-et-unième siècle marquera un tournant pour les missiles tactiques et les UAV en ce qui concerne leur acceptabilité financière. Les fournisseurs de missiles tactiques s'orientent actuellement vers une politique d'efficacité qui doit permettre de réduire leurs coûts unitaires de façon considérable. Avec les améliorations spectaculaires prévues pour les senseurs multispectre et les liaisons de données sécurisées à large bande, les UAV prendront toute leur importance en tant que moyens de reconnaissance, capables de fournir des images de la cible de haute qualité, en temps réel. Ces deux réunions ont eu pour objectif de capter l'état actuel des connaissances dans ces domaines techniques en évolution rapide.

Ces réunions de spécialistes ont atteint leurs objectifs. Les différentes sections de ce compte-rendu de conférence seront riches d'enseignement pour tous ceux qui sont actuellement responsables:

- de l'achat et de la mise en œuvre tactique des UAV et des missiles tactiques;
- de la conception et du développement des UAV et des missiles tactiques;
- de la recherche fondamentale en UAV.

Les présentations couvrant l'intégration des sous-systèmes dans les missiles tactiques ont traité un certain nombre d'exemples de l'intégration réussie de senseurs avancés, de systèmes de guidage-pilotage et de systèmes de navigation. Les méthodes d'essais des missiles, y compris les enseignements tirés des essais du Penguin Mk2 par la Norvège, ont fait l'objet d'une session supplémentaire.

La réunion sur les UAV était axée sur des questions relatives à la conception, aux charges utiles aux technologies associées, et aux opérations. Les systèmes spécifiques suivants ont été décrits: le système autonome français d'alerte lointaine contre les missiles anti-navire; le Phénix; le "heliwing" de Boeing; la Crécelle, et le démonstrateur d'UAV à rotor basculant de l'US Navy.

Contents

	Page
Executive Summary	iii
Synthèse	iv
Theme	viii
Acknowledgements	ix
Flight Vehicle Integration Panel	x
	Reference
Introductory Remarks: "Introduction — The Turning Point" by L.M. Nicolai	I
Keynote Address 1 by Col. M.S. Francis	K1
Keynote Address 2 by Col. M. Akçay	K2
Penguin MK2 MOD7 Integration in the Sikorsky S-70B Helicopter Integration and Live Fire Testing by A.C. Sollie and S. Spitz	1
Improved Engagement Envelope of a Tactical Missile with an Integral Rocket/Ramjet Engine by M. Lauzon	2
Operationally Representative Testing of Modern Tactical Weapons by D.H. Bergevin	3
Analysis of Wrap-Around Fin and Alternative Deployable Fin Systems for Missiles by G.L. Abate and G. Winchenbach	4
Linear Stability Analysis of Unguided Missiles with Wrap-Around Tail Fins in Free Flight by Ö. Tanrikulu, C. Önen, G. Mahmutyazicioğlu and İ. Bektaş	5
Détermination de coefficients aérodynamiques avec des résultats d'essais en vol (Practical use of Flight Tests Results for Estimations of Aerodynamic Coefficients) by G. Schmitt	6
Paper 7 Cancelled	
A Navigation System Concept for a Modern Anti-Ship Missile by Ø. Hoelsæter and B. Jalving	8
Control of a Supersonic Air to Ground Missile with Very Lightly Damped Bending Modes by J.P. Friang, J.P. Bonnet and G. Duc	9

Monte Carlo Simulation Studies of Unguided and Guided Missiles based on Probabilistic Modelling of Aerodynamic Coefficients by A.O. Merttopçuoğlu, H.H. Özdamar and M.K. Özgören	10
The Future for UAVs in NATO by R.C. Michelson	11
Lessons Learned in the Development and Operation of Remotely Piloted Helicopters by R.G. Austin	12
Paper was Classified and not available for publication	13
Aerodynamics of the Armor X7 UAV by V. de Brederode, P.A. Jorge, J.R. Marcelino and R. Patraquim	14
Paper 15 Cancelled	
Technology and Application of Modern Drone Systems by J. Bäcker, M. Möhring and V. Schlenkrich	16
Enabling Technology for UAVs by R.C. Michelson	17
High Performance Data Link for Unmanned Air-Vehicles by W.W. Rochus and D. Garcia	18
Unmanned Tactical Aircraft: A Lockheed Martin Perspective by A.J. Chaput, T.S. Albin, D.M. Hosmer and S.R. Weigel	19
Paper 20 was Classified and not available for publication	
An Exploratory Study of the Human-Machine Interface for controlling Maritime Unmanned Air Vehicles by L. van Breda	21
Multiple UMA's In-Flight Management by C. Siardi	22
ARMOR Projet — Autonomous Flight Capability by P. Lourtie, J.R. Azinheira, J.P. Rente and P. Felfício	23
The MARVEL Maritime UAV by J.-F. Pelous and J.B. Barlow	24A
Le système de drone marine MARVEL by J.-F. Pelous and J.B. Barlow	24B
Conception et développement d'un système d'appontage maritime automatique d'un véhicule générique de type VTOL by B. de Ferrier and C. Reboulet	25
Turkish Unmanned Air Vehicle Developments by Ü. Kaynak	26
Système d'alerte autonome déporté contre missiles antinavires basse et très basse altitude by S. Fesland and P. Nigron	27
Paper 28 not available for publication	

The Phoenix Target Acquisition and Surveillance System by R.W. Dennis	29
CRECERELLE: un système d'avion léger télépiloté de nouvelle génération, pour des missions de reconnaissance, de surveillance et d'acquisition d'objectifs by G. Thin and P. Durieux	30
PREDATOR: Medium Altitude Endurance by L. Ernst	31

Theme

The 21st century, will be a turning point for tactical missiles and UAVs with regard to their affordability. NATO will insist on more affordable systems and the tactical missile suppliers will respond with equal effectiveness at cheaper unit costs. With dramatic improvements in multi-spectral sensors and secure, wide-band data links, UAVs will provide high quality, real time, target imagery to anywhere on the battlefield. Recoverable and autonomous UAVs will expand their traditional role of reconnaissance and also demonstrate their capability of complementing manned aircraft in performing strike warfare. Reconnaissance and strike UAVs will offer NATO a dramatic improvement in affordability by reduced operation and support costs.

Thème

Le 21^{ème} siècle marquera un tournant pour les missiles tactiques et les UAV en ce qui concerne leur acceptabilité budgétaire. L'OTAN insistera sur la nécessité de disposer de systèmes plus abordables et les fournisseurs de missiles tactiques devront répondre en mettant à disposition des produits d'efficacité égale mais à moindre coût unitaire. Avec les améliorations spectaculaires prévues dans le domaine des senseurs multispectraux et les liaisons de données sûres à large bande, les UAV pourront transmettre des images de la cible à n'importe quel point du champ de bataille. Les UAV autonomes et récupérables permettront d'élargir leur rôle traditionnel d'engin de reconnaissance et aussi de faire apparaître leur aptitude au soutien des avions pilotés dans les frappes aériennes. Les UAV de reconnaissance et de frappe permettront à l'OTAN de faire un grand pas vers des coûts acceptables en réduisant les coûts d'exploitation et de maintenance.

Acknowledgements

The Flight Vehicle Integration Panel wishes to express its thanks to the National Authorities of Turkey for the invitation to hold these meetings in their country as well as to TUBITAK and the Middle East Technical University for providing the facilities and personnel which made these meetings possible. We also wish to thank the United States Air Force European Office of Aerospace Research and Development as sole supporter for a session related to missile aeroballistics.

Flight Vehicle Integration Panel

Chairman: Dipl.-Ing. Horst WÜNNENBERG
Mgr. of Flight Physics & Predesign
DORNIER Luftfahrt GmbH
P.O. Box 1103
D-82230 Wessling
Germany

Deputy Chairman: Mr. Barry TOMLINSON
Flight Dynamics &
Simulation Dept.
Flight Systems Department
Defence Research Agency
Bedford, MK41 6AE
United Kingdom

TECHNICAL PROGRAMME COMMITTEE

Mr. S. BAILLIE
Flight Research Laboratory
Institute for Aerospace Research
National Research Council
Montreal Road
Ottawa, Ontario K1A 0R6
Canada

Dr. L. NICOLAI
Program Manager
Lockheed Advanced Development Co.
P.O. Box 250
Sunland, CA 91401
United States

HOST NATION COORDINATOR

Prof. N. ALEMDAROGLU
Middle East Technical University
(O.D.T.U.)
Aeronautical Engineering Department
06531 Ankara
Turkey

PANEL EXECUTIVE

John B. WHEATLEY, LTC, USA

Mail from Europe:
LTC J.B. WHEATLEY
AGARD-OTAN/FVP
7, rue Ancelle
92200 Neuilly-sur-Seine
France

Mail from US and Canada:
AGARD-NATO/FVP
PSC 116
APO AE 09777

AGARD Specialists' Meeting On Subsystem Integration For Tactical Missiles and Design and Operation of Unmanned Air Vehicles Introduction – The Turning Point

Leland M. Nicolai
Lockheed Martin Skunk Works
1011 Lockheed Way
Palmdale, California 93599

The remainder of this century is viewed as the turning point for tactical missiles and UAVs. For tactical missiles the next few years will see a new stable of precision tactical weapons that are affordable. Industry will be expected to field new weapons at very challenging unit cost targets. For UAVs the next few years will bring vindication and respect.

The tactical missile affordability issue was recently high lighted with the cancellation of the AGM-137 Tri-Service Standoff Attack Missile (TSSAM) in the US. The TSSAM was to be a low signature, air-launched cruise missile for standoff attack of high value targets. When the TSSAM program was started in 1985 the unit cost target for the 2250 lb cruise missile was \$400K (US). When the program was cancelled in December 1994 the unit cost for 4000 units was \$2.136M. The requirement for TSSAM still exists and the US Air Force and Navy have launched the Joint Air-to-Surface Standoff Missile (JASSM) program with a unit cost target of less than \$600K.

The current precision air-to-surface tactical weapons under development are (all \$ in 1995 US):

- Joint Air-to-Surface Standoff Missile (JASSM): A replacement for the cancelled AGM-137 TSSAM at a unit cost < \$600K.

- Joint Standoff Weapon (JSOW): A stealthy glide weapon at a unit cost < \$100K for the baseline (GPS guidance plus CEBs).

- Joint Direct Attack Munition

(JDAM): A GPS/INS tailfin kit for standard bombs at a unit cost < \$20K.

- Conventional Armed Standoff Missile (CASOM): Performance similar to JASSM at a unit cost < \$1M.

UAVs have been fighting for respect for decades. In the past UAVs had a real and perceived inferiority with manned aircraft. The UAVs with their automation and artificial intelligence could not handle uncertain or unforeseen events such as target uncertainty or emergencies. Manned aircraft with the human brain aboard could handle such events. The technology available today in the form of sensors and wideband data links can transmit target scene imagery real time to a remote vehicle manager. The remote vehicle manager can view the transmitted imagery, make a decision, interrupt the autonomous operation of the UAV and tell it what to do next in the case of uncertain or unforeseen events.

This real time transmission of imagery (termed telepresence) to a remote vehicle manager essentially eliminates the real inferiority that UAVs have had compared to manned aircraft as it puts the human brain onboard the UAV. Telepresence opens the door for a recoverable UAV performing tactical strike and support missions and is the foundation for a new ARPA initiative called Unmanned Tactical Aircraft or UTA.

Tactical reconnaissance is being per-

formed today by UAVs. Figure 1 shows the current and future stable of reconnaissance UAVs being pursued by the Defense Airborne Reconnaissance Office (DARO). The General Atomics Predator shown in Figure 2 is performing the DARO Tier 2 mission with its recce missions over Bosnia. Its payload of 450 lb includes a synthetic aperture radar (SAR) which provides one-foot resolution from 15000 feet with a 6.2 mile slant range. The Predator has a 70 knot cruise speed and 24 hour endurance at 25000 ft altitude. Its price is \$3.2M per copy.

The Lockheed Martin Tier 3—Darkstar shown on Figure 3 is currently in development. The first of two prototypes is scheduled to fly by the end of 1995. The Darkstar features low signature airframe and sensors in order to get closer to defended targets for better imagery and targeting. The Tier 3—has a 300 knot speed and 12 hour endurance at 50000 ft with a 1000 lb payload. The payload is either a SAR or EO/IR camera with one-foot resolution for SAR and EO, and two-foot resolution for IR in the spot mode. The resolution is three-foot for all sensors in the wide-area search. The coverage is as shown on Figure 1. The Tier 3— price tag is \$10M per copy.

The Teledyne Ryan Tier 2+ is in concept development and is shown on Figure 4. The Teledyne endurance UAV is designed for 42 hour endurance at 65000 feet with a 2000 lb payload. The payload will feature standoff radar, EO and IR sensors with one-foot resolution in the spot mode and three-foot resolution in the search mode. The data link will permit transmission at 50 megabits per second allowing real time imagery by satellite link. The Tier 2+ cost target is \$10M per copy.

The near term demonstrations and operational deployment of the endurance UAVs plus the proposed ARPA UTA demonstrations of telepresence should eliminate the perceived inferiority of UAVs so that they can take their rightful place as equal to manned aircraft. The UAV would offer a greatly reduced LCC due to minimal flying required during peacetime training.

The future for UAVs is certainly bright as the Tier-XXX is fielded next century and the UTAs perform tactical strike and support missions in concert with manned aircraft.

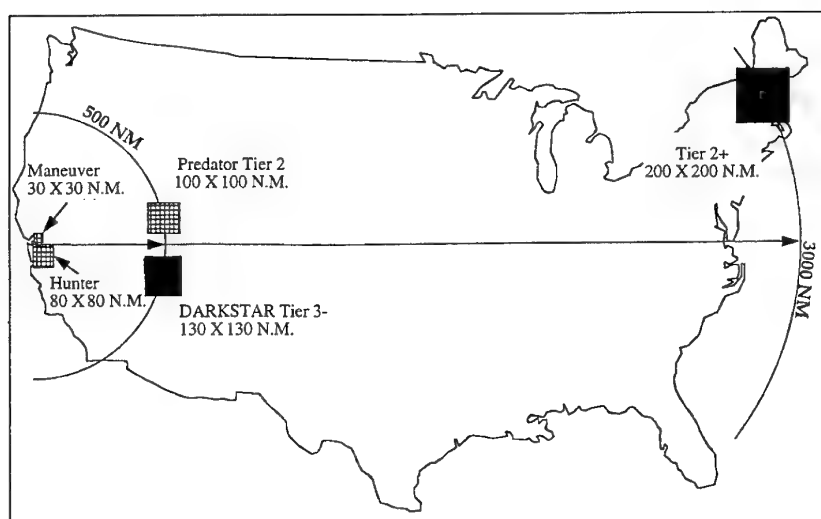


Figure 1 Area coverage of DARO endurance UAVs

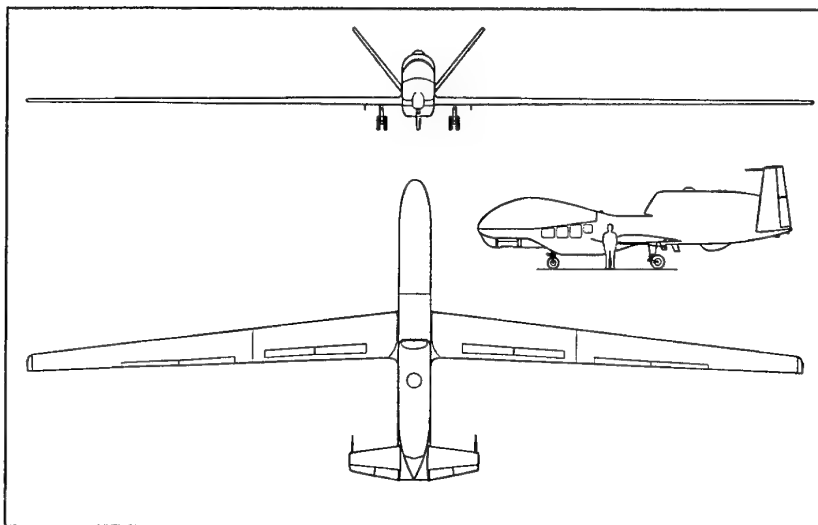
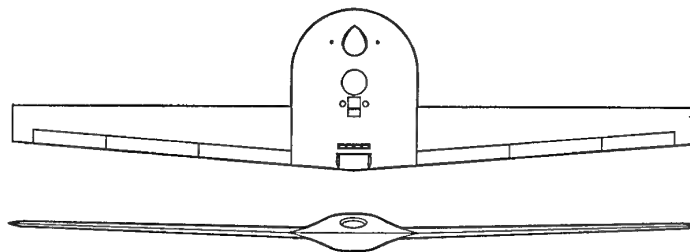


Figure 2 Teledyne Ryan Tier 2+ Configuration



Specifications

Length	15 ft.
Span	69 ft.
Height	5 ft.
Max. gross weight	8,600 lbs.
Speed	Subsonic
Altitude	More than 45,000 ft.
Radius of action	More than 1,000 nautical miles
Sensors	Radar or electro-optic
Mission	Reconnaissance/surveillance

Figure 3 Lockheed Martin Tier 3—Darkstar UAV

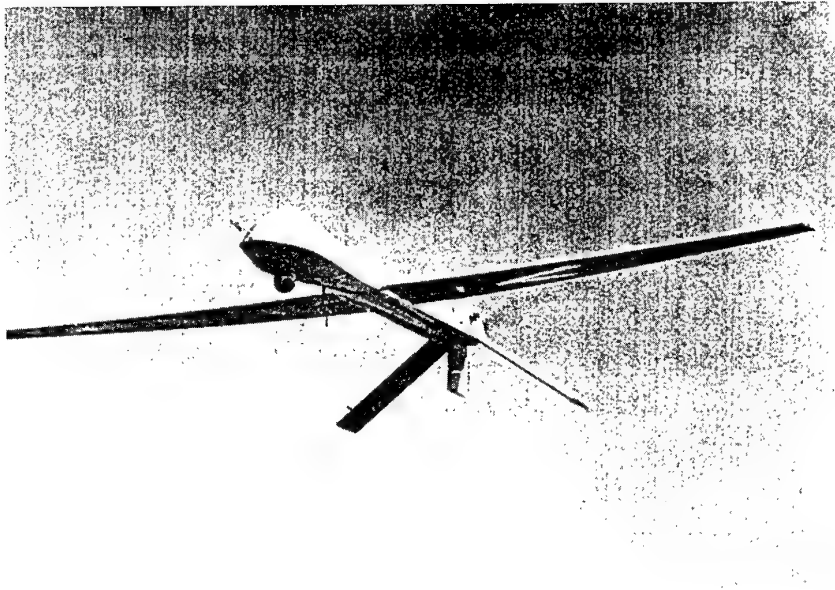
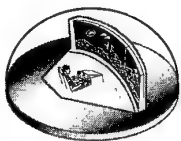


Figure 4 General Atomics Tier 2 Predator UAV

UNMANNED TACTICAL AIRCRAFT

by

Col. Michael S. Francis
Director Unmanned Tactical Aircraft
ARPA/TTO, 3701 N. Fairfax Drive
Arlington, VA 22203-1714, USA

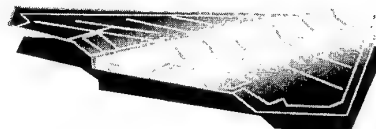


Unmanned Tactical Aircraft

Presentation to
AGARD Specialists' Meetings

Col Michael S. Francis

October 9, 1995
Tübitak, Ankara, Turkey



Outline

Unmanned Tactical Aircraft

- ◆ **Background**
- ◆ **The UTA Vision**
- ◆ **Initial Focus**

“The UTA Study” - Our Motivation

Unmanned Tactical Aircraft

- ◆ **Understand the Potential of Unmanned Tactical Aircraft**
 - Force Effectiveness and Multiplication
 - New Capabilities
 - Impact on Force “Affordability”
- ◆ **Understand the Enabling Technologies**
 - Current/Projected Limitations
 - Resolution of Deficiencies
- ◆ **Identify Near-Term Demonstration Opportunities**

Fully Leverage and Exploit the Information Revolution

Unmanned Tactical Aircraft-What is it?

Unmanned Tactical Aircraft

- ◆ UTA is not a cruise missile or a UAV - it is a general purpose tactical aircraft
 - With remote operator
 - With full aircraft payloads and systems
- ◆ UTA is uninhabited, but otherwise functions like a piloted vehicle
- ◆ UTA captures the benefits of manned and unmanned operation
 - The remote operator control higher level mission functions
 - The air vehicle has mostly autonomous modes augmented by operator override based on judgment
 - The remote operator's mission interface fused many sources of tactical information including data from the aircraft sensors and avionics systems
- ◆ UTA can be designed for enhanced performance without pilot constraints



KEEP THE OPERATORS HEAD IN THE COCKPIT
- LEAVE THE REST OF HIM AT HOME

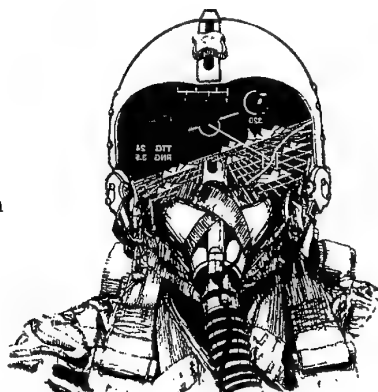


The Human Factor

Unmanned Tactical Aircraft

The Contribution

- ◆ Critical Decisions
 - Life or Death
 - Safety
 - Mission Planning
 - Tactics
- ◆ Data Interpretation
- ◆ Information Synthesis
- ◆ Direct Sensing (WVR)
- ◆ Manual Control

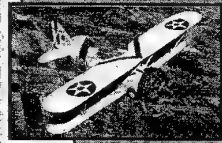


The Penalty

- ◆ Environmental Adaptation
 - Oxygen
 - Pressurization
- ◆ Heat of Battle Effectiveness
 - Workload
 - Stress
- ◆ Human Interfaces
 - Displays
 - Switches
 - Comfort
- ◆ Safety/Level of Risk
- ◆ Susceptibilities
 - Motion Sickness
 - Disorientation (e.g., Vertigo)
- ◆ Limitations
 - Acceleration (g's)
 - Gravitational Orientation
 - Endurance
- ◆ Training and Proficiency
- ◆ Additional Infrastructure
 - Aircrew Support Systems
 - Search and Rescue

Aircraft Autonomy

Unmanned Tactical Aircraft



- Inherent Stability



P-51

- Stability
- S/L Flight (Autopilot)



F-16

- Stabilization
- Flight Path
– Limited Maneuver
- Navigation Decision



TIER III -



F-117

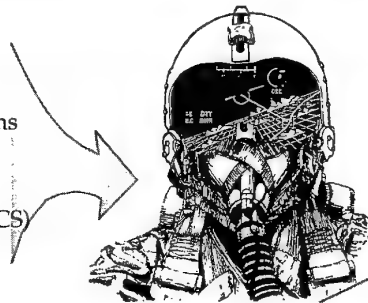
- Self-Stabilization
- Flight Path/Maneuver
- Navigation - Precise
- Auto Replan
- Terrain Avoidance
- Self Diagnosis
- Reconfigurability (Repair)
- Takeoff and Landing
- Turbulence/Buffer Control
- Aggressive Maneuver
- Data Synthesis for Decision

The Information Age

Unmanned Tactical Aircraft

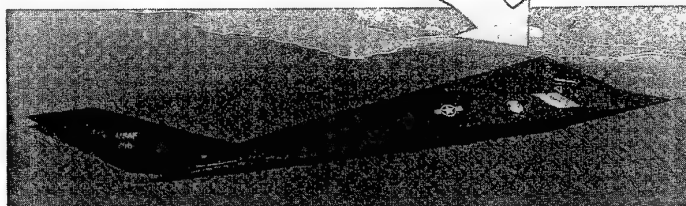
Off-Board Information

- ◆ Satellite Imagery
- ◆ Advanced Communications
- ◆ Surveillance UAVs
- ◆ Command and Control Platforms (JSTARS, AWACS)
- ◆ Other C³ Nodes
- ◆ GPS



On-Board Sensors

- ◆ Radar
- ◆ Infrared
- ◆ Visual Imagery
- ◆ Targeting Systems



Robust Control

- ◆ Digital FBW/FBL
- ◆ Vectored Thrust
- ◆ Reconfigurable Systems

Advanced Digital Processing

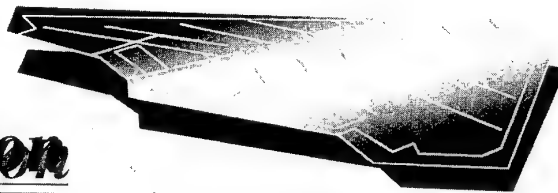
- ◆ Navigation
- ◆ Mission Functions
- ◆ Displays

Anecdotes

Unmanned Tactical Aircraft

- ◆ The Lockheed L-1011 Demonstrated Virtually Hands-Off Intercontinental Flight from Throttle Up to Power Off 25 Years Ago
- ◆ A Buffalo Hunter RPV with a Television Camera Demonstrated Live Bomb Drops 25 Years Ago
- ◆ A Large Classified UAV Recovered Autonomously from Catastrophic Control Systems Failures on Final Approach on Two Consecutive Missions Several Years Ago
- ◆ The F-117 Today can Fly a Complete Mission from Wheels Up to Wheels Down without Pilot Input Except Weapons Release Consent
- ◆ The F-16 Fighter is so Automated it would be Virtually Impossible to Fly without Systems On
- ◆ The Pilot in an F-22 will be an "Executive Systems Director" for High Level Mission Functions
- ◆ A 5 Gbps COTS Computer will be Available this Fall

The UTA Vision



Unmanned Tactical Aircraft

- ◆ **Expanded Range of Mission Options**
 - Extremely Hazardous Operations (e.g. SEAD)
 - Targets Inappropriate for Cruise Missiles (Low Value, Last Minute Decisions Required)
 - Imprecise Target Information and Targets of Opportunity
 - Politically Sensitive Missions
- ◆ **More Affordable Air Power**
 - Lower Acquisition Costs - Eliminate Man-Related Requirements, Shorter Life
 - Significantly Lower O&S Costs (≈ 50%) (New CONOPS, Manned Interface, Wartime Surge Capability)
 - Exploit 'End of Life' Assets
- ◆ **Tactical Deterrence**
 - Fundamentally Superior Air Vehicles
 - Larger Force due to Decreased Unit Cost
 - A New Class of Weapon Systems
- ◆ **Full Exploitation of The Information Revolution**
 - Operator as "The Center of Information"

System Concept

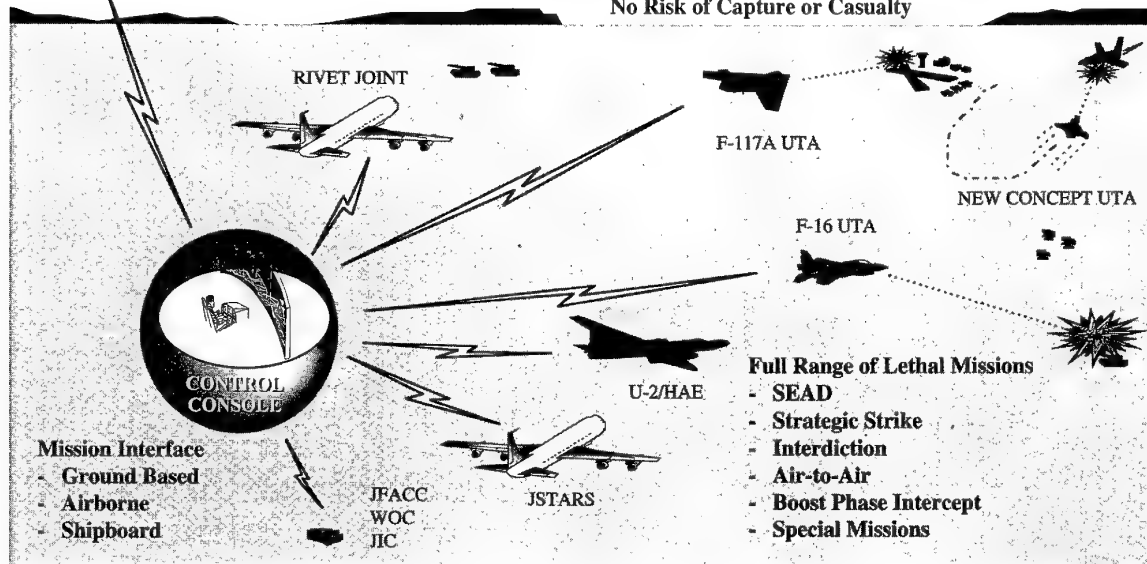
Unmanned Tactical Aircraft

Information Exploitation

- Offboard Theater Sensors
- Offboard National Sensors
- Theater Databases
- Onboard Sensors

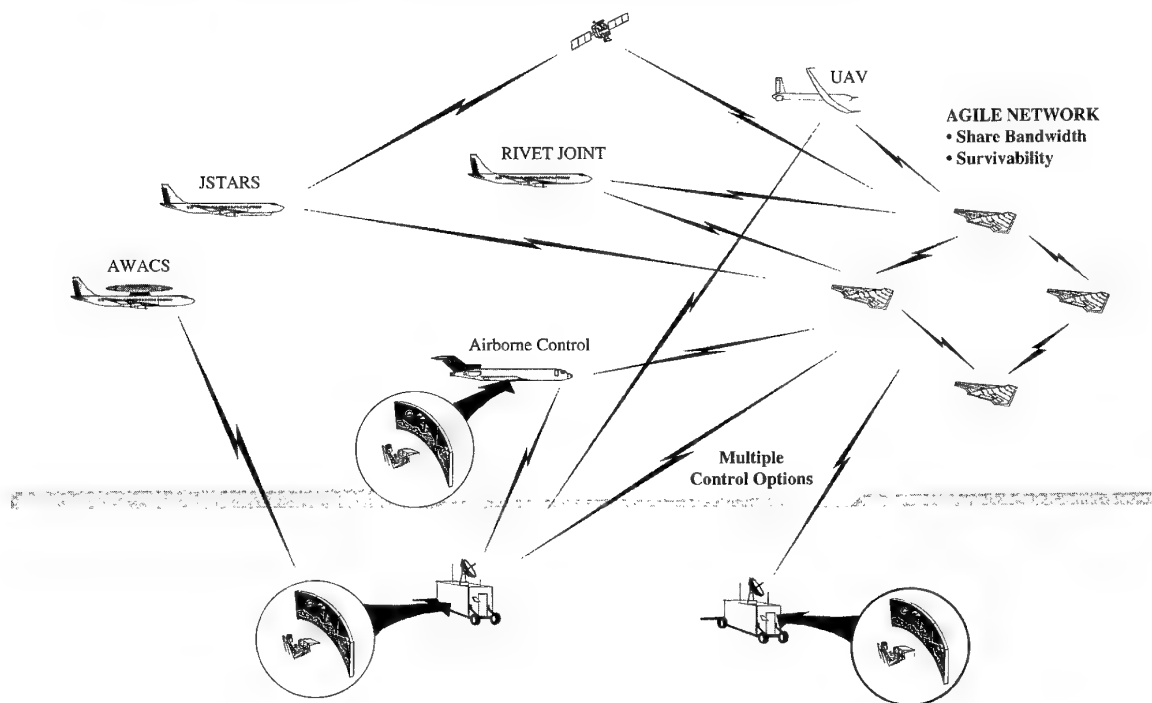
*Keep the Pilot's Head in the Cockpit
Leave the Rest of Him at Home*

No Risk of Capture or Casualty



UTA - An Agile System

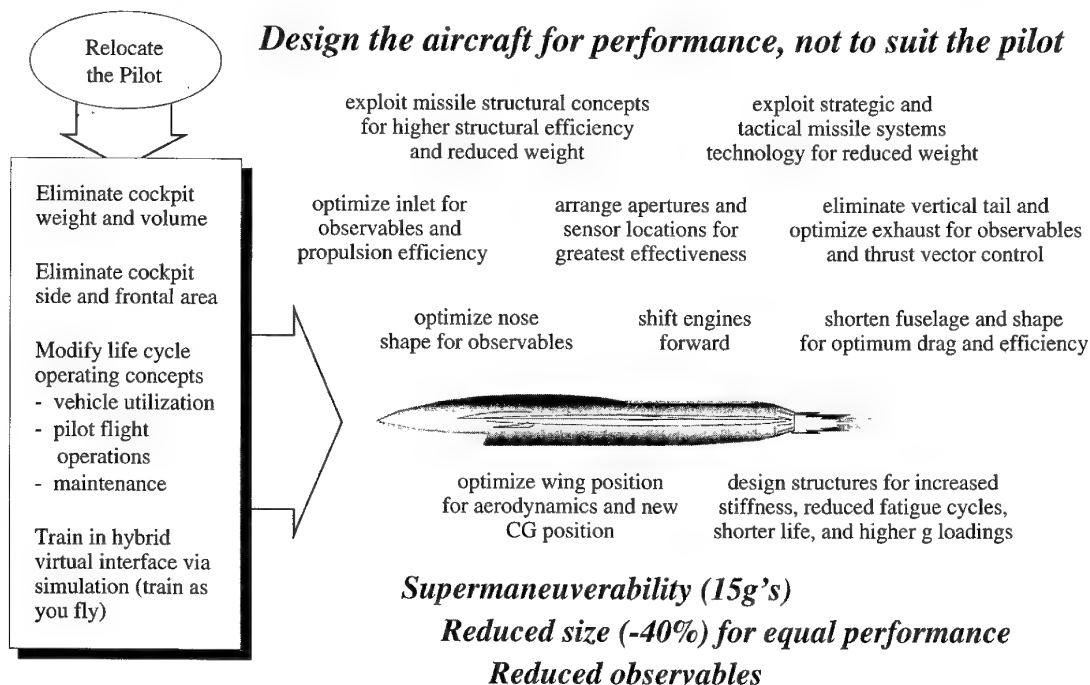
Unmanned Tactical Aircraft



Revolutionary Design Potential

Unmanned Tactical Aircraft

Design the aircraft for performance, not to suit the pilot

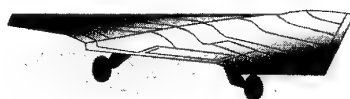


Unmanned Tactical Aircraft

Unmanned Tactical Aircraft

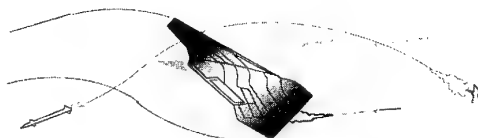
◆ LOW COST PLATFORM

- Minimal Onboard Avionics
- Inherent Stealth
 - Size
 - Shape

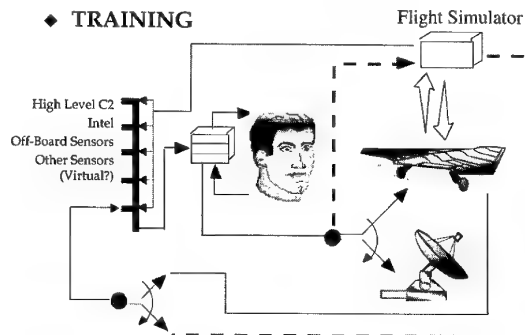


- "Good Enough" Sensors
- General Purpose Aircraft

◆ EVOLVED MISSIONS:

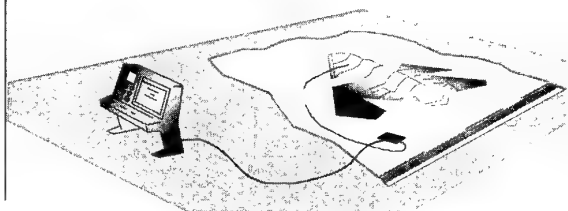


◆ TRAINING



◆ MAINTENANCE CONCEPT:

- Aircraft Maintained in Flight Ready Storage
- Periodic Checks and Service
- Occasional Training / Exercises



Evolution of the UTA

Unmanned Tactical Aircraft

Near Term

- ◆ **Communications**
 - Link Oriented
 - Bandwidth vs Vehicle Trades
- ◆ **Command and Control**
 - Evolved Control Station
 - Limited Number of Aircraft
- ◆ **Air Vehicles**
 - Existing Manned Platforms or Derivatives
 - End of Life Assets
- ◆ **Missions**
 - Niche Applications
 - Relatively Simple

The Future

- ◆ **Communication - Robust**
 - Network Oriented
 - Agile and High Capacity
- ◆ **Command and Control**
 - Optimized Operator Interface
 - Large Vehicle Fleet
- ◆ **Air Vehicles**
 - Low Cost Platforms
 - Low O&S Requirements
 - “Surge” Fleet for Wartime Contingency
- ◆ **Missions**
 - Broad Mission Applications
 - Complex Functionality

Key Program Elements

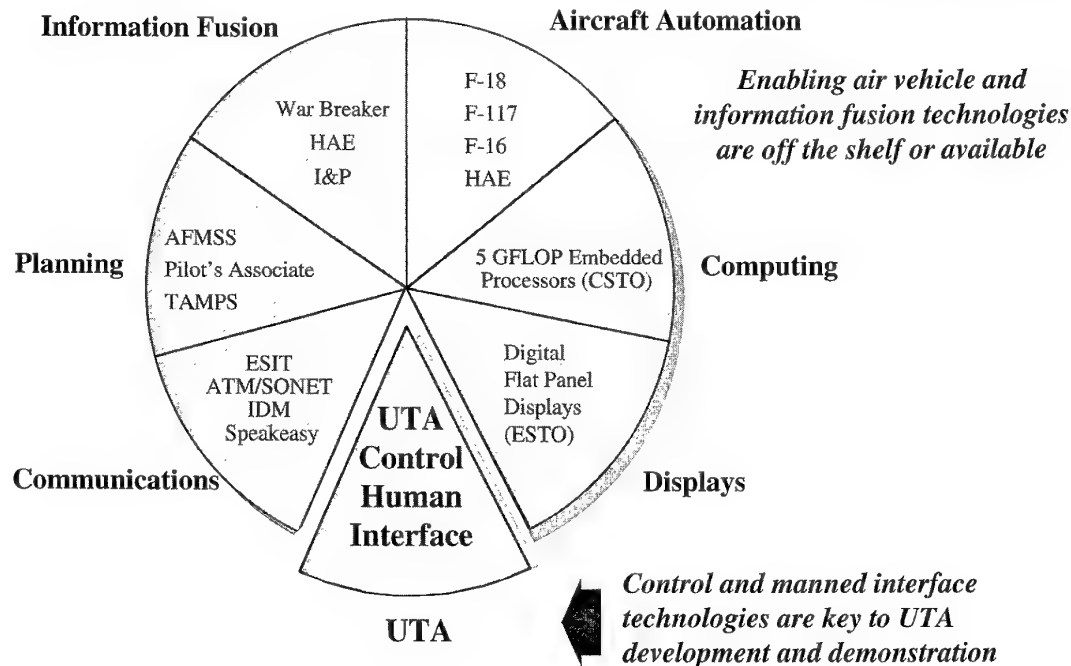
Unmanned Tactical Aircraft

– The Near Term –

- ◆ **Robust, Meaningful Demonstrations (...Dispel the Skeptics)**
 - Routine aircraft functions – repeatedly (takeoff, landing, navigation)
 - Mission essential functions (e.g., aerial refueling)
 - Communications integrity
 - Rapid reaction and replan
 - Flexible human intervention
- ◆ **A Product with Legacy**
- ◆ **Acceptance and Exploitation of the Capability**
 - User “Buy-In”
- ◆ **Identify the Affordability Paradigm**

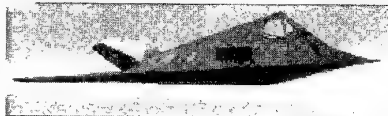
Core Technologies

Unmanned Tactical Aircraft



Demonstration Platforms Examined

Unmanned Tactical Aircraft



F-117: Night Ground Attack

PROS

- Almost Fully Integrated
 - Digital FCS
 - Highly Automated

CONS

- Night Missions Only
- Unique, Expensive Asset
- Direct Manned Mission Threat



F-16: Wild Weasel or Fixed Strike

PROS

- Pressing Military Need
- Minimal Bandwidth Required
- All Weather Aircraft
- Aircraft Availability
 - End of Life Assets

CONS

- Extensive Technical Effort



F-18: Attack Recce

PROS

- TO&L Already Automated
- Aircraft Availability
- Unpopular Manned Missions

CONS

- Limited Payload Capability (Mission Impact)
- Potential Extensive Integration



Special Purpose/Unique Design

PROS

- Flexible Mission Options
- Low Cost Potential
- No Mission Bias

CONS

- User Acceptance More Difficult
- New/Highly Modified Airframe
- No Safety Pilot for Initial Ops

UTA Technologies for the Future

Unmanned Tactical Aircraft

- ◆ **Low Cost Manufacturing Processes**
 - Composite Structures for Modular Aircraft
 - “Store-and-Fly” Technologies
- ◆ **Advanced Digital Communications**
 - Distributed Bandwidth Communications
 - Agile Networks
- ◆ **Advanced Flight Control**
 - Fly-By-Light
 - Advanced Vectored Thrust
 - Vortex Management
- ◆ **Limited Life Component Technologies**
 - Low Cost Sensors
- ◆ **High-g Air Breathing Propulsion Systems**

UTA - Its' Time Has Come

The Washington Post
11th Year No. 150 SATURDAY, JUNE 3, 1995

U.S. Jet Shot Down Over Bosnia; Pilot Missing
Serbs Free Some Western Hostages; Clinton Ponders Military Options

DAVID A. FULGHUM/WASHINGTON

European and Middle Eastern nations see both military and civil applications for the Pentagon's new crop of long-range unmanned aerial vehicles

20th Anniversary Special October 17, 1994

USAF's McPeak Urges 'Revolutionary' Fighter Research Envisions Aircraft Without Pilots, Radar Systems

By THERESA HITCHENS
Defense News Staff Writer

WASHINGTON — The U.S. Air Force must look beyond a replacement for its F-16 multirole fighter to more exotic aircraft, including unmanned vehicles, as it explores plans for its future combat fleet, according to Gen. Merrill McPeak, outgoing Air Force chief of staff.

Army, Air Force Tussle Over UAVs

By FRANK OLIVIERI
Defense Staff Writer

WASHINGTON — The U.S. Air Force is trying to wrest control of tactical unmanned aerial vehicles (UAVs) from the Army, which uses them for battlefield reconnaissance, according to military officials.

At stake is how tactical UAVs should be controlled in the air-space above the battlefield and which service will control them. The disagreement is reminiscent of the battles that raged last year between the Air Force and Army over close air support during the Balkan conflict. Officially, both services support the existing structure for close air support, but privately the Army chafed at its dependency on the Air Force for battlefield air-ground attack planes.

A military official who helps plan the use of UAVs in the force said, "The Army is concerned about airspace issues. (Army leaders) like to operate with the altitude of 'This is the area. We own it. Keep out of it unless you want to hit us.' The Air Force feels very uncomfortable with the sea-and-sky engine."

Gen. Joseph Babbitt, commander of Air Combat Command, is leading the Air Force in calling for the operation of all UAVs within an air-battle order (ATO), according to Air Force officials. An ATO is a plan for air operations in a combat theater.

JAPAN: MULTIPURPOSE UNMANNED AIRCRAFT

In fiscal year 1995, the Japan Defense Agency (JDA) will launch two programs designed to produce small, unmanned multipurpose aircraft to enhance Japan's air defense capability while reducing troop numbers and risks to military personnel.

JDA will invest approximately 500 million yen (\$5 million) in this program during fiscal year 1995; overall research costs for fiscal years 1995-2000 are estimated at between 10 and 100 billion yen (\$100 million to \$1 billion). Three aircraft manufacturers—Mitsubishi Heavy Industries, Kawasaki Heavy Industries, and Fuji Heavy Industries—are expected to submit applications for participation in the aircraft development program. The plane is not expected to enter into service until after fiscal year 2000 (NIKKAN KOGYO SHIMBUN 23 Jan 95).

JOURNAL OF COMMERCE
April 27, 1995 Pg. 2B

Supersonic Plane Test Is Successful in China

BEIJING — China has successfully conducted its first test flight of an unmanned, supersonic plane, the Liberation Army Daily said Wednesday.

The test flight was conducted recently at an unidentified experimental base deep in the desert, the newspaper said.

"This marks our development of unmanned, supersonic planes," the newspaper said.

The plane, which was remotely controlled from the ground, flew at supersonic speeds at a height of about 32,800 feet and made several maneuvers, it said.

An air force experimental base spent four years developing the plane. The newspaper did not give further details.

IMPACT OF THE NEW GEOPOLITICAL ENVIRONMENT AND TECHNOLOGICAL ADVANCES ON MISSILE DESIGN

Col. Mehmet AKÇAY
T.A.F., Kara Kuvvetleri Komutanlığı
Head, Planning & Project Management Section
Teknik & Proje Yönetim Daire Bşk.
Bahçelievler, Ankara, Turkey

Defence materiel is more or less developed and procured according to standard project management systems. The development of such systems starts with the threat analysis and ends with its disposal. Recent changes in the political and the strategic situations in the world resulted in new military scenarios. In parallel to the new advances in technology, new military scenarios lead to more damaging and advanced types of weapon systems. Yet sharply decreasing defence budgets put limits to these developments.

1. INTRODUCTION

New military needs and advances in technology lead to missile systems that are more costly than ever before. On the other hand the technological advances make it possible to produce new system that are more capable, modular and meeting higher performance goals. A cost effective missile design requires the use of fast and sophisticated aerodynamics and flight mechanics tools to optimize the configuration. The configuration is determined by not only aerodynamics but also considerations of various disciplines, such as internal aerodynamics, aero thermodynamics, aeroacoustics, structural loads, flight mechanics and all types of signature.

Use of the Total Missile Damage Concept, tandem warheads, smokeless and low signature propellants, beam-riding guidance systems, GPS navigations and fiber optics based guidance systems, absorbent structural materials for stealth are some of the more important examples of technological advances that have occurred in missiles.

Also mobility of targets are increasing rapidly and it is required that the system reaction times must be shorter than before. Therefore, existing tools need to be improved and new tools must be generated to achieve the required performance targets.

As a result of the new geopolitical structure and technological advances new missiles must have high penetrativity, high efficiency and high flexibility in addition to their affordability and availability characteristics.

2. PROGRAM DEVELOPMENT UNDER THE NEW THREAT ENVIRONMENT

The acquisition process for major defense systems starts with the mission area analysis and ends with its disposal (1). The flowchart of a standard project management system is shown in Fig.1. At the end of each phase, the need for the programme is reassessed, using milestone decision reviews, by The Secretary of Defense or the Service Secretary as required, before additional resource is authorized. At each review, the decision authority can choose to continue the present phase, proceed to the next phase, or cancel the program.

The methodology used in Research and Development programs is quite similar to that explained above for major defense systems acquisition process (2). The flowchart of this R&D methodology is explained in Fig.2. Military needs in the postulated geopolitical scenarios of peace, crisis and war that are adopted to the mission needs constitute the basis for the system concept development. A key feature is that if there is a change in military priority, in the geopolitical scenario, or there are other changes, the planner should determine the necessary programme modifications.

Development of military needs depends on a detailed threat analysis. Missiles can be given as a good example for military needs. The new political and strategic situation and newly emerging missile technologies are the two basic factors taken into consideration to carry out a correct threat analysis.

The New World Geopolitical and Threat Environment

The disarmament activities after the collapse of the USSR have significantly changed the political and strategic situations in the World. Many counts of missiles and guns have been destroyed in the Western and Eastern Blocks respectively. In order to control the armament proliferation, the number and types of guns in each region have been determined. Treaties like Missile Technology Control Regime (MTCR) put limit on the range and warhead types of the missiles. As a result, the risk of mass destructions of larger armies have been decreased drastically, especially for NATO countries. However, new changes in the regional political structures created new dangers and assigned new roles to the NATO and the United Nations (2,3). These changes and the new roles are as follows;

- a. Increasing local conflicts
- b. Multinational peace keeping operations
- c. Regional conflict management using limited size national troops
- d. National point defense tasks against terrorist attacks
- e. Surveillance, reconnaissance, inspection and control activities in buffer zones in connection with boycott, disarmament measures and further defence activities.

According to the geopolitical scenarios, as described for peace, crisis and war, a system concept recommendation matrix is given in Fig.3. For example, surveillance and monitoring systems would be of high priority for peace, while improved weaponry would be emphasized for war. Key Research and Technology Development Programme recommendations would be prioritised in a similar manner (2). In result of these, R&D programmes are managed according to a nine step flowchart as shown in Fig.4.

The above mentioned conditions, in addition to the declining defence budgets as shown in Table 1 forced many nations to decrease their armed forces in terms of number of personnel and metarial (4). On the other hand, armed forces started to ask for better quality, more sensitive and cheaper weapon systems (5). Due to the regional conflicts,

transportation of highly qualified troops and metarial from one place to another becoming increasingly important. As a result, many of the weapon systems are started to be designed as air transportable and air droppable. Therefore, it is necessary to design these systems as usable in diverse geographical areas under very different climatic conditions during day and night. Furthermore the agility of the targets necessitates high precision weapon systems to hit their targets. All These require the use of intelligent and autonomous weapon systems with minimum human interference, a development that leads to the use of minimum man power and maximum automation.

The number of killed people in conflicts normally arises political anger in international arenas. For this reason, non-lethal weapons such as oxidizers for metal made materials, stickers for attackers, chemical agents which blind or faint the people temporarily and ect. are becoming increasingly important for the future developments.

Finally, invisible and inaudible activities receive highest importance and priority in the future.

3. IMPACT OF NEW TECHNOLOGIES ON MISSILE DESIGN

A lot of new technologies have emerged in recent years. Some of these technologies have significant impact on aeromechanical design of missiles (3). However the basic configurations of missiles are not significantly altered and more or less remain the same as shown in Fig.5. Interactions of various technology areas in the design of modern missiles can be seen in Fig.6. In the following, some of the basic developments that effect the design of new missile systems will be explained in detail.

3.1 Lethal Payload

The terminal accuracy achieved must match with the characteristics of the lethal payload carried by a missile. (6).

The design goal for any warhead and the associated fuzing used to initiate it is to deliver as much damaging agent as possible to the target. A warhead might typically be only about 10 % of the launch mass of the air defence missile. On detonation, only about 10 % of the warhead products actually strike

the air target. Any means of increasing the ratio of lethal payload to the launch mass would clearly be desirable. One means of improving this ratio would be to use the entire missile as a source of damaging agents. This can be achieved by breaking up the missile prior to intercept, thus creating a cloud of fragments which may potentially strike the target. This is called as "The Total Missile Damage Concept". Trajectory shaping must be arranged according to the miss distance and tailored very well to apply this concept. Another way to increase the effectiveness of warhead is to use aimable warheads. Aimable warheads, which can be detonated in a preferred direction, have the potential of directing more of their damaging agents towards the target than conventional axisymmetric designs. This has to be studied carefully in terms of aeromechanical and guidance considerations.

3.2. Warheads

Frontal part of the missiles consist of the warhead, so that, outer shape and weight of the warhead will influence the design of a missile. Submunition warheads are designed to be used in Multiple Launch Rocket Systems to put the target area under fire. Separation of submunition from a missile body is a problem area to be studied. During the last decade, armour technology has been further developed, such as the reactive armour, multilayer armour, composite armour and smart armour. Consequently much new progress has occurred in armour piercing technology. Tandem warheads and high L/D and high velocity penetrators have been developed. The extensive increase in missile velocities creates aerodynamic heating of the sensor domes(4). For IR domes active cooling or the use of covers might be a solution. The use of ceramic or fiber reinforced materials creates some favorable advantages in terms of aerothermal and aeroelastic properties including weight reduction factor.

3.3 Propulsion Units

New turbo propulsion units for low-velocity vehicles and smokeless and low signature propellants are the new challenges for designers in this field (7).

The combination of these systems can lead to

new missile designs with different flight paths. Very high missile velocities obtained by means of new propellants cause aerothermal problems on the frontal part of the missile.

3.4. Guidance

Beam-riding guidance systems and very cheap and powerful electronic components, and PC's lead to more intelligent and autonomous missiles or to more elaborated launch and guidance units (3,6).

New data links like laser beam or glass fiber-optics give the opportunity for a more precise homing and for transmission of a lot of data acquired. High power television cameras or improved IR, MW or Radar Sensors with high sensitivity give the opportunity to make better picture scanning, processing and interpretation. All these new developments can provide better opportunities to identify a target with much higher precision on greater range.

The use of GPS for navigation has become common and leads also to much higher precision. Laser and radar altimeters are of much higher precision and are much more independent of the environment than the classical ones.

For high velocity missiles, the use of classical control surfaces is a problem because of the high temperatures caused by the aerodynamic heating, mainly in the wing tips. In such cases, to develop new control mechanisms becomes necessary. The methods of thrust vector control, injection technique, pyrotechnique force control, and grid lines are the new control techniques currently under study.

3.5 Stealth

Stealth will be taken to mean the reduction of target detectability in the electro-optical as well as the radiofrequency bands. There are two broad levels of stealth (5).

Partial stealth, in which major scattering points such as air intakes, cockpits and radomes are treated to reduce radar echoes and hot areas such as exhaust of turbine motors are masked. Partial stealth might reduce the RCS of a typical fighter aircraft from around 10 m^2 to around 1 m^2 and a cruise missile to 0.1 m^2 . Yet, performance is not significantly affected. These measures are not excessively expensive and

can be applied to substantial numbers of targets.

Full stealth with special target shaping, meticulous care taken to deal with every scattering point and generous use of radar-absorbent materials, including absorbent structural materials. Equally elaborate measures may be taken to reduce IR radiation and optical visibility, including visual camouflage.

Signature management becomes a predominant requirement, and as the unconventional configurations are used to mask IR sources, aerodynamics is compromised and performance is reduced. Development and production costs are very high and are only affordable by rich and technologically developed nations.

3.6 Integrated Design

In order to achieve higher velocities, it is necessary to reduce the drag of a configuration. This leads to the integration of intakes and sensors with the body and conformal carriage of stores.

For long range, low velocity vehicles, there is a trend to develop low velocity vehicles, stealthy configurations. This forces the designers to optimize the missile geometry in terms of its aerodynamic shape and its signature. The same problems must also be solved for dispenser weapons with their unconventional non-circular cross section shapes (1).

Parachutes and gliders used to decelerate submunition or loads are another point of interest with their complicated aerodynamics and flight patterns.

The targets or missions are mainly the same but the geopolitical scenarios changes the distribution of these targets all over the world. Technical developments have increased the mobility of the possible targets so that the new combat situations require new characteristics from the missiles.

The targets and the missions that are expected to be important for missiles can be classified (1) and given in Table 2.

4. MISSILE TYPES OF INTEREST

Missile types are classified according to the new target structures and their specific characteristics have been derived according to the corresponding mission.

4.1 Tactical Ballistic Missiles (TBM)

INF treaty froze the situation by setting a range threshold of 500 km or less. The current range, about 30 km of unguided Multiple Launch Artillery Rocket Systems are intended to increase their range up to 100-150 km. Because their unguided characteristics some guidance elements has to be used to increase their hit probabilities.

For the long range ballistic missiles because of very high velocities in atmospheric heights, these missiles have similar problems to those of space vehicles. Maneuverability will be a subject to be studied for TBM's. The characteristics to be considered for the future TBM are as follows:

Modular warhead capability (explosive to submunition)

Good accuracy with terminal guidance (use of GPS)

Excellent penetration capabilities in the current air defence system.

Limited payload mass.

4.2 Ballistic Missile Defense

Under the Ballistic Missile Defense, early warning systems, Hawk Air Defense System and Patriot Missile Systems are being improved and modified, in order to intercept missile attacks such as Scud class ballistic missiles(5).

The main improvement for Patriot Systems occurred in their radars of Patriot Systems. Under this, three major improvements have been accomplished. Which are;

- a. Engagement with stealthier targets
- b. More lethal intercept capability
- c. Improved system reliability

New program in this field is the Extended Range Interceptor missile (ERINT) which provides significantly improved capabilities against missile threats. Here, the selected missile uses hit-to-kill technology to destroy attacking ballistic missiles, especially those carrying weapons of mass destruction. The new ceramic radome is lighter and less expensive than the older radome. The ceramic radome is a high-strength ceramic composite that has improved performance

characteristics in every critical area.

4.3 Hypersonic and High Velocity Missiles

Demands for high kinetic energy, short reaction time and high penetrability can be satisfied by reaching high velocities. According to different target and mission types several classes of high velocity missiles can be defined. Because of very high velocities, in addition to aerodynamic and flight mechanic problems, aero thermal heating, severe stress distribution and erosion created by dust grain and rain are some problems to be studied in detail.

4.4 Hypersonic Missiles-Short Range

High velocity short range missiles can carry their energy to longer distances than projectiles and they have the maneuverability. They can be used against targets like TBM, missiles, aircraft, tanks and helicopters. To reduce the reaction time while keeping the possibility to aim at targets approaching from any direction, vertical launch followed by a fast turn manoeuvre to almost horizontal flight is used in most cases. The velocity of these missiles lies between Mach 6 to 8. Aero elastic structure and control devices are subjects to be studied. The selection of surface material and guidance unit are two other subjects for researcher.

4.5 Hypersonic Missiles-Medium to Long Range

High velocity missiles for medium to long ranges have similar features to those of short range missiles. The speed will be a little lower (around Mach 4 to 6) and typical cruise height would be between several hundred to several thousand meters. The aim in developing such systems is to obtain better penetrability without using stealth features. If the speed is low, the level of signature will gain more importance with increasing range. The aerothermal heating is still important for radome. If air breathing propulsion unit is used for this type of missile, optimisation of drag becomes very important and this leads to unconventional missile design with a body having non-circular cross section.

4.6 Subsonic Cruise Missiles

This kind of weapon is more dedicated to relatively fixed and high value targets. They are cheap and effective stand off weapons. They have the range between 100 to 1000 km with up to 500 kg payloads. To build such a system in a more cost effective manner, it is necessary to use low cost airframe and propulsion technology. In the future, stealthy design, excellent accuracy using electroptics and thermal imaging, terrain following, thermal imaging and INS/GPS hybrid midcourse guidance are desired. On the other hand, the vulnerability and penetration capabilities are probably not so good, due to their low speed.

4.7 Supersonic Cruise Missiles

Velocity, flight profile and maneuverability of a weapon system describe its penetration capability.

To enhance the penetration capabilities, supersonic stand off weapons can be designed for particularly nuclear versions.

4.8 Hypersonic Projectiles

Penetrators shot from electro thermal or electromagnetic rail or coil guns are mainly intended to be used as antitank weapons or as ditch for TBM and for air defense as a kind of an improved shell.

These kinetic energy projectiles require relatively high mass and very high velocities of around Mach 6 to 10. Since the velocity decreases rapidly their range is limited to several kilometers.

Generally, these projectiles are fired from gun tubes with sabots. Separation of projectile from sabot creates some aerodynamic and trajectory problems. High L/D ratios causes some aeroelastic deformations, also.

The hit probability, especially for air targets can be increased considerably by using guided projectiles. A favourable guidance principle is the collision point oriented line of sight guidance. The control devices may consist of lateral thrust system or of a bending nose. The main problem is the prediction of drag and the correlation of flight path between theoretical and experimental values.

4.9 Dispensers

The main task of a dispenser is to carry a load and to drop it after some distance. This load consists of submunitions of different kind, a penetrator with an acceleration device, nonlethal agents that has to be transported and distributed. There are dispensers that are carried only as stores, others with free-flight without propulsion for short ranges. For longer ranges, they need propulsion unit. They have a typical flight height around 100 m with terrain following capability. Their average velocity is around transonic regime and there is tendency to increase their velocities to low supersonic regime. Stand-off characteristic is a high value of interest for dispensers. For long range dispensers, system must have sufficient penetrability. The unconventional design structure and control surfaces creates highly separated flow field around missiles. Store carriage and store separation is a subject of study.

4.10 Submunitions

There is a wide variety of submunition types. Their targets may be tanks, tank formations, armored vehicles, bridges, runways and other subjects of the infrastructure. Penetrators, mines and other similar weapons can be carried as a kind of submunition by a dispenser. In some cases payload has to be distributed regularly over a certain area, in some others the flight time and range of submunition have to be extended to allow a longer detection time of a suitable target. In order to stabilize the flight condition of submunition after ejection, some retarders, parachutes or gliders have to be integrated on to the submunition. There is strong interference effects after ejection between , the dispenser and submunition, between the submunitions and between the flight regulators and submunitions. Complicated flow conditions occur around a submunition which require detailed acrodynamic studies.

4.11 Fiber Optic Guided Missiles

The new technology of broad band signal transmission by optical fiber over distances up to about 100 km offers the chance to develop systems completely with new features. The missile carries an IR or visible light camera which transmits the pictures in

real time to a screen where the information is used by the launch crew to guide the missile. In this way a very high precision in the flight performance can be reached. This allows surgical strikes with conventional warheads or with non-lethal agents. The missile may be launched from a protected position and can reach protected areas, hidden places or points within narrow streets in cities. The new and cheaper turbo engines for missiles offer control of thrust and provide adaptable speed and, therefore, allow for a good coordination of connected missions.

4.12 Reconnaissance and Observation Vehicles

Drones of different kind and for different types of mission have been used for a quite long time. Because of the new demands in situations like out of area missions, confined and low-level confrontations, disarmament, armistice supervision, inspection, or boycott control, there will be increasing requirement for vehicles of this type. The design goals imagined by possible users often sound very fabulous. An ideal observation vehicle would be invisible and inaudible, would have unlimited flight range and mission time while having high manoeuvrability, and it would observe and transmit any relevant optical, acoustical and other information from protected and hidden areas, even from the inside of the buildings. To meet, at least to some extent these fantastic ideas, one has to develop a vehicle that has an extremely low signature not only in the various electromagnetic frequencies but also in the acoustic regime. It needs a lift producing device capable to carry the necessary sensors and the transmission system.

4.13 Supply Gliders

As mentioned before, safe and accurate delivery of supply or general loads in confined and insecure areas has gained increasing importance under the new scenarios. For this several concepts have been developed recently. A possible configuration consist of a glider and of different devices to assure for a soft and accurate landing. The freight may have a weight of up to 5 tons. The flight range will be 3 to 5 times the drop altitude which means up to about 50 kilometers. A minimum of manoeuvrability is needed. Since the

system must be as cheap as possible, standard components have to be used. Similar to submunitions with parachutes the aeromechanical challenge consists of the sufficient description of the aerodynamic behaviour of the glider and the load and also consists of the flight mechanical description of the coupled and heavily interfering unsteady system, especially as far as the maneuvers are to be concerned.

4.14 Multi-Purpose Missiles

Because of decreasing budgets, closer international cooperation, smaller independent operational units and higher geographical and seasonal flexibility, troops often don't have the opportunity to be equipped for all they wanted. They rather need missiles that are appropriate against several types of targets and that are fit for all-weather missions. The weapon systems have to be adaptable easily to new or improved components, also of other nations, which means a very modular set-up, and they have to be of good transportability. For missiles, an ideal system would be the one with exchangeable warheads allowing dosable effects for different missions and perhaps with exchangeable guidance units with sensors that are optimal for different environments and targets. In this way the number of different missile systems necessary for different targets should be reduced considerably.

5. DESIGN AND DEVELOPMENT DEMANDS

From the description of new targets and scenarios, a list of missile types of present interest was derived and given above. If one summarizes the design and development goals associated with them, one can find several general tactical design and development demands. In many cases technological objectives can be directly derived from them. The major ones are the following:

5.1. High Penetrativity

It means low detectability of the missile or low change for defense for the attacked target.

This can be realized by

- High velocity which leaves not enough time to an attacked enemy to react properly

- Low altitude flight and pop-up maneuvers which also lead to unawareness

- Statistical maneuvers like sea-weaving or screw-shaped flight that make it difficult for a defensive missile or the other measures to find their target

- Low signature features (stealthy missile) in all sensor regions that could be relevant for a detection.

5.2. High Efficiency of the Mission

It means to have a high probability to hit the target with a correctly operating missile and to give the warhead an optimal change to produce the desired effect. Several aspects are of importance here. Which are:

- High precision directly at or after launch asks for small deviations of the trust vector, and small interferences during the start phase which allows high hit probability for very short distances already,

- Low structural aeroelastic or thermal loads during the flight for all components by active or passive cooling, and by optimizing the flight path that guarantee the proper operation

- Intelligent guidance realized by an autonomous system of a precisely working sensor and advanced software or by integrating the human guide into the loop by using a very good data link

- Precisely working control devices allow high precision maneuvers at the appropriate time and should provide high hit and kill probabilities even for high velocity flight or for long ranges

- High kinetic energy at the target if penetration is planned.

5.3. High Flexibility of the Missile System

It is of increasing importance because of the new political situation. It makes possible for the user a wider field of action and reduces the overall cost.

Important aspects are

- Adaptability of the system to increased demands of advanced technologies without a new development phase by using the high modularity of the system.

- Development of multi-purpose systems, also supported by the high modularity and decreasing cost for acquisition, maintenance and logistics.

- High transportability and mobility including flexible installation, modularity of the complete system and low-weight components.

- Suitability for actions within a wide range of regions, environmental conditions and international cooperations without larger adaptations.

6. CONCLUSION

The tactical demands explained in Section 5 constitute also the main criteria for the missile system design. To meet these tactical demands experts have to first derive special aeromechanical demands to accomplish. Consequently, these aeromechanical design criteria are the preconditions within this special technological field to meet the tactical demands. Some important points of missile design are:

- Sufficiently exact prediction of all aeromechanical characteristics for all relevant geometries and flight conditions

- Sufficiently exact prediction of all aeromechanical and other aeromechanical reactions to changes in those parameters

- Securing a sufficiently high (or low) stability for all flight conditions in spite of changing center of gravity, and for unfavourable aerodynamic shapes like submunitions, dispensers or stealth configurations or for aerodynamically optimized but unconventional geometries

- Development of relatively optimal aerodynamic shapes for the complete missile or for components (wings, rudders) within the limits set by aeromechanical or other design demands

- Optimization of the shape to create a minimum (or, for retarders-maximum) drag

- Description of flow parameters in areas that are of interest for other specialists (after body flow, plume, intake)

- Development of control devices with exactly defineable and fastly reactable build-up of lateral forces for all flight conditions

- Reaching a fast and high maneuverability by bank-to-turn or skid-to-turn control

- Integrated aerodynamical and flight mechanical simulation of unsteady or other highly time dependent maneuvers

- Development of methods to reduce the aerodynamical, mechanical and aeroelastical loads of

the surface and the structure or development of materials to endure these stresses

- Development of methods to reduce the aerothermodynamic loads of surfaces, structures and components by constructive measures, by active or passive cooling, by finding aerothermally optimized flight paths or development of new materials able to stand those stresses

- Development of IR domes and of radomes suitable for high velocities

- Design of stealthy missiles with low signature levels in all possible domains (this is often already a primary demand)

- Simulation of plume emission and transmission characteristics.

REFERENCES

1. Project Management, by Dr. R.L. Martino, MDI Publications, 1968.
2. Extended Air Defence Past 2000 Volume II, AC/224 (AG VI)-D/B NIAG-D (93) 13, October 1993.
3. Hennig, P., Lacau P.G. "Aeromechanical Design of Modern Missiles",
AGARD Report 804, June 1994.
4. "Genel Ekonomik Göstergeler ve Savunma Bütçesi ile İlgili Bilgiler Broşürü"
K.K.K. 1191, ANKARA 1995
5. O'Neil, M.R. "Statement to the House National Security Committee", USA
Ballistic Missile Defense Organization, April 4, 1995.
6. Hurst, K.A. "Future Precision Guided Anti-Air Weapons- A Research Overview"
AGARD CP 524, December 1992. (Classified).
7. Leisch, S., Dunn, B., "Extending Range With The Boron Solid Fuel Ramjet
Engine (U)" AGARD CP 526 May 1992. (classified).
8. Chun, P.A. "Summary of The AQM 127 A Supersonic Low Altitude Target (SLAT)
Program" AGARD CP 526 May 1992. (Classified).

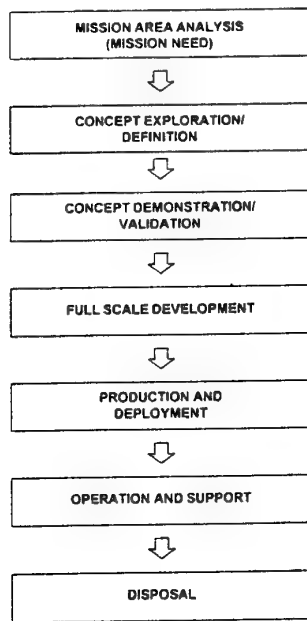


Figure 1. Acquisition Process for Major Defense Systems (1)

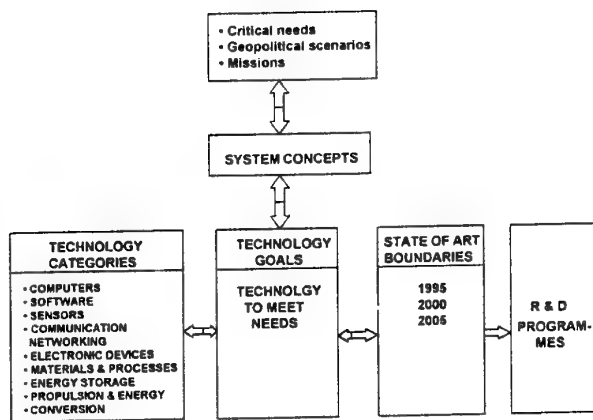


Figure 2. Relating Mission Needs, System Concepts and Key Technologies (2)

SCENARIOS GEOPOLITICAL PHASE	THEATRE	REGIONAL	BORDAR	OUT OF AREA
PEACE				
CRISIS				
WAR				

Figure 3. The Twelve Cell Matrix for Geopolitical Scenarios (2)

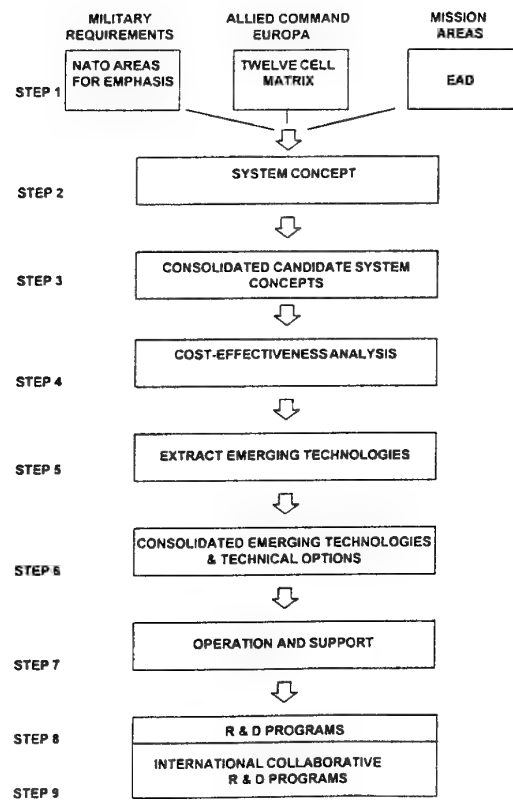


Figure 4. R & D Program Evolution Sketch (2)

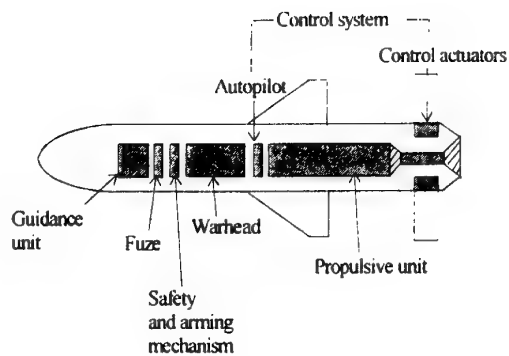


Figure 5. Layout of a typical guided weapon (3)

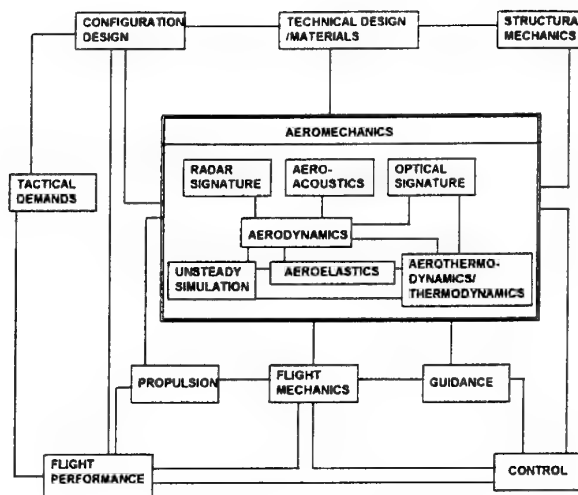


Figure 6. Sketch of interactions of technology areas in the design of modern missiles (3)

COUNTRY	YEARS				
	1990	1991	1992	1993	1994
USA	5.60	5.00	5.15	4.77	4.34
GERMANY	2.82	2.33	2.16	1.95	1.80
BELGIUM	2.42	2.35	1.89	1.81	1.79
DENMARK	2.05	2.07	2.00	1.97	1.87
FRANCE	3.56	3.56	3.41	3.40	3.35
HOLLAND	2.62	2.50	2.47	2.29	2.19
GREAT BRITAIN	4.06	4.25	3.84	3.62	3.36
SPAIN	2.84	1.73	1.58	1.74	1.58
ITALY	2.13	2.13	2.05	2.07	2.07
ICELAND	-	-	-	-	-
CANADA	2.03	1.92	1.92	1.88	1.74
LUXEMBURG	1.08	1.15	1.17	1.05	1.12
NORWAY	3.22	3.10	3.37	3.15	3.17
PORTUGAL	3.14	3.08	3.01	2.94	2.96
TURKEY	3.11	3.83	3.87	4.11	4.08
GREECE	5.81	5.42	5.63	5.52	5.55

Table 1. Defense Spendings of NATO Countries for Last Four Years (4)
(Percent of GNP)

Target	Desired Characteristics of Missile
Little armoured individual targets or formations (trucks, bridges, runways, launchers, infra structures)	Short to long range scattered ammunition manoeuvres at low altitude
Bankers and shelters	Medium to long range high kinetic energy
Tanks	Short to medium range fast reaction time high kinetic energy manoeuvres at low altitudes
Helicopters	Short and medium range fast reaction time possibly high kinetic energy
Fighter airplanes (Mostly low-level flight) Offensive missiles of different type	Short to medium range fast reaction time high manoeuvrability
Cruise missiles (Terrain-following or low level flight)	Short to medium range fast reaction time high manoeuvrability
Sea targets (above sea surface)	Medium to long range sea weaving manoeuvres
Sea targets (below sea surface)	Medium range surface effects
Tactical ballistic missiles (TBM)	Short to long range fast reaction time high manoeuvrability
Radar installations or detectors	Fast reaction time high manoeuvrability against moving targets
Defense missiles	Short range fast reaction time high manoeuvrability
Highly accurate drop of loads (supply)	Low cost
Delivery of non-lethal weapons	Short range very high reliability
Observations of battle fields	Short range low signature
General surveillance (Snipers, gun positions, troop movements)	Short to medium range Low signature Long operation time

Table 2. Desired characteristics of Missiles.

PENGUIN MK2 MOD7 INTEGRATION IN THE SIKORSKY S-70B HELICOPTER INTEGRATION AND LIVE FIRE TESTING

Are Christian Sollie
Senior Principal Engineer
NFT Aerospace Group
P.O. Box 1003
N-3601 Kongsberg, Norway

Steve Spitz
United Technologies
Sikorsky Aircraft
6900 Main Street
Stratford, CT 06601-1381, USA

SUMMARY

The paper describes the Penguin MK2 MOD7 (AGM-119B) anti-ship missile integration in the Sikorsky S-70B helicopter. Innovative design techniques allowed use of existing aircraft and missile hardware. Only software development was required to integrate the Penguin missile with the S-70B aircraft. The paper discusses briefly the system integration testing and presents some of the test results. The system integration testing was based on extensive simulation of mathematical models and a low-cost instrumentation of a captive carry flight test range in the Long Island Sound, USA. Finally, some test results from a live firing demonstration performed at USN NAWCAD, Patuxent River are given.

1. INTRODUCTION

The Penguin MK2 MOD7 Missile (AGM-119B) is a fire and forget IR homing anti-ship missile designated for helicopter launch. The Penguin MK2 MOD7 was integrated in the US Navy SH-60B LAMPS MKIII helicopter in the late 1980's and became operational in 1993.

The integration to be discussed in this paper is for a Sikorsky Aircraft S-70B naval helicopter which is an international derivative of the USN SH-60B helicopter. The S-70B aircraft has a similar airframe to the SH-60B aircraft but a different avionics suite. Only the Missile Control System was added to the standard avionics configuration.

The Penguin missile was originally designed for operation in Norwegian fjords and coastal waters. This operation puts strong demands both on the missile's ability to avoid land obstacles and the correct positioning of the seeker field of regard. The missile is therefore equipped with an Inertial Navigation System (INS) and a digital autopilot with trajectory shaping. The missile INS components provide sufficient stability for a missile flight, therefore the overall missile navigation performance is

governed by the alignment of the INS reference frame. The paper will discuss more details on the design and flight testing of the alignment system.

To ensure alignment filter robustness and performance during dynamic flight, and to verify sufficient targeting and weapon control, it was necessary to perform captive carry flight testing over water on an instrumented range. A cost effective solution was to instrument a test facility on the Long Island Sound which is in the vicinity of the Sikorsky Aircraft, Stratford CT, facility. The instrumentation consisted of a mobile telemetry ground system and three commercial GPS receivers with PC compatible software for differential position reference.

The Penguin MK2 MOD7 integration on the Sikorsky Aircraft S-70B helicopter was completed by live firing at the NASA Wallops Island test range. The test set-up and the main test results will be presented.

2. SYSTEM GENERAL DESCRIPTION

2.1 Missile general description

The Penguin Mk2 Mod7 (AGM-119B) Missile is a true fire-and-forget missile which combines precision inertial guidance with a high-resolution IR-seeker in order to locate, identify and home on targets. The missile does not require any in-flight guidance from the launching platform during flight. All data needed to achieve a successful result, such as target position (or bearing to target), desired flight profile and seeker mode, have all been entered into the missile from the helicopter mission computer prior to launch.

Using inertial navigation for mid-course guidance, the missile flies to a pre-determined position relative to computed target position ready to start searching for the target. When the target is detected the missile seeker optimizes the hit-point based on the distribution of the IR signal.

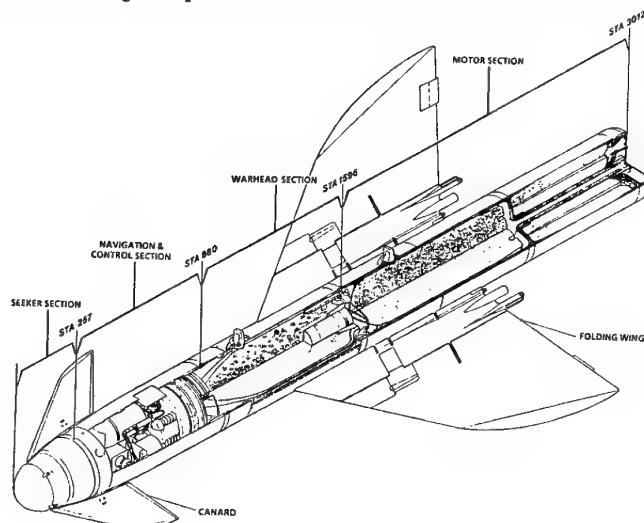


Figure 2.1. Penguin Mk2 Mod7 Missile

The missile, which is of conventional aerodynamic design, has a rolling airframe with cruciform wings, has a high subsonic speed and cruises at a low nominal altitude. Although originally built for use from helicopters, the Mk2 Mod7 missile maintains the integrity of earlier Penguin ship-launched models, and may be deployed from any static or slow-moving platform (e.g. ships and shore installations). The two-stage rocket motor (booster and sustainer) will ensure successful take-off during the launch sequence.

A 120 kg warhead with 43 kg high explosive (HE) and a delayed action fuze mechanism, will inflict serious damage on any medium-size or smaller combatant.

Missile characteristics:

Designation:	Penguin Mk2 Mod7
Overall length:	3020 mm
Diameter:	280 mm
Wing span:	Deployed: 1420 mm Folded: 760 mm
Launch weight	395 kg
Warhead weight	120 kg (43 kg HE)
Guidance:	Midcourse inertial, programmable flight path. Terminal passive IR.
Cruise speed:	High subsonic
Operational range:	> 3 nautical miles < 18 nautical miles
Firing arc:	360°

2.1.1 Missile Seeker

The seeker consists of a mechanically scanning, infrared pseudo-imaging system with the capability of autonomously searching the target area, acquiring and classifying the target, and switching from search mode to a terminal tracking mode. Search width may be selected from one of three options to counteract reduced target data quality and obstacles in the target area. At a fixed distance from target intercept point, the seeker is automatically activated and starts scanning a strip of the sea surface ahead of the missile. After first having established an infra-red reference level based on the environmental conditions in the search area, the seeker scans the sea surface in search for the target, recognized as an IR contrast. Upon detection of such signal, the signal is automatically validated for ship-like characteristics. If positively confirmed as a ship, the seeker will enter the tracking mode for terminal guidance as the seeker maps out the target contrast against the sea background, independent of target hot-spots. After making an altitude pop-up to gain a favourable angle of attack, the seeker will guide the missile to an impact point close to the target water-line, thus inflicting maximum damage in the target. The all-digital processing facilitates efficient schemes for discriminating between decoys and ships, giving the seeker a very high resistance against IR counter measures in the search phase as well as in the tracking phase. The seeker has been made indifferent to changes in temperature and humidity and thus maintains all-weather capability.

2.1.2 Missile Navigation and Control System

To fully utilize the features in the target seeker, the missile is equipped with an inertial navigation system (INS) with accuracy well within the seeker's search geometry and a digital autopilot with the capability of trajectory shaping.

The missile INS consists of an inertial measurement unit (IMU) and a navigation processing system (NAPS). The IMU has a semi-strapdown mechanization with a gimbal in the roll axis due to the missile rolling airframe. Sensor outputs are sampled by the NAPS at a fixed rate, compensated and then used to perform update of the navigation solution, see figure 2.3. During the alignment phase (pre-launch phase) the missile is using a local geographic reference frame, while during free flight (after launch) the missile is navigating in a Wander Azimuth reference frame.

The IMU gyro output is compensated for known errors (calibration data established in the IMU production line), corrected for earth rate, earth curvature (transport rate) and Schuler tuning and then used to update the Direction Cosines and Euler angles. Accelerometer output is compensated with the calibration parameters, as for the gyros, corrected for the Coriolis effects and integrated.

Prior to launch, the missile navigation reference system is continuously aligned to the helicopter navigation reference system. Corrections to the missile navigation system is estimated by the Alignment Filter (ref. paragraph 2.3) and used to update the NAPS computation scheme. Estimates of both misalignment, velocity error and certain IMU sensor errors are used for correction.

In general a navigation system performance is a function of both the quality of the INS sensors and how well the INS reference frame has been aligned. For the Penguin missile, with its INS, the experience has been that errors caused by the uncertainty in alignment have often been more significant than the accuracy of the INS itself. The transfer alignment for helicopter applications is further discussed in section 2.3.

The complete position reference of the missile flight trajectory, from separation to predicted target impact, is computed prior to launch. During set-up and planning of a Penguin launch the missile trajectory, as computed by the missile system, is continuously updated and displayed for the operator on the helicopter Multi Function Display. The operator may at any time modify the set-up to improve the tactical scenario. During the launch sequence the missile is given the final targeting data and trajectory data.

The missile trajectory, separated in the vertical and the horizontal planes, consists of arc segments and straight lines. Where applicable, turn manoeuvres are co-ordinated with dive manoeuvres to maximize use of the energy.

Figure 2.4 shows the vertical trajectory and figure 2.5 shows some examples of horizontal trajectories.

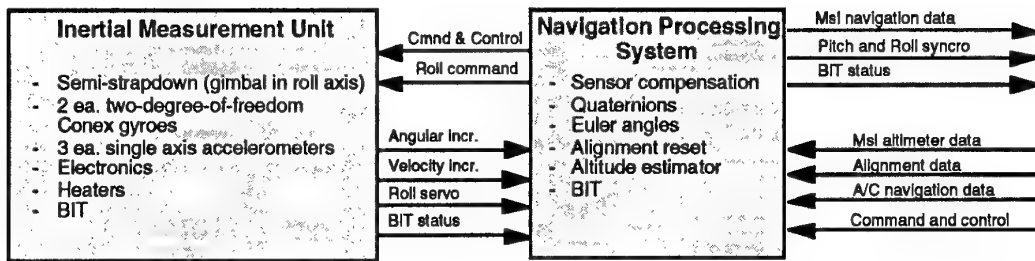


Figure 2.2. Missile Inertial Navigation System (INS).

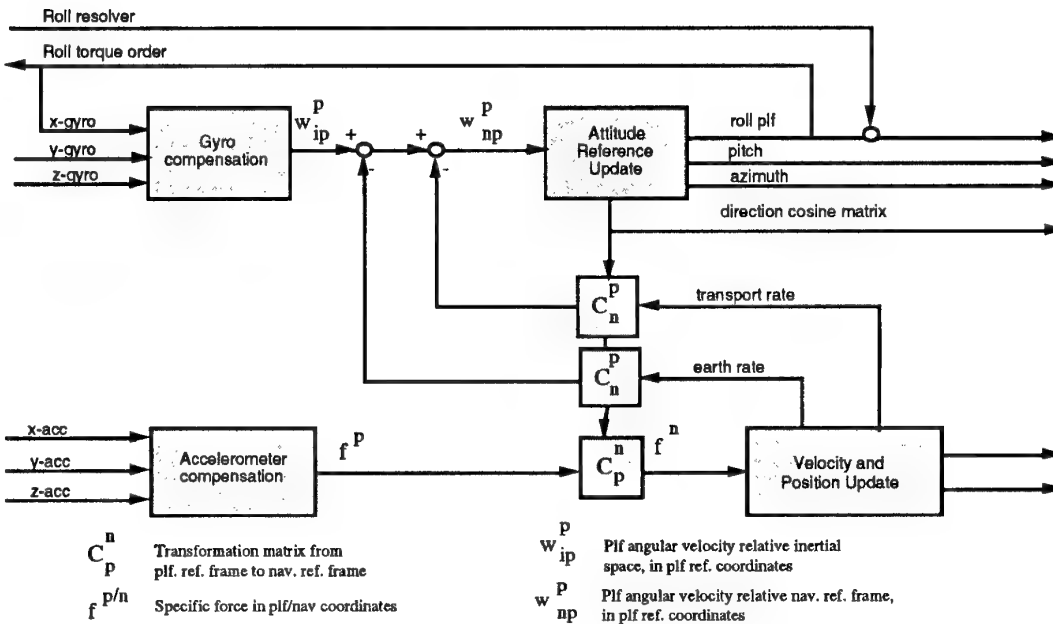


Figure 2.3. Penguin Missile Navigation Processing System (NAPS).

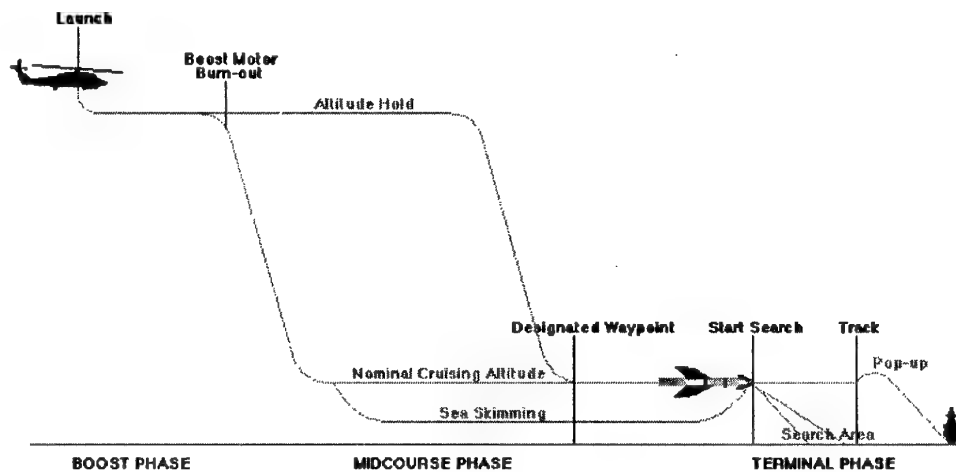


Figure 2.4. Examples of Missile Vertical Trajectories (not to scale)

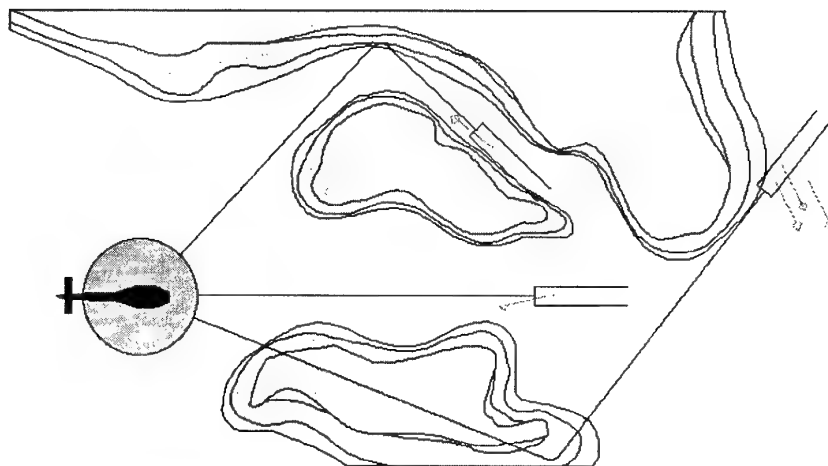


Figure 2.5. Examples of Missile Horizontal Trajectories (not to scale)

2.2. Helicopter Description

2.2.1. General

The Sikorsky Aircraft S-70B helicopter is a derivative of the USN SH-60B Seahawk helicopters. The primary missions are:

Anti-Submarine-Warfare (ASW), Anti-Surface-Warfare (ASuW), Search and Rescue (SAR) and Surveillance. A drawing of the S-70B helicopter is shown in figure 2.6 with key dimension and weight given in table 2.1. A total of 265 Sikorsky S-70B helicopters are today in service in the following countries: USA, Spain, Australia, Japan, Taiwan and Greece.



Figure 2.6. Sikorsky S-70B helicopter with Penguin Missile mounted

Length overall, rotor and tail pylon folded	12,47 m
Width, rotors folded	3,26 m
Height overall, pylon folded	4,04 m
Weight, empty	6.191 kg
Weight, maximum gross weight	9.926 kg

Table 2.1. Sikorsky S-70B key dimensions and weight.

2.2.2. Avionics Configuration

The integrated mission system is designed around a dual redundant MIL-STD-1553B data bus with sensors, armament, control and display and weapons as subsystems. Only the ASuW mission, which is linked to the Penguin MK2 MOD7 integration, will be covered in this paper. The following subsystems are directly or indirectly utilized in the control and launch of a Penguin MK2 MOD7 missile:

Navigation Sensors:

Doppler Radar, Attitude and Heading Reference System (AHRS) No.1 and No.2, Radar Altimeter

Mission Sensors:

Search Radar, Tactical Data Processor (2), Multi Function Displays (2), Control Display Units (4), Display Control Panels (2)

Weapons Management:

Armament System Controller (ASC), Armament Control Panel, Jettison Control Panel, Missile Control System

Since the helicopter mission systems are highly integrated all data required by the missile systems are available from the Tactical Data Processor (TDP). The missile integration will therefore remain unchanged if the functionality of the existing systems are replaced by other models. Also, helicopter targeting data to the missile system is transferred on the MIL-STD-1553 data bus. The source of the targeting data may therefore be any targeting sensor integrated in the TDP: search radar, infra-red sensor, third party targeting or even manually entered data.

2.3. Penguin Missile Integration in the S-70B Helicopter

The Penguin missile is mounted to a Missile Launch Adapter (MLA) on the forward left stubwing. The MLA contains the Missile Control System (MCS) which is the electrical interface between the helicopter and the missile and a standard BRU-14 bomb rack with an AERO-1A extension adapter, see figure 2.7 and figure 2.8.

The MCS contains the following units:

- Alignment Unit (ALU) for signal interface between the missile and the helicopter, launch sequence control, transfer alignment, missile trajectory calculations and built-in-test.
- Power Units for supplying power to both the ALU and the missile during captive flight.
- Umbilical Release Unit for retraction of the missile umbilical cable during launch sequence
- Wing Lanyard Assembly for release of the wing folding mechanism after separation
- Cables

2.3.1. Mechanical Interface

The missile is mounted to the BRU-14/AERO-1A bomb rack with two lugs. The AERO-1A adapter is used to achieve 30 in lug spacing. Four sway braces prevent any movements of the missile when mounted to the MLA.

The missile is gravity released from the BRU-14 bomb rack. Missile motor ignition occurs 2-3 meters below the aircraft, and is controlled by the missile sequence controller to prevent any booster motor plume impingement on the aircraft.

2.3.2. Electrical Interface

A block diagram of the electrical interface between the helicopter and the Penguin missile system is shown in figure 2.9. The shadowed units indicate helicopter avionics subsystems that required software modification to control the Penguin missile system.

No additional helicopter avionics sub-systems were required for integration of the Penguin missile except for the MCS. Control of missile modes and inspection of missile status are performed on the existing Control Display Units (CDU) and Multi Function Display (MFD). Arming and launch control is performed on the existing Arming and Launch Panel. All interface signals required between the helicopter and the MCS were obtained by adapting existing torpedo control signals.

2.3.3. Penguin Missile Transfer Alignment

As described in paragraph 2.1, the Penguin missile uses an inertial navigation system (INS) for guidance purposes. Prior to launch the navigation reference frame of the missile INS must coincide with the helicopter's computed navigation reference frame. The process of aligning the missile navigation reference frame to the helicopter reference frame is called Transfer Alignment and is performed by an Alignment System. The purpose of the Alignment System is to:

- Establish the missile navigation reference frame, and maintain this until missile launch.
- Initialize the missile velocity

In addition to (a) and (b) above the Alignment System will also estimate corrections to certain inertial sensor calibration parameters to account for turn-on to turn-on variations. The estimation process is located in the MCS while the correction process is located in the missile navigation computer. The alignment process is split into three main parts:

- Initial Roll Alignment:** This process takes place immediately after power on. The missile roll gimbal is slaved to zero degrees.
- Coarse Alignment:** The Coarse Alignment is an initialization process for the Fine Alignment process. Pitch, roll and azimuth data from the helicopter avionics are used to correct the missile direction cosine matrix. Low pass filtered doppler radar velocities, rotated with the present missile direction cosine matrix, are used to initialize the output of the specific force integration in the navigation computer.
- Fine Alignment:** Correction data to the missile navigation computer is estimated based on velocity and azimuth data from the missile INS and the helicopter navigation sensors. The estimation is performed by a recursive minimum variance estimator (Kalman Filter), see figure 2.10.

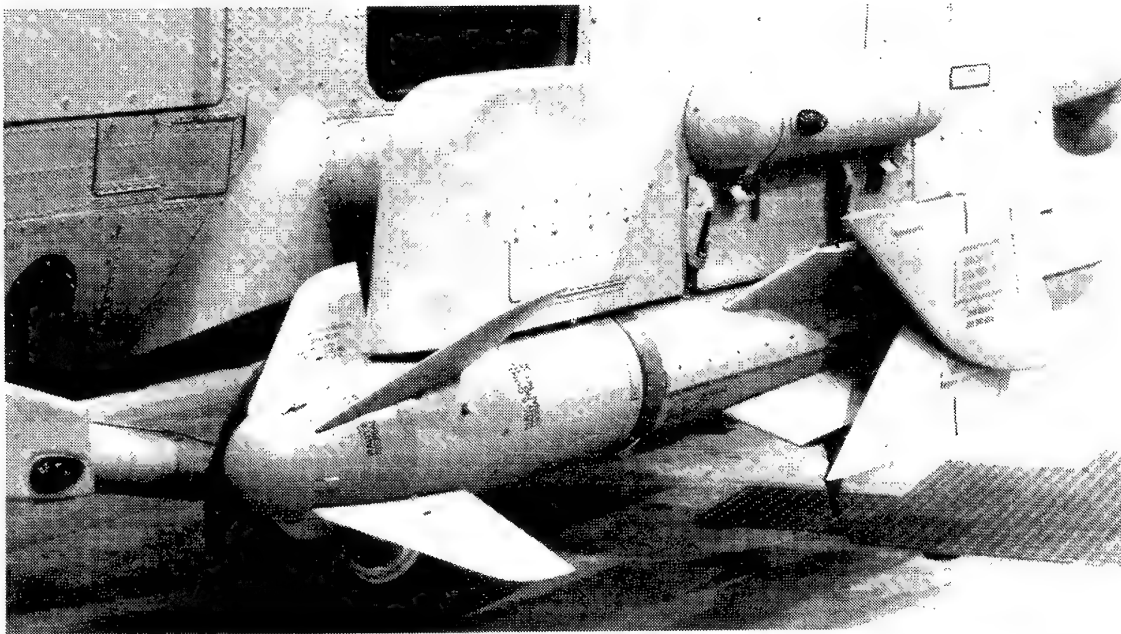


Figure 2.7. Penguin Missile Launch Adapter mounted to the S-70B helicopter

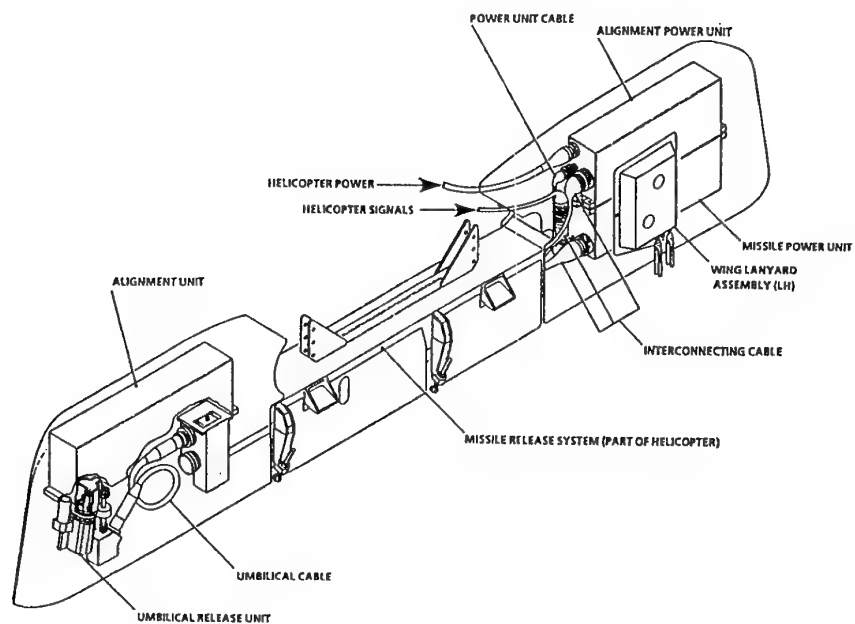


Figure 2.8. Cut-through drawing of the Missile Launch Adapter (MLA)

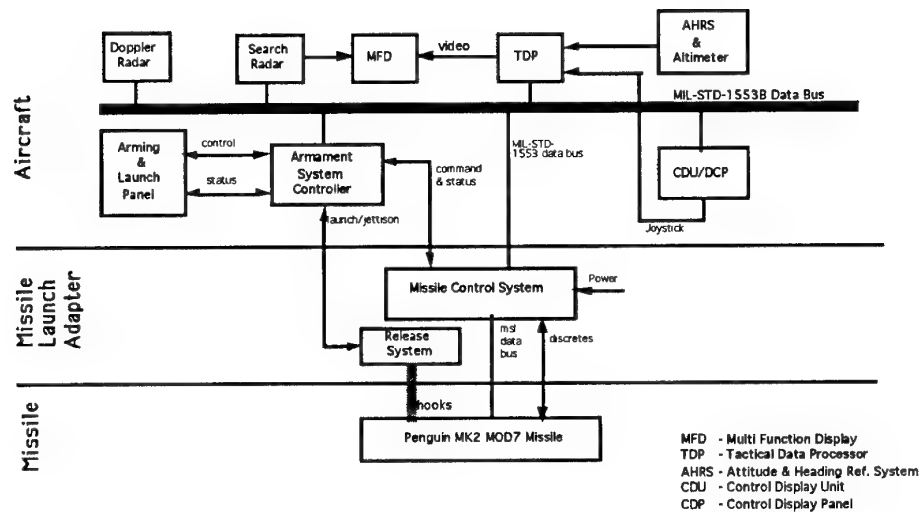


Figure 2.9. Block diagram of the interface between the helicopter and the missile system.

The reset function closes the loop in the feedback system. A linearized model is therefore used to describe the error development in the Kalman filter. The Prefilter computes an average of the deviation between the helicopter and missile velocity and azimuth angles. The Prefilter also computes the time variant elements of the system matrix of the error model used by the Kalman filter and averages these over the filter interval. No attempts were made to compensate the transition matrix for exact averaging time. The effect by doing this was analysed and found to have insignificant effect on the performance. The lever arm effect, which is an important factor in a fighter aircraft application, was analysed and also found to have insignificant effect on the navigation data comparison between the missile and the helicopter. The challenges, not in priority, when designing and testing the Alignment System were:

- a. Adjustment of the Kalman Filter measurement noise level and process noise level to match the actual performance.
- b. Find criterias for when estimation could occur with respect to reliable data, and when only time update (prediction) of the filter could be performed.

- c. Find criteria for alignment performance, i.e., when sufficient alignment for a missile launch had been achieved.
- d. Tune the filter characteristics with respect to robustness.

The main challenge, however, was that the four challenges above do interact and can not be separated. The challenge was solved using the Penguin Alignment Simulator (PALSIM) in combination with captive carry flight testing. Test data from captive carry flights were used to update and validate the simulator and to verify actual alignment performance. The PALSIM was used for post-simulations, design and test of software modifications based on test data, and for pre-simulations to establish additional flight procedures. This is illustrated in figure 2.11.

The end product was an Alignment Filter that does not put any restrictions on the helicopter flight envelope, is insensitive to temporary transient errors that are inherent in any doppler radar and AHRS, provides sufficient performance within minimum alignment time and is stable for any helicopter mission time.

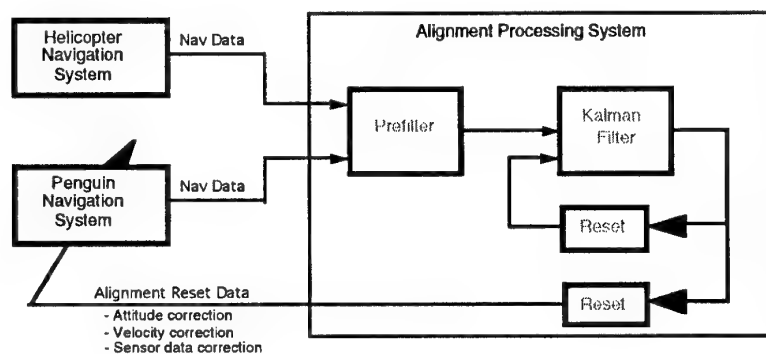


Figure 2.10. Block diagram of the missile alignment filter (Fine Alignment).

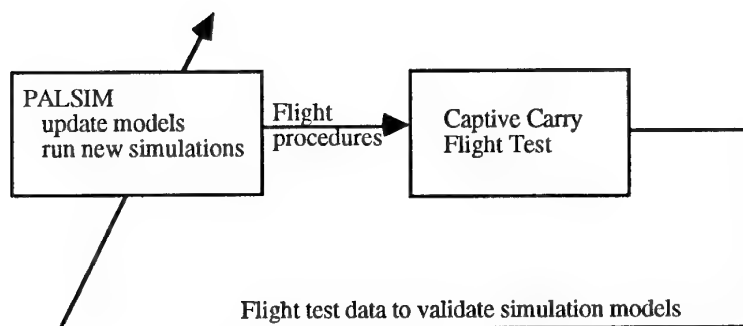


Figure 2.11. Interaction between simulations and actual flight test data

3. TEST AND VERIFICATION

The Penguin MK2 MOD7 had previously been integrated in the USN SH-60B helicopter. The SH-60B helicopter has identical airframe to the S-70B helicopter with the exception of radar radome size and some antenna configuration. The difference in airframe was, by analysis, found to have insignificant effect on the aerodynamic flowfield at the missile station. The missile captive carriage and separation from the S-70B helicopter were therefore qualified by similarity.

The SH-60B and S-70B helicopters, however, have quite different avionics configurations. All integration testing performed was therefore related to the avionics integration. The avionics integration effort was highly based on mathematical modelling of the avionics systems and simulations. The Penguin Alignment Simulator and the missile telemetry system played a central part of the simulation analysis.

3.1. Special Test Equipment

3.1.1. Penguin Alignment Simulator

The Penguin Alignment Simulator (PALSIM) is a simulation system for design, analysis and test of the missile alignment and navigation system. It contains a mathematical model of the helicopter avionics system, the missile navigation system and the Missile Control System (MCS). The MCS application software may be simulated in a close to real environment. Expensive flight testing can therefore be reduced to a minimum. The first generation of PALSIM was presented in the AGARD Guidance and Control 46th Symposium in Norway 1988. A block diagram of the PALSIM is shown in figure 2.1.

The helicopter trajectory generator contains a simplified dynamic model of the launch platform. Based on trajectory reference input elements (desired helicopter velocity vector and altitude) the model computes the "true" helicopter navigation data.

The helicopter navigation model contains approximate models of the helicopter doppler navigation radar system and attitude and heading reference system (AHRS). The Penguin navigation model contains correction for lever arm effects, a model of the missile inertial measurement unit and a model of the missile altimeter. The navigation computer program of the missile

model contains the missile Navigation Processing System (NAPS) software also residing in the operational Missile System

The doppler radar model computes the helicopter velocity in a body axis reference frame. Errors are added in accordance with the specification for the doppler radar. The output velocity includes velocity bias errors, velocity scale factor error, random noise and correlation effects (due to sequential sampling of four doppler beams). The model of the helicopter attitude and heading reference system computes the measured helicopter azimuth (true heading) angle and the helicopter pitch and roll angle. Magnetic heading bias errors are implemented as a look-up table. Helicopter pitch and roll are not used by the missile alignment system, therefore a simplified model (random noise) is modelled. A time delay has been included for the helicopter navigation data to represent the mission computer processing time and data bus transmission delay.

During the captive carry flight test program tests were planned and prerun using PALSIM. The flight profiles were then "flown" and the test data used to update and improve the PALSIM model. The primary objective for the PALSIM is test and analysis of the alignment system, but the PALSIM is also used to simulate the missile navigation accuracy and stability during missile free flight. Using operational flight program software in a simulated environment that has been sufficiently tuned to actual test data provides access to data not available through the missile telemetry system.

The PALSIM system may be used in two configurations: as a Monte Carlo simulation system and as a Hardware-in-the-Loop simulation system. When used as a Monte Carlo simulation system a model of the MCS is used. This model contains all MCS operational software except interface software. When used as a Hardware-in-the-Loop simulation system a production MCS is used. The MCS can not differ from a PALSIM simulation and an actual captive carry flight. Monte Carlo simulations were done to analyse the statistical behaviour of the filter. Input to the filter consists of data infected with normal distributed Gaussian noise, and output from the Monte Carlo simulation is expected to show a similar statistical characteristic.

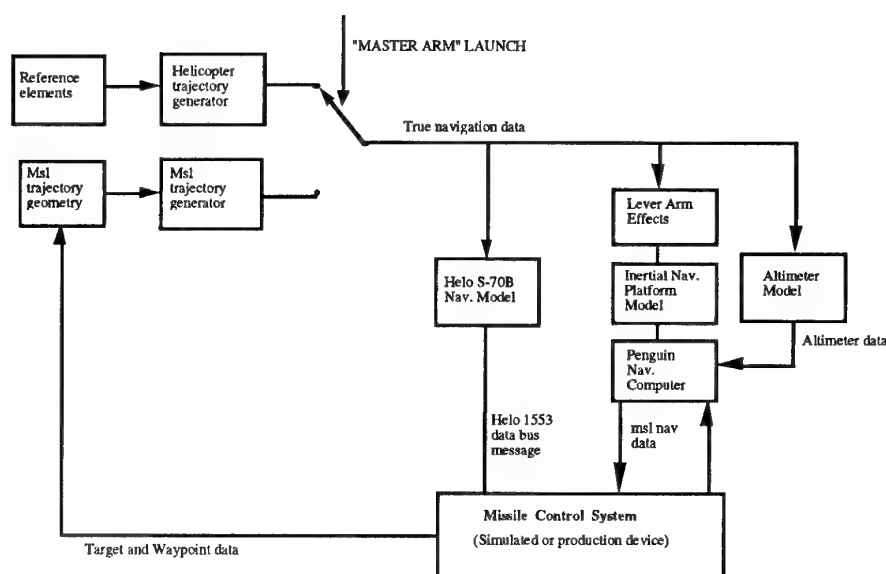


Figure 3.1. Block diagram of the Penguin Alignment Simulator (PALSIM)

3.1.2. Telemetry Ground Equipment

The Penguin MK2 MOD7 missile may be configured with a telemetry section as a replacement for the warhead section when recording and/or monitoring of missile internal data is essential, e.g. test firings and captive carry flight testing.

The missile telemetry section contains a telemetry processing system (TEPS), a transmitting antenna and a battery unit. The TEPS receives data from the missile data bus plus a number of analog signals. The data is formatted, coded and modulated before being transmitted to ground. The telemetry data stream contains approximately 1000 data bus signals sampled with a rate up to 100 Hz and approximately 50 analog signals sampled with a rate up to 7 kHz.

The telemetry signal is received and processed by the Telemetry Ground Equipment. The Penguin Telemetry Ground Equipment used in previous Penguin programmes was based on a VAX-730 computer. The system was installed in a standard transportation container with air-condition and utility hardware. Transportation required use of truck and C-130 air lift. It was decided to convert the telemetry ground processing to a system based on standard PC's. The ground equipment was also supplemented by a portable telemetry tracking antenna. Figure 3.2 shows a block diagram of the upgraded Telemetry Ground Equipment configuration.

The Pulse Code Modulated (PCM) output signal from the telemetry receiver is fed both to a tape recorder and to the PC

Server. Time reference is either from an internal IRIG-B source, a GPS receiver which is part of the Telemetry Ground Equipment or range time if telemetry data shall be correlated with other range data such as tracking data. The time reference is also stored with the TM data on the tape recorder for later use. The PC Server may be run in either a real time application or in a post-processing application. In real time application either telemetry data is output over a Local Area Network (LAN) to PC laptop real time displays, or telemetry data are converted to analog form for output on a strip-chart recorder. The real time display screens may at any time be dumped to a laser printer. A number of critical flight parameters can also be transferred on a serial line to a serial line receiver, e.g. a computer in a range control room for correlation with other range data. A key feature is the cancellation of telemetry drop outs: false data caused by a weak signal strength or erroneous transmission will never be displayed.

The standard configuration uses three PC laptop real time displays but other units may be added to the LAN. All data information is equally available for all of the real time displays, each of the displays may therefore display any desired information. A number of different pre-defined screens are available for each of the real time displays and switching between the screens is done by a simple keystroke.

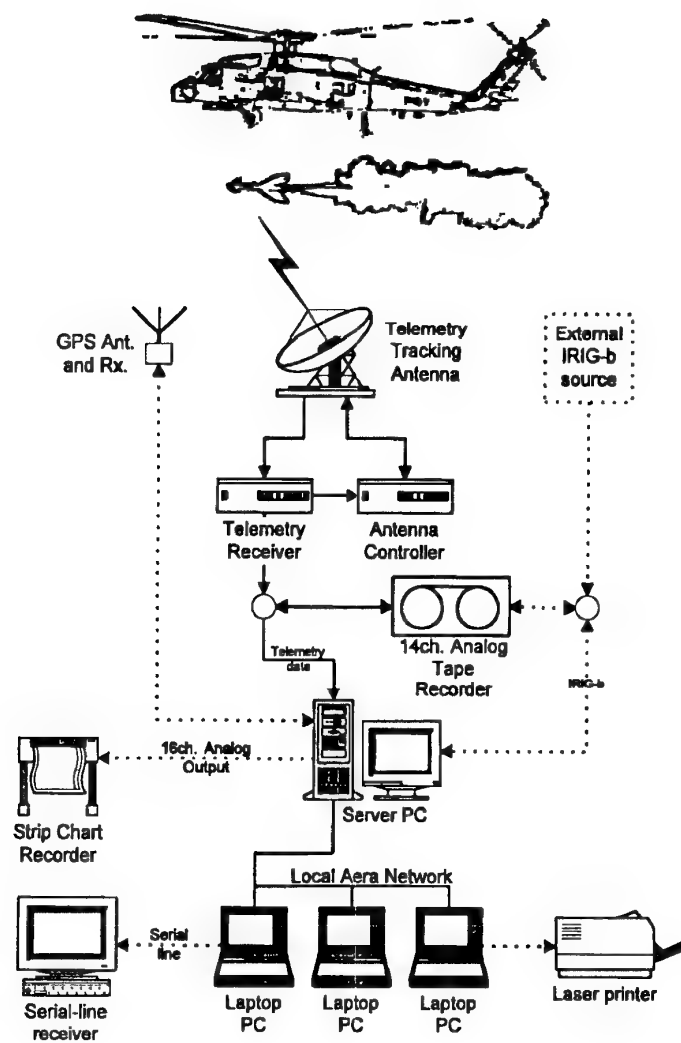


Figure 3.2. Telemetry Ground Equipment.

3.2. Integration Tests

To guarantee success the integration testing was performed in phases. Each of the phases were completed before the next one was started. The majority of the testing was done without using live missile electronics. A flow diagram of a Weapon System Integration Program, with the period of each phase indicated, is shown in figure 3.3.

Both the aircraft avionics system and the missile system were tested separately in appropriate laboratory environments. Both static and dynamic environments were simulated. A Penguin

Missile System Simulator (simulated Missile + Missile Control System) was upgraded from earlier programs, and a Penguin Missile Simulator (missile only) was developed to support the aircraft integration tests. The simulators prevented the need for actual missile hardware at an early stage of the testing, and also provided correct missile interface and response for testing on prototype aircraft mission avionics equipment. The Penguin Missile Simulator was also successfully used throughout the test program to verify correct aircraft electrical interface prior to missile load, and will now be offered to customers as an Operational-level test equipment.

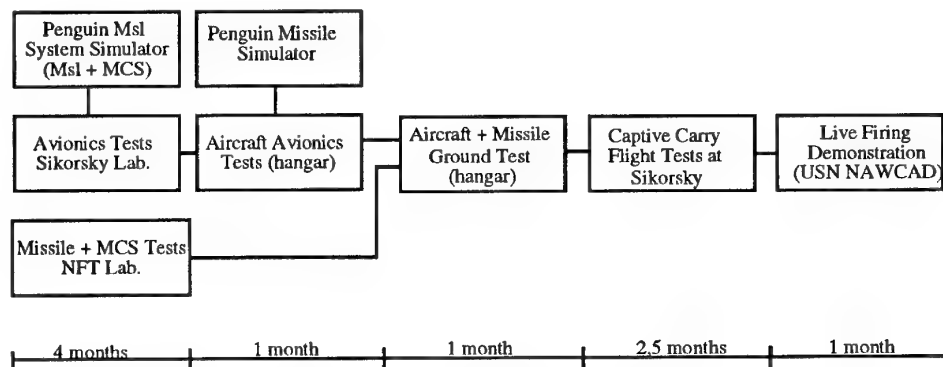


Figure 3.3 System Integration flow diagram.

3.2.1. Captive Carry Flight Test

The main objective of the captive carry flight test was to:

- Tune the missile alignment system to match the helicopter navigation system with respect to performance and robustness.
- Verify the alignment filter sensitivity to helicopter manoeuvres.
- Verify aircraft search radar performance in a dynamic environment with respect to both tracking accuracy and time to establish a track in different environments.
- Verify missile waypoint and trajectory calculations in a dynamic environment with actual helicopter targeting and navigation data input.
- Verify the tactical display with dynamic input data with respect to human interface requirements.

The captive carry flight testing was performed over water in the vicinity of Sikorsky Aircraft Stratford facility, see figure 3.4. The captive carry flight testing was performed over a period of less than 2.5 months, with a total of less than 15 flights including a Weapon System Performance Test where no modifications to the system were done. Using the Long Island Sound as the test range was based on program cost and test range availability. Only weather restrictions would limit use of the range and only a limited investment would be required to instrument the range. Effort was rather put into data analysis tools and wide use of mathematical models rather than expensive measurement equipment. The range instrumentation is shown in figure 3.4 with instrumentation equipment list given in table 3.1. Investment was limited to 3 ea. GPS antennas/receivers with IBM PC compatible software for Differential GPS computations.

Helicopter instrumentation:	MIL-STD-1553B data bus monitor with recording facility. Recording of search radar video. Video recording of MFD display. GPS antenna/receiver with recording facility (IBM PC computer with SW).
Missile instrumentation:	Missile telemetry (missile data bus signals and analog/discrete signals).
Target instrumentation:	GPS antenna/receiver with recording facility (IBM PC computer with SW).
Ground instrumentation:	Missile Telemetry Ground Equipment. GPS antenna/receiver with recording facility (IBM PC computer with SW) used as reference for GPS Differential post-processing.

Table 3.1. Captive Carry Flight Test instrumentation.

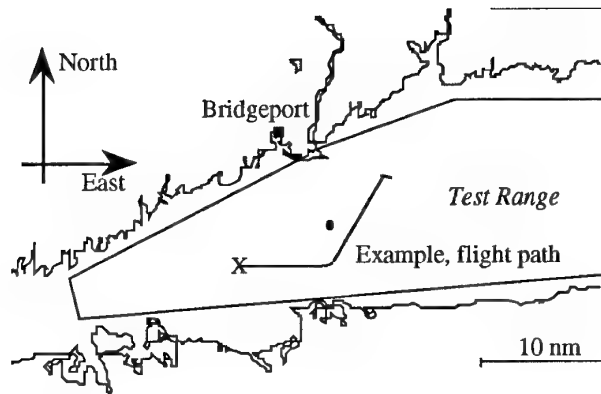


Figure 3.4. Captive Carry Test Range Test Range.

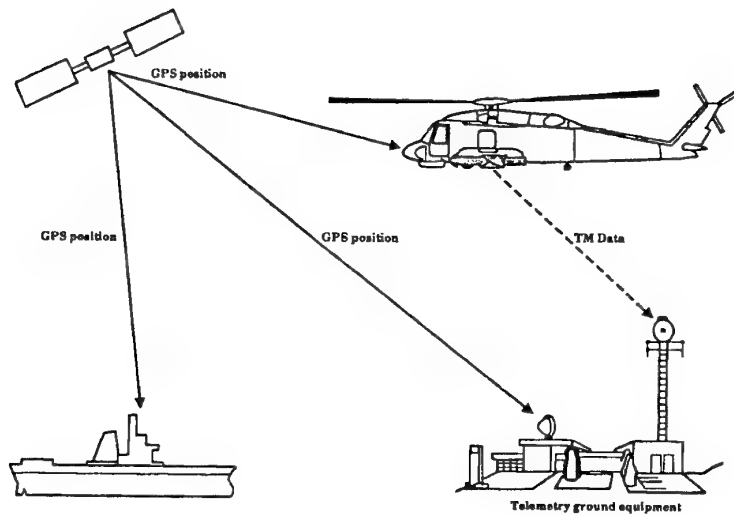


Figure 3.8. Long Island Sound test range instrumentation

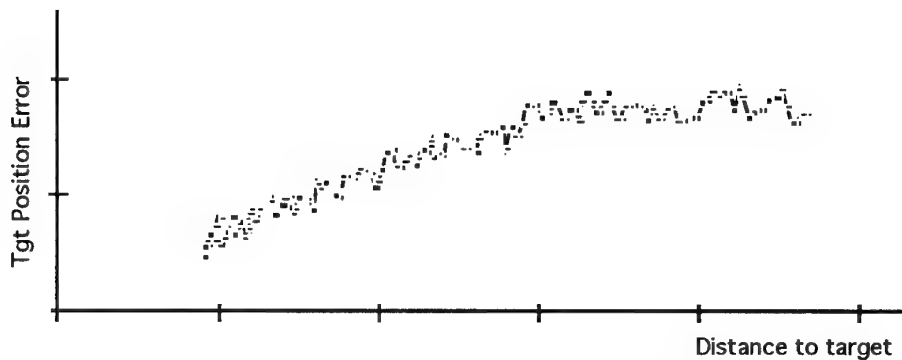


Figure 3.6. Typical error in target position as function of distance to target.

The helicopter search radar is an essential part of the S-70B/Penguin MK2MOD7 weapon system. It is therefore important to test the search radar with respect to the applicable mission in a dynamic environment. Using the test range as described above, any ship or boat above a certain size could be used for testing of the radar's tracking capability. A passenger ferry, for instance, would have the necessary size but also a fairly predictable speed, course and departure schedule, thus planning of test procedures would be easy. The helicopter flight profiles were planned to achieve different search radar aspect angles of the "target" (radar cross section) and different target course relative to the aircraft heading. Various helicopter manoeuvres during radar tracking were also performed to validate the radar's sensitivity with respect to initiate "dead-reckoning", time to establish a new track and time for the new track to converge. Figure 3.6 shows a typical example of how the target tracking converges as the helicopter approaches the target in a straight and level helicopter flight.

The Alignment System had been extensively tested with the PALSIM simulator (ref. paragraph 3.1.1) prior to the captive carry flight testing. The simulator, however, contained mathematical models of the helicopter navigation system which needed to be validated by actual dynamic flight data. Also, a simulator can never give a 100% correct representation of the real world, therefore it was necessary to verify the simulated results with actual flights. The captive carry flight tests did not reveal any big surprises, however, some minor tuning of certain filter constants and some additional filter logic were necessary:

- a. Since the helicopter AHRS azimuth is used for both radar tracking and missile alignment it is important that the missile azimuth alignment is performed with minimum time delay. Flight testing revealed a slightly different AHRS characteristic than anticipated and modelled. The PALSIM models were updated and new simulations were run in different dynamic environments. Based on the simulations the alignment filter was modified to put more weight on the helicopter azimuth measurements and less weight on estimation of azimuth related INS sensor errors.
- b. The aircraft has two AHRS's of which the output data may deviate from one another. In case of a primary AHRS failure the system switches to the secondary AHRS. A reset function was therefore implemented in the Kalman filter to account for the possible change in azimuth reference data: both azimuth misalignment and related estimates were reset

and the gains were increased. The alignment estimation is recovered within minimum time.

- c. A similar situation as in case (b) above may occur if a sea bias correction is entered or changed. The missile MCS was modified to survey the sea bias data from the helicopter and, if a change occurs, the alignment filter velocity estimates are reset and the filter gains are increased. The alignment estimation is recovered within minimum time.
- d. Based on a number of captive carry flight tests, with different missile uploads, the mechanical alignment was found to be better than originally modelled in the PALSIM. After updating the model, and re-run of simulations, the alignment filter was tuned to represent the findings.
- e. The alignment Kalman filter processes noise and measurement noise, except for azimuth related noise characteristics which is covered above, needing only minor tuning to give a best match with respect to robustness and performance.

Figure 3.7(a) shows helicopter and missile azimuth measurements prior to, during and after a turn manoeuvre. Figure 3.7(b) shows alignment Kalman filter standard deviation in azimuth for the same time period. Figure 3.7(c) shows how missile azimuth is corrected to match the helicopter azimuth after completion of the turn manoeuvre. The oscillation in missile azimuth is caused by vibration induced by the helicopter rotor.

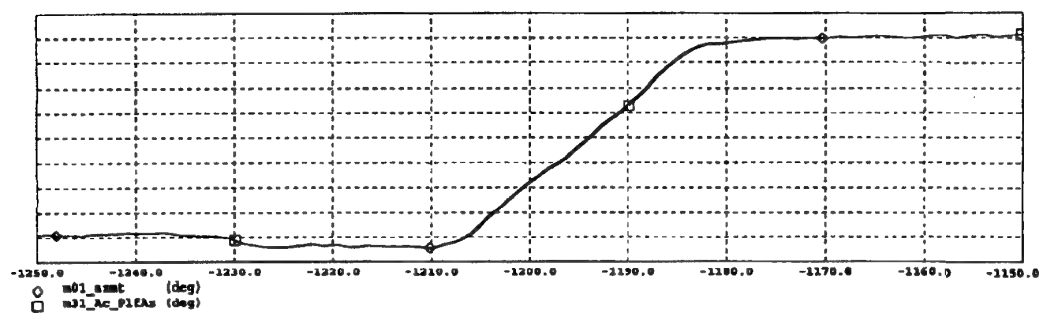


Figure 3.7(a) Helicopter and Missile azimuth during and after a turn manoeuvre.

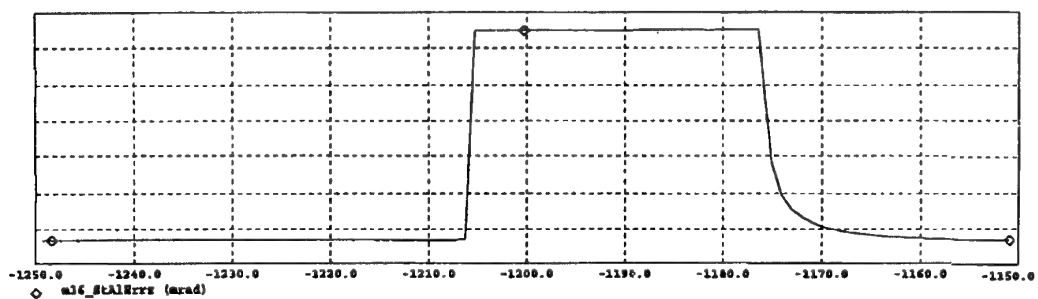


Figure 3.7(b) Standard deviation in azimuth misalignment, uncertainty in azimuth misalignment is increased during turn manoeuvres.

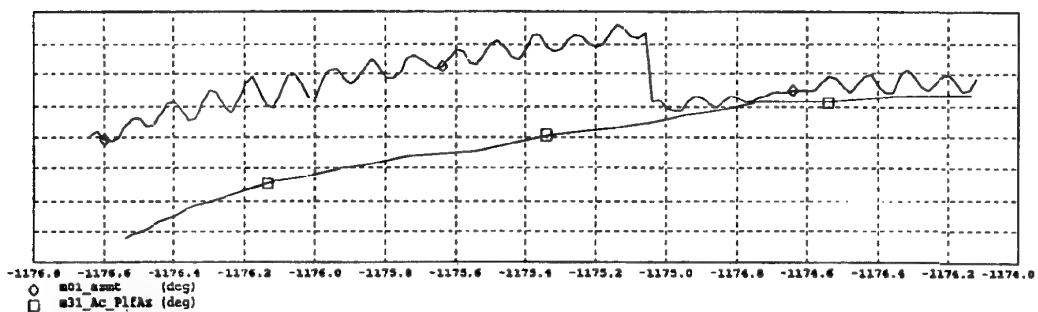


Figure 3.7(c) Missile azimuth is corrected to match the helicopter azimuth (m01_azm is missile azimuth, m31_Ac_PlfAz is helicopter azimuth).

Accurate missile alignment is only a means to achieve accurate missile navigation. The missile has a test mode where missile navigation can be initiated during captive carry just as if the missile was launched. Each of the test runs performed during the captive carry flight test contained a simulated missile launch in order to record missile navigation data for performance analysis. Data from all of the tests were finally used to compute statistical numbers for the achieved missile navigation performance. Estimated missile navigation error for each of the test runs were computed based on:

- Difference between the missile computed position and the helicopter GPS position.
- Difference between missile velocity and helicopter velocity, integrated over a fixed time period.

All navigation tests were done in straight and level flight, independent of the alignment flight profile. This was done both to keep the navigation scenario the same for all of the tests (comparable results) and to provide the best possible conditions for the helicopter navigation system which was used as a reference.

When comparing missile navigation data with GPS data it is important to note that the missile INS is aligned to the helicopter heading reference which may deviate from actual true north. This has no effect on the weapon system performance since the targeting data is given in the same reference frame. The comparison of missile navigation data with range data, however, will be affected. Since GPS position is given in a true north/east reference frame there will be a difference between the GPS position and the missile INS position even with a perfect aligned INS with no sensor errors. The difference in azimuth reference causes a development in position difference which is linear with range and is not, for a captive carry flight with no acceleration during the navigation phase, possible to separate from the azimuth misalignment. Integration of the missile and helicopter velocity difference was therefore judged as a more reliable source for navigation performance. Figure 3.8 shows a typical development of the velocity deviation between the helicopter and the missile.

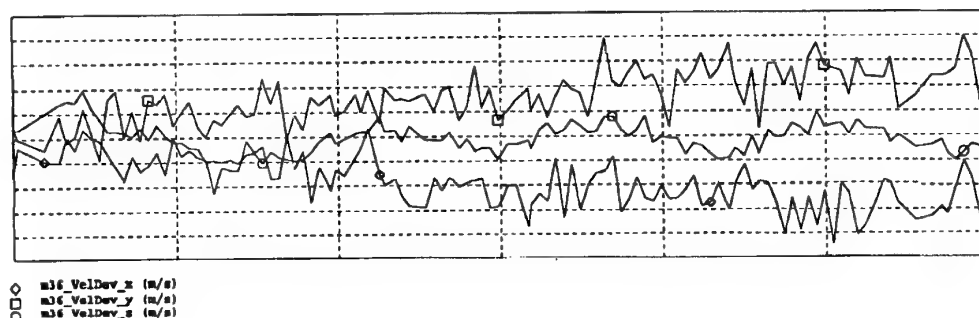


Figure 3.8. Difference between missile and helicopter velocity in north, east and down directions as function of time during the navigation test (no corrections from the alignment system)

3.2.2. Live Firing Test

A Live Firing Test must, for understandable reasons, be performed in a restricted area for range safety considerations. USN NAWCAD, Patuxent River, MD, in co-operation with NASA Wallops Island, have all the necessary facilities for conducting a live missile firing. The live firing of Penguin Mk2 Mod7 from the S-70B helicopter was performed at this facility. The test instrumentation at NASA Wallops Island is depicted in figure 3.9.

The target was instrumented with heaters to create the IR signature, high speed cameras for missile impact coverage, temperature sensors for monitoring the heaters and GPS receivers for target position reference. The missile was instrumented with a telemetry transmitter, a Flight Termination System (FTS) and a radar transponder to ease range radar tracking. Two different radars were assigned for missile tracking. The launch helicopter was instrumented with a NAWC Mid-Atlantic-Tracking-System (MATS) for high accuracy real time position reference and a radar transponder for range radar tracking in addition to the instrumentation package used for the captive carry flight tests.

A common problem with test firings data analysis, when examining the weapon system accuracy, is to separate the missile navigation error from the helicopter targeting error. The

weapon system accuracy is measured by the range radar tracking. These data are, however, given in a reference system that is rotated relative the helicopter and missile reference frame. A more reliable parameter is the seeker search angle in which the target is detected. This angle is directly related to a lateral miss distance since the seeker search geometry is fixed. The lateral miss distance, provided by the seeker, can then be used to compensate radar tracking for rotation. The helicopter targeting error may be found from helicopter and target GPS position measurements. These data, however, suffer from the same rotational error as the radar tracking data.

The missile was launched in a Designate Waypoint mode (operator selectable waypoint). After separation from the helicopter the missile accelerated from launch speed to Mach 0.9, performed the offset turn, the straight leg towards the waypoint turn, waypoint turn and finally the straight leg towards the target. The seeker was activated in the last straight leg and the target was detected and acquired only a short distance to the right of the predicted impact position. All phases of the missile operation, including the pre-launch activities (alignment, targeting and missile set-up), performed well.

Figure 3.11 shows the missile ground track as reported by the telemetry and the range radar tracking. Figure 3.12 shows the same situation in the target area. Predicted impact position is indicated by (1) and actual target impact position is indicated by

(2). The solid line shows the radar tracking which lost track of the missile in the terminal phase and continued with dead-reckoning. The dotted line, which shows the missile ground track reported by telemetry, has been corrected for the estimated reference systems deviation.

The weapon system position error, visible as required missile flight path correction in the terminal phase, was minor and made separation of the missile navigation error from the

helicopter targeting error an academic task. The resultant cross range position error was comparable with estimated radar tracking uncertainty, and also within the uncertainty involved in rotation of the reference systems.

The live firing test was a success with respect to both missile performance, aircraft performance and missile integration.

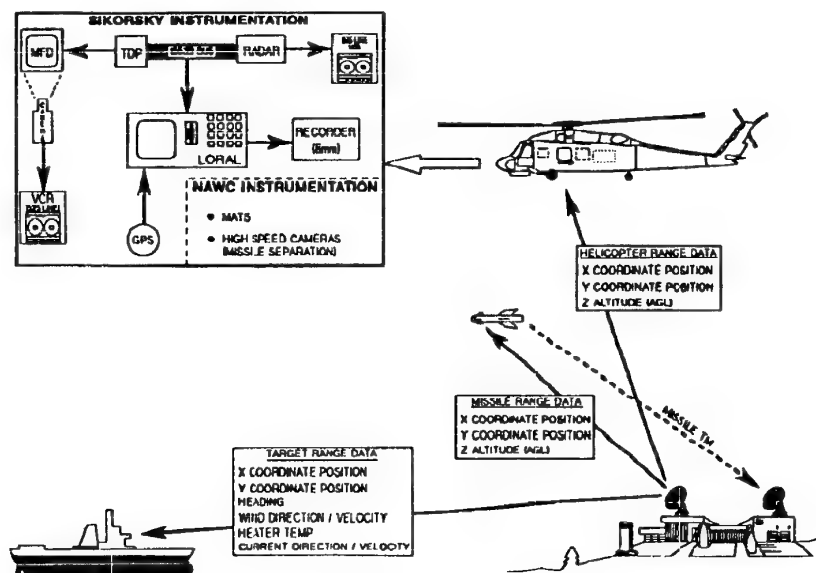


Figure 3.9. Live Firing test instrumentation (telemetry and range radar tracking)

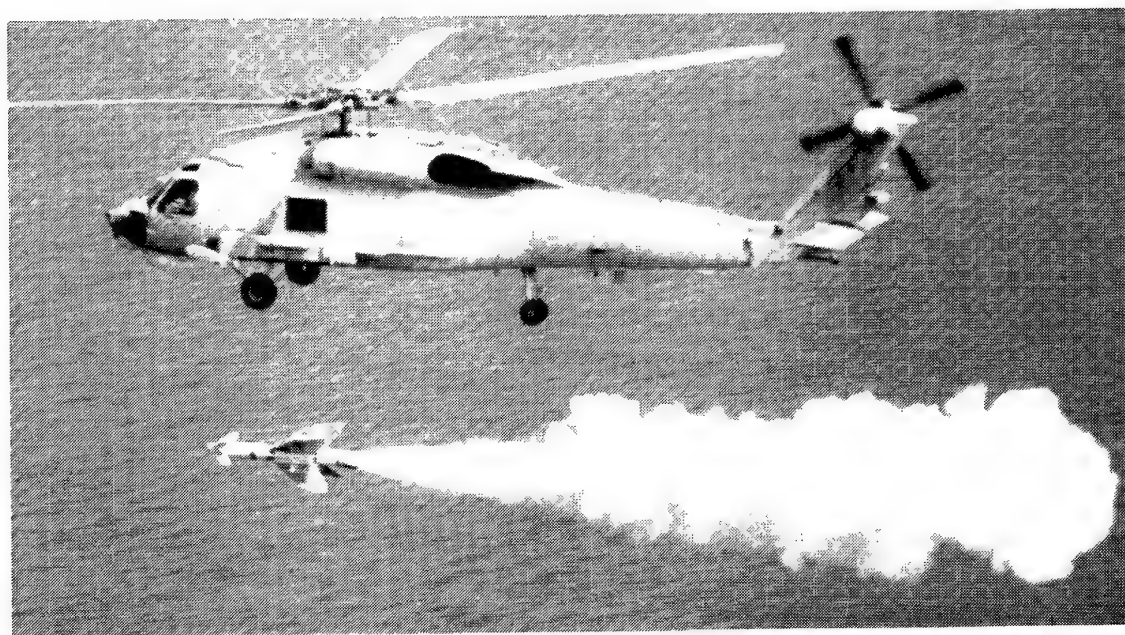


Figure 3.10. Picture from live firing test, immediately after missile boost motor ignition.

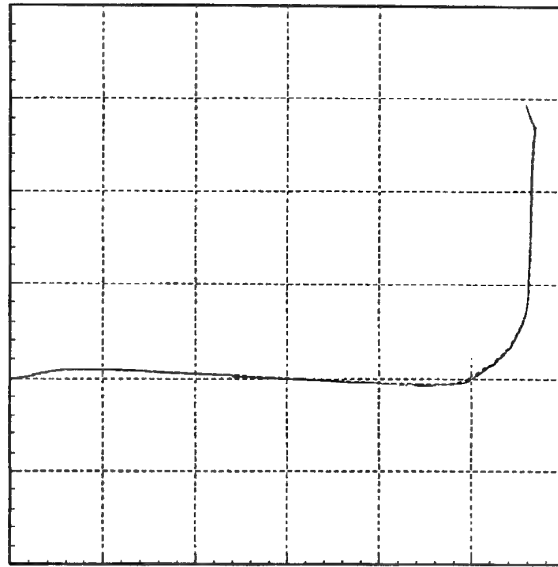


Figure 3.11. Missile north/east ground track as reported by radar tracking and missile telemetry.

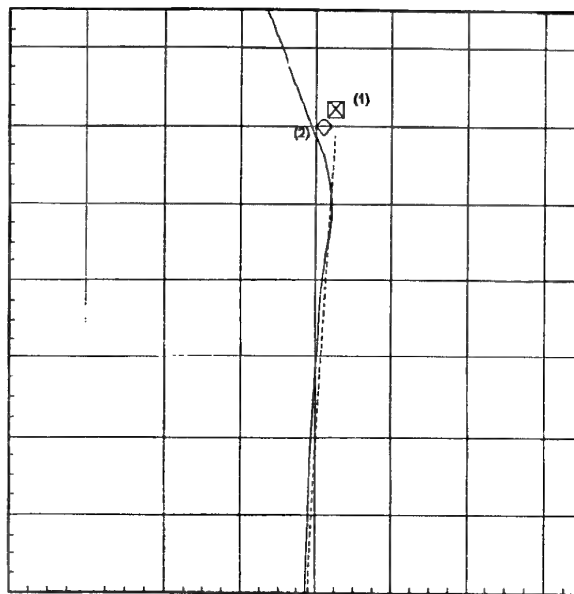


Figure 3.12. Missile north/east ground track as reported by radar tracking and missile telemetry in the missile terminal phase. Dotted line is missile position reported by telemetry, solid line is missile position reported by range radar tracking. Symbol (1) is predicted target impact position, symbol (2) is actual target impact position.

Improved Engagement Envelope of a Tactical Missile with an Integral Rocket/Ramjet Engine

M. Lauzon
Defence Research Establishment Valcartier
P.O. Box 8800
Courcellette, Quebec, Canada
G0A 1R0

SUMMARY

A trade-off study on mission effectiveness identified definite benefits of the solid fuel integral-rocket-ramjet engine over the solid rocket motor for a medium-range air-to-air tactical missile. A six-degrees-of-freedom trajectory simulation model was first developed to assess the performance and operating envelope of the solid rocket motor and the ramjet engine for tactical air-to-air missile applications. The 6DOF simulation code includes a fully algebraic model for ramjet propulsion, a model for missile guidance based on the law of proportional navigation and a three-degrees-of-freedom target trajectory model. It can be used to evaluate missile kinematic performance and effectiveness against a maneuvering target. Results show that ramjet propulsion improves three important performance characteristics of a missile, namely, the time-of-flight (average velocity), maximum range and end-game maneuverability for longer range missions. The solid rocket motor, with its high thrust output and low burn time, gives the tactical missile a higher average velocity and hence a better maneuverability for shorter range engagements. A missile time-of-flight envelope with a non-maneuvering target at 10 km altitude shows that the IRR missile offers a time-of-flight advantage for launch ranges greater than 25-35 km and improves the missile maximum range capability by 40%. The IRR engine also extends the $3 g_n$ maneuverability boundary by 50% in slant range.

LIST OF SYMBOLS

a_n Coefficients in $\dot{r} = a \dot{m}_a^n$
 C_D, C_p Drag and pressure coefficients
 DOF Degree-of-freedom
 DR Ducted rocket
 DREV Defence Research Establishment Valcartier
 g_n Gravitational constant [m/s^2]
 HTPB Hydroxyl-terminated-polybutadiene
 IRR Integral-rocket-ramjet
 \dot{m}_a Inlet air mass flow rate [kg/s]
 NSW Normal shock wave
 OSW Oblique shock wave
 \dot{r} Solid fuel regression rate [m/s]
 SFRJ Solid fuel ramjet
 SRM Solid rocket motor

1. INTRODUCTION

The missile subsystems must be designed and integrated to ensure that the missile meets prescribed mission requirements. An assessment of global missile effectiveness as a function of sub-system design can be performed cost-effectively by modelling the missile system within a trajectory simulation code. In support of research activities in the field of missile propulsion at DREV, a 6DOF trajectory simulation capability was acquired and improved to assess benefits of both the conventional solid rocket motor and the ramjet engine on missile performance and effectiveness. A systems approach is required particularly for modelling the ramjet propelled missile because the performance of the airbreathing engine depends strongly on its flight path. The simulation tool contains all the necessary elements to model this dependence in a straight forward manner.

The DREV six-degrees-of-freedom (6DOF) trajectory simulation code was selected as the baseline. The 6DOF code contains the usual components of a trajectory simulation tool. By providing a complete description of the missile translational and angular dynamics, the tool serves as a generic trajectory simulation platform for the study of other topics of interest (present and future), such as:

- effect of missile incidence on ramjet engine performance,
- effect of the guidance system on the missile dynamic response,
- effect of the control system (aerodynamic surfaces, thrust vectoring) on the missile dynamic response, and
- reaction jet control course correction system for a long-range artillery rocket (Ref. 1).

Finally, the well organized code structure facilitates the integration of new models.

The 6DOF code in its original version did not possess the required capability to model a guided ramjet propelled tactical missile against a maneuvering target. The original version had been developed to model an unguided projectile propelled by solid rocket motor propulsion only (Ref. 1). An algebraic model of the subsonic ramjet engine was identified and

implemented. The model describes the main engine components in sufficient details to account for engine adaptability to varying flight conditions. The ramjet model is also computationally efficient to allow the 6DOF code to perform parametric studies in a reasonable time frame. Finally, with the addition of a missile guidance model and a 3DOF target trajectory model, the 6DOF code can now be used to assess the performance of a tactical missile in an engagement against a maneuvering target.

After completion of the modifications to the 6DOF code, a preliminary trade-off study was performed to identify benefits and compare operating envelopes of solid rocket motor and ramjet propulsion systems for a medium-range air-to-air tactical missile concept. The missile concept was propelled by either a conventional solid rocket motor (SRM missile) or a solid fuel integral-rocket-ramjet (IRR missile).

The ramjet engine benefits mostly medium to long-range missions. Straight and level flight simulations at 10 km altitude (no engagement) show that the IRR missile travels faster than the SRM missile for distances greater than 20 km, and extends the 3 g_n boundary to 50% longer ranges. In co-altitude engagement simulations at the same altitude, the IRR missile also presents a higher performance (time-of-flight, closing velocity, range) than the SRM missile for launch ranges to target typically above 25-35 km. The sustain-level thrust of the ramjet engine suits the longer time-of-flight and smaller average axial acceleration of medium and long-range missions. For smaller launch ranges, the SRM missile offers a higher average speed because the solid rocket motor delivers a high thrust impulse over a short duration. Finally, the tactical missile offers an increase of over 40% in maximum launch range with the ramjet engine over the solid rocket motor. The ramjet propulsion and guidance models implemented in the 6DOF code are discussed separately. The final section presents the results of the preliminary trade-off study.

2. RAMJET ENGINE

A brief description of the ramjet engine summarizes critical operational issues to be included in the ramjet propulsion model.

While the engine internal flow is complex, the mass flow rate of air and fuel through the ramjet engine remains limited by the choked nozzle. The supersonic flow entering the engine inlet is compressed through a system of reflecting OSW (free-stream speed above design Mach number, by design) and through a normal shock wave (supercritical operating mode, by design).

The flow velocity reduces to subsonic speeds before entry into the combustion chamber. Mass addition from the walls (solid-fuel ramjet) or from a separate gas generator (ducted rocket) as well as heat addition from the combustion process both increase the flow speed up to the combustor exit plane. The flow accelerates further in the convergent section of the nozzle up to Mach 1 at the nozzle throat and expands supersonically down the divergent nozzle section. A choked nozzle guarantees subsonic flow in the combustor and ensures a near-optimum thrust output. Because air intake conditions vary with missile velocity and flight path, the engine internal flow adjusts constantly to satisfy the choked nozzle condition. This capacity to adapt of the ramjet engine must be included in the numerical model to realistically represent the dependence of engine performance on flight conditions.

In summary, the ramjet propulsion model must incorporate a capability to dynamically satisfy the choked nozzle condition at all times during the trajectory by changing the profile of the OSW in the intake duct and the position of the NSW in the diffuser.

The role of the air intake duct and diffuser is to supply a subsonic flow of air to the combustion process. The flow enters the combustion chamber with speeds typically of Mach 0.2 to 0.3. The compression of a supersonic flow over the limited volume must occur through a series of shock waves. The departure from an isentropic compression is usually expressed as a total pressure loss, and this approach is adopted in the present ramjet model.

The ramjet engine inlet is assumed to operate above the design Mach number and in a supercritical mode. Inlet operation in the subcritical mode is detrimental to engine performance because the resulting reduction in captured air flow decreases engine thrust output. In practice, the inlet design includes a safety margin against sub-critical operation (the supercritical margin), because a lack of control mechanisms such as variable geometry denies the possibility for actively maintaining supercritical operation.

The propulsive power of the ramjet engine comes from the energy added to the airflow in the combustor by the combustion of a fuel. In a solid-fuel ramjet engine, the combustion takes place within a diffusion flame located near the fuel surface. Some of the energy released from the combustion process serves to vaporize the solid fuel. The inlet air and vaporized fuel feed the combustion process. As the fuel vaporizes, the fuel surface regresses and the combustor

inner diameter increases. In the ducted rocket engine, the fuel is injected in the combustor through a suitable supply system to mix with the incoming air. A suitable insulant protects the inner combustor walls from the intense heat generated by the combustion process. The present ramjet numerical model, in its first version, describes the combustion process with a single equilibrium point for simplicity.

A missile propelled by an airbreathing ramjet engine requires an initial boost phase to accelerate to the ramjet engine start-up speed (typically between Mach 2 and 3). Because of different operating conditions, the booster and ramjet nozzles have different throat diameters. Except where specifically stated, the subsequent discussion uses the term nozzle to refer to the ramjet nozzle.

Proper operation of a ramjet engine requires both a sufficient mass flow rate and a sufficient pressure head at intake to drive the ramjet internal flow through the sonic nozzle throat. These two conditions are combined in the requirement for a ramjet start-up speed, defined as a function of altitude. The size of the booster also depends on the missile velocity at launch (typically Mach 0.9). The solid rocket motor model of the original code is used to compute the missile trajectory during the boost phase.

3. RAMJET PROPULSION MODEL

The algebraic ramjet propulsion model of Amichai (Ref. 2) was selected for implementation in the 6DOF code. The model accounts for ramjet engine adaptability to varying flight conditions but remains computationally efficient. Engine thrust is computed as a function of flight conditions using information on the engine internal geometry and using specified or computed total pressure efficiency factors. The original ramjet model of Amichai was first modified to improve the treatment of the supersonic inlet, to add a simple model of the ducted rocket engine and to implement a scheme for inlet-combustor matching using the secant iterative method. Inlet-combustor matching refers to the procedure by which the location of the normal shock wave (NSW) in the diffuser and the pressure coefficient across the system of reflecting oblique shock waves (OSW) are iterated upon to maintain the nozzle choked at all times during ramjet engine operation.

Within the ramjet model, the engine is divided in two sections, namely the combustor/nozzle and the inlet/diffuser. The computation of the flow conditions in the combustor/nozzle section assumes a choked nozzle while the inlet/diffuser flow is computed

separately. Indices I and N identify the flow conditions at the combustor upstream end obtained from either the inlet/diffuser (I) or the combustor/nozzle (N) sections respectively. The profile of the system of reflecting OSW and the position of the NSW in the diffuser are iterated upon using the secant method (two iteration cycles), thereby varying flow conditions I, until the difference between conditions I and N is less than a user-specified residue. Residues of 10^{-5} are obtained within less than five steps with the secant method. More specifically, iterating on the position of the NSW adjusts the flow speed M_i while iterating on the pressure coefficient across the system of reflecting OSW adjusts the total pressure P_{T_i} . Inlet-combustor matching is achieved at convergence of conditions I and N, and the resulting internal flow then represents the engine state at a particular trajectory point. The total pressure at the nozzle throat, which equals the free-stream total pressure minus losses in the inlet and combustor, is at convergence of the two iteration cycles (NSW and OSW cycles) the required pressure to drive the total flow of air and fuel at sonic speed through the nozzle throat.

3.1 Intake Model

The intake and diffuser compress the flow from supersonic to subsonic speeds before entry to the combustion chamber. To simplify the treatment of the inlet, the model does not describe the compression through the detailed system of reflecting OSW but rather through a single OSW only. Indeed, well-known two-dimensional flow relations describe the single OSW compression over a 2D wedge shaped inlet, while a semi-empirical relation (Ref. 2) approximates the compression over an axisymmetric conical inlet. After the single OSW, a diffuser accelerates the supersonic flow up to a NSW for the final compression to a subsonic flow. The remaining diffuser section decelerates the subsonic flow up to the sudden expansion with a final rapid expansion into the combustor. The diffusion of the flow is computed for an isentropic flow, complemented by an efficiency factor for total pressure loss. The strength (pressure coefficient) across this single OSW and the NSW position inside the diffuser are iterated upon to achieve inlet-combustor matching.

The intake model currently assumes a supercritical intake and operation above the inlet design Mach number. The first assumption implies that the air capture area remains fixed throughout the flight of the missile. With the second assumption, the ramjet model tracks the position of the NSW in the diffuser and aborts if the NSW is expelled upstream out of the intake duct.

3.2 Combustor Model

The ramjet combustion model computes the mass flow rate of injected fuel and the flow conditions at the combustor exit. An empirically based power-law equation computes the regression rate of the SFRJ fuel surface as a function of the air intake mass flow rate. Relations describing the change of the flow properties across the combustor are obtained by applying the principles of conservation of mass, momentum and energy. The associated control volume is the combustor itself, from the sudden expansion to the nozzle entrance plane. The combustor flow is axisymmetric and the flow is assumed to be one-dimensional for simplicity.

The energy conservation principle applied to the combustor accounts for the energy released to the flow by the combustion process. A rigorous evaluation of the amount of energy released must be performed by modelling the fluid flow and the combustion finite-rate chemistry. A less time consuming approach is to compute the equilibrium conditions of a given mixture of fuel and air at each integration time step of the simulation, during ramjet engine operation.

For its first version, the ramjet model uses a still simpler approach. Equilibrium conditions are computed for only one fuel-air ratio and only one temperature and pressure for each reactant (fuel and air). The selected reactants conditions and fuel-air ratio are assumed to be typical over the duration of engine operation. The conditions at the combustor exit are set equal to these equilibrium conditions, after including a combustion efficiency factor. The equilibrium code gives the total temperature, gas constant and the ratio of specific heats of the combusted mixture, while the combustion efficiency factor is user-specified.

The ramjet model also accounts for total pressure losses and other loss mechanisms (such as heat transfer, boundary layer effects and wall friction) using global efficiency factors. Some factors are computed implicitly in the model while others are user-specified. A complete description of the ramjet model can be found in Ref. 3.

4. GUIDANCE MODEL

Simplified models for missile navigation, guidance and control and for the target trajectory have been implemented in the 6DOF code to add a capability to simulate the missile trajectory during an engagement against a maneuvering target. The missile seeker provides the target-to-missile relative angular displacement. Since the true angular displacement is

given exactly as a function of time by the 6DOF trajectory simulation, the use of a real sensor is modelled by including two error components, the gimbal boundary limit and a constant target-missile angular position error. Both are user-specified. Target tracking ends when the maximum gimbal boundary is reached.

The target-to-missile angular position change measured by the sensor is fed to the guidance system. The guidance module evaluates the corrective missile lateral acceleration required for a future encounter with the target according to the proportional navigation guidance law. The seeker provides the rate-of-change of the line-of-sight angle while a doppler radar provides the closing velocity. The control lateral acceleration vector is oriented in the direction of the vector of the rate-of-change of the line-of-sight angle plus an angular error contribution, if specified.

The lateral acceleration computed from the guidance law is commanded to the missile control system. Implemented controls include an ideal control, aerodynamic control (tail or wing surfaces), thrust vector control (TVC) and coupled tail/TVC control. The ideal control provides exactly the required lateral corrective force computed by the guidance law. This control is also independent of flight conditions, is assumed to be located at the vehicle CG and hence induces no missile pitching and, finally, does not contribute additional missile drag.

Aerodynamic control provides a lateral corrective force from the deflection of external surfaces (aerodynamic control coefficient derivatives must be supplied). A symmetrical deflection of the control surfaces provides a lateral force, a pitching moment and increases the missile total drag force. Control effectiveness now depends on the geometry of the control surfaces and on the flight conditions. A maximum deflection angle limits the effectiveness of aerodynamic control in the numerical model. The control deflection necessary to provide the required lateral corrective force is computed using a specific logic. This corrective force is however applied to the missile equations of motion only after a specific time delay to account for the missile overall time constant.

Thrust vector control improves missile effectiveness in close-in combat. A short-range missile usually acquires its turning capability by flying at a high angle of attack. The possible missile controls (canards, tails, thrust vector and/or reaction jets) pitch the missile to the required angle of attack. For the initial missile flight early after launch, aerodynamic control by itself

cannot pitch the missile to sufficiently high incidence because of the low missile speed (low dynamic pressure). Thrust vector control on the other hand can provide the required pitching moment by deflecting the high momentum exhaust gas.

The primary limiting factor of the thrust vector control is its dependence on engine thrust. In fact, the time required for the maneuver must not exceed the motor burn time. The ramjet engine however has a longer burn time than the solid rocket motor and, hence, would allow the thrust vector control unit to operate for a longer time. Given this possible application of thrust vector control to missiles propelled by a ramjet engine, a simplified movable nozzle thrust vector control was implemented in the 6DOF code. This thrust vector control can operate alone or can be coupled to a tail control.

5. MISSILE PROPULSION TRADE-OFF STUDY

A preliminary trade-off study was performed to investigate the implications of propulsion (conventional rocket motor and ramjet engine) on the overall missile effectiveness. For the purpose of this study, two generic medium-range air-to-air tactical missile concepts were established using simplified design procedures. The first concept uses a conventional rocket motor while, in the second concept, the rocket motor is replaced by a solid-fuel IRR engine. The performance of each concept was evaluated using the improved 6DOF code and compared.

5.1 Missile Concepts

Figure 1 shows the concept of the medium-range air-to-air tactical missile propelled by a conventional solid rocket motor (denoted as the SRM missile). The radome, target seeker, warhead and flight control system occupy the front half of the missile while the propulsion unit is attached behind the control system. The missile overall length is 3630 mm and its nominal diameter is 200 mm. Table I summarizes the physical and performance characteristics of the conceptual SRM missile. The missile mass reduces from 232 kg at launch to 169 kg at burn-out. The length of the cylindrical propellant grain was limited to 1300 mm to ensure that the missile does not exceed the aeroheating limit, arbitrarily set to Mach 4 at 10 km altitude. A total thickness of 10 mm was allocated for the insulant and combustion chamber casing. The nozzle throat area was sized to ensure that the maximum pressure is 12.4 MPa. The solid rocket motor contains a standard non-aluminized HTPB/AP propellant (a reduced-smoke propellant, where AP refers to ammonium perchlorate) with a burn rate of 14 mm/s at 6.9 MPa. The motor produces an average thrust of 20.9 kN over a burn time

of 7.05 s, for a total impulse of 147 kN s at sea level. The motor specific impulse is 240 s at sea-level, characteristic of reduced-smoke propellants.

Figure 2 shows the variant of the SRM missile concept propelled by a solid fuel IRR engine. The engine uses a side-mounted inlet because the front section of the missile is occupied by the radome. However, this configuration limits the maximum deflection angle of the wing control surfaces. The ramjet combustion chamber contains the booster and ramjet solid fuels.

The booster and the ramjet engine cannot use a nozzle of the same throat area. The booster requires a small throat area to operate at high pressures, and to produce a sufficiently large thrust to quickly accelerate the missile away from the launch aircraft. The throat area required for the booster is however too small for subsequent ramjet operation. The total pressure head required to drive a sonic flow through the booster nozzle throat would largely exceed the total pressure of the air supplied by the intake. Accordingly, the ramjet engine must operate with a nozzle of larger throat area. Hence, the IRR engine uses a dual nozzle, where the smaller nozzle of the booster is inserted within the ramjet nozzle and is ejected after booster operation and before ramjet ignition.

Table II summarizes the physical and performance characteristics of the IRR missile while Figure 3 describes the solid fuel ramjet engine. The missile mass reduces from 232 kg at launch to 191 kg at booster burn-out, and to 172 kg at ramjet burn-out. The length of the cylindrical booster propellant grain was set to 1600 mm to ensure that the end-of-boost missile speed is sufficiently high for ramjet start-up. A high speed at ramjet ignition implies that the total pressure head of the intake air is sufficiently high to drive the sonic flow through the ramjet nozzle throat. The booster nozzle throat area was sized to ensure that the maximum pressure is 12.4 MPa during the boost phase. The ramjet booster and rocket motor of the SRM missile both contain the same propellant. The booster produces an average thrust of 20.6 kN over a burn time of 4.73 s, for a total impulse of 97 kN s and a specific impulse of 240 s at sea-level. The booster propellant mass of the IRR missile is less than in the SRM missile because the ramjet solid fuel must be contained in the combustor total volume.

The ramjet engine burns a pure HTPB solid fuel grain cast inside the combustion chamber. The nozzle throat area is 0.0025 m² during the boost phase and 0.0120 m² during ramjet operation. A trajectory simulation using the improved 6DOF code has shown

that, when launched at 5 km altitude, at a speed of Mach 1.2 and an elevation of 20°, the IRR engine burned for 43.7 s, producing an average thrust of 3.65 kN (a sustain-level thrust, compared with 20.6 kN for the booster). The 19 kg and 1500 mm long fuel grain produces a total impulse of 159 kN s, yielding a high specific impulse of 859 s. The ramjet propulsion model assumes an instantaneous ignition and does not describe variations in ignition time between different fuels. Further details on this simulation can be found in Ref. 3.

The combustion model for the solid-fuel ramjet engine computes the fuel regression rate as a function of intake air mass flow rate using a power law equation. This equation contains two user-specified empirical constants. No experimental data was readily available on the regression rate of HTPB propellant in a ramjet combustor with air mass flow rates typical of those encountered in the current concept engine (typically 5 kg/s). Accordingly, the two coefficients were taken from experimental data (Ref. 4) on the overall regression rate of a different fuel (PE) for lower air mass flow rates (0.3 kg/s). The estimated coefficients a and n are 0.0033 and 0.61 respectively for a regression rate in mm/s and the air mass flow rate in g/s. For a typical air mass flow rate of 5 kg/s, the resulting regression rate of HTPB fuel is 0.6 mm/s in the ramjet combustor.

The combustion model of the current ramjet propulsion model requires the state of the combusted mixture at the combustor exit. A representative total temperature of 2000 K, a ratio of specific heats of 1.23 and a gas constant of 292 J/kg-K were obtained using a thermochemical equilibrium code and typical reactants conditions (Refs. 3, 5).

5.2 6DOF Code Input Files

The missile mass properties, aerodynamic coefficients and booster performance must be specified in addition to the ramjet engine geometry and performance data. Aerodynamic coefficients of the SRM missile were obtained using the aero-prediction code AP-81 (Ref. 6). The same aerodynamic coefficients were assumed for the IRR missile configuration, except for the drag coefficient. A user-specified factor increases the missile drag based on intake status (open/closed). The performance of the solid rocket motor is evaluated separately and specified as an input to the 6DOF code.

One input file contains all the necessary information on the ramjet engine required by the numerical model, as well as intake drag contribution. The dimensions of all engine internal stations are specified. The density of

the selected HTPB fuel is 971.56 kg/m³ (from Ref. 2). User-specified efficiency factors describing intake flow losses have been realistically set to 0.96. Except for the large total pressure loss across the NSW, the inlet total pressure recovery is then 0.92 (0.96²) times the total pressure loss across the OSW (typically 0.90), or 0.83. This value of total pressure recovery is typical of missile supersonic inlets (Ref. 7).

The 6DOF code requires three factors to compute the IRR missile drag (inlet closed, inlet open, ramjet on). From Table III, the zero-lift drag coefficient of the IRR configuration with inlets closed is set to 30% larger than the coefficient of the configuration without inlets, and 10% larger when the inlet is open. During ramjet operation, the total missile drag decreases by 15% because of a reduction in the missile base drag. The three " F_{CD} ..." factors are representative of generic airbreathing missiles (Ref. 7).

5.3 Inlet-combustor Matching

Figure 4 indicates the rapid convergence achieved by the secant method to match the I and N conditions (at the combustor entrance plane, station 3) for Mach number and total pressure. A successful convergence is achieved within five steps for both iteration cycles. This rapid convergence with the secant method contributes to reducing the overall simulation computing time. Inlet-combustor matching is achieved at convergence of these cycles, indicating that the total pressure of the intake air corresponds to the required pressure to drive the flow of air and fuel through the sonic nozzle throat.

5.4 Trade-off Study - Results

The present section analyzes and compares the performance of the SRM and IRR missile concepts to highlight benefits and identify an operating envelope for each propulsion system.

5.4.1 Effect of booster size

The relative sizing of the booster propellant and ramjet fuel grains in a solid fuel IRR engine is constrained by the volume available in the combustor. Figure 5 shows the effect of varying the booster propellant mass on the IRR missile speed as a function of the distance travelled. The first missile contains the baseline booster (described earlier) while the second missile contains 15% more booster propellant (by weight) and therefore less ramjet fuel. The missile travels at a constant altitude of 10 km.

The IRR missile with a larger booster accelerates to a higher end-of-boost speed than the baseline missile since the thrust developed by a rocket motor (the

booster) exceeds largely that of the ramjet engine. The missile with the larger booster also maintains a higher speed up to ramjet burn-out, but ramjet burn-out occurs earlier due to the smaller ramjet fuel mass carried. Accordingly, the higher range in a true level flight is achieved by maximizing the ramjet propellant and with the minimum boost propellant mass required to ensure ramjet start-up. This conclusion should not however be extended to apply to all IRR missile engagement scenarios because, in some cases, the missile could well benefit from a larger size booster and its increased initial acceleration. Hence, the relative sizing of the booster and ramjet fuel grains in a solid fuel IRR is mission-specific.

5.4.2 Flight Mach number

The sustain-level thrust and the longer operating time of the ramjet engine is suited to long-range missions. Figure 6 compares missile speed as a function of distance travelled for both IRR and SRM concepts and for two altitudes (7.5 km and 10 km). The x-axis title is purposely labeled "distance" travelled to emphasize that this distance should not be interpreted as a launch range-to-target. With a moving target, a gain in distance travelled is not equivalent to a gain in launch range because time-of-flight to the target must also be considered. For a missile-target engagement, this distance travelled will represent the distance between the missile launch point and the intercept point.

Each missile is launched at a speed of Mach 1.2 and maintains a level flight trajectory. The IRR missile achieves a lower end-of-boost speed because of the smaller booster total impulse. The SRM missile starts decelerating immediately after booster burn-out, but the IRR missile continues to accelerate due to the sustain thrust produced by the ramjet engine. With regard to flight speed, the SRM missile travels with a higher average speed for ranges below approximately 20 km because the total impulse delivered by its rocket motor exceeds that of the IRR engine. The IRR missile on the other hand maintains a higher speed above the 20 km threshold and also travels for a 60% longer range than the SRM missile before reaching the arbitrary minimum flight speed limit of Mach 0.95. Missile range depends strongly on flight altitude, increasing by 40% with a 2.5 km altitude change.

5.4.3 Time-of-flight

Figure 7 presents the time-of-flight as a function of the distance travelled for the same flight conditions as in Fig. 6. The SRM missile travels with a larger average speed and hence a lower time-of-flight below a threshold range of 25 km. The average speed and time-of-flight advantage of the IRR missile increases

steadily with distance travelled above this threshold range.

The performance of the IRR missile against a moving target depends on the time-of-flight and average speed. A sufficient speed advantage (Fig. 6) over a moving target is critical to allow the missile to intercept the target, especially in a tail chase. Similarly, the missile time-of-flight controls the total range travelled by the target before being intercepted. If the time-of-flight is high, the target can reach the no-escape zone outer boundary before being intercepted.

5.4.4 Turning capability

The IRR engine improves end-game maneuverability at longer ranges by maintaining high missile speed. Figure 8 indicates the turning capability in g_n 's achievable during each trajectory of Fig. 6. Although Fig. 6 indicates a gain in speed with altitude, the turning capability can be larger or smaller at the lower altitude as it depends on the local dynamic pressure. The SRM missile has a greater turning capability for distances smaller than the threshold range of approximately 20 km. The IRR missile also maintains a minimum 3 g_n maneuverability for 50% longer ranges than the SRM missile.

5.4.5 Performance against a non-maneuvering target

The performance of the SRM and IRR missiles against a non-maneuvering target are compared for various initial missile-to-target ranges. Each missile is launched at Mach 1.2 and at an altitude of 10 km against a non-maneuvering target travelling at the same altitude and speed in a tail chase (target aspect angle of 0°). Figure 9 presents the missile-target closing velocity as a function of launch range. The SRM missile performs better than the IRR missile for ranges smaller than 15 km. The IRR missile however intercepts targets up to a 60 km range, which represents a 50% increase over the SRM missile maximum intercept range at this altitude.

Figure 10 presents the time-of-flight and f-pole distance as a function of launch range for the same scenario. The SRM missile intercepts its target in a shorter time due to its higher average velocity below a launch range of 25 km and the IRR missile performs better above this range. The f-pole distance is very similar with either the SRM or the IRR missiles up to the maximum launch range of the SRM missile because the flight times are similar. The f-pole distance was computed by assuming that the aircraft maintains the same course after launching the missile.

5.4.6 Performance against a maneuvering target

The relative performance of the IRR and SRM missiles follows a similar trend when the missiles engage a maneuvering target. Each missile is launched at a speed of Mach 1.2 in a co-altitude engagement against a maneuvering target at 10 km altitude. The target maintains a constant speed of Mach 1.2 but pulls a $5 g_n$ turn at missile launch to a 90° heading (slicing target).

Figure 11 shows the closing velocity between the missile and target as a function of launch range for each missile. The IRR missile again has a greater speed advantage than the SRM missile above a threshold range. This range is now lower at 10 km, compared with 15 km in an engagement against a non-maneuvering target (Fig. 9). Also, for a given launch range, higher closing velocities are achieved against the maneuvering target (Fig. 11) than against the non-maneuvering one (Fig. 9) because the 90° heading change of the target in Fig. 11 actually reduces missile range and flight time to intercept. This example shows that when selecting and optimizing a propulsion system for a particular tactical missile, trade-off studies must be performed using a set of engagement scenarios representative of the missile role.

A comparison of Figs. 9 and 11 also shows that both the IRR and SRM missiles can intercept the target at longer launch ranges against a slicing target with a 90° turn than against the non-maneuvering target. Indeed, the missile uses only its speed advantage against a non-maneuvering target in a tail chase (Fig. 9), but can use both its speed and maneuverability advantages against the slicing target (Fig. 11). Hence, if the target is approaching the missile maximum range boundary at missile launch, the target should maintain a straight course to reach the outer boundary quickly.

Figure 12 presents the time-of-flight and f-pole distance as a function of launch range for the scenario of Fig. 11. The SRM missile offers a time-of-flight advantage over the IRR missile for launch ranges below 30 km, compared with 25 km in Fig. 10 for a non-maneuvering target. The threshold range observed in Figs. 11 and 12 do not have to agree because the time-of-flight advantage (Fig. 12) depends on the distance travelled during the intercept. Finally, from Fig. 12, the IRR missile offers an increasing f-pole advantage with launch range over the SRM missile for ranges greater than 35 km.

5.4.7 Time-of-flight envelope/non-maneuvering target

A total of three missile performance parameters are of particular interest to the pilot: the time-of-flight, maximum range and terminal velocity. Reducing the

time-of-flight to intercept means an increased speed advantage, thereby improving f-pole distance. The maximum range represents the engagement outer boundary, while the terminal velocity governs missile maneuverability during end-game and the no-escape zone. The IRR missile offers improved end-game maneuverability, as shown in Fig. 8, for long ranges. A time-of-flight envelope shows missile performance in a realistic operating environment in terms of the other two parameters, time-of-flight and maximum range, for a large number of initial target locations.

Figure 13 shows the time-of-flight envelope generated for both the IRR and SRM missiles. The non-maneuvering target, initially located at coordinates (0,0), travels in the direction shown at a constant speed of Mach 1.2 and at a constant altitude of 10 km. The missile is launched at any (x,y) point in the direction of the target initial position, at also a speed of Mach 1.2 and an altitude of 10 km. Each contour line represents a constant time-of-flight to intercept. For example, both IRR and SRM missiles intercept the target after a flight of approximately 30 s when launched at the position (-20,20) km. The contour lines are also skewed to the left because intercepts can be achieved at greater ranges when the target aspect angle is greater than 90° . To generate the envelope, the domain was divided into 33 nodes in the x-direction (from -80 km to +80 km) and 17 nodes in the y-direction (from 0 km to 80 km). Engagement simulations were performed using the 6DOF code for each initial position of the missile. A total of 560 simulations were performed in batch mode to generate the envelope of Fig. 13.

Although all the engagements performed to generate the envelope are co-altitude, the missile does not maintain a truly constant altitude. The proportional navigation guidance law requires a change in the line-of-sight angle to effect a normal acceleration command. The missile loses altitude in the first part of the trajectory due to the gravity pull, but the normal acceleration commanded by the missile guidance increases with time from zero at launch, as the rate-of-change of the line-of-sight angle increases. The missile pitches up to the target altitude in the final part of the engagement. The ramjet model properly accounts for the effect of changing altitude on engine performance.

The envelope confirms that the IRR missile offers a time-of-flight advantage over the SRM missile for longer ranges. The IRR missile intercepts the target in a shorter time than the SRM missile for flight times greater than about 35 s. The value of the threshold range depends on the missile initial position, hence on

the engagement scenario. The time-of-flight advantage increases i) largely with launch range because the IRR missile then maintains a higher average velocity and ii) slightly from tail-on to head-on target aspects.

The IRR engine also improves missile maximum range capability. As shown in Fig. 13, the IRR missile can successfully intercept targets at launch ranges 40% greater than the SRM missile. The last contour level (75 s and 65 s for the IRR and SRM missiles respectively) is near to but does not represent the truly maximum range boundary.

6. CONCLUSIONS

A 6DOF trajectory simulation code was acquired and improved to assess missile performance and effectiveness in a realistic operating environment. The code can model the trajectory of a missile propelled by either a conventional rocket motor or a solid fuel integral-rocket-ramjet engine. Modifications to the original version were required to implement i) a model of missile guidance and control based on the law of proportional navigation and ii) an algebraic ramjet propulsion model. Improvements to the selected ramjet model included i) a 2D intake model and ii) a numerical procedure based on the secant method to achieve a true inlet-combustor matching by iterating on the position of the normal shock wave in the diffuser and on the pressure coefficient across the reflecting oblique shock waves. The combustion model was purposely kept simple and future improvements are planned. The improved 6DOF code represents a cost-effective tool to assess missile performance and define the missile operating envelope. Further work remains in the areas of inlet and combustion modelling but a conservative assessment of ramjet engine performance is already possible with appropriate efficiency factors.

A preliminary trade-off study was performed using the improved 6DOF code to investigate the preferred operating envelopes of the conventional rocket motor and of a solid fuel IRR engine for a tactical missile. Two generic 200 mm medium-range air-to-air tactical missile concepts were established, one for each propulsion system. The ramjet engine delivers a sustain level thrust but with a high specific impulse when compared to the conventional rocket motor. From a simulated trajectory, the booster delivers an average thrust of 20.6 kN with a specific impulse of 240 s using a reduced smoke HTPB/AP, compared with 3.65 kN and 859 s for the ramjet engine. The IRR missile average speed depends on booster propellant to ramjet fuel ratio, and the optimum ratio is mission specific.

Ramjet propulsion improves three important performance criteria of a missile system, namely, the time-of-flight (average velocity), maximum range and end-game maneuverability. The ramjet engine however is for longer range missions, with its higher specific impulse and sustain type thrust profile. The conventional solid rocket motor, with its high thrust output and low burn time, gives the tactical missile a higher average velocity and hence a better maneuverability for shorter range engagements. A time-of-flight envelope generated for both missiles against a non-maneuvering target at 10 km altitude shows that the IRR missile offers a time-of-flight advantage for flight times greater than 35 s, which corresponds to a 25 to 35 km launch range. The envelope also shows that the solid fuel IRR engine improves the missile maximum range capability by 40%. The IRR engine also extends the $3 g_n$ maneuverability boundary by 50% in slant range.

7. REFERENCES

1. Lauzon, M., "6DOF Trajectory Modelling of a Guided Long-Range Artillery Rocket", DREV Memorandum No. 3200/94, March 1994.
2. Amichai, O., "Performance of Solid-Fuel Ramjet Guided Projectile for USM 5"/54 Gun System", Report No. NPS67-82-002CR, Naval Postgraduate School, Monterey, March 1982.
3. Lauzon, M., "An Algebraic Ramjet Propulsion Model for Efficient Missile Trajectory Simulation", DREV-TM-9443, January 1995.
4. Currie, T.C., "Computational Fluid Dynamics for Solid-Fuel Ramjet Flowfield Analysis - a State-of-the-art Review", Contractor Report, ECS-Power Systems Inc, September 1990.
5. Gordon, S. and McBride, B.J., "Computer Program for Calculation of Complex Chemical Equilibrium Compositions, Rocket Performance, Incident and Reflected Shocks, and Chapman-Jouguet Detonations", NASA SP-273, 1971.
6. Devan, L. and Mason, L.A., "Aerodynamics of Tactical Weapons to Mach Number 8 and Angle of Attack 180°, Part II - Computer Program and Users Guide", NSWC TR 81-358, September 1981.
7. "Ramjet and Ramrocket Propulsion Systems for Missiles", AGARD-LS-136, October 1984.

TABLE I
SRM Missile Concept

<u>Missile</u>	
Mass at launch	232 kg
Mass at end-of-boost	169 kg
<u>Booster</u>	
Propellant grain	1300 mm long, 25 mm ID, 190 mm OD
Nozzle throat area	.0027 m ²
Nozzle exit plane area	.0246 m ²
Propellant mass	63 kg
Propellant characteristic velocity	1524 m/s
Propellant regression rate	0.104 P _c ^{0.31} mm/s (P _c in Pa) (14 mm/s at 6.9 MPa)
Maximum operating pressure	12.4 MPa
Burn time	7.05 s
Average thrust*	20.9 kN
Average operating pressure	4.98 MPa
Specific impulse*	240 s
Total impulse*	147 kN s
* at sea level	

TABLE II
IRR Missile Concept

<u>Missile</u>	
Mass at launch	232 kg
Mass at end-of-boost	191 kg
Mass at ramjet burnout	172 kg
<u>Booster</u>	
Propellant grain	1600 mm long, 25 mm ID, 140 mm OD
Nozzle throat area	.0025 m ²
Nozzle exit plane area	.0270 m ²
Propellant mass	41 kg
Propellant characteristic velocity	1524 m/s
Propellant regression rate	0.104 P _c ^{0.31} mm/s (P _c in Pa) (14 mm/s at 6.9 MPa)
Maximum operating pressure	12.4 MPa
Burn time	4.73 s
Average thrust*	20.6 kN
Average operating pressure	5.38 MPa
Specific impulse*	240 s
Total impulse*	97 kN s
<u>Ramjet</u>	
Propellant grain	1500 mm long, 140 mm ID, 190 mm OD
Nozzle throat area	.0120 m ²
Nozzle exit plane area	.0260 m ²
Fuel mass	19 kg
Burn time**	43.7 s
Average thrust**	3.65 kN
Specific impulse**	859 s
Total impulse**	159 kN s

* at sea level

** free-flight simulation: missile launched at 5 km altitude, speed of Mach 1.2 and 20° elevation angle

TABLE III
6DOF Inputs for the Ramjet Model

RAMJET MODULE INPUTS:

1	Ramjet engine type: (1) - SFRJ; (2) - DR/LFRJ
3.630	Missile body length [m]
0.1	Missile body nominal radius [m]
2	Inlet type: (1) - conical and axisymmetric; (2) - 2D rectangular
20.	Wedge angle [deg], for 1 st estimate of C_p at ramjet start-up
1.5	Ramjet combustor length [m]
10.e-03	Inlet frontal area [m ²]
1.	Ratio of inlet capture area to inlet frontal area
5.5e-03	Diffuser entrance area [m ²]
1.5e-02	Diffuser exit area [m ²]
0.0033	Coefficient a in the SFRJ solid-fuel regression equation ($\dot{r} = a \dot{m}_a^n$)
0.61	Exponent n in the SFRJ solid-fuel regression equation ($\dot{r} = a \dot{m}_a^n$)
971.56	Ramjet fuel density [kg/m ³]
14.e-02	Combustor inner diameter, at end-of-boost [m]
19.e-02	Combustor outer diameter, at ramjet burnout [m]
12.e-03	Ramjet nozzle throat area [m ²]
2.6e-02	Ramjet nozzle exit plane area [m ²]
0.74	Combustion efficiency factor
0.96	Ramjet nozzle efficiency factor
0.96	Diffuser efficiency factor (up to NSW)
0.96	Diffuser efficiency factor (from NSW to diffuser end)
3.15e-02	Reference area for the thrust coefficient [m ²]
.073	Stoichiometric fuel-air ratio of ramjet fuel/air mixture (DR/LFRJ engine)
.025	Minimum fuel-air ratio for combustion (for HTPB fuel in this case)
2500.	Ideal total temperature [K]
1.23	Ratio of specific heats of the combustion products
292.	Gas constant of the combustion products [J/kg-K]
0.	Inlet bleed in % of inlet air mass flow rate
18.	Total fuel mass (DR/LFRJ engine) [kg]

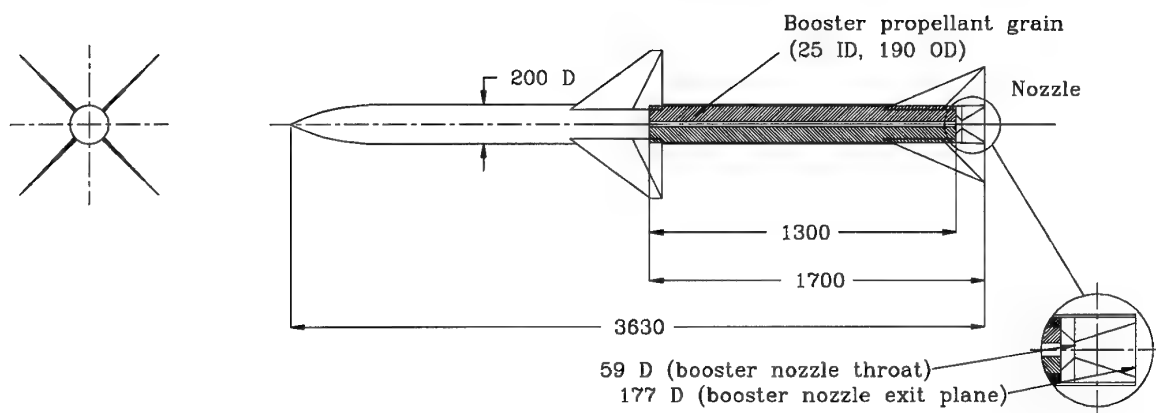
ADDITIONAL INPUTS FOR 6DOF RAMJET PROPULSION MODULE

30.	Drag coefficient increase with ramjet inlet(s) closed*
10.	Drag coefficient increase with ramjet inlet(s) open*
15.	Drag coefficient decrease during ramjet operation*
10	Calling frequency of the ramjet module**

NOTES

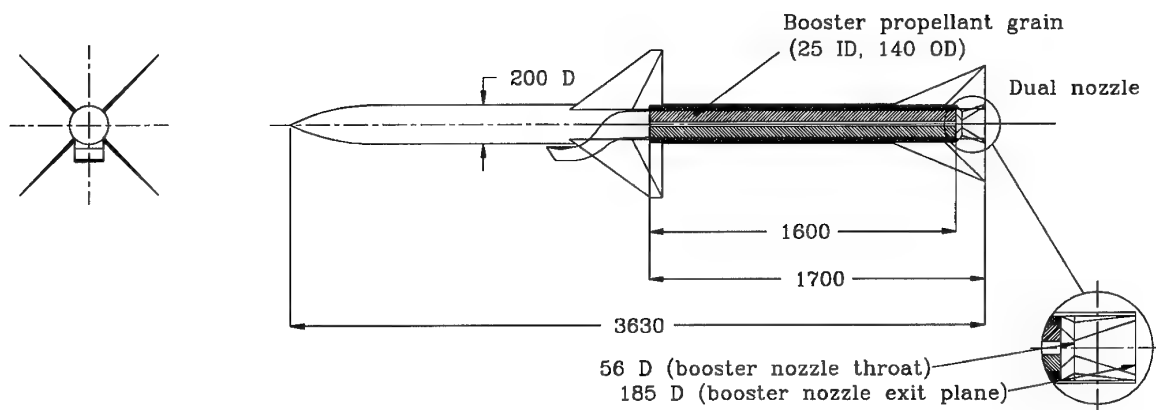
* % of drag coefficient of missile without air inlets ($C_{D-no\text{inlet}}$);

** in units of integration time step of the 6DOF simulation



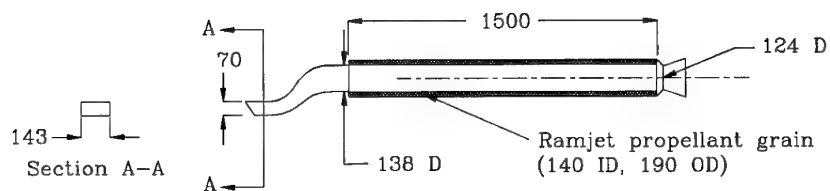
All dimensions in mm

Figure 1 - SRM Missile concept



All dimensions in mm

Figure 2 - IRR Missile concept



All dimensions in mm

Figure 3 - Solid fuel IRR engine concept

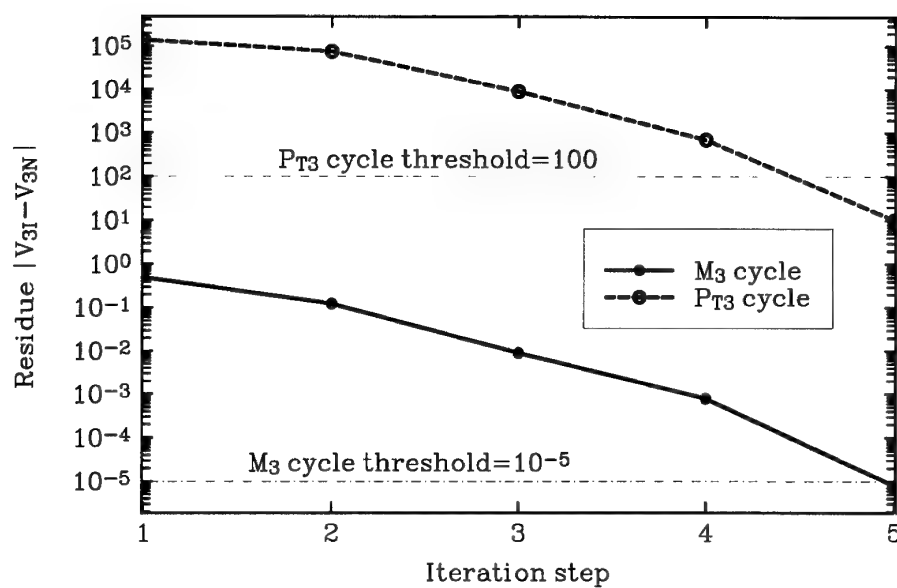


Figure 4 - Inlet-combustor matching convergence rate

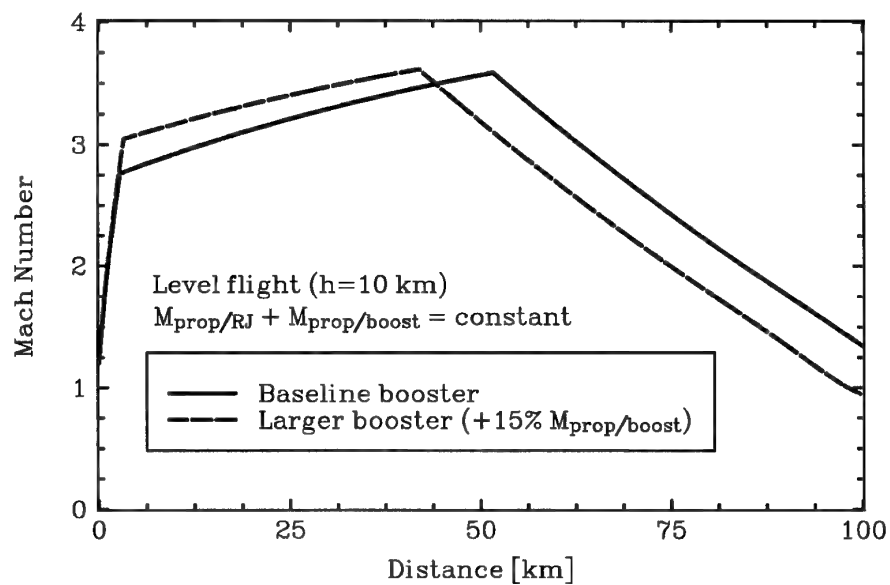


Figure 5 - Effect of booster size on IRR missile speed

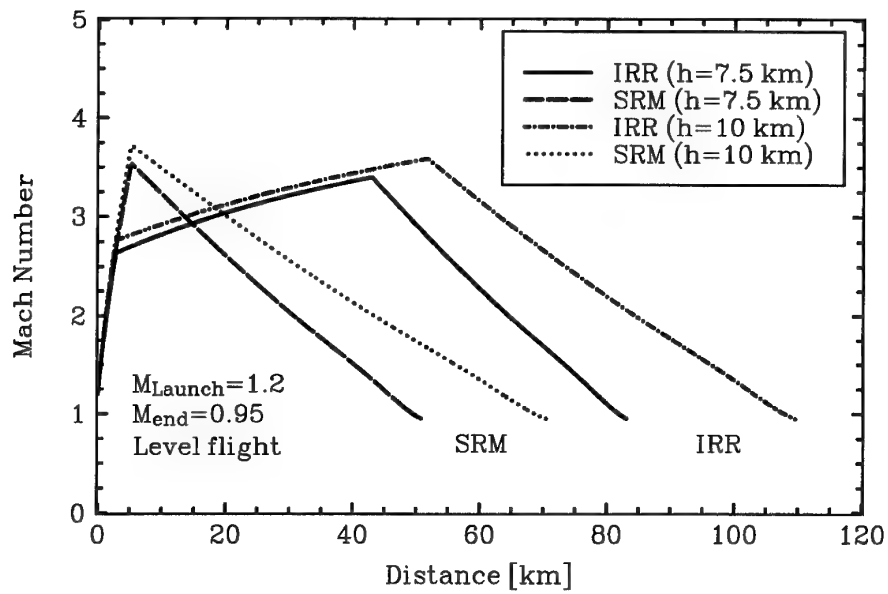


Figure 6 - Effect of propulsion system on missile speed

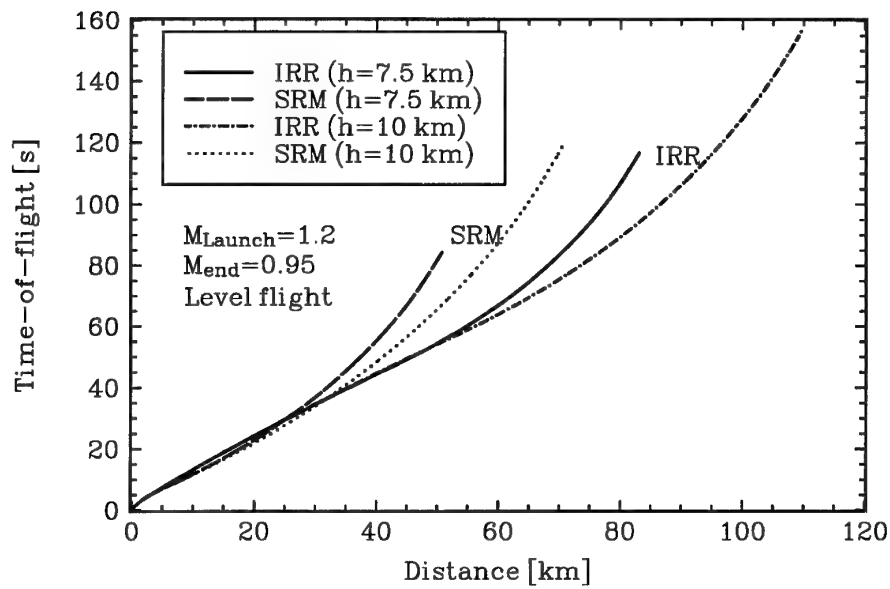


Figure 7 - Effect of propulsion system on flight time

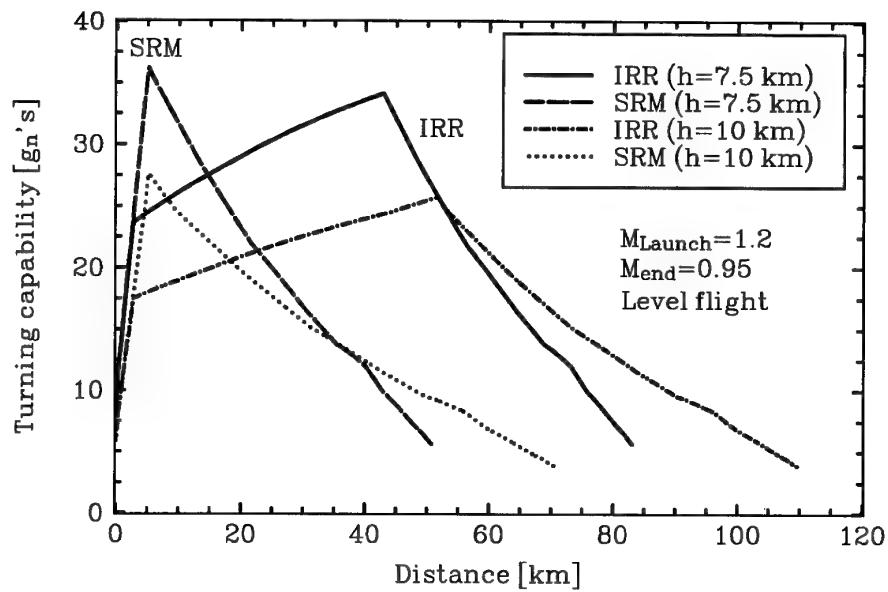


Figure 8 - Effect of propulsion system on missile maneuverability

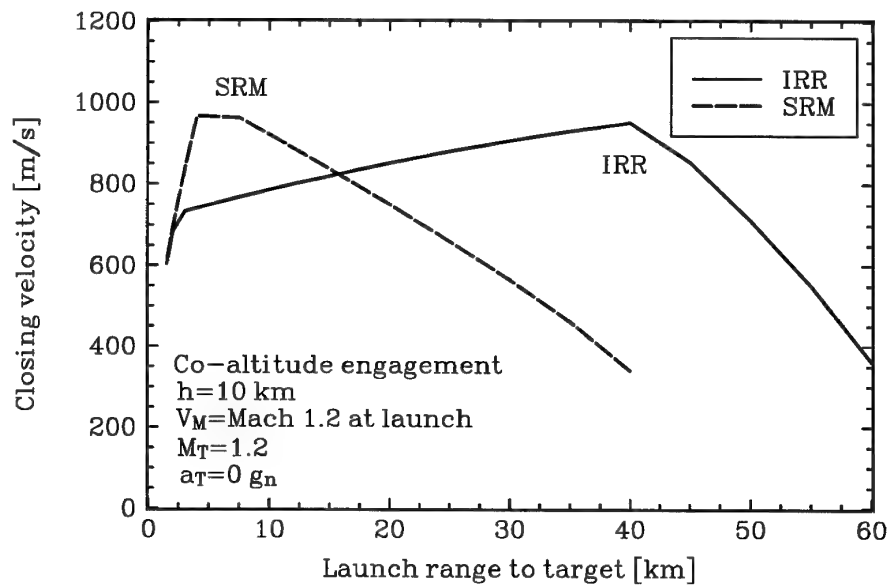


Figure 9 - Closing velocity advantage (non-maneuvering target)

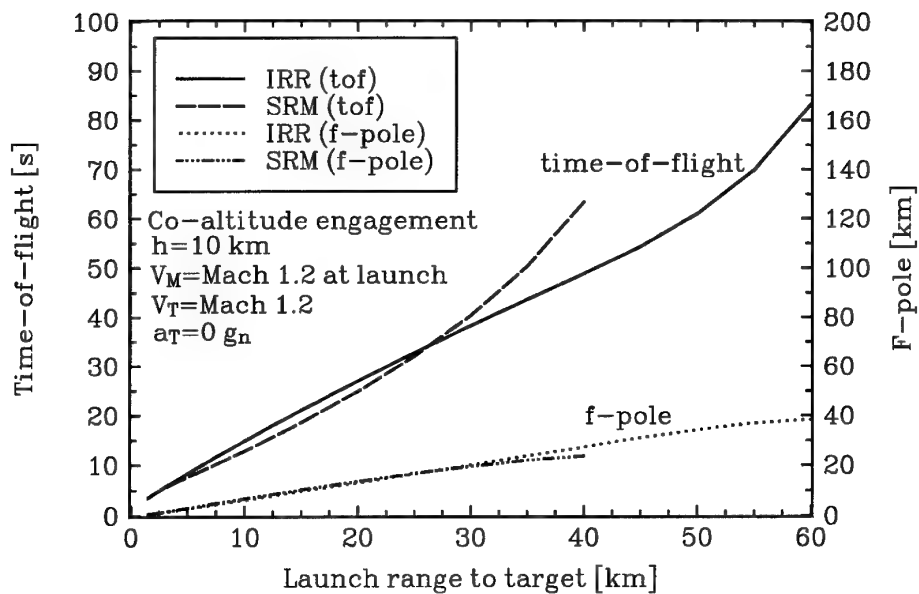


Figure 10 - Time-of-flight and f-pole advantages (non-man.target)

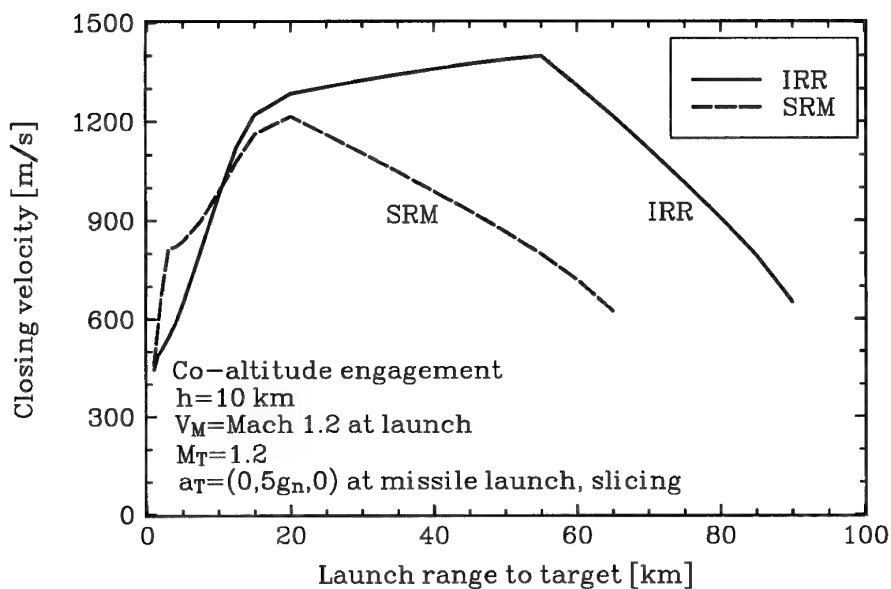


Figure 11 - Closing velocity advantage (maneuvering target)

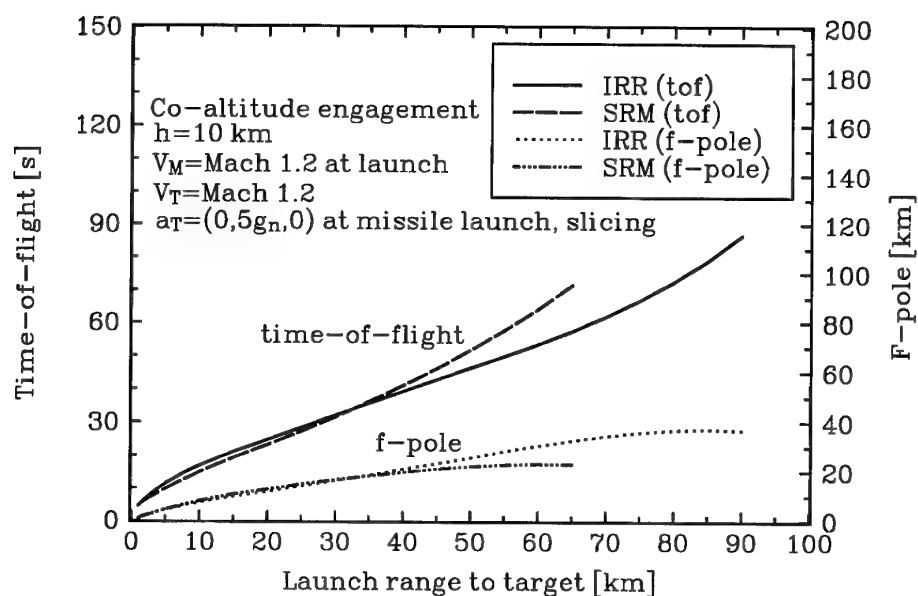


Figure 12 - Time-of-flight and f-pole advantages (man. target)

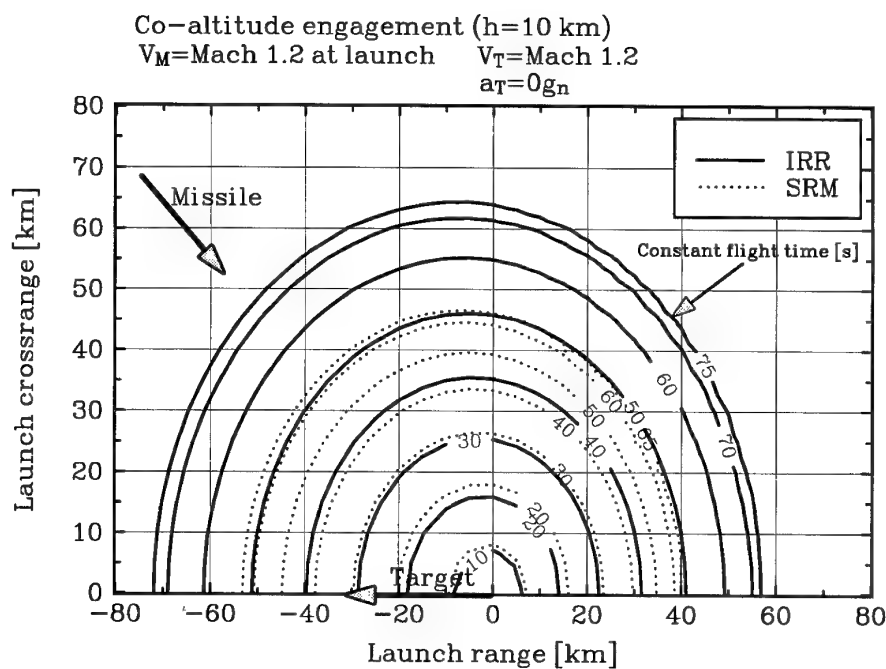


Figure 13 - Time-of-flight envelope (non-maneuvering target)

OPERATIONALLY REPRESENTATIVE TESTING OF MODERN TACTICAL WEAPONS

Dean H. Bergevin
501 Range Squadron/CC
6067 Box Elder Ln
Hill AFB, Utah 84056-6067
United States

1. SUMMARY

Increased weapon sophistication, interaction between different weapon capabilities, and increased weapon cost have led to increased reliance on large scale multiple objective test and training exercises. This combination can simultaneously obtain high value training and weapons test data with minimum expenditure of weapon assets.

This paper details the experience of Utah Test and Training Range (UTTR) in supporting increasingly sophisticated weapons test and training programs conducted by the U.S. Air Force. Objectives, procedures, and test equipment used by such Air Force Air Combat Command programs as the Weapon Systems Evaluation Program (WSEP) and Conventional Air Launched Cruise Missile are discussed. WSEP tests multiple precision guided munition types, including the sophisticated High Speed Anti-Radiation Missile (HARM), Maverick, and Have Nap missiles. All tests are conducted using aircraft and aircrews from operational units in a realistic "war game" environment against realistic targets to provide unmatched training for multiple fighter and bomber squadrons. Fiscal year 1994 WSEP tests involved nine fighter units and over 150 weapons at UTTR. Strategic and tactical cruise missile tests are also conducted using operational aircraft, crews, and equipment flying long range routes simulating wartime requirements. Simulated missile launch areas add operational realism. Missile profiles are designed to exercise missile launch, enroute guidance, and terminal attack capabilities. Weapons data are collected and used to evaluate accuracy, effectiveness, and reliability.

Methods, procedures, and test range equipment used by UTTR to support tactical missile tests are discussed. Constraints necessary to meet

range safety requirements are discussed, as well as methods used to minimize the constraints.

2. INTRODUCTION

The United States Air Force Air Combat Command (ACC) operates combat-coded fighters, bombers, tankers and reconnaissance aircraft and provides nuclear-capable forces for US Strategic Command¹. In order to accomplish its mission, ACC must constantly train the crews who maintain, load, and fly the aircraft, as well as periodically assess the performance of the weapons used. ACC uses multiple methods to accomplish the task, including continuous unit training exercises, and periodic multi-unit training exercises, competitions, and weapons system evaluation programs. Unit and multi-unit training exercises typically use Air Combat Maneuvering Instrumentation systems with computer simulated gun and missile firings for air-to-air training, and small practice bombs for air-to-ground training. Well known examples are the Red Flag exercises at Nellis Air Force Base (AFB). The weapon systems evaluation programs differ in that ACC combines weapons testing with operational training in an intense exercise to test "end-to-end" system readiness. The crews obtain valuable training on the weapons they would use in combat, while data are also accumulated and analyzed to evaluate weapons performance and measure effects of long term storage, handling, and maintenance procedures. Examples are the Combat Archer Air-to-Air Weapon System Evaluation Program (WSEP) at Tyndall AFB and the Combat Hammer Air-to-Ground WSEP at Eglin AFB and UTTR. Modern, high performance weapons challenge test range capabilities, since the range must safely accomplish the tests and collect the necessary weapon performance data while minimizing the constraints to training scenario realism.

This paper discusses the general support requirements necessary to successfully incorporate both test and training objectives into weapon system evaluations. It also provides examples of specific test range support required, scenarios used, and data gathered for some representative air-to-surface weapon system evaluations conducted at UTTR.

3. TEST REQUIREMENTS

Effective combination of test and training objectives in a weapon systems evaluation requires test range locations that can accommodate the extended "footprints" for multiple high performance operational weapons. The weapon footprint is the surface area that can be reached by the weapon, given the energy available to the weapon at launch and the methods available to terminate flight in case of a malfunction. Weapons footprint size can be limited by controlling the launch parameters or determining stringent termination conditions. However, such constraints greatly detract from combat realism, severely limiting the training value of the test. The permissible launch parameters and constraints are associated with a "shoot box." If the missile is fired within the shoot box and within permissible constraints, then it can be contained within the footprint. Combat realism and training value are greatly enhanced if the available shoot box accommodates a variety of representative launch locations, speeds, altitudes, and off-boresight angles relative to the target, encompassing as much of the weapon firing envelope as possible.

Weapons system evaluation tests can also enhance training realism by using multiple participants, including operationally representative attacking and defending aircraft formations. Support elements such as "wild weasel" electronic combat aircraft, Airborne Warning and Control (AWACS) aircraft, and air refueling tankers are also employed.

Strategic and conventional cruise missile test realism is enhanced by having terrain following or high altitude training routes available to enter the test range, coupled with representative terrain and targets for cruise missile profiles within the test range boundaries.

The test scenarios can optimize training value by incorporating a realistic battlefield environment and realistic weapons employment scenarios to the maximum extent possible. One

method for incorporating operational realism is to use Multiple Threat Emitter System (MUTES) radar simulators, the Threat Reaction Analysis and Indicator System (TRAINS), and other threat simulators to exercise the electronic combat capabilities of the operational aircraft and pilot. These systems are also used in conjunction with launches of "Smoky Sam" simulated surface-to-air missiles to provide a realistic simulation of enemy ground defensive systems, and to evaluate the pilot's responses to the threats.

Weapons used in the evaluations consist of multiple samples drawn from operational inventories. Performance degradation due to manufacturing defects or effects of long term storage can be discovered by analyzing performance data acquired during the weapon test. Identification and correction of the problems vastly increases confidence that weapon inventories will perform reliably and with known capabilities when they are drawn upon to meet operational requirements.

Evaluation of the weapon system performance typically requires Time Space Position Information (TSPI) tracking of the weapon by radars or other tracking systems for at least part of the flight profile, although range safety considerations require that the weapon be tracked from launch to impact (see below). If sufficient internal space is available, the weapon carries a tracking augmentation device, such as a radio frequency (RF) transponder. If space is not available, radar skin track or optical track of the weapon is used. High accuracy (± 1 meter) tracking data is usually required at the weapon fusing and impact points. This terminal phase TSPI data is acquired with unmanned, remotely controlled, high-speed film or video camera arrays.

Thorough evaluation of weapon system performance usually requires employment of a telemetry (TM) package, if it can be installed within the weapon. This TM package typically takes the place of the weapon warhead or some of the fuel. For long range or high performance weapons, the TM package typically also incorporates a flight termination system that can be independently controlled from ground or airborne flight safety stations.

4. SAFETY REQUIREMENTS

A fundamental analysis required for safety is the footprint analysis. The footprint analysis begins by evaluating the kinetic and potential energy available to the weapon at each point, or at crucial points, along its flight path. The evaluation of available energy assumes that the missile suffers a catastrophic failure or commanded termination at the given point. The energy calculation determines where the weapon debris would impact the ground given the worst case failure mode or the expected result of the termination command.

A simple example of a footprint analysis can be conducted for a single stage sounding rocket that is launched in a near vertical trajectory to reach the maximum possible altitude. In the worst case scenario, a failure of the rocket guidance controls immediately after launch could cause it to follow any possible random trajectory. Since we do not know what the specific failure might be, we must assume that the rocket will fail in a manner to cause it to fly in any random direction, with the horizontal distance traveled to be any value up to the maximum capability of the rocket. The resulting circular footprint is illustrated in Figure 1.

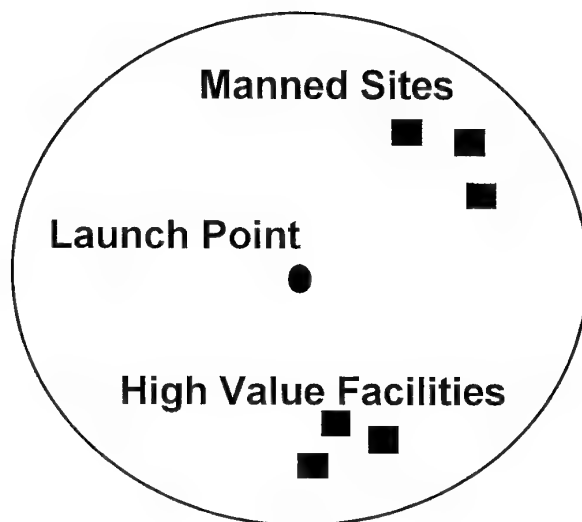


Figure 1

Circular Footprint

The safety officers have two choices for managing the footprint. First, they can position the launch site and specify the allowed launch conditions such that rocket impact anywhere within the safety footprint will not cause unacceptable damage. Second, a commanded termination system can be installed to destroy the rocket if it deviates substantially from the expected flight path. Commanded termination, in the form of terminated thrust, increased drag, and/or fragmentation, can substantially decrease the footprint size.

Each weapon has unique characteristics that profoundly change the safety constraints and dictate how the weapon footprint can be accommodated within the range air and surface space. As an example, the Air-Launched Cruise Missile (ALCM) employs a nuclear warhead

which is replaced with an instrumentation package during weapons evaluation exercises. However, the Conventional Air-Launched Cruise Missile (CALCM) version of the weapon replaces the nuclear warhead with a 454 Kg conventional blast fragmentation warhead (with the same destructive effect as a 970 Kg bomb). The live warhead requires that the weapon flight path be constrained to well-controlled air and ground space because of the potential for collateral damage if the weapon fails before reaching its intended target. These concerns require the range to provide extremely reliable real-time TSPI tracking and display, constant monitoring of weapon health, and positive safety control in the form of a commanded flight termination system. UTTR has for these reasons provided a three-dimensional weapon tracking display at the range safety officer's

station, and air vehicle tracking displays using three different TSPI tracking sources. The safety displays also graphically display critical command termination system parameters such as battery conditions, signal strength, etc. Real-time displays of missile TM data also allow the test engineers to monitor flight control responses, evaluate missile performance, and detect failures during the flight.

5. RANGE INSTRUMENTATION

Range instrumentation support requirements for weapons evaluation tests present unique challenges. Since by definition the weapons employment scenarios must be as operationally realistic as possible, the test range instrumentation used to control the tests, maintain range safety, and gather needed weapons data for evaluation must be reliable, effective, and unobtrusive.

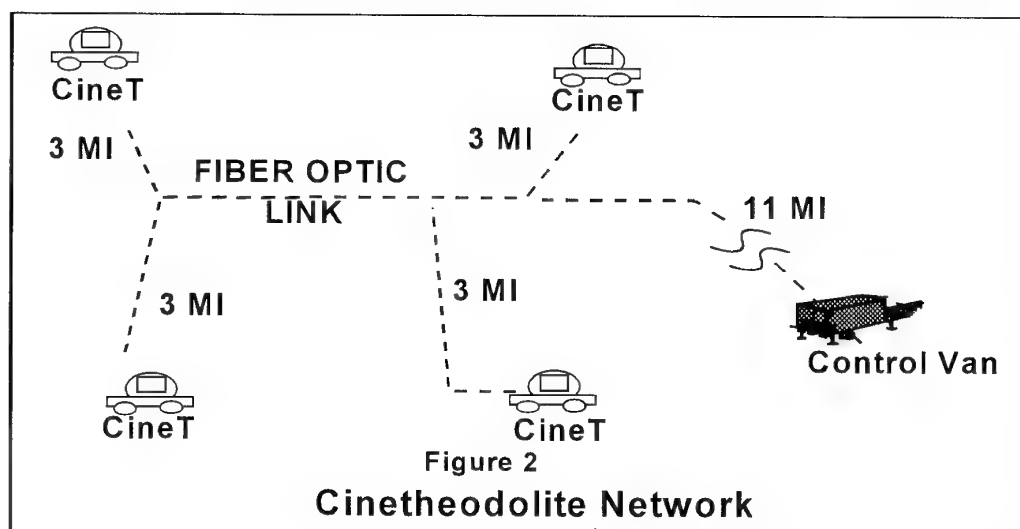
Test data acquisition at UTTR utilizes fixed telemetry reception sites with wide coverage of the range airspace. Coverage "holes" are covered using mobile telemetry acquisition vans that can be positioned prior to the test. The mobile telemetry vans must be usable either in a manned or unmanned mode, depending upon the test scenario and missile footprint size. Test requirements for some weapons require telemetry data acquisition through impact. This requirement necessitates placement of the mobile telemetry vans near the actual weapon impact point.

TSPI tracking of the launch aircraft is usually performed utilizing metric radars or multi-lateration tracking systems such as the Global Positioning System. Safety management at UTTR is greatly enhanced by using the High Accuracy Multi-Object Tracking System (HAMOTS) as a source of TSPI data. This system uses uniquely coded tracking beacons on participating aircraft, allowing each aircraft to be identified and tracked separately. TSPI tracking of weapons is more difficult than for manned aircraft because the weapon typically combines small size and high performance with inadequate internal space to install tracking aids. Some specially configured tracking instrumentation systems are employed to track the weapons and supply the data needed for range safety control and weapons evaluation. They are:

Tracking radar modifications: The TPQ-39 C-band metric tracking radar at UTTR was

modified by replacing the boresighted video tracking camera with a Forward Looking Infrared (FLIR) camera. This enables the radar operator to more easily track a rocket or turbojet propelled weapon, even in light clouds or against background terrain. The radar was also modified to add an operator controlled joystick, which allows the operator to break radar track on the launching aircraft prior to weapons launch, manually track the weapon using the FLIR and joystick until it separates well away from aircraft, and then revert to automatic track using radar returns from the weapon skin.

Cinetheodolite modifications: Two arrays of four cinetheodolites each were converted to remote control operation, and one array was fitted with auto-tracking FLIR cameras. The remote control modifications were developed by White Sands Missile Range. Each array of four modified cinetheodolites are connected via fiber-optic cable to a central van housing remote control operator stations. The modifications allow the cinetheodolites to be operated within the weapon safety footprint without endangering the operators. A schematic representation of a remotely controlled cinetheodolite array is shown in Figure 2. Standoff distances of up to 48 Km between the cinetheodolite and the control van have been demonstrated. An added benefit of the conversion is the capability to generate real-time TSPI information using computer analysis of the azimuth and elevation position recorded by each tracking mount. The real-time TSPI information is generated within the control van and is distributed over range communications nets, allowing other tracking systems (such as tracking radars) to automatically acquire the target. Conversely, any other available tracking data source can supply data to the central control van, allowing the remotely controlled cinetheodolites to rapidly acquire and track the target. In addition to the other benefits, it has been found that the FLIR camera systems allow the cinetheodolites to detect and track rocket propelled weapons at much longer ranges than would be expected from visual spectrum cameras. The remotely controlled cinetheodolites have demonstrated the capability to track rocket propelled weapons from up to 42 Km away in clear, low humidity atmospheric conditions.



6. TARGET CONFIGURATIONS

Targets should confer some operational realism for operational tests; they should accurately simulate some target that may be found in a wartime situation. For example, many of the video guided weapons are designed to be effective against large structures such as aircraft hangars, bridges, or buildings. These targets represent a challenge for test range support, since even simulated structures are expensive. At a minimum the structures must be able to withstand possible range weather conditions, such as wind, rain, or snow loads, prior to use in a test. The best approach is to provide a simulated structure that can be used multiple times as a target, usually by making it easily repairable. A method used at UTTR and other test ranges is to produce a simulated building using surplus sea containers. Sea containers are relatively large cargo containers used commercially to transport goods over long distances using multiple transportation methods. Sea containers generally have standardized exterior dimensions and incorporate a steel or aluminum frame. The target building is constructed by stacking and welding together multiple containers. If required, a uniform exterior finish can be supplied by adding a repairable coating, such as stucco, to simulate various building types. An example building is shown in Figure 3.

Test programs typically employ inert warheads where possible to limit the target damage and increase the probability that the target can be repaired and reused. The targets are also

constructed to facilitate damage repair. For instance, a building constructed of sea containers can be repaired by replacing damaged containers as required, and then repairing the exterior finish. An alternative method used to produce target buildings is to use pre-cast concrete pillars and panels. This produces a more robust building, but damage can still be repaired by removing and replacing damaged pillars and panels. Figure 4 shows an example of this construction method. A third method is to use pre-cast concrete bridge sections joined together to produce stand-alone buildings or bunkers. Again, the buildings are repairable by replacing the pre-cast components. An example of this target type is shown in Figure 5.

Another difficult target type is the simulated radar target for air-to-ground anti-radiation missiles. Operational evaluation test scenarios need multiple targets that simulate not only a realistic mix of radio frequency emitter types, but also employ some simulated emitter responses to the weapons threat. The threat emitters must be capable of remote control and the controllers must be able to obtain test aircraft position information that allows them to employ counter tactics such as shutting the emitters off or switching frequencies. The scenario also requires utilization of a target area within which extraneous radio frequency emissions can be carefully monitored and controlled. Otherwise even tracking radars and communications systems used for test control and for test data acquisition can become targets! The anti-radiation weapon target area

requirements are met at UTTR by implementing a specialized target area called TS-4. A schematic of the TS-4 target area is shown in Figure 6. This impactable target area was designed to support testing of both autonomous loitering and direct attack anti-radiation weapons. All communications and remote control functions for the target area utilize buried fiber-optic lines. All TSPI and telemetry data are acquired either by remotely controlled systems within the target area's 22 mile (35Km)

diameter, or manned sites located outside the target area. The target area is located well within positive control restricted airspace that spans from ground level to 17,678 meters above mean sea level. Additional unpopulated expanses outside the target area, but within the restricted airspace, allow a wide latitude in allowable launch conditions. A typical large shoot box provided in support of recent weapons evaluation tests is shown schematically in Figure 7.

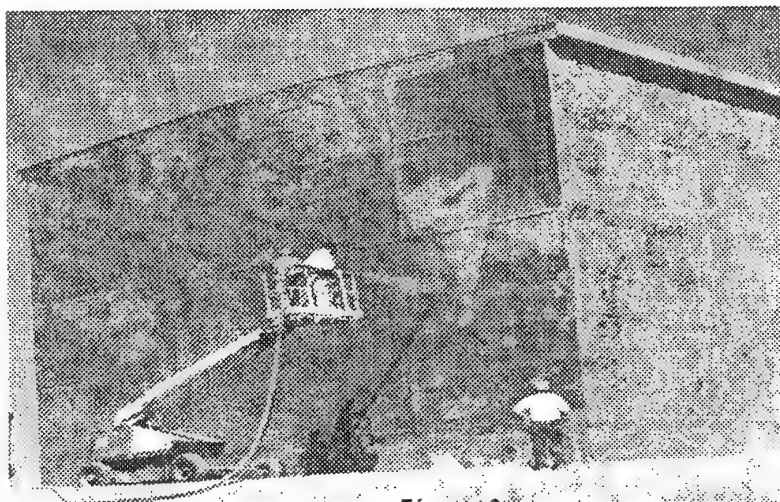


Figure 3

TARGET BUILDING MADE OF SEA CONTAINERS

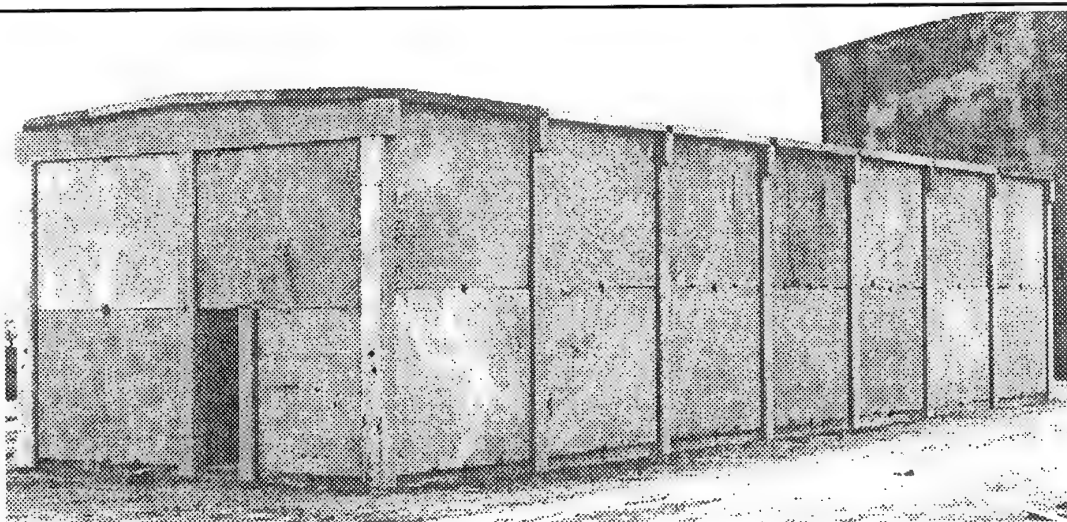


Figure 4

TARGET BUILDING MADE OF PRE-CAST SECTIONS

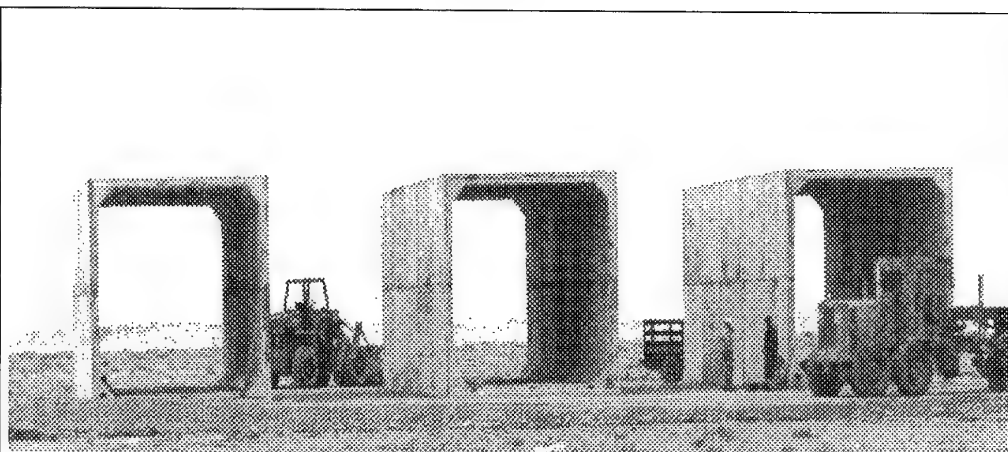


Figure 5
TARGET MADE OF CONCRETE BRIDGE SECTIONS

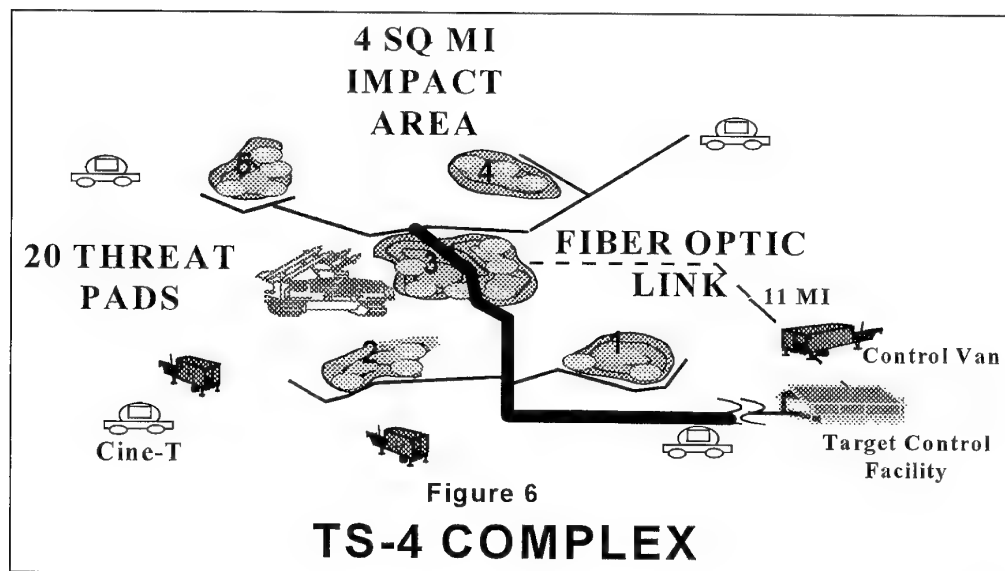
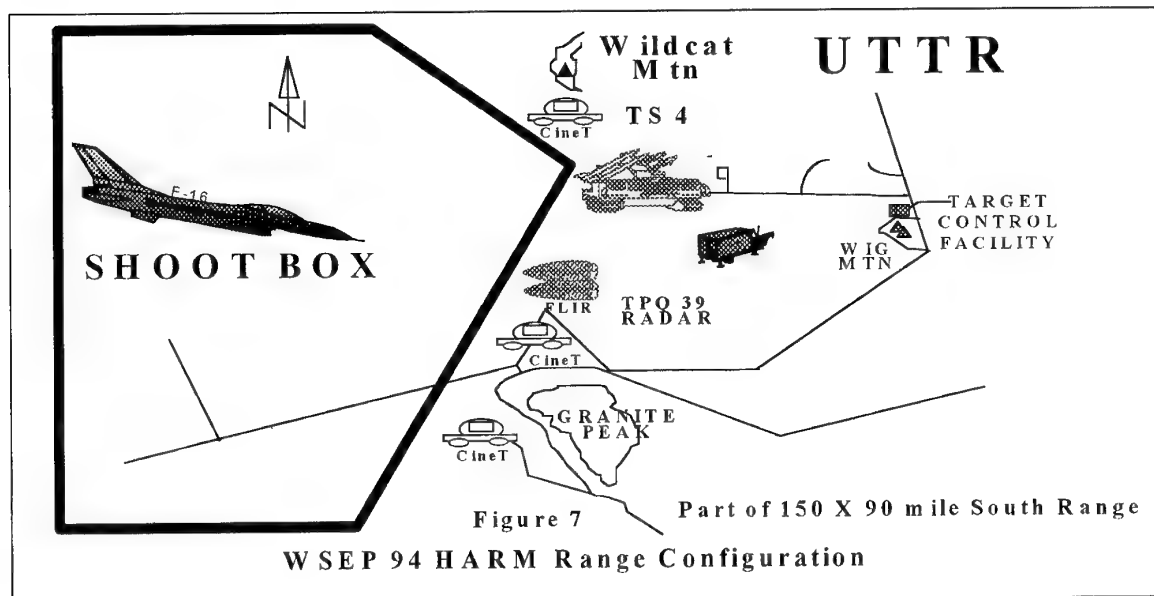


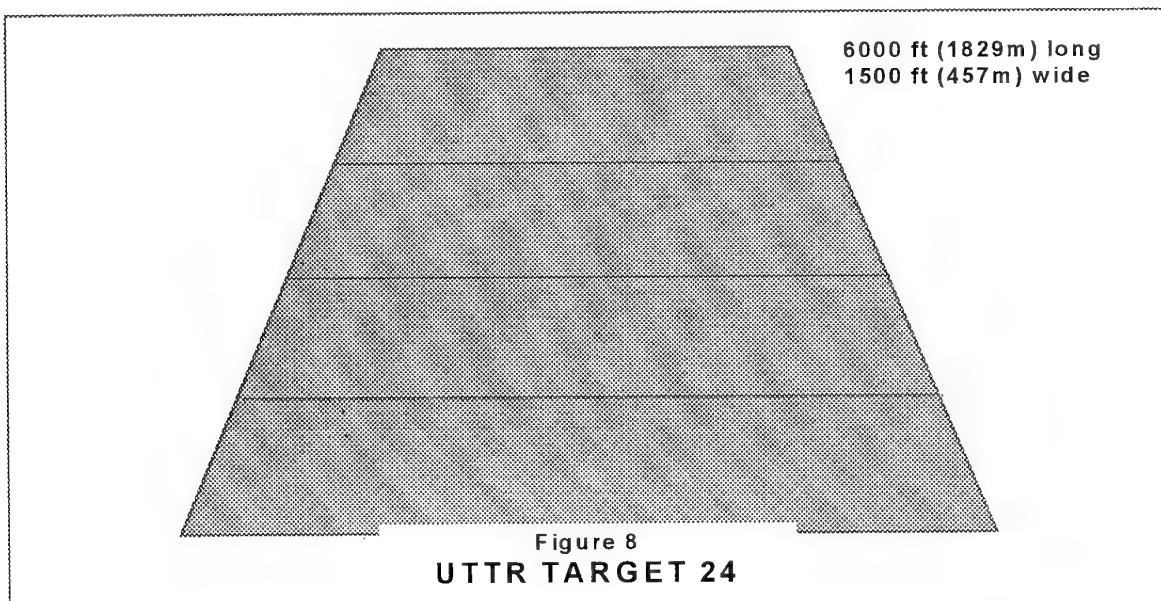
Figure 6
TS-4 COMPLEX



Some weapons require other types of specialized targets. An example is the submunition dispensing class of weapons, such as the Cluster Bomb Unit (CBU) gravity weapons, the Joint Direct Attack Munition (JDAM)ⁱⁱ, the Joint Standoff Weapon (JSOW)ⁱⁱⁱ, and other projected weapons.^{iv} These systems need a target area which can support instrumentation for analyzing weapon separation from the launch aircraft, as well as dispersion, impact, and functioning of the submunitions. The target area must also allow for recovery/ disposal of all unexploded submunitions after the test. The target surface must be capable of withstanding submunition impact and detonation, but be easily repaired and maintained. Example target areas are

shown in Figure 8. These target pads are optimized for independent analysis of multiple sequential deliveries (up to four), and represents UTTR target area 24.

The Air-to-Ground Missile (AGM)-65 Maverick missile requires still another type of targets for operationally realistic tests. These targets typically include stationary or remotely controlled tanks arrayed to represent either friendly or enemy tanks. The tank targets typically have operating engines, or some form of infrared signature augmentation, to increase the target realism. These arrays require the pilots to distinguish between friendly and enemy forces before launching the weapons.



7. OPERATIONS CONDUCT

Typical developmental weapons test and evaluation (DT&E) differs substantially from operational weapons evaluations test and evaluation (OT&E). Airborne participants in a typical DT&E weapons test consist of a launch aircraft and a chase aircraft, with some additional support aircraft, such as tankers or airborne data relays. The launch and chase aircraft fly a tight formation (within strict safety constraints) along a carefully pre-determined flight path to a pre-determined shoot box. The small shoot box typically allows the weapon to be launched along a carefully controlled launch heading from pre-approved altitude, airspeed, and dive angle conditions. The weapon then travels along a well determined flight path with a known safety footprint to impact the pre-selected target.

In contrast, OT&E tests can employ complex tactical scenarios which are constructed to gain the maximum combined test and training benefit from each weapons launch. The scenario does not constrain the participants to pre-determined flight paths, but only identifies targets, expected threats, and potential threat responses scenario. This allows the test participants much more freedom to employ weapons tactics. For example, the participants in a weapons evaluation may consist of a classical four-ship formation^v with two or more of the aircraft carrying live weapons. If the tactical scenario requires attack of an active radar complex, for example, the scenario may also employ supporting Wild Weasel aircraft to aid in identifying and prioritizing targets. The attacking formation can be met by a defensive four-ship element which use air-to-air tactics, with electronically simulated missiles and guns, to defend the target area. MUTES and TRAINS sites are used to provide "threat density" sufficient to force the attacking formation to employ evasive tactics and electronic warfare countermeasures. Small unguided "Smoky Sam" missiles can be fired to simulate surface-to-air threats. Range safety and range control officers actively monitor the scenario and transmit warnings or commands as the aircraft approach or exceed the allowable weapon shoot box boundaries. As the attacking aircraft approaches the shoot box, the range control officer calls "red" or "green" range conditions. Red range conditions mean that the range is not ready for a missile launch, while green range conditions mean that approval can be given to arm the weapon. If the missile is equipped with telemetry, the data are checked by range personnel to ensure that all of its

required systems, particularly the command-destroy system, are operational. If the weapon condition is acceptable, permission to launch is relayed to the pilot. The pilot is then free to fire at one of several "shootable" targets provided. Depending upon the target type, remote target control may be available, allowing the target operators to employ defensive tactics that the launch aircraft must counter. Once the weapon is launched, range TSPI and TM systems track it on its flight into the target. The weapon is typically tracked using two or three independent TSPI sources, since complete loss of weapon track is a criteria for a commanded termination. The weapon is also destroyed if tracking and telemetry data predict that it will leave the permissible footprint area. The TSPI sources are internetworked so that any tracking source can be fed to all other tracking sources to acquire track, or re-acquire if track is lost. In some instances where the weapon cannot be reliably tracked by TSPI sources, a chase aircraft will follow the weapon to the target to ensure that the weapon trajectory meets safety requirements. If the weapon successfully attacks the target, telemetry, high speed high accuracy film cameras, and the video measurement analysis system (VMAS) are used to provide data used for the post-flight probability-of-kill analysis. The VMAS can also be used to provide real-time video of target impacts.

Weapon system evaluation of bomber launched strategic and tactical cruise missiles is managed somewhat differently from evaluations of shorter range tactical missiles and bombs. Much of the training for the bomber crew and support personnel is conducted away from the test range as missions are prepared and weapons are loaded at the bomber's home base. Once airborne, the bomber flies a complex long range profile to the weapon launch point at the weapons test range. Once the weapon is released, the bomber typically exits the range and returns to base along the pre-planned profile. The weapon meanwhile uses its on-board navigation system and sensors to fly an independent profile to a pre-planned target. The target can be either a simulated enemy facility or a set of pre-planned coordinates, depending upon the test requirements. Data is collected from telemetry downlinks both to determine missile performance and to evaluate range safety. An example of a typical cruise missile scenario is shown in Figure 9.

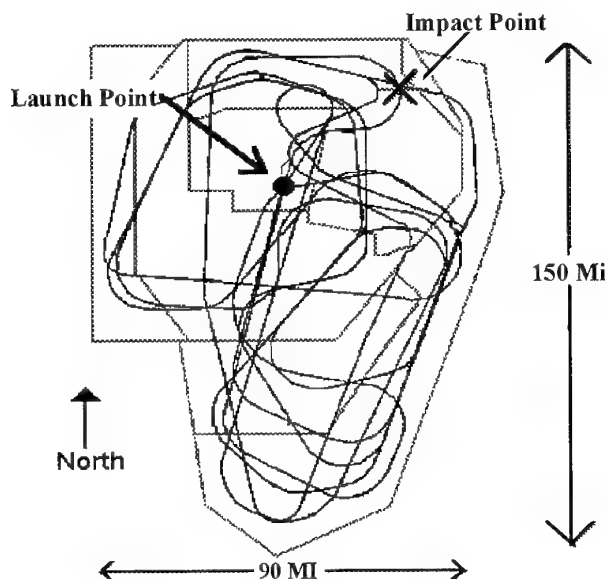


Figure 9
Typical Cruise Missile Profile

8. RESULTS

8.1 Weapon Systems Evaluation Program

Last year, in the largest Combat Hammer Air-to-Ground Weapon Systems Evaluation Program (WSEP) to date, the ACC demonstrated in 21 successful launches that the HARM weapon is a proven fire-and-forget winner. The 1993, 1994, and 1995 WSEP HARM tests used instrumented missiles in a simulated combat environment against a variety of live targets, thoroughly testing the missiles, the pilots, and their target acquisition methods. The HARM missiles repeatedly hit the bulls-eye, demonstrating their suppression of enemy air defenses (SEAD) capability while gathering valuable missile performance data. Capt Krafcik, HARM Program Manager, said: "Shooting HARM at other ranges is great for a development program, but their restrictions are not favorable to operational testing. We were delighted to help get more realistic HARM training at UTTR." Since using HARM to its fullest potential can substantially decrease the exposure of friendly forces to enemy fire, the added benefit of realistic training on a large range is critical to increasing the success of friendly forces during wartime.^{vi}

HARM was included in the UTTR WSEP program after demonstration tests were successfully completed in December 1993. The

two test launches validated UTTR's capability to track and acquire data for high performance missiles launched at low altitude or substantially off-axis from the target. (Off-axis profiles occur when the launch aircraft is not pointed in the direction of the intended target at launch.) Now pilots can practice tactics using HARM's low altitude and off-axis launch capabilities to launch a strike at a target radar while performing combat maneuvers, increasing the survivability rate of the strike aircraft.^{vii}

The WSEP program requires the use of UTTR because of the uniquely large combination of restricted airspace and land area available as a safety footprint. Range Safety personnel determine the footprint requirements after reviewing the missile performance capabilities and analyzing possible failure modes. HARM's high velocity gives it a very large footprint compared to its shoot box. The added WSEP requirement of realistic combat training can only be facilitated by a range big enough to allow for dynamic maneuvering with live-fire under simulated combat conditions. WSEP also requires simultaneous tracking of multiple aircraft and small uncooperative missiles. The UTTR is the only place in the United States where the Air Combat Command can enjoy a 1100 m² overland HARM shoot box, with

launches within the shoot box restricted only by operational aircraft and missile limits.^{viii}

The unprecedented flexibility given WSEP at the UTTR surprised both the planners and pilots. The first missions were flown very close to the old restrictions. It took several reminders that "you don't have to worry about that anymore!" for them to realize their tactical missions could be planned with only minimal range considerations. Major Sipher of Eglin's 86th FWS, the Air-to Ground WSEP Systems Operations Officer, stated that the "UTTR outclassed other candidate ranges by leaps and bounds. The UTTR provided a shoot box which allowed a highly flexible air-to-ground tactical environment with airspace extending from the surface to 15,240 meters, any aspect angle launch profiles, and ranges out to 30 nautical miles (55 Km). This was the best shoot environment seen to date!"^{ix}

WSEP pilots launched or dropped approximately 180 munitions during the 1994 two week exercise. In addition to HARM, weapons tested included AGM-130s, GBU-10/12/15/24/27s, and Maverick missiles.^x Similar results were obtained during the 1995 WSEP tests, which included the first operational F-15E launch of an AGM-65 and an AGM-130. Air Combat Command has already used data obtained from these tests to make operational readiness decisions, and to institute corrections to system reliability and effectiveness that were identified as a result of the test program.

8.2 Cruise Missiles

All types of cruise missiles have been successfully flown to impact or recovery at the UTTR. These have included submarine, ground, and air launched cruise missiles; Advanced Cruise Missiles; and Conventional Air Launched Cruise Missiles. The evaluation results so far have been superior in terms of identifying problems and advantages under live-fire conditions for: missile targeting, guidance, control, survivability, reliability, accuracy, probability of kill (Pk). The evaluation also encompasses mission operations from takeoff to missile launch to landing, including aircrew environmental-ergonomic concerns. This has allowed weapon employment using realistic operational scenarios made possible only with a flexible large-footprint range environment.

The results? Warfighter customers are unanimous in their accolades for this type of test. Operationally representative testing of modern tactical weapons results in many advantages over alternative test and training methods. One advantage is that evaluation of weapon performance during the tests results in identification of deficiencies caused by

manufacturing defects or long-term storage. Identification and correction of weapon deficiencies greatly increases confidence that the operational inventory of weapons will perform reliably when called upon. In addition, operationally representative testing results in greatly enhanced training for the participating aircrews. Use of realistic scenarios allows participation by multiple aircraft, including support aircraft. Expenditure of each expensive weapon results not only in training the aircrew that launched it, but in training multiple other participant aircrews. In short, operationally representative testing of modern tactical weapons is a key to successful employment of those weapons today and on into the 21st century!

ⁱ *Airman Magazine* (September 1993): p. 14.

ⁱⁱ *Air Force Magazine* (May 1994): p. 131.

ⁱⁱⁱ Ibid

^{iv} David A. Fulghum, "TSSAM Follow-on to Take Shape this Year," *Aviation Week and Space Technology* (February 27, 1995): p. 49.

^v James P. Coyne, "Fighting in Fours," *Air Force Magazine* (April 1993): p. 60.

^{vi} Captain Jeffrey S. Davis, "In HARMS Way!," *MRTFB Gazette*, (May 1995): p. 4.

^{vii} Ibid

^{viii} Ibid

^{ix} Ibid

^x Ibid

ANALYSIS OF WRAP-AROUND FIN AND ALTERNATIVE DEPLOYABLE FIN SYSTEMS FOR MISSILES

Gregg L. Abate* and Gerald Winchenbach**
 Weapon Flight Mechanics Division
 Wright Laboratory, Armament Directorate
 101 W Eglin Parkway, Suite 219
 Eglin AFB, FL 32542

SUMMARY

This paper will present aerodynamic results of investigations of wrap around fin missile configurations. The investigations were carried out at Wright Laboratory's Armament Directorate, Eglin AFB, FL. The investigations have shown that instabilities exist in the form of an undamped side moment induced by the pitching motion of the missile, a roll moment at zero degrees angle-of-attack, and a roll moment reversal through Mach 1. This paper will also present data for alternative deployable fin designs.

List of Symbols

A	= reference area (typ. $\pi d^2/4$)
b	= fin span
c	= fin chord
CG	= center of gravity
$C_{m\alpha}$	= pitching moment coefficient derivative per $\sin \alpha$
C_n	= side moment
$C_{np\alpha}$	= Magnus moment
$C_{n\alpha}, C_{nsm}$	= slope of side moment vs. $\sin \alpha$
C_p	= pressure coefficient
d	= reference length (typ. diameter)
l, m, n	= moment about x, y, z axis
M	= Mach number
p/p_∞	= pressure ratio
p, q, r	= missile roll, pitch, yaw angular velocities
\bar{q}	= dynamic pressure
x, y, z	= spatial coordinates
α	= angle of attack
θ, ψ, ϕ	= angular coordinates

* Aerospace Engineer

** Senior Scientist

This paper is a work of the US. Government and is not subject to copyright protection in the United States.

INTRODUCTION

The purpose of this research effort is to better understand the aerodynamics associated with wrap around fin (WAF) missile configurations as well as to investigate alternative solutions to the problem of missile fin stowage. The data contained herein is a culmination of tests conducted on free flight models at the Aeroballistic Research Facility (ARF) and analysis using computational fluid dynamics (CFD) techniques.

1. Background

Missile configurations which employ wrap around fins have been studied extensively over the years. Such configurations offer excellent packaging advantages for tube-launched and dispenser launched applications. Aerodynamically, such configurations can present problems in the form of roll reversal through Mach 1, roll moments at 0° angle-of-attack, and the generation of a side force/moment when at angle-of-attack. Although such configurations have been tested extensively through the years, results have merely shown cause-and-effect relations for various WAF components (i.e. fin opening angle, leading/trailing edge geometry, fin attachment method, fin planform, etc.) and offered little towards the complete understanding of the aerodynamic cause of such anomalies.

Studies of WAF configurations date back to the mid 1950's where much of the same phenomena discussed above was first noticed. Dahlke^{1,2,3,4} documented wind tunnel tests in which parametric studies of WAF configurations were tested at Mach numbers ranging from 0.3 to 3.0. The Navy became interested in wrap around fin configurations and investigated unique methods of aerodynamic control. One of these methods involved the use of fin slots to help alleviate known aerodynamic problems. Daniels in the early 1970's investigated fin slots to help alleviate spin-yaw lock-in which can lead to catastrophic failure^{5,6,7,8}.

The Air Force Armament Directorate became interested in WAF configurations in the mid 1980's^{9,10}. These free-flight tests were conducted at the Aeroballistic

Research Facility (ARF)^{11,12} and clearly showed the dynamic motions associated with WAF configurations (see Figure 1). This Figure shows the angular motion about the center of gravity (CG) of the model as viewed from behind as it flies downrange (the circles represent discrete data points and the lines represent the fit motion profile). Figure 1a represents a dynamically stable missile configuration with straight fins. Note the elliptic pattern of motion and that the magnitude damps as the model traverses the range. Figures 1b-1d show the motion of a WAF missile. What stands out immediately is the circular motion pattern. This is due to the presence of a small side moment when the model is at angle of attack. This side moment, which if of sufficient magnitude, can cause a dynamic instability as illustrated in Figure 1.

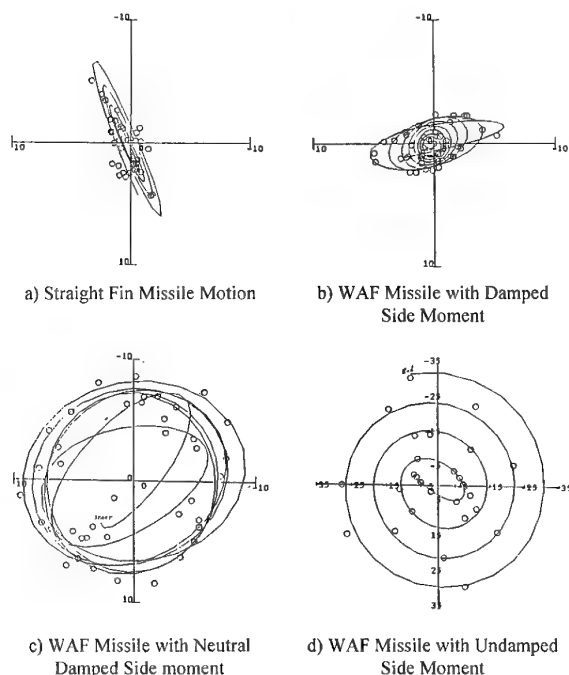


Figure 1. Free-Flight Motion Patterns

Another aspect of WAF aerodynamic anomalies that is dramatically shown in aeroballistic tests^{9,10} is the roll moment dependence with Mach number as shown in Figure 2. Here we see the roll vs. down range distance (the slope being the roll rate) for a typical WAF missile. For the subsonic tests, the WAF model rolls with the fins cupped into the flow (clockwise looking from rear) and for supersonic tests, the models roll with the fins cupped away from the flow (counterclockwise looking from the rear). Of great concern are those shots whose flight Mach number is close to Mach 1. Here we see roll reversals of the models as their flight Mach number crosses from supersonic to subsonic. This phenomena is of great

concern to designers of missiles in order to avoid spin-yaw resonance.

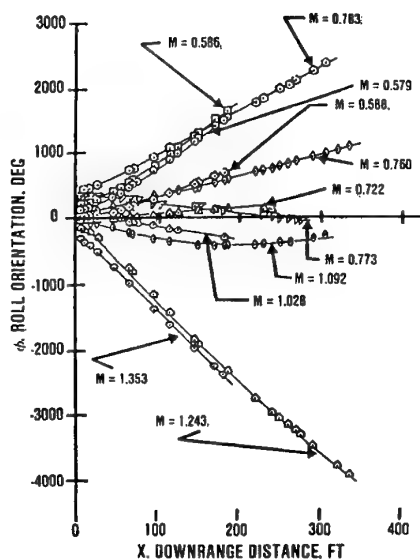


Figure 2. Wrap Around Fin Roll Motion

RESEARCH PROGRAMS

The following research programs described herein were all conducted by the Aerodynamics Branch of Wright Laboratory Armament Directorate. The first four programs describe results of free flight tests conducted in the ARF and the fourth program describes results from a CFD analysis. The first three free-flight programs employed the same basic missile shape (see figure 3) with variations in the fin region; all fin designs had the same planform area. Note that for the tests of offset fins, the planform is of a clipped delta. For tests which used wrap around fins, a rectangular fin was used. The wrap around fin span is determined by the missile body and the span was chosen to give consistent planform area (see Figure 4). Typical flight Mach numbers for the first three free flight tests ranged from 0.6 to 1.8.

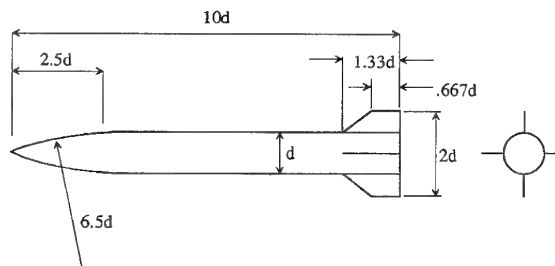


Figure 3. US Air Force Basic Research Model

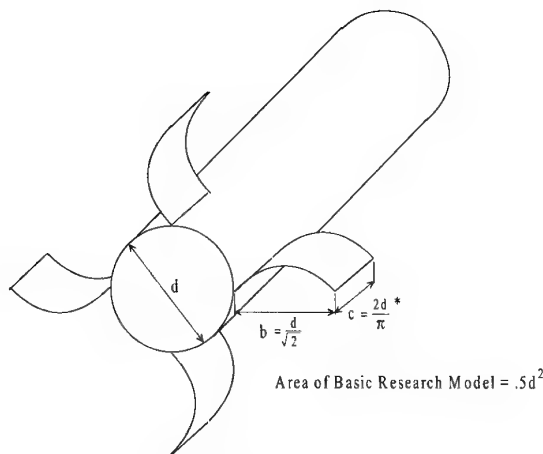


Figure 4. Wrap Around Fin Geometry

1. Offset Fins

In an effort to preserve the packaging advantages of WAF missile configurations but eliminate adverse flight characteristics, it has been proposed to deploy a fin which is flexible enough to fold around the body yet stiff enough when deployed to provide aerodynamic control surfaces. The U.S. Army Missile Command (MICOM) investigated such a configuration¹³ in which a bi-convex cross-section fin constructed of flexible steel could be folded around a missile body and deployed to a cruciform shape. However, the amount of bend required of such a fin, especially at the attachment point, could cause material failure and/or have other adverse affects if stowed for long periods of time. One potential way of alleviating these problems is to deploy such a fin to some angle less than perpendicular (90°). Hence, the resulting configuration was termed an "offset fin." Four offset fin configurations were tested¹⁴ in this program which are shown in Figure 5. The 0° model was constructed slightly different as the severe offset decreased the static stability. For this configuration, a heavier nose was used to move the CG far enough forward to maintain stability. In the presentation of the results however, the pitch moment derivatives are referenced back to the 'nominal' configurations.

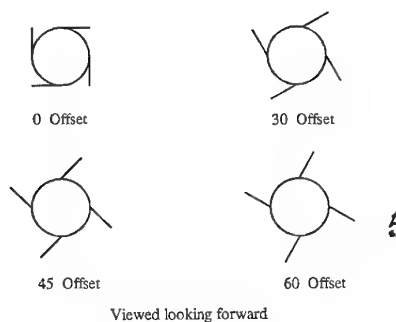


Figure 5. Offset Fin Models

2. Slotted Fins

Slotted fins are fins in which some of the area has been removed to allow flow through the fins. As previously mentioned, Daniels⁵⁻⁷ investigated fin slots in an effort to reduce the inherent instabilities of current wrap around fin designs. Fin slots were also investigated on the Air Force basic research model¹⁵. Figure 6 depicts a typical WAF configuration with fin slots.

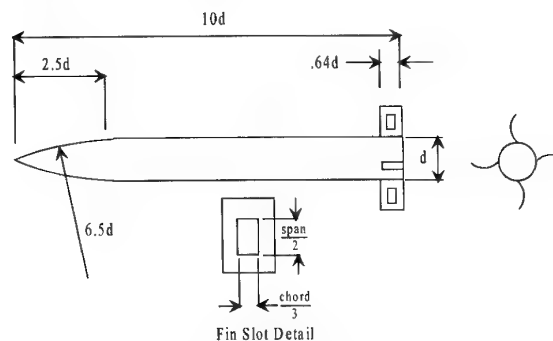


Figure 6. Slotted Fin Model

3. Base Cavities

One of the aerodynamic anomalies of wrap around fins is the presence of a side force when the missile is at angle of attack. The flow asymmetry in the fin region causes this small force when at an angle of attack and can result in a significant side moment which tends to lead to lunar angular motion of the missile. Reference 16 presented data suggesting that cavities in the base of a missile configuration with wrap around fins reduced both the side moment and the coning motion to near-zero levels. Therefore, it was also decided to test similar cavities on WAF missile configurations for which there were already significant data available¹⁷.

Figure 7 depicts the model configuration used for these tests. For these tests, the base of the models had a one half caliber extension with a semi-hemispherical cavity. The shape of this cavity is similar to the one described in Reference 16.

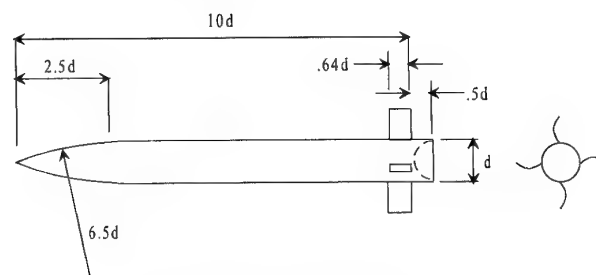


Figure 7. Base Cavity Model

4. Other Configurational Variations

Further tests to define the effects of various configurational changes, i.e., length-to-diameter ratio (l/d), fin sweep angle, fin root chord length, and fin thickness have also been accomplished¹⁸. The configurational variations used in those tests are listed in Table 1; however, all models used the 2.5 caliber ogive nose consistent with the basic research configuration already discussed. Although these tests only included 25 flights, it is believed that the design of experiments process provided reasonable trends over the Mach number range tested (Mach 1.5-3.0). The results of these tests are presented in Reference 18 and will not be discussed in detail in this paper.

Table 1. Design Factors

Design Factor	Design Level
Fin Sweep Angle	0°, 22.5°, 45°
Fin Thickness	0.04, 0.07, 0.10 inches
Length-to-Diameter Ratio	7.5, 10, 12.5
Mach Number	1.50, 2.25, 3.00
Root Chord Length	0.53, 0.71, 1.08 inches

5. CFD Analysis

As discussed, extensive testing has been done on wrap around fin configurations through the use of wind-tunnels and aeroballistic ranges which have identified the aerodynamic anomalies previously mentioned. Results from these tests quantify these anomalies for the particular configuration of interest and have shown cause-and-effect relations for various WAF components (i.e. fin opening angle, leading/trailing edge geometry's, fin attachment method, fin planform, etc.). Complete understanding of the aerodynamic cause of these anomalies is still not known however. Conventional analysis tools have not been able to accurately predict the aerodynamics associated with curved WAF configurations. Analysis through the use of programs such as Missile DATCOM and the NWL code¹⁹ usually suffice for preliminary analysis but side force/moment predictions can not be determined for WAF configurations.

Previous CFD studies of missile configurations with wrap-around fins have shown general agreement with experimental data but always lacked accuracy in roll moment and side force/moment determination²⁰. The accuracy of the CFD results are greatly determined by how accurately the configuration is modeled (i.e. grid resolution). Closer examination into these analysis revealed that the fins were usually modeled as being "infinitely thin." Since the aerodynamic anomalies of interest are inherent to the WAF geometry, it is important to model (grid) the fin area as accurately as possible.

Therefore, it was decided to analyze a generic wrap around fin missile configuration using CFD paying particular attention to the details in the fin region²¹. That is, fins would be modeled with thickness and computational points clustered tightly within the fin region. Program EAGLE²² (Eglin Arbitrary Geometry impLicit Euler) was utilized for all the analysis contained herein. EAGLE is a collection of codes which contain a grid code, surface generation code, and a flow solver code. Although "Euler" is inherent in its name, program EAGLE does have a thin-layer Navier-Stokes flow solver as well as a Full Reynold's Averaged Navier-Stokes (FRANS) solver.

A series of computations were performed at Mach numbers ranging from 0.3 to 3.5. Direct output from the program contains pressure data on all fin surfaces and the integrated forces and moments. Output files can also be directly imported into a post-processor (YAPP)²³ for interactive flow visualization.

RESULTS

1. Offset Fin

The complete aerodynamic coefficients and stability derivatives for the four offset fin configurations tested are presented in Reference 14. However, the pitch moment derivatives are plotted vs. Mach number herein, see Figure 8. Also plotted here for comparison purposes are the baseline aerodynamics²⁴. As described in Reference 14, there is no appreciable difference in drag for the four offset fin configurations. However, as shown in Figure 8 there is a decrease in the static stability as the offset angle decreases. Note here that the zero degree offset model's center of gravity was further forward than the other configurations. However, the data shown in Figure 9 are converted to the same reference CG.

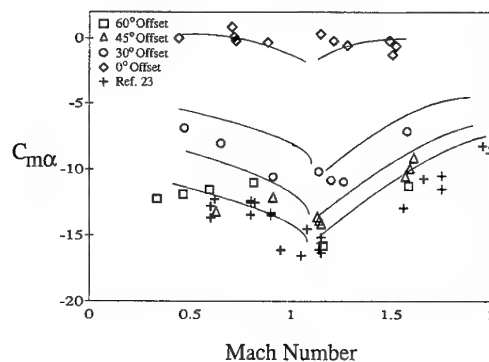


Figure 8. Offset Fin Pitch Moment Coefficient vs. Mach Number

Figures 9 shows representative motion plots for the zero and 60 degree offset fin configurations. These angular motion profiles are about the center of gravity of the projectile viewed from the rear. The typical motion pattern for a damped straight-fin missile is similar to that of Figure 9-a. Whereas the typical motion of a wrap around missile configuration is similar to that of Figure 9-b. This lunar angular motion is caused by the out-of-plane side moment generated when the missile is at angle-of-attack. It is seen then that as the fins are offset from 60° to 0° there is a tendency of the missile to behave like a WAF configuration Which is due to the increasing asymmetry of the fin region.

The inclusion of the side moment due to pitch angle was necessary in order to adequately fit the measured motion patterns of the 0° , 30° , and some of the 45° offset models. The tendency of the motion to develop into a circular pattern provides a clue to the possible presence of this side moment. Both Murphy²⁵ and Nicolaides²⁶ have studied the consequences of a side moment due to pitch on the dynamic stability of a finned missile and showed that if this side moment was of significant magnitude then the angular motion would be undamped.

2. Slotted Fin

The aerodynamic coefficients and stability derivatives extracted from the experimentally measured trajectories are presented in Reference 15. The data shown in Figure 10 illustrates that there is about a 33% decrease in the magnitude of $C_{m\alpha}$ for the slotted fin in the supersonic region. This difference increases to 67% in the transonic region. Also shown in Figure 10 is the slotted fin data with the fin area normalized to the solid fin area. That is, the slotted fin data has been reduced 17% (the amount of fin area removed) to try and separate fin area effects from slot effects. Here it is seen that approximately one half of the pitching moment loss is due to removed area in the supersonic region and one fourth of the pitching moment loss is due to removed area in the transonic region.

The side moment vs. Mach number data is shown in Figure 11. A reduction in the side force of 50% is immediately noticed for the slotted fin configuration vs. the solid fin configuration. Again, this derivative is normalized to represent the reduced area of the slotted fin but it is seen that the overall reduction in side force is much greater leading one to believe that the slots are mostly responsible for the reduction vs. reduced wetted area.

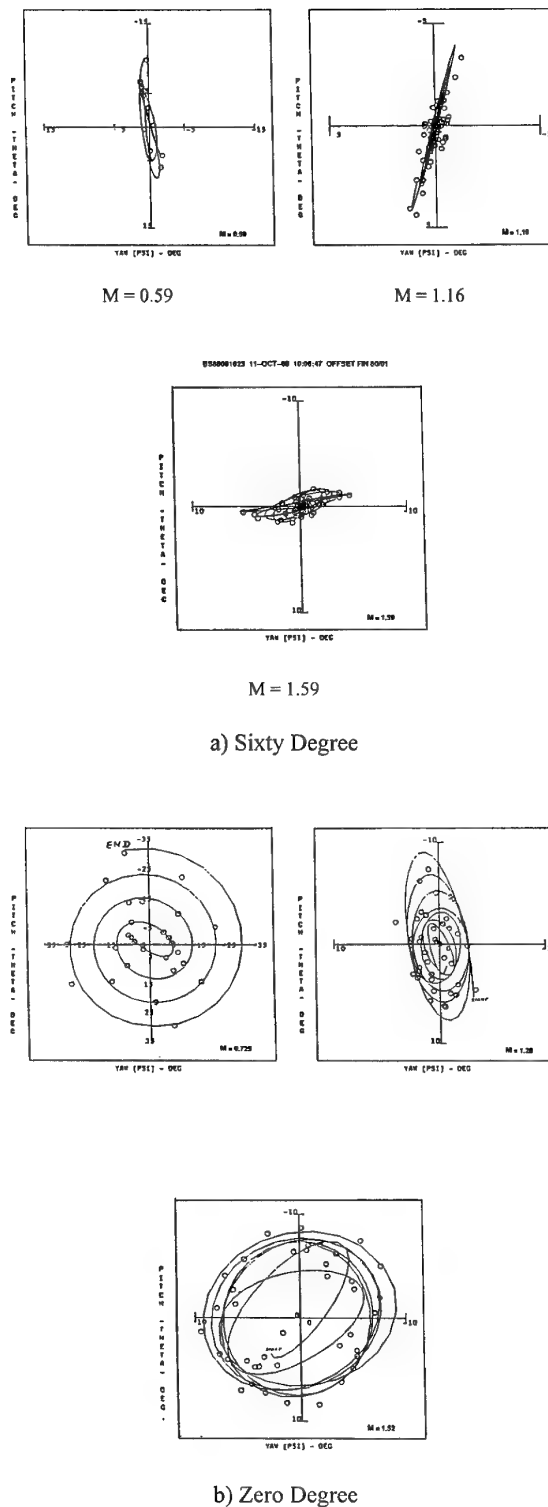


Figure 9. Sixty Degree & Zero Degree Offset Angular Motions

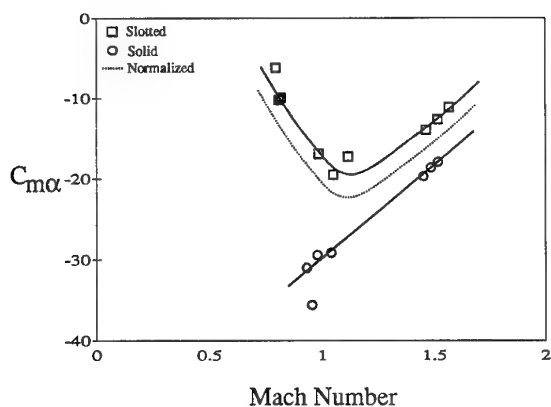


Figure 10. Slotted Fin Pitch Moment Coefficient vs. Mach Number

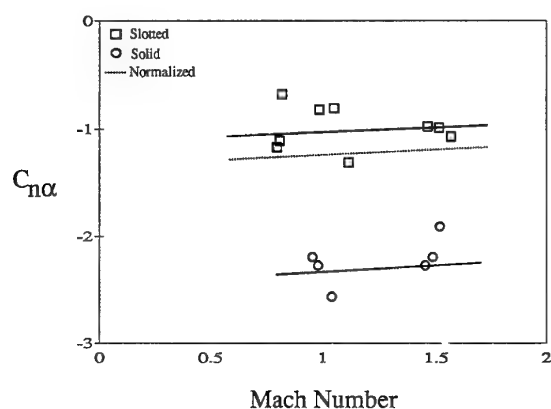
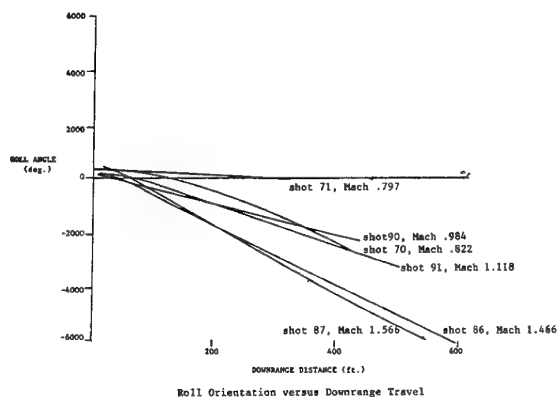


Figure 11. Slotted Fin Side Moment Coefficient vs. Mach Number

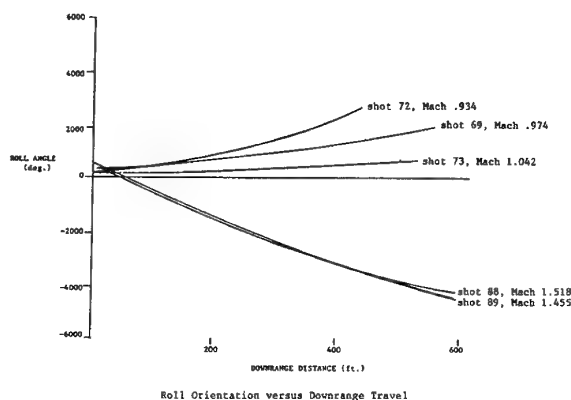
Figure 12 plots the roll orientation vs. downrange distance for the slotted and solid fin configurations. Note that the solid fin model in Figure 12-b demonstrates the classical roll rate dependence with Mach number (see for example Figure 2). Interestingly, the roll rate for the slotted fin configuration does not show this dependence (Figure 12-a)

3. Base Cavity

Reference 17 presents the aerodynamic results for the base cavity models. In that Reference it is shown that there are no significant drag differences between the baseline and base cavity aerodynamics and only minor variations in the normal force and pitching moments. These reductions did show significant sensitivity to both side moment, $C_{n\alpha}$, and Magnus moment, $C_{np\alpha}$. However, the combined magnitudes of the out-of-plane moments were not large enough to cause a dynamic instability.



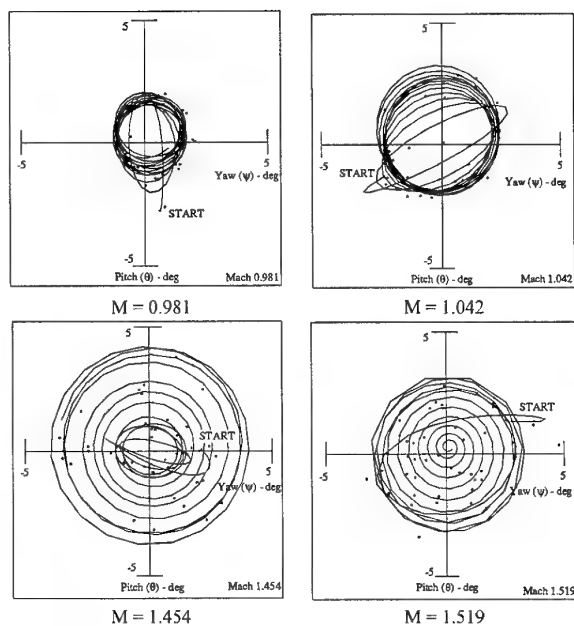
a) Slotted Fin



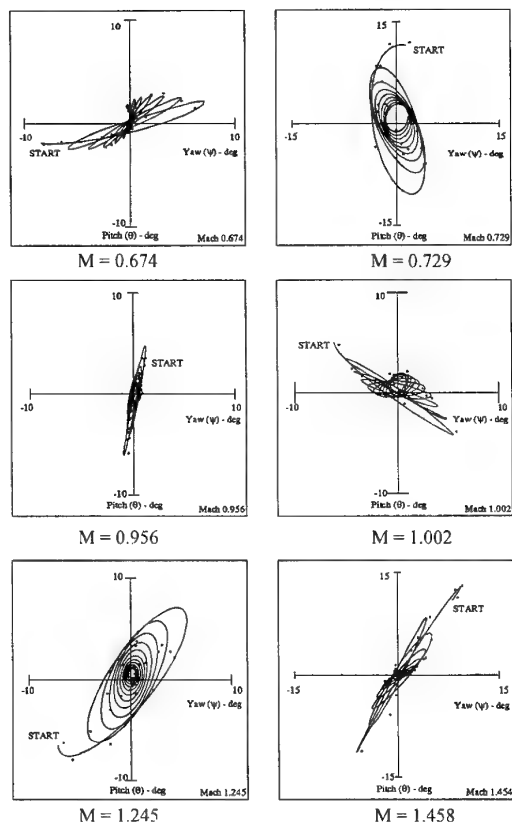
b) Solid Fin

Figure 12. Slotted & Solid WAF Roll Motion

Figures 13 shows the corresponding angular motion profiles about the center of gravity with and without base cavities. Here we see the effects of the side moment most clearly as demonstrated by the base cavity model. Note the circular motion of the missile which is the classical effect of the side moment as caused by the asymmetric fin configuration at angle of attack. Compare that motion profile to the one with a base cavity also shown in Figure 13. Obviously the presence of the cavity has greatly affected the dynamics of the model.



a) Without Cavities



b) With Cavities

Figure 13. Effect of the Base Cavity on the Angular Motion

4. CFD Analysis

a. Infinite Body

Rather than be concerned with what goes on far upstream or far downstream, the initial analysis focused on the fins themselves. That is, a wrap-around fin geometry was modeled on an infinitely long body. This was done to: 1) isolate the effects of the fins, 2) accurately model the fin geometry (i.e. thickness), 3) devote more points to the fin region, and 4) ignore base flow effects. The analysis utilized an Euler code, which neglects viscous effects, which is most appropriate for this configuration.

A 10% thick bi-convex airfoil shape was utilized for the fin cross-section. This would provide not only the thickness effects under investigation, but a simple CFD geometry with which to model. That is, it is easily "gridable" and would not present the flow solver any problems. The bi-convex airfoil shape is rotated through 90° to model the fin curvature. The root intersects the body at 45° and is blended into the cylindrical body. Details of the grid used in the CFD calculations are presented in Reference 21 and will not be elaborated on herein.

Euler flow solutions were calculated at Mach numbers ranging from 0.35 to 3.5. The flow visualization tool YAPP²³ was then utilized to gain insight into the associated flow physics. Also studied were force and moment data associated with the configuration. This data were determined from integrating pressure on the fin surface only. No pressure acting on the body was considered in the force and moment calculations. In that respect, the only meaningful forces calculated are the normal and side forces. Axial (or drag) forces are present only as a result of wave drag in supersonic conditions; subsonically, there were no axial forces present (inviscid flow solution). The only meaningful moment data is the roll moment (about the body axis). Yawing and pitch moments are meaningless for this infinite body case.

Figure 14 shows the variation of rolling moment coefficient as a function of Mach number for this baseline configuration as well as for additional configurations which will be discussed later. First, it is seen that for the case of $0^\circ \alpha$, there exists a rolling moment that varies as a function of Mach number. In addition, the direction of this rolling moment changes direction near Mach 1. This trend is in complete agreement with previous wind tunnel and experimental data.

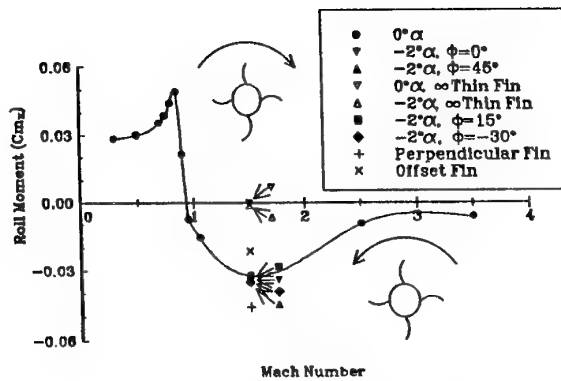


Figure 14. CFD Roll Moment vs. Mach Number

In addition to the $0^\circ \alpha$ case, it was of interest to investigate the effect of angle of attack and roll orientation on this configuration. At a Mach number of 1.5, the same configuration was analyzed at $-2^\circ \alpha$ for various roll orientations. The results indicate a slight increase in the magnitude of the rolling moment (as seen in Figure 14). This effect of roll angle on roll moment while at $-2^\circ \alpha$ angle of attack is shown in Figure 15. As shown, there is only a 5% change in roll moment as roll orientation is varied.

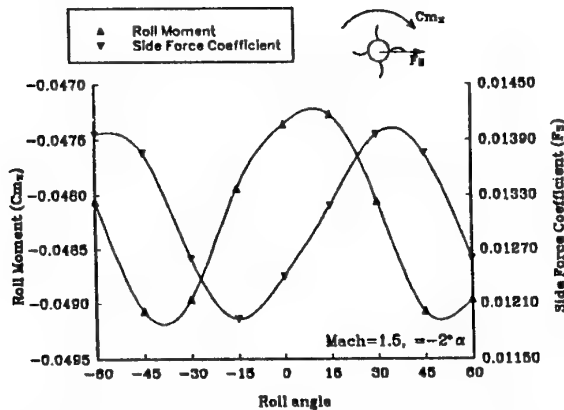


Figure 15. CFD Roll Moment & Side Force vs. Roll Angle

The fact that a roll moment was present for this configuration leads us to ask why no roll moment was observed in previous CFD studies of WAF configurations. As stated earlier, those configurations were modeled with "infinitely thin" fins. That is boundary conditions were applied to grid points within the flow. Additionally, those simulations were of the complete missile configuration where relatively few grid points were available for the fin region. With this in mind, our configuration of interest was modeled as having infinitely thin fins at Mach 1.5.

As seen in Figure 14, there is no rolling moment for this case. Additionally, at $-2^\circ \alpha$, there is a slight, almost negligible, increase in the rolling moment. This analysis seems to indicate that fin thickness contributes significantly to the roll tendencies of wrap around fin configurations.

In addition to the roll motion anomalies associated with WAF's, there is also the generation of a side force/moment. The baseline results indicate that there are no lift or side forces while at $0^\circ \alpha$ as expected. However, at $-2^\circ \alpha$, there are lift and side forces present. Figure 15 shows the side force variation as a function of roll orientation. Here it is seen that there is a 20% variation in side force depending on the roll orientation. Even though the magnitude of this side force may be small, its effect on side moment can lead to undamped coning motion of a missile. Incidentally, previous CFD results on infinitely thin fins indicate the presence of a side moment also²⁰. It can be concluded then that the generation of a side force/moment is mainly a function of the WAF geometry (i.e. asymmetric fin shape and attachment).

b. Fin Attachment

In an effort to investigate the aerodynamics associated with the fin/body junction, an analysis was conducted on wrap around fins which intersect the body at 90° . That is, a typical WAF geometry with the fins not fully deployed. Due to the asymmetry of the WAF geometry, a complete 4-fin model was used. A CFD solution was performed at Mach 1.5 and $0^\circ \alpha$. Figure 16 depicts this configuration with shading depicting pressure contours. Interestingly, the magnitude of the roll moment increased as shown again in Figure 14.

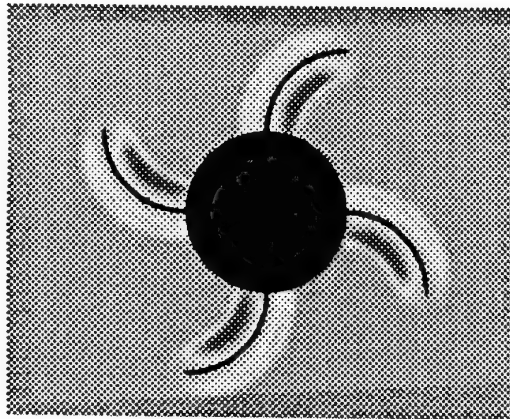


Figure 16. CFD Pressure Contours, Perpendicular Fin, $0^\circ \alpha$, $\phi=0^\circ$

This result leads one to question how fin curvature vs. fin attachment affects WAF aerodynamics. In this respect a simulation of an offset fin configuration was performed. Figure 17 shows the pressure shading associated with the Mach 1.5, $0^\circ \alpha$ case. Here the magnitude of the rolling moment is decreased by nearly 50% as shown in Figure 14. The only indications given as to why this happens is the high pressure region underneath the fin that is closest to the body. As a result we see a dependence of the roll moment that is both a function of the fin curvature and also the fin attachment. It is easy to see that the fin attachment can cause a roll moment due to the asymmetry of the fin/body junction.

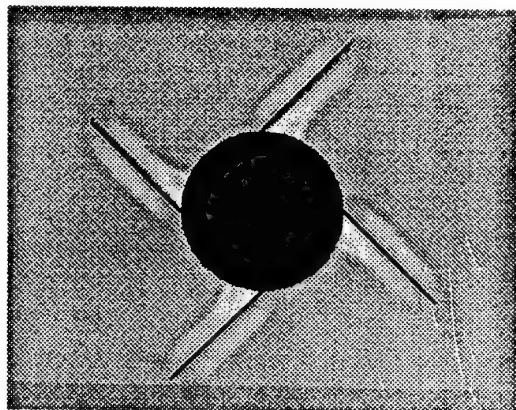


Figure 17. CFD Pressure Contours, Offset Fin, $0^\circ \alpha$, $\phi=0^\circ$

c. Fin Alone

The investigation up to this point indicates that there are some unique aerodynamics associated with curved fins. In order to understand these effects, analysis was conducted on curved fins alone; isolated from the blockage effects of the body. Again, the same 10% thick bi-convex airfoil was used. For this investigation, several simulations were done at Mach numbers ranging from .25 to 1.5. All runs were carried out at $0^\circ \alpha$. Interestingly, the results indicate the presence of a normal force. The direction of this normal force indeed changes direction at Mach 1. The results are shown in Figure 18. Therefore the mere curvature of the fins themselves lead to the rolling moment at $0^\circ \alpha$ and that rolling moment changes direction through Mach 1.

In order for a lift force to be produced on the fin there has to be a pressure differential and the computed chord-wise pressure distributions in Reference 21 provide insight into this phenomena. There it was shown that a definite difference in the pressure distributions on the upper and lower surfaces existed. The difference between the two ΔC_p 's, integrated over the fin surface, provided

the lift force and the direction of this force changes for subsonic/ transonic vs. supersonic flow conditions.

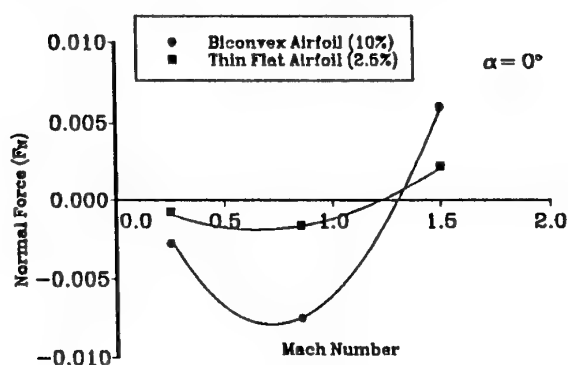


Figure 18. CFD Fin Alone Normal Force vs. Mach Number

In Reference 21 it was also postulated that the effect of the pressure distribution being higher and lower than a normalized distribution and ultimately reversing in subsonic and supersonic flow is similar to the converging/diverging nozzle flow. Figure 19 shows the classic result for a converging/diverging nozzle where the flow is sonic in the throat and where there are no shocks present. Also shown is the pressure distribution along that nozzle.

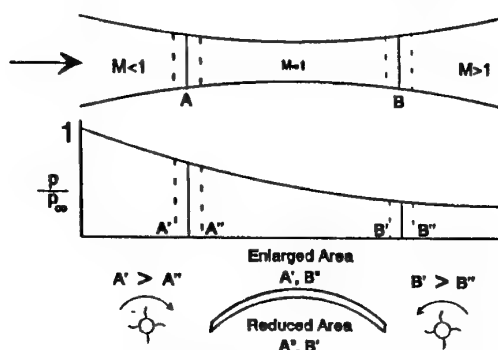


Figure 19. CFD Converging/Diverging Nozzle Analogy

Consider first a point in the subsonic section (A). A pressure slightly higher (A') and a pressure slightly lower (A'') are also shown. The location of A' and A'' in the converging/diverging nozzle are as indicated. Here it is seen that the lower pressure corresponds to the smaller cross-section and the higher pressure correspond to the larger cross-section. In other words, the flow under the WAF (concave side) acts as if it is being slightly compressed (resulting in a lower pressure) while the flow over the fin (convex side) acts as if it is slightly expanded (resulting in a higher pressure). This same analogy can be extended to the supersonic conditions (B, B', and B''). This time

however, as the flow passes under the WAF, the air is slightly compressed and the resulting pressure is higher than the normalized case. Similarly, as the flow passes over the WAF the air is slightly expanded and the pressure is slightly lower than normal. As a result of this phenomena, there is a net force which, when applied to a wrap around fin missile configuration, produce roll moments that are entirely consistent with experimental results.

DISCUSSION

1. Free-Flight Tests

The free-flight tests conducted under this program (Offset fin, Slotted Fin, and Base Cavity) give aerodynamic data on alternative wrap around fin configurations. The underlying goal of all these tests was to evaluate the configurations vs. WAF and determine any advantage of their use.

The study of offset fins was motivated by an innovative fin deployment scheme coupled with the need to reduce stress concentrations and increase shelf life. Additionally, the fact that the resulting fin configuration has straight fins rather than curved fins could lead to insight about curvature effects vs. fin asymmetry effects for missile configurations. It is seen from the results that as the fin offset decreased from 90° (90° being a conventional missile/fin configuration) the stability decreases indicating less effective fin area for aerodynamic stability. Additionally, the magnitude of a side moment grows from near-zero levels for the 60° case to relatively strong levels for the 30° and 0° cases. This indicates that the fin asymmetry is partially responsible for the generation of side moments at angles of attack and that the stronger this asymmetry the stronger the resulting side moment.

The results of the CFD analysis (which was performed subsequent to the free-flight tests) provided additional insight into the effect of fin asymmetry vs. fin curvature. The results showed that both fin curvature and fin asymmetry contributed to rolling moment; however, the effects of curvature were more pronounced in roll.

The study of the slotted fin configuration was an attempt to reduce or eliminate the lunar motion typical on WAF configurations. The motivation was previous results from NSWC which documented that the inclusion of fin slots minimized spin-yaw resonance. The results here indicate that indeed there is a reduction of the magnitude of the side moment and that the spin rate-Mach number dependence is reduced. Most likely there exists some optimal slot and/or fin shape that would reduce the side force to acceptable levels without adversely affecting the

pitch stability or drag. Analysis of the governing flow physics for fin slots would be required to exploit their effects.

The motivation behind the base cavity tests (Reference 16) was to investigate the possible reduction of coning motion for wrap around fin missiles through use of a base cavity. Having studied wrap around fin configurations for many years, it was perplexing to understand how base cavities could reduce or eliminate such motion. It has been well accepted that the asymmetry of the fins while the vehicle is at angle-of-attack produces the out-of-plane force and moment and if this moment is of sufficient magnitude the vehicle will be dynamically unstable^{25,26}.

Since both the out-of-plane side moment and the Magnus moment act in the same plane and that base geometry can significantly affect the Magnus moment, it was speculated that the base cavities produce an effect that is masking the side moment in Reference 16. The high spin rates (due to the 2° fin cant) causes a Magnus moment to be present and the cavities could alter this moment in a manner to counteract the out-of-plane side moment.

2. CFD Analysis

A generic wrap around fin was modeled on an infinitely long body to investigate the aerodynamics of curved fins. This allows for isolating the effects of the fins from that of the body. An Euler flow solver was used in this study to not only perform initial analysis's quickly but to be able to isolate effects of viscosity in future work.

The results of a four fin wrap around configuration on an infinitely long body yielded the following results:

- Roll moments were determined at $0^\circ \alpha$
- The roll moment varied as a function of Mach number and was consistent with experimental observations.
- "Infinitely thin" fins used in CFD modeling are inadequate for predicting roll moments of wrap around fin configurations.
- A side force was present when the model was at angle of attack..
- The side force is at least partially produced by the asymmetric fin attachment geometry associated with WAF's.

- Roll moment generation is due partially to fin attachment geometry and partially fin curvature.
- Curved fins inherently produce lift. The direction of which reverses through Mach 1.
- The converging/diverging nozzle analogy helps explain the direction of lift and why it reverses through Mach 1.

CONCLUSIONS

The underlying goal of this research was to investigate possible alternative configurations to wrap around fins as well as better understand the flow physics to alleviate aerodynamic anomalies. To that end significant progress was made.

One viable alternative to wrap around fins is the use of FLEX fins which deploy straight fins to some offset angle less than perpendicular. For moderate offsets (45° - 60°), there is little adverse effects due to the asymmetry and performance does not significantly suffer.

Another potential improvement to wrap around fins is the use of slots. It was shown that fin slots reduce the out-of-plane moment and decrease the roll rate dependence with Mach number. More research needs to be performed however to optimize the slot size and geometry for a configuration of interest.

The use of base cavities also has some promise for the reduction of circular motion of WAF configurations. Although not completely understood at this point, there is sufficient evidence indicating that a base cavity can affect WAF aerodynamics for a spinning missile in a positive manner.

Finally, the use of CFD proved to be very useful in studying WAF aerodynamics. With this tool and sufficient post processors, one is able to study the flow in the fin region in detail. The interactions of the fin with other fins as well as the body in subsonic, transonic, and supersonic conditions can be investigated. With sufficient analysis and experimental data, root causes can be determined for such things as side moment and roll vs. Mach number dependence. Design changes can then be easily offered to allow missile designers the packaging advantages of WAF's without the associated aerodynamic problems.

REFERENCES

1. Dahlke, C. W., and Deep, R. A., "Techniques for Roll Tailoring for Missiles with Wrap Around," AIAA Paper 83-0463, January 1983.
2. Dahlke, C. W., "Experimental Investigation of Several Wraparound Fins on Bodies of Revolution from Mach 0.3 to 1.3," Data Report, US Army Missile Command, Redstone Arsenal, AL, September 1971, Report No. RD-TM-71-12.
3. Dahlke, C. W., "The Aerodynamic Characteristics of Wrap-Around Fins at Mach Numbers of 0.3 to 3.0," Technical Report, US Army Missile Command, Redstone Arsenal, AL, October 1976, Report No. RD-77-4.
4. Humphrey, J. A., and Dahlke, C. W., "A Summary of Aerodynamic Characteristics for Wrap Around Fins from Mach 0.3 to 3.0," Technical Report, US Army Missile Command, Redstone Arsenal, AL, March 1977, Report No. RD-77-5.
5. Daniels, P., "The Effect of Fin Slots and Fin Tabs on the Dynamic Stability Characteristics of the Navy Low Drag Bomb," Technical Report, US Naval Weapons Laboratory, Dahlgren, VA, May, 1970, Report No. TR-2403.
6. Clare, T. A., and Daniels, P., "Effect of Fin Slots on the Static and Dynamic Stability Characteristics of the Finned Bodies," Technical Report, US Naval Weapons Laboratory, Dahlgren, VA, June, 1971, Report No. TR-2582.
7. Daniels, P., "Minimization of Lock-In Roll Moment on Missiles via Slots," NSWC TR-3250, January 1975.
8. Daniels, P. and Hardy, S. R., "Roll-Rate Stabilization of a Missile Configuration with Wrap Around Fins in Incompressible Flow," Technical Report, Naval Surface Weapons Center, Dahlgren, VA, December, 1975, Report No. TR-3346.
9. Winchenbach, G. L., Buff, R. S., Whyte, R. H., Hathaway, W. H., "Subsonic and Transonic Aerodynamics of a Wraparound Fin Configuration," AIAA Paper 85-0106, January 1985.
10. Kim, Y. H., Winchenbach, G. L., "Roll Motion of a Wraparound Fin Configuration at Subsonic and Transonic Mach Numbers," AIAA Paper 85-1777, August 1985.
11. Kittyle, R. L., Packard, J. D., Winchenbach, G. L., "Description and Capabilities of the Aeroballistic

Research Facility," Air Force Armament Laboratory Technical Report, AFATL-87-08, May, 1987.

12. Fischer, M. A., Hathaway, W. H., "Aeroballistic Research Facility Data Analysis System (ARFDAS)," AFATL-TR-88-48, September 1988.

13. Koenig, Walter, "A Preliminary Flexible Fin Deployment Simulation," ARAED TR 88-70, August 1988.

14. Abate, G. L., and Hathaway, W. H., "Aerodynamics of Missiles with Offset Fin Configuration," AIAA Paper 89-3367, August 1989.

15. Abate, G. L., and Winchenbach, G. L., "Aerodynamics of Missiles with Slotted Fin Configurations," AIAA Paper 91-0676, January 1991.

16. Sjöquist, A., "Wrap Around Fins - Neat and not so Nasty," Paper presented at the 13th International Symposium on Ballistics, Stockholm, Sweden, June, 1992.

17. Abate, G. L., and Hathaway, W. H., "Aerodynamic Test and Analysis of Wrap Around Fins with Base Cavities," AIAA Paper 94-0051, January 1994.

18. Swenson, M. W., and Abate, G. L., "Aerodynamic Test and Analysis of Wrap Around Fins at Supersonic Mach Numbers Utilizing Design of Experiments," AIAA Paper 94-0200, January 1994.

19. Moore, F. G., "Aerodynamics of Guided and Unguided Weapons, Part 1 - Theory and Application," NWL TP-3018, December 1973.

20. Vitale, R. E., Abate, G. L., Winchenbach, G. L., Riner, W., "Aerodynamic Test and Analysis of a Missile Configuration with Curved Fins," AIAA Paper 92-4495, August 1992.

21. Abate, G. L., and Cook, T., "Analysis of Missile Configurations with Wrap Around Fins Using Computational Fluid Dynamics," AIAA Paper 93-3631, August 1993.

22. Lijewski, L., Cippola, J., et al, "Program Eagle User's Manual, Vols. I-IV," Air Force Armament Laboratory Technical Report, AFATL-88-117, September 1988.

23. Belk, D. M., Maple, R. C., "Visualization of Vortical Flows with Yet Another Post Processor," AIAA Paper 93-0222, January 1993.

24. West, K. O., and Whyte, R. H., "Free-Flight and Wind Tunnel Test of a Missile Configuration at Subsonic and

Transonic Mach Numbers with Angle of Attack up to 30 Degrees," Paper 39, 11th Navy symposium on Aeroballistics, Tevose, PA, August 1978.

25. Murphy, C. H., "Free Flight Motion of Symmetric Missiles," US Army Ballistic Research Laboratory, Aberdeen MD, BRL Report 1216, July 1963.

26. Nicolaides, J. D., "Free Flight Dynamics," University of Notre Dame, South Bend IN, 1968.

Linear Stability Analysis of Unguided Missiles with Wrap-Around Tail Fins in Free Flight

Ö. Tanrikulu, C. Önen, G. Mahmutyazıcıoğlu & İ. Bektaş

Scientific and Technical Research Council of Turkey

Defense Industries Research and Development Institute

TÜBİTAK-SAGE

P. K. 16, Mamak

Ankara 06261

TURKEY

1. SUMMARY

A large number of tube launched unguided missiles of NATO such as 70 mm Mk 66, 122 mm FIROS, 127 mm Mk 71, 160 mm RAYO and 227 mm MLRS have wrap-around tail fins (WAF). These missiles have more complicated flight mechanics when compared to the ones with flat and straight tail fins. This is due to the fact that WAF lack mirror symmetry. Detailed free flight mechanics analysis of such missiles were performed with particular emphasis given to the effect of out-of-plane static moment stability derivative $C_{m\dot{\phi}}$ on dynamic stability. In this study, combined effects of $C_{m\dot{\phi}}$ and Magnus moment stability derivative $C_{m\dot{\phi}p}$ on dynamic stability are explored. Aerodynamics and flight mechanics of a simple configuration with WAF are examined as a case study.

2. INTRODUCTION

Most of the current unguided missiles have tube launchers due to packaging, storage and transportation conveniences. In case of aerodynamically stabilized unguided missiles, tail fins are hinged and have spring driven lock mechanisms. Tail fins are in their folded position when the missile is inside the launcher and they are instantly deployed just after launch by the action of aerodynamic forces and lock mechanisms. The most important disadvantage of tube launching is that tail fins are required to fit into a small volume. This puts restrictions on dimensions of them which can indirectly cause problems in external configuration design for satisfactory range, dispersion and stability performance. Tail fins that wrap-around missile

body in their folded position have been used for some time to overcome the limited space problem. On the other hand, flight mechanics of missiles with WAF are much more complicated compared to the ones with flat and straight tail fins. WAF aerodynamics and flight mechanics have been the subject of many studies during the past decades. Important results of this research are summarized in the third section of this paper. The fourth section focuses on different aspects of WAF aerodynamics that are relevant to this study such as lack of mirror symmetry (Maple-Synge analysis), roll direction dependent aerodynamics and Magnus phenomena. Theoretical aspects of linear dynamic stability analysis are presented in section five, where combined out-of-plane and Magnus moment effects will be emphasized. Practical implications of this theory will be discussed in section six based on a case study of a simple WAF configuration.

3. WAF RESEARCH

Start of intense research on WAF flight mechanics can be dated back to 1969 when The Technical Cooperation Program (TTCP) was set up between US Armed Forces, United Kingdom, Canada and Australia during a meeting at Eglin Air Force Base. The purpose of TTCP was experimental investigation of WAF aerodynamics. One of the significant outcomes of TTCP is a report that was published by Dahlke and Craft of US Army Missile Research Development and Engineering Laboratory in 1973, [1]. Dahlke and Craft carried out systematic wind tunnel tests of twenty four configurations

with four WAF that were obtained by combining three body and sixteen fin shapes. The aim was to obtain insight about effects of certain geometric parameters (after body shape; chord length, leading and trailing edge shapes, leading and trailing edge sweep angles, dihedral angle and thickness of tail fins; fin-body gap) on aerodynamics of WAF in a Mach number range of 0.3 to 3.0 and an angle of attack range of -6° to $+6^\circ$, Figure 1. Dahlke and Craft determined that static stability characteristics $C_{Z\alpha}$, $C_{m\alpha}$ and x_{CP} (static force and moment stability derivatives and location of center of pressure from missile nose) of an unguided missile with WAF and with flat fins with the same projected area are similar. In all configurations that were tested WAF had 10% higher drag coefficient C_D when compared to the corresponding cases with equivalent flat tail fins simply due to the increased frontal area.

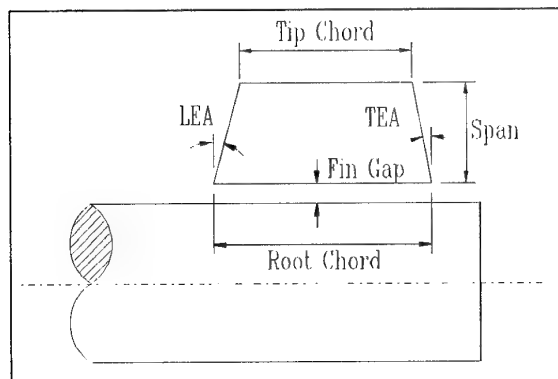


Figure 1. Wrap-around fin geometrical parameters.

Dahlke and Craft pointed to the fact that unguided missiles with WAF have a non zero induced roll moment C_{l_0} even at zero total angle of attack. They did not provide any explanation for the mechanism that generates C_{l_0} , but focused on the relationship between tail fin geometry and this moment. In all cases C_{l_0} was a highly oscillatory function of Mach number and angle of attack, and changed sign around transonic region. At subsonic speeds the fin force related with C_{l_0} acted towards fin center of curvature while at supersonic speeds it acted in the reverse direction. Dahlke and Craft, observed that leading edge sweep angle, aspect ratio and thickness of tail fins significantly altered C_{l_0} . They showed that C_{l_0} had considerable effect on roll rate history of unguided missiles which was given as a possible explanation to unexpected instabilities that were often observed in practice.

Dahlke and Craft also investigated out-of-plane static moment stability derivative $C_{m\beta}$ that unguided missiles with WAF can theoretically generate due to lack of mirror symmetry. They found out that $C_{m\beta}$ of negligible magnitude existed regardless of details of WAF geometry. Humphrey and Dahlke published another report in 1977, [2], where they presented an extensive compilation of aerodynamic data of the models used by Dahlke and Craft.

An important report on flight mechanics of unguided missiles with WAF was published by Stevens of Naval Weapons Laboratory of US NAVY in 1973, [3]. Stevens carried out Maple-Synge analysis and showed that it is mathematically possible to obtain stability derivatives such as $C_{m\beta}$, $C_{m\dot{\beta}}$, $C_{m\ddot{\beta}}$ and $C_{m\alpha\beta}$ in case of WAF. These derivatives are out-of-plane static and damping moment and in-plane Magnus moment stability derivatives respectively. Stevens also noted that WAF have different roll damping stability derivatives $C_{l_{p-}}$, $C_{l_{p+}}$ depending on direction of roll. He then proceeded to investigate linear free flight mechanics of unguided missiles with WAF using a procedure which is similar to the one presented in reference [4]. Stevens derived static and dynamic stability criteria for a general WAF model which turned out to be much more complicated than those of straight finned missiles. He simplified his analysis by considering $C_{m\beta}$ as the only significant WAF out-of-plane effect. The reduced criteria showed that static stability is not affected by WAF, while dynamic stability and resonance magnification factor changed drastically with $C_{m\beta}$. He stated that an unguided missile with WAF becomes dynamically unstable if magnitude of $C_{m\beta}$ takes a value which is higher than about 10% of that of $C_{m\alpha}$ when in-plane Magnus moment stability derivative $C_{m\beta\dot{\beta}}$ is neglected. Stevens also found out that unguided missiles with WAF exhibited circular trajectories in α versus β plane in case of both stable and unstable flight. Same type of motion pattern is also observed for unguided missiles with flat-fins in case of yaw-pitch-roll lock-in, catastrophic yaw-pitch-roll or significant nonlinear out-of-plane damping moments, [5].

A direct continuation of the work discussed in above paragraph was published by Stevens, On and Clare of Naval Weapons Laboratory of US Navy in 1974, [6]. The major aim of this

report was comparison of flight performance of a 127 mm unguided missile with wrap-around and flat tail fins. The authors pointed out to the fact that unguided missiles are required to have high roll rotational speed especially during powered flight to reduce dispersion due to inertial, aerodynamic and thrust asymmetries. They stated helical launcher rails and fluted nozzles as two major alternatives for obtaining roll during powered flight and canted tail fins as the most commonly used solution to keep roll rate above resonance roll rotational speed during free flight. Stevens, On and Clare presented WAF that induce a static roll moment even at zero total angle of attack as an alternative to flat canted fins which are difficult to manufacture accurately. At the end of their analysis, they concluded that aerodynamic side effects due to WAF do not have any significant effect on static and linear dynamic stability while they considerably improved dispersion performance and reduced the risk of nonlinear yaw-pitch-roll coupling.

Daniels and Hardy of Naval Surface Weapons Center of US Navy published a paper on roll behavior of unguided missiles at high angles of attack in 1975, [7]. They noted that WAF induce larger roll rotational speeds at high angles of attack compared to flat fins which can be dangerous in terms of Magnus instability. They conducted wind tunnel tests of a sting mounted freely rolling model for angles of attack between 0° and 90° and measured steady-state roll rate both for WAF and flat fins. They suggested that WAF can be modified by using slots, fences and tabs so that they have the same roll moment characteristics as the corresponding flat fins. Hardy continued his work on this subject later with a report published in 1977, [8]. He again used wind tunnel testing and focused on modeling of nonlinear roll behavior using a second order differential equation. Hardy used a least-squares curve fitting procedure to identify linear and nonlinear aerodynamic roll coefficients: roll moment due to cant C_{l_s} , linear roll damping C_{l_p} , cubic roll damping $C_{l_{p^3}}$ and induced roll moment $C_{l_{4\gamma}}$. He found out that these data are sufficient to describe nonlinear roll behavior at high angles of attack.

Catani, *et al.* investigated aerodynamics of 122 mm FIROS unguided artillery missile which has four WAF, [9]. They used

wind tunnel, water table and flight tests and examined effects of after body, nose and tail fin geometries on flight mechanics. They especially concentrated on the relationship between geometry of fin housing cavity and drag coefficient C_D . Catani *et al.* determined that cavity induced drag amounts to a significant proportion of total drag. They noted that C_D in case of open cavity flow is much larger than that induced by closed cavity flow. They modified the original cavity shape of 122 mm FIROS and as a result maximum range increased from ~ 20 km to ~ 25 km which is an important result.

As was discussed in above paragraphs, flight mechanists were aware of existence of C_{l_0} in case of WAF from the very beginning of the research in this field. However, for a long time period they could not provide any meaningful explanation for the mechanism that induces C_{l_0} . The first attempt on this subject matter was made by Bar-Haim and Seginer of Israel Institute of Technology-Technion who published an important paper in 1983, [10]. They focused their attention to subsonic flow speeds and zero total angle of attack. They proposed that C_{l_0} is generated by radial velocity components induced by wake of the missile on asymmetric WAF. They tried to prove their hypothesis qualitatively by using potential techniques. They modeled the missile body as a source distribution along its axis which is justified at zero total angle of attack and negligible fin-body interference. They modeled the missile wake as a solid integral part of the body. Three types of wakes were considered: jet-off wake, jet-on wake and the wake in case of a sting-mounted wind tunnel missile model. They determined the flow over WAF by using a linear vortex lattice method that is restricted to zero total angle of attack as well. Bar-Haim and Seginer used one of the missile geometries that were extensively tested by Dahlke *et al.* as their test case. They obtained good correlation between numerical and experimental data. They found out that moving WAF upstream and/or increasing trailing edge angle reduces C_{l_0} since interaction between wake and WAF is reduced. They also investigated relationship between C_{l_0} and, span and dihedral angle of WAF parametrically. Bar Haim and Seginer determined that $C_{l_0, \text{jet-on}} > C_{l_0, \text{jet-off}} > C_{l_0, \text{sting}}$ and that $C_{l_0, \text{jet-on}}$ and $C_{l_0, \text{jet-off}}$ have opposite signs at subsonic flows. They did not provide any explanation for the mechanism of C_{l_0} generation at

supersonic flow speeds but suggested that '*... the shock wave focusing on the concave side of the curved fin with the resultant pressure difference acting in the direction of the convex surface...*' may be a possible answer.

Winchenbach and his colleagues investigated flight mechanics characteristics of an unguided missile with WAF by using aeroballistic range testing and published several papers, [11]-[13]. They noted that many unguided missiles with WAF had significant stability problems which were related to the lack of mirror symmetry. These instabilities were often detected only after the start of dynamic testing stage and caused delays in project schedules. Winchenbach *et al.* had difficulties in aerodynamic data identification of a configuration with WAF since they did not include any moments related with WAF such as $C_{m\beta}$, C_{l_0} , C_{p-} and C_{p+} into their aerodynamic model. Inclusion of these coefficients improved the quality of their curve-fits significantly. They also determined that $C_{m\beta}$ had a profound influence on dynamic stability especially at supersonic speeds. They concluded that '*... this side moment is symptomatic of WAF configurations and should be of particular concern to the designer...*'.

A recent contribution to WAF research was made by Vitale, *et al.* who investigated aerodynamics of two unguided missile configurations with WAF by using empirical and computational aerodynamics methods (three dimensional Euler), and aeroballistic range testing, [14]. Their work is interesting in two respects: Firstly, it shows that research on WAF flight mechanics is far from being complete. Secondly, one of the missile configurations examined can be associated with extended range MLRS. Vitale *et al.* focused their attention to the nature of $C_{m\alpha}$, $C_{m\beta}$, C_D and C_{l_0} at high supersonic Mach numbers 2.75 to 5.15. They found out that in this Mach number region there is a complex shock structure between WAF which have direct consequences especially in terms of $C_{m\alpha}$ and C_{l_0} . They determined that interaction between WAF due to shocks becomes less significant as Mach number increases.

Another recent study on WAF aerodynamics was made by Edge of US Army Research Laboratory who used experimental and

computational methods (three dimensional Navier-Stokes) to examine the flow field around the standard TTCP configuration at zero total angle of attack and a Mach number range of 1.3 to 3.0, [15]. He also found out that complex shock patterns exist over WAF at supersonic Mach numbers. His results indicate that shock interaction between WAF is responsible for generation of C_{l_0} at this flow regime.

4. WAF AERODYNAMICS

Compared to other flight vehicles such as aircraft, helicopters and guided missiles, it is easier to determine aerodynamic characteristics of unguided missiles since they have a higher level of geometrical symmetry, namely rotational symmetry and mirror symmetry. If a missile is rotated along its longitudinal axis by an angle ϕ after which configuration of the missile is the same as the original configuration, then the missile is said to have undergone a covering operation. If a succession of such rotations with $\phi = 2\pi/n$, ($n = 1, 2, 3, \dots$), results in n covering operations, then the missile is said to have n -gonal rotational symmetry. If there exists a plane parallel to longitudinal axis of the missile such that the missile part on one side is the mirror image of the part on the other side, then that plane is called a plane of mirror symmetry. In Figure 2 cross sectional views of two different unguided missile configurations each with four tail fins are shown. Configuration A has 4-gonal rotational symmetry and four planes of mirror symmetry which are shown with dashed lines. This type of geometry is known as cruciform geometry. Configuration B with four WAF also has 4-gonal rotational symmetry, but it lacks mirror symmetry.

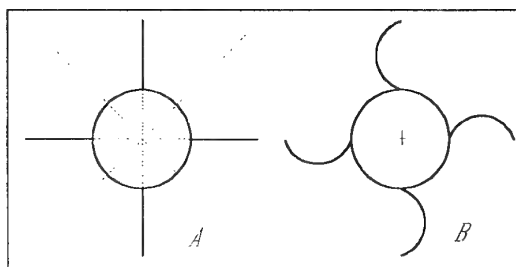


Figure 2. Missiles with and without mirror symmetry.

Maple-Synde analysis is an important mathematical tool which utilizes symmetry properties to explore functional form of aerodynamic forces and moments, [16]. Basics of the analysis will be outlined briefly in the following paragraphs:

Consider an unguided missile in free flight over non rotating flat earth. Rotational attitude of the missile is specified by yaw-pitch-roll Euler rotating frame based (321) sequence which is defined as follows:

$$F_v \xrightarrow{\psi} F_m \xrightarrow{\theta} F_n \xrightarrow{\phi} F_b$$

ψ , θ and ϕ are yaw, pitch and roll angles respectively. F_v denotes the vehicle fixed vertical reference frame. The third unit vector of F_v is expressed as $\bar{u}_3^{(v)}$ and it points downwards parallel to the vector of gravitational acceleration \bar{g} . $\bar{u}_1^{(v)}$ points to north and $\bar{u}_2^{(v)}$ points to east. F_b denotes the body fixed reference frame, unit vectors of which coincide with the axes of principle moments of inertia of the missile, Figure 3. Another important reference frame in the sequence is the aeroballistic reference frame F_n which yaws and pitches but does not roll with the missile. Equations of motion are expressed in F_n for mathematical convenience. Air trajectory reference frame F_w does not appear in the above sequence but will be utilized in this study to define the aerodynamic drag, lift and side forces. $\bar{u}_1^{(w)}$ is directed along velocity vector \bar{v}_C of center of mass C of the missile. Centers of all four reference frames are attached to C .

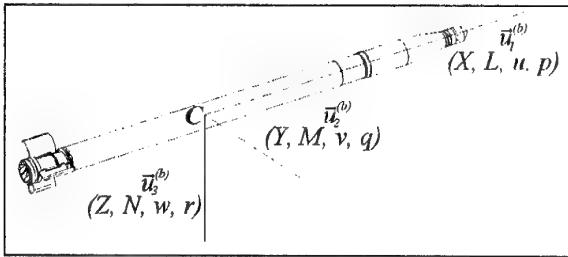


Figure 3. Body fixed reference frame F_b .

Components in F_b of \bar{v}_C , relative rotational velocity $\bar{\omega}_{(b/v)}$ of F_b with respect to F_v , external aerodynamic moment \bar{M}_A and components in F_b and F_w of external aerodynamic force \bar{F}_A are denoted with standard symbols in flight mechanics:

$$\bar{v}_C^{(b)} = \begin{Bmatrix} u \\ v \\ w \end{Bmatrix} \quad \bar{\omega}_{(b/v)}^{(b)} = \begin{Bmatrix} p \\ q \\ r \end{Bmatrix}$$

$$\bar{M}_A^{(b)} = \begin{Bmatrix} L \\ M \\ N \end{Bmatrix} \quad \bar{F}_A^{(b)} = \begin{Bmatrix} X \\ Y \\ Z \end{Bmatrix} \quad \bar{F}_A^{(w)} = -\begin{Bmatrix} D \\ C \\ L \end{Bmatrix}$$

Relative rotational position of F_w with respect to F_b is defined by angles of attack and sideslip, α and β respectively:

$$\alpha = \tan^{-1}\left(\frac{w}{u}\right) \quad \beta = \sin^{-1}\left(\frac{v}{V}\right)$$

where V is speed of C , $V = \sqrt{u^2 + v^2 + w^2}$.

In flight mechanics analysis non dimensional generalized force, moment and velocity components are used based on the reference length $\lambda = D$, reference area $S = (\pi/4)D^2$ and free stream dynamic pressure $q_\infty = (1/2)\rho_\infty V^2$, (D and ρ_∞ are missile diameter and free stream density respectively):

$$C_F = \frac{F}{q_\infty S} \quad C_m = \frac{M}{q_\infty S \lambda}$$

$$\gamma = \frac{u}{V} \quad \beta \approx \frac{v}{V} \quad \alpha \approx \frac{w}{V}$$

$$\frac{p\lambda}{2V} \quad \frac{q\lambda}{2V} \quad \frac{r\lambda}{2V} \quad \frac{\dot{\beta}\lambda}{2V} \quad \frac{\dot{\alpha}\lambda}{2V}$$

Maple-Synge analysis is performed by using complex combinations of non dimensional transverse aerodynamic forces, moments and translational and rotational velocity components:

$$C_F = C_Y + iC_Z, \quad (4.1)$$

$$C_t = C_m + iC_n, \quad (4.2)$$

$$\xi = \beta + i\alpha, \quad (4.3)$$

$$\mu = \left(\frac{q\lambda}{2V}\right) + i\left(\frac{r\lambda}{2V}\right) \quad (4.4)$$

Non dimensional aerodynamic force and moment components are assumed to have the following functional forms:

$$C_{(F,t,x,l)} = \sum_{ijkl} (f, t, x, l)_{ijkl} \left[\gamma, \left(\frac{p\lambda}{2V} \right) \right] \xi^i \bar{\xi}^j \mu^k \bar{\mu}^l, \quad (4.5)$$

In above equation f_{ijkl} , t_{ijkl} , x_{ijkl} and l_{ijkl} are complex functions and the bar (-) denotes complex conjugate of the related quantity. Figure 4 shows a covering operation for a 4-gonal missile. Original and final configurations of the missile are represented by F_n and F_b respectively. Functional form of aerodynamic forces and moments can not change during such a rotational transformation. Using this information one can determine the admissible terms in series expansions (4.5) for general n -gonal rotational symmetry. Some of these terms are known to be small or zero due to aerodynamical reasons. In case of an unguided missile with three or more WAF ($n \geq 3$), widely used linear transverse aerodynamic force and moment expansions based on Maple-Syngé rotational symmetry analysis are as follows:

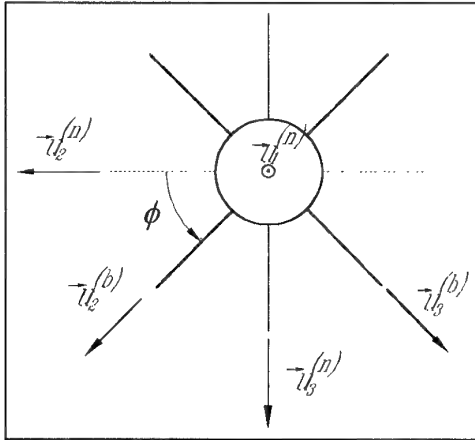


Figure 4. F_n and F_b frames in covering operation.

$$C_Y = C_{Y\beta}\beta + C_{Y\alpha}\alpha + C_{Yq}\left(\frac{q\lambda}{2V}\right) + C_{Yr}\left(\frac{r\lambda}{2V}\right) + C_{Yap}\alpha\left(\frac{p\lambda}{2V}\right) + C_{Y\beta p}\beta\left(\frac{p\lambda}{2V}\right), \quad (4.6)$$

$$C_Z = C_{Z\alpha}\alpha + C_{Z\beta}\beta + C_{Zq}\left(\frac{q\lambda}{2V}\right) + C_{Zr}\left(\frac{r\lambda}{2V}\right) + C_{Z\beta p}\beta\left(\frac{p\lambda}{2V}\right) + C_{Zap}\alpha\left(\frac{p\lambda}{2V}\right), \quad (4.7)$$

$$C_m = C_{m\alpha}\alpha + C_{m\beta}\beta + C_{mq}\left(\frac{q\lambda}{2V}\right) + C_{mr}\left(\frac{r\lambda}{2V}\right) + C_{m\beta p}\beta\left(\frac{p\lambda}{2V}\right) + C_{map}\alpha\left(\frac{p\lambda}{2V}\right), \quad (4.8)$$

$$C_n = C_{n\beta}\beta + C_{n\alpha}\alpha + C_{nq}\left(\frac{q\lambda}{2V}\right) + C_{nr}\left(\frac{r\lambda}{2V}\right) + C_{nap}\alpha\left(\frac{p\lambda}{2V}\right) + C_{n\beta p}\beta\left(\frac{p\lambda}{2V}\right). \quad (4.9)$$

Maple-Syngé rotational symmetry analysis also shows that the stability derivatives in above equations are related to each other as follows:

$$C_{Y\beta} = C_{Z\alpha} \quad C_{Y\alpha} = -C_{Z\beta} \quad C_{Yq} = C_{Zr} \quad C_{Yr} = -C_{Zq}$$

$$C_{m\beta} = C_{n\alpha} \quad C_{m\alpha} = -C_{n\beta} \quad C_{mq} = C_{nr} \quad C_{mr} = -C_{nq}$$

$$C_{Y\beta} = C_{Z\alpha} \quad C_{Y\alpha} = -C_{Z\beta} \quad C_{Yq} = C_{Zr} \quad C_{Yr} = -C_{Zq}$$

$$C_{Yap} = -C_{Z\beta p} \quad C_{Y\beta p} = C_{Zap} \quad C_{map} = -C_{n\beta p} \quad C_{m\beta p} = C_{nap}$$

If the unguided missile in question with n -gonal rotational symmetry also has n planes of mirror symmetry, then transverse linear aerodynamic force and moment expansions can be shown to be much simpler by using a Maple-Syngé analysis similar to the one presented above:

$$C_Y = C_{Y\beta}\beta + C_{Yr}\left(\frac{r\lambda}{2V}\right) + C_{Yap}\alpha\left(\frac{p\lambda}{2V}\right), \quad (4.10)$$

$$C_Z = C_{Z\alpha}\alpha + C_{Zq}\left(\frac{q\lambda}{2V}\right) + C_{Z\beta p}\beta\left(\frac{p\lambda}{2V}\right), \quad (4.11)$$

$$C_m = C_{m\alpha}\alpha + C_{mq}\left(\frac{q\lambda}{2V}\right) + C_{m\beta p}\beta\left(\frac{p\lambda}{2V}\right), \quad (4.12)$$

$$C_n = C_{n\beta}\beta + C_{nr}\left(\frac{r\lambda}{2V}\right) + C_{nap}\alpha\left(\frac{p\lambda}{2V}\right). \quad (4.13)$$

A comparison of equations (4.6)-(4.9) and (4.10)-(4.13) shows the amount of complication introduced into transverse aerodynamics by WAF.

A widely used linear expansion for the roll moment of a configuration with WAF is as follows:

$$C_l = C_{l_0} + C_{l_{p\pm}} \left(\frac{p\lambda}{2V} \right) + C_{l_\delta} \delta. \quad (4.14)$$

As this equation indicates roll aerodynamics of configurations with WAF is also more complicated. Firstly, WAF induce a roll moment C_{l_0} which is non zero even at zero total angle of attack. Results of research on this moment was summarized in the literature survey section. Secondly, WAF configurations have different roll damping stability derivatives depending on roll rotation direction: $C_{l_{p-}}$ and $C_{l_{p+}}$. One can easily understand this phenomenon by using physical reasoning, Figure 5. Roll rotation dependence may well be extended to other stability derivatives such as $C_{m_{\beta p\pm}}$ and $C_{m_{\alpha p\pm}}$.

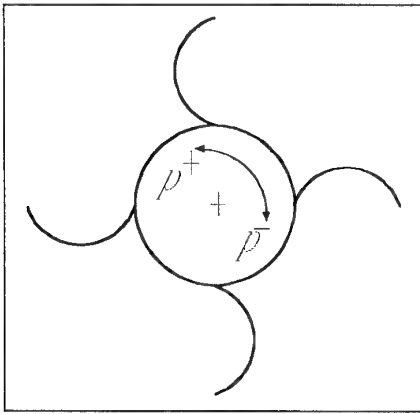


Figure 5. Roll direction dependent aerodynamics.

Magnus phenomena have profound influence on dynamic stability of rolling missiles. Magnus force due to $C_{Z_{\dot{p}}}$ is usually about 5-10% of the static force due to C_{Z_α} , but the associated out-of-plane moment due to $C_{m_{\dot{p}}}$ is still very important in terms of dynamic stability. On the other hand, it is difficult to determine $C_{m_{\dot{p}}}$ accurately which has led flight mechanists to consider $C_{m_{\dot{p}}}$ as the only significant out-of-plane effect in their stability analysis of configurations with WAF. Engineers usually come across with Magnus phenomena during

their undergraduate fluid mechanics courses while they study lifting and non lifting potential flows around cylinders in uniform flow, [17]. A similar potential Magnus force also acts on rolling missiles at non zero total angle of attack and this can be predicted for simple configurations and incompressible flow by using the Method of Bryson, [16]. Unfortunately, there are some viscous Magnus mechanisms as well which are difficult to determine by using analytical, computational and even experimental methods since they are very sensitive to ξ , p , geometry, free stream Mach and Reynolds numbers M_∞ and Re_∞ respectively, [18]-[30]:

- Asymmetric boundary layer over body.
- Asymmetric vortex shedding over body.
- Fin-body interference.
- Fin-cant.
- Base pressure difference of fins.
- Interaction of asymmetric vortex wake of body and fins.

In references [18]-[30], attention was focused on missile configurations with mirror symmetry. A recent study which investigated Magnus characteristics of a missile configuration with WAF was performed by Corby and Berry, [31]. They developed a special test rig that allowed accurate measurement of forces and moments acting on rolling missile configurations. They investigated a guided missile which becomes fin stabilized by deployment of four WAF after a brief spin stabilized launch stage. Corby and Berry did not present any new results related to effects of lack of mirror symmetry on Magnus characteristics.

5. WAF DYNAMIC STABILITY

Vectorial equations of motion of an unguided missile in free flight can be expressed as follows, [32]:

$$D_v \bar{H}_C = \bar{M}_A, \quad (5.1)$$

$$m D_v \bar{v}_C = \bar{F}_A + m \bar{g}. \quad (5.2)$$

\bar{H}_C is the vector of absolute angular momentum about C ; m is mass of the missile and D_v denotes differentiation with respect to time in F_v . Three translational and three rotational scalar equations of motion can be obtained from (5.1) and (5.2).

Rotational equations of motion are going to be expressed in F_n :

$$I_a \ddot{\tilde{p}} = \tilde{L}, \quad (5.3)$$

$$I_t \ddot{\tilde{q}} + I_a \tilde{p} \tilde{r} = \tilde{M}, \quad (5.4)$$

$$I_t \ddot{\tilde{q}} - I_a \tilde{p} \tilde{q} = \tilde{N}. \quad (5.5)$$

I_a and I_t are axial and transverse moments of inertia respectively. (\sim) denotes components of a vector in F_n . Translational equations of motion that are expressed in F_n are as follows:

$$m(\ddot{\tilde{u}} + \tilde{q}\tilde{w} - \tilde{r}\tilde{v}) = \tilde{X} + m\tilde{g}_1, \quad (5.6)$$

$$m(\ddot{\tilde{v}} + \tilde{u}\tilde{r}) = \tilde{Y} + m\tilde{g}_2, \quad (5.7)$$

$$m(\ddot{\tilde{w}} - \tilde{u}\tilde{q}) = \tilde{Z} + m\tilde{g}_3. \quad (5.8)$$

In the equations presented above components of gravitational acceleration in F_n are,

$$\tilde{g}^{(n)} = \begin{Bmatrix} -g \sin \theta \\ 0 \\ g \cos \theta \end{Bmatrix}. \quad (5.9)$$

Mathematical simplicity is obtained by expressing the first translational equation of motion in F_v rather than in F_n :

$$m\dot{\tilde{V}} \approx -D. \quad (5.10)$$

The six scalar equations of motion (5.3)-(5.5), (5.10), (5.7) and (5.8) represent dynamics of a time varying and nonlinear system. Several simplifications are introduced into the analysis to determine stability criteria that can be used in engineering design:

- Total angle of attack ξ is assumed to be small which allows aerodynamic decoupling of axial and transverse equations of motion, $\gamma \approx 1$. Linear expansions are used for generalized aerodynamic forces, (4.6)-(4.9) and (4.14).

- Aerodynamic properties are assumed to be constant which is based on the fact that M_∞ is a slowly varying function of time. Roll rotational speed p is assumed to vary slowly with time as well. Independent variable is changed from time t to non dimensional distance variable s :

$$s = \frac{1}{\lambda} \int_{t_0}^t V dt. \quad (5.11)$$

- The four transverse equations of motion, (5.4), (5.5), (5.7) and (5.8), are reduced into a single equation of motion by using complex variables, (4.1)-(4.4).

The resulting complex scalar transverse equation of motion is,

$$\ddot{\tilde{\xi}} + [H + i(I - P)]\dot{\tilde{\xi}} - [(M + PU) + i(N + PT)]\tilde{\xi} = G, \quad (5.12)$$

where $\tilde{\xi}$ is the complex angle of attack in F_n and i is the unit imaginary number. (\cdot) denotes differentiation with respect to s and coefficients of the equation are as follows:

$$H = -\left[C_{z\alpha}^* + 2C_D^* + \frac{1}{2k_t^2} (C_{m\dot{q}}^* + C_{m\dot{\alpha}}^*) \right], \quad (5.13)$$

$$I = -\left[C_{z\beta}^* + \frac{1}{2k_t^2} (C_{m\dot{r}}^* + C_{m\dot{\beta}}^*) \right], \quad (5.14)$$

$$P = \frac{I_a \tilde{p} \lambda}{I_t V}, \quad (5.15)$$

$$M = \frac{1}{k_t^2} C_{m\alpha}^*, \quad (5.16)$$

$$N = \frac{1}{k_t^2} C_{m\beta}^*, \quad (5.17)$$

$$T = \frac{1}{2k_a^2} C_{m\dot{p}}^* - C_{z\alpha}^* - C_D^*, \quad (5.18)$$

$$U = C_{z\beta}^* - \frac{1}{2k_a^2} C_{m\dot{\alpha}}^*, \quad (5.19)$$

$$G \approx \frac{\lambda}{V^2} \tilde{g}_3 P. \quad (5.20)$$

In above equations:

$$k_{a,t} = \sqrt{\frac{I_{a,t}}{m\lambda^2}} \quad C^* = \left(\frac{\rho S \lambda}{2m} \right) C$$

Equation (5.12) is a second order linear differential equation with constant coefficients and its solution can be expressed as,

$$\tilde{\xi} = \tilde{\xi}_g + K_1 e^{i\phi_1} + K_2 e^{i\phi_2}, \quad (5.21)$$

where,

$$\tilde{\xi}_g = -\frac{G}{(M+PU) + i(N+PT)}, \quad (5.22)$$

$$K_j = K_{j0} e^{\lambda_j s}, (j=1,2), \quad (5.23)$$

$$\phi_j = \phi_{j0} + \phi'_j s, (j=1,2), \quad (5.24)$$

$$\lambda_j + i\phi'_j = \frac{1}{2} \left\{ -H + i(P-I) \mp \sqrt{4(M+PU) + H^2 - (I-P)^2 + i[2H(I-P) + 4(N+PT)]} \right\},$$

$$(j=1,2). \quad (5.25)$$

In equation (5.21) $K_j e^{i\phi_j}$ terms represent homogeneous solution while $\tilde{\xi}_g$ is the particular solution due to gravity. Stability of an unguided missile with WAF in free flight can be examined by using equation (5.25). After a few derivations one can obtain the following expression for modal damping factors:

$$\lambda_j = -\frac{1}{2} \left\{ H \mp \frac{2(N+PT) - H(P-I)}{\sqrt{(P-I)^2 - 4(M+PU)}} \right\}, (j=1,2). \quad (5.26)$$

Dynamic stability of the missile is assured if both of the modal damping factors $\lambda_j (j=1,2)$ have negative values during all phases of flight:

$$\lambda_j \leq 0, (j=1,2). \quad (5.27)$$

Inequality (5.27) is equivalent to following inequalities:

$$H \geq 0, \quad (5.28)$$

$$|H| \geq \frac{2(N+PT) - H(P-I)}{\sqrt{(P-I)^2 - 4(M+PU)}}. \quad (5.29)$$

If inequality (5.29) is expanded, one can obtain a quadratic stability condition in terms of the gyroscopic roll P :

$$T(T-H)P^2 + (UH^2 + 2TN - HN + THI)P + (MH^2 + N^2 + NHI) \leq 0, \quad (5.30)$$

$$(P - P_{dyn1})(P - P_{dyn2}) \leq 0. \quad (5.31)$$

Inequalities (5.28) and (5.31) indicate that an unguided missile with WAF in free flight is dynamically stable if it has positive in-plane damping and its roll rotational speed stays in an interval which is specified by P_{dyn1} and P_{dyn2} . Actual roll rotational speeds corresponding to P_{dyn1} and P_{dyn2} can be determined as,

$$P_{dynj} = \frac{I_t}{I_a} \frac{V}{\lambda} P_{dynj}, (j=1,2). \quad (5.32)$$

In case of a missile which has both rotational and mirror symmetry, $I = 0$, $N = 0$ and $U = 0$. Hence, (5.30) becomes:

$$T(T-H)P^2 + MH^2 \leq 0. \quad (5.33)$$

This is a quadratic inequality as well, but $P_{dyn1} = -P_{dyn2}$ in contrast to the more general case. In case of a stability analysis of a missile with WAF in which $C_{m\beta}$ is considered as the only significant out-of-plane effect, inequality (5.30) is reduced to,

$$-HNP + MH^2 + N^2 \leq 0. \quad (5.34)$$

This is a linear inequality in terms of P , which specifies the upper and lower limits of roll rotational speed for dynamic stability for $p > 0$ and $p < 0$ respectively.

6. CASE STUDY

A missile configuration similar to the basic finner was selected as the subject of this case study, Figure 6. The only difference of the present configuration from basic finner is that it has four WAF rather than four straight fins. $C_{Z\alpha}$, $C_{m\alpha}$, $C_{mq} + C_{m\dot{\alpha}}$ and C_D data of basic finner were calculated by using *MISSILE DATCOM*. $C_{Z\alpha}$, $C_{m\alpha}$, $C_{m\beta}$ and C_{mq} data of the test case configuration were calculated by using a three dimensional panel code, *PANEL3D*. $C_{Z\alpha}$ and $C_{m\alpha}$ data obtained from *MISSILE DATCOM* and *PANEL3D* for the two different configurations were seen to be in good match. Transonic and supersonic $C_{m\beta\beta}$ data of basic finner which was determined by aeroballistic range testing was available from literature, [4]. Subsonic $C_{m\beta\beta}$ data of basic finner was estimated by using the Method of Bryson, [16]. $C_{m\beta\beta}$ data of the test case configuration was assumed to be the same as that of basic finner. Reference and inertial data of the test case configuration are presented in Table 1 and Table 2 respectively:

Table 1. Reference data.

$D[m]$	$S[m^2]$	$a_o[m/s]$	$\rho_o[kg/m^3]$
0.02	3.14×10^{-4}	344	1.225

Table 2. Inertial data.

$m[kg]$	$I_a[kgm^2]$	$I_i[kgm^2]$	$x_{CM}[m]$
0.15	8.3×10^{-6}	3.5×10^{-4}	0.122

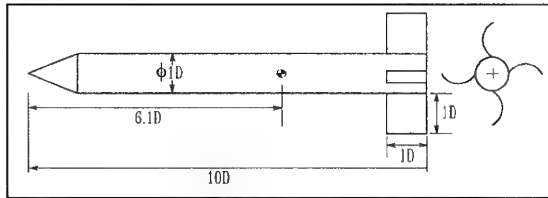


Figure 6. Geometry of the test case missile.

Variation of aerodynamic data with M_∞ are presented in Figure 7-Figure 12.

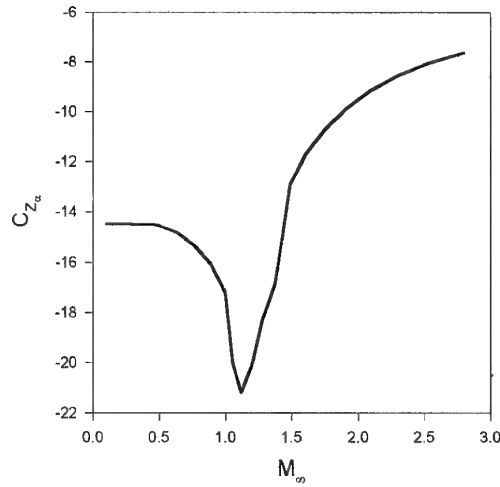


Figure 7. Variation of $C_{Z\alpha}$ with M_∞ .

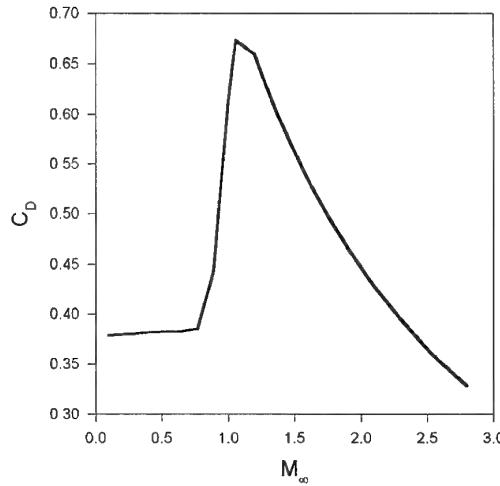


Figure 8. Variation of C_D with M_∞ .

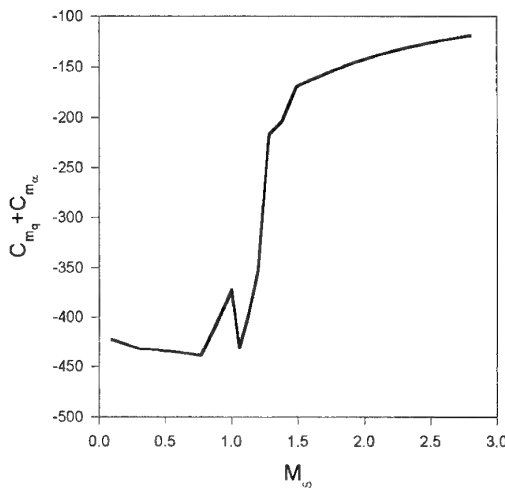


Figure 9. Variation of $C_{mq} + C_{m\dot{\alpha}}$ with M_∞ .

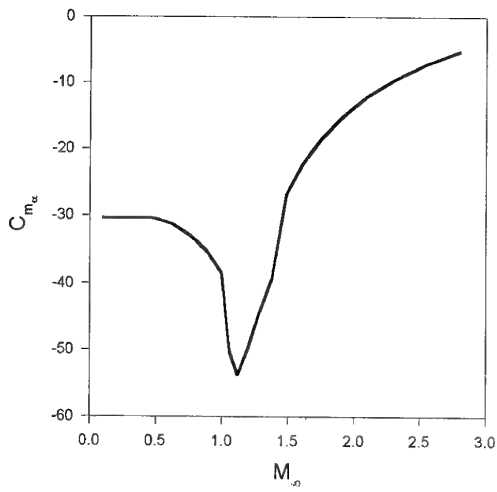


Figure 10. Variation of $C_{m\alpha}$ with M_∞ .

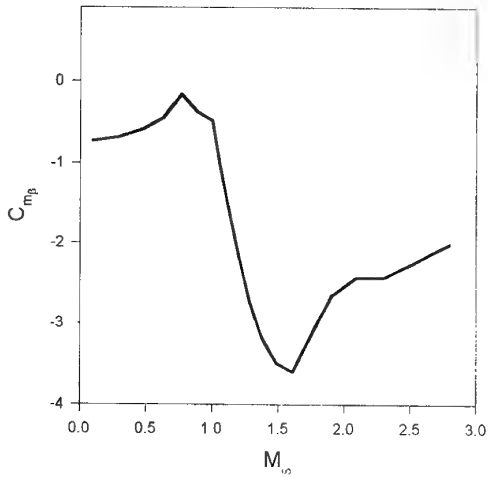


Figure 11. Variation of $C_{m\beta}$ with M_∞ .

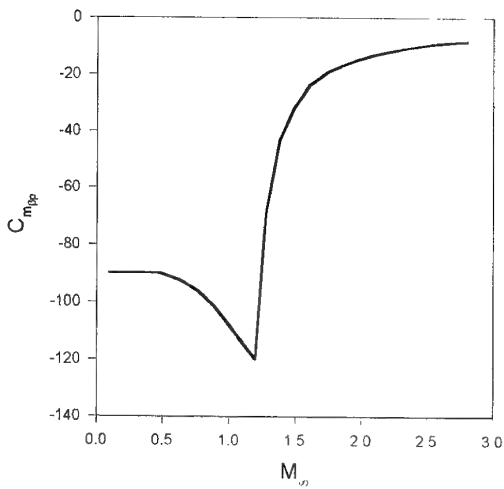


Figure 12. Variation of $C_{m\beta p}$ with M_∞ .

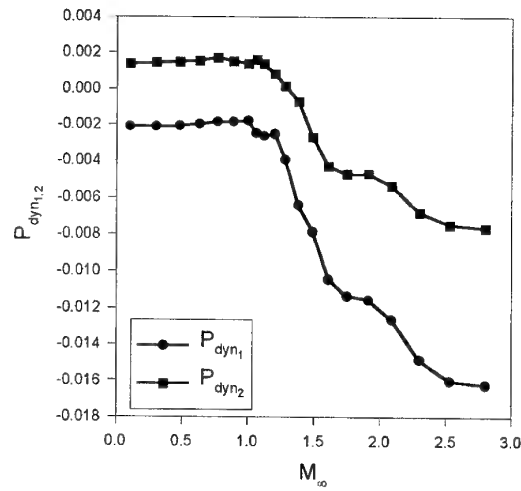


Figure 13. Variation of $P_{dyn1,2}$ with M_∞ , ($C_{m\beta}$, $C_{m\beta p}$ present).

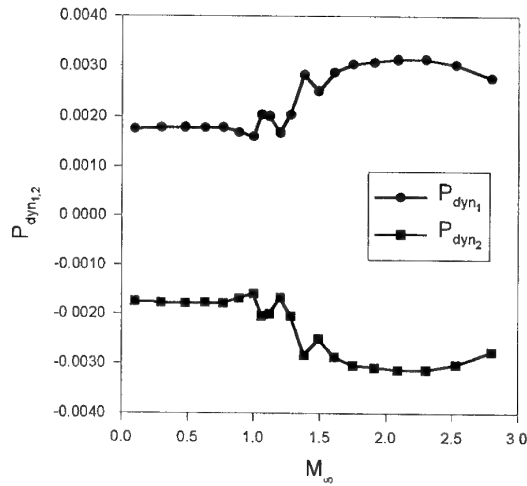


Figure 14. Variation of $P_{dyn1,2}$ with M_∞ , ($C_{m\beta p}$ present).

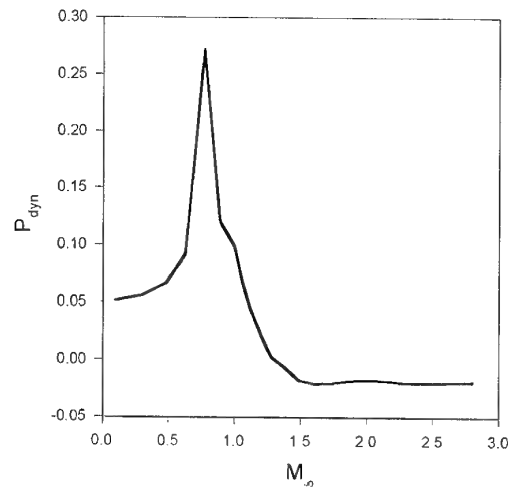


Figure 15. Variation of P_{dyn} with M_∞ , ($C_{m\beta}$ present).

Variation of $P_{dyn1,2}$ with M_∞ in cases of both $C_{m\beta\beta}$ and $C_{m\beta}$ present, only $C_{m\beta\beta}$ present and only $C_{m\beta}$ present are given in Figure 13-Figure 15. In Figure 13 and Figure 14, the configurations that lie between the P_{dyn} curves are stable. In Figure 15, the P_{dyn} curve is the upper boundary of the stability region.

7. DISCUSSION & CONCLUSION

The case study performed in above section is alarming since it shows that one can arrive at completely wrong conclusions about dynamic stability of a missile configuration with WAF if effects of $C_{m\beta}$ and $C_{m\beta\beta}$ are not considered at the same time. A comparison of Figure 13 and Figure 14 shows that effect of $C_{m\beta}$ on dynamic stability is significant even at subsonic speeds where its magnitude is relatively small. At supersonic speeds $C_{m\beta}$ causes a complete change of the dynamic stability picture: P_{dyn1} and P_{dyn2} are both negative. Effect of lack of mirror symmetry is more pronounced in supersonic region with increasing M_∞ since magnitude of $C_{m\alpha}$, $C_{mq} + C_{m\dot{\alpha}}$ and $C_{m\beta\beta}$ decreases while that of $C_{m\beta}$ increases. This can have serious implications in terms of external configuration design of a missile with WAF if maximum range performance has priority since high M_∞ at rocket motor burn-out becomes unavoidable. Research on linear stability analysis of configurations with WAF should be extended with consideration of effects of $C_{m\tau}$ which can easily be obtained by panel methods. Another area which requires further investigation is roll direction dependent aerodynamics: $C_{m\beta p\pm}$, $C_{m\omega p\pm}$.

REFERENCES

1. Dahlke, C. W., Craft, J. C., "The Effect of Wrap-Around Fins on Aerodynamic Stability and Rolling Moment Variations", US Army Missile Research Development and Engineering Laboratory, RD-73-17, July 1973.
2. Humphrey, A. J., Dahlke, C. W., "A Summary of Aerodynamic Characteristics for Wrap-Around Fins from Mach 0.3 to 3.0", US Army Missile Research Development Command, TD-77-5, March 1977.
3. Stevens, F. L., "Analysis of the Linear Pitching and Yawing Motion of Curved Finned Missiles", Naval Weapons Laboratory, NWL TR-2989, October 1973.
4. Murphy, C. H., "Free Flight Motion of Symmetric Missiles", Ballistic Research Laboratories, Report No. 4216, July 1963.
5. Murphy, C. H., "Symmetric Missile Dynamic Instabilities-A Survey", AIAA JGCD, Vol. 4, No. 5, September-October 1981, pp. 464-471.
6. Stevens, F. L., On, T. J., Clare, T. A., "Wrap-Around vs Cruciform Fins: Effects on Rocket Flight Performance", AIAA Paper No. 74-777, August 1974.
7. Daniels, P., Hardy, S. R., "Roll Rate Stabilization of a Missile Configuration with Wrap-Around Fins", AIAA JSR, Vol. 13, No. 7, December 1975, pp. 446-448.
8. Hardy, S. R., "Nonlinear Analysis of the Rolling Motion of a Wrap-Around Fin Missile at Angles of Attack from 0° to 90° in Compressible Flow", Naval Surface Weapons Center, NSWC/DL-TR-3727, September 1977.
9. Catani, U., Bertin, J., De Amicis, R., Masullo, S., Bouslog, S., "Aerodynamic Characteristics for a Slender Missile with Wrap-Around Fins", AIAA JSR, Vol. 20, No. 2, January 1982, pp. 122-128.
10. Bar Haim, B., Seginer, A., "Aerodynamics of Wrap-Around Fins", AIAA JSR, Vol. 20, No. 4, August 1983, pp. 339-345.
11. Winchenbach, G. L., Buff, R. S., Whyte, R. H., Hathaway, W. H., "Subsonic and Transonic Aerodynamics of a Wrap-Around Fin Configuration", AIAA JGC, Vol. 9, No. 6, November-December 1986, pp. 627-632.
12. Kim Hoon, Y., Winchenbach, G. L., "Roll Motion of a Wrap-Around Fin Configuration at Subsonic and Transonic Mach Numbers", AIAA JGCD, Vol. 9, No. 2, March-April 1986, pp. 253-255.
13. Whyte, R. H., Hathaway, W. H., Buff, R. S., Winchenbach, G. L., "Subsonic and Transonic Aerodynamics of a Wrap-Around Fin Configuration", AIAA 23rd Aerospace Sciences Meeting, AIAA-85-0106, January 1985.
14. Vitale, R. E., Abate, G. L., Winchenbach, G. L., Riner, W., "Aerodynamic Test and Analysis of a Missile Configuration with Curved Fins", AIAA Paper-92-4495-CP, 1992.

15. Edge, H. L., "Computation of the Roll Moment for a Projectile with Wrap-Around Fins", AIAA JSR, Vol. 31, No. 4, July-August 1994, pp. 615-620.
16. Nielsen, J. N., "Missile Aerodynamics", McGraw-Hill, 1960.
17. Anderson, J. D., "Fundamentals of Aerodynamics", McGraw-Hill, 1991.
18. Benton, E. R., "Wing-Tail Interference as a Cause of Magnus Effect on a Finned Missile", Journal of Aerospace Sciences, Vol. 29, November 1962, pp. 1358-1367.
19. Benton, E. R., "Supersonic Magnus Effect on a Finned Missile", AIAA Journal, Vol. 2, No. 1, January 1964, pp. 150-155.
20. Platou, A. S., "Magnus Characteristics of Finned and Non Finned Missiles", AIAA J, Vol. 3, No. 1, January 1965, pp. 83-90.
21. Uselton, J. C., Carman, J. B., "A Study of the Magnus Effects on a Sounding Rocket at Supersonic Speeds", AIAA JSR, Vol. 8, No. 1, January 1971, pp. 28-34.
22. Platou, A. S., "Wind Tunnel Magnus Testing of a Canted Fin or Self Rotating Configuration", AIAA J, Vol. 10, No. 7, July 1972, pp. 965-967.
23. Seginer, A., Rosenwasser, I., "Magnus Effects on Spinning Transonic Finned Missiles", AIAA JSR, Vol. 23, No. 1, January-February 1986, pp. 31-38.
24. Sahu, J., "Transonic Navier-Stokes Computations for a Spinning Body of Revolution", ASME Publication, Vol. 103, 1990, pp. 87-97.
25. Martin, J. C., "On Magnus Effects Caused by the Boundary Layer Displacement Thickness on Bodies of Revolution at Small Angles of Attack", Journal of Aeronautical Sciences, Vol. 24, March 1957, pp. 421-429.
26. Swanson, W. M., "The Magnus Effect: A Summary of Investigations to Date", Journal of Basic Engineering, Vol. 83, September 1961, pp. 461-470.
27. Power, H. L., Iversen, J. D., "Magnus Effects on Spinning Bodies of Revolution", AIAA J, Vol. 11, No. 4, April 1973, pp. 417-418.
28. Vaughn, H. R., Reis, G. E., "A Magnus Theory". AIAA Paper No. 73-124, 1973.
29. Fletcher, C. A. J., "Negative Magnus Forces in the Critical Reynolds Number Regime", AIAA JA, Vol. 9, No. 12, December 1972, pp. 826-834.
30. Seginer, A., Ringel, M., "Magnus Effects at High Angles of Attack and Critical Reynolds Numbers", AIAA JSR, Vol. 23, No. 3, May-June 1986, pp. 237-244.
31. Corby, N., Berry, J., B., "A Wind Tunnel Rig for the Measurement of Magnus Force and Moment on Spinning Models", in "Missile Aerodynamics", AGARD CP-493, April 1990, No. 13.
32. Önen, C., Tanrikulu, Ö., Mahmutyazıcıoğlu, G., "Flight Mechanics of Unguided Missiles with Wrap-Around Fins", TÜBİTAK-SAGE, 93/4-7, SI 94/31, 22192, November 1994.

Détermination de coefficients aérodynamiques avec des résultats d'essais en vol

Practical use of flight tests results for estimations of aerodynamic coefficients

G. SCHMITT

MATRA DÉFENSE

37, avenue Louis Bréguet - B.P. n° 1
78146 Vélizy-Villacoublay Cédex
France

ABSTRACT

At the end of a missile development, the flight tests, limited in quantity have to validate the overall missile performances. They are particularly used for the validation of the aerodynamic characteristics. After them, some improvements of the aerodynamic modeling or even adjustments of the aerodynamic design can be initiated.

The identification of the missile aerodynamics is important to establish its operational performances by running of simulations. It allows the limitation of the expensive flight tests to the minimal number needed to perfect the guidance and control functions embedded in the missile.

The aerodynamic coefficients are not directly measured in flight, but computed from measured flight datas.

Some results obtained with a long range cruise missile are therefore presented. The comparison with wind tunnel test data are explained and are satisfactory.

RESUME

Les essais en vol de missile, exécutés en nombre restreint, sont destinés à valider le bon comportement d'ensemble de l'engin. En particulier, ils permettent de valider le bon comportement aérodynamique. Ils peuvent être à l'origine d'amélioration du modèle aérodynamique ou même d'ajustements de la configuration aérodynamique.

L'identification de l'aérodynamique de l'engin est importante pour établir sa performance dans son domaine d'emploi à partir de simulations et limiter le nombre d'essais en vol onéreux à la mise au point des fonctions embarquées dans le missile.

Les coefficients aérodynamiques ne sont pas directement mesurés, mais déduits des paramètres mesurés en vol.

Des résultats obtenus avec un missile de croisière de longue portée sont présentés à titre d'illustration. Ils sont en bonne corrélation avec les résultats d'essais en soufflerie.

I. INTRODUCTION

Dans le développement des missiles, les essais en vol revêtent une importance très grande, car ils permettent de vérifier en conditions réelles la bonne exécution de l'ensemble des fonctions implantées dans l'engin : navigation, guidage, pilotage, propulsion ...

D'un coût onéreux, les essais en vol se font en nombre limité et il n'est guère possible de couvrir tout le domaine de vol opérationnel de l'engin. L'évaluation de la performance du missile repose par conséquent sur la simulation numérique incluant une représentation de chacun des composants de l'engin.

La performance en portée et en vitesse de l'engin dépend pour partie de l'efficacité aérodynamique modélisée à partir d'essais en soufflerie. Les conditions du vol libre étant différentes de la soufflerie, il convient de recalculer le modèle aérodynamique à partir de mesures faites en vol, afin que la simulation du missile puisse rendre compte de l'ensemble de ses performances.

Ce document présente la méthodologie de restitution de l'aérodynamique à partir de mesures faites au cours d'un vol ainsi qu'un cas d'application.

NOTATIONS

M :	nombre de Mach du missile
x, y, z :	coordonnées du centre de gravité du missile dans un repère terrestre
ϕ, θ, ψ :	angles d'Euler, caractérisant la position angulaire du missile par rapport à une référence terrestre
$\delta l, \delta m, \delta n$:	braquages des gouvernes en roulis, tangage et lacet
p, q, r :	vitesse de rotation du missile par rapport à un repère terrestre, exprimées en repère missile
$\dot{p}, \dot{q}, \dot{r}$:	accélérations angulaires
V_x, V_y, V_z :	vitesse du missile par rapport à un repère terrestre

$\gamma_x, \gamma_y, \gamma_z$:	effort spécifique en repère missile
m :	masse du missile
[j] :	matrice d'inertie du missile
I_{xx}, I_{yy}, I_{zz} :	termes diagonaux de j
p_0 :	pression statique à l'altitude de vol
$C_{xRI}, C_{yRI}, C_{zRI}$	
$C_{mRI}, C_{nRI}, C_{lRI}$	coefficients aérodynamiques évalués avec les données de la Référence Inertielle
G :	centre de gravité du missile
A :	positionnement de la Référence Inertielle
P :	poussée du moteur
S réf, L réf :	données de référence aérodynamiques
α, β :	incidence, dérapage
Z :	altitude du missile
ω :	régime moteur
$C_{x_a}, C_{y_a}, C_{z_a}, C_{l_a}, C_{m_a}, C_{n_a}$	coefficients aérodynamiques évalués avec le modèle aérodynamique
Cx :	coefficient de traînée
Cy :	coefficient de force latérale
Cz :	coefficient de portance
Cm :	coefficient de moment de tangage
Cn :	coefficient de moment de lacet
Cl :	coefficient de moment de roulis

Ces coefficients sont définis en axes missile.

II. INFORMATIONS DISPONIBLES

Les informations disponibles pour restituer un vol d'essais proviennent des senseurs embarqués à bord de l'engin et des détecteurs de poursuite du champ de tir.

Moyens extérieurs :

Les moyens de mesure extérieurs à l'engin permettent une restitution de la trajectoire du véhicule testé :

- le radar mesure la trajectoire de l'engin (x, y, z) dans un repère terrestre
- les caméras et cinéthéodolites assurent une localisation (x, y, z) dans un repère terrestre ; utilisées lors de séparations sous avion, les caméras permettent à faible distance de moins de 10 m, une évaluation de l'attitude relative de

l'engin par rapport à l'avion (angles d'Euler ϕ, θ, ψ)

- les mesures météorologiques caractérisent l'atmosphère au moment du vol par les paramètres suivants : vent V_v (direction et amplitude), pression statique et température ; ces mesures recalent le modèle d'atmosphère utilisé pour le calcul des coefficients aérodynamiques au cas où le véhicule testé ne dispose pas de capteurs de pression pour mesurer la pression dynamique et la pression d'arrêt

Moyens internes télémésurés :

Pour remplir sa mission, l'engin est équipé d'une panoplie de senseurs afin d'assurer correctement les fonctions de navigation, guidage et pilotage. L'évaluation des coefficients aérodynamiques repose essentiellement sur les informations des capteurs de navigation et de pilotage. Les mesures de ces senseurs sont collectées par un équipement de télémessure et envoyées au sol.

La liste suivante contient les mesures les plus importantes réalisables à bord du véhicule de test, mais toutes ne sont pas nécessairement réalisées :

- senseurs inertiels
 - vitesses angulaires p, q, r par des gyromètres
 - efforts spécifiques $\gamma_x, \gamma_y, \gamma_z$ par des accéléromètres
- La position (x, y, z), la vitesse (V_x, V_y, V_z) et l'attitude (ϕ, θ, ψ) inertielles ou par rapport à la terre en sont déduites si les senseurs sont de la classe navigation.
- senseurs de pilotage
 - braquages des gouvernes $\delta_l, \delta_m, \delta_n$ par des potentiomètres
 - incidence α et dérapage β par des girouettes
 - pressions statique p_0 et dynamique p_i par une centrale anémométrique pour évaluer le Mach M
 - régime moteur ω en cas de propulsion autre que par moteur fusée
 - débit de carburant par un débitmètre

III. EQUATION DE LA DYNAMIQUE

Le principe de restitution des coefficients aérodynamiques repose sur l'équation fondamentale de la dynamique :

$$m \cdot \ddot{\Gamma} = \Sigma F = F_p + F_a$$

$$I \cdot \ddot{\Omega} = m_p + m_a$$

m masse de l'engin

Γ effort spécifique

F_p force de propulsion

F_a résultante aérodynamique

I matrice d'inertie

Ω accélération angulaire de l'engin

m_p moment de la propulsion au centre de gravité

m_a moment aérodynamique au centre de gravité

La matrice d'inertie I est en général assimilée à une matrice diagonale dont les termes diagonaux sont I_{xx} , I_{yy} , I_{zz} .

IV. DÉTERMINATION DES COEFFICIENTS AÉRODYNAMIQUES

L'objet de la restitution aérodynamique du vol est la comparaison entre les coefficients aérodynamiques obtenus par deux voies différentes :

A. Le modèle aérodynamique du missile

Les six coefficients aérodynamiques s'écrivent :

$C_{x_a} = C_x (M, \alpha, \beta, Z, \delta_l, \delta_m, \delta_n, \dots)$ Traînée

$C_{y_a} = C_y (M, \alpha, \beta, \delta_l, \delta_m, \delta_n, \dots)$ Portance latérale

$C_{z_a} = C_z (M, \alpha, \beta, \delta_l, \delta_m, \delta_n, \dots)$ Portance

$C_{l_a} = C_l (M, \alpha, \beta, \delta_l, \delta_m, \delta_n, p, \dots)$ Roulis

$C_{m_a} = C_m (M, \alpha, \beta, \delta_l, \delta_m, \delta_n, q, x_G, \dots)$ Tangage

$C_{n_a} = C_n (M, \alpha, \beta, \delta_l, \delta_m, \delta_n, r, x_G, \dots)$ Lacet

Les paramètres entre parenthèses doivent être estimés pour chaque point de vol :

M : Mach

α et β : incidence et dérapage

$\delta_l, \delta_m, \delta_n$: Braquages en roulis, tangage et lacet

p, q, r : vitesses angulaires en roulis, tangage et lacet

x_G : position du centre de gravité

D'autres paramètres peuvent intervenir, tels que présence ou non de propulsion, etc ...

B. L'utilisation des équations de la dynamique vues précédemment

$$F_a = m \cdot \ddot{\Gamma} - F_p = \frac{1}{2} \gamma \cdot p_0 \cdot M^2 \cdot S_{\text{réf}} \cdot (C_x, C_y, C_z)$$

$$m_a = I \cdot \ddot{\Omega} - m_p = \frac{1}{2} \gamma \cdot p_0 \cdot M^2 \cdot S_{\text{réf}} \cdot L_{\text{réf}} (C_l, C_m, C_n)$$

p_0 pression statique à l'altitude de vol

$S_{\text{réf}}, L_{\text{réf}}$ grandeurs de référence

$\gamma = 1,4$ rapport des chaleurs massiques

On obtient ainsi :

$$C_{x_{RI}} = \frac{m \cdot \ddot{x} - F_{px}}{\frac{1}{2} \gamma \cdot p_0 \cdot M^2 \cdot S_{\text{réf}}}$$

$$C_{y_{RI}} = \frac{m \cdot \ddot{y} - F_{py}}{\frac{1}{2} \gamma \cdot p_0 \cdot M^2 \cdot S_{\text{réf}}}$$

$$C_{z_{RI}} = \frac{m \cdot \ddot{z} - F_{pz}}{\frac{1}{2} \gamma \cdot p_0 \cdot M^2 \cdot S_{\text{réf}}}$$

$$C_{l_{RI}} = \frac{I_{xx} \cdot \ddot{p} - m_{px}}{\frac{1}{2} \gamma \cdot p_0 \cdot M^2 \cdot S_{\text{réf}} \cdot L_{\text{réf}}}$$

$$C_{m_{RI}} = \frac{I_{yy} \cdot \ddot{q} - m_{py}}{\frac{1}{2} \gamma \cdot p_0 \cdot M^2 \cdot S_{\text{réf}} \cdot L_{\text{réf}}}$$

$$C_{n_{RI}} = \frac{I_{zz} \cdot \ddot{r} - m_{pz}}{\frac{1}{2} \gamma \cdot p_0 \cdot M^2 \cdot S_{\text{réf}} \cdot L_{\text{réf}}}$$

La détermination des coefficients aérodynamiques par ces deux méthodes réclame la connaissance, en chaque point de vol, d'un certain nombre de grandeurs physiques. Celles-ci sont soit directement mesurées et transmises à des enregistreurs au sol, soit, en l'absence de mesures directes, calculées à partir de modèles utilisant d'autres grandeurs physiques plus facilement accessibles comme indiqué ci-dessous.

V. DÉTERMINATION DES GRANDEURS PHYSIQUES NÉCESSAIRES AUX CALCULS DES COEFFICIENTS AÉRODYNAMIQUES

A. Modèle de propulsion (F_p, m_p)

La force de propulsion F_p n'est pas directement

mesurée. Selon le mode de propulsion retenu, son amplitude est une fonction plus ou moins complexe du temps de vol, des conditions de vol (Mach M, altitude Z, ...), du régime moteur ω ...

$$F_p = F_p(t, M, Z, \omega, \dots) = (F_{px}, F_{py}, F_{pz})$$

La projection de la force de propulsion (F_{px} , F_{py} , F_{pz}) dans le repère lié à l'engin dépend du montage mécanique et éventuellement de la présence de gouvernes de jet.

$$m_p = F_p \wedge PG$$

P point d'application de la poussée

G position du centre de gravité

B. Modèle de cellule

Les caractéristiques massiques de la cellule concernent la masse, l'inertie et le centrage :

- la masse est une fonction du temps de vol. Des pesées avant tir donnent la masse finale et l'évolution de la masse au cours du vol propulsé est évaluée par une fonction forfaitaire du temps ou estimée grâce à la mesure de consommation du propulseur par un débitmètre.
- la matrice d'inertie, réduite le plus souvent à une forme diagonale, est une fonction calculée à partir de la masse ; elle évolue de manière analogue à la masse ; les estimations des inerties peuvent être recalées par des mesures des caractéristiques pendulaires de l'engin suspendu.
- le centrage évolue en fonction de la masse de l'engin. Son estimation est faite avec les procédés utilisés pour définir la masse et les inerties.

C. Modèle d'atmosphère

Les efforts aérodynamiques sont proportionnels à la pression statique. Celle-ci, ainsi que la vitesse du son, peuvent être évaluées selon deux procédés :

- la mesure de la pression dynamique ($p_i - p_0$) par une centrale anémométrique qui fournit directement le facteur multiplicateur des efficacités aérodynamiques $\frac{1}{2} \gamma \cdot p_0 \cdot M^2$
- un modèle d'atmosphère permet de déterminer à partir des estimations d'altitude et de vitesse aérodynamique, la pression statique, la vitesse du son et le Mach

Le modèle d'atmosphère est en général recalé par une mesure ponctuelle faite par l'installation de tir : température et pression statique.

D. Estimation des accélérations

Les équations de la dynamique mettent en évidence l'accélération angulaire $\dot{\Omega}(\dot{p}, \dot{q}, \dot{r})$ et la force spécifique $\Gamma(\gamma_x, \gamma_y, \gamma_z)$.

$\dot{\Omega}(\dot{p}, \dot{q}, \dot{r})$ accélération angulaire en roulis, tangage, lacet

$\Gamma(\gamma_x, \gamma_y, \gamma_z)$ force spécifique en roulis, tangage, lacet

Pour les besoins du pilotage, les engins disposent en général d'un bloc gyrométrique qui mesure la vitesse angulaire $\Omega_m(p_m, q_m, r_m)$ et le plus souvent d'accéléromètres pour la mesure des efforts spécifiques $\Gamma_m(\gamma_{xm}, \gamma_{ym}, \gamma_{zm})$. Pour des engins rudimentaires dont la panoplie des senseurs fonctionnels est plus réduite, un équipement spécifique de test est en général développé et comporte ces senseurs.

L'accélération angulaire $\dot{\Omega}$ est estimée par filtrage et dérivation de la détection en vitesse angulaire

$$\dot{\Omega} = \frac{\dot{\Omega}_m \cdot s}{1 + a \cdot s + b \cdot s^2}$$

La bande passante du filtre est suffisante pour bien restituer l'accélération angulaire aux fréquences inférieures à 10 Hz et éliminer le bruit de mesure situé aux fréquences élevées.

La force spécifique est mesurée par les accéléromètres. Cependant, la force spécifique impliquée dans l'équation de la dynamique correspond au centre de gravité de l'engin, alors que les accéléromètres se trouvent en général à une position différente. Les effets de cet écart de position peuvent être corrigés :

$$\Gamma = \Gamma_m + \dot{\Omega} \wedge AG + \Omega_m \wedge \Omega_m \wedge AG$$

$\Gamma(\gamma_x, \gamma_y, \gamma_z)$ force spécifique estimée au centre de gravité

$\dot{\Omega}(\dot{p}, \dot{q}, \dot{r})$ accélération angulaire estimée

$\Omega_m(p_m, q_m, r_m)$ vitesse angulaire mesurée par les gyromètres

$\Gamma_m(\gamma_{xm}, \gamma_{ym}, \gamma_{zm})$ force spécifique mesurée par les accéléromètres

A position des accéléromètres

G position du centre de gravité

E. Estimation de la position

L'estimation de la position est nécessaire pour identifier les coefficients aérodynamiques, car les efforts aérodynamiques dépendent de l'altitude et de la vitesse.

L'estimation de la position est réalisée par des moyens internes ou externes au véhicule testé :

- les moyens externes (radar, caméras, cinétodolites ...) spécifiques du champ de tir sont toujours utilisés quand la distance de l'engin au moyen de mesure ne dépasse pas 20 km pour assurer une précision de mesure de l'ordre de 100 m. La précision peut être améliorée grâce au montage de répondeur ou réflecteur sur le véhicule de test.
- les moyens internes sont utilisés en complément des moyens externes. Leur coût rapporté à celui du véhicule testé est relativement important et ils ne sont souvent pas spécifiquement implantés pour les besoins de test. Les équipements de localisation embarqués sont variés : équipements de navigation inertiels, GPS, radioaltimètre, baroaltimètre, ...

L'estimation de position peut être améliorée par la fusion des mesures de plusieurs senseurs externes ou internes.

Pour la restitution de l'aérodynamique, la précision de localisation souhaitée est de l'ordre de 100 m à 300 m pour l'altitude. La localisation est souvent exploitée pour estimer par dérivation la vitesse de l'engin avec une erreur inférieure à 10 m/s.

F. Estimation de la vitesse

La vitesse intervient par son carré dans l'expression des efforts aérodynamiques et sa connaissance est donc vitale pour l'estimation des efficacités aérodynamiques

La grandeur incriminée est la vitesse par rapport à l'air V_a :

$$V_a = V - V_v$$

V_a vitesse aérodynamique

V vitesse inertielle ou vitesse par rapport à la terre

V_v vitesse du vent

La centrale anémométrique est le meilleur équipement pour extraire les coefficients aérodynamiques à partir des efforts aérodynamiques car l'écart entre la pression statique et la pression d'arrêt donne directement le

$$\text{coefficient } \frac{1}{2} \gamma \cdot p_0 \cdot M^2$$

$$p_i - p_0 = \frac{1}{2} \gamma \cdot p_0 \cdot M^2$$

p_0, p_i pression statique et pression d'arrêt
 M Mach

$\gamma \simeq 1.4$ rapport des chaleurs massiques

La mesure de la pression dynamique ($p_i - p_0$) permet d'éviter le recours à l'estimation de l'altitude pour déterminer les coefficients aérodynamiques. Elle est surtout indiquée pour les engins évoluant à faible vitesse et pour lesquels la vitesse du vent V_v peut être significative vis-à-vis de la vitesse de translation V de l'engin.

Les autres méthodes permettant de reconstituer la pression dynamique consistent à déduire la pression statique à partir de l'altitude estimée et d'un modèle d'atmosphère et à évaluer le Mach, donc la vitesse aérodynamique à partir de la vitesse de translation et de la vitesse du vent moyen mesuré sur le champ de tir au moment du vol.

La vitesse de translation peut être déduite par filtrage et dérivation de la localisation effectuée avec les moyens du champ de tir.

Si l'engin testé dispose de moyens de navigation suffisants (inertiels, GPS, ...) la navigation du véhicule fournit la vitesse de translation avec une erreur de un à quelques mètres par seconde (jusqu'à 10 m/s pour une navigation inertielle médiocre d'un missile tactique).

La reconstitution de la vitesse aérodynamique par la vitesse inertielle et une estimation du vent moyen ne prennent pas en compte les rafales de vent.

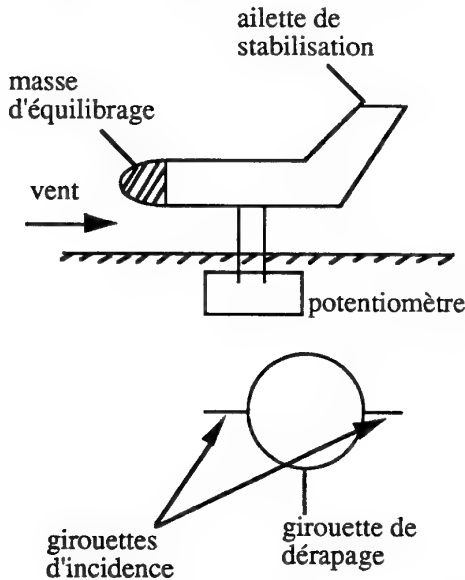
Le recours à une centrale anémométrique pour estimer la pression dynamique est onéreux, car au prix de la centrale, il faut ajouter les coûts d'implantation sur le véhicule et d'étalonnage en soufflerie.

G. Estimation de l'incidence α et du dérapage β

L'estimation des coefficients aérodynamiques résultants en effort et en moment n'exige pas la connaissance de l'incidence et du dérapage. Cependant, la maîtrise du guidage-pilotage ainsi que l'évaluation de la portée de l'engin nécessitent la connaissance de l'amplitude des mouvements angulaires et de leur effet sur la traînée. En conséquence, l'estimation des gradients aérodyna-

miques par rapport à l'incidence et au dérapage est primordiale pour assurer la performance du véhicule testé.

La mesure de l'incidence et du dérapage peut être faite grâce à l'implantation de girouettes sur le vecteur. Cette opération nécessite un important travail en soufflerie pour le choix de l'implantation des girouettes et leur étalonnage. Ces girouettes sont au moins au nombre de 2 et de préférence 3 ou 4 pour mesurer l'incidence et le dérapage. Ce nombre a tendance à grandir avec le domaine d'évolution de l'incidence et du dérapage.



La mesure brute du potentiomètre est corrigée en fonction de la caractéristique d'étalonnage relevée en soufflerie pour rendre compte de l'incidence et du dérapage de l'engin par rapport à l'écoulement infini amont.

En l'absence de girouettes, l'incidence et le dérapage peuvent être estimés à partir de l'attitude de l'engin et de sa vitesse aérodynamique. Cette opération n'est réalisable que si le véhicule de test dispose d'une centrale de navigation inertielle. La procédure utilisée est la suivante :

- le vecteur vitesse aérodynamique est la différence entre le vecteur vitesse inertiel estimé par la navigation et l'estimation du vecteur vitesse du vent
- l'incidence et le dérapage sont les angles entre l'axe de roulis de l'engin et le vecteur vitesse aérodynamique défini ci-dessus

Il est possible pendant les phases de vol stabilisé

de reconstituer l'incidence et le dérapage selon le même procédé sur un engin équipé d'une centrale d'attitude en utilisant la vitesse inertielle déduite de la poursuite effectuée avec les moyens de mesure du champ de tir.

La précision de ce procédé d'estimation dépend de la justesse des hypothèses faites sur le vent et de la qualité de la navigation du véhicule testé, en particulier de la dérive de l'estimation de la vitesse inertielle par rapport à celle de l'attitude de l'engin. Plus l'engin est lent, plus l'obtention de bons résultats avec cette méthode devient délicate.

Hormis les rafales de vent, ce procédé permet une très bonne estimation des variations à court terme de l'incidence et du dérapage, et la méthode reste toujours précise pour l'évaluation des gradients des efficacités aérodynamiques dès lors qu'elle est effectuée à partir de différentes phases de vol stabilisé, proches dans le temps (écarts de quelques secondes).

Pour les engins rustiques équipés de senseurs gyrométriques et accélérométriques n'autorisant pas une navigation correcte, il est possible d'évaluer les variations rapides d'incidence et de dérapage par les formulations suivantes :

$$\dot{\alpha} = qm + \frac{\gamma z + g_z}{V}$$

$$\dot{\beta} = rm - \frac{\gamma y + g_y}{V}$$

- $\dot{\alpha}, \dot{\beta}$ dérivées de l'incidence et du dérapage
- qm, rm vitesses de tangage et de lacet mesurées par les gyromètres
- V vitesse estimée de l'engin par la poursuite des moyens externes
- g_y, g_z projection de la pesanteur sur les axes de lacet et de tangage
- $\gamma y, \gamma z$ effort spécifique au centre de gravité en lacet et tangage

Compte tenu de la qualité des senseurs, cette méthode n'est applicable qu'à des variations significatives et rapides de l'incidence et du dérapage (commandes en échelons, ...).

VI. EXPLOITATION DES DONNÉES DE VOL

A. Coefficients aérodynamiques restitués

Le modèle aérodynamique mis au point à partir des mesures en soufflerie est complexe et doit rendre compte du torseur aérodynamique à tout instant. Les coefficients d'efficacité dépendent

d'un grand nombre de paramètres (p_0 , M , α , β , p , q , r , δl , δm , δn , ...). Les estimées instantanées de ces paramètres sont bruitées et le niveau de bruit est particulièrement élevé sur la mesure du moment, car elle découle de l'évaluation de l'accélération angulaire.

C'est pourquoi, la meilleure estimation des coefficients aérodynamiques est obtenue grâce à l'analyse d'un grand nombre de points de vol stabilisé (accélération angulaire nulle). Une telle procédure est retenue pour identifier les coefficients d'efforts C_x , C_y , C_z : le modèle est simplifié grâce à la faible valeur des vitesses et accélérations angulaires et un moyennage des détecteurs permet de réduire l'influence des bruits de mesure. La concordance en un grand nombre de points de vol des estimations des coefficients aérodynamiques faites à partir du vol avec les sorties du modèle aérodynamique excité par les mêmes paramètres de vol confère à ce dernier une grande crédibilité.

La restitution des coefficients d'effort est importante pour l'évaluation des performances de l'engin en terme de portée, de vitesse et de manoeuvrabilité. Si l'évaluation des coefficients de portance est relativement aisée, la tâche se révèle plus complexe pour le coefficient de traînée, car l'effort mesuré par l'accéléromètre longitudinal est le résultat de la propulsion et de la traînée. L'estimation du coefficient de traînée dépend donc pendant la phase de vol propulsé, de la connaissance du niveau de poussée.

L'écart entre la vitesse inertielle et la vitesse aérodynamique est souvent mal évalué, car le vent n'est pas ou mal mesuré dans les conditions du vol et cela peut entraîner des erreurs d'estimation de plus de 5 % sur l'aérodynamique.

La restitution des coefficients de moment est plus importante pour caractériser la pilotabilité que pour définir la performance (portée, vitesse). L'analyse des phases de vol stabilisé permet d'obtenir des renseignements sur les braquages d'équilibre et même sur les gradients de moments grâce à l'examen de plusieurs points d'équilibre. La précision requise pour le pilotage est de l'ordre de 10 %.

L'analyse des transitoires est plus délicate, car la modélisation aérodynamique est plus complexe à cause de l'évolution d'un grand nombre de paramètres et l'estimation des accélérations angulaires est pénalisée par les bruits de mesure des gyromètres. Cependant, à cause des rapides variations des braquages des gouvernes, il est

possible d'identifier le gradient de moment des gouvernes sur de brusques mises en manoeuvre.

B. Application au missile de croisière Apache

Ce missile effectue sa croisière à Mach 0.8. Après son largage sous avion, il rallie son altitude et son Mach de croisière. Pour des raisons de discrétion, il vole à faible altitude en suivi de terrain et manoeuvre à vitesse constante.

De configuration bank-to-turn, à ailes déployables, ce missile manoeuvre principalement en tangage, mais peut aussi réaliser des facteurs de charge en lacet en maintenant un dérapage équilibré.

La propulsion est assurée par un turboréacteur qui fonctionne pendant tout le vol.

Le vol analysé ci-après débute par un largage à moyenne altitude et se poursuit par des manoeuvres préprogrammées afin de décrire le domaine de facteur de charge opérationnellement prévu. Ce vol spécifique a pour but la caractérisation des performances aérodynamiques de la cellule pilotée.

Le missile est équipé d'une télémessure retransmettant au sol les informations suivantes :

- la position, la vitesse et l'altitude ainsi que les mesures des senseurs inertiels (forces spécifiques et vitesses angulaires) issues du bloc de navigation inertielle
- la pression statique p_0 et le Mach M déduits des mesures d'une perche anémométrique spécialement installée pour ce vol
- l'incidence et le dérapage mesurés par des girouettes spécialement installées pour ce vol et calibrées par des essais préalables en soufflerie à l'échelle 1
- les braquages des gouvernes mesurés par des potentiomètres
- la vitesse de rotation du turboréacteur mesurée par un tachymètre

L'autopilote du missile contrôle les mouvements angulaires autour des trois axes : roulis, lacet, tangage. Les deux gouvernes horizontales servent au contrôle du roulis et du tangage, et les dérives verticales supérieures au contrôle du lacet ; les dérives verticales inférieures assurent la stabilité en lacet.

Les résultats obtenus en vol sont comparés à ceux obtenus avec le modèle aérodynamique, élaboré à partir d'essais en soufflerie de l'ONERA. Deux campagnes ont été effectuées, avec une maquette à l'échelle 0,25, et une autre à l'échelle 1 avec un turboréacteur réel en fonctionnement.

C. Analyse des résultats

Les résultats les plus fiables correspondent à des points de vol stabilisés. Les planches n° 1 à 5 représentant les évolutions de l'incidence α , du dérapage β et des braquages en fonction du temps, mettent en évidence les nombreux et importants transitoires entre les périodes de vol stabilisé.

L'engin évoluant à faible incidence, l'aérodynamique est assez linéaire et il suffit d'identifier quelques points en incidence et dérapage pour vérifier les principales caractéristiques aérodynamiques :

- la portance et la traînée
- les stabilités autour des trois axes
- les efficacités aérodynamiques des gouvernes

Ces vérifications sont faites par comparaison de points de vol pour lesquels un seul des paramètres (α , β) varie, l'autre restant sensiblement constant. Ainsi, l'identification des coefficients aérodynamiques à dérapage nul est réalisée à partir de points de vol tels que $-2^\circ < \beta < 2^\circ$.

1. Aérodynamique à dérapage nul $\beta \simeq 0$ (planches n° 6 à 8)

Pour la portance, une comparaison directe est réalisée entre les efforts restitués par les accéléromètres au centre de gravité et ceux estimés par le modèle aérodynamique excité par les paramètres d'état du vol (α , β , p , q , r , δ_l , δ_m , δ_n , ...). Dans le cas présent, la mesure en vol met en évidence un léger déficit en portance. Il est attribué à l'effet de torsion des ailes plus important en vol réel qu'en soufflerie. Il était prévu, mais les essais en vol ont permis de le quantifier précisément.

Les dépouillements ont été réalisés avec deux définitions différentes du point de vol : le premier (n° 1) part d'une mesure de l'atmosphère par la perche anémométrique donnant les pressions statique et totale, le Mach et la température totale. Le second (n° 2) utilise un modèle d'atmosphère recalé par une mesure (p_0 , T) sur le champ de tir. La première restitution se révèle plus proche du modèle aérodynamique. La comparaison des deux

démarches permet d'évaluer l'apport en précision de mesure de la perche anémométrique.

L'évaluation de la traînée est plus délicate à cause de la présence de la propulsion assurant une vitesse de croisière constante. L'estimation de la traînée est tributaire de la connaissance de la poussée du turboréacteur, calculée à partir du régime moteur et du point de vol (altitude et Mach). Dans le cas présent, la restitution ainsi réalisée de la traînée est très proche de son modèle aérodynamique.

Aux points de vol stabilisés, les accélérations angulaires mesurées sont nulles. Les moments aérodynamiques calculés avec le modèle aérodynamique excité par les données des points de vol stabilisés révèlent l'écart entre la modélisation et le vol réel et permettent d'évaluer s'il y a lieu d'apporter des ajustements au modèle.

L'examen de la voie tangage montre que les conditions d'équilibre en vol (incidence α et braquage en tangage δ_m) définissent dans le modèle aérodynamique un coefficient de moment C_m faible et sensiblement constant sur la plage d'incidence examinée. En conséquence, le modèle aérodynamique représente bien la stabilité de la cellule et l'efficacité des gouvernes, mais il convient de corriger légèrement le C_m global d'un ΔC_{m0} constant.

2. Aérodynamique à incidence constante

L'engin en vol en palier effectue des manœuvres en lacet dans le plan horizontal. L'exploitation de points de vol stabilisés à différents dérapages montre que la prédiction de la portance latérale par le modèle aérodynamique est bonne et légèrement inférieure à la réalité (planche n° 9).

La précision de la stabilité est également satisfaisante. La cellule est bien symétrique ($C_n = 0$ pour $\beta = 0$) et un peu plus stable que ne le prévoyaient les essais en soufflerie puisque les évolutions du moment de lacet en fonction du dérapage restituées à partir du vol et du modèle aérodynamique ne sont pas parallèles (planche n° 10).

L'évolution du roulis induit $Cl(\beta)$ est bien prédite par le modèle aérodynamique puisque les coefficients déduits du vol et du modèle aérodynamique ont des caractéristiques parallèles. Le décalage constant ΔCl constaté est cohérent avec la tolérance de calage mécanique des ailes droite et

gauche. Cet écart ΔC_l ne doit donc pas être pris en compte dans la définition nominale du coefficient de roulis, mais comme une tolérance sur ce coefficient (planche n° 11).

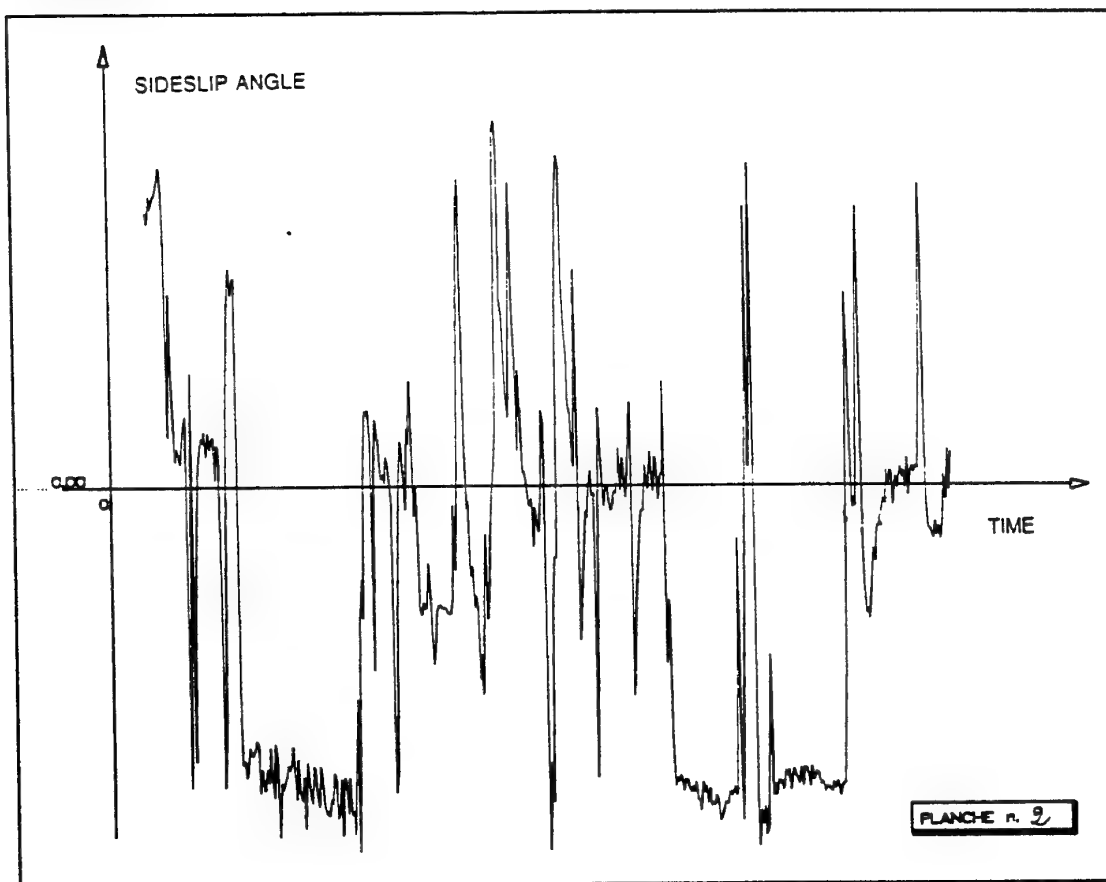
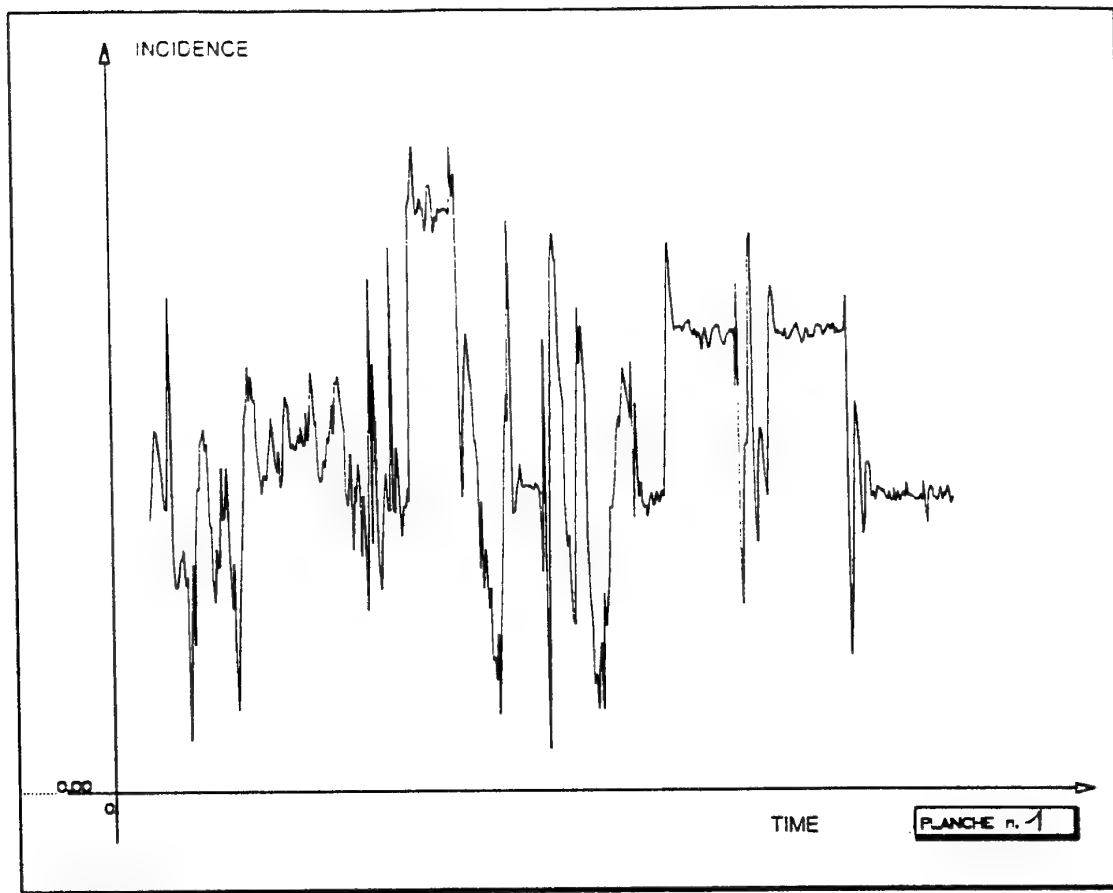
VIII. CONCLUSION

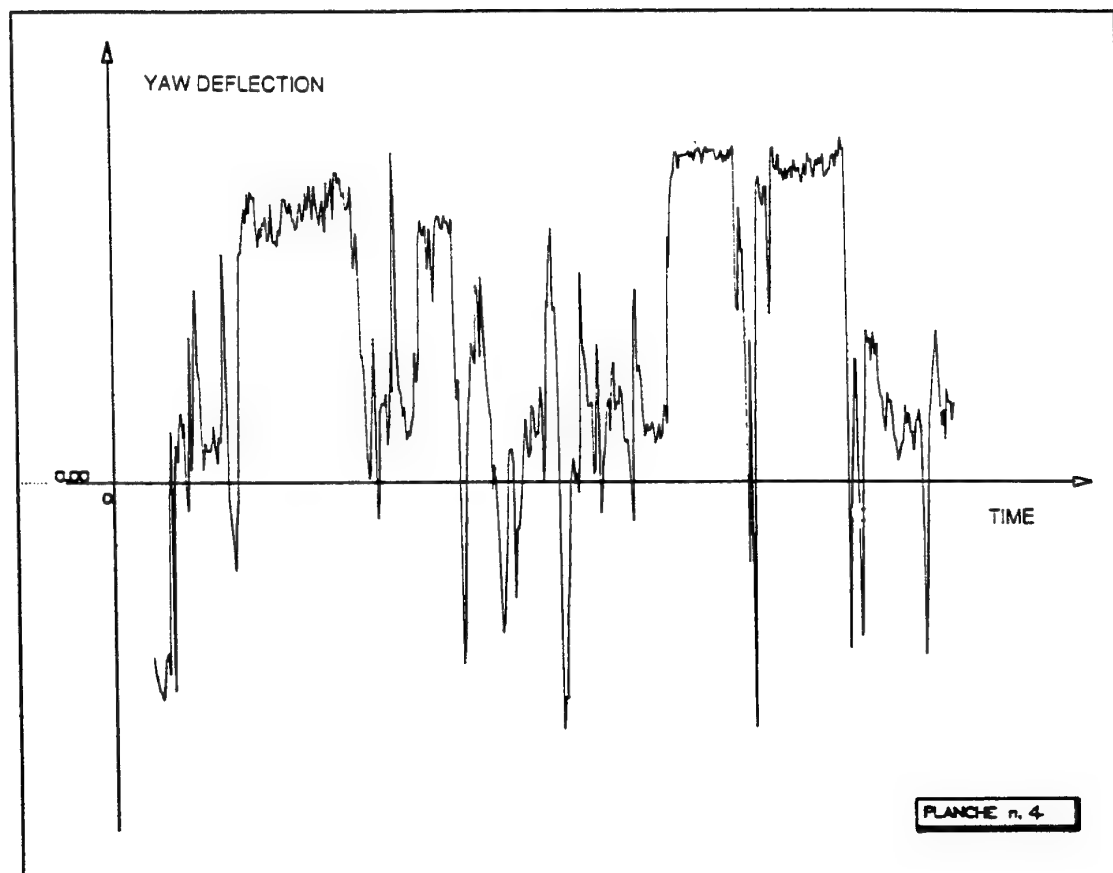
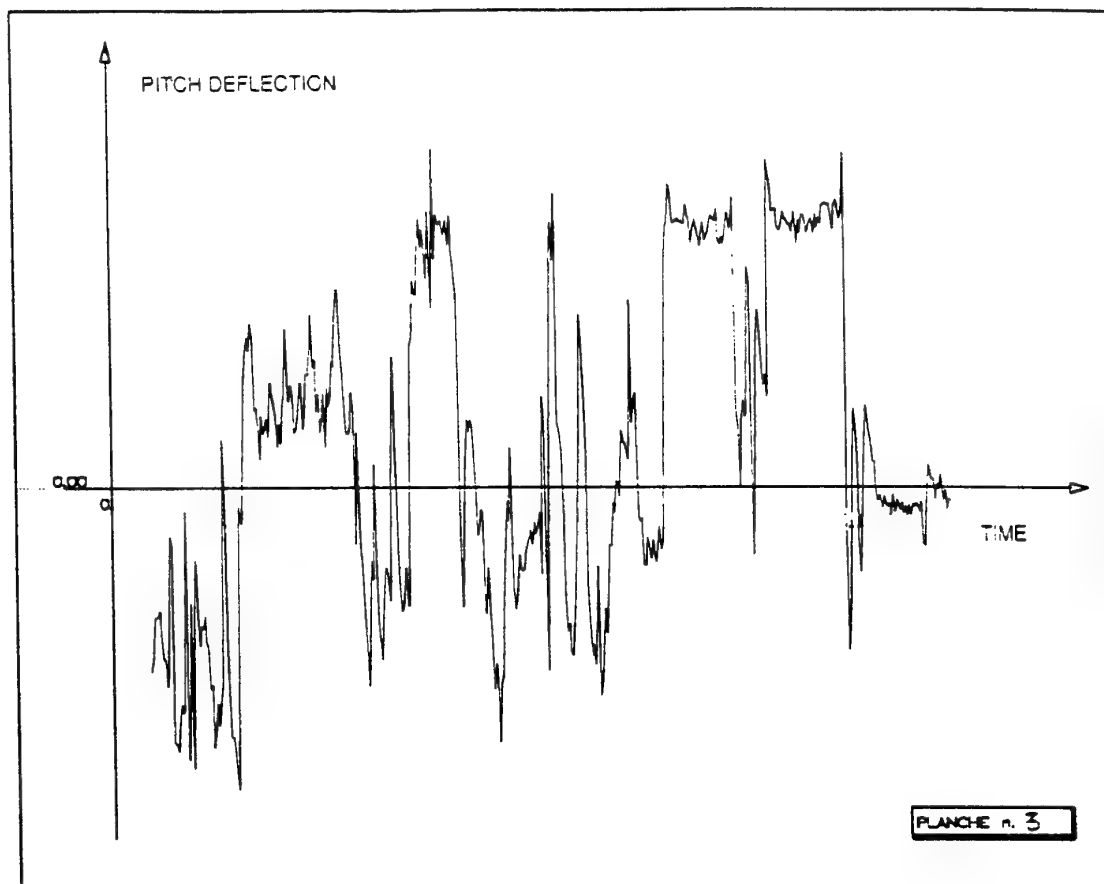
L'utilisation de données télémessurées provenant de références inertielles permet d'effectuer une estimation précise des forces aérodynamiques exercées sur un missile pendant un essai en vol.

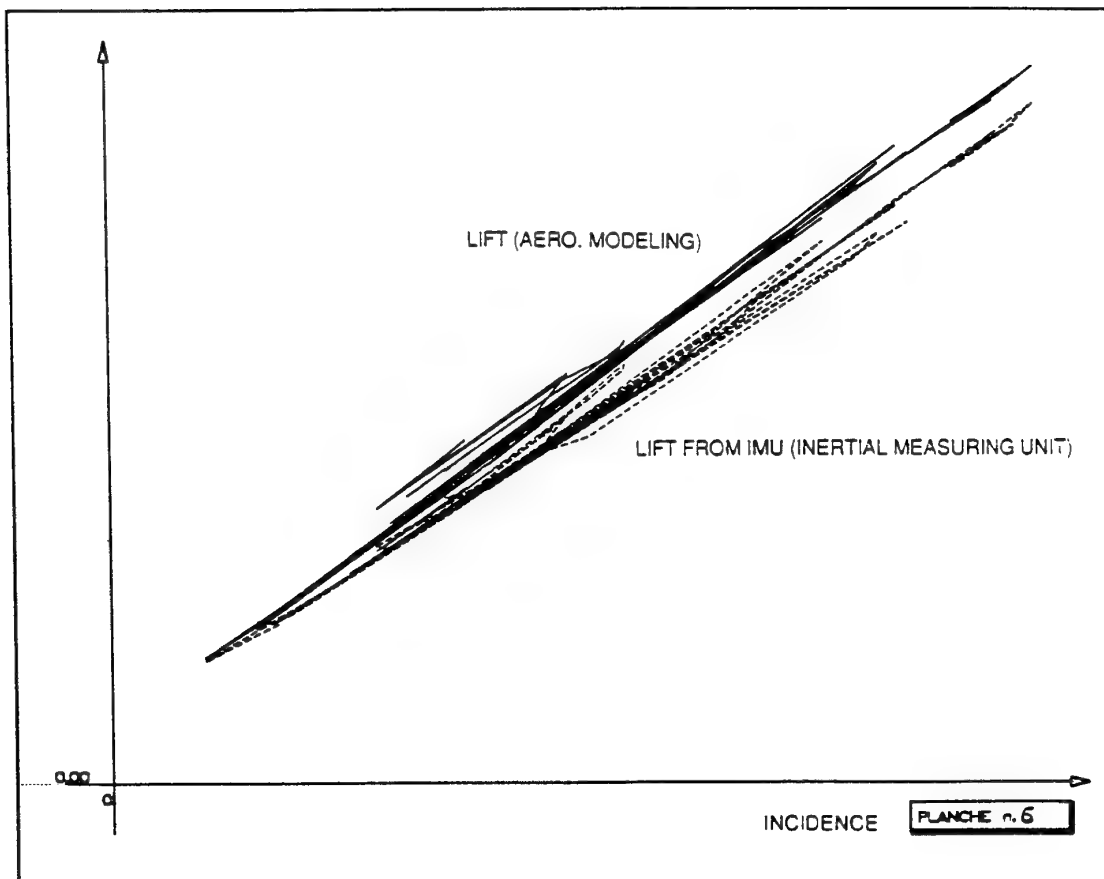
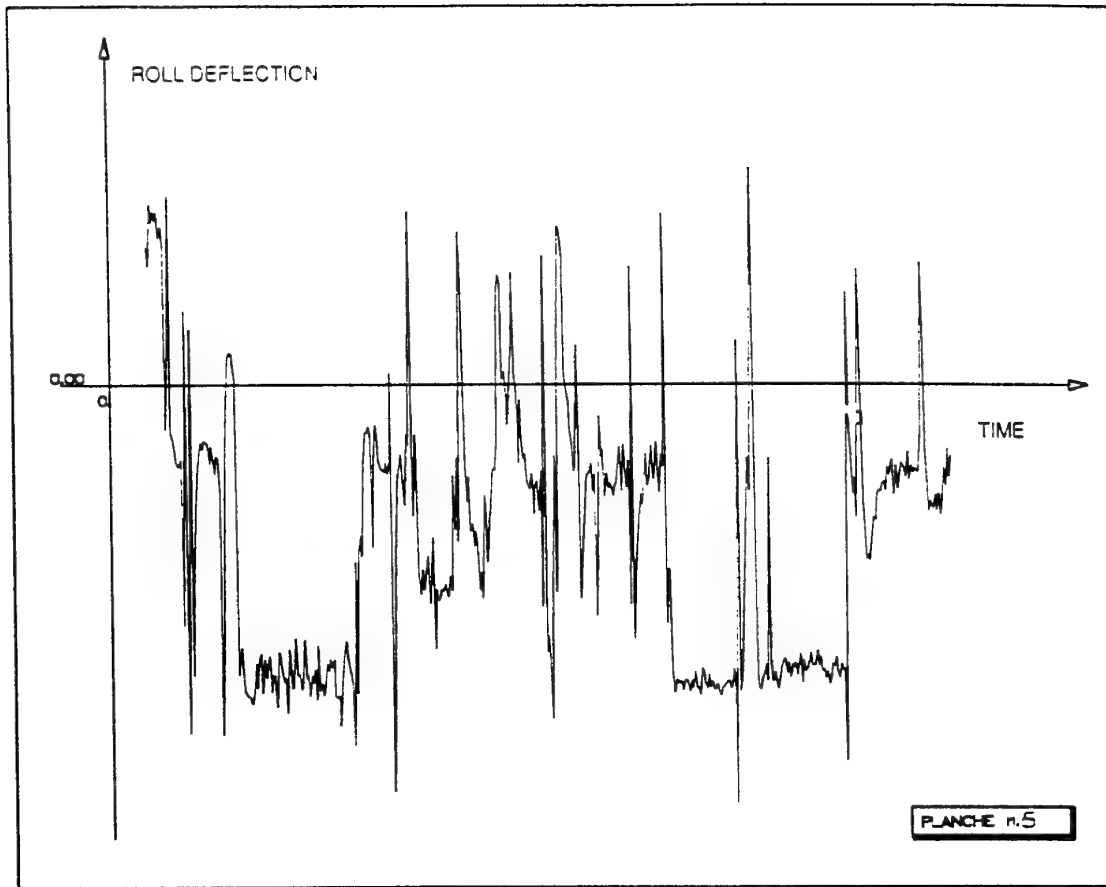
La qualité de la restitution, pour les missiles subsoniques en particulier, est améliorée par la présence d'une perche anémométrique et de sondes d'incidence et de dérapage.

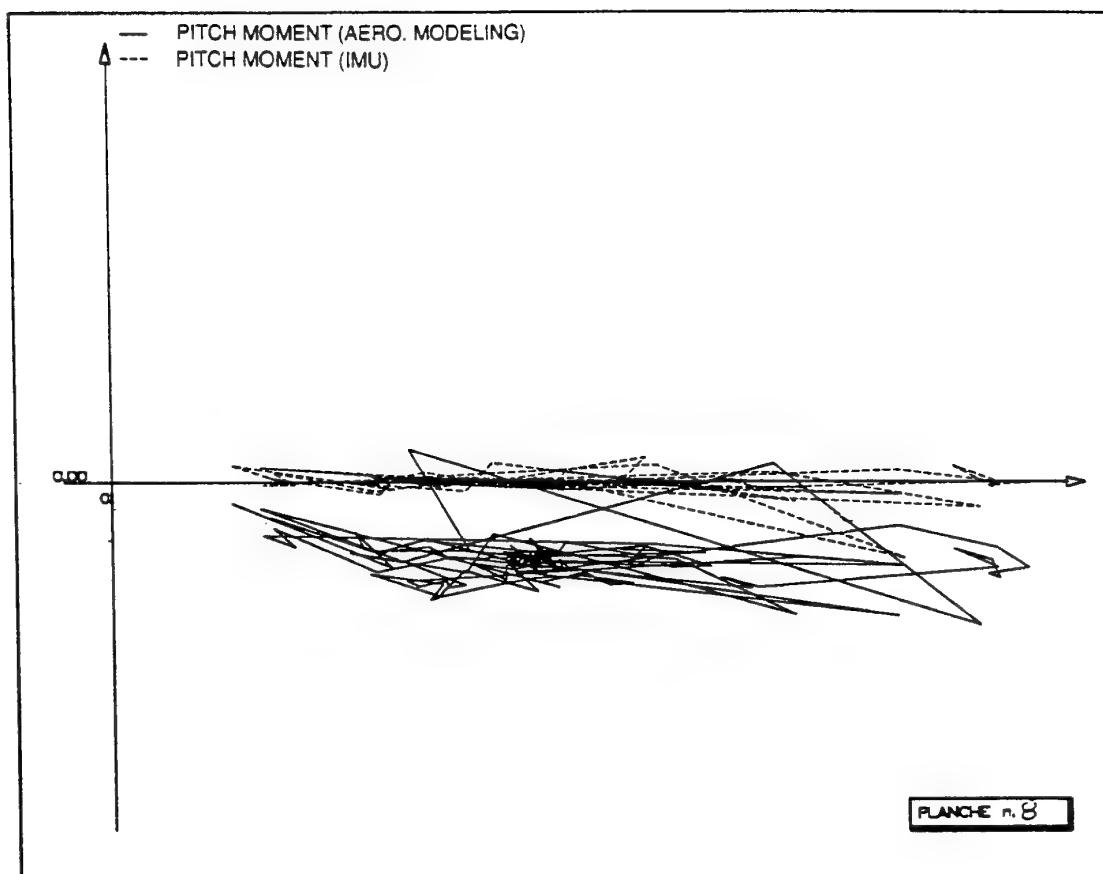
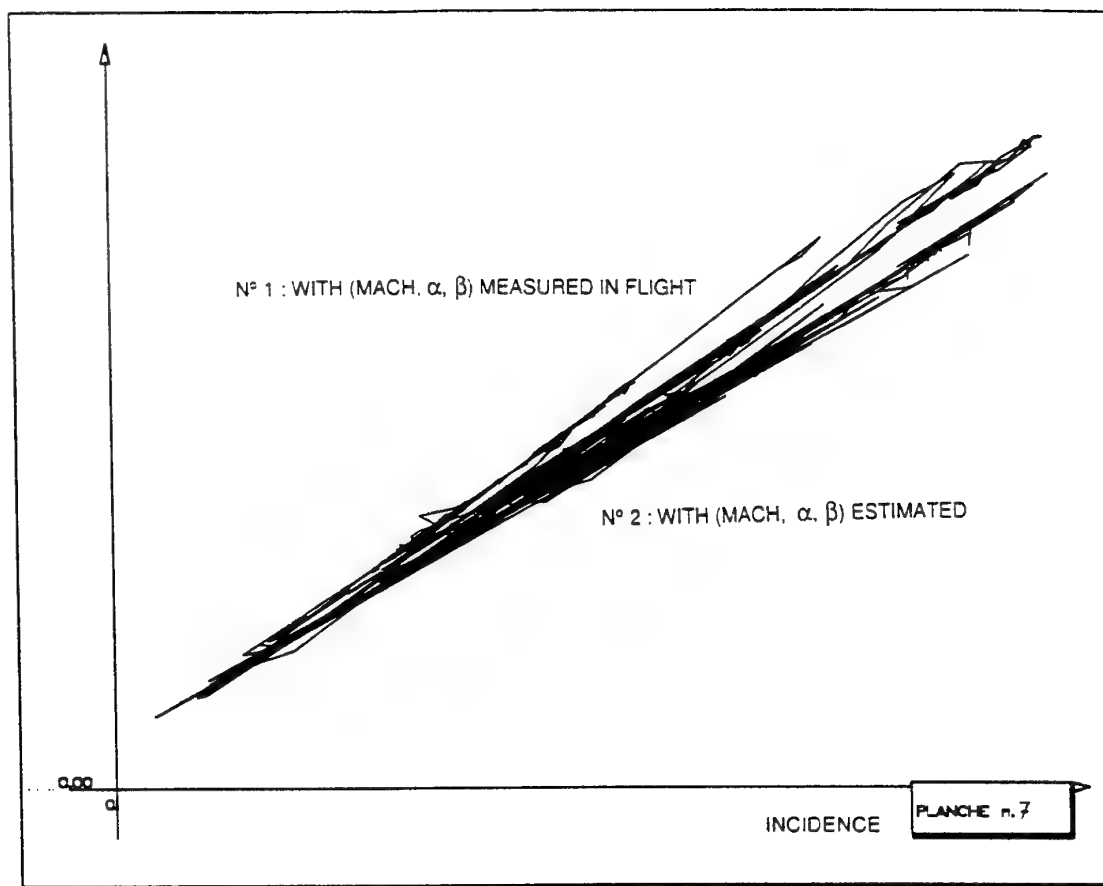
L'analyse pendant les phases transitoires est possible, en tenant compte de la position physique des capteurs dans le missile. Elle est affinée, dans le cas de missiles de croisière, avec les périodes de vol stabilisé.

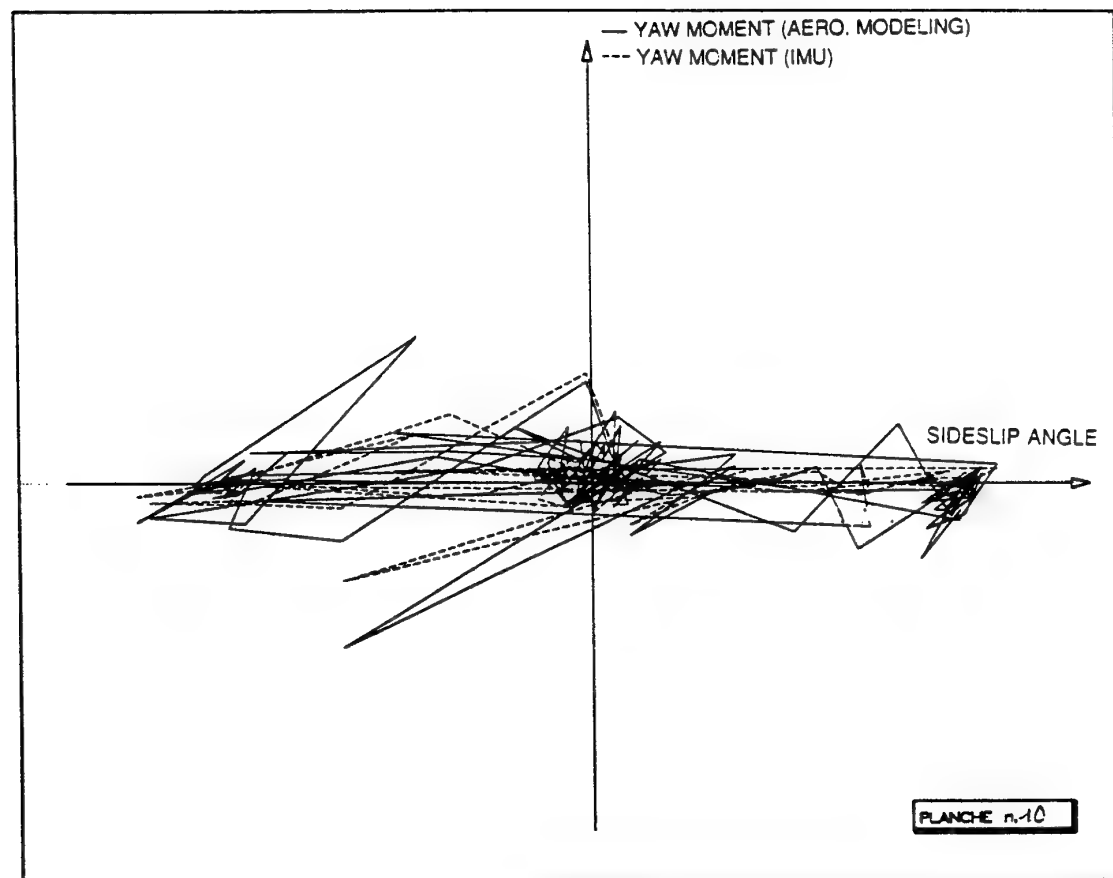
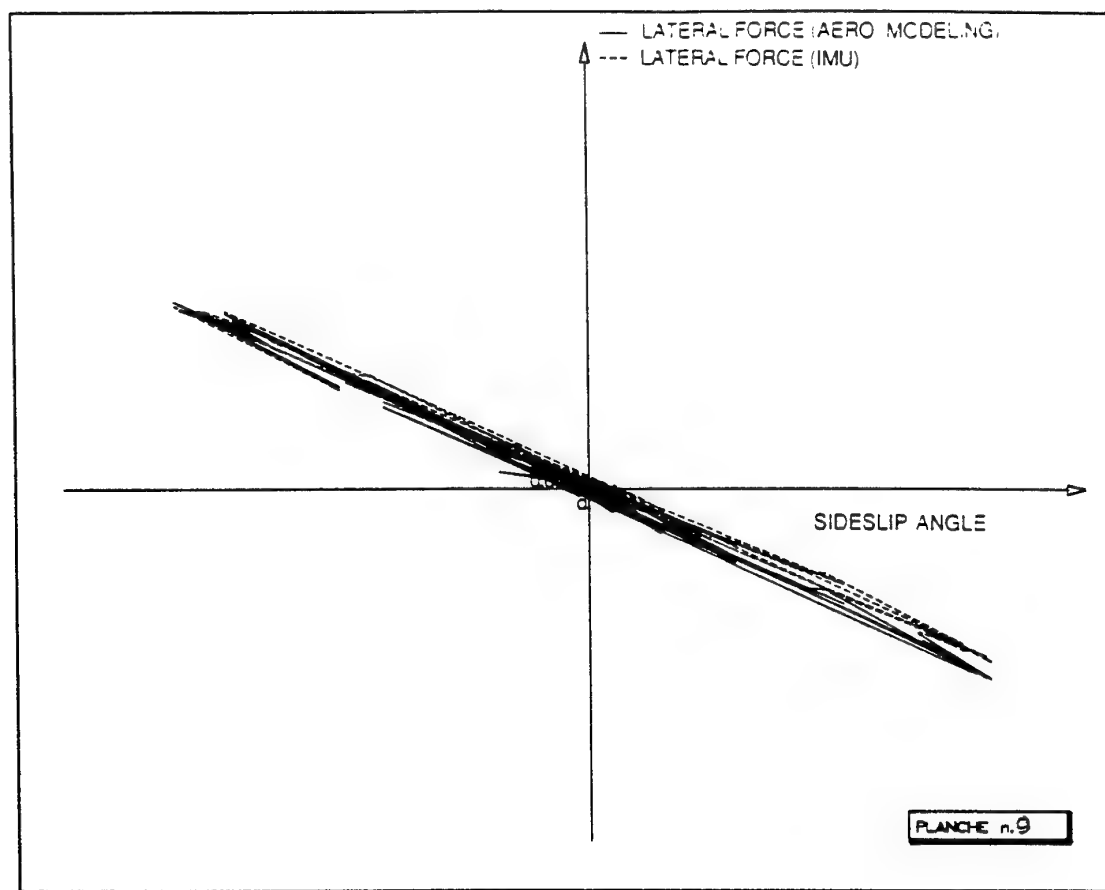
Dans le cas du missile Apache, l'analyse d'un essai en vol de durée importante a permis de constater que le modèle aérodynamique élaboré à partir des résultats de soufflerie était très proche des caractéristiques réelles, et de procéder aux ajustements mineurs nécessaires.

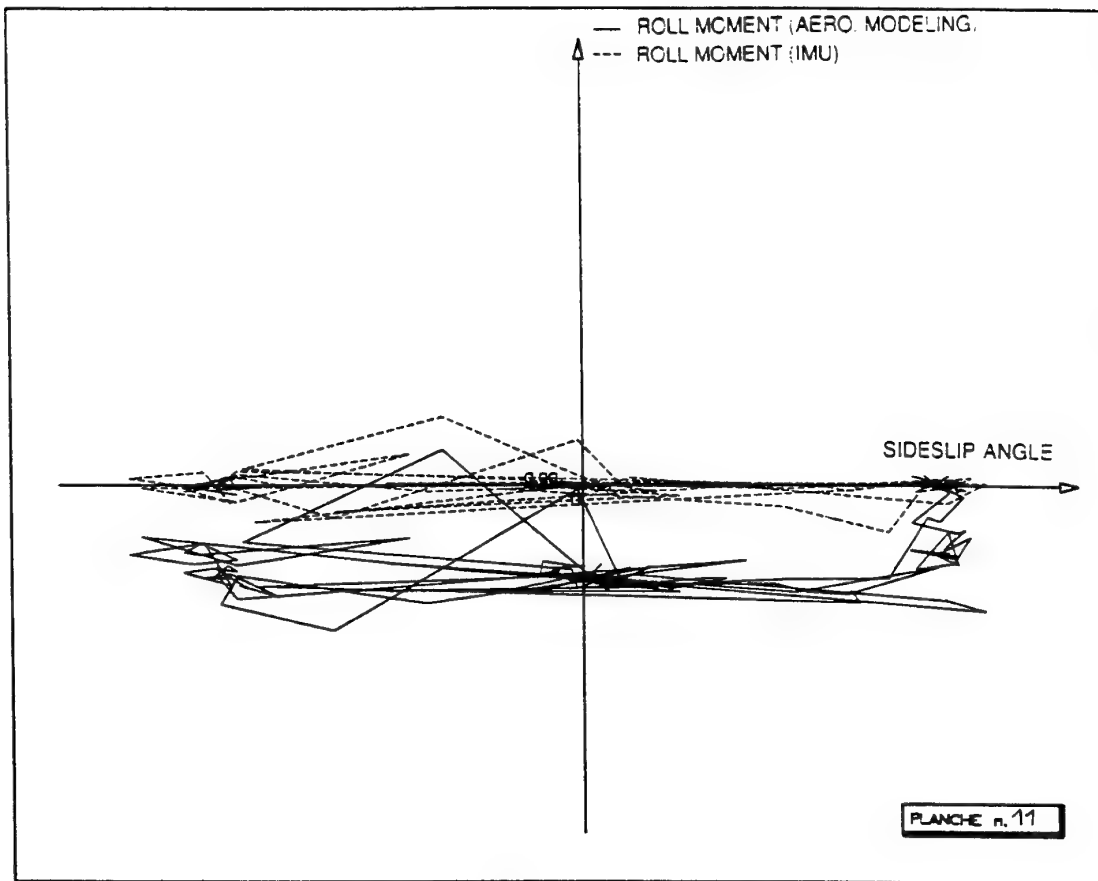












A NAVIGATION SYSTEM CONCEPT FOR A MODERN ANTI-SHIP MISSILE

Ø. Hoelsæter

B. Jalving

Division for Electronics

Norwegian Defence Research Establishment

P.O. Box 25, 2007 Kjeller, Norway

1 SUMMARY

A navigation system concept for a modern anti-ship missile has been investigated. The navigation system can be divided into several subsystems. At open sea altitude measurements are used in a Kalman filter to limit the inertial navigation system (INS) error propagation. Correspondingly, terrain contour matching (TERCOM) position updates are used when flying over land. A method for estimating the sea state and predicting extreme wave heights, which is useful in choosing sea skimming altitude, is also discussed. Finally, a model based compensator, which reduces the dynamic errors of the INS attitude references used for seeker stabilization, is described. The paper presents the theory of the various subsystems and how they are integrated. Results from tests with real data as well as simulations are presented.

2 INTRODUCTION

Norway has developed and produced several versions of the Penguin anti-ship missile. The Norwegian Defence Research Establishment (NDRE) and the Norwegian company NFT are currently developing a new missile based on new and advanced technology. The missile is intended for use on Fast Attack Crafts (FAC), frigates and in coastal missile batteries.

The missile will have a bank-to-turn (BTT) control strategy. It will be equipped with a turbojet engine enabling long range capability. Increased range means increased time of flight and thus stricter specifications for the navigation system. The new missile will have an infrared seeker, which by nature is relatively near sighted. Complicating matters further, the navigation system must be capable of dealing with the dynamics of a very agile missile.

The navigation system provides the guidance and control loops with estimates of missile position, velocity and orientation. The guidance system leads the missile to a preprogrammed point where it opens its imaging-IR seeker. Several factors influence the probability of the target appearing in the seeker field of view. A missile flying 100 km at high subsonic speed will have a time of flight of about 330 seconds. With no datalink allowing target data updates during the flight, the predicted target position uncertainty will easily become much larger than a typical navigation error. Designing a very accurate navigation system without being able to reduce the errors in the expected target position will thus be of little use and therefore not cost-effective.

The use of GPS in cruise missiles and smart bombs is increasing. A properly integrated GPS-INS system will give a position accuracy that far exceeds the requirements of a typical anti-ship missile. An advantage of this solution is that the INS-misalignment can be estimated using GPS-velocities, thus giving better conditions for the seeker unit. However, the missile will no longer be completely autonomous, and it might be vulnerable to jamming. Our objective has been to design a navigation system that is robust, autonomous and with a position uncertainty that does not severely affect the probability of the target appearing in the seeker field of view.

The Norwegian coastline is characterized by long fjords and numerous islands. This provides the opportunity of applying map-aided navigation methods and tactical route planning. The navigation system will consist of a modern inertial navigation

system, terrain contour matching (TERCOM) and shoreline detection. A laser altimeter provides the input to TERCOM and the shoreline detection system. During open sea flight, the inertial navigation system will be aided by the altitude measurement. This limits the navigation error.

Sea state estimation is employed because prediction of maximum wave height enables the missile to fly as close to the sea surface as possible and thus reducing the risk of being intercepted. The theory behind sea state estimation using a missile altimeter is discussed in fairly detail, since few publications on the matter exist.

The navigation system provides attitude references used for stabilizing of the seeker unit. Due to agile maneuvering, a model based compensator will be used to reduce the dynamic errors caused by time delays in the navigation system.

3 INERTIAL MEASUREMENT UNIT

In recent years optical gyros characterized by low cost, power and weight has become available. NDRE and NFT has tested several candidate inertial measurements units (IMU) intended for the tactical missile market. Both ring laser gyro and fiber optic gyro based systems have proven satisfactory performance. For tactical missiles, strapdown systems has replaced gimbal systems due to simpler structure, lower cost and higher reliability. Below the INS specifications assumed in the simulations are listed (all values are standard deviations or spectral densities in the case of white noises) :

Accelerometer bias :	$b_a = 200 \mu g$
Accelerometer scale factor error :	$\tau_a = 0.02 \%$
Accelerometer coloured noise :	$\delta f = 50 \mu g$
Accelerometer white noise :	$v_a = 50 \mu g / \sqrt{Hz}$
Acc. noise corr. time :	$T_f = 60 s$
Gyro bias :	$b_g = 1 \text{ } ^\circ/h$
Gyro coloured noise :	$\delta \omega = 0.35 \text{ } ^\circ/h$
Gyro noise corr. time :	$T_w = 100 s$
Gyro white noise :	$v_g = 0.07 \text{ } ^\circ/h / \sqrt{Hz}$
Gyro scale factor error :	$\tau_g = 0.02 \%$
Initial misalignment	$\epsilon_N = \epsilon_E = 0.3 \text{ mrad}$
	$\epsilon_D = 3 \text{ mrad}$

4 REDUCING NAVIGATION ERRORS AT OPEN SEA

In order to reduce the position uncertainty we have to concentrate on the most important error sources, for instance misalignment in the horizontal plane. In the alignment phase prior to the flight, the misalignments, ϵ_N, ϵ_E and ϵ_D , will be estimated to a relatively accurate level. During the flight the misalignments will however increase due to gyro drift. Misalignment cause the accelerometer measurements in the IMU coordinate system to be wrongly transformed to the navigation coordinate system, hence giving rise to position errors. In a situation where the missile is flying straight and level, ϵ_D does not contribute to increased velocity errors because there are no acceleration in the horizontal plane. In the launch phase, the accelerations will be transformed incorrectly giving an initial

velocity error. This launch-phase generated velocity error will propagate during the entire flight. If we assume the missile to fly in a north direction, the east position error due to ϵ_D will be:

$$\delta p_E(\epsilon_D, t) \approx \epsilon_D \cdot v_m \cdot t \quad (1)$$

where v_m is the inertial missile velocity.

Misalignment in the horizontal plane give rise to position errors in the same plane, because the 1g acceleration measurement is incorrectly transformed to the navigation coordinate system. Thus, the position errors due to horizontal plane misalignment can be written:

$$\delta p_N(\epsilon_E, t) = \frac{1}{2} \cdot g \cdot \sin(\epsilon_E) \cdot t^2 \quad (2)$$

$$\delta p_E(\epsilon_N, t) = \frac{1}{2} \cdot g \cdot \sin(\epsilon_N) \cdot t^2 \quad (3)$$

where g is the acceleration of gravity

Because of the t^2 dependency, it is important to reduce the misalignment for long flight distances. Because of gyro bias and gyro random walk the variance of the misalignments increase during the flight. In a situation where the sensitive axis of the x and y-gyros coincide with the north and east axis, the position error due to gyro bias can be written :

$$\delta p_E(b_{gx}, t) = \frac{1}{6} \cdot g \cdot b_{gx} \cdot t^3 \quad (4)$$

$$\delta p_N(b_{gy}, t) = \frac{1}{6} \cdot g \cdot b_{gy} \cdot t^3 \quad (5)$$

where b_{gx} and b_{gy} are biases in the x and y-gyro.

If the missile is maneuvering in the horizontal plane, the misalignments ϵ_N and ϵ_E will cause a component of the horizontal acceleration to be measured as a vertical acceleration. After integration, this will show up as an INS-altitude error. The vertical position error due to the misalignment can be expressed as

$$\delta p_D = \int_0^t \int_0^t a_h \sin(\epsilon) dt dt = \frac{1}{2} a_h \sin(\epsilon) \cdot t^2 \quad (6)$$

where a_h is a constant acceleration in the horizontal plane and ϵ is the misalignment about an axis in the horizontal plane being perpendicular to the acceleration. Figure 1 gives an example of the INS altitude error during and after the launch phase and a 90° turn.

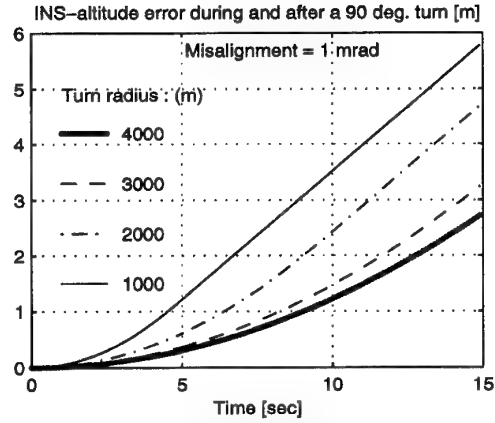
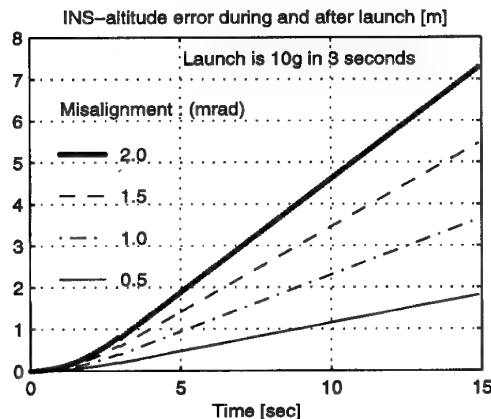


Figure 1 INS altitude error due to misalignment and accelerations

The misalignment about an axis being perpendicular to the acceleration is observable through altitude measurements. After a maneuver in the horizontal plane, the difference between the INS-altitude and measurements from either a laser- or radar altimeter can be used in a Kalman filter for estimation of the misalignments. This is of course only possible when flying over the sea. Over land, the missile altitude can not be measured exactly enough due to uncertainties in the map and missile position.

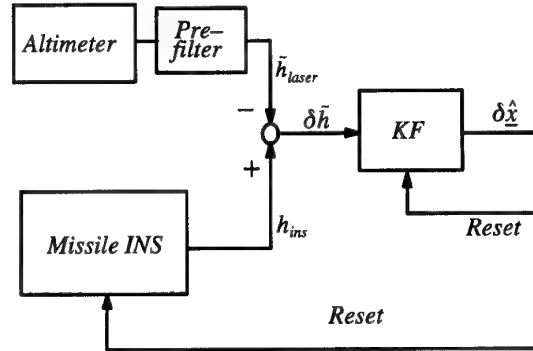


Figure 2 The altimeter will be integrated with the INS using a Kalman filter

The INS errors was modelled in state-space form as :

$$\delta \dot{\underline{x}} = A \delta \underline{x} + C \underline{v} \quad (7)$$

where $\delta \underline{x}$ represents the error states in the INS, and \underline{v} is white noise. The model consists of 27 states. Among the states are position and velocity errors, misalignment and different types of sensor errors (e.g gyro bias and angular random walk). The most important parameters and their standard deviations for a relevant INS are listed in Section 2. The error equations for a strapdown INS can be found in e.g [1]. In our simulations, the Kalman filter used the same model as in (7), which means that it is an optimal filter. The results are therefore the best obtainable. The process model used in the Kalman filter can be written :

$$\delta \dot{\underline{x}} = A \delta \underline{x} + C \underline{v} \quad (8)$$

This Kalman filter will be denoted *the navigation filter*.

The measurement used in the filter was modelled as :

$$y = \delta \tilde{h} = \delta h + v = \tilde{h}_{laser} - h_{ins} \quad (9)$$

where δh is the true altitude error and v is measurement noise. The measurement was lowpass filtered in order to reduce the influence of wave noise. This is described in Section 5. The

measurement noise will have a relatively complex nature, being influenced by the altimeter, the seastate and the lowpass filter.

In the Kalman filter used in our simulations the measurement noise was approximated as being white noise with spectral density

$$V = 2\sigma_n^2 T_n \quad (10)$$

where $T_n = \frac{1}{f_c}$, f_c is the low pass filter cut-off frequency, and σ_n is the approximate standard deviation of the noise. We have assumed the use of a laser altimeter being developed at NDRE. If this altimeter is not stabilized in pitch and roll, the reflections from the sea will be weak if the pointing angle exceeds about 10° . The reflected signal strength is however a function of the sea state. We have assumed the measurements to be invalid during turns where the pointing angle exceeds 10° . When the measurements during turns are considered invalid, only the prediction part of the KF equations is computed.

Flight paths over open sea are often characterized by long straight lines. This of course, gives no acceleration in the horizontal plane. The missile therefore has to perform a few extra maneuvers to make the misalignments observable. A bank-to-turn missile will have a roll angle:

$$\phi = \text{atan}\left(\frac{a_h}{a_v + g}\right) \quad (11)$$

where a_h and a_v are accelerations in horizontal and vertical directions respectively. The required acceleration levels mean that altitude measurements can only be expected before and after a turn. This implies that turns should be separated with straight lines to enable measurements. Another aspect is that angular velocities excites scale factor errors in the gyros. A bank-to-turn missile performing e.g. a zigzag maneuver will have positive and negative angular velocities in roll, with zero mean. An asymmetric scale factor error in the x-gyro will contribute to roll misalignment in this case. The y-gyro will, however, measure an angular velocity with nonzero mean. This means that even a symmetric scale factor error in the y-gyro will contribute to pitch-misalignment. In the flight path design there must then be a tradeoff between being able to estimate the misalignment and avoiding excitation of other error sources.

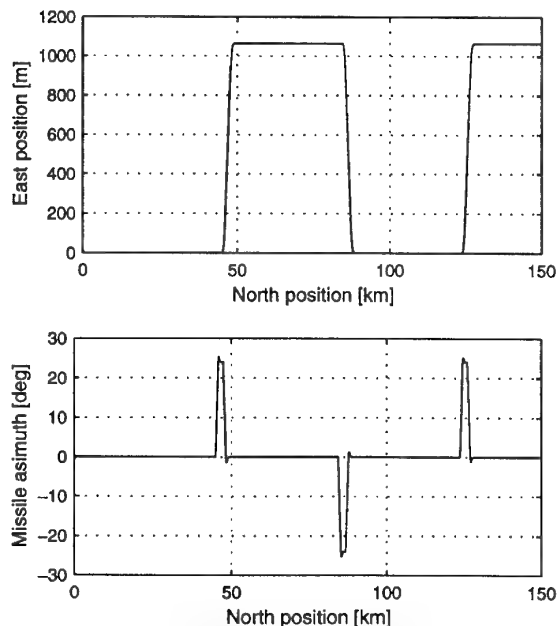


Figure 3 Trajectory used for estimating misalignments in the horizontal plane

The flight path in figure 3 is an example of a simple but effective way of flying. The acceleration levels during the turns reaches about 40 m/s^2 . The deviation from the nominal path is relatively small and the time of flight is only slightly increased compared with a straight trajectory. The maneuvers does not start too early as there is little to gain when the misalignments are small. If the alignments are expected to be poor at launch time, the maneuver could start earlier. The optimum trajectory will of course be a function of the quality of the INS (e.g. scale factor errors and gyro drift), the missile dynamics and the sea state. The sea state applied in the simulation and the low pass filtering of the altimeter measurements are discussed in Section 5.

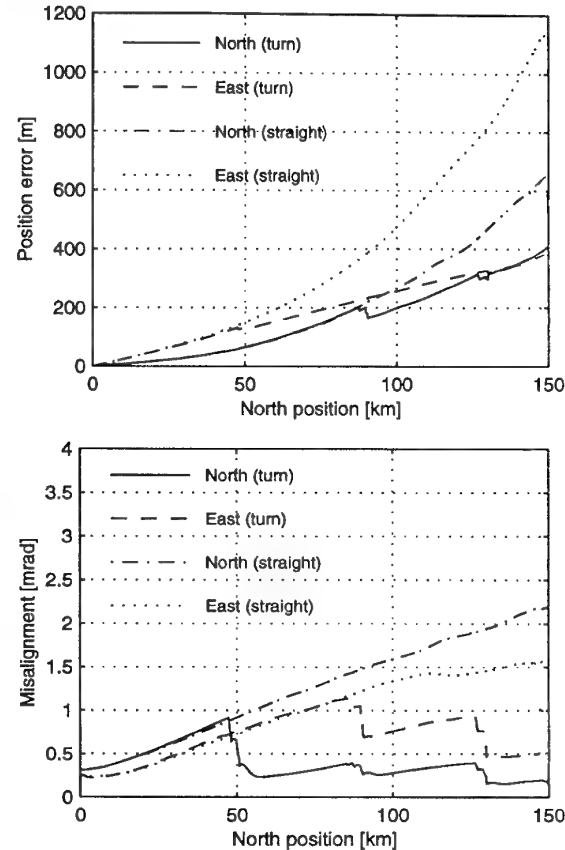


Figure 4 Comparison of the INS errors when flying straight and curved trajectories.

From figure 4 it can be seen that the position errors are reduced by about 60% in the east direction when a curved trajectory is compared to a straight trajectory. It should however be noted that the improvement is a function of the altimeter measurement noise and thus the sea state.

5 SEA STATE ESTIMATION

The main reason for employing sea state estimation is that prediction of maximum wave height enables the missile to fly as close to the sea surface as possible and thus reducing the risk of being intercepted. Secondly, model based filtering of the altimeter will reduce the measurement noise to a certain extent which is beneficial to the navigation filter described in the preceding Section.

5.1 Statistical description of sea waves

Sea waves are highly irregular and nonrepeatable in time and space. The energy transferred from winds to the surface spreads in space, and hence the waves propagate in different directions, although the predominant wave energy moves in the same direction as the wind. Waves which are called swell often travel from neighboring generating areas and are superimposed

on the local waves. The resulting wave configuration is complicated. Hence, waves should be characterized by a probabilistic approach.

There exist a comprehensive literature on waves. Most of it focus on marine applications. The wave theory presented in this paper is mainly drawn from [2,3,4].

Linear theory is usually used to represent wind generated waves. The wave elevation of a long-crested sea propagating along the positive x -axis can be written as the sum of a large number of wave components, i.e.

$$\zeta(t, x) = \sum_{j=1}^N A_j \sin(\omega_j t - k_j x + \epsilon_j) \quad (12)$$

Here A_j , ω_j , k_j and ϵ_j mean respectively the wave amplitude, circular frequency, wave number and random phase angle of wave component number j . The random phase angles are uniformly distributed between 0 and 2π and time invariant. For deep waters ω_j and k_j are related by the dispersion relationship $k_j = \omega_j^2/g$, where g is the acceleration of gravity. The wave amplitude A_j of wave component j is related to the wave spectral density function $S(\omega_j)$ as

$$A_j^2 = 2S(\omega_j)\Delta\omega \quad (13)$$

where $\Delta\omega$ is a constant difference between successive frequencies. Expression (12) repeats itself after a time $2\pi/\Delta\omega$. For simulation purposes this problem is circumvented by choosing ω_j at random in the frequency interval $\Delta\omega$.

The different wave spectra can be classified by their wave spectrum moments

$$m_k = \int_0^\infty \omega^k S(\omega) d\omega \quad (14)$$

The instantaneous wave elevation is Gaussian distributed with zero mean and variance $\sigma^2 = m_0$. The mean wave period is defined as

$$T_1 = 2\pi \frac{m_0}{m_1} \quad (15)$$

while the average zero-crossing period is given by

$$T_2 = 2\pi \sqrt{\frac{m_0}{m_2}} \quad (16)$$

The significant wave height H_s is a statistical parameter defined as the average of the highest one-third of the wave heights. It is widely used to represent the severity of a sea. By assuming the wave height Rayleigh distributed, it can be shown that

$$H_s = 4.01 \sqrt{m_0} \quad (17)$$

5.1.1 Standard Wave Spectra

The wave spectrum can be estimated from wave measurements since the random wave process can be assumed stationary for a time period ranging from 0.5 hour to 10 hours, by far exceeding the duration of a missile flight. However, a long range missile may fly into several sea states, especially in coastal waters.

Several wave spectral formulations have been proposed in the literature. For open sea conditions, for instance, the 15th ITTC (International Towing Tank Conference) recommended the use of the ISSC (International Ship and Offshore Structures Congress) spectral formulation for a fully developed sea, refer to [5] for details.

The spectrum used in the simulations presented in Figure 4 is the JONSWAP spectrum, which is based upon an extensive measurement program in the North Sea. It was adopted as an ITTC standard by the 17th ITTC, [6]. The JONSWAP spectrum

is used to describe non-fully developed sea, hence the spectral density will be more peaked than for those of the fully developed spectra. The spectrum is of the form

$$S(\omega) = A\omega^{-5} \exp(-B\omega^{-4})\gamma^Y \quad (18)$$

where

$$A = \frac{155H_s^2}{T_1^4} \quad B = \frac{944}{T_1^4} \quad (19)$$

In [7] it is suggested that $\gamma = 3.3$ and

$$Y = \exp\left(-\left(\frac{0.191\omega T_1 - 1}{\sqrt{2}\sigma}\right)^2\right) \quad (20)$$

where

$$\sigma = \begin{cases} 0.07 & \text{for } \omega \leq 5.24/T_1 \\ 0.09 & \text{for } \omega > 5.24/T_1 \end{cases} \quad (21)$$

This formulation can be used with other characteristic periods by substituting

$$T_1 = 0.834T_0 = 1.073T_2 \quad (22)$$

T_0 is also referred to as the modal period.

The wave frequency ω_e observed by an altimeter mounted to a missile flying with forward speed U is given by

$$\omega_e = \omega_0 + \frac{\omega_0^2}{g} U \cos \beta \quad (23)$$

where β is the direction of the waves relative to the missile's velocity vector.

5.2 Linear Approximations to the Wave Spectra

5.2.1 2nd-order transfer function approximation

The wave model in (12) is far too comprehensive to be used in a sea state estimator. For the linear system

$$\zeta(s) = h(s)\eta(s) \quad (24)$$

where $\eta(s)$ is a zero-mean Gaussian white noise process with power spectrum $P_\eta(\omega) = 1.0$ and $h(s)$ is a transfer function, the power spectral density function of $\zeta(s)$ is given by

$$P_{\zeta\zeta}(\omega) = |h(j\omega)|^2 P_\eta(\omega) = |h(j\omega)|^2 \quad (25)$$

Linear wave model approximations has been reported in the literature, for instance [8,9]. The transfer function

$$h(s) = \frac{C_2 s}{s^2 + 2\zeta s + \omega_e^2} \quad (26)$$

has the corresponding power spectral density function

$$P_{\zeta\zeta}(\omega) = \frac{C_2^2 \omega^2}{(\omega_e^2 - \omega^2)^2 + 4\zeta^2 \omega^2} \quad (27)$$

where C_2 is a constant describing the wave intensity and ζ is a damping coefficient. (26) and (27) differ slightly from the models found in literature by the fact that the variance and the significant wave height do not vary with ω_e . That is essential in order to arrive at a model valid for all wave directions and missile speeds.

Reasonable values for C_2 and ζ can be found by letting the power spectrum of the linear model approximate $S(\omega)$ of the JONSWAP spectrum. This is done by minimization of

$$J = \int_0^\infty (P_{\zeta\zeta}(\omega) - S(\omega))^2 d\omega \quad (28)$$

Figure 5 shows how the linear wave spectrum approximates the JONSWAP spectrum for $H_s = 3.5$ m and $T_0 = 7.7$ s.

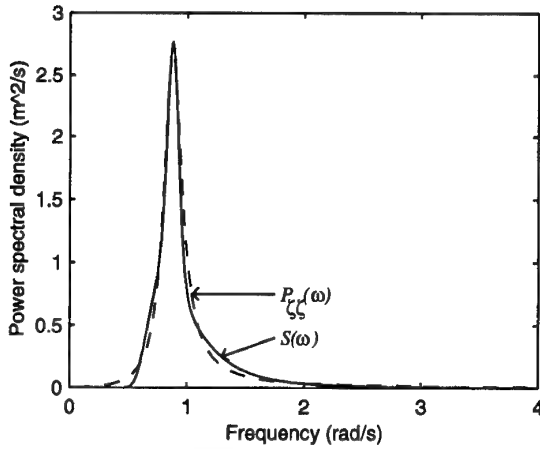


Figure 5 JONSWAP spectrum and 2nd-order linear approximation.

5.2.2 State-Space Model

Since the frequency of encounter, ω_e , is a function of missile speed, missile course, wave direction and wave frequency as shown in (23), ω_e used in (26) must be estimated. Relatively complex models for the rate of change in ω_e including the missile speed, wave direction and missile heading can be derived, however, simulations revealed that the complex models did not have superior performance to the simple model

$$\dot{\omega}_e = C_3 \eta \quad (29)$$

when used in a Kalman filter.

The laser altimeter measurement is modeled as

$$y = \hat{h} + \delta h + \zeta + v \quad (30)$$

where \hat{h} is the INS height, δh is the INS height error, ζ is the wave height and v is altimeter measurement error modelled as white noise. The navigation filter estimates δh well. The δh estimation process in the sea state filter is modelled as a first order markov process with a time constant $T_{\delta h}$ roughly corresponding to the δh settling time. $T_{\delta h}$ should be sufficiently large to prevent δh from picking up some of the wave motion.

A second order linear state space model can be obtained from (26). Combining this with the models for ω_e and δh , we get the nonlinear model

$$\begin{bmatrix} \dot{x}_1 \\ \dot{x}_2 \\ \dot{\omega}_e \\ \dot{\delta h} \end{bmatrix} = \begin{bmatrix} 0 & \hat{\omega}_e & 0 & 0 \\ -\hat{\omega}_e & -2\zeta & 0 & 0 \\ 0 & 0 & 0 & 0 \\ 0 & 0 & 0 & -\frac{1}{T_{\delta h}} \end{bmatrix} \begin{bmatrix} x_1 \\ x_2 \\ \omega_e \\ \delta h \end{bmatrix} + \begin{bmatrix} 0 \\ C_2 \\ C_3 \\ C_4 \end{bmatrix} \eta \quad (31)$$

where $x_2 = \hat{\zeta}$. This model was used in a continuous-discrete extended Kalman filter, [10].

5.3 Prediction of wave height

5.3.1 Estimation of wave variance

The accuracy of the wave height prediction is dependent upon a good estimate of $m_0 = \text{var}(\zeta)$, refer to (14). An estimate of m_0 can be calculated in real time by using the recursive formula

$$\hat{m}_{0,i} = \hat{m}_{0,i-1} \frac{i-1}{i} + \frac{x_{2,i}^2}{i} \quad (32)$$

The accuracy of the estimate improves with time. Generally, 20–30 seconds of flight time is required before the estimate settles properly. Instead of using the estimated wave height x_2

in (32) one could simply use $\tilde{y} - \hat{h}$ where \tilde{y} is the laser altimeter measurement and \hat{h} is the INS height. Simulations indicate less accurate estimates with this solution due to noisy and biased measurements.

A long range missile in coastal waters may experience considerable changes in the severity of the sea state. Thus, when calculating \hat{m}_0 one should put most emphasis on the most recent measurements. This can be achieved by either low pass filtering \hat{m}_0 or introducing some kind of moving average in which (32) is reset at specified intervals or after certain incidents.

5.3.2 Prediction of extreme waves

The theory presented in this Section is mainly based upon [2]. Waves are considered to be an ergodic Gaussian process with zero mean. Furthermore the wave spectra are assumed narrow banded and the wave peaks statistically independent. Given these assumptions it can be derived theoretically that the wave height, h , is Rayleigh distributed:

$$f(h) = \frac{h}{4m_0} e^{-h^2/8m_0} \quad (33)$$

The distribution shown in Figure 6, has a peak value for

$h = 2\sqrt{m_0}$. The wave amplitude, which limits the lowest possible missile altitude, is assumed to be half the wave height. The expression for the significant wave height H_s in (17) is derived using (33). The cumulative distribution function is given by

$$F(h) = P(H \leq h) = 1 - e^{-h^2/8m_0} \quad (34)$$

The validity of using the Rayleigh distribution in predicting wave heights is thoroughly discussed in [2]. It is concluded that the results based upon the Rayleigh distribution yields acceptable accuracy. In fact, the effect of the narrow-band spectrum assumption can be ignored as far as the estimation of the extreme wave height is concerned.

The objective is to estimate the largest wave height that is likely to occur in n wave height observations. The extreme wave height in n observations, denoted Y_n is a random variable and has its own probability density function

$$g(y_n) = n[f(h)[F(h)]^{n-1}]_{h=y_n} \quad (35)$$

while the cumulative distribution function is

$$G(y_n) = [F(h)^n]_{h=y_n} \quad (36)$$

The probability density functions for $f(h)$ and $g(y_n)$ for $H_s = 3.5$ m are shown in Figure 6.

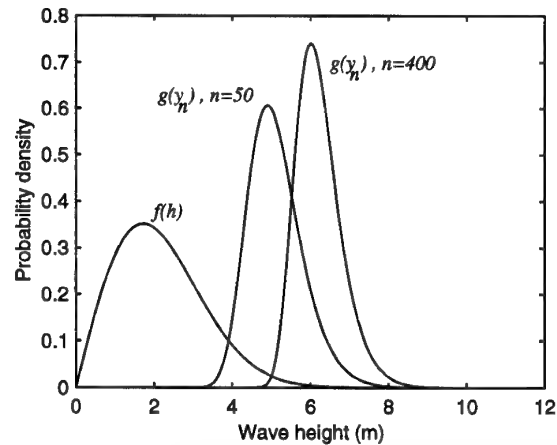


Figure 6 The wave probability density function $f(h)$ and the extreme value probability function $g(y_n)$ for $n = 50$ and $n = 400$.

From (33) and (35) the most probable extreme wave height to occur in n observations can be deduced

$$\bar{y}_n = 2\sqrt{2\ln n}\sqrt{m_0} \quad (37)$$

\bar{y}_n is the value for which $g(y_n)$ has its peak. For a missile flight it is more meaningful to express the extreme wave height in terms of remaining time of flight than as a function of the number of wave height observations. If one assumes constant wave direction relative to the missile, we have

$$n = \frac{t_f}{T_{2,e}} = \frac{t_f}{2\pi} \sqrt{\frac{m_2}{m_0}} \quad (38)$$

where t_f is time of flight and $T_{2,e}$ is the zero-crossing wave period observed by the missile altimeter. To account for possible changes in wave directions and thus observed zero-crossing period, the right side of (38) may be multiplied by an "uncertainty" parameter $\gamma > 1$.

The probability of $y_n < \xi_{\max}$ can be found by solving

$$\int_0^{\xi_{\max}} g(y_n) dy_n = [F(\xi_{\max})]^n = 1 - \alpha \quad (39)$$

where α can be interpreted as a risk parameter. In [2] ξ_{\max} as a function of α is derived

$$\xi_{\max} = 2\sqrt{2\ln\left(\frac{n}{\alpha}\right)}\sqrt{m_0} = 2\left[2\ln\left(\frac{t_f}{2\pi\alpha}\sqrt{\frac{m_2}{m_0}}\right)\right]^{1/2}\sqrt{m_0} \quad (40)$$

In Figure 7 the extreme wave amplitude $A_{\max} = \xi_{\max}/2$ for varying α and remaining time of flight t_f is plotted. The risk parameter α should be chosen weighting the probability of hitting a wave against the probability of being intercepted at a certain altitude.

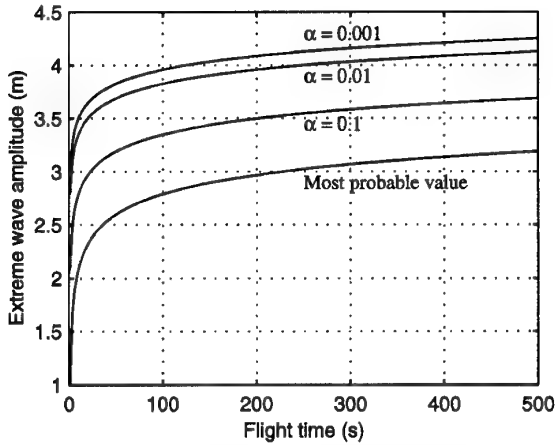


Figure 7 Extreme wave amplitude as a function of the probability α of being exceeded and the most probable extreme wave height. $H_s = 3.5$ m, $T_{2,e} = 0.54$ s, $\beta = 60^\circ$.

5.4 Integration with the navigation filter

5.4.1 Integration considerations

The estimated height \hat{y} from the sea state filter is low-pass filtered and sent to the navigation filter described in Section 4. The second order butterworth low-pass filter has a cut-off frequency of 0.5 Hz. The choice of cut-off frequency is based on anti-aliasing considerations. A lower cut-off frequency would establish δh more accurate by averaging out measurement and wave noise. However, additional phase lag on the measurement cause stability problems in the navigation filter.

The navigation filter in Section 4 utilizes information about δh for the estimation of INS error sources. Hence, it may seem

natural to use $\delta \hat{h}$ from the sea state filter as a navigation filter measurement. However, simulations revealed that this strategy suffered from instability.

Instead of applying the estimated height from the sea state filter as input to the navigation filter one could simply use the raw altitude measurement. This solution is more vulnerable to measurement noise and occasional altimeter anomaly (wild points). Model based filtering is generally superior to other methods with regard to robustness and performance.

5.4.2 Simulation results

The sea state chosen for the simulations presented in this paper was characterized by

$$H_s = 3.5 \text{ m} \quad T_0 = 7.7 \text{ s} \quad (41)$$

According to [11,12] this is a likely sea state in the Norwegian sea in winter time. The performance of the navigation filter degrades slightly with increased sea state. Correspondingly, the variance of the sea state filter innovation process increases with the significant wave height. However, extensive simulations has shown robust and good performance for the whole range of possible sea states.

For the simulations shown in Figure 4 the wave direction was assumed to be 60° . This implies a frequency of encounter $\omega_e = 11.0$ rad/s. For comparison, head sea would have implied $\omega_e = 21.2$ rad/s. Due to the low-pass filtering of the estimated measurement, the higher frequency of encounter the better performance of the navigation filter because the mean missile height is more rapidly established.

5.5 Sea state filter simulation results

5.5.1 Results from real data

The sea state filter has postprocessed height data obtained from the NDEA candidate laser altimeter when flown over sea. Figure 8 shows the altimeter wave measurement and the estimated wave height of the Kalman filter.

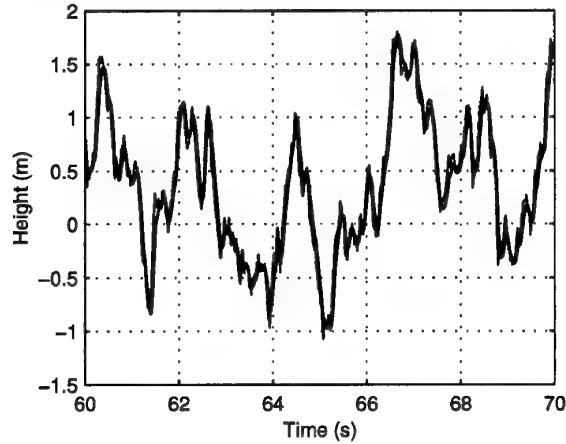


Figure 8 Raw altimeter measurements (thin line) and predicted height (thick line) from the sea state filter.

5.5.2 Simulation example

In Figure 9 the results from a simulation example is presented. Altimeter measurements were generated using (12), (23) and a simple missile model. The Kalman filter model is given by (30) and (31). During missile turns there are no measurements available, as can clearly be seen on the innovation process. After a turn the wave direction relative to the missile's velocity vector and thus the observed wave frequency changes. In the figure the estimated frequency of encounter $\hat{\omega}_e$ is shown. The estimate is held constant when there are no measurements. After a turn the INS height error is changed in steps. The filter succeeds in estimating δh . When the sea state filter is inte-

grated with the navigation filter, $\hat{\delta h}$ follows δh as δh approaches zero.

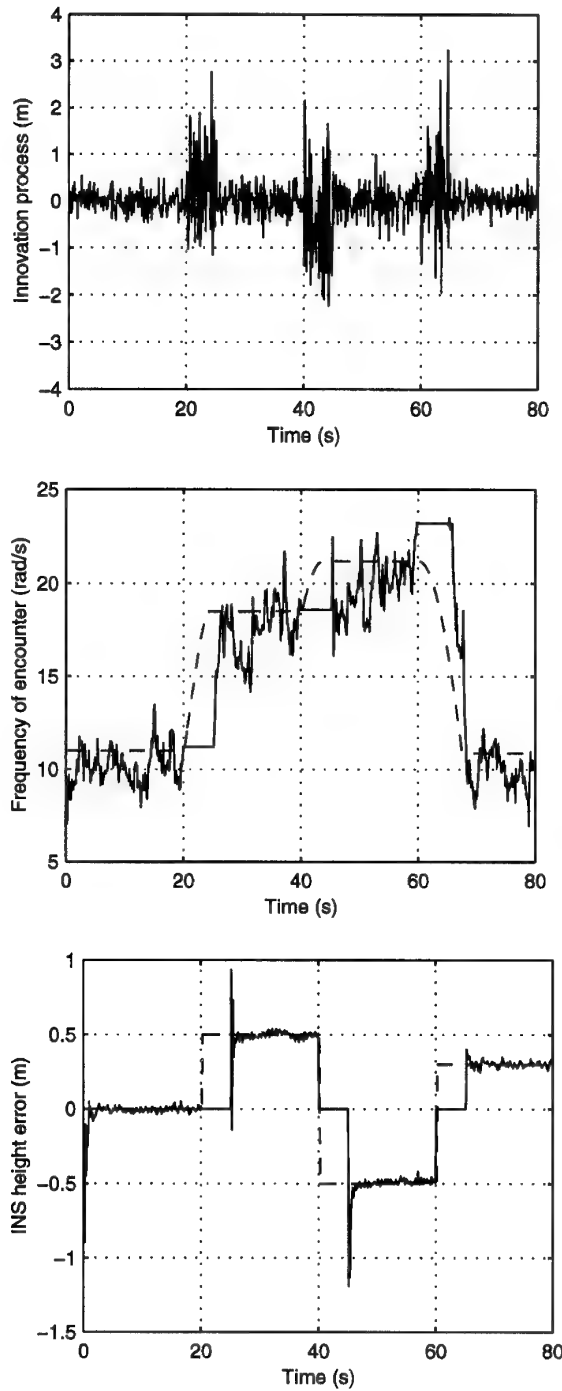


Figure 9 Sea state filter simulation example.

6 REDUCING NAVIGATION ERRORS OVER LAND

The Norwegian coastal terrain is characterized by numerous fjords and islands. In general, it could be said that the variance of the terrain is high. One of the roles for the new missile will be in coastal missile batteries. The missile may then have to fly a long distance over land before it reaches the sea. Using its laser altimeter, the missile can compare a measured terrain profile with an onboard stored map. This is the well-known method called TERCOM (Terrain Contour Matching). Several

papers have been published on this topic, e.g. [2] and [3]. After a few TERCOM-updates, the position error will be relatively small as the missile reach the sea. In Norway, the DLMS-DTED (Digital Terrain Elevation Data) maps have a horizontal resolution in the area of 100 meter, and this of course limits the accuracy of the position error measurements. Shoreline maps often have a resolution of about 10 meters (uncertainty of tides and ice deposit not accounted for), but have no information about the terrain between the shorelines. The laser altimeter developed at NDRE has proved its ability to detect shorelines. The principle is that the reflected signal from the sea is much weaker than that from terrain areas. The obtained land/no-land profile can be matched to the shoreline maps in a TERCOM-type of manner. This will increase the position accuracy even further. Only the terrain profile matching will be discussed further in this paper.

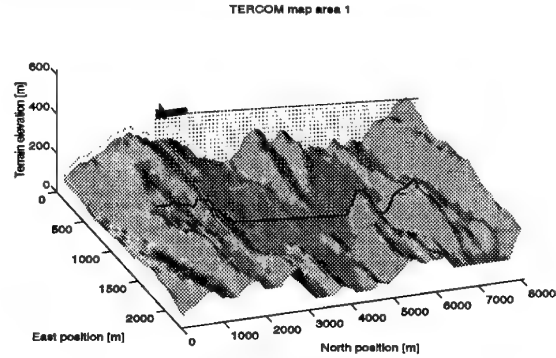


Figure 10 The terrain profile is measured with either a laser or radar altimeter

The Mean Absolute Difference (MAD) correlation algorithm is commonly used in TERCOM systems:

$$C(\Delta N, \Delta E) = \sum_{i=1}^n |\hat{h}_{terr}(i) - h_{map}(\Delta N, \Delta E, i)| \quad (42)$$

ΔN and ΔE are perturbations around the expected missile position, and n is the number of discrete terrain elevation measurements. For visualization purposes the C_v matrix can be converted:

$$C_v = -C + \max(C) \quad (43)$$

The $\Delta N, \Delta E$ combination giving the maximum of C_v will then be a position error measurement.

In the simulations the $\Delta N, \Delta E$ perturbations had the same step-size as the map resolution. The position error was expected to be within ± 1100 meters in both the north and east directions. This means that the measured profile was compared with 576 different map profiles starting within this area.

The primary laser altimeter measurement is the distance \tilde{l} from the missile to the terrain along the z_b -axis. We then assume a non-stabilized laser altimeter, hence the z_b -axis is not necessarily parallel with the down axis in the navigation coordinate system. The z_b -axis can be expressed as

$$\underline{v}_3^b = [0 \ 0 \ 1]^T \quad (44)$$

This vector can be represented in the navigation coordinate system:

$$\underline{v}_3^n = R(\psi, \theta, \phi) \cdot \underline{v}_3^b \quad (45)$$

where $R(\psi, \theta, \phi)$ is the transformation matrix from the body coordinate system to the navigation coordinate system. The position where the laser hits the terrain is given by

$$\underline{\tilde{p}}_{terr}^n = \underline{\tilde{p}}^n + \tilde{l} \cdot \underline{v}_3^n \quad (46)$$

where \tilde{p}^n is the INS missile position. The measured terrain elevation above sea level is then

$$\tilde{h}_{terr} = \tilde{p}_{terr}^n \cdot [0 \ 0 \ 1]^T \quad (47)$$

We have used a modified version of equation (42) where the elevation mean values of both the measured terrain profile and the map profiles are removed:

$$C(\Delta N, \Delta E) = \sum_{i=1}^n |(\tilde{h}_{terr}(i) - \bar{h}_{terr}) - (h_{map}(\Delta N, \Delta E, i) - \bar{h}_{map}(\Delta N, \Delta E))| \quad (48)$$

The motivation is to make the algorithm insensitive for vertical INS-errors and at the same time enable measurement of the vertical INS position error. When the best fitting map profile from (48) is found, then the INS-vertical error during the measurement period can be computed. The total output from the TERCOM system becomes:

$$\underline{y} = [\delta p_z \ \delta p_y \ \delta p_x] = [\Delta N_{best} \ \Delta E_{best} \ \bar{h}_{terr} - \bar{h}_{map}(\Delta N_{best}, \Delta E_{best})] \quad (49)$$

Equations (44)–(47) computes the terrain elevation profile for arbitrary laser pointing angles. Hence, the TERCOM algorithms can principally run during turns when pitch and roll angles are different from zero. Simulations show, however, that this should be done with care as the measured terrain profile becomes a function of the missile to terrain distance. In other words, the matching process goes from being a 2D-problem to a 3D-problem. This is especially so in Norway because of the highly dynamic mountain like terrain common along the coast. A relatively small altitude error can for instance cause the laser to hit a mountain top and not the valley behind the top.

6.1 Simulation example

Extensive simulations show that when using a profile length of 5–10 km it is easy to find areas along the Norwegian coastline that is suitable for TERCOM. The uniqueness of the measured profile is in general very good. Figure 12 shows the typical result of a simulation where the missile is performing three TERCOM updates along its trajectory. The trajectory is shown in Figure 11. The terrains are taken from the Ørland area not far from Trondheim. The position error measurements (north, east, down) were sent to a 27 state Kalman filter for optimal estimation of the INS-errors. The results shown are from a Monte-Carlo simulation using 100 runs. The INS error parameters were as described in Section 3. No alignment phase was simulated before the flight, and the initial error parameters were assumed uncorrelated. Thus, the error growth is slightly faster than what would have been the case if an alignment phase had been included.

The terrain elevation measurements were generated from the DLMS-DTED maps, adding white noise with standard deviation $\sigma_m = 10$ meters. The profile length was about 6 km and the distance between the measurements was approximately 90 m.

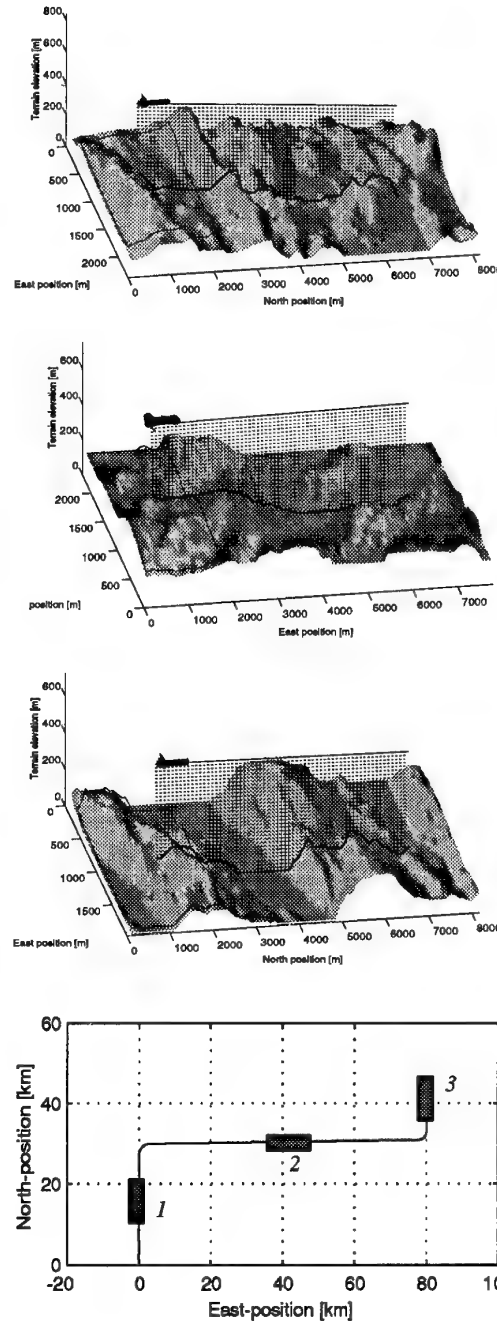


Figure 11

The simulated flight used three TERCOM updates. The terrains were taken from the Ørland area near Trondheim.

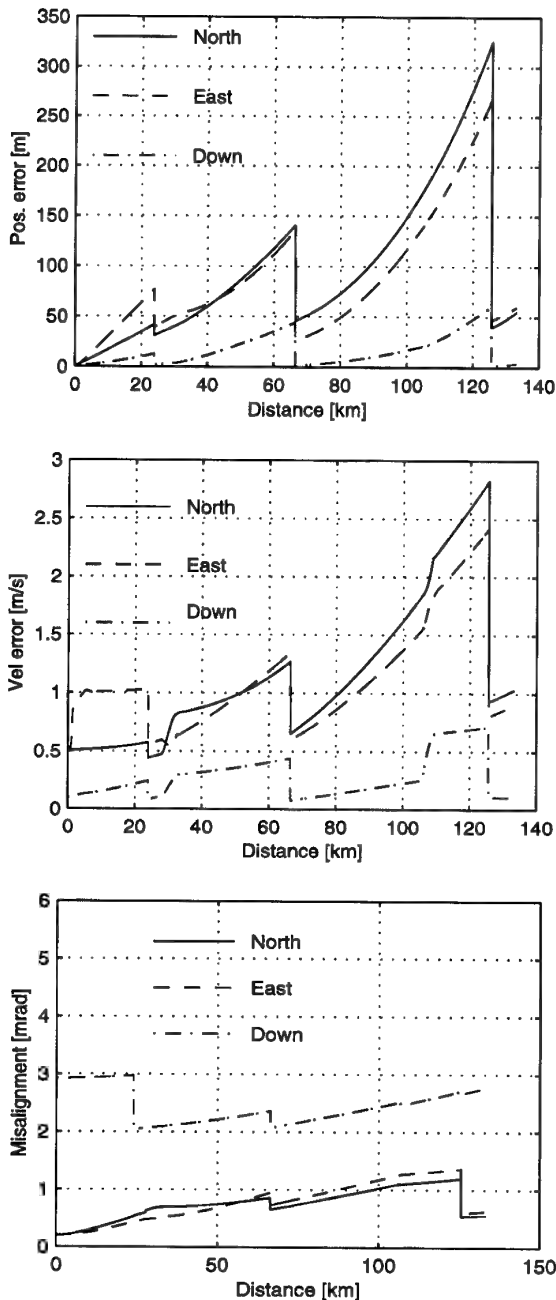


Figure 12 The TERCOM updates greatly improved the overall navigation performance.

6.1.1 Real data tests

The TERCOM strategy has also been tested using real data. The laser altimeter was mounted on a Twin Otter airplane flying at about 70 m/s. The plane was equipped with an encrypted GPS-receiver integrated with a missile type INS. The flight shown here was from the Austevoll area outside Bergen in the western part of Norway. This area is not especially suitable for TERCOM. It can be seen from figure 13 that the area has a lot of small islands. When the sea is relatively flat, the reflections are weak and loss of valid measurements may occur. The loss of measurements is in fact a good land/sea indicator. In figure 13, 'GPS' is the airplane altitude and 'laser' is the measured airplane to terrain distance. Figure 14 shows a visualization of the correlation matrix C_v . The best correlation is found fairly close to the zero-error point.

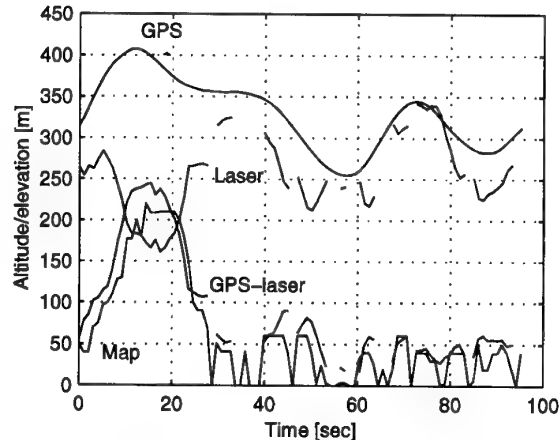


Figure 13 Measured terrain profile and map profile for the flight over Austevoll.

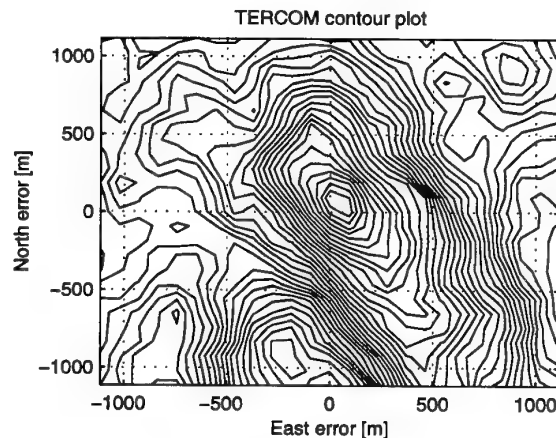


Figure 14 Contour plot of the C_v matrix for the flight over Austevoll

The work done so far on TERCOM leads us to the preliminary conclusion that TERCOM is well suited for use along the Norwegian coast.

7 REDUCING DYNAMIC ANGULAR ERRORS

The new anti ship missile will be a very agile missile. This means that the angular velocities may become very large, especially in the terminal phase when the seeker is activated. The seeker optical axis servo reference value is given by (the pitch axis is used as an example) :

$$\theta_{servo} = \theta_m - \theta_{seeker} \quad (50)$$

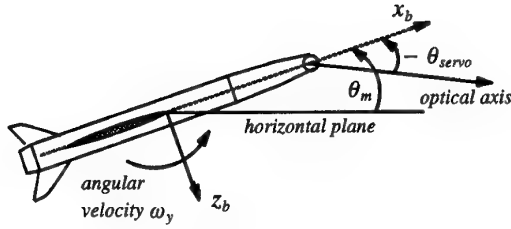


Figure 15 Pitch angles

where θ_{servo} is the seeker's servo reference for the angle between the optical axis and the missile body. θ_{seeker} is the desired angle between the optical axis and the horizontal plane. θ_m is the missile body pitch angle. θ_m is an output from the INS. Measurement errors in θ_m due to missile dynamics will be transferred to the optical axis. This is highly undesirable as the measured missile to target line of sight will be corrupted by the maneuvers. The line of sight measurements will be used for estimating the position and velocity of the target vessel.

There will always be some angular errors as a function of the maneuvers because the angular measurements from the INS are not available in absolutely real time. There are three major reasons for this. The first is what we call latency, τ_l . This is the time from initiating the readout of the IMU internal registers to the data is available at the output. The output from the IMU is discrete angular and velocity increments. The second source is the finite IMU sampling frequency. If we assume a zero order hold, the sampling will give a mean time delay :

$$\tau_s = \frac{1}{2f_s} \quad (51)$$

where f_s is the sampling frequency.

The third delay is the strapdown navigation computation time, denoted τ_n . This involves transforming and integrating the IMU-measurements from the IMU coordinate system to the navigation coordinate system. With todays computers this should however be more or less negligible. The total delay is given by:

$$\tau = \tau_l + \tau_n + \tau_s \quad (52)$$

For a constant angular velocity, the angular error is given by

$$\delta\theta = \dot{\theta} \cdot \tau \quad (53)$$

A bank-to-turn missile will often experience a maximum roll rate of several hundred %/s. The angular rates in yaw and pitch are usually much lower due to the control strategy and the higher moments of inertia. The INS delay τ can be measured, and the delay sources are expected to be long-term stable. If the delays are known, we can model the angular dynamics of the missile and then estimate the angular error. Thus, the angular outputs from the INS can then be compensated for using the estimated errors. The angular error compensation principle is shown in Figure 16.

It suffices for the missile model to include angular dynamics. The model initially consisted of one decoupled system for each axis. However, a bank-to-turn missile has considerable inertial as well as aerodynamic coupling between the different axes. For instance, the unwanted moment about the z_b -axis due to inertial coupling is given by the Euler equations :

$$M_z = \omega_x \omega_y (I_y - I_x) \quad (54)$$

where I_y and I_x are moments of inertia of the y- and x axis.

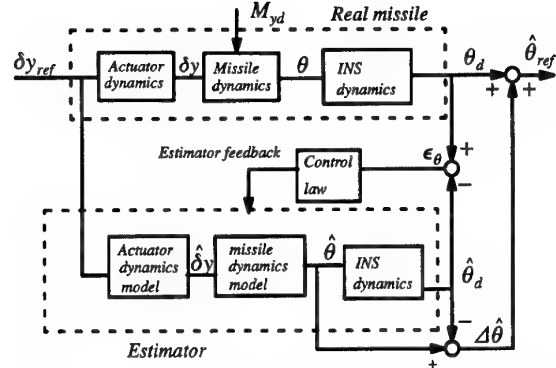


Figure 16 Dynamic angular error estimator overview

As the moment of inertia is usually much larger about the y-axis than for the x-axis, M_z may, depending on the control strategy, become very large. This effect is also very easy to model and it was therefore included in the estimator model. Aerodynamic coupling is also significant, but was omitted due to its modelling complexity. An example of aerodynamic coupling is the rolling moment due to a combination of the angle of attack and sideslip. The inertial moments on the other axis were also omitted since the moments of inertia of the y and z-axis are very close to each other and thus almost cancels in the Euler equations. The gyroscopic and reactional moments from the turbojet engine are not modeled in the estimator. They are however included in the true missile simulation model. The structure of the estimator single axis models was as in figure 17 (pitch axis used as an example). The disturbance M_{yd} is assumed to be pitching moments not modeled in the estimator.

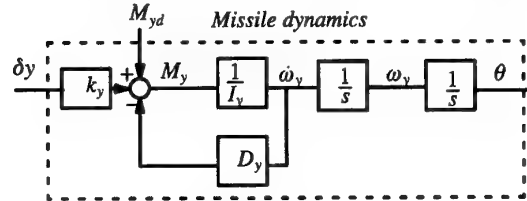


Figure 17 Simplified pitch axis model used in the estimator

The generic missile model used in the simulations has very close to neutral stability in pitch for small angles of attack. That means there is only very small pitching moments as long as the angle of attack stay small. However, the pitch moment curves for missiles are usually highly nonlinear for higher angles of attack. Thus, the simple model in figure 17 is most valid for relatively low-g maneuvers.

The estimator feedback control problem was solved by using simple PD-controllers for the error signal in pitch, roll and azimuth. The controller parameters was designed by using traditional frequency analysis. A more sophisticated solution would involve a Kalman filter. The PD-solution was chosen for its simplicity and low computational requirements. The computation time for the estimator should be far less than the time delay τ . The roll, pitch and azimuth control outputs were decomposed to fictitious fin deflections and added to the estimated fin deflections.

For testing the dynamic angular error estimator, the *true missile* was simulated using a complex and detailed missile model. This model includes all known missile dynamics, also nonlinear effects and aerodynamic coupling not modelled in the estimator. The estimator was implemented in Matlab/Simulink.

An overview of the system used in the simulations is shown in figure 18.

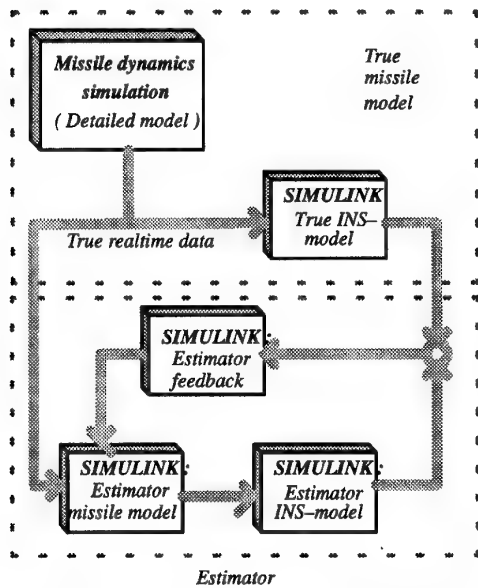


Figure 18 Overview of the system used in our simulations.

The INS error dynamics were assumed to be known, hence the INS-model in the simulator and estimator are identical. In the simulations, a very conservative model was used :

$$G_{ins}(s) = \frac{e^{-0.005s}}{1 + 0.005s} \quad (55)$$

The 5 ms time constant was intended to account for INS error dynamics that might be encountered during laboratory tests. Figure 19 shows an example where the missile is performing a zigzag maneuver. Figure 20 shows that without the model based compensator, the angular error in roll becomes very large. The errors are far beyond acceptable limits. When the INS angular data are compensated for using the estimated error, the results are much better and the total errors are within acceptable limits. The missile might be subjected to more agile bank-to-turn maneuvers than in Figure 19. For such maneuvers, a more detailed model including more of the inertial and aerodynamic coupling might be needed.

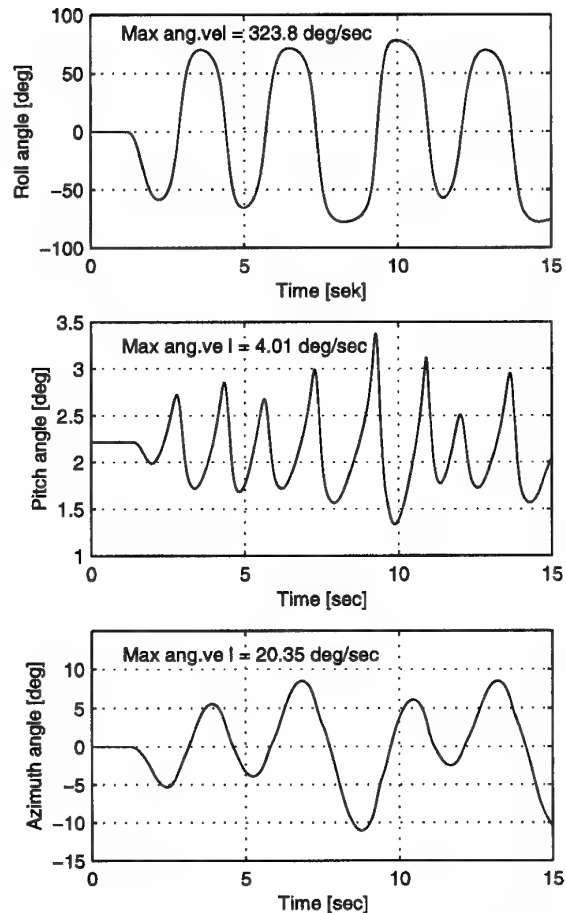


Figure 19 Angular dynamics for a missile performing zigzag maneuvers

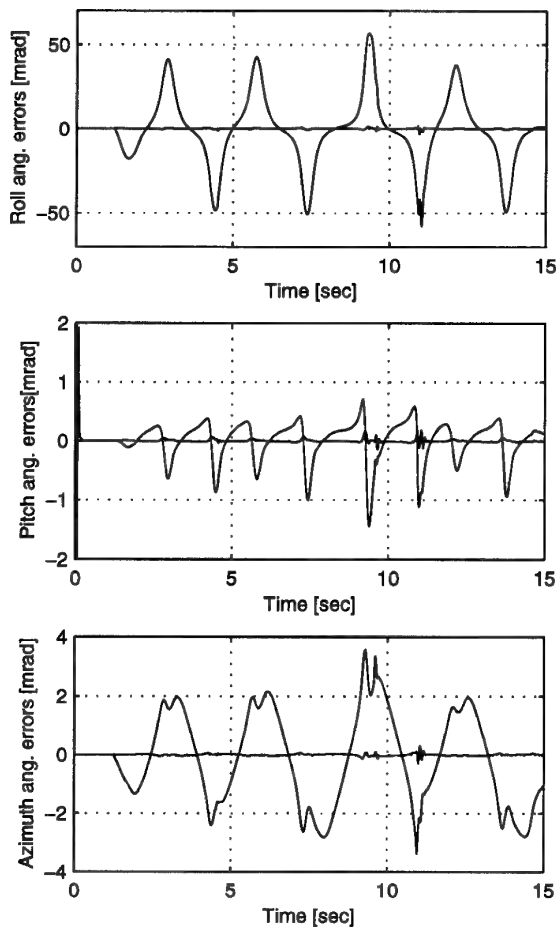


Figure 20 Angular errors with and without compensation using the estimated errors.

8 CONCLUSION

A navigation system concept consisting of four subsystems has been proposed.

Simulations indicate that INS attitude errors when flying over open sea can be substantially reduced by employing altimeter measurements in a Kalman filter. Reduced attitude errors bring about limited position error propagation. The actual improvement is dependent upon the missile trajectory and the sea state. The Norwegian coastline is well suited for TERCOM. The TERCOM strategy has been verified using real data. TERCOM position error updates provide an efficient and robust method for limiting INS position errors.

Simulation and real data tests indicate that the sea state can be estimated using a simple model. Estimated wave variance is used in prediction of the maximum wave height that is likely to occur during a missile flight. This is useful when deciding the missile altitude during sea skimming.

The agile maneuvering of the new anti-ship missile necessitate reduction of the dynamic errors in the INS angular data used for seeker stabilization. A model based compensator for this purpose has been proposed.

References :

1. Britting, K. "Inertial Navigation systems". John Wiley & Sons, 1971, (ISBN 0-471-10485-X)
2. Ochi, M. K., "Stochastic Analysis and Probability Prediction in Random Seas", in "Advances in Hydroscience", 13, pp. 217-375, 1982.
3. Faltinsen, O. M., "Sea Loads on Ships and Offshore Structures", Cambridge University Press, Cambridge 1990.
4. Fossen, T. I., "Guidance and Control of Ocean Vehicles", John Wiley & Sons Ltd., 1994.
5. 15th ITTC, "Report of the Seakeeping Committee", in "Proceedings of the 15th International Towing Tank Conference", The Hague, pp. 55-70, 1978.
6. 17th ITTC, "Report of the Seakeeping Committee", in "Proceedings of the 17th International Towing Tank Conference", The Hague, pp. 531-534, 1984.
7. Hasselman K., "Measurements of wind-wave growth and swell decay during the Joint North Sea wave project", Deutsche hydrographische Zeitschrift, 1973.
8. Sælid, S., Jenssen, N. A. and Balchen J. G., "Design and Analysis of a Dynamic Positioning System Based on Kalman Filtering and Optimal Control", IEEE Transactions on Automatic Control, AC-28(3): 84-101, 1983.
9. Holzruter, T. and Strauch, H., "A commercial Adaptive Autopilot for Ships: Design and Experimental Experience", in "Proceedings of the 10th IFAC World Congress", Munich Germany, pp. 226-230, July 27-31, 1987.
10. Gelb, A. (editor), "Applied Optimal Estimation", The MIT Press, Cambridge 1992.
11. Dannevig, Petter, "Sjøboka - Vær, vind og sjø på Norskekysten" (in Norwegian), Nordangers nautiske håndbøker.
12. Børresen, J. A., "Vindatlas for Nordsjøen og Norskehavet" (in Norwegian), Universitetsforlaget/ Det norske meteorologiske institutt.
13. Golden, J. P., "Terrain Contour Matching (TERCOM): a cruise missile aid", SPIE Vol 238 Image Processing for Missile Guidance, pp. 10-18, 1980.
14. Baird, C. A. and Abramson, M.R., "A comparison of several digital map-aided navigation techniques", IEEE, CH2110-5/84/0000-0286, 1984,

Control of a Supersonic Air to Ground Missile with Very Lightly Damped Bending Modes

J.P. Friang^{1,2}, J.P. Bonnet¹, G. Duc²

¹AEROSPATIALE – MISSILES
2 à 18 rue Béranger
92320 Chatillon-sous-Bagneux, France

²ECOLE SUPERIEURE D'ELECTRICITE
Service Automatique
Plateau de Moulon
91192 Gif-sur-Yvette Cedex, France

1. SUMMARY

In this paper, an autopilot is designed to control a missile with very lightly damped bending modes, using the loop-shaping H_∞ design procedure of McFarlane and Glover. Robustness in the face of large modelling uncertainties (including parameter and bending modes) is then investigated using real μ -analysis. The autopilot of the Bank To Turn (BTT) missile developed by AEROSPATIALE (French Aerospace Industrial National Company) is finally validated on a non linear simulator: this will show the performances and the robustness of our design.

2. INTRODUCTION

Loop-shaping H_∞ design has been first proposed by McFarlane and Glover [1,3]. It leads to a procedure which have interesting properties: the design is based on selecting pre- and post- compensators to shape the open-loop transfer function, according to the classical rules of Automatic control; a particular H_∞ problem is then involved where the optimal value γ_{\min} of the H_∞ criterion is *a priori* known (no γ -iteration is therefore required). Furthermore it usually leads to designs which exhibit a good level of robustness and performance, with balanced input / output behaviours.

In this paper, the loop-shaping H_∞ design is applied to the stabilisation of a BTT flexible missile. For this process, the flight control system is designed in a usual way, *i.e.* choosing one of the linearized models of nonlinear equations of motion. Mixed μ -analysis (real and complex scalars) [4,5] is then performed to guarantee stability despite gain, phase and delay uncertainties, aerodynamic deviations and bending modes uncertainties.

The paper is organized as follows. Section 3 describes the missile model and the design objectives. Section 4 is a summary of the loop-shaping H_∞ design. Section 5 describes the application to the autopilot. Section 6 is devoted to robustness analysis while the autopilot is finally validated on a non linear simulator in Section 7.

3. MISSILE MODEL AND DESIGN OBJECTIVES

This paper is concerned with a BTT flexible missile. Local linearization at various flight conditions leads to the following dynamic model in terms of the motion equations:

$$\dot{\alpha} = q + \frac{QS}{mV} \left(C_{z\alpha} \alpha + C_{z\eta} \eta_{ex} + \frac{L}{V} C_{zq} q \right) \quad (1.a)$$

$$\dot{q} = \frac{QSL}{I_y} \left(C_{m\alpha} \alpha + C_{m\eta} \eta_{ex} + \frac{L}{V} C_{mq} q \right) \quad (1.b)$$

$$\dot{\beta} = -r + \frac{QS}{mV} \left(C_{y\beta} \beta + C_{y\zeta} \zeta_{ex} + \frac{L}{V} C_{yr} r \right) \quad (1.c)$$

$$\dot{r} = \frac{QSL}{I_z} \left(C_{n\beta} \beta + C_{n\zeta} \zeta_{ex} + \frac{L}{V} C_{nr} r \right) \quad (1.d)$$

$$\dot{p} = \frac{QSL}{I_x} \left(Cl_{\alpha\beta} + Cl_{\xi} \xi_{ex} + \frac{L}{V} Cl_p p \right) \quad (1.e)$$

$$\dot{\Phi} = p \quad (1.f)$$

$$a_z = V(\dot{\alpha} - q + p\beta) ; a_y = V(\dot{\beta} + r - p\alpha) \quad (1.g)$$

where α , q and η_{ex} denote the angle of attack, the pitch rate and the executed elevator deflection; β , r and ζ_{ex} denote the sideslip angle, the yaw rate and the executed rudder deflection; a_z and a_y are the normal and lateral accelerations (at the centre of gravity); Φ , p , ξ_{ex} are the bank angle, the roll rate and the executed aileron deflection; m , Q , I_x , I_y , I_z , V , S , and L are the mass of the missile, the dynamic pressure, the 3 moments of inertia, the missile velocity, the reference area and the reference length, respectively.

The uncertain aerodynamic coefficients are the following: $C_{z\alpha}$, $C_{z\eta}$, C_{zq} (*resp.* $C_{m\alpha}$, $C_{m\eta}$, C_{mq}) are the normal force (*resp.* moment) coefficients; $C_{y\beta}$, $C_{y\zeta}$, C_{yr} (*resp.* $C_{n\beta}$, $C_{n\zeta}$, C_{nr}) are the lateral force (*resp.* moment) coefficients; Cl_p , Cl_{ξ} and $Cl_{\alpha\beta}$ are the roll moment coefficient, the roll moment efficiency and the Dutch roll, respectively.

The cross-coupling between the dynamics of the yaw channel and the pitch and roll channels are characterized by the terms $Cl_{\alpha\beta}$, $p\alpha$ and $p\beta$ in Equations (1.e), (1.g). In the BTT technique, the autopilot is designed so that the resulting roll rate dynamics are faster than those of the yaw and pitch channels: this allows to reduce the cross-coupling effects.

Aeroelasticity is the interaction between flight control systems and structural dynamics. Modern missiles including long fuselages and new composite materials, aeroelasticity becomes a significant phenomenon: the flexible missile fuselage introduces a lot of flexible modes outside (but very close to) the bandwidth, with a very low damping (between

10^{-3} and 10^{-2}). Two modes on pitch and yaw channels are therefore added to Model (1) (Figure 1). For the pitch channel, the acceleration and rate measures (by inertial unit) due to aeroelasticity a_{zel} and q_{el} are obtained from the executed deflection η_{ex} by a fourth order model. The global acceleration and rate measures are then:

$$a_{zg} = a_z + a_{zel} ; q_g = q + q_{el} \quad (1.h)$$

A similar model is used for the yaw channel, to obtain the global acceleration and rate measures a_{yg} and r_g . From a control point of view, the plant measurements are a_{zg} , q_g , a_{yg} , r_g , Φ and p , while the plant inputs are η_{ex} , ζ_{ex} and ξ_{ex} (Figure 1). The control plant model (1) has to be augmented by actuators dynamics, that are commonly assumed to be described by a second order model between η_{ex} (resp. ζ_{ex} and ξ_{ex}) and η_{co} (resp. ζ_{co} and ξ_{co}) where η_{co} , ζ_{co} and ξ_{co} denote the commanded elevator, rudder and aileron deflections. Finally a first order Padé approximation is added to each actuator to model the various delays in the feedback loop.

The considered control scheme is depicted in Figure 1. The rate feedback allows to stabilize the system, while ensuring an admissible damping. The required rise time and overshoot are mainly achieved by the acceleration feedback which includes integral actions. The motivation of the control design consists in ensuring relatively fast regulation dynamics while guaranteeing satisfactory stability and performance robustness.

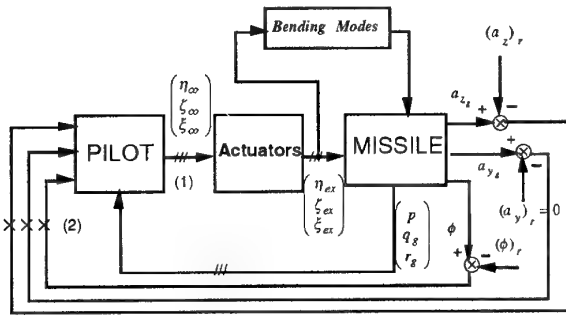


Figure 1. Control Scheme

The same missile autopilot has to be applied for the stabilized flight and for different manoeuvres. To synthesize the missile autopilot we have thus selected a family \mathbf{P} which includes 4 models, each of them corresponding to a representative manoeuvre:

- P_N : Nominal model
- P_0 : Stabilized flight
- P_1 : Pull up flight
- P_2 : Diving flight

The choice of P_N (which is used to design the control law) is an important point: it has to be selected to avoid conservatism in the uncertainty modelling, to optimise the performances on

each model of \mathbf{P} , and to insure the robustness of the control law. The *a priori* knowledge about the process has been used to select for P_N a model between P_0 and P_2 .

The controller has to insure the following specifications for all the family \mathbf{P} :

- 66% settling time: lower than a pre-specified value (denoted τ in the following) for the pitch channel; lower than 0.8τ for the roll channel.
- Sideslip angle β as small as possible.
- Limitations on the first and second derivatives of η_{ex} , ζ_{ex} and ξ_{ex} .
- Gain, phase and delay margins: at least 6 dB, 30° , 0.05τ for the Outer and Equivalent Loops (points 2 and 1 on Figure 1 respectively).
- Reasonably damped closed loop responses with respect to a step demand (pitch and roll channels).

4. LOOP-SHAPING H_∞ DESIGN

Let $G(s)$ represent the $p \times m$ real rational transfer-function matrix of a stable system. The H_∞ norm of $G(s)$ is:

$$\|G(s)\|_\infty = \sup_{\omega} \sqrt{\lambda_i [G(-j\omega)^T G(j\omega)]} \quad i=1, \dots, n \quad (2)$$

where $\lambda_i(A)$ denote the eigenvalues of the matrix A (and $\lambda_i[G(-j\omega)^T G(j\omega)]$ are called the singular values of $G(j\omega)$).

Consider the block diagram of Figure 2, where the block 2×2 transfer function matrix $P(s)$ relates the input vector w and control vector u to the output vector e and measurement vector y :

$$P(s) = \begin{bmatrix} P_{11}(s) & P_{12}(s) \\ P_{21}(s) & P_{22}(s) \end{bmatrix} \quad (3)$$

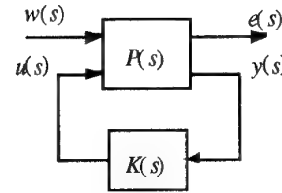


Figure 2. Standard H_∞ Problem

When a controller $K(s)$ is connected from $y(s)$ to $u(s)$, it is simple to establish that the closed loop transfer matrix from $w(s)$ to $e(s)$ is:

$e(s) = F_l(P(s), K(s))w(s)$ where $F_l(P, K)$, which is called the lower linear fractional transformation (LFT) of P and K is:

$$F_l(P, K) = P_{11} + P_{12} K (I - P_{22} K)^{-1} P_{21} \quad (4)$$

The standard H_∞ problem is: for γ given, find $K(s)$ such that the closed loop system of Figure 2 is stable, and $\|F_l(P, K)\|_\infty < \gamma$.

In this paper, a particular H_∞ problem is considered [1,2], which corresponds to the block diagram of Figure 3.

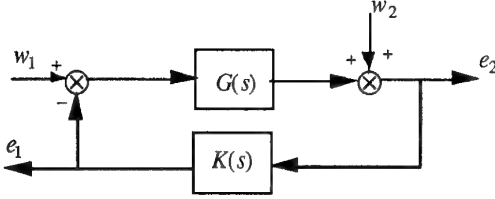


Figure 3. A Particular H_∞ Problem

The transfer matrix of the closed loop system is:

$$\begin{pmatrix} e_1 \\ e_2 \end{pmatrix} = \begin{pmatrix} KSG & KS \\ SG & S \end{pmatrix} \begin{pmatrix} w_1 \\ w_2 \end{pmatrix} \quad (5)$$

where $S(s) = (I + G(s)K(s))^{-1}$ is called the sensitivity function.

The corresponding H_∞ problem is then: for γ given, find $K(s)$ stabilising such that:

$$\left\| \begin{pmatrix} KSG & KS \\ SG & S \end{pmatrix} \right\|_\infty < \gamma \quad (6)$$

As an advantage, the minimal value γ_{\min} of γ can be *a priori* computed, while formulae involving 2 Riccati equations are available to construct any controller achieving a value γ arbitrarily close to γ_{\min} . Let $\{A, B, C\}$ be a state space minimal realisation of $G(s)$; one obtains:

$$K(s) = \gamma^2 B^T X (sI - A + BB^T X - \gamma^2 ZYC^T C)^{-1} ZYC^T$$

where:

$$A^T X + XA - XBB^T X + C^T C = 0$$

$$AY + YA^T - YC^T CY + BB^T = 0$$

$$Z = ((1 - \gamma^2)I_n + YX)^{-1}$$

$$\text{and } \gamma > \gamma_{\min} = \left(1 + \sup_i \lambda_i(YX)\right)^{1/2}$$

Furthermore some robustness result can be connected with this approach. Let $G(s) = \tilde{M}(s)^{-1} \tilde{N}(s)$, where $\tilde{M}(s), \tilde{N}(s)$ are stable and proper transfer matrices such that $\tilde{M}(j\omega)\tilde{M}(-j\omega)^T + \tilde{N}(j\omega)\tilde{N}(-j\omega)^T = I$. Controller $K(s)$ will stabilise all perturbed plants belonging to the following family:

$$P_\varepsilon = \begin{cases} P = (\tilde{M} + \Delta_{\tilde{M}})^{-1} (\tilde{N} + \Delta_{\tilde{N}}) \\ \text{with } \left\| \begin{pmatrix} \Delta_{\tilde{M}} & \Delta_{\tilde{N}} \end{pmatrix} \right\|_\infty < \varepsilon \end{cases} \quad (8)$$

where $\varepsilon = \gamma^{-1}$. ε and γ are therefore simultaneously related to performances (since γ is the H_∞ -norm of the closed loop system) and robustness (since ε defines the "size" of the family P_ε). Value of ε between 0.3 and 0.5 (γ between 2 and 3) are generally considered to be satisfying.

In order to tune the performances, a loop-shaping procedure is generally performed before solving the H_∞ problem (6). To this end, $G(s)$ is replaced by $G_a(s) = W_2(s)G(s)W_1(s)$ (Figure 4.a) where $W_1(s)$ and $W_2(s)$ are pre- and post-compensators selected following the classical rules of Automatic Control: for instance integral action can be introduced to achieve zero steady state error, but one can also increase the open loop gain at low frequencies for performances, or add low pass filters to increase the roll-off at high frequencies.

The H_∞ problem to be solved is now:

$$\left\| \begin{pmatrix} KS_a G_a & KS_a \\ S_a G_a & S_a \end{pmatrix} \right\|_\infty < \gamma \quad (9)$$

where $S_a(s) = (I + G_a(s)K(s))^{-1}$.

As a result, the final controller is $K_f(s) = W_1(s)K(s)W_2(s)$ (see Figure 4.b).

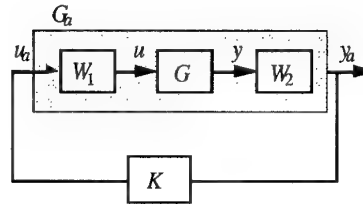


Figure 4.a Loop-Shaping procedure: compensators for shaped plant $G_a(s)$

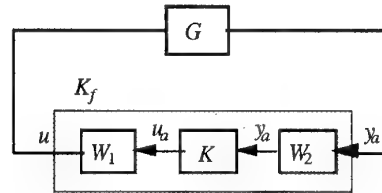


Figure 4.b Loop-Shaping procedure: controller for unshaped plant $G(s)$

5. DESIGN OF THE CONTROL LAW

The main feature of the nominal model P_N is an exact decoupling between pitch and yaw / roll channels. It is therefore more convenient to design separately an autopilot for the pitch channel (Pc) and one for the yaw / roll channel (YRc). One consequence is that the robustness indicator ε_{\max} of each separately designed autopilot will be greater than the one obtained by designing a unique autopilot for all channels.

To design the control law, bending modes are considered as neglected dynamics. *Note however that on pitch and yaw channels the natural frequency of the first bending mode is less than 3 times the crossover frequency.* Fifth order low pass filters are *a priori* introduced in the loop-shape to reduce the open-loop gain in such a way that the resonance of the bending mode remains below 0 dB. Stability of the closed-loop is then ensured. This will also reduce the high frequency noise, such as the sensor noise, and improve the robustness against other high frequency model uncertainties, such as other neglected dynamics, sampling time delay,...

5.1 Loop-Shaping

5.1.1 Pitch channel (Pc)

Since only the first output a_{zg} has to track the demand, the following post-compensator $W_{2_{Pc}}$ has been chosen:

$$W_{2_{Pc}} = \begin{pmatrix} k_{Pi1} \frac{s + \beta_{Pi1}}{s} & 0 \\ 0 & \alpha_q \end{pmatrix} \quad (10)$$

The scalar gain α_q in $W_{2_{Pc}}$ allows to adjust the bandwidth of the rate feedback. The post-compensator also includes a PI controller on the normal acceleration to achieve zero steady-state error.

The pre-compensator $W_{1_{Pc}}$ includes a fifth order low pass filter. The obtained stability margin is $\varepsilon_{\max} = 0.36$.

5.1.2 Yaw /Roll channels (YRc)

Since the first output a_{yg} has to be maintained to zero and the third output Φ has to track the demand, the following pre- and post-compensators $W_{1_{YRc}}$ and $W_{2_{YRc}}$ have been chosen:

$$\begin{aligned} W_{1_{YRc}} &= \text{diag} \left(F_2(s); \frac{1}{1 + \tau_3 s} \right) \\ W_{2_{YRc}} &= \text{diag} \left(k_{Pi2} \frac{s + \beta_{Pi2}}{s}; \alpha_r; k_{Pi3} \frac{s + \beta_{Pi3}}{s}; \alpha_p \right) \end{aligned} \quad (11)$$

$W_{2_{YRc}}$ includes a PI controller on the lateral acceleration a_{yg} and the bank angle Φ . The scalars α_r and α_p allow to adjust the bandwidth of the rate feedback.

$W_{1_{YRc}}$ includes a fifth order low pass filter $F_2(s)$ on the yaw channel and a first order low pass filter to increase the roll-off on the roll channel. The obtained stability margin is $\varepsilon_{\max} = 0.28$.

5.2 H_∞ Controllers

5.2.1 Pitch channel (Pc)

A H_∞ optimal controller K_1 is then generated for the shaped plant. It results in $W_{1_{Pc}} K_1$ having 15 states, which can be reduced to 8 states without significant degradation by using the Aggregation Method [9]. The controller of the plant is then given by $K_{f1} = W_{1_{Pc}} K_1 W_{2_{Pc}}$, and has 9 states variables. The singular value of the corresponding shaped plant $P_{s1} = W_{2_{Pc}} P_{0_{Pc}} W_{1_{Pc}}$ and the resulting Equivalent-Loop singular value are shown on Figure 5. As expected by the good value of ε_{\max} , the loop shape is not significantly altered by the inclusion of the H_∞ controller (*i.e.* the singular value obtained for $K_{f1} P_{0_{Pc}}$ remains close to this of P_{s1}).

5.2.2 Yaw/Roll channels (YRc)

A H_∞ optimal controller K_2 is then generated for the shaped plant. $W_{1_{YRc}} K_2$ has 22 states, which can be reduced to 14 states without significant degradation by the Aggregation Method. The controller of the plant is then $K_{f2} = W_{1_{YRc}} K_2 W_{2_{YRc}}$, and has 16 states variables. The singular values of the corresponding shaped plant $P_{s2} = W_{2_{YRc}} P_{0_{YRc}} W_{1_{YRc}}$ and the resulting Equivalent-Loop singular values are shown on Figure 5. Again the loop shape is not significantly altered by the H_∞ controller.

Finally, the order of the global controller (for the 3 axes) is 25. *Henceforth K_f denotes the global autopilot obtained by the association of K_{f1} and K_{f2} .*

The Equivalent-Loop Bode plots with the first two bending modes on pitch and yaw channels are shown on Figure 6.

6. ROBUSTNESS ANALYSIS

6.1 LFT's and μ analysis

Linear Fractional Transformations (*LFT*'s) provide a general concept to include uncertainties on transfer matrices or state-space realizations [5]. Consider the general structure of Figure 7.a, where M and Δ are either real, complex or transfer matrices, with M partitioned as:

$$M = \begin{pmatrix} M_{11} & M_{12} \\ M_{21} & M_{22} \end{pmatrix} \quad (12)$$

Assuming the invertibility of $I - M_{11}\Delta$, the upper *LFT* is defined by:

$$\mathcal{F}_u(M, \Delta) = M_{22} + M_{21}\Delta(I - M_{11}\Delta)^{-1}M_{12} \quad (13)$$

As a special case, any rational transfer matrix $G(s)$ with state-space realization $\{A, B, C, D\}$, $\dim(A) = n \times n$ can be expressed as an *LFT*:

$$\begin{aligned} G(s) &= D + C(sI - A)^{-1}B = \mathcal{F}_u(M, s^{-1}I_n) \\ \text{with } M &= \begin{pmatrix} A & B \\ C & D \end{pmatrix} \end{aligned} \quad (14)$$

Following this idea, any transfer matrix $G(s, \delta_1, \dots, \delta_k)$ which rationally depends on s and uncertainties $\delta_1, \dots, \delta_k$ can be expressed as an *LFT* [11]:

$$G(s, \delta_1, \dots, \delta_k) = \mathcal{F}_u \left(M, \text{diag} \left\{ s^{-1} I_n ; \Delta_1 \right\} \right) \quad (15)$$

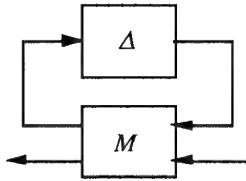
$$\Delta_1 = \text{diag} \left\{ \delta_1 I_{n_1}, \dots, \delta_k I_{n_k} \right\}$$

where M is a state-space realization of $G(s, \delta_1, \dots, \delta_k)$ with supplementary inputs and outputs in order to connect the uncertainties $\delta_1, \dots, \delta_k$ (Figure 7.b).

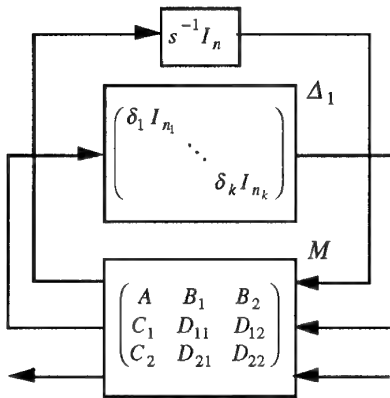
A fundamental property is that any interconnection of *LFT*s is again an *LFT* [5]. Collecting all uncertainties of a closed-loop system therefore again results in the general structure of Figure 7.b.

Consider now the set of uncertainty matrices:

$$\mathbf{D} = \left\{ \Delta_1 = \text{diag} \left\{ \delta_1 I_{n_1}, \dots, \delta_k I_{n_k} \right\} / \delta_i \in \mathbb{R} \text{ or } \mathbb{C}, |\delta_i| \leq 1 \right\} \quad (16)$$



a) General Structure



b) Structure with Parametric Uncertainties

Figure 7. LFT Structure

The structured singular value (ssv) of a complex matrix M (whose dimensions are compatible with Δ_1), with respect to the set \mathbf{D} is [4]:

$$\mu(M) = \left(\inf \left\{ k \in [0, \infty] / \exists \Delta_1 \in \mathbf{D} : \det(I - k \Delta_1 M) = 0 \right\} \right)^{-1} \quad (17)$$

The fundamental result concerning robust stability analysis using μ is that the system of Figure 7.b remains stable for any $\Delta_1 \in \mathbf{D}$ if and only if:

$$\forall \omega \in \mathbb{R} \quad \mu(\omega) = \mu \left(\mathcal{F}_u \left(\begin{pmatrix} A & B_1 \\ C_1 & D_{11} \end{pmatrix}, \frac{1}{j\omega} I_n \right) \right) < 1 \quad (18)$$

In fact $\mu(\omega)^{-1}$ represents the size of the smallest parameter perturbation which brings one closed-loop pole on the imaginary axis at $\pm j\omega$. Robust stability is therefore guaranteed for any δ_i such that $|\delta_i| < \min_{\omega} (\mu(\omega)^{-1})$.

In the following, such an analysis is applied to guarantee robust stability against different kinds of uncertainties. The μ -Tools software [8] has been used to obtain upper and lower bounds for $\mu(\omega)$, which has been regularized by adding a small amount of (generally 10%) complex uncertainty to each real uncertainty [7, 10].

6.2 Gain, phase and delay margins

Gain and phase margins were evaluated at Points 1 (Equivalent Loop) and 2 (Outer Loop) on Figure 1, for each model of the family \mathbf{P} with the first 2 bending modes. For the single input pitch channel, the margins were deduced from classical analysis using Nyquist plots of the open-loop transfer function. For the yaw / roll channel, they were obtained by μ -analysis as explained in the following.

6.2.1 Gain margins

Diagonal gain uncertainties at Point 1 or 2 were considered by successively using direct and inverse multiplicative models:

$$\text{diag}\{k_1; k_2\} = I + \Delta_d = (I + \Delta_i)^{-1} \quad (19)$$

Let $H_o(s)$ be the open-loop transfer function at the point (1 or 2) where the margins are to be evaluated. Define $S(s) = (I - H_o(s))^{-1}$, $T(s) = -H_o(s)(I - H_o(s))^{-1}$ and:

$$\mu_1 = \min_{\omega} (\mu(T(j\omega)))^{-1} ; \quad \mu_2 = \min_{\omega} (\mu(S(j\omega)))^{-1} \quad (20)$$

where the ssv are computed assuming diagonal real uncertainty. The system remaining stable for any diagonal Δ_d such that $\overline{\sigma}(\Delta_d) < 1$ or any diagonal Δ_i such that $\overline{\sigma}(\Delta_i) < 1$, the following gain margins are deduced:

$$k_1, k_2 \in]1 - \mu_1, 1 + \mu_1[\cup]1 / (1 + \mu_2), 1 / (1 - \mu_2)[\quad (21)$$

6.2.2 Phase margins

Diagonal phase uncertainties were similarly considered:

$$\text{diag}\{e^{j\varphi_1}; e^{j\varphi_2}\} = I + \Delta_d = (I + \Delta_i)^{-1} \quad (22)$$

Computing the ssv as in (20) but assuming diagonal complex uncertainty, the following phase margins are deduced:

$$|\varphi_1|, |\varphi_2| < \sup \{ 2 \text{Arcsin}(\mu_1 / 2), 2 \text{Arcsin}(\mu_2 / 2) \} \quad (23)$$

Contrary to the gain margins, these phase margins are somewhat conservative: in fact assuming diagonal uncertainty does not take into account the particular structure of the diagonal uncertainty matrices $\Delta_d = \text{diag}\{e^{j\varphi_1} - 1; e^{j\varphi_2} - 1\}$ and $\Delta_i = \text{diag}\{e^{-j\varphi_1} - 1; e^{-j\varphi_2} - 1\}$.

6.2.3 Delay margins

Uncertainties on both delays of the yaw / roll channel were considered by using the following *LFT*:

$$e^{-(\tau_0 + \tau_1 \delta)s} \approx \frac{2 - (\tau_0 + \tau_1 \delta)s}{2 + (\tau_0 + \tau_1 \delta)s} = \mathcal{F}_u \left(M, \text{diag} \left\{ \frac{1}{s}; \delta \right\} \right)$$

$$M = \begin{pmatrix} A & B_1 & B_2 \\ C_1 & D_{11} & D_{12} \\ C_2 & D_{21} & D_{22} \end{pmatrix} = \begin{pmatrix} -2/\tau_0 & -\tau_1/\tau_0 & -2 \\ -2/\tau_0 & -\tau_1/\tau_0 & 0 \\ -2/\tau_0 & -\tau_1/\tau_0 & -1 \end{pmatrix} \quad (24)$$

Two independent *LFT*'s of the type (24) are connected to the closed-loop system, and the corresponding *ssv* is computed. Robust stability is then guaranteed if each delay remains below $\tau_0 + \tau_1 \min(\mu(\omega))^{-1}$.

Table 1 gives the single input margins (gain, phase and delay) of the Equivalent and Outer Loops obtained on the pitch channel (*Pc*) for each model of the family **P**. Similarly, Table 2 gives the multivariable margins obtained for the yaw / roll channel (*YRc*). As the multivariable phase margins are somewhat conservative, all these values are satisfactory.

	Equivalent Loop			Outer Loop		
P_N	8.2 dB	76°	0.66 τ	11 dB	63°	$> 0.5 \tau$
P_0	7.8 dB	80°	0.96 τ	12 dB	71°	$> 0.5 \tau$
P_1	6.6 dB	78°	0.78 τ	8.2 dB	70°	$> 0.5 \tau$
P_2	8.6 dB	62°	0.36 τ	9.2 dB	45°	$> 0.5 \tau$

Table 1: Gain, Phase and Delay Margins (Pitch Channel)

	Equivalent Loop				Outer Loop			
P_N]-13	7.8[dB 33°	0.07 τ]-20	11.5[dB 26°	$> 0.5 \tau$
P_0]-28	7.8[dB 40°	0.1 τ]-30	10.7[dB 37°	$> 0.5 \tau$
P_1]-15	7.8[dB 32°	0.07 τ]-30	11[dB 26°	$> 0.5 \tau$
P_2]-30	6.5[dB 34°	0.09 τ]-30	8.5[dB 34°	$> 0.5 \tau$

Table 2: Gain, Phase and Delay Margins
(Yaw / Roll Channels)

6.3 Robustness to Parametric Perturbations

H_∞ methods can not take explicitly into account real parametric robustness objectives, so it is important to analyse the robustness of the design in the face of such uncertainties.

Each of the 15 aerodynamic coefficients C_i in (1.a)-(1.e) is assumed to be constant, but unknown, in the interval

$[C_{i_0}(1-p_i) \ C_{i_0}(1+p_i)]$; C_i is then represented as $C_i = C_{i_0}(1+\delta_i p_i)$ where p_i is the nominal dispersion and $\delta_i \in \mathbb{R}$, $|\delta_i| \leq 1$ represents the normalized uncertainty associated with C_i (depending on the coefficient, the nominal dispersion p_i is between 10% and 45%).

The state space model of the plant can now be written-as:

$$\begin{cases} \dot{x} = (A + \sum_{i=1}^n \delta_i \bar{A}_i)x + (B + \sum_{i=1}^n \delta_i \bar{B}_i)u \\ y = (C + \sum_{i=1}^n \delta_i \bar{C}_i)x \end{cases} \quad (25)$$

and the corresponding closed-loop plant is transformed into the *LFT* structure of Figure 7.b (For this study parametric uncertainties δ_i enter linearly in the state space equations of the closed loop, so that they are represented by non repeated scalar blocks in Δ_1). The *LFT* structure is created using Morton's method [6].

Moreover the values of the natural frequencies of the bending modes are assumed to be accurate to within 15% and the values of damping ratio to within 50%; those data will then also be dissipated.

To this end the first bending mode is modelled by:

$$\ddot{q} = ku - \omega_0 (2\xi_0 \dot{q} + \omega_0 q) \quad (26)$$

with $u = \eta_{ex}$ for the pitch channel, $u = \zeta_{ex}$ for the yaw channel, and k is a scalar gain.

The frequency ω_0 and the damping ratio ξ_0 are then replaced by perturbed values:

$$\omega_p = \omega_0 + \delta_\omega \omega_1 \quad \text{and} \quad \xi_p = \xi_0 + \delta_\xi \xi_1 \quad (27)$$

The corresponding *LFT* structure (see Figure 8) is then [11]:

$$\frac{k}{s^2 + 2\xi_p \omega_p s + \omega_p^2} = \mathcal{F}_u \left(M, \text{diag} \{ s^{-1} I_2; \delta_\xi; \delta_\omega I_2 \} \right)$$

$$M = \begin{pmatrix} A & B_1 & B_2 \\ C_1 & D_{11} & D_{12} \\ C_2 & D_{21} & D_{22} \end{pmatrix} = \begin{pmatrix} 0 & 1 & 0 & 0 & 0 & 0 \\ -\omega_0^2 & -2\xi_0 \omega_0 & -\omega_0 & -\omega_0 & -1 & k \\ 0 & 2\xi_1 & 0 & 0 & 0 & 0 \\ \omega_1 & 0 & 0 & 0 & 0 & 0 \\ \omega_1 \omega_0 & 2\xi_0 \omega_1 & \omega_1 & \omega_1 & 0 & 0 \\ 1 & 0 & 0 & 0 & 0 & 0 \end{pmatrix} \quad (28)$$

Connecting this *LFT* with the one obtained by Morton, a new *LFT* is obtained, which allows to analyse stability of the closed loop in the face of simultaneous uncertainties on aerodynamic and bending modes coefficients. To this end, the real *ssv* for each model P_i of the family **P** with by the same controller K_f is computed.

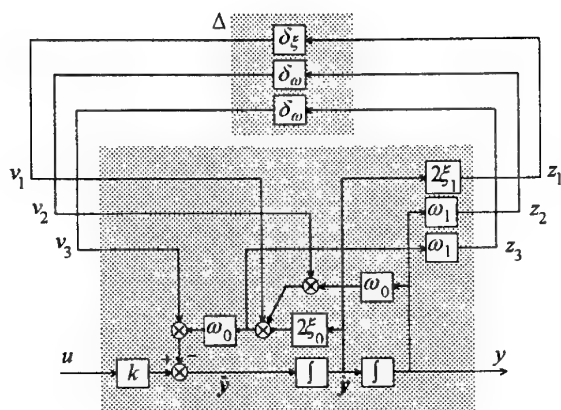


Figure 8: LFT of the 2nd order model

The plots of $\mu(\omega)$ upper and lower bounds for Model P_0 (P_c and YR_c) are shown on Figure 8. Similar curves are obtained for P_1, P_2, P_N . The maxima of $\mu(\omega)$ upper bounds (with the corresponding frequency ω) are listed in Table 3 for each model of P (P_c and YR_c).

The maximal values of $\mu(\omega)$ upper bounds being less than 1 (for each model of P), stability is guaranteed for uncertainties higher than the nominal dispersions.

	Pitch Channel Maximal Value of $\mu(\omega)$ [lower upper] bound frequency	Yaw / Roll Channels Maximal Value of $\mu(\omega)$ [lower upper] bound frequency
P_N	[0.74 0.88] $\tau\omega = 25.0$	[0.60 0.71] $\tau\omega = 28.5$
P_0	[0.76 0.87] $\tau\omega = 24.9$	[0.60 0.71] $\tau\omega = 28.4$
P_1	[0.73 0.88] $\tau\omega = 25.0$	[0.61 0.70] $\tau\omega = 28.4$
P_2	[0.74 0.88] $\tau\omega = 25.0$	[0.60 0.71] $\tau\omega = 28.5$

Table 3: Robustness to Parametric Uncertainties

7. NON LINEAR SIX DOF EVALUATION

A complete nonlinear six Degrees Of Freedom (DOF) simulation, including the nonlinear actuators and the bending modes, is finally used to validate the design. All classical manoeuvres have been successfully tested. As an example, Figure 9 (*resp.* Figure 10) shows the missile responses to a sharp turn (*resp.* diving flight) with dispersions on aerodynamic and bending modes coefficients. Specifications in terms of settling time, overshoot and decoupling are verified, while actuators outputs remain below the limitation values (this property was also verified for the first and second derivatives). Finally gain and delay margins were also

verified by introducing perturbations on gains and delays in the simulation.

8. CONCLUSION

An autopilot for a flexible missile was successfully designed using the loop-shaping H_∞ procedure. Real μ analysis was then used to compute multivariable stability margins and to check the robustness of the design against uncertainties on the aerodynamic coefficients and the bending modes: it proved the stability of a family P of linear models, despite the nominal dispersions. Including the uncertainties and the nonlinear models, the validation in a six DOF simulation of the missile motions confirms the performances and the robustness of the computed autopilot.

9. REFERENCES

- [1] D. McFarlane and K. Glover, "Robust Controller design Using Normalised Coprime Factor Plant Descriptions", *Lecture Notes in Control and Information Sciences*, Springer Verlag, (1990).
- [2] K. Glover and D. McFarlane, "Robust Stabilisation of Normalised Coprime Factors Plant Description with H_∞ Bounded Uncertainty", *IEEE Trans. Autom. Control*, vol. 34, pp. 821-830, (1989).
- [3] D. McFarlane and K. Glover, "A Loop Shaping Design Procedure Using H_∞ -Synthesis", *IEEE Trans. Autom. Control*, vol. 37, pp. 759-769, (1992).
- [4] J.C. Doyle, "Analysis of Control Systems With Structured Uncertainty", *IEEE Proc. Part. D*, vol. 129, pp. 242-250, (1982).
- [5] J.C. Doyle, A. Packard and K. Zhou, "Review of LFTs, LMIs, and μ ", *30th Conf. on Decision & Control*, pp. 1227-1232, Brighton, (1991).
- [6] B.G. Morton, "New Applications of μ To Real Parameter Variation Problems", *24th IEEE Conf. on Decision & Control*, pp. 233-238, (1985).
- [7] A. Packard and P. Pandey, "Continuity Properties of The Real / Complex Structured Singular Value", *IEEE Trans. Autom. Control*, vol. 38, pp. 415-428, (1993).
- [8] G.J. Balas, J.C. Doyle, K. Glover, A. Packard and R. Smith, " μ Analysis And Synthesis Toolbox", The Math Works Inc., (1993).
- [9] J.M. Siret, G. Michalesco and P. Bertrand, "On The Use of Aggregation Techniques", in *Handbook of Large Scale Systems Engineering Applications*, M. Singh and A. Titli Edts, pp. 20-37, North-Holland, (1979).
- [10] G. Ferreres, V. Fromion, G. Duc and M. M'Saad, "Application of Real / Mixed μ Computational Techniques to a H_∞ Missile Autopilot", *Int. Journal of Robust and Nonlinear Control*, to be published.
- [11] S. Font, *Méthodologie pour Prendre en Compte la Robustesse des Systèmes Asservis : Optimisation H_∞ et Approche Symbolique de la Forme Standard*, Thèse de Doctorat, Supélec et Paris-Sud, (1995).

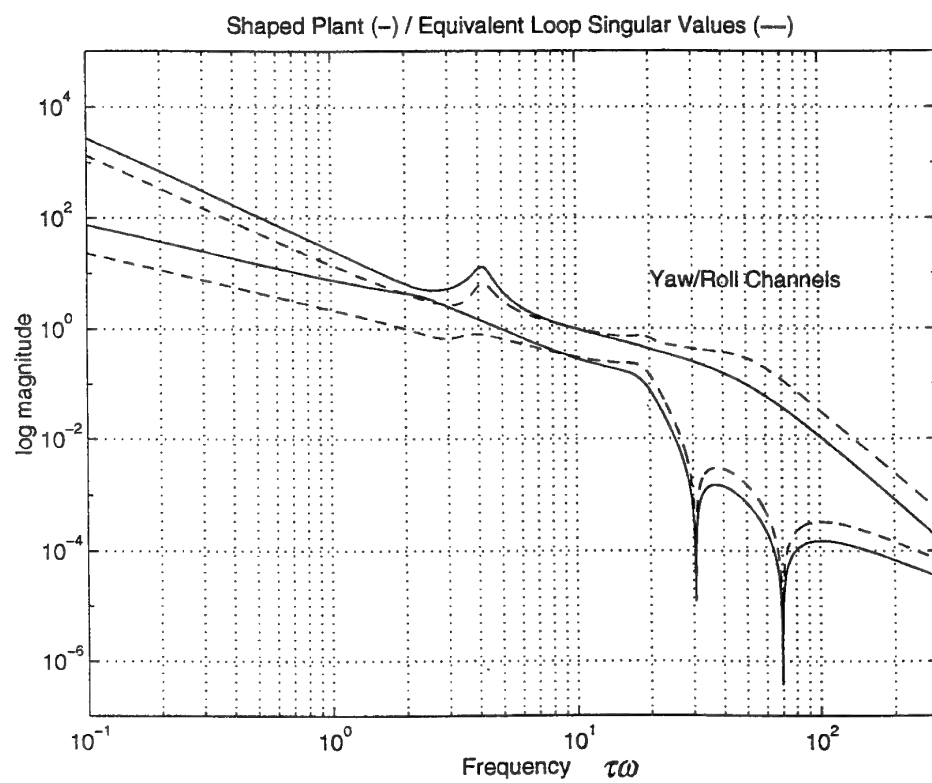
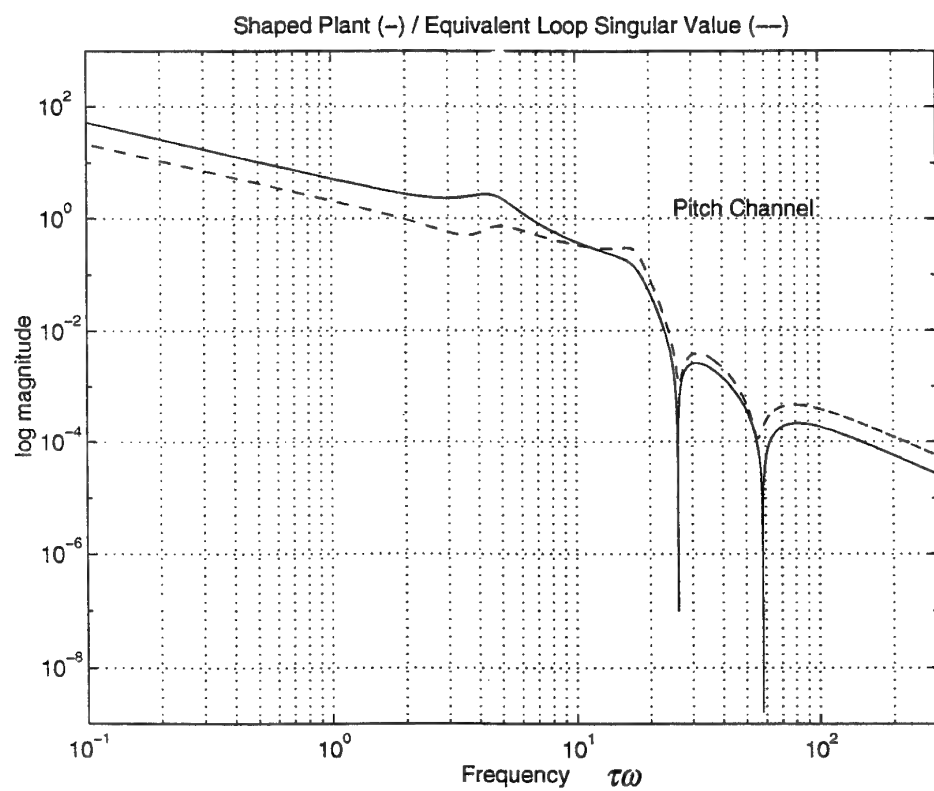


Figure 5. Equivalent – Loop singular values, Pitch Channel / Yaw Roll Channels

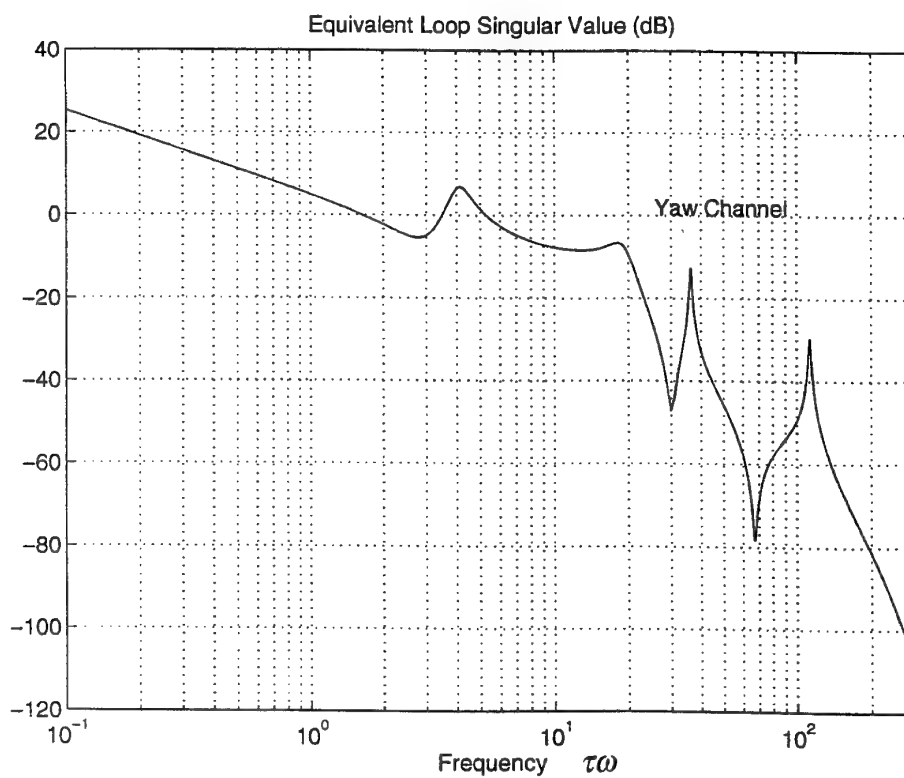
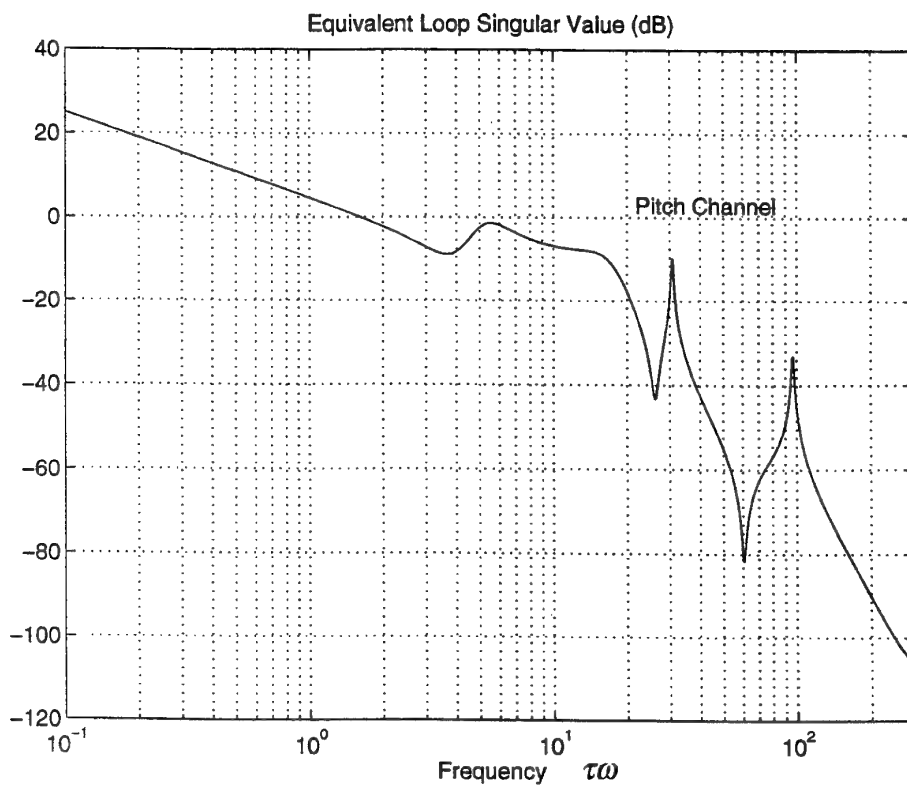


Figure 6. Equivalent – Loop Bode plots, Pitch Channel / Yaw Channel
with the two first bending modes

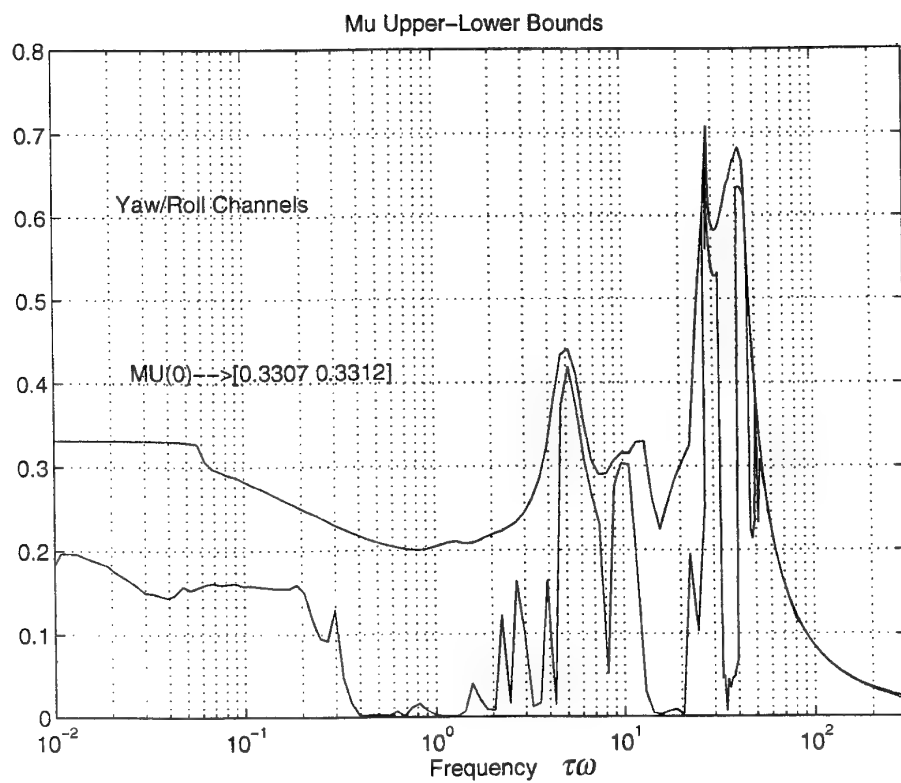
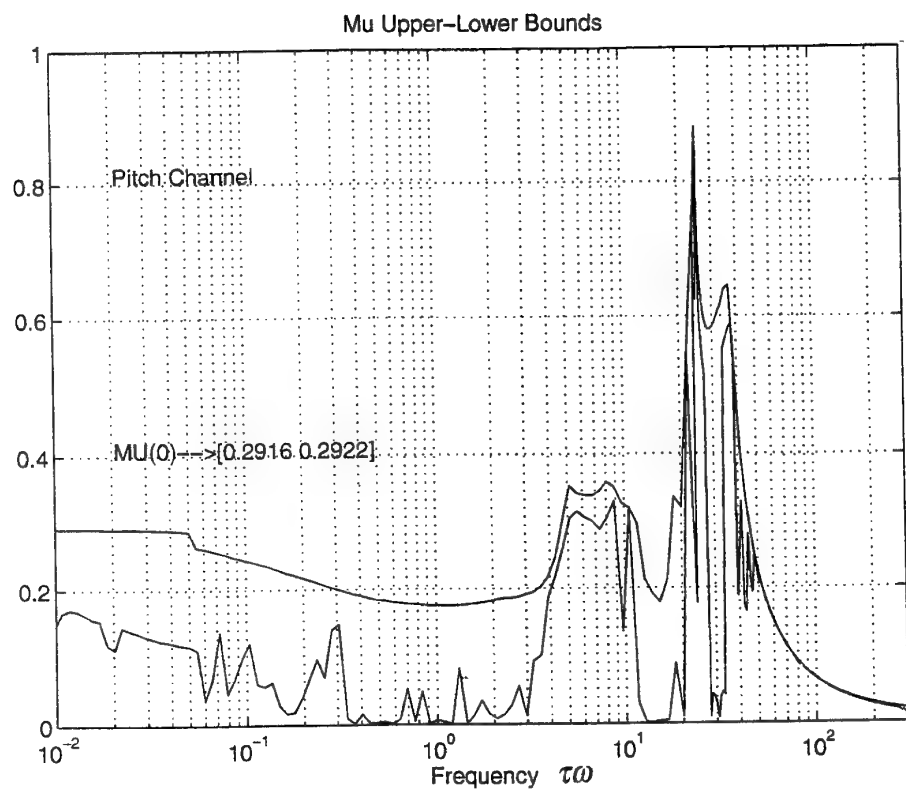


Figure 8. μ Upper and Lower Bounds for Model P_0 , Pitch Channel / Yaw Roll Channels

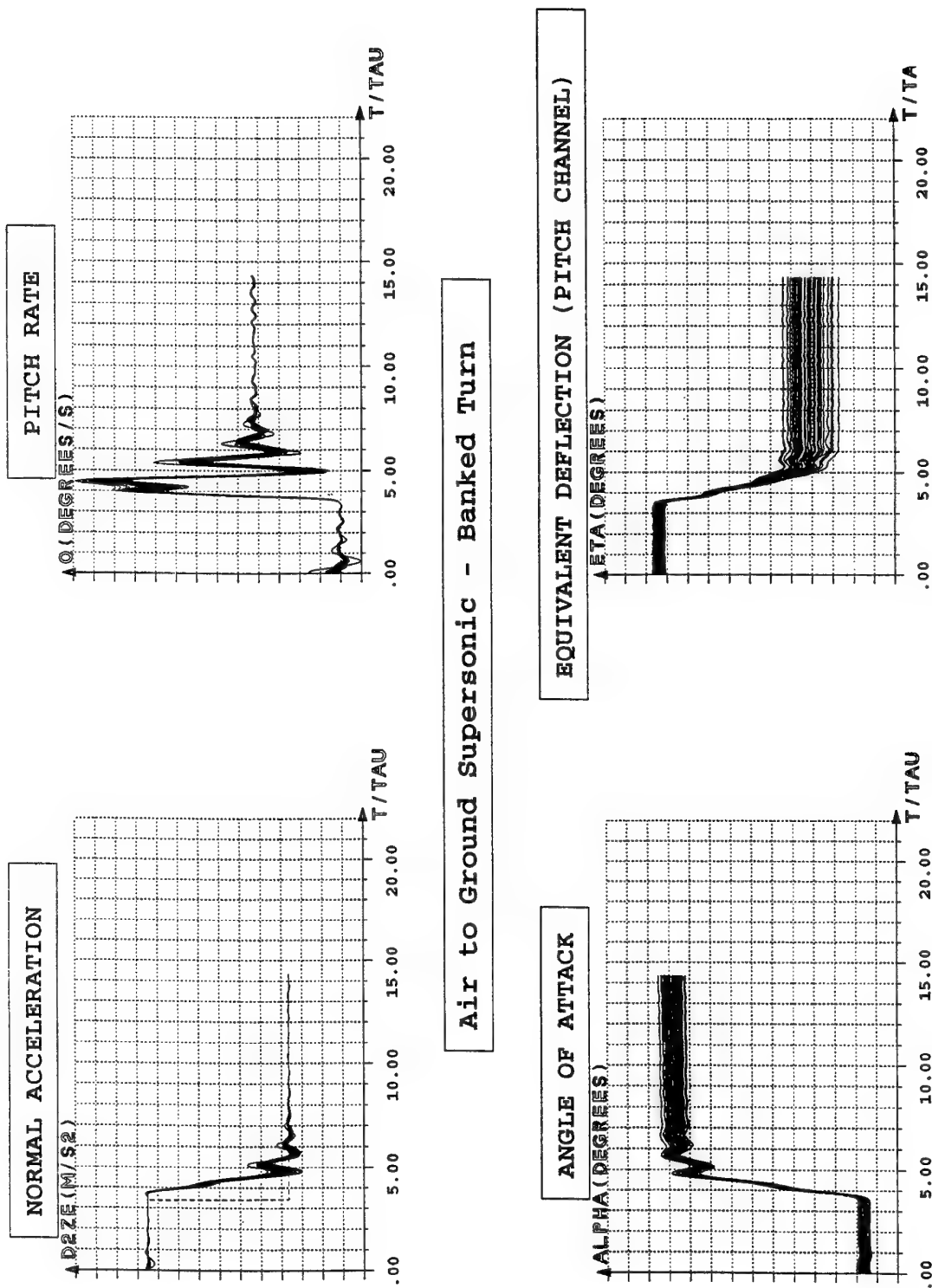


Figure 9. Missile Responses to a sharp turn a) Pitch Channel

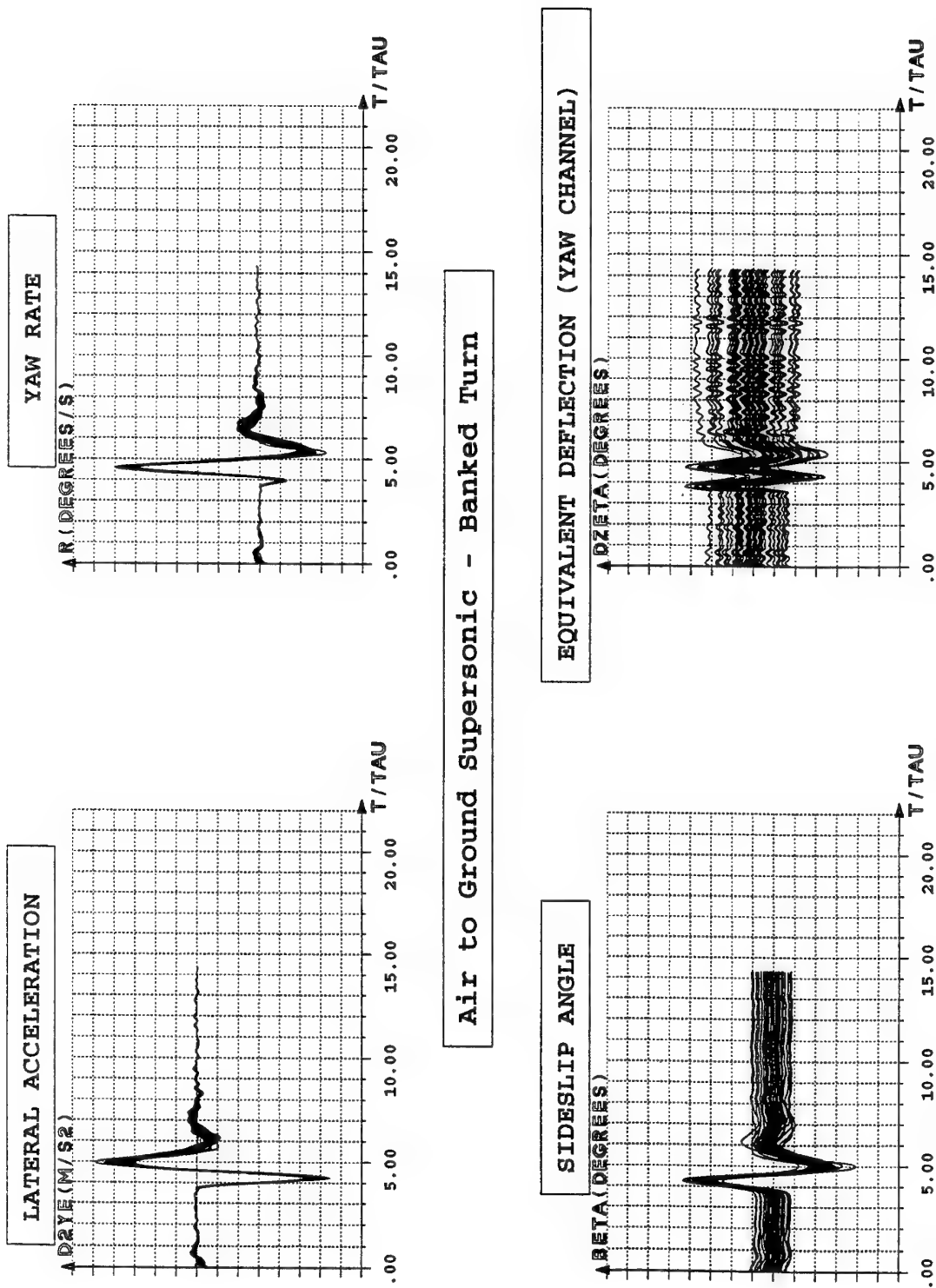


Figure 9. Missile Responses to a sharp turn b) Yaw Channel

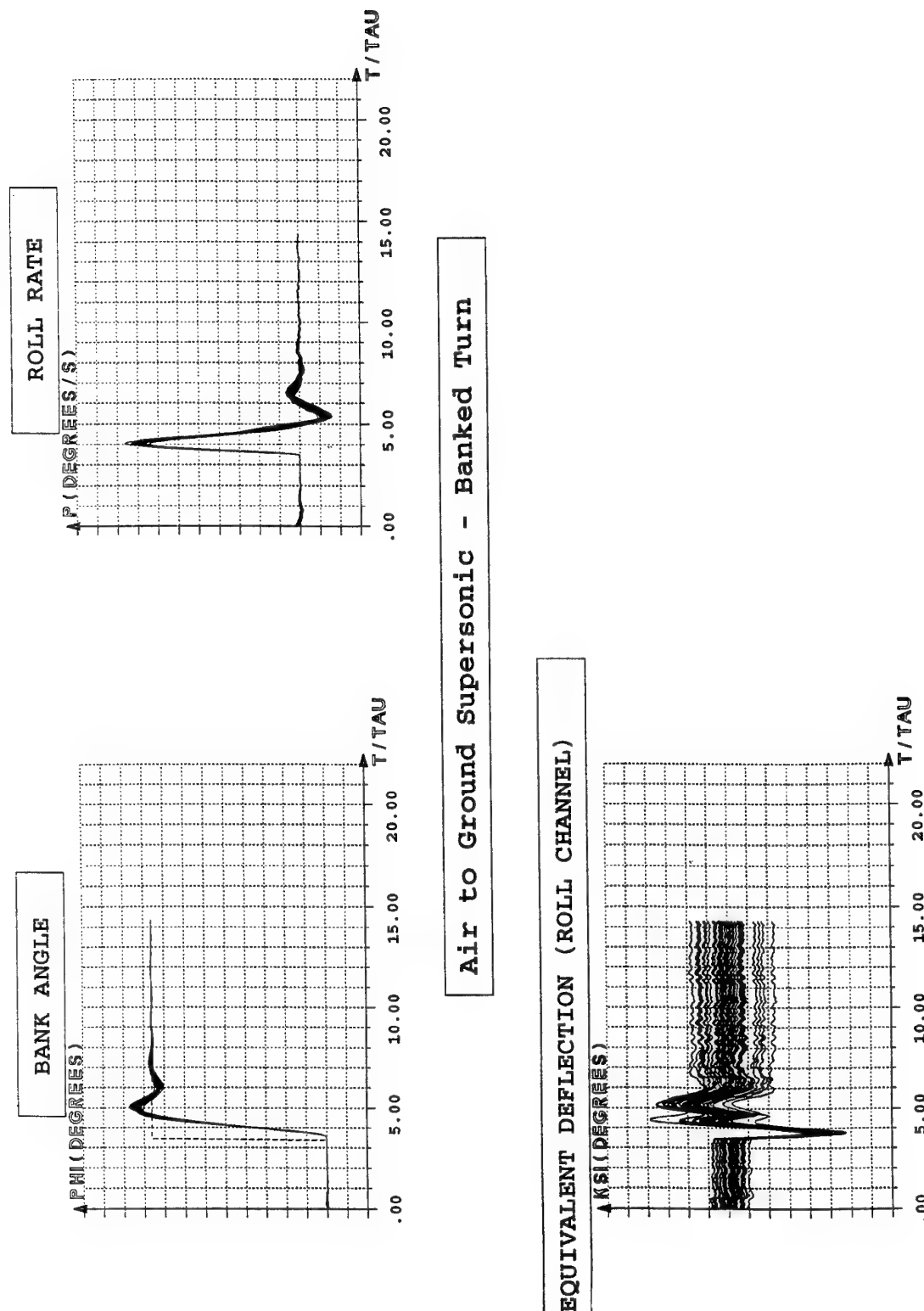


Figure 9. Missile Responses to a sharp turn c) Roll Channel

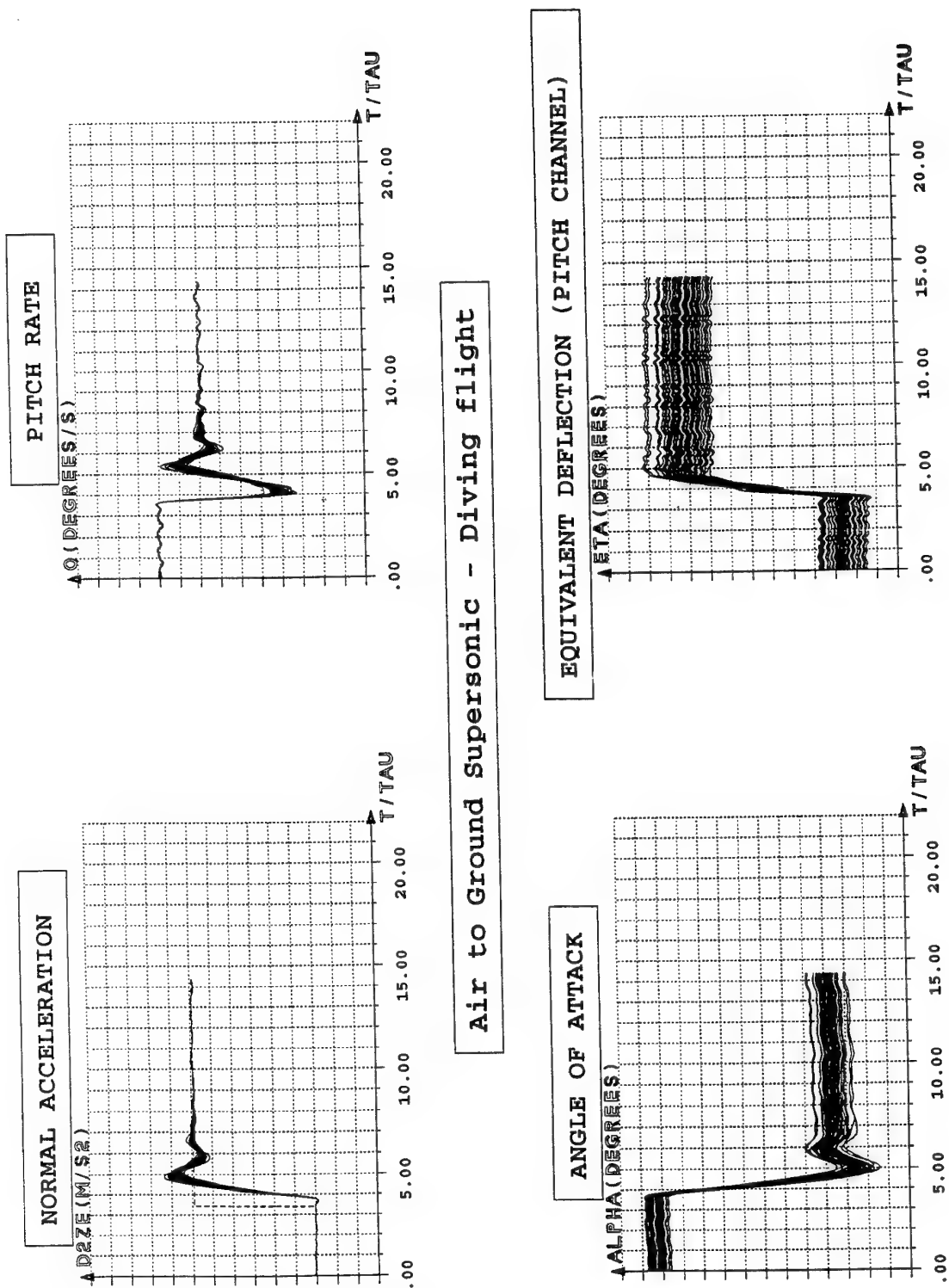


Figure 10. Missile Responses to a diving flight a) Pitch Channel

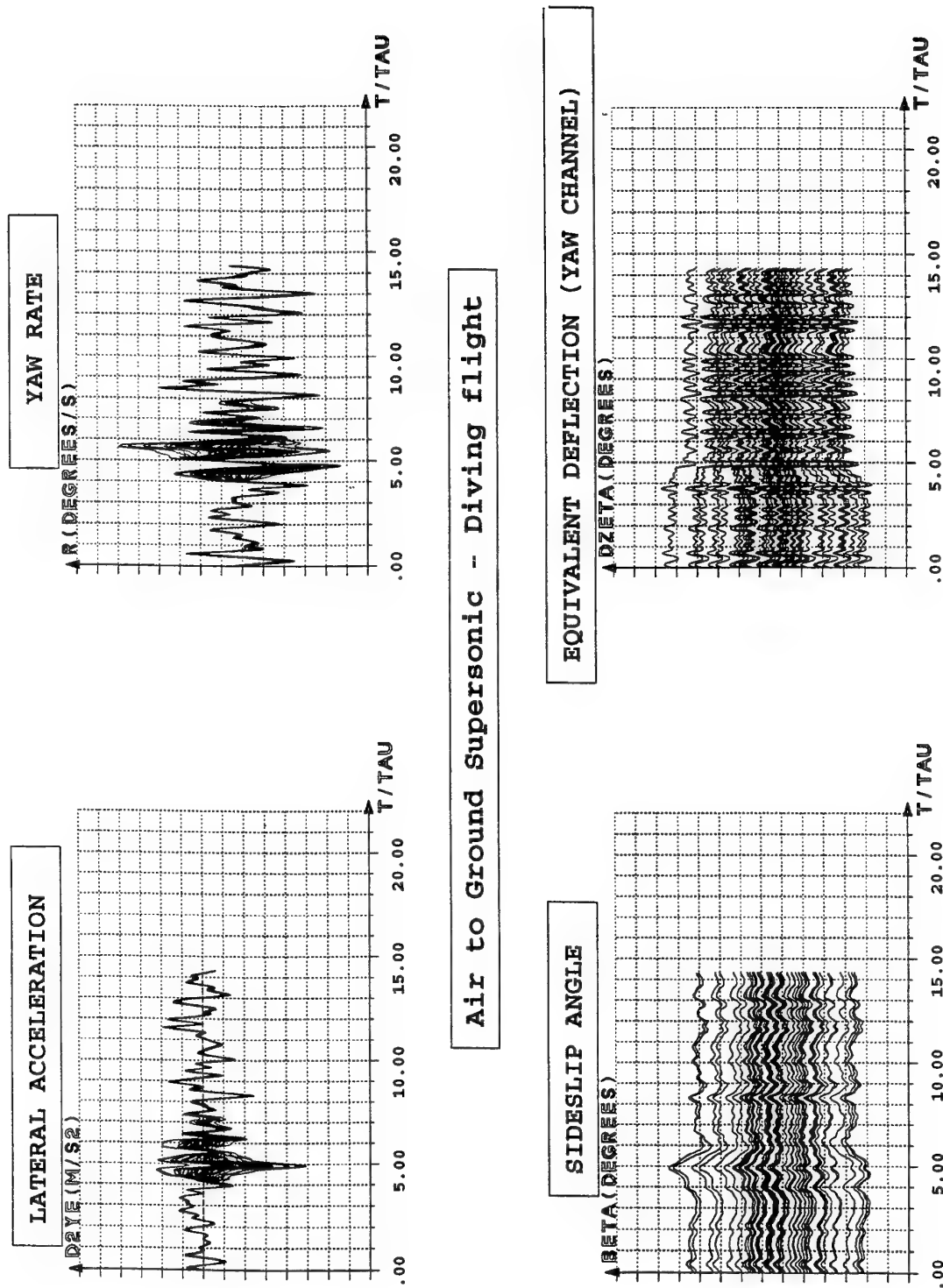


Figure 10. Missile Responses to a diving flight b) Yaw Channel

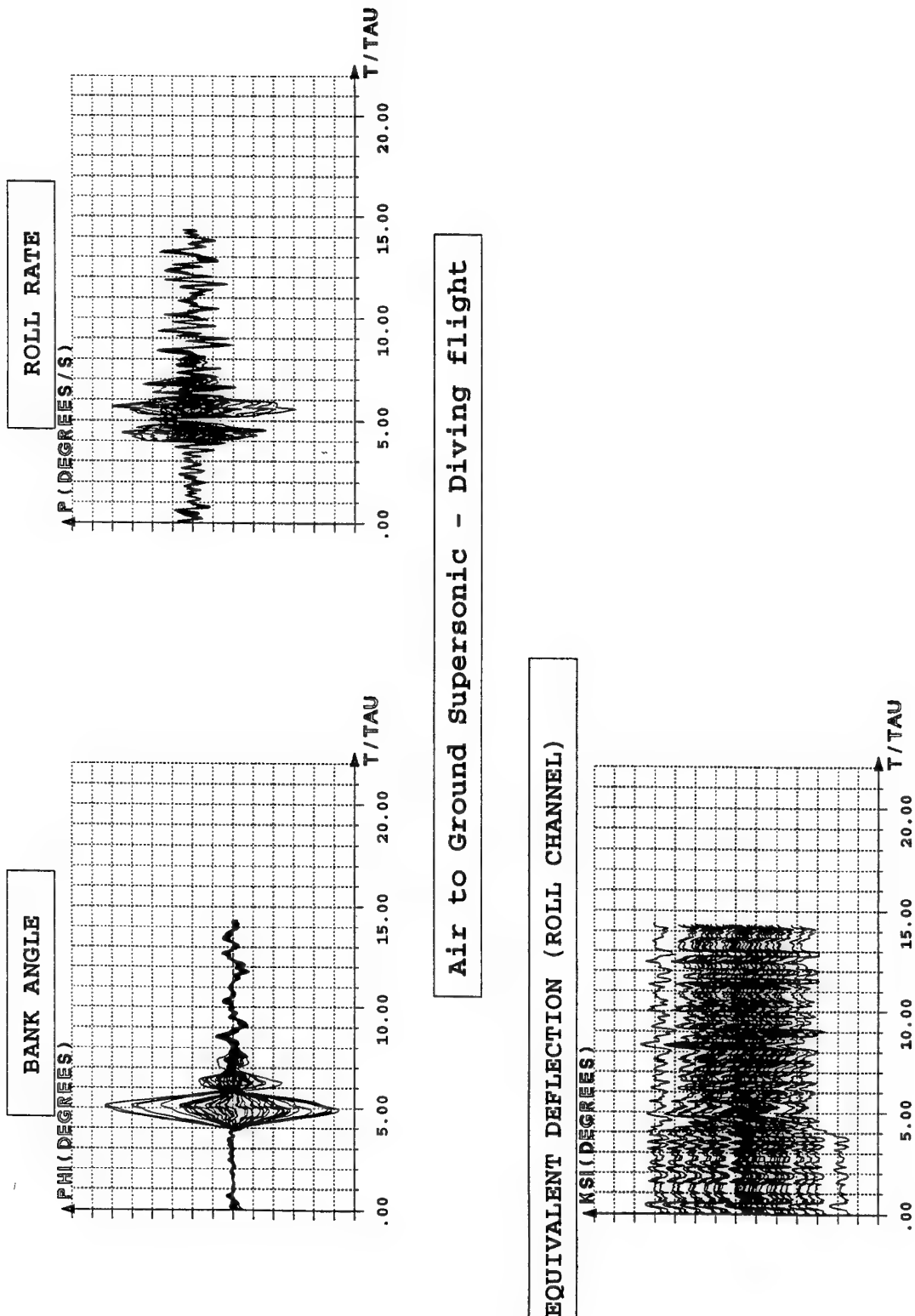


Figure 10. Missile Responses to a diving flight c) Roll Channel

MONTE CARLO SIMULATION STUDIES OF UNGUIDED AND GUIDED MISSILES BASED ON PROBABILISTIC MODELLING OF AERODYNAMIC COEFFICIENTS

A.Osman MERTTOPÇUOĞLU
ROKETSAN Missiles Industries Inc.
P.O. Box:30, Elmadag
06780 Ankara, TÜRKİYE

Hüda H. ÖZDAMAR
ROKETSAN Missiles Industries Inc.
P.O. Box:30, Elmadag
06780 Ankara, TÜRKİYE

M. Kemal ÖZGÖREN
Middle East Technical University
Mechanical Eng. Dept.
06531 Ankara, TÜRKİYE

SUMMARY

The main motivation underlying this work is to develop a methodology by which the effect of aerodynamic estimation errors on flight simulation problems are investigated. A "family" is defined as a predetermined class of similar missile configurations for which a reference aerodynamic data is available. The error is defined as the difference between the results of the "available computational method" and the reference data. Then the statistical characteristics of the errors in the aerodynamic coefficients are determined assuming Gaussian probability distribution for the members of the "family". For a proposed missile configuration which fits to the "family", the aerodynamic coefficients are first obtained using the "available computational method". Afterwards, the errors in these aerodynamic coefficients are estimated using the statistical characteristics determined above.

LIST OF SYMBOLS

\hat{C}	: Covariance Matrix of \bar{x}
C_m, C_n	: Pitch and yaw moment coefficients
$C_{m\alpha}, C_{n\beta}$: Pitch and yaw derivatives
C_x, C_y, C_z	: Axial, side and normal force coefficients
$C_{y\beta}, C_{z\alpha}$: Side and normal force derivatives
f	: Probability density function
\hat{L}	: Transform matrix into \bar{y} domain
M	: Mach number
\bar{x}	: Random variable vector
\bar{y}	: Transformed random variable vector
α, β	: Angle of attack and angle of sideslip
δ	: Control deflection angle
\bar{e}	: Error vector
$\hat{\Lambda}$: Diagonal Standard deviation matrix of \bar{y}
$\bar{\mu}$: Mean value vector of \bar{x}
σ	: Standard deviation values of \bar{y}
Subscripts	
c	: of calculated (nominal) data
i	: of ith configurations
r	: of reference data

1. INTRODUCTION

In a preliminary design stage, one needs to make flight simulations of the proposed missile. For this purpose, since the missile is not materialized yet, one necessarily uses an available computational method to determine the aerodynamic coefficients. Obviously, these computed coefficients will contain some uncertainties. Then, one would like to see the effects of these uncertainties on the simulated flight of the missile. Thus, it would be possible to judge the reliability of the simulations and based on this judgment one could take

healthier decisions to improve the design of the missile. Furthermore, in the case of a guided missile, it would become possible to check autopilot robustness against aerodynamic uncertainties. Under the cover of this paper, a method based on a statistical analysis is illustrated [1]. By the aid of this method one can statistically show the effects of uncertainties in the aerodynamic coefficients on the simulations of unguided and guided missile flights.

A Monte Carlo error analysis procedure is proposed in this work, in order to investigate the flight mechanics under the influence of indeterminate aerodynamic coefficients. The main concern is to provide a computational method to the designer to enable him to deal with aerodynamic uncertainties, especially at a preliminary stage of the design. The method is based on a probabilistic error model from which a subsequent trajectory sensitivity analysis follows in the scope of the work. The treatment is extended to cover both unguided and guided missiles.

2. FAMILY DESCRIPTION

Aerodynamic estimation methods make similar mistakes for similar missile configurations. An error in the prediction of an aerodynamic coefficient comes from an obvious inability of that method to account for some physical aspects of gas dynamics around the body. However, this deficiency will be repeated for similar missile configurations, under similar conditions. Corollary of this fact states that an aerodynamic estimation error model to be established for a certain prediction tool under certain conditions, is likely to be over a range of similar missile configurations.

A "family", under the cover of this work, is defined as a predetermined class of similar missile configurations for which a reference aerodynamic data is available. This reference data may originate from flight tests or wind tunnel tests or advanced computational methods. The error is defined as the difference between the results of the "available computational method" and the reference data. Under the light of the fact discussed in the previous paragraph, which has also led to the definition of "family", a correlation must exist between the error values belonging to the "family" members.

Another correlation, which is used in this work, is among the aerodynamic coefficients at different Mach numbers. Although aerodynamic coefficients are treated as random numbers, the preservation of the physical pattern as Mach number changes is also considered. The variation of these random numbers should reflect the physical appearance of the actual coefficients. This fact is also taken into account thus the resultant error model includes correlation among the coefficients at several Mach numbers.

3. RANDOM DATA GENERATION

Let \bar{x} be the n th order random variable vector of concern. In the present work, elements of \bar{x} correspond to the values of an aerodynamic coefficient at different Mach numbers. For \bar{x} , a covariance matrix \hat{C} , and a mean value vector $\bar{\mu}$ are defined as

$$\bar{\mu} = E\{\bar{x}\}$$

$$\hat{C} = E\{(\bar{x} - \bar{\mu})(\bar{x} - \bar{\mu})^T\}$$

where $E\{\}$ is expected value operator.

With predetermined elements $\bar{\mu}$ and \hat{C} , the probability density function of \bar{x} is defined as a multivariable jointly normal distribution, which may be expressed as [2].

$$f_{\bar{x}} = a \exp \left\{ -\frac{1}{2} [(\bar{x} - \bar{\mu})^T \hat{C}^{-1} (\bar{x} - \bar{\mu})] \right\}$$

$$\text{where } a = (2\pi)^{-\frac{n}{2}} \det^{\frac{1}{2}}(\hat{C})$$

The reasons for the selection of a Gaussian distribution function may be stated as follows :

- It is simple to construct due to the fact that information on mean value and covariance matrix is sufficient.
- It is suitable to the use of linear transform techniques.
- Most natural random phenomena, originated from large number of independent sources, may readily be shown to obey the normal distribution equation.

For our purpose, the random variable vector is defined as

$$\bar{x} = \bar{x}_c + \bar{e}$$

where \bar{x}_c is the calculated value of \bar{x} , by the available prediction tool, and \bar{e} is the error vector, which corresponds to the unknown (random) part to the coefficient vector. Let \bar{e}_i be the error vector of the i th member of the "family". For a "family" having N members, with $\bar{x}_{r,i}$ denoting the reference aerodynamic coefficient associated with the i 'th member, error vector is found as,

$$\bar{e}_i = \bar{x}_{r,i} - \bar{x}_{c,i}, \quad i = 1, 2, \dots, N$$

In the above expression $\bar{x}_{c,i}$ are again the calculated vectors for each member. Since each \bar{e}_i represents an occurrence in the prediction error within the "family" of interest, it may also represent an occurrence in the prediction error for the new configuration which is also similar to the members of the "family". So, a set of random vectors for the new configuration is defined as

$$\bar{x}_i = \bar{x}_c + \bar{e}_i, \quad i = 1, 2, \dots, N$$

Given the above set, the mean value vector and the covariance matrix are calculated as

$$\bar{\mu} = \frac{1}{N} \sum_{i=1}^N \bar{x}_i$$

$$\hat{C} = \frac{1}{N} \sum_{i=1}^N (\bar{x}_i - \bar{\mu})(\bar{x}_i - \bar{\mu})^T$$

There are several library routines in the computer domain now, that generate normally distributed random numbers. However, their usage is generally limited to the independent number vectors. So, in order to generate jointly normal random vectors, some transformations are required. Let,

$$(\bar{x} - \bar{\mu})^T \hat{C}^{-1} (\bar{x} - \bar{\mu}) = \bar{y}^T \hat{\Lambda}^{-2} \bar{y}$$

by definition. This transformation is such that $\hat{\Lambda}$ is a diagonal matrix, whose diagonal elements are standard deviation values, σ_i , of random elements of vector \bar{y} . By this definition elements of \bar{y} are independent random variables.

Structure of covariance matrix enables this transformation. Upon singular value decomposition of \hat{C}

$$\hat{C} = \hat{L} \hat{\Lambda}^2 \hat{L}^T$$

\hat{L} is the required orthonormal transformation matrix, where $\hat{\Lambda}$ is already defined. It turns out that,

$$\bar{y} = \hat{L}^T (\bar{x} - \bar{\mu})$$

$$\bar{x} = \hat{L} \bar{y} + \bar{\mu}$$

The probability density function of \bar{y} is given as,

$$f_{\bar{y}} = a \exp \left\{ \bar{y}^T \hat{\Lambda}^{-2} \bar{y} \right\}$$

Here, a is the same as before since $\det(\hat{C}) = \det(\hat{\Lambda})$. The disjoint property of \bar{y} leads to the following implementation:

$$f_{\bar{y}} = \prod_{j=1}^n \frac{1}{\sqrt{2\pi\sigma_j}} \exp \left\{ \frac{-y_j^2}{2\sigma_j^2} \right\} = \prod_{j=1}^n f_{y_j}$$

if σ_j are, by definition, the standard deviation values of y_j .

At this point, the overall procedure can be summarized as follows.

- Given "family" of N members calculate the quantities $\bar{\mu}$, \hat{C} .
- Create a normal random vector \bar{y} , with zero mean and standard deviation values σ_j for each y_j .
- Transform it into the \bar{x} domain.
- Form an ensemble on \bar{x} for a Monte Carlo analysis. To do this, repeat the \bar{x} generation process several times.

The Monte Carlo analysis here can be seen as a means of transformation to reach a distribution in the trajectory domain from the aerodynamic coefficient domain. The applications will follow in later sections.

A special case is that the covariance matrix \hat{C} is rank deficient. Let,

rank $(\hat{C}) = \text{rank}(\hat{\Lambda}) = r < n$
and $\sigma_j = 0$ with $r < j \leq n$.

So, upon singular value decomposition, some diagonal elements of $\hat{\Lambda}$ vanish. However, since the orthonormality of \hat{L} is not affected, transformations are still valid. Besides, the disjoint property of $f_{\bar{y}}$ implies that corresponding component \bar{y} can be dealt with separately. It can be shown that in the limiting case f_{y_j} behaves as indicated below:

$$\lim_{\sigma_j \rightarrow 0} \frac{1}{\sqrt{2\pi\sigma_j}} \exp \left\{ \frac{-y_j^2}{2\sigma_j^2} \right\} = \delta(y_j)$$

Thus, the density function turns out an impulse function which tells that the corresponding \bar{y} components form the deterministic modes of the distribution. So, although \hat{C}^{-1} does not exist in the rank deficient case, the definition of Gaussian distribution is still valid. However, it can be noted that the corresponding components of \bar{y} take place in the null space of \hat{C} , and accordingly have no contribution to \bar{x} . So it turns out that only the first r columns of \hat{L} become useful.

4. UNGUIDED APPLICATIONS

In order to cover the error analysis procedure discussed so far a generic missile configuration is introduced here. For this application, a rather general set of configurations is selected as a family; i.e. conventional missiles with slender bodies, with pointed noses and with cruciform tails. 11 configurations are selected as members. As the "available computational method", MISSILE DATCOM is used [3]. Compilation of the necessary reference data is realized by other means.

This test case is worked out using the coefficients C_x , $C_{z\alpha}$ and $C_{m\alpha}$. A covariance matrix and a mean value vector is calculated for each coefficient. In order to set out the Monte Carlo analysis a total number of 100 coefficient-Mach curves are generated for each coefficient. Each coefficient vector comprises 27 values of the coefficient at different Mach number. However, degree of freedom at the random number generation system (also number of non-zero singular values) is necessarily taken to be 11, which is the number of reference configurations. A sample of generated curves (10 curves of C_x) is given in Figure 1. In Figure 2, there is shown the mean value and standard deviation curves of C_x , beside the nominal curve.

Table 1 lists some data used in the unguided simulation applications. Total 100 simulations are performed in this analysis. MATRIXx software[4] is chosen as the simulation environment. Standard atmosphere model is used to obtain atmosphere data. A thrust misalignment factor is introduced as a disturbance source to the simulations. Lateral aerodynamics is calculated by means of the symmetry considerations (i.e. $C_{y\beta} = C_{z\alpha}$, $C_{n\beta} = -C_{m\alpha}$). Finally, the damping derivatives are taken with their nominal values. For the specified application, trajectory dispersions (in y and z directions, and in Mach Number) with 40 samples are shown in Figure 4. The impact plane, with hit points (for all the 100

samples) around the nominal hit point, with mean impact point and with the 50% region can be seen in Figure 3.

5. GUIDED APPLICATIONS

The missile defined in this section is implanted with autopilots which are functioning in pitch, yaw and roll directions. Then the configuration is controlled so as not to deviate from its nominal ballistic trajectory. The gains of the autopilots are calculated as a result of a linear quadratic regulator design, and are allowed to be scheduled as a function of distance. Roll autopilot is assumed to function efficiently, so that no spin is considered throughout the flight. The control is achieved by means of the surfaces located at the tail of the missile. This makes the aerodynamics of the missile more complicated as the coefficients become the functions of not only Mach number but also α and δ . So each coefficient requires data presented in the form of 3-dimensional matrices. However, no correlation data is available in the α and δ domains. The way followed here is to assume a strong correlation between the coefficients and their zero α and δ counterparts, so, the 3-dimensional scale matrices are defined as follows:

$$S_m(M, \alpha, \delta) = \frac{C_m(M, \alpha, \delta)}{C_{m\alpha}(M)}$$

The procedure is that, first the random coefficients vectors are obtained as in the unguided case, then these vectors are multiplied by scale-matrices to obtain 3-dimensional C_x , C_z , C_m matrices, then, it is assumed that longitudinal and lateral aerodynamics are similar and uncoupled, which in turn supplies C_y and C_n data.

The deviations from the trajectory are expressed in a cross plane taken perpendicular to the trajectory. y -cross axis is defined to be in this plane and parallel to the ground, while z -cross axis is in the plane and perpendicular to both the nominal trajectory and y -axis. Deviation curves of several simulations (40 samples taken here) in y -cross and z -cross directions are given in Figure 5.

Besides, control deflection history curves are also illustrated in the same figure for both autopilots. The impact plane appearance is as in Figure 6. In the figure, hit points (100 samples), the nominal hit point, the mean hit point and the 50% region are given.

Since autopilots are designed with nominal aerodynamic coefficients, another question is how the stability of the control is effected due to aerodynamic uncertainty. The real part of the most dominant eigenvalue is taken as the stability margin. Figure 7 shows the autopilot robustness probability in the longitudinal plane for different instances of the trajectory. Positive stability margins imply temporary instability probabilities for a portion of flight. The situation in the lateral plane is similar, so it is not separately illustrated.

6. CONCLUSION AND RECOMMENDATIONS

In this analysis, a Monte Carlo Simulation technique is used in order to analyze the effect of errors in the aerodynamic coefficients on the flight simulations of an unguided and guided missile. Monte Carlo technique can be seen as a means of transformation to correlate the outputs of a nonlinear system to its inputs in probabilistic terms. The success of this work

depends on the definition of the input domain (which covers the uncertainties in the aerodynamic coefficients) as close to physical reality as possible.

For instance, a randomly generated coefficient vs. Mach number curve should have a trend as similar as possible to a one which may occur in nature. The method developed in this work provides a means to define the input domain according to this principle.

The output of the analysis is the dispersion of the expected trajectory in a probabilistic sense. In this work, the results of both unguided and guided analyses are presented in various ways. Of course, the results of such analyses are case dependent. The main purpose here is to illustrate how the designer can draw any conclusion by using this error analysis method. The output of the Monte Carlo simulations can be post-processed in various ways. Eventually, this processed data will lead to some design decisions. The application of this method can provide the following possibilities to the designer:

- To find out the error envelope of the flight variables.
- To observe the scattering characteristics of the flight variables about their nominal value.
- To perform an error tolerance analysis in the presence aerodynamic uncertainties.
- To deduce the sensitivity of the trajectories to the aerodynamic coefficients.
- To perform robustness tests on the autopilots against uncertainties in the aerodynamic coefficients.
- To make CEP analysis and try to identify what share of the dispersion of the simulated trajectories is due to the aerodynamic uncertainties.
- To define flight variables in terms of probability density functions.

In a proper application with the availability of real reference data, the designer can take more advantage of the method, if he or she can

- develop error models to consider error variations as the functions of not only the Mach Number, but also α , β , δ .
- form the "family" to include larger number of similar configurations.

ACKNOWLEDGEMENTS

This work was supported by NATO AGARD Flight Mechanics Panel under the support project T77. Authors also wish to acknowledge ROKETSAN Missiles Industries Inc. for providing its conveniences throughout this work.

REFERENCES

1. Final Report of the NATO/AGARD Support Project T-77, "Statistical Characterization of Errors in Aerodynamic Coefficients and the Study of Their Effects on the Flight Simulations of Unguided and Guided Missiles via the Monte Carlo Method", M.K.ÖZGÖREN, A.O. MERTTOPÇUOĞLU, Jan. 1995.
2. "Probability, Random Variables, and Stochastic Processes", A. Papoulis, Mc. Graw-Hill, 1965
3. MISSILE DATCOM, Wright Laboratory, Wright Patterson Air Force Base, Ohio USA 1991.
4. MATRIXx, Xmath/SystemBuild Version 4.0, Integrated System Inc. Santa Clara USA, 1994

Table 1 : Data About Simulations

Empty Mass : 950 kg	Total Length : 3.9 m
Empty Ix : 30 kg.m ²	Diameter : 0.6 m
Empty Iy : 525 kg.m ²	Total Impulse : 1.8 MN.sec
Empty CoM (from back) : 2 m	Thrust Misalignment Angle : 0.2 deg.
Full Mass : 1650 kg	Launch Angle : 45 deg.
Full Ix : 50 kg.m ²	Launch Velocity : 55 m/s
Full Iy : 1250 kg.m ²	Launch Altitude : Sea level
Full CoM (from back) : 1.65 m	Launch Spin Rate (Unguided Case) : 2 rev/sec.

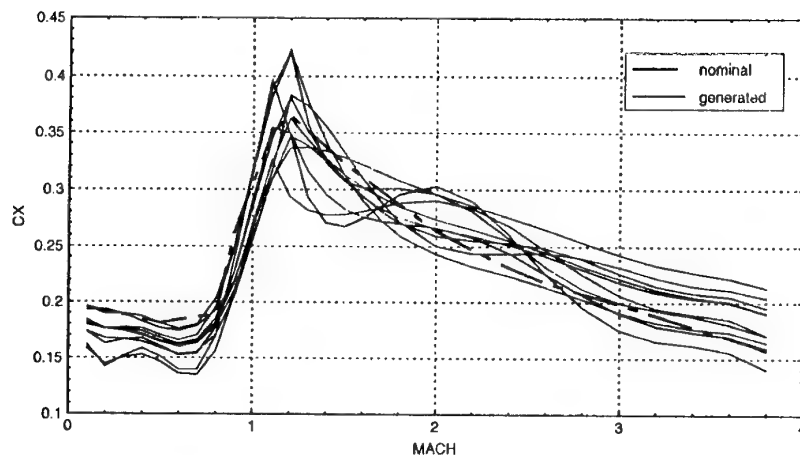


Figure 1 : Nominal and Generated Cx Curves

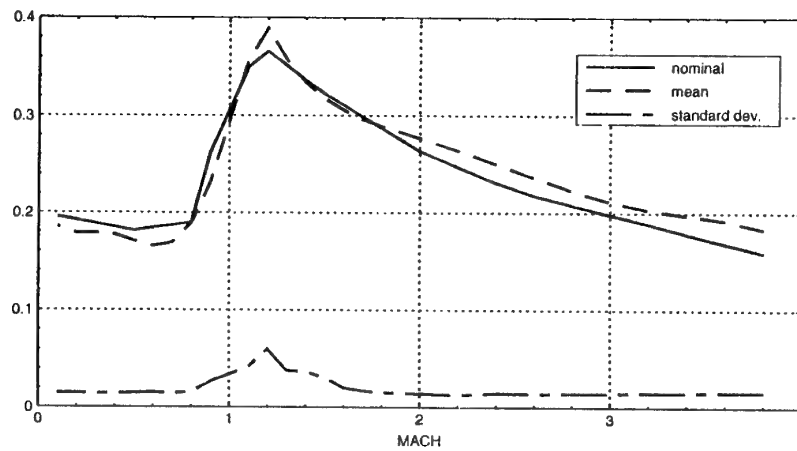


Figure 2 : Nominal, Mean and Standard Deviation of Cx

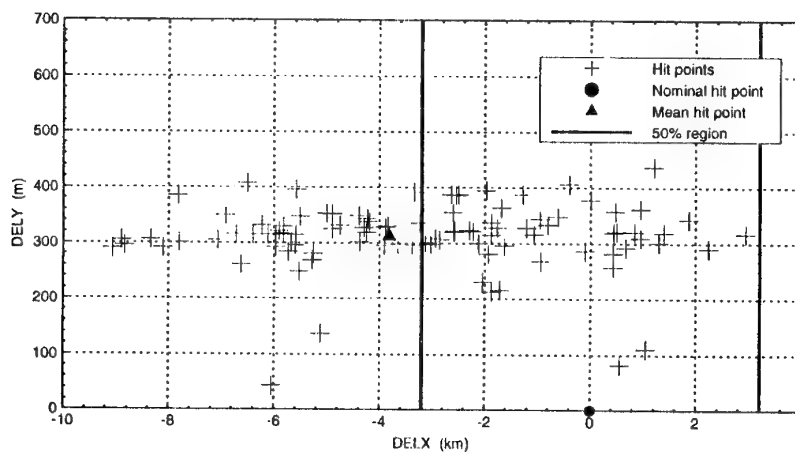


Figure 3 : Dispersion in Unguided Application

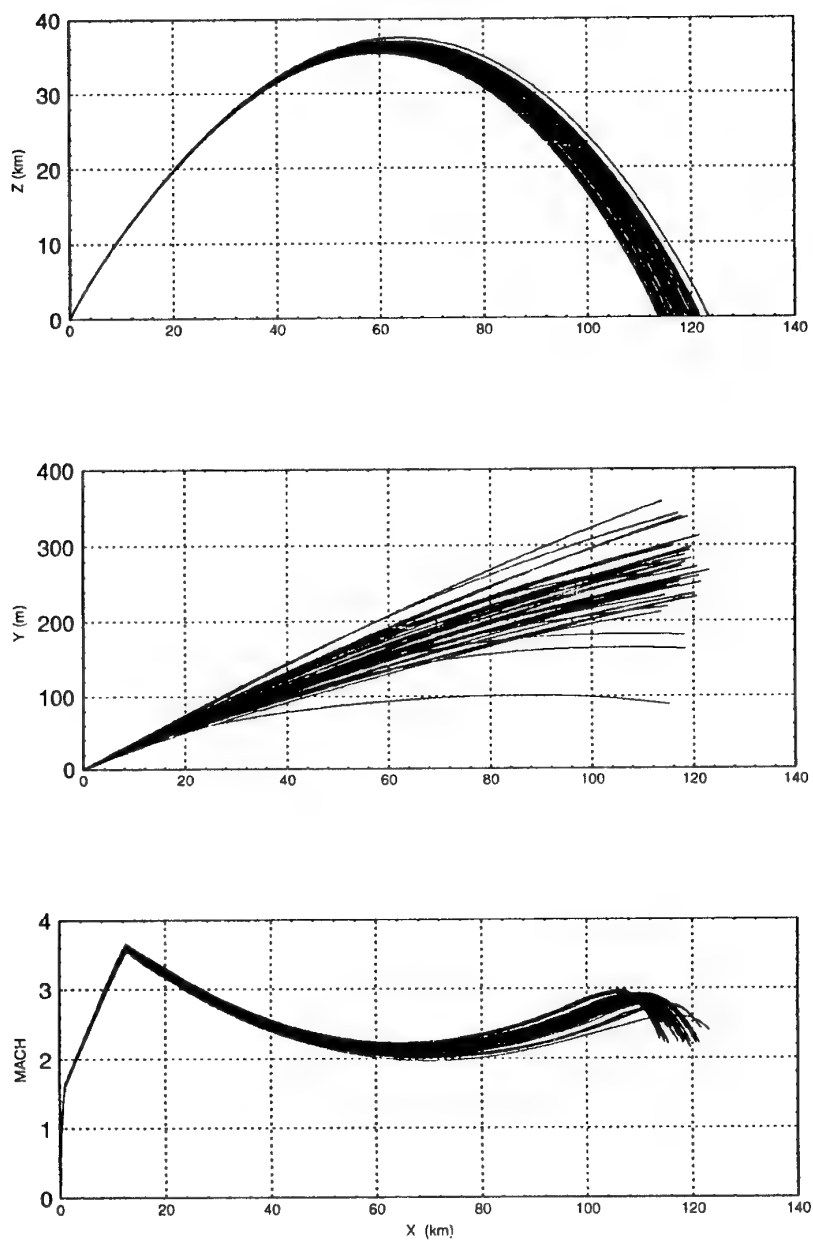


Figure 4 : Trajectory Envelope for Unguided Application

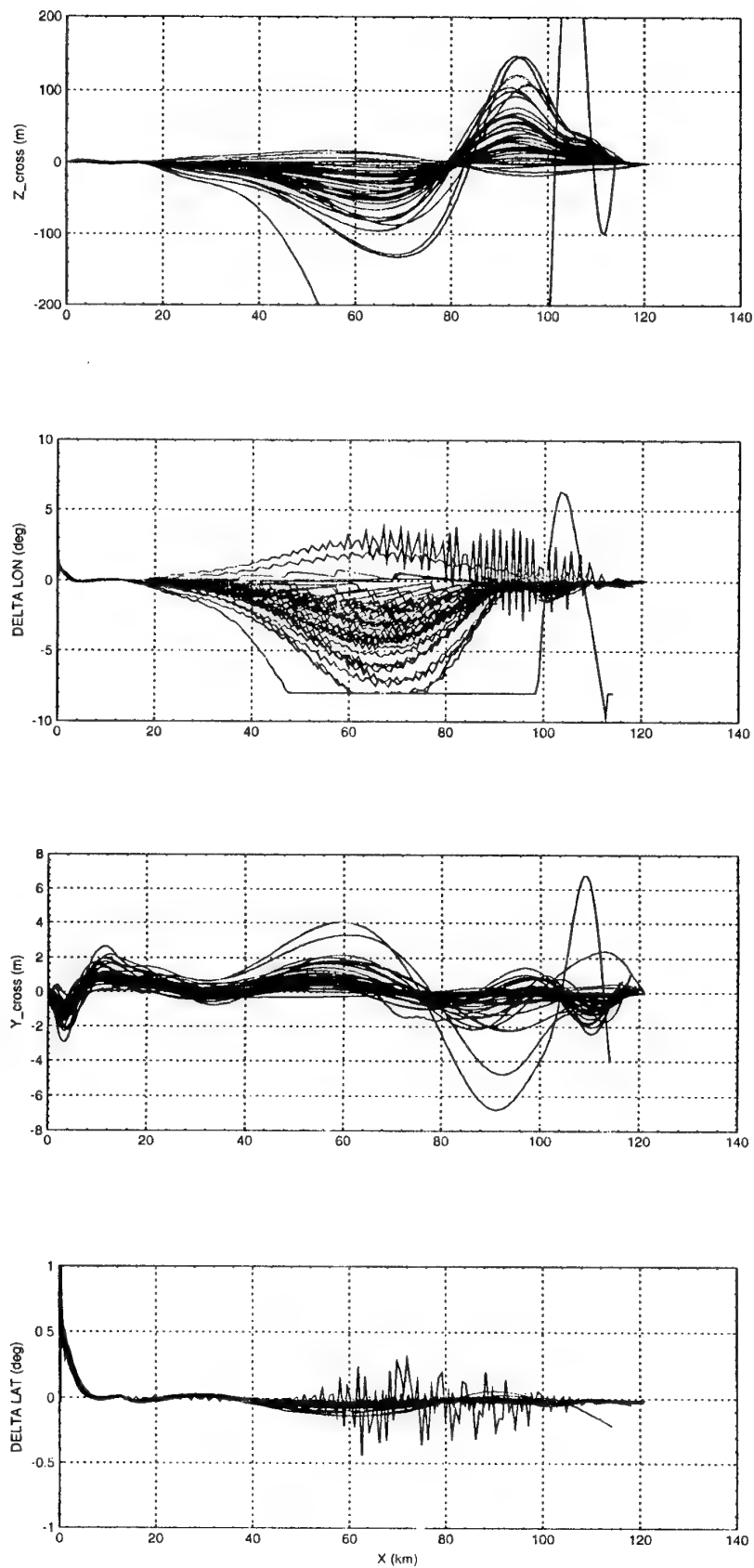


Figure 5 : Trajectory Envelope for Guided Application

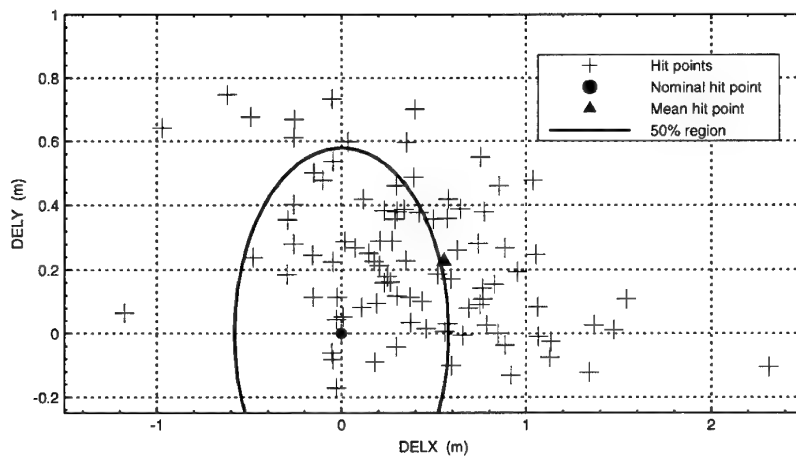


Figure 6 : Dispersion in Guided Application

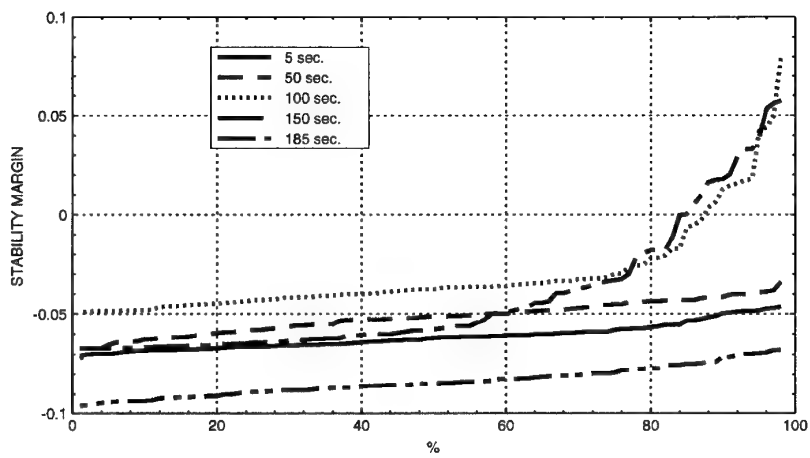


Figure 7 : Longitudinal Autopilot Robustness

The Future for UAVs in NATO

Robert C. Michelson

*Principal Research Engineer
Georgia Tech Research Institute
Atlanta, Georgia 30332*

INTRODUCTION

The face of NATO is changing in the light of the demise of the Soviet Block, however the need for NATO is perhaps more critical today than ever before due to the fragmented warring factions that have arisen in the absence of the stabilizing oppression of the Soviet Union and the Warsaw Pact. Unfortunately, these changes are occurring in the face of a global recession that has prompted the Nations to reconsider past levels of military spending. The demise of the Soviet Union is viewed as a reason to draw down forces and rely on existing (and sometimes antiquated) defense infrastructures.

Advances in machine intelligence and robotics can be leveraged to offset the negative impact of economically-induced factors affecting the Nations' forces during the next decade. Particularly in the areas of reconnaissance, intelligence, early warning, and even certain lethal operations, the use of Unmanned Aerial Vehicles (UAV) is predicted to be a major factor in the maintenance of an affordable military presence.

Low intensity conflicts along the borders of the Nations (as already witnessed in Bosnia) are expected to continue. Coupled with the need to continue certain NATO activities more effectively, is the occurrence of expanded missions that will arise due to increased trade in contraband as the Economic Community facilitates a more open Europe. Both land-based and maritime UAVs have a definite place within the NATO infrastructure, but currently the individual Nations do not have a clear or unified road map to define their use.

Given a coordinated plan for the use of UAVs by the Nations, what critical technologies must be put in place over the next few years to allow UAVs to meet the challenges of the missions expected by the year 2000? How will the predicted burgeoning of the commercial market for UAVs by the year 2000 affect NATO interests in this technology, and how can NATO leverage this commercial market for its own benefit?

This paper will identify both the military and commercial UAV missions expected by A.D. 2000. The analysis will consider the particular regional requirements posed by the geography of the member nations.

The contribution of the commercial sector to the development of these emerging technologies and

industry's use of UAVs for commercial applications such as overnight package delivery, security, or natural resource inspection will be a major factor considered by this paper.

NATO STRATEGIC PLAN

Before one can assess the future for UAVs in NATO, the future for NATO must first be defined. At their meeting in London in July 1990, NATO's Heads of State and Government agreed on the need to transform the Atlantic Alliance to reflect the new European situation. While reaffirming the basic principles upon which the Alliance was based, they realized that the developments taking place in Europe would have a far-reaching impact on the way NATO would function in the future. A new strategic environment would require a new strategic plan.

Since 1989, profound political changes have taken place in Central and Eastern Europe which have radically improved the security environment of the North Atlantic Alliance and its neighbors. The former satellites of the USSR have fully recovered their sovereignty. The Soviet Union and its Republics are undergoing radical change. The three Baltic Republics have regained their independence. Soviet forces have withdrawn from Hungary, Czechoslovakia, Poland and Germany. The Warsaw Pact nations have become nonaligned and there is even discussion about former foes joining NATO! The political division of Europe that was the source of the military confrontation of the Cold War period has ended. Further ameliorating the tension in Europe is the substantial progress in arms control that has already enhanced stability and security by lowering field of strategic nuclear arms levels and increasing military transparency and mutual confidence.

In spite of the improved security environment of today's Europe, NATO still faces real and ongoing threats. The risks facing NATO are different from what they were a decade ago. The threat of a simultaneous, full-scale attack on all of NATO's European fronts has effectively been removed and thus no longer provides the focus for Allied strategy. Particularly in Central Europe, the risk of a surprise attack has been substantially reduced. In contrast with the predominant threat of the past, the remaining risks to Allied security come from multiple, often unrelated sources of low-intensity conflict rising out of ethnic oppression or economic forces. As such, sources of future NATO risk are harder to predict and assess.

NATO has traditionally been concerned with threats to its member nations that are military in nature. Alliance security interests will be affected by other risks of a wider nature, including proliferation of weapons of mass destruction, disruption of the flow of vital resources, and acts of terrorism and sabotage. In the future, national threats such as the interdiction of contraband may warrant the attention and coordinated, concerted efforts of NATO forces to protect the populace. The NATO infrastructure that is in place to support military police actions could easily be turned to the suppression of terrorist acts and the drug trade.

The new NATO strategy can be summarized in a three-pronged approach to conflict prevention, abatement, and resolution. The three central elements to this strategy are: a) dialog, b) cooperation, and c) physical defense. According to the 1995 NATO handbook¹,

"The Alliance's active pursuit of dialogue and cooperation, underpinned by its commitment to an effective collective defence capability, seeks to reduce the risks of conflict arising out of misunderstanding or design; to build increased mutual understanding and confidence among all European states; to help manage crises affecting the security of the Allies; and to expand the opportunities for a genuine partnership among all European countries in dealing with common security problems."

Clearly, dialog and cooperation are preferable alternatives to physical defense, but misunderstandings though apparent acts of aggression can stop dialog and cooperation. Often adequate situational awareness (intelligence) is key to averting misunderstandings. Unmanned aerial reconnaissance vehicles can play a central role in information gathering to avoid or defuse misunderstandings that could lead to military action. Also, should military actions become inevitable, unmanned aerial reconnaissance vehicles can shorten the engagement significantly, as demonstrated in the Gulf War.

How UAVs will Fit into the Alliance's Force Posture

The Allies have agreed to move away, where appropriate, from the concept of forward defence towards a reduced forward presence, and to modify the principle of flexible response to reflect a reduced

reliance on nuclear weapons. This new force posture has significant implications for the use UAVs by NATO.

As the Allies pull in their talons, they will need to sharpen their eyes in order that they be able to go on the defensive quickly with conventional weapons or deploy their remaining nuclear assets without false alarm. Real-time reconnaissance across borders can only be done effectively from the air or space. The reaction time to divert satellite imagery for specific intelligence purposes may be too long logistically, or may conflict with the priorities already set by the owner of the satellite. Few nations are willing or able to bear the expense of intelligence satellites, however all of them can afford UAV reconnaissance systems.

Another consideration is the implication of foreign over-flights, be they over Allied countries or NATO's neighbors. Reconnaissance over-flights by manned fighters could send the wrong message and actually exacerbate ongoing dialog and cooperation—not to mention the risk to the pilot and the political repercussions were he to be shot down.

The 1995 NATO handbook states that based on the security objectives and strategic principles of the new European environment, "the organization of the Allies' forces must be adapted to provide capabilities that can contribute to protecting peace, managing crises that affect the security of Alliance members, and preventing war, while retaining at all times the means to defend all Allied territory and to restore peace."²

To realize the objectives stated by NATO doctrine, the size, readiness, availability and deployment of the Alliance's military forces will have to reflect a strictly defensive mission and adapt to the new strategic environment and its arms control agreements, by reducing the overall size of the Allied forces, while not diminishing its readiness.

Unmanned aerial vehicles can play a major role in resolving the contradiction of a smaller force with the readiness of a larger one by supplanting many manned aircraft missions with less expensive and less labor-intensive unmanned ones. The logistics burden required to train and support a fighter pilot and his aircraft is enormous compared to that of an unmanned system which, for many missions, can supply the same function better and for less cost.

Those missions which are dull, dirty, or dangerous (D³) are ideally suited for unmanned systems. Consider reconnaissance missions (typically very dull

¹ Anon., "The Alliance's Strategic Concept," Agreed by the Heads of State and Government participating in the meeting of the North Atlantic Council in Rome on 7-8 November 1991, as found in Appendix IX, Paragraph 26 of the *NATO Handbook*, 1995.

² *ibid.*, Paragraph 45.

from the pilot's perspective), or a situation in which aircraft may have to operate in nuclear, biological, or chemically dirty environments where the entire hazard is to the pilot, not his machine. Similarly, dangerous missions into territory where NATO does not have air superiority, risks not only the man, but the expensive non-expendable aircraft with its payload. When the NATO forces are forced to shrink due to economic and treaty pressures, the value of the remaining pilots increases by a factor that is directly proportional to the draw-down in the force. In the future, can NATO risk to send pilots on D³ missions other than those which are pilot-essential?

Unmanned aerial vehicles can be organic assets controlled by the local NATO commanders. This is possible due to the size and cost of typical UAV systems. Because UAVs can be organically controlled, they can provide quicker intelligence information to the units that have the need to know it. This then translates into shorter reaction times in response to new regional threats. This is entirely consistent with the notion that the conflicts which NATO will encounter in the future will be local rather than centrally-orchestrated and strategically executed.

To ensure that at this reduced force level the Allies' forces can be effective in managing crises and in countering aggression against any Ally, they will require enhanced flexibility and mobility. In order to do this, those forces available must include ground, air, and sea contingents in sufficient numbers and possessing the ability to react rapidly to a wide range of eventualities, many of which are unforeseeable. Though largely controlled from land-based forces or larger ships at sea (e.g., the battleship Missouri during the Gulf War), UAV assets have been shown to be deployable by smaller combatant units. Mobility of smaller land, air, and sea units can be increased if their situational awareness can be increased through better real-time intelligence that is directed to their own immediate information needs. A platoon will hesitate to cross the next hill if it does not know what awaits them on the other side. Theatre-wide information assets (satellites or AWACS) do not fill this information need with the speed or resolution necessary to make the fighting force move and react quickly.

In the event of a major conflict, the forces of the Allies must be structured to permit their military capability to build up rapidly. This ability to build up by reinforcement, by mobilizing reserves, or by reconstituting forces, must be in proportion to potential threats to Alliance security. Readiness will become a greater problem as the interval of peace is protracted. It takes time to train new pilots, but aerial robots can be pressed into service as quickly as then can be built.

Having an industry that can "shift gears" from producing 100 tractors per day to one that can produce 100 UAVs per day is a very real possibility. Flexible manufacturing is a key to NATO readiness after a period of defense cut-backs, treaty limitations, and relative peace, but it only has optimum effect when done in support of unmanned systems that can be deployed immediately— if the allied nations could build 100 new fighter aircraft per day, there would not be enough trained personnel to fly them proficiently. Simply knowing that NATO could respond rapidly with an armada of reconnaissance and lethal drones would be a deterrent to aggressors.

In the future, UAVs will be smarter and harder to counter militarily. Autonomous UAVs will be able to gather information (either intelligence before a military action, or battle damage assessment after an engagement has taken place) at close range with impunity. Lethal UAVs will seek out and destroy their targets with calculated tenacity and precision. Fully autonomous systems ("thinking machines") will be literally unstoppable through conventional means of deception or jamming. An aggressor who knows that stirring the NATO hornet's nest will result in a swift response by pain-inflicting or ultimately lethal swarms of expendable flying robots, will consider his actions with much deliberation.

AT WHAT COST?

How can NATO afford the cost of new UAV systems when a draw down in the U.S. and European forces is under way? Perhaps the real question is "how can NATO *not* afford to invest in UAV systems?" Consider the economic ramifications already incurred by using manned aircraft in reconnaissance flights as part of Operation Deny Flight, when drones could serve as NATO's eyes to scramble jets that are either in a perpetual state of readiness at bases within striking distance, or are orbiting at a safe stand-off range:

In the first 780 days of Operation Deny Flight, NATO forces logged:³

"No-Fly" Zone fighter sorties flown over Bosnia-Herzegovina	= 20,824
Close Air Support and Air Strike sorties over Bosnia-Herzegovina	= 20,920
Sorties by NAEW, tanker, reconnaissance, and support aircraft	= 19,146
<i>Total Number of Missions</i>	<i>= 60,890</i>

³ Anon., NATO Release Number: 95-16, dated 2 June 1995, HQ AFSOUTH, Naples.

The cost for this many flight hours over the Bosnian region is enormous, not only in operational costs, but also in lost aircraft and risk of death to the pilots. Consider that thus far during Operation Deny Flight, attacks against NATO aircraft were as follows:

On 17 December 1994, a French Etendard IVP jet on a NATO reconnaissance flight over Bosnia-Herzegovina was hit by ground fire and returned safely to air base in Italy. The aircraft which had taken off from the French aircraft carrier Foch received tail damage. The pilot was not injured.

On 15 April 1994, a French Etendard IVP reconnaissance aircraft safely returned to the French carrier Clemenceau after being hit by ground fire over the Gorazde area.

On 16 April 1994, the pilot of a Sea Harrier from the British carrier HMS Ark Royal safely ejected over Gorazde after his aircraft was hit while attempting to conduct a close air support mission.

On 8 March 1994, a Spanish CASA 212 transport aircraft, on a routine flight from Zagreb to Split, made a successful emergency landing at Rijeka Airport (Croatia) after being hit by ground fire while flying over Croatia. Four passengers on the aircraft were slightly injured by shrapnel.

On 2 June 1995, a U.S. Air Force F-16C was shot down over Bosnia. The pilot survived the crash of his aircraft, but had to evade enemy forces for six days in northwest Bosnia-Herzegovina.⁴ Special Operations forces called upon to risk their lives to extract the downed airman. Their search and rescue mission was successful. The single-seat aircraft was flying a routine Operation Deny Flight mission when it was observed by accompanying aircraft to be shot down by a missile, at about 1300 GMT. The aircraft was based at Aviano, Italy, as part of the Operation Deny Flight force.

Most recently on 31 August 1995, two French pilots were forced to eject from their aircraft over Bosnia for reasons yet to be determined at the time of this writing. No word as to their condition is known.

The costs associated with manned operations are often not appreciated. Consider the downing of the U.S. Air Force F-16C on 2 June, 1995. Not only did the Allied forces lose millions of dollars in aircraft and mission equipment, but consider the costs involved in the rescue of the downed pilot and the diversion of resources from NATO's primary mission in Bosnia due to the presence of an American pilot on Bosnian soil. The following quote from Commander-in-Chief, Allied Forces Southern Europe (CINCSOUTH) Admiral Leighton W. Smith Jr, U.S. Navy⁵ indicates the extent of the massive rescue effort mounted. Admiral Smith proudly reports:

"The numbers of aircraft are not that important, but you can see we had Cobras, we had CH-53s, we had Harriers off of the KEARSARGE as part of a TRAP package — that's basically a recovery of aircraft and personnel. We had the suppression of enemy air defence cover, with close air support, and fighter cover with A-10s, F-15s, we had F-16s, F-18s, the whole shootin' match up there, E-111s, EA-6Bs, and we had additional special operations forces that were backing them up. NATO — all of these were NATO forces, obviously — we had NATO AWACS up, we had tankers up. All of this was pulled together in roughly two hours and forty-five minutes after initial contact with the young man on the ground, we began launching the package that was going to eventually retrieve him."

Note that a few Predator UAVs have been performing high altitude reconnaissance over Bosnia for some time under U.S. control. The Predator is a high-altitude, long endurance reconnaissance UAV. Two have been lost to date. Both were lost during combat action over Bosnia during July of 1995, and in both cases, the only economic impact was the loss of the UAV (a cost less than one fifth of that incurred by the June 1995 crash and rescue of the F16 pilot). When the Predators went down, there were no multi-million dollar, high risk rescue attempts. There were no lives lost.

There may be an even more compelling reason to be using more UAVs in Bosnia, and that is the threat of hostage-taking. As has already been demonstrated, United Nations (UN) peacekeepers have been used as political pawns when they were freely taken as hostages. UAVs can not be taken hostage, but downed pilots can. This puts NATO in an awkward position at the negotiating table.

⁴ Transcript of CINCSOUTH Press Conference, 20 Grosvenor Square, London, June 8, 1995, Subject: RESCUE OF F-16 PILOT.

⁵ *ibid.*

Costs vs. Savings

Life cycle analyses show UAV systems to be more economical than manned systems for given missions, but there is an investment to be made in producing the initial systems. Where will this investment come from?

The answer lies with the private sector of the nations' economies. Some projections indicate that the market for UAVs by the year 2000 will be worth approximately \$10 Billion (U.S.) annually,⁶ and surprisingly the majority of this will be for civil applications. These applications will include aerial inspection of resources (e.g., insect damage in pulp wood forests), inspection of utilities (e.g., pipelines), or as an aid to the day-to-day operation of industry (e.g., reconnaissance for fishing fleets).

If NATO is willing to jump-start the process by investing in critical enabling technologies, and working to develop international agreements whereby UAV operation becomes acceptable across borders in either specified corridors or internationally regulated in manned air space, then industry will invest in the manufacturing infrastructure. In this win-win scenario, NATO benefits from decreased fly-away costs for UAV systems, the nation's economies benefit from the manufacturing jobs created as well as the new UAV-based industries that will ensue.

NATO countries such as France, Portugal, Spain, Italy, and Iceland with large coastal regions will benefit from UAV operations in support of maritime monitoring, contraband interdiction, and fisheries. Other nations such as Turkey which border unstable neighbors like Iran and Syria will benefit particularly from the less expensive, but more comprehensive border monitoring that can be achieved with UAVs. Package delivery to remote sections of eastern Turkey or to snowbound reaches of Norway might emerge as profitable markets. The safe spraying of pesticides on German sugar beet crops are within the realm of possibility for commercial UAVs during peace time. Even nations with highly developed infrastructures such as the United States could benefit from more

advanced and less expensive methods of traffic surveillance, utility inspection, and border patrol.

Seven critical enabling technologies are proposed as necessary for advancement of UAV systems by the year 2000. These are *Photonics*, *Acoustic Charge Transport (ACT)*, *Wafer-Scale Integration of Dissimilar Technologies*, *Full Spectrum*, *Ultra-Resolution Sensors*, *Smart Skins*, *microelectromechanical systems (MEMS)*, and *Knowledge-Based Systems*. Clearly many other areas require advancement, particularly the area of propulsion. However other areas are already receiving funding and with respect to propulsion, the technological leaps to be made in the area of Wafer-Scale Integration of Dissimilar Technologies using the other six enabling technologies, will lessen the need for more efficient propulsion systems as the air vehicles and mission equipment packages get smaller, lighter, and more capable. NATO needs to take the first step by investing in research to move these enabling technologies forward. The initial investment will be returned to NATO as it leverages the future commercial market.

SUMMARY

NATO has recognized that the security climate in Europe has changed for the better, but it faces the contradictory situation of having to reduce the size of its force while maintaining its ability to respond to crises quickly and effectively on multiple fronts. In the short term unmanned aerial vehicles present a way to realistically achieve both requirements without excessive cost. In the long term, UAV technology is expected to yield even better levels of readiness and response to crises, with the added feature that they themselves could become a non-nuclear deterrent as they evolve into fully autonomous agents of NATO. Industrial participation in the manufacture of civil UAVs is key to the affordable use of UAVs by NATO. It is incumbent upon NATO to invest in academic and industrial research to develop the enabling technologies that will create an economically viable market based upon UAV capabilities necessary to both military and civil applications.

⁶ Wagaman, R. T., "Worldwide Use of UAVs," Proceedings of the UV-95 Conference, Le Méridien, Paris, France, 8 - 9 June 1995.

LESSONS LEARNED IN THE DEVELOPMENT AND OPERATION OF REMOTELY PILOTED HELICOPTERS

R.G. Austin
Aeronautical Consultant
3 Shepherds Hill
Bracknell, RG12 2LS, United Kingdom

SUMMARY

Lessons learned, both in development and operation, of rotary wing UAVs over a period of some 25 years are described.

In particular it has been found that airvehicle compactness and vertical flight capability offers operational versatility not available to fixed-wing systems.

There is no cost or reliability penalty to pay for this though design must take account of the dependence of the VTOL UAV on an accurate height sensor and the demands of scale (compared with manned systems) on the technology.

1. INTRODUCTION

A number of different types of unmanned airvehicle systems (UAVs) are in limited use by the armed forces of several countries and their use is predicted to expand considerably within the next decade.

None of these systems are based upon a rotary wing airvehicle, although in the field of manned military aircraft, rotary wing types are believed to account for one third of the total fleets.

Is this not surprising, especially in view of the fact that many of the problems of the current fixed wing (FW) UAVs occur in the launch and recovery phases of flight? Also, for many missions, such as target designation, an ability of the airvehicle to remain at a fixed point in space is highly desirable.

There is a view that rotary wing UAVs would be too slow, unreliable and expensive to acquire and operate.

Is that view correct? This paper attempts to answer that question whilst briefly describing some of the attributes of the rotary wing UAV experienced by the author, and some lessons learned, during 25 years of engagement in their development and

operation.

The author is indebted to Westland Helicopters Limited and to M.L. Aviation Limited for their permission to release the information contained in this paper but the views expressed are those of the author and not necessarily representative of those of the Companies.

Although by 1967 the author had gained some twenty years of experience in the design and development of the several different configurations of manned helicopters, it was not until that year that his interest turned to unmanned systems. This was in response to a need by the United Kingdom Ministry of

Defence (UK MOD) for a vertical take-off and landing (VTOL) UAV for surveillance roles. An analysis showed that the most suitable configuration was a small helicopter utilising two coaxial counter-rotating rotors to lift what the author called "the plan-symmetric helicopter (PSH)". That is, the whole airvehicle, rotor system and body, is completely symmetric in plan view.

It was this configuration which was proposed to UK MOD, thus beginning the work which was to culminate almost 25 years later in the delivery of an operationally capable system to the first customer, the Swedish Government. Its development and its characteristics are the subject of this paper.

Interestingly, the majority of rotary wing UAV projects have adopted the counter-rotating rotor system, though it appears that, apart from the author, only Canadair with their Sentinel project have adopted the full PSH configuration.

2. NOTE

The Westland submission to the UK MOD was for a system utilising a PSH with a body shaped essentially as a prolate spheroid of height to diameter ratio of about 3 to 1. It would have a mass of about 200kg and be powered by

a Rover free-power turbine engine of 55KW.

Much detailed design work was carried out on this airvehicle and its associated ground control station (GCS) and other supporting systems. This included flight simulation, and analysis of detectability, vulnerability and surveillance performance. Although this UAV did not proceed to hardware, the analysis, simulation and wind tunnel testing of this period were a useful guide to future possibilities and pitfalls.

We were recognisably treading new ground in this form of airvehicle configuration, particularly as far as the control and stability were concerned. It was therefore decided to build the smallest and cheapest airvehicle (on a budget of £5,000!) that would carry an automatic flight control and stability system (AFCS) with the necessary power supplies to demonstrate control of pitch, roll and yaw axes. This UAV, named "MOTE", shown in fig.1. had a maximum mass of 15kg and was powered by two model aircraft engines each of 0.75KW. Many other components from the model world were pressed into service, including the radio command equipment.

We were quite scared that the aircraft would be difficult, or even impossible, to control, yet we dared not risk crashing it - we had only one! So we tethered it loosely by cords attached to the undercarriage for the first check flight.

As soon as the lift came onto the rotors the aircraft performed a hideous dance, which depressed us all, but the cords prevented it turning over or escaping. Subsequent viewing in slow motion of the video recording of the "flight" indicated that all was steady until one or other of the cords became tensioned and thus changing the dynamics of the system. We decided to gamble everything on a free flight.

Superstition disregarded, this was tried on Friday 13 June 1975. To our great relief, a perfectly controlled flight ensued, to be followed by two or three more that morning.

A number of subsequent flights, used to fine-tune the AFCS derivatives, confirmed our predictions of the very low gust response of the configuration and, within the limitations of its small power margin, the ease of positioning it in the sky.

The lessons from MOTÉ then were:-

- a. tethering, unless by the more sophisticated means adopted by Canadair, so changes the dynamic characteristics of the aircraft as to be worthless.
- b. the predictions of purity of control and low gust response of the configuration were confirmed.
- c. continuing tests showed that the use of model components were not acceptable in the longer term due to their low resistance to wear and lack of reliability.
- d. the use of glues to lock mechanical components frequently failed. These glues are, of course, used with success in many other applications, and we never discovered the reason for their failure in MOTÉ, but we resolved to eschew their use in the future.

3. WISP

The UK MOD were impressed with the success of MOTÉ but, of course, it had no useful function other than as a limited research vehicle. Accordingly we were excited to be awarded a contract by MOD to build three airvehicles and a small ground control station (GCS). The airvehicles were to carry monochrome TV cameras with a down-link to return images to the GCS.

WISP, shown in fig.2., adopted the same mechanical configuration as MOTÉ but was scaled up and better engineered to accept the power of two 3KW twin-cylinder 2-cycle engines and an all-up-mass of 32kg. The body was an all-enveloping glass-reinforced plastic shell of ellipsoid shape with a rotor pylon above to mount the two rotors. The AFCS was identical with that of MOTÉ but better housed. The rotors were of the same wooden construction; the gearbox, as in MOTÉ, was comprised of a light alloy sheet casing, containing a system of unlubricated tufnol gears and nylon drive belts.

The videocon tubed TV camera was arranged to be driven in elevation through an angle of 110° i.e. the sight line being capable of direction from 10° above the horizontal to 10° behind the vertical. Provision was made to incorporate stabilisation of the camera in pitch but this was never incorporated. The camera mounted a fixed focus lens of $30^\circ \times 40^\circ$ field of view. After fairly extensive rig running, the first flight of the first aircraft took place in December 1976 followed by 2 others in March and June

respectively of 1977.

These aircraft ably demonstrated their potential as camera platforms as good pictures were returned in spite of the lack of camera stabilisation. The range at which targets could be identified was, however, quite limited due to the inability of the optical system to reduce the field of view.

Very little vibration was apparent in the aircraft body and in particular in the camera bay, due, no doubt, to the artifice of suspending the body from a carefully tuned rubber suspension beneath what was termed the "mechanical module". This, however, comprising the rotors, transmission and power plants did vibrate. The ability to rapidly remove the mechanical module for servicing and test running before re-inserting it into the airframe was of considerable maintenance advantage.

The configuration of WISP as an oblate ellipsoid was adopted primarily to enable the payload camera to have the ability to see forward as well as downward, unlike the WIDEYE project in which the camera was stabilised to see only in a vertically downwards direction. This choice also resulted in a much lower drag configuration, in spite of a lengthy rotor pylon, compared with the prolate body proposed for WIDEYE as wind tunnel tests of a range of configurations showed - fig.3.

Another advantageous effect of the "flatter" body was that it produced a lower centre of mass of the aircraft and offered the opportunity of providing a wider undercarriage base. This became obviously of enormous practical advantage in operations from rough or sloping ground.

The large angular range of the camera in elevation enabled an assessment to be made of the operational penalty incurred in restricting that range. Limiting the camera sight-line to the vertical only was found to be impractical in seeking targets, in maintaining a stand-off surveillance, and in the approach to landing. An effective 60° range was necessary and a full 90° effective range was highly desirable.

The aircraft were operated at up to 200 metres tape height. No suitable altimeter was available, so the control of height was obtained manually. This was achieved with practice provided that the aircraft was

within sight of the operator. With the aircraft out of sight, the operator found difficulty in using the image from the camera to judge height. Large changes in height could take place before the operator recognised it. Here, the fixed wing aircraft offers an advantage as a significant change in height can only result from a change in pitch attitude which is instantly recognisable by the operator, through the TV image, or by a gyro system. In addition, pressure altitude is fairly readily measured on a fixed wing aircraft but is not easy to measure on a helicopter. Thus altitude control can be readily achieved on a fixed wing aircraft automatically through a combination of pitch angle sensed by gyro and barometric height measurement, with the possibility of manual reversion should the automatic system fail.

The helicopter UAV therefore needs an accurate height sensor. EMI offered the possibility of an altimeter using a laser system and they were contracted to develop and deliver 3 prototypes. Unfortunately these did not arrive until the WISP programme was about to be terminated.

The endurance of WISP was only of order $\frac{1}{2}$ hour and within this, the aircraft proved quite reliable, apart from the gearbox. The single cylinder engines vibrated badly and tended to shake loose from their mounting on the sheet metal gearbox casing, and the dry gears were relatively inefficient and ran quite hot.

Of the several lessons learned from WISP, the following were probably the most important:-

- a. As a camera platform, the co-axial rotor configuration was markedly superior to the penny-farthing type tried by other organisations.
- b. A wide angular range in elevation for the camera sight line was operationally necessary.
- c. The ability of the configuration to fly with equal facility in all directions without rotating was of considerable tactical advantage.
- d. A low aircraft CG coupled to a wide undercarriage base was operationally necessary for ground stability in all terrains.
- e. The practical value of modular construction in maintenance.
- f. The "dry" gearbox carried over from MOTE used too much aircraft volume and

operating close to its limiting PV value, was overheating. It was not a viable long-term solution.

- g. The importance of an accurate height measuring instrument was realised both for operation at altitude and as a landing aid.
- h. Though the airvehicle is only one element of the System, its design has considerable impact on the complexity of the other system elements.

4. WIDEYE

The relative success of WISP encouraged UK MOD in 1977 to place a contract on Westlands for 4 prototypes of the larger WIDEYE aircraft with a parallel contract being placed on GEC Marconi to provide the TV payload stability sensors and the Ground Control Station. A change in the Westland Company structure at this point resulted in the author accepting a change in his area of responsibility within the Company and meant that he temporarily left development work of UAVs.

The WIDEYE programme, soon to be known as Project Supervisor, was cancelled by the UK MOD at the end of 1979. No lessons can be learned from the WIDEYE/SUPERVISOR programme except perhaps that Engineering, and Aero-Engineering in particular, is a demanding discipline.

5. SPRITE

In 1980, the author joined ML Aviation. After a year of assessment MLA decided, with some encouragement from UK MOD, to begin the private venture development of the SPRITE System intended for sale initially in Military markets and subsequently in Civil Markets as a versatile, low cost, surveillance system.

A small team of professional aeronautical engineers were assembled and development began in 1981. As a totally new venture, the SPRITE aircraft gave the opportunity to begin afresh and produce a new, well considered and integrated system design - making good use of the lessons learned in MOTE and WISP, and of the considerable advance in electronics technology during the period 1975-1981. In this time, development of silicon chip technology achieved increases in performance of circuit components and of sub-systems such as power generation, radio equipment, gyros, and electro-optic sensors whilst reducing their size and mass and increasing their reliability.

The task was seen to be to design an airvehicle which:

- a. gave the specified performance (70kts max speed, 2 hours endurance)
- b. carried a range of alternative sensors of adequate performance
- c. had a radar cross section of no more than 0.05m²
- d. made minimum demands on handling and support equipment
- e. was an easy 2-man lift when fully fuelled
- f. could complete 100, two-hour sorties between overhauls
- g. could be carried in a small/medium sized all-terrain land vehicle which also housed the Ground Control Station. This was capable of being operated by only two persons with a minimum of skill.

Aspects (a), (c) and (d) all pointed towards the adoption of the oblate ellipsoid body of WISP rather than the prolate form of WIDEYE. A number of scale models were constructed in order to measure the non-dimensional aerodynamic and the radar reflective characteristics of bodies of that general form but with slight variations. A best compromise was selected.

In order to achieve the required absolute values of aerodynamic drag and pitching moment and an acceptable radar signature, it was necessary to reduce the body size to a diameter of 600mm, depth of 300mm and an overall airvehicle height of 1 metre.

These conclusions as to size were also confirmed by the transport aspect (g) and the desirability of minimising the airvehicles' optical signature.

This density of packaging (125kg/m³) could only be obtained with practical access for maintenance and means of rapidly interchanging payloads (b) by adopting a totally modular air-vehicle. Thus the airvehicle was constructed of four major modules (see fig 4)

These are:-

- 1. The Body
- 2. The Electronic module (The Brains)
- 3. The Mechanical module (The Brawn)
- 4. The payload (or Business) module.

The last three being replaceable within 2 minutes.

Each module is itself comprised of a number of removable sub-modules.

This modular construction was also adopted for the Systems installed in the Ground Control Station i.e. Power supply, controls, Data links and displays etc., so that the same equipment (with specific customer variations) could be installed in the various types of ground vehicles operated by different customers.

The System was the subject of a very rigorous design and test programme, appropriate design standards and specifications being prepared at the outset. The airvehicle, for example, was designed to meet the appropriate sections of the British Civil Airworthiness Requirements 29 for rotorcraft. Further information on the SPRITE System may be found in ref 1.

SPRITE Systems have been operated in the UK, USA, Germany and Sweden in a range of terrains and weather conditions by day and by night, using monochrome or colour TV, low light level TV and Thermal Imagers.

A view of a SPRITE airvehicle with a Thermal Imager payload mounted is shown, with the payload cover removed, in fig 5; whilst fig 6 shows a detached lowlight level TV payload with mini-lights fitted.

What are the lessons that have been learned with SPRITE?

These fall into the categories of technical and operational and while many are just confirmation of the predicted; they are none-the-less important for that.

5.1 Technical Lessons

5.1.1. Altimeter

The only technical mistake that was made in the design of SPRITE was the adoption of a laser system in the height control loop for measurement of airvehicle height. The advantages that it offered were a virtually zero probability of detection and a high degree of accuracy from a mature system already in use on oil rigs for the measurement of wave height. In practice, the system worked well over solid surfaces in all but very high temperatures, and gave a rapid and accurate response which enabled the height of the aircraft to be set to a few centimetres. Thus, for example, the aircraft could be set to maintain station, say 50cms

above a heaving ship's deck, rising and falling exactly in "formation" with the ship.

Unfortunately this performance was not maintained over water or over certain types of fir trees which absorbed or deflected the laser energy, thus registering a lack of contact. This caused the automatic flight control system (AFCS) to put the aircraft into a rapid descent, until contact was re-established when a rapid climb was demanded. Roller-coaster progress of this sort was, of course, unacceptable, and the laser system was replaced by a combined radio/acoustic altimeter.

It was, as has been previously said, possible to demand the height of the aircraft "manually" provided that other height cues were available. For landing within the sight of the operator, this was achieved with practice. An interesting phenomena was that in training almost all new operators held a high rate of descent far too late until checked by the instructor. The inference made was that operators assessed the height of the aircraft above ground in terms of numbers of airvehicle body heights (1 metre), so that a vertical descent 10m/s or more was held down to 10 metres above ground which then required a 2g deceleration in order to save the undercarriage! Had the body height been, say, 3 metres as in the case of a manned-size helicopter, a gentler descent would, it is believed, have been demanded.

The automatic descent system in SPRITE, therefore scheduled a vertical rate of descent for landing in direct proportion to the airvehicle height above ground, or more accurately, 15cms below ground to ensure a positive touch-down.

5.1.2. Data Links

The encoder/decoder/transmitter/receiver units form interchangeable modules in both airvehicle and ground station. The uplink transfers instructions to the airvehicle autopilot whilst the downlink transfers sensor images (depending upon the payload type) and airvehicle housekeeping data to the GCS. To maintain the ability to send new instructions to the airvehicle it is important that the uplink be inviolate. For example, in SPRITE, as in other UAVs, if loss of uplink is experienced, the airvehicle will proceed on a program of searching for the link and in the event that contact is not re-established, the flight may be terminated; and in the case of SPRITE, an automatic

landing procedure is activated.

SPRITE activities involved flying on occasions, close to, and into, the main beam of various forms of electro-magnetic emissions, whether intentionally or by accident.

Although this could not directly affect the control of the airvehicle, very high power emissions on a nearby frequency could drown the incoming command signals and cause initiation of link-lost procedure. In SPRITE, therefore, we adopted the use of two parallel data links in widely separated bands, with logic in the airvehicle to select the better signal. This worked very well after we had obtained satisfactory antennae solutions, and offered other advantages such as system redundancy and a safer means of transfer from one GCS to another.

5.1.3. Gearbox and Transmission

In SPRITE, the gearbox comprises 5 spur gears to accept and combine the drive from the two 5KW engines (the airvehicle can maintain flight on either engine), and effect a reduction from the engine speed of 8000rpm to the rotor speed of 1600rpm. The gearbox casing, of a light alloy casting, mounts the gear shafts within roller bearings. In this case, the square/cube law is working for us and the gearbox casing is therefore very stiff and does not suffer the problems of distortion found in larger helicopters, while the larger surface area/volume ratio allows oil circulation for cooling and lubrication to be achieved by a simple flinger-ring. No failures or significant wear were experienced in any gearbox throughout the 9-year programme.

The transmission shafts and rotor hubs also performed sterling service except on two occasions, in each case after some 10 reversals, or 20 plus flying hours. Both failures were caused by manufacturing faults not caught by inspection, one on a rotor blade spindle, the other on the upper rotor shaft. In each case failures were at a bearing mounting where the standard radius had not only been omitted but a deep score mark from the cutting tool had occurred. This led us not only to re-appraise the quality control but to recognise that aberrations in the machining processes were more critical in the small components - i.e. an adverse scale effect. We therefore carried out a re-design of all bearing mountings in order to increase the fillet

radii well in excess of those in the standard design manuals even though this meant introducing a form of abutment washer to support the bearings (fig 7).

5.1.4. Electronic Systems

The electronic systems were concentrated in the airvehicle largely in the electronics module comprising:

- a. Gyros: vertical and directional attitude gyros plus an azimuth rate gyro
- b. Height sensor
- c. Data link receivers and transmitter with decoders and encoders
- d. Logic circuits which received the commands from the GCS and, interpreting the information from the on-board sensors, instructed the control systems to maintain or change aircraft speed, height or direction
- e. Payload interface circuits which controlled the several alternative payloads and interpreted the data from them for transmission
- f. Housekeeping circuits which monitored the internal state of the airvehicle e.g. rotor speed, fuel state, data link performance, temperatures, etc and initiated contingency measures
- g. Power conditioning for all the above

The electronics module forms a quarter segment of the airvehicle and is so compact that the cable runs and screening are extremely short, thus minimising EMC problems and keeping cable weight low, though of course internal screening and earthing required rigorous attention.

Other electronic systems, of course, constituted the various alternative payloads, their sensors and their stabilisation. These payloads included:-

- a. TV, monochrome or colour
- b. Low light level TV
- c. Thermal Imagers (Infra Red)

and in development:-

- d. Radio relay
- e. NBC Monitor
- f. Electronic Countermeasures
- g. Laser designator
all including a TV system

5.1.5. Modular Construction

The decision to make the airvehicle very compact achieved largely through the adoption

of a 4-modular construction, paid dividends in many ways.

Construction was easier as each type of module was assembled in its own appropriate environment and separately tested for satisfactory operation. The four modules were brought together to form a complete airvehicle at the last moment.

The ability, especially during development, to substitute modified modules enabled changes to be made and assessed with a minimum of interference to the flight programme.

However, this advantage brought an interesting problem of identification of an aircraft and its build standard. No longer was it possible to call up an aircraft, but instead an assembly of modules e.g. EO2/MO5/BO3/PAO4 were identified on the flight documents.

5.1.6. Reliability

It is arguable as to what level of reliability is required of a military UAV System. Simplistically it is often argued that no highly trained and expensive human life is at risk, and usually being much cheaper than a manned aircraft the UAV can be considered to be expendable. Therefore, it is argued, the level of reliability can be much lower than that of an airborne manned system.

The author does not accept that simple argument. The failure of a UAV to complete a military mission of importance could result in the subsequent loss of many lives. The author does not presume to know the answer, which may only be determined after many years of real operational experience.

Experience, so far, has indicated that there is no reason that the mechanical systems in a rotary wing UAV will be any less reliable than the equivalent in a manned helicopter given similar development effort, and there is no pressure for them to be more reliable.

The exception may be the engines and we therefore duplicated them with sufficient power to sustain flight on one engine.

The UAV, however, has a greater dependence upon its electronic systems as there is no option of manual reversion in the event of an electronic control failure.

Duplexing of electronics, fortunately, is easier than duplexing mechanical systems and this may be an option to consider. SPRITE already does this to a degree.

Provided that basic reliability is "designed in", the level of proven reliability in UAVs will depend upon the investment thought to be justified in reliability testing. (see also section 5 ref 2; section 2.3 ref 3)

5.2 Operational Lessons

5.2.1. General

Trials at home and abroad largely confirmed our expectations of the operational advantages but some unexpected bonuses arose.

The low detectability predicted was demonstrated, though this caused a problem for the publicity department's photographers! The blob-like shape did not attract the eye as a profile of straight lines would do. Also, even if detected visually, its flight direction was not at all obvious.

The stability in turbulence and the insensitivity to wind direction of the configuration impressed most observers and enabled the System to be operated under wind conditions where most other UAVs and light aircraft would have been grounded.

5.2.2. In surveillance work, the ability of the airvehicle to approach a target and come to a stop out of detectable range, and to set up and maintain surveillance from the best angle whether determined by incident light, terrain, or target geometry was a considerable asset.

The ability to rapidly change payloads whilst refuelling between sorties - for example from a colour TV system to a ILLTV system at dusk was found to be of great advantage operationally.

5.2.3. In reconnaissance, the ability to remain covert and to adapt the airvehicle's speed to the terrain or density of possible targets, right down to the hover if necessary, was found to be of immense value.

5.2.4. In artillery operations, the correction of fall of shot proved to be very easy and effective with the airvehicle being able to remain at a fixed and advantageous, viewpoint. Simulation of laser target designation indicated the same advantage.

(A laser designator/TV System payload was designed for SPRITE but not built)

5.2.5. Airfield Damage Reporting

Operational analysis results of airfield damage reporting missions were tested in a number of exercises. It was confirmed that a full surveillance, and the determination of the best repair strategy, could be completed within ½ hour without risk to operators from UXBs or anti-personnel weapons.

The low light level TV payloads were found to be very effective systems, complementary to the more expensive Thermal Imager payloads.

Good ground images were obtained under starlight conditions and with the two 60 watt lamps switched on, good pictures could be obtained under overcast conditions from heights of 200 metres.

5.2.6. Naval Operation

The advantage of a small VTOL vehicle in operating from naval vessels was amply demonstrated over a range of sea conditions. Here insensitivity to wind direction and a low gust response came into their own as did the deck stability provided by an airvehicle with a low centre of mass and wide undercarriage base. Area search over water, however, demanded a wider sensor field of view and greater transit speeds than land reconnaissance.

Here, airvehicle speeds of about 150kts were desirable together with a side-to-side scan of the sensor and preferably enhanced by a pattern recognition facility.

Design calculations have shown that such a speed capability is possible in a small co-axial rotor helicopter configuration (ref 3 - see para 3.3) though this may be at the expense of a somewhat increased radar signature.

5.2.7 Other Roles

The UAV is a tool, and like other tools it may be found to have more uses than originally expected, depending upon the operator's ingenuity. The author is sure that we have yet to see exploited the full range of roles of which the UAV is capable, especially one with the versatility conferred by vertical flight.

Moreover, it became obvious to us that the cheaper UAV is more likely to be riskable in attempting novel uses, and the more

user-friendly UAV confers greater confidence in its operators in coping with the unexpected operational opportunity.

Two such examples with SPRITE, included:

- a. landing remotely, with the operator cued only by the TV picture, in order to regard a small stationary object at close quarters; and
- b. a vertical climb out from a small enclosed site with the camera rotating through 360° to give all-round coverage, the range of view increasing as the airvehicle climbed.

5.3 Costs

Comparing, as far as suitably comparable programmes are visible, the development of a rotary wing UAV System may be expected to take a little longer and cost more than the "equivalent" fixed wing System, largely due to the testing required to establish the fatigue life of the mechanical systems.

In practice, however, history records the development of fixed wing based systems being protracted due to problems with the launch and recovery methods.

A full, though basic, SPRITE System was operating within 2 years of the start of the programme, operating abroad within 4 years and equipped with a range of alternative payloads within a further two.

Subjectively, development and production costs of the basic airframe may be greater for the VTOL System, but those costs for its payloads are less due to the more benign environment to which they are subjected in the VTOL UAV. The total airvehicle costs are likely to be similar.

The ground equipment costs for the VTOL UAV System are markedly less than for the fixed wing System, requiring no launch or recovery equipment or vehicles to transport them, nor subsystems in the GCS to monitor those phases of the UAV flight.

Operating costs for the VTOL System will remain lower than for the fixed wing system so long as replacement items or repairs are needed for the FWUAV after each sortie, and a large number of land vehicles are needed for its support.

Manning levels for the VTOL UAV System are observably a small proportion of those required to operate the FWUAV System.

6. SUMMARY OF LESSONS LEARNED

SPRITE operations confirmed and extended the lessons learned with MOTE and WISP. They are principally:

- 6.1 As part of a UAV System the plan-symmetric helicopter provides an extremely stable camera platform, with low gust response and insensitivity to wind direction.
- 6.2 The PSH UAV System offers versatility in a wide range of roles with ease and economy of operation from both land and sea.
- 6.3 There are no unsolved technical problems preventing its military procurement and operation.
- 6.4 The airvehicle offers a very low probability of detection and provides the advantage of covert operation.
- 6.5 It is dependent upon the inclusion of an accurate and reliable height sensor - more so than its FW counterpart.
- 6.6 Operation from naval vessels and from uneven terrain is greatly assisted by an airvehicle with a low C of M and a wide undercarriage base. This is readily achieved with the oblate ellipsoidal form of body.
- 6.7 A rapidly changeable range of payloads greatly enhances operational versatility whilst retaining the advantages of a small and low cost airvehicle.
- 6.8 It is highly desirable that the imaging sensors in each payload are trainable through a full lower hemispherical field of regard, to make full use of the airvehicle's unique flight characteristics.
- 6.9 The smaller airvehicle, with its lower system inertia is more user-friendly and therefore more readily adaptable to novel uses.
- 6.10 Full modular construction is of particular advantage in the airvehicle, providing ease of maintenance within a very compact body. The serviceability of each module can, and should be, proven separately. The system also offers the availability of cannibalisation in service. Aircraft operating records, however, become more complex.
- 6.11 As in any UAV System the safe operation is totally dependent upon the

reliability of the electronics systems and consideration should be given to providing paralleled functions particularly for the command links.

- 6.12 The small scale of the mechanical elements demands a recognition of scale effects in manufacture.

7. CONCLUSIONS

The notion expressed in the introduction to this paper that rotary wing UAVs may be thought to be slow, unreliable and expensive has been shown by experience to be untrue.

Rotary wing UAVs offer adequate speed for their appropriate roles, and are potentially cheaper to operate and no less reliable than their fixed wing counterparts. Moreover, they offer a much greater versatility, and better sensor platform than the fixed wing based system.

Successful development, however, demands an understanding of the technical and operational lessons previously learned, some of which have been detailed in this paper.

Their future now depends upon the recognition of their advantages and their procurement by Military agencies.

8. REFERENCES

Conference Proceedings:

1. Austin R.G. and Pugh C.C. "The SPRITE System": Seventh Bristol International RPV Conference September 1988 - Paper 7.
2. Austin R.G. and Ryrie P.A. "The SPRITE System - an update": Eighth Bristol International RPV Conference April 1990 - Paper 13.
3. Austin R.G. "One Man's View": Tenth Bristol International RPV Conference March 1993 - Paper 20.

9. LIST OF ILLUSTRATIONS

1. MOTE RPH
2. WISP RPH
3. Drag of ellipsoidal bodies of various aspect ratios
4. The four modules of SPRITE airvehicle
5. SPRITE RPH with Thermal Imager Payload
6. Low light level TV payload
7. Typical revision of bearing mount.

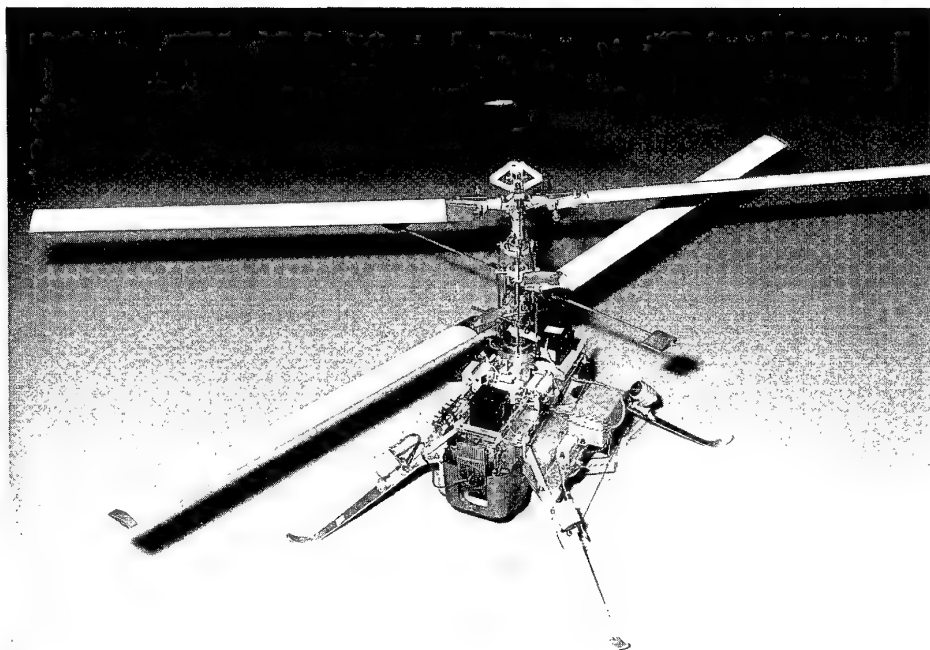


Fig. 1 MOTE RPH

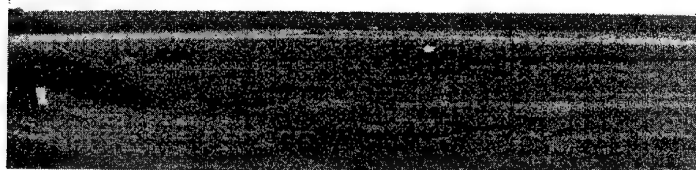
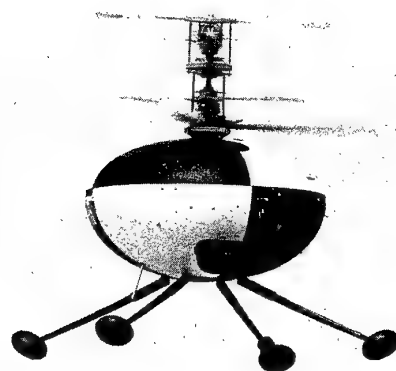


Fig. 2 WISP RPH

DRAG OF ELLIPSOIDAL BODIES
OF CONSTANT VOLUME AND VARIOUS
ASPECT RATIO COMPARED WITH A SPHERE

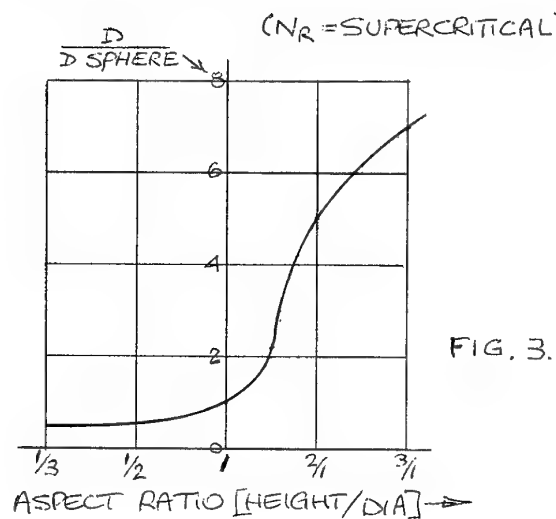


Fig. 3 Drag of ellipsoidal bodies of various aspect ratios



Fig. 4 The four modules of SPRITE airvehicle

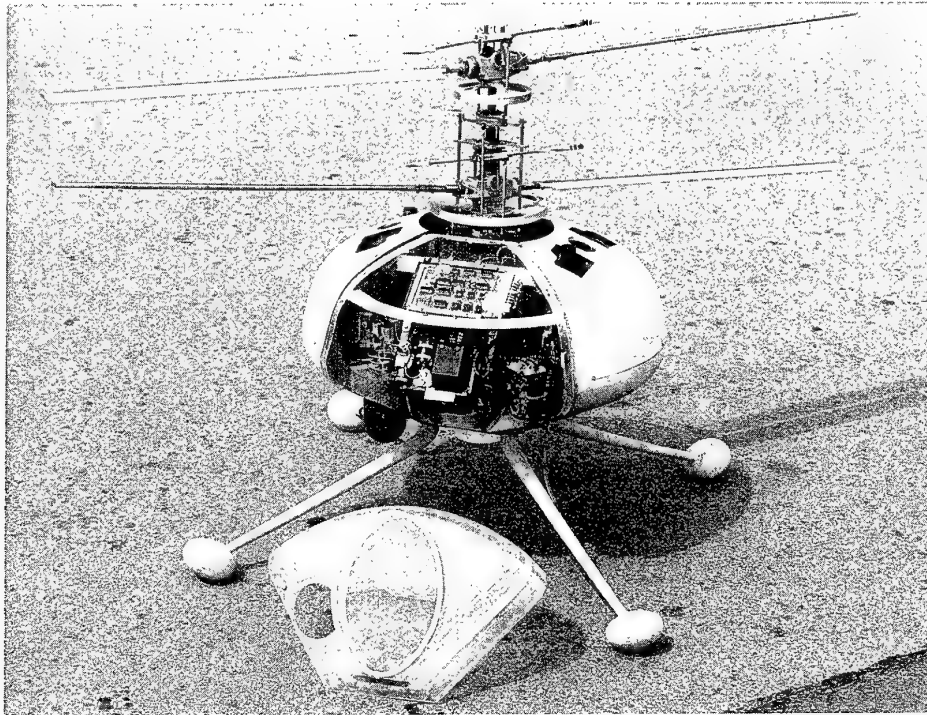


Fig. 5 SPRITE RPH with Thermal Imager Payload

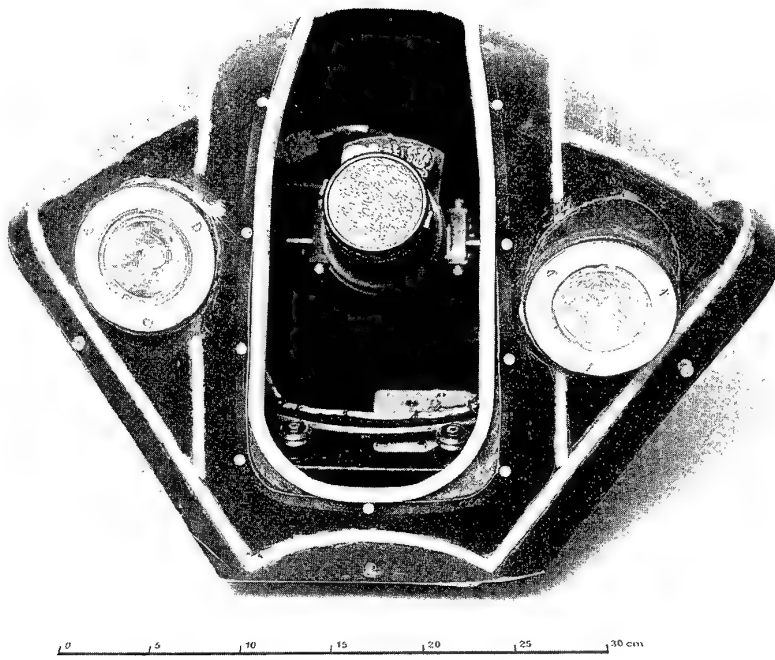


Fig. 6 Low light level TV payload

TYPICAL REVISION OF BEARING MOUNT
(HALF SECTIONAL VIEW)

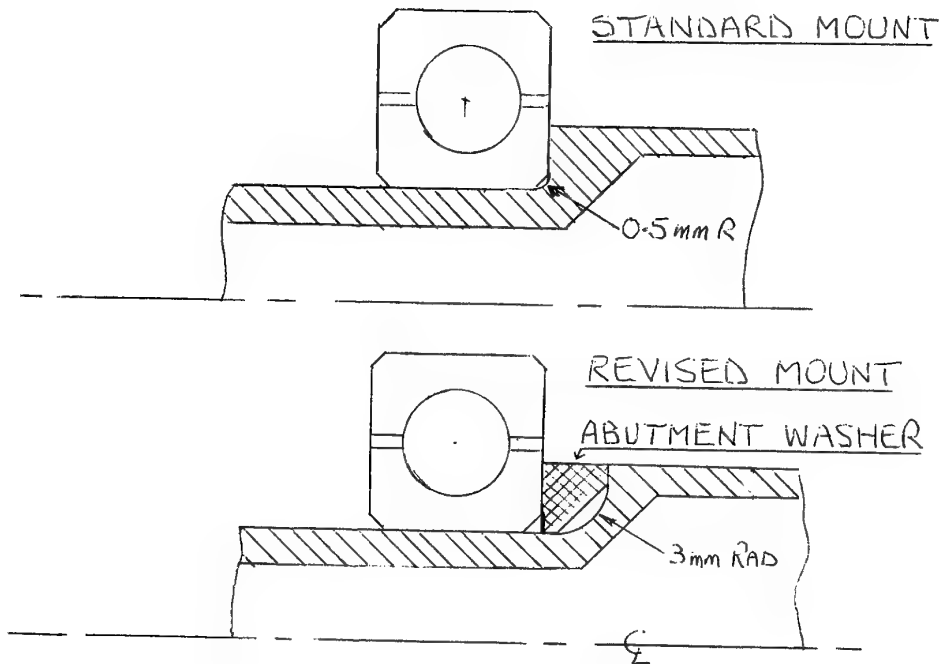


Fig. 7 Typical revision of bearing mount

AERODYNAMICS OF THE ARMOR X7 UAV

by

V. de Brederode¹, P.A. Jorge², J.R. Marcelino² and R. Patraquim³

Mech. Eng. Dept.
Instituto Superior Técnico
Technical University of Lisbon
P-1096 Lisboa Codex
Portugal

Summary

The paper reports the most significant aspects of the aerodynamic design and testing of a low speed UAV which is being developed in Portugal as a joint University / Industry project.

Starting from a baseline configuration of the air-vehicle aimed at complying with mission requirements in terms of endurance and range, a parametric sensitivity study is carried out for defining the optimum lay-out of the lifting surfaces. The family of the wing aerofoils is selected from the Wortmann series and a new aerofoil is designed for the tip section. Predicted and wind-tunnel results for the fuselage and inner-wing panels are reported and discussed and an assessment of the aerodynamic behaviour of the whole configuration is made.

1. Introduction

A joint University / Industry UAV project is currently under way in Portugal: the ARMOR project - Robotized Aeronets for Observation and Reconnaissance Missions. Project objectives are twofold:

- design, construction, prototype testing and operation of an UAV system mainly intended for observation and reconnaissance missions in the civil field, viz. forest firewatch, home-waters patrol for fisheries control, oil-spillage detection, smuggling prevention, etc.
- development of aerospace design capabilities in the country.

Project participants are the Mechanical Eng. Dept. of IST — Instituto Superior Técnico (Faculty of Engineering) of the Technical University of Lisbon, as leading institution, IST's Electrical Eng. Dept., the Polytechnic Institute of Setúbal and OGMA - Portugal Aeronautical Establishment, S.A.

1. Associate Professor
2. Research Assistant
3. M.Sc. Student

Numerical studies and laboratory experiments are being carried out in the different scientific disciplines pertaining to such an aerospace project — aerodynamics, composite structures, flight mechanics, control and robotics, navigation, data and image links — and a half-scale model (3 m span) of the ARMOR X7 air-vehicle is undergoing flight tests.

The present paper details project developments in the aerodynamics field; a companion paper [1] dwells upon the autonomous flight capability aspects of the air-vehicle. Mission requirements and the reasonings behind the baseline configuration of the air-vehicle are presented in Section 2 of the paper; Section 3 deals with the optimum lay-out of the lifting surfaces, Section 4 concerns the selection and the design of the family of aerofoils and Section 5 documents the shaping and the wind-tunnel testing of the fuselage and presents an assessment of the full configuration; conclusions are drawn in Section 6.

2. Mission requirements and baseline configuration lay-out

Given the lack of aerospace design experience in the country, a low-altitude medium endurance air-vehicle of conventional configuration and conventional wheeled take-off and landing was sought for a start.

Based on historical data for such a sort of vehicles the following parameters were set as a goal:

- Flight speed for endurance: ≈ 60 knots ≈ 30 m/s
- Flight height above terrain: 1-2 km
- Range: 400 km for patrolling out to the extreme end of the EEZ (200 nm)
- Endurance: 15 hrs. from full to dry fuel tanks
- Gross TOW: 200 kg (empty weight: 120 kg; payload: 50 kg; fuel weight: 30 kg)
- Span: 6 m with detachable wing outer panels for ease of ground handling, storage and transportation.

In a quest for safety duplicated control surfaces, 2 engines driving 2 separate 500 W alternators and a dual uplink were required.

Although the platform is mainly aimed at endurance, consideration also has to be given to range performance, so that the design point should result from a weighted sum of endurance and range. Assuming, at the conceptual design phase, a comfortably achievable endurance lift coefficient $C_{L_E} = 1.1$, for a parabolic drag polar of the type

$$C_D = C_{D_0} + \frac{C_L^2}{\pi k AR}$$

where k is the overall vehicle efficiency, a range lift coefficient of $C_{L_R} = C_{L_E} / \sqrt{3} \approx 0.6$ results. A design $C_L = 1$ then sounds like a reasonable and round figure to choose for an initial sizing of the air-vehicle. For an average weight $\bar{W} \approx 185$ kg and for flight at a density altitude of 1000 m — $\rho_{ISA} = 1.1$ kg/m³ —, this C_L value leads to a wing area $S = 3.6$ m² from what follows a wing aspect ratio $AR = 10$.

Despite the natural laminar flow (NLF) aerofoils to be used on the lifting surfaces and the intended laminar flow fuselage, a cautious $C_{D_0} = 0.015$ was taken in view of the large drag contribution expected from the ventral dome required for housing the revolving video camera.

For an estimated k of 90% all the above numerical values are seen to come into close agreement at endurance conditions, for which the quadratic drag contribution is 3 times the zero lift drag:

$$C_{L_E} = \sqrt{3\pi k AR C_{D_0}} = \sqrt{3\pi \times 0.9 \times 10 \times 0.015} \approx 1.13$$

The overall drag at endurance then turns out as $C_{D_E} = 4C_{D_0} = 0.060$, the lift to drag ratio as $(L/D)_E \approx 18$ corresponding to a maximum range $(L/D)_R = 2/\sqrt{3} (L/D)_E \approx 21$ and, from Breguet's endurance equation at constant angle of attack, $E \approx 18.5$ hours for an assumed propeller efficiency $\eta = 70\%$, a specific fuel consumption $sfc = 0.4$ kg/kWh ≈ 0.65 lb/HP/h — data for the IRM type 190 DR engines were taken as a guide — and not taking into account the fuel expenditure required for driving the electric generators.

These initial sizing considerations led to the design, construction and tests of a half-scale model of a X1 configuration, shown in Fig.1, with 2 wing-mounted pusher engines, a T-tail and a tandem wheels with outriggers arrangement for the landing gear, which didn't prove well in ground runs and was subsequently replaced by a conventional tricycle gear.

Six paper studies later the present X7 configuration emerged, with the 2 engines driving the same propeller shaft, twin-booms and an inverted U-tail: Fig.2; the wing lay-out is basically the same as for the X1. Advantages of the latter configuration are the avoidance of an asymmetrical power condition following failure of one of the engines, a lighter structure as the engines bulk-head is incorporated as one of the fuselage mainframes, and an

aerodynamically cleaner wing. The propulsive arrangement is presently being bench-tested. The nose gear is retractable; an assessment of the pros-and-cons of a retractable vs. fixed main gear with faired wheels clearly favoured the latter solution, given the requirements of wet wing inner panels, detachable outer panels and the configuration of the fuselage [2].

The aerodynamic design and analysis of the X7 configuration is the subject of the remainder sections of the paper.

3. Optimum lay-out of the lifting surfaces

The optimum lay-out of the lifting surfaces was searched in the line of the parametric sensitivity studies reported in [3]. Endurance and range were the key variables to maximize, reference values being taken as 15 hours and 1500 km (15 hours at a flight speed of about 100 km/h); the 'range' designation is only used in view of Breguet's range formula, but the word should be understood as referring to 'distance flown' and not to 'range', as such.

Given the non-negligible amount of power required for driving the electric generators compared with the power required for propelling the air-vehicle, Breguet's range and endurance equations were duly modified to account for that extra sink of power. The starting equation, including a constant electrical power term P_e , then takes the form:

$$\frac{dW}{dt} = -c (P + P_e)$$

where W stands for the aircraft weight and t for time, c is the engine specific fuel consumption and $P = DU/\eta$ is the engine power required from aerodynamic considerations, with D the air-vehicle's drag, U the flight speed and η the propeller efficiency. The resulting (and lengthy) range and endurance equations are presented in [3].

The most significant dimensions of the X7 baseline configuration, illustrated in Fig.2, are, as noted in the previous section: wing area $S = 3.6$ m², wing span $b = 6$ m, a 2 m span rectangular wing inner panel, 2 m wing outer panels tapered at $\lambda = 0.6$ with a 4° dihedral and a stabilizer volume coefficient of 0.58. Trimmed conditions were always imposed, a constant 10% static margin value was assumed given the stability requirements of the platform, a parasite drag coefficient $C_{D_{par}} = 0.010$ was considered, to which corresponds an equivalent parasite area $S_\pi = 0.036$ m², and a Wortmann FX 67-K-150/17 aerofoil was taken as representative of an average aerofoil to be used along the wing span, for which experimental data are available in [4].

The MultOp code (a Multiple-Lifting-Surface Optimization Program), developed by Ilan Kroo [5, 6], was used as the main tool in the concept study phase of the project. MultOp is a fast running code based on a vortex lattice modelling of a set of trapezoidal lifting surfaces and on a Lagrange multipliers methodology, which allows evaluation of the circulation distribution

that produces minimum drag subjected to lift, trim, stability and weight constraints. The original code was complemented to account for the aerofoils' pitching moment about the aerodynamic center and for a non-zero equivalent parasite area and to compute range and endurance as referred to above. In this way it became possible to compare the performance of, and select from, a set of air-vehicles of fixed overall dimensions optimized over a range of lift coefficients.

The sort of information so obtained is depicted in Fig. 3 for the baseline configuration, under the form of Endurance vs. Range curves over a C_L range from 0.6 to 1.5 in 0.05 increments, where it is made clear the performance degradation due to a $P_e = 1$ kW electrical power generation: maximum range decreases from 2140 to 1750 km and maximum endurance from 19.6 to 15.5 hours; also the C_L values for maximum range and endurance at $P_e \neq 0$ are slightly lower than the ones corresponding to $(C_L/C_D)_{\max}$ and to $(C_L^{3/2}/C_D)_{\max}$ — e.g. C_L for maximum range decreases from about 0.76 to 0.68.

Defining a Figure of Merit as a weighted sum of Endurance and Range, conveniently non-dimensionalized by the reference values, i.e.

$$FoM = w_E \frac{E}{E_{\text{ref}}} + w_R \frac{R}{R_{\text{ref}}}$$

the design C_L could be obtained from the point of tangency of the E/E_{ref} vs. R/R_{ref} curve with the $FoM = \text{const.}$ straight line, with a slope controlled by the relative weights of endurance and range. Such a geometrical construction is shown in Fig. 4 for $w_E = 80\%$ and $w_R = 20\%$, from which a design $C_L = 1.14$ is obtained.

Both Figs. 3 and 4 show the baseline vehicle to slightly exceed the required goals for range and endurance, meaning that the mission could be accomplished with a bit less of fuel; in fact, by decreasing the fuel weight from the original 30 kg to just 29 kg the design point is precisely reached, as shown by the full line in Fig. 5, but at an overall C_L of 1.18 requiring a local $c_{l_{\max}} = 1.25$, which suggests the use of high-lift aerofoils. The original Wortmann aerofoil was thus replaced by the high-lift NASA NLF(1)-1015, designed for a high-altitude, long-endurance (HALE) UAV [7], and exhibiting an inevitably higher moment coefficient about the aerodynamic center: $c_{m_{ac}} = -0.22$ for the NLF(1)-1015 compared to -0.09 for the FX 67-K-150 — for this example study only the low-drag bucket behaviour of both aerofoils was considered and, for simplicity, extended beyond their upper limits. The result of using the NLF(1)-1015, as shown by the dashed curve in Fig. 5, is a slight degradation in performance brought about by the increased trim drag required from an aft-loaded aerofoil: the stabilizer download required to trim close to the design point is now about 6 % of the total lift instead of an upload of about 2 % as for the FX 67-K-150; also the maximum local c_l across the span is now 1.37,

which already lies outside the low-drag bucket. The necessary wing area might, however, be smaller, leading to a smaller and lighter vehicle. The effects of the wing planform parameters, such as wing area, span and aspect ratio, on the performance characteristics of the air-vehicle thus need be assessed next.

The parametric sensitivity study reported in [3] led to the conclusion that best performance would be achieved with a vehicle of the smallest wing area and the largest span (implying a high aspect ratio wing) compatible with other requirements and constraints. That study is now carried a step further taking into consideration the spanwise station where the largest c_l 's occur, aiming at a sound stall behaviour, and the desired cruise speeds. The effects of up and down variations around the baseline values for wing span at constant aspect ratio and at constant wing area and for wing area at constant wing span are shown as Figs. 6.a), b) and c), respectively — these three figures are all drawn at the same scales for better visualization of the relative influence of each of the parameters; a constant equivalent parasite area, not constant parasite drag coefficient, was assumed throughout this parametric sensitivity study, as it concerns the assessment of the influence of the wing planform parameters on the performance of a vehicle with fixed drag producing components.

The general trends shown in these figures are easily understood in view of Breguet's range and endurance equations for operation at constant C_L and constant S_π and assuming a parabolic drag polar, from which the following proportionalities yield [3]:

$$R \propto (SAR)^{1/2} = b$$

$$E \propto (SAR)^{3/4} = b^{3/2}$$

$$C_{L_{R,E}} \propto (AR/S)^{1/2} = b/S$$

deviations from these general trends are due to electric power generation.

In Fig. 6.a) the increase in range with the wing dimensions is due to an increase in the vehicle efficiency brought about by a diminishing influence of the parasite drag effects: $C_{D_{\text{par}}} = S_\pi/S$; this increased aerodynamic efficiency, coupled to a lower wing-loading, acts so as to produce increased endurances. The increase in both performance parameters with an increase in wing span at constant wing area in Fig. 6.b) results from the increased vehicle efficiency produced by a higher aspect ratio wing. In Fig. 6.c) the small influences of an increase in wing area at constant span are only associated with the generation of electric power, the sole aerodynamic effect being a shift of both maximum range and endurance to lower C_L values.

These trends suggest that the performance curve for the baseline configuration in Fig. 5 could be shifted to lower operational C_L 's in the vicinity of the design point

simply by slightly increasing the wing area at constant span. Increasing S from the original 3.6 m^2 value to 3.8 m^2 does in fact allow us to meet all our requirements, as shown in Fig. 7: the E, R design point is closely met at an overall $C_L = 1.1$, $c_{l_{\max}}$ across the span is about 1.2, which lies well within the low-drag bucket region of the Wortmann aerofoils, and the point of tangency of the $ForM$ 80%/20% line is achieved at $C_L \approx 1.07$; the average flight speed along the mission is $\bar{U} \approx 100 \text{ km/h}$ and the required average engine power, including a $P_e = 1 \text{ kW}$ contribution, is $\bar{P} \approx 6.6 \text{ HP}$, showing that safe one-engine-only operation is guaranteed.

The optimum spanwise c_l distribution at a configuration $C_L = 1.1$ is shown as a dotted line in Fig. 8 for the just selected $b = 6 \text{ m}$, $S = 3.8 \text{ m}^2$ wing and assuming, as for the baseline configuration, a $1/3$ span rectangular inner panel and $\lambda = 0.6$ tapered outer panels; the stabilizer upload required to trim is fairly negligible, giving no quantifiable trim drag, apart from the form drag resulting from the presence of the stabilizer itself.

A sounder spanwise c_l distribution, in terms of stall behaviour, is shown as a full line in Fig. 8, with $c_{l_{\max}}$ occurring at a quarter semi-span and with the ailerons' stations less loaded than in the former case. This latter distribution was achieved with a $\lambda = 0.9$ tapered wing inner panel and a taper of $\lambda = 0.7$ for the outer panels; it requires a circa 4° wing wash-out in the outer one third span and a stabilizer setting at nearly $+5^\circ$ to compensate for the wing downwash.

This is the final configuration of the lifting surfaces. Ailerons are located in the outer one-third span and, for redundancy, the middle one-third span is equipped with flaperons, capable of operating also as air-brakes. Given the large amount of systematic and reliable experimental data available for the Wortmann aerofoils and the fact that, once selected the $b = 6 \text{ m}$ and $S = 3.8 \text{ m}^2$ configuration presented above, this series does comply with all our requirements within the low-drag-bucket region, the Wortmann series of aerofoils was selected as a basis in the present design experiment. This point will now be taken further in the following section of the paper.

As illustrated by the above discussed effect of a 3 % reduction in fuel weight (from 30 to 29 kg, i.e. a $1/30$ reduction), and as already stressed in [3], efficiency of the engine-propeller assembly is the most crucial parameter governing the air-vehicle performance. Once determined, from careful flight test experiments, the correct values for the configuration $C_{D_{par}}$, for the engine specific fuel consumption, for the propeller efficiency and for the electrical power demand, the methodology just presented points to ways of determining the best configuration of the lifting surfaces for achieving the design goal.

4. Wing and tail aerofoils

The following sequence of Wortmann flapped aerofoils was initially chosen for the wing: FX 67-K-170/17 for the inner one-third span panel evolving to the FX 67-K-150/17 at two-thirds span and to the FX 60-126 at the tip; the tip aerofoil was chosen in view of its high absolute stall angle of attack and gentle stall, as stressed by Prof. Wortmann himself [8], and its renowned low Reynolds number behaviour, which makes it a preferred aerofoil among the aeromodeller community [9] — that aerofoil was thus selected for the X7 1:2 scale flying model: half the size, half the speed of the prototype. For checking if these three aerofoils would produce an aerodynamically uniform wing, compatibility of their characteristics at varying Reynolds numbers was first assessed resorting to Mark Drela's XFOIL analysis and design code [10]; this code, specially suited to the analysis of low Reynolds number aerofoils with transitional separation bubbles, is based on an inviscid linear-vorticity panel method coupled to a two-equation lagged dissipation integral method for the viscous layers and an e^9 -type transition prediction criterium. One difficulty with the prediction of the real fluid flow behaviour of the Wortmann aerofoils stems from the fact that their published coordinates [4] do produce physically unrealistic wiggles and spikes in the C_p distributions, as illustrated in Fig. 9 for the FX 60-126 at $\alpha = 3^\circ$. A priori smoothing out of the aerofoils coordinates then becomes mandatory, and that was achieved using a least-squares polynomial and cubic spline program [11]; the required coordinates adjustment is, at most, of 0.04% c , and so hardly perceivable within graphical accuracy, but the resulting C_p distributions become much more physically sounder, as also shown in Fig. 9. A comparison between XFOIL's predictions and experimental data is presented in Fig. 10 for the FX 67-K-150 operating at $Re = 1.5 \times 10^6$; XFOIL generally overpredicts the aerofoils' performances (higher lifts, lower drags), but the predicted results are quite reliable in relative terms.

The predicted polar plots for the three above mentioned Wortmann aerofoils are compared in Fig. 11.a) for chord Reynolds numbers related to the local operational c_l by

$$Re = \sqrt{\frac{2}{\rho}} \frac{\bar{W}}{S} \frac{c}{v} \frac{1}{\sqrt{c_l}} = 1.86 \times 10^6 \frac{c(m)}{\sqrt{c_l}}$$

and their C_p distributions at $\alpha = 3^\circ$ are shown in Fig. 11.b). The aerodynamic characteristics of the two thicker aerofoils are seen to be nearly coincident but the C_p distribution of the thinner one is clearly different, which would lead to spanwise flows inducing crossflow instabilities tending to promote an early transition.

The FX 60-126 was then replaced by another aerofoil with a closer similitude to the FX 67-K-170 and 150 ones. That new aerofoil was the S1045, designed on purpose by Michael Selig using his multipoint inverse PROFOIL code [12, 13], an incompressible potential

flow inverse design method based on conformal mapping and coupled to a direct integral boundary layer analysis method. Starting from a velocity distribution approaching that of the FX 67-K-150, the aerofoil shape was optimized by iteratively switching from PROFOIL, for interactive design, to XFOIL, for detailed analysis; the aerofoil was required to be 12% thick, to exhibit a $c_{m_{ac}}$ not larger than the FX's, to have its low-drag bucket in the c_l range predicted to occur in the tip stations, as from Fig. 8, and to have low aft-load for minimizing ailerons' hinge-moments. The aerodynamic characteristics of the S1045 are compared with those of the Wortmann's in Fig. 11. At $Re = 7.5 \times 10^5$ transition occurs at about 65% c for $\alpha = 0^\circ$, upstream of the ailerons' hinge line, and $c_{l_{max}} \approx 1$.

A 12% thick symmetrical aerofoil was sought for the stabilizer and the double-fins, as a compromise between aerodynamical and structural requirements. Candidate aerofoils could have been the 14% thick (too thick) Eppler e521 [14] and the 10% thick (too thin) Selig-Donovan SD8020 [15], the latter one designed for the low Reynolds number of operation of model aeroplanes; XFOIL's predicted polars for these two aerofoils are shown in Fig. 12 for the local cruise Re of about 6.2×10^5 . A new 12% thick aerofoil is then in the process of being designed, following the aforementioned methodology for the S1045 — call it the PAJ1, as from the initials of one of the paper co-authors; preliminary XFOIL's predicted polar results for that aerofoil, aimed at exhibiting a flat roof-top C_p distribution at $\alpha = 0^\circ$ similar to the e521's one, are included in Fig. 12.

5. Fuselage and inner-wing flow fields

In this section a comparison is made between numerical predictions and wind-tunnel experiments for the flow field about the fuselage/wing inner-sections of the baseline configuration. Predictions were made using VSAERO, a commercially available low-order panel method code allowing for wake relaxation and for viscous/inviscid interaction [16]. The reported experiments were performed in IST's low-speed, blow-down, 1.35×0.80 m wind-tunnel using the center body of the X7 half scale flying model; the wind-tunnel and flight model Reynolds numbers are about the same: $Re \approx 10^6$ per metre. The location and extent of boundary layer transition and the occurrence of flow separations were assessed both for the no-propeller and the running propeller situations.

Fig. 13 shows VSAERO's predictions of the pressure coefficient C_p and of the skin-friction coefficient C_f distributions along the fuselage upper surface in the symmetry plane — the non-smooth behaviour of the C_f curve at some locations is a consequence of the surface tangential discontinuities resulting from the necessity of braking the fuselage down to 16 different patches for including the wing fairings, the ventral dome and the engine inlets, which also impairs the predicted location

of transition [17]. An inflow factor of 0.1 was assumed, which corresponds either to a steady shallow climb or to a level and slightly accelerated flight condition; surface distributions downstream of the 'actuator disk' are meaningless. The pressure gradient is favourable up to the fuselage maximum height section and extends beyond that point for the running propeller case, thus ensuring large extensions of laminar flow, as substantiated by the sudden jump in C_f from one control point to the next one, indicative of the occurrence of transition. For the four times higher Reynolds number of the full scale prototype, although the C_f level was expectably lower, transition was predicted to occur at the same stations in result of the destabilizing effect of the installed adverse pressure gradients.

Such a late transition was not achievable in the wind-tunnel experiments as the boundary layer was tripped at the junction between the downstream end of the payload compartment top cover and the fuselage main body. Predicted and experimentally observed locations of transition are in fairly good agreement, though, on the wing upper surface, as shown in Figs. 14, 15 and 16 for a configuration $\alpha = 0^\circ$.

In the VSAERO plot of Fig. 14 transition is identified by the sudden change from a dark to a light gray color. The computed flow behaviour in the vicinity of the wing tips might be misleading, though, as the geometry of the wake filament lines springing from the blunt tips was only defined in a simple but crude way; anyway, a correct description of this complicated tip vortex flow would call for a more elaborate prediction scheme, e.g. based on the parabolised Navier-Stokes equations [18]. Close to the tips, transition instead of occurring further downstream than on the wing inner sections, as a result of the predicted milder adverse pressure gradients, is experimentally observed to move towards the leading-edge due to contamination of the wing upper-surface by the wrapping tip vortex flow, as documented in the china-clay visualizations [19, 20] of Fig. 15. A transition region of some extent, instead of a transition line, was clearly identified at this low Reynolds number by probing the boundary layer flow with a stethoscope; the two lines shown in Fig. 16 delimiting the transition region refer, the upstream one, to the onset of transition, as identified by a single frequency whistle, and, the downstream one, to complete disruption into turbulence, characterized by a broad band roar and generally identified with the transition line.

Wool tuft visualizations of the fuselage and wing upper-surface flow fields are documented in Figs. 17.a) and b) at an extreme angle of attack of 9° for both the no-propeller and the running propeller cases, respectively; to that configuration $\alpha = 9^\circ$ it should still be added the wing 6° setting angle on the fuselage and accounted for the -5° zero lift angle of the FX 60-126 aerofoil, which sums up to an absolute angle of attack of 20° . The separated flow in the neighbourhood of the wing-fuselage intersection for the no-propeller situation is seen to become well attached with a running propeller, which demonstrates the faired junction to be operating properly.

VSAERO's predictions of the C_p distribution on the complete X7 configuration are illustrated in Fig. 18 for 2 viscous/inviscid iterations and 2 wake relaxation iterations. This figure depicts the favourable pressure gradients acting over most of the fuselage top surface, as required for achieving the intended laminar flow fuselage, the spanwise running of the isobars on the wing upper surface, leading to small cross-flows and to a sound stall development, and the well-behaved stabilizer/fins junction.

6. Conclusions

The paper documents the aerodynamic design of the ARMOR X7 UAV presently being developed in Portugal as a joint University / Industry project.

Starting from a definition of the mission requirements in terms of endurance, range, flight speed and altitude, a baseline configuration of the air-vehicle was proposed: a vehicle of the conventional aft-tail type, with a pusher propeller, twin booms and an inverted U-tail, a gross take-off weight of 200 kg and a 6 m span wing. The layout of the lifting surfaces of that baseline configuration was optimized in terms of a figure of merit defined as a weighted sum of endurance and range. The parametric sensitivity study then performed led to the conclusion that the baseline configuration slightly exceeded the performance requirements and that the design point could be achieved with a bit less of fuel than originally thought (3% less) and a larger wing area: 3.8 m² instead of the original 3.6 m²; the Wortmann 15% thick aerofoil taken as a guide at this conceptual design phase was also found to meet the requirements. That study demonstrated the correctness of the methodology for optimizing the layout of the lifting surfaces once more reliable data on engine specific fuel consumption, propeller efficiency, parasite drag is obtained from careful flight tests.

Aerodynamic compatibility of the series of Wortmann aerofoils originally considered for the wing was assessed using Drela's XFOIL analysis code; the proposed tip aerofoil was found to exhibit characteristics different from the two inner ones and a new aerofoil was then designed on purpose by Michael Selig, iteratively switching from his PROFOIL inverse design code to XFOIL. The main characteristics of that new aerofoil are presented and shown to comply well with the requirements. Preliminary results are presented for a 12% thick symmetrical aerofoil for the stabilizer and fins which still is in the design stage.

The flow about the fuselage / wing inner panels was assessed both numerically and in a wind-tunnel. The fuselage was shaped so as to produce large extensions of laminar flow; that requirement was shown to be met and improved with a running propeller. VSAERO's predictions of transition on the inner-wing upper surface are shown to be in qualitative agreement with experiments using both the china-clay technique and probing the boundary layer flow with a stethoscope.

Flow separations in the wing / fuselage junction were experimentally found to be discouraged with a running propeller even at extreme angles of attack. The location of transition and the stall development are to be assessed next in flight using the X7 half-scale flying model.

Acknowledgments

We are grateful to Prof. Michael Selig for his design of the S1045 aerofoil, for the supply of Morgan's aerofoil coordinates smoothing program and for his continuing assistance.

The reported work was sponsored by the Portuguese Ministry of Defense and by the PEDIP Program; R. Patraquim benefits from a Praxis XXI grant.

References

1. Lourtie, P., Azinheira, J.R., Rente, J.P. and Felício, P.: "ARMOR Project — Autonomous Flight Capability", AGARD FVP95 Specialists' Meeting on the 'Design and Operation of Unmanned Air Vehicles', Ankara, 1995.
2. Marcelino, J.R.: "Considerations on the Main Gear Configuration for the ARMOR X7 Prototype", ARMOR internal report, 1994.
3. Brederode, V.de and Pina, H.L.: "Concept Study of a Short-Range UAV", 10th RPV's Intern. Conf., Bristol, 1993.
4. Althaus, D. and Wortmann, F.X.: *Stuttgarter Profilkatalog I*, Friedr. Vieweg & Sohn, 1981.
5. Kroo, I.: "A General Approach to Multiple Lifting Surfaces Design and Analysis", AIAA Paper 84-2507, 1984.
6. Kroo, I.: "MultOp - Multiple Lifting Surface Optimization", Desktop Aeronautics, USA, 1991.
7. Maughmer, M.D. and Somers, D.M.: "An Airfoil Designed for a High-Altitude, Long Endurance Remotely Piloted Vehicle", 5th AIAA Applied Aerod. Conf., 1987.
8. Wortmann, F.X.: "Einige Laminarprofile für Segelflugzeuge", OSTIV Congress, OSTIV Publ. no.VII, 1963.
9. Revel, G.: "Un Profil Célèbre et sans Surprise: le Wortmann FX 60-126", *Model Mag.*, no. 401, pp. 84-85, 1985.
10. Drela, M.: "XFOIL: An Analysis and Design System for Low Reynolds Number Airfoils", in Mueller, T.J. (Ed.): *Low Reynolds Number Aerodynamics*, Conf. Proc., Springer-Verlag, 1989.

11. Morgan, H.L., Jr.: "Computer Program for Smoothing and Scaling Airfoil Coordinates", NASA TM 84666, 1983.
12. Selig, M. and Maughmer, M.D.: "Multipoint Inverse Design Method Based on Conformal Mapping", AIAA J., vol. 30, no. 5, pp. 1162-1170, 1992.
13. Selig, M. and Maughmer, M.D.: "Generalized Multipoint Inverse Airfoil Design", AIAA J., vol. 30, no. 11, pp. 2618-2625, 1992.
14. Eppler, R.: *Airfoil Design and Data*, Springer-Verlag, 1990.
15. Selig, M.S., Guglielmo, J.J., Broeren, A.P. and Giguère, P.: *Summary of Low-Speed Airfoil Data*, vol. 1, SoarTech Publ., 1995.
16. "VSAERO Program", Analytical Methods Inc., USA, 1994.
17. Almeida, H., Brederode, V.de, Marcelino, J.R.: "Aerodynamic Design, Analysis and Tests of the ARMOR X7 UAV", 11th RPVs Intern. Conf., Bristol, 1994.
18. Eça, L.: "Numerical Solution of the Parabolised Navier-Stokes Equations for Incompressible Tip Vortex Flows", Ph.D. thesis, Inst. Sup. Técn., 1993.
19. Richards, E.J. and Burstall, F.H.: "The 'China Clay' Method of Indicating Transition", ARC R&M no. 2126, 1945.
20. Moir, I.R.M.: "Recent Experience in the RAE 5 metre Wind Tunnel of a China Clay Method for Indicating Boundary Layer Transition", paper no. 1391, The Aeron. J., Jan. 1986.



Fig. 1 ARMOR X1 half-scale flying model.

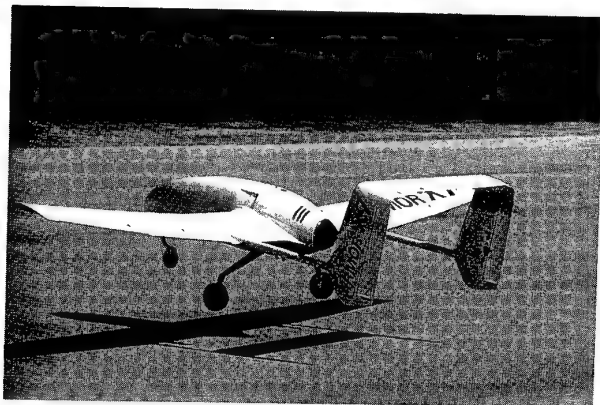


Fig. 2 ARMOR X7 half-scale flying model.

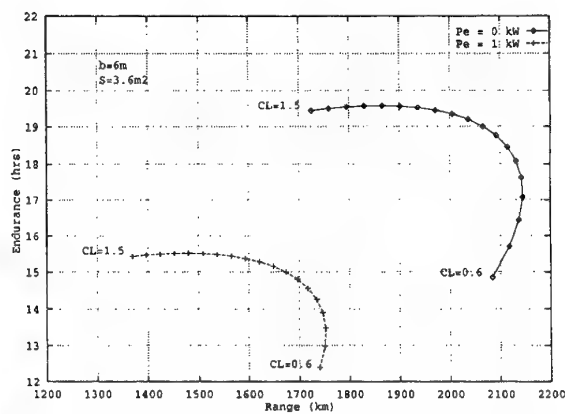


Fig. 3 Endurance vs. Range curves for the baseline configuration: effect of electrical power generation.

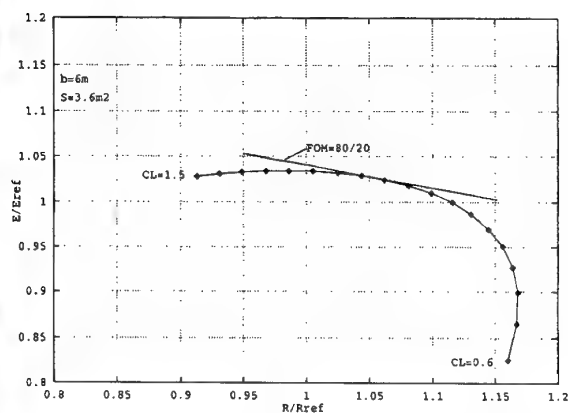


Fig. 4 Non-dimensional performance of the baseline configuration and location of the FoM design point.

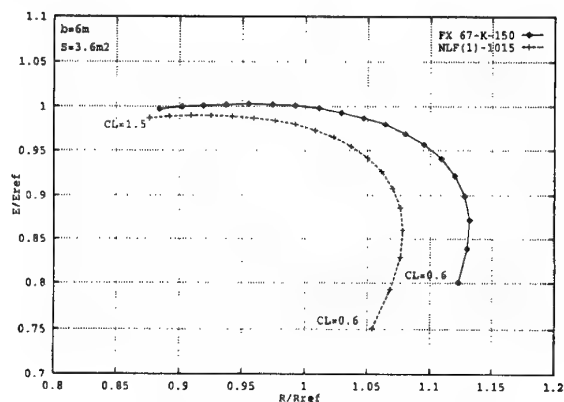


Fig. 5 Non-dimensional performance curves for the baseline configuration with 29 kg of fuel and for the Wortmann and NASA NLF aerofoils.

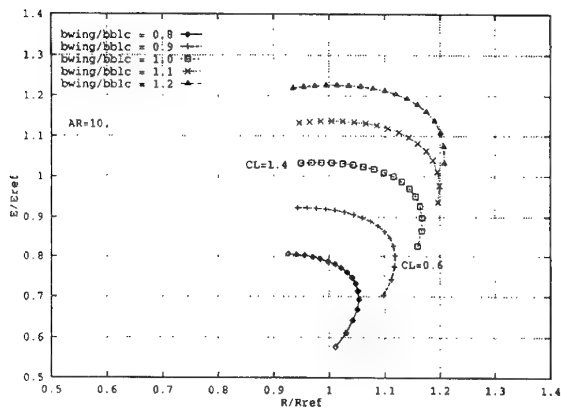
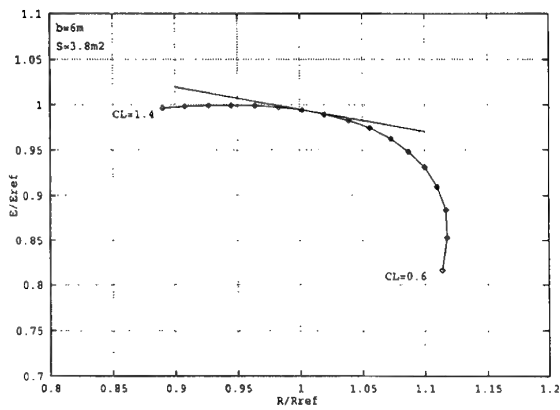
a) Effect of varying b at constant AR .

Fig. 7 Performance of the increased area configuration.

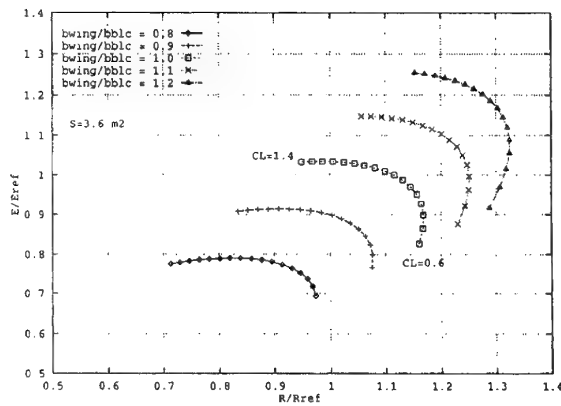
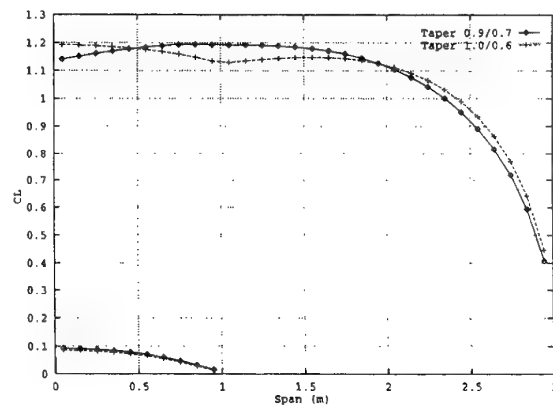
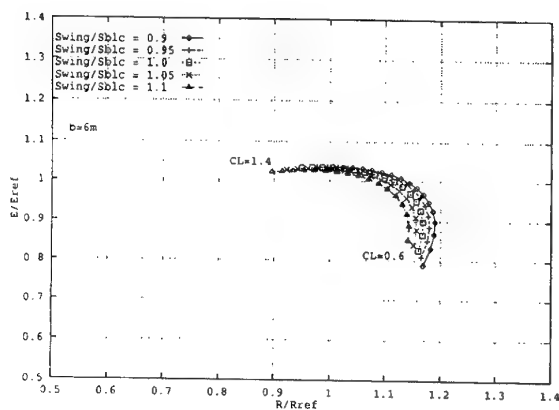
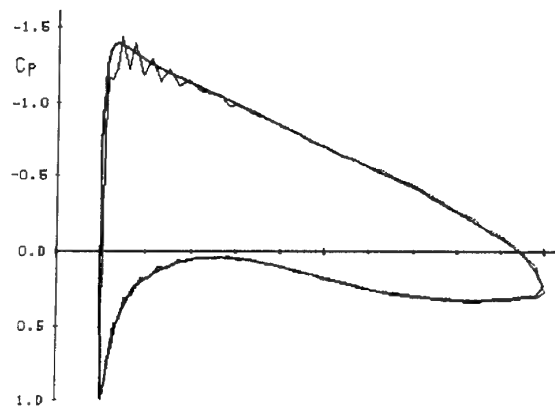
b) Effect of varying b at constant S .Fig. 8 Spanwise c_l distribution on the wing and stabilizer for two combinations of taper ratios.c) Effect of varying S at constant b .Fig. 9 C_p vs. x/c distributions for the original and the smoothed Wortmann FX 60-126 at $\alpha = 3^\circ$.

Fig. 6 Effect of the wing planform parameters on the performance characteristics.

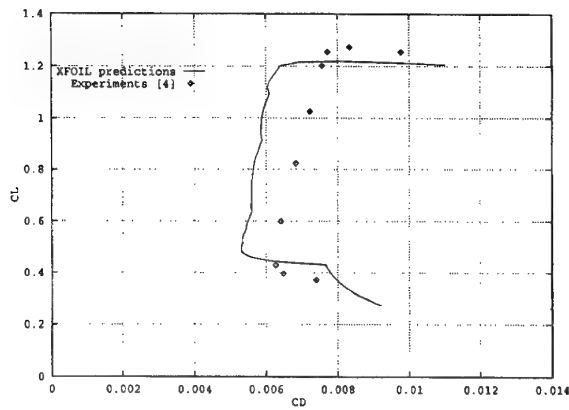


Fig. 10 Comparison between XFOIL predicted and experimental polars for the FX 67-K-150 at $Re = 1.5 \times 10^6$.

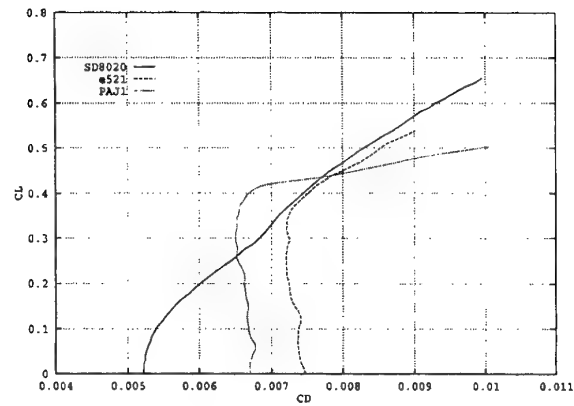
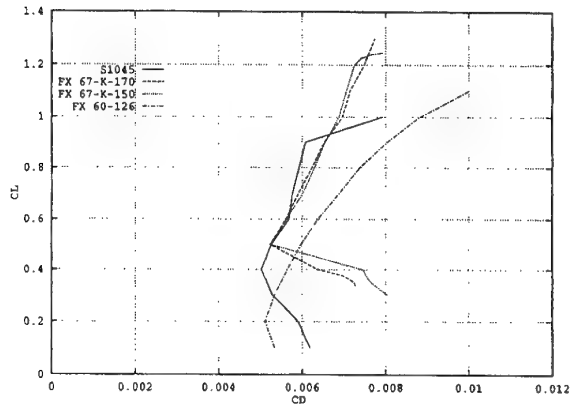


Fig. 12 Polars for candidate tail aerofoils at $Re = 6.2 \times 10^5$.



a) Polars at varying Re .

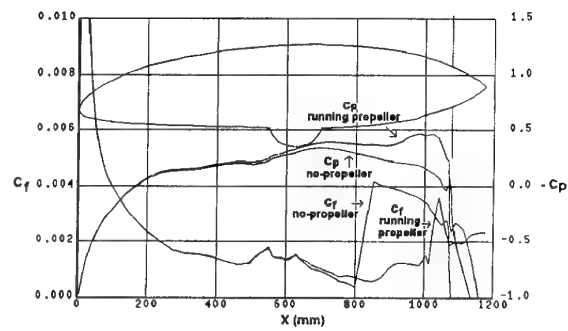
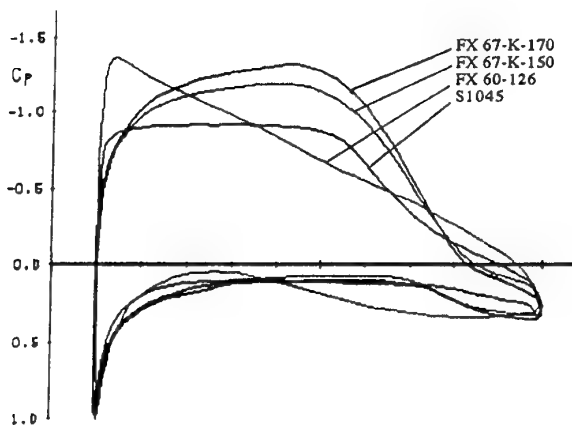


Fig. 13 VSAERO predictions of the C_p and C_f distributions along the symmetry plane of the fuselage upper surface at $\alpha = 0^\circ$.



b) C_p vs. x/c distributions.

Fig. 11 XFOIL predicted characteristics of the FX 67-K-170, FX 67-K-150, FX 60-126 and S1045.

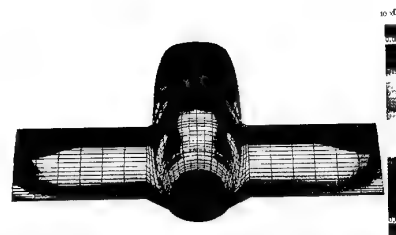


Fig. 14 VSAERO predictions of the C_f distribution on the upper surfaces of the fuselage and of the wing inner sections at $\alpha = 0^\circ$.



Fig. 15 China clay detection of transition on the upper surfaces of the fuselage and of the wing inner sections at $\alpha = 0^\circ$.



a) No-propeller.

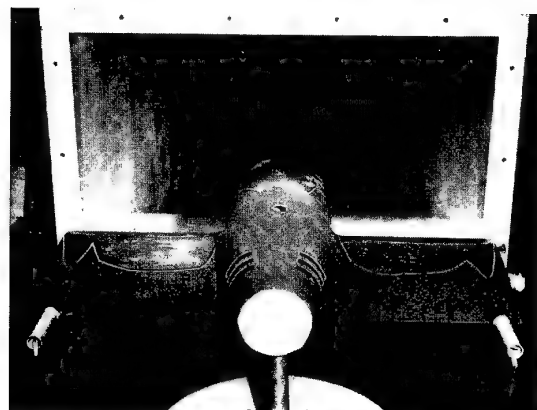
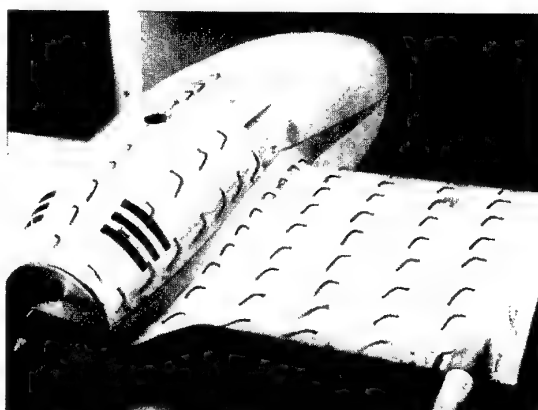


Fig. 16 Stethoscope detection of the transition regions on the inner-wing upper-surface at $\alpha = 0^\circ$.



b) Running propeller.

Fig. 17 Wool tuft visualization of the wing / fuselage junction flow at $\alpha = 9^\circ$.

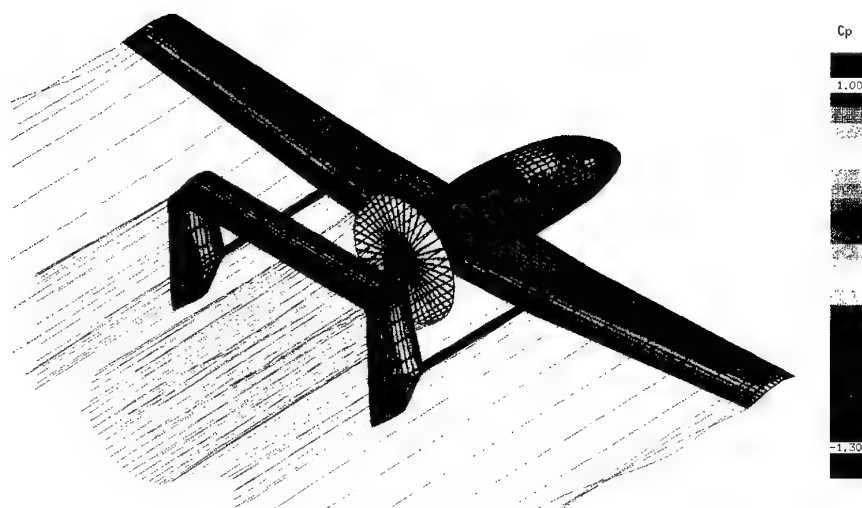


Fig. 18 VSAERO prediction of the surface pressure field on the complete configuration.

Technology and Application of Modern Drone Systems

by J. Bäcker, M. Möhring, V. Schlenkrich
STN ATLAS ELEKTRONIK GmbH
Unmanned Aerial Vehicles
Hünefeldstraße 1-5
D-28199 Bremen

Table 1 shows the appropriate assignments of payloads, design characteristics and missions to the a.m. tasks.

Table 1: Design characteristics and applicable payloads for drones			
TASK	BASIC DESIGN	PAYLOADS	
reconnaissance	reusable	o E/O (TV, IR) o SAR o direction finding receiver o meteorological	o data link payload/ target data to ground operator
surveillance	reusable		payload / mission control from ground station
target localization	reusable	o E/O (TV, IR) o SAR	
electronic warfare	reusable / fire & forget	o jammer	o up + downlink o uplink
relay	reusable	o receiver transmitter	o data link
defence / target combat / suppression	fire & forget	o SAR o E/O	o warhead
recce / strike combination	expendable	o SAR	o warhead o data link target data mission control

1. Introduction

Modern drones represent robotic systems which pick up situations in their environment by sensor payloads, assess them by preprogrammed mission logic and react according to their predefined mission. Some functions of the air vehicle may be controlled or supervised interactively by operators from a ground control station.

Typical tasks for drone systems are

- o reconnaissance
- o surveillance
- o target localization
- o electronic warfare
- o target combat

in adverse environmental conditions, e.g. considerable threat by enemy air defence systems (ADS).

The different tasks lead to two major designs for the air vehicle:

- o the reusable drone, e.g. for recce missions
- o the expendable / fire and forget drone, e.g. for combat missions.

These design criteria determine the range of the necessary ground equipment, e.g. for drone refurbishing, number of staff as well as the training effort.

Due to the threat by ADS, the drones should have low signatures in the frequency bands of visual, infrared, acoustic and radar sensors to minimize the probability of being detected and jammed or shot down.

In accordance with the mission and the environmental requirements, different payloads must be integrated, which may be sensors, data links or warheads.

There are some special requirements which lead to a High Altitude Long Endurance (HALE) drone or a fast flying missile-like drone. However, all the tasks shown in Table 1 can be covered by small, light-weight drones with fixed wings and with a take-off-weight up to 150 kg. The available sensor technologies lead to payloads of less than 50 kg. The flight velocity has to be adjusted to the sensor performance to achieve complete terrain coverage and sufficient integration time for data exploitation. The flight velocity of about 50 m/s to 70 m/s takes this into account. In addition, a flight endurance of more than four hours becomes possible. The reusable drones are operator-controlled (not piloted) if they are equipped with data link capabilities. This permits changes of the preprogrammed flight path according to events during mission as well as homing / landing control facilities.

There is also a demand for a low weight / easy-to-operate drone with a take-off weight of less than 25 kg for close range recce.

Therefore this paper will present two drone systems which are the basis for the drone family of STN ATLAS Elektronik, covering the entire range of the a.m. applications:

- o The TAIFUN defense drone, representing the fire and forget type and the

- o BREVEL system for real-time reconnaissance and target localization, representing the reusable type.

2. Drone Systems and Applications

2.1 The TAIFUN Defense Drone

Main tasks and mission sequence

The TAIFUN is a fire and forget drone. It is designed to engage tanks, armoured vehicles, other high-value vehicles and individual targets, which are part of command posts, logistic facilities or artillery unit at firing sites.

The mission is preprogrammed. The mission program comprises the flight path, the search area, the target types to be engaged and data for sensor control and navigation update. After launch, the TAIFUN operates autonomously. It searches for targets in a predefined search area. Depending on the special task and the available recce information, this search area is very small (e. g. 500 m * 500 m) or covers a region of more than 1000 km². The TAIFUN is equipped with a mmW seeker for target acquisition, target classification and homing. The actual situation found in the search area cannot be predicted. Therefore the flight control computer (FCC) changes the preprogrammed mission during flight, in accordance with deployment, amount and behaviour of the acquired targets. The drone can stay above and monitor an area until the expected targets appear. It can recover from target homing mode, climb and search again if a target classification is not verified with sufficient reliability during terminal dive. If more than one individual targets are detected, all targets are mapped and the target with the highest value will be selected for engagement. The steep dive homing leads to a precise hit. The hit point is controlled by the FCC according to target type.

System overview

The TAIFUN system consists of

- o 1 ground control unit (GCU) loaded on a 5 t-truck.
The GCU is equipped for communication, mission planning, mission programming and crew training. The equipment is installed in a standard shelter.
- o 8 storage, transport and launch containers (Container)
This is a 8 ft * 8 ft * 10 ft container which can be handled with all military and civil logistic means. Nine drones are stored inside under controlled environmental conditions. Lift gears are mounted to the front side for loading and unloading the container onto and from trucks. They are also used to lift the container for launching. The container is linked to the GCU by a fibre optics interface to program the drones.

- o 72 drones TAIFUN (9 per container)

TAIFUN Air vehicle characteristic

The air vehicle design is a cross-wing type. The advantage of this design is a precise homing capability and a no-bank-to-turn flight, which makes sensor stabilization easier. During storage in the container, the wings are folded. Gas springs unfold the wings after launch. The air vehicle is launched from the container by means of a solid state booster. Cruise flight propulsion is by a 32 kW heavy-fuel piston engine. The basic air vehicle is made of glassfibre and carbonfibre combined with radar absorbing materials. Its radar cross section is less than that of a pigeon. The FCC is equipped with GPS and a strap-down INS. The payload consists of a mmW seeker and a shaped charge and is installed in the front section. The dimensions are 2.1 m (length), 2.3 m (wing span) and 1.0m (height). With the a.m. payload the take off weight is 135 kg.

The TAIFUN mmW seeker

The TAIFUN seeker is a SAR radar operating in the 35 GHz frequency range. The doppler beam sharpening (DBS) mode provides high-resolution data of targets and terrain images which are used for navigation update. The various radar modes permit target classification, target homing, home on jam and moving target indication. Flight trials with a seeker preprototype of DASA ULM demonstrated the online target classification as well as a high-resolution imaging. Normally a considerable integration time and computing time is necessary to produce high-resolution radar images. This sensor provides the images online after a "single look" with a 0.5 m * 0.5 m resolution.

The Terrain Aided Navigation (TAN)

The TAN principle consists in matching a radar image of the terrain with a digital map stored in the flight control computer. The digital map is based on the Digital Land Mass System (DLMS) which provides terrain elevation and terrain feature data as a standard. Typical features are roads, railway tracks, forest edges, river banks etc.. The radar measures terrain elevation and computes terrain images during the search flight. After matching the radar image, the drone position is calculated with the relevant antenna boresight angles. Captive flight trials demonstrated an update accuracy better than 150 m CEP.

Hit performance

A shaped charge, which penetrates even reactive composite armour, has been designed and tested. The test target included an add-on armour to ensure performance also when used against future tanks. The total weight, including fuze sensor and safety unit is less than 25 kg.

6-DOF simulations of the terminal dive into moving targets show the precision of the sensor and of the steering manoeuvres of the air vehicle.

Program status

The TAIFUN master plan shows the start of the development phase in 1996. All major components have already been proved by hardware trials in previous phases.

2.2 The BREVEL Drone System

The BREVEL is a drone system for real-time reconnaissance and target localization. It is a reusable drone. The BREVEL is equipped with a forward-looking infrared sensor.

The system comprises the BREVEL Air Vehicle, the Ground Control Station, the Launch Vehicle, the Recovery Vehicle, the Refurbishing Vehicle and the Data Link Vehicle.

The Ground Control Station comprises three operator bays with displays for mission planning and mission control including a digital map, for the sensor images and image evaluation as well as a control and communication terminal. All components are installed in a cabin. The Launch Vehicle carries a container for transport and booster launch of the drone. Launch is specified for wind velocities of up to 15 m/s and additional gusts of +/- 10 m/s. A control unit gives a Go / NoGo indication after preflight check and controls the launch sequence. After landing, the BREVEL is recovered by a crane vehicle and transported to the Refurbishing Vehicle. The latter is used for system check after storage, post flight check and refurbishing including all field maintenance of the air vehicle. All work can be done inside the cabin.

The telescope mast system of the ground data link is mounted on a trailer. It is linked to the Ground Control Station by a fibre optic cable. After orientation with the vehicle navigation system and a north seeking gyro, the slaved antenna can also be used to measure the air vehicle position.

The preprogrammed BREVEL mission is operator supervised. The operator can take over the control of the air vehicle and / or the sensor and switch back to the flight control computer at any time.

BREVEL Air vehicle dimensions and characteristics

BREVEL has a modular, compact and tailless configuration with low-set wings. With a length of 2.2m, a span of 3.4 m and a height of 0.9 m the BREVEL is a very small bird in comparison to other drones. The air frame is

made of radar absorbing and radar transparent composite materials. It can be launched by a booster at any wind direction. For de-icing, the exhaust heat of the two-stroke piston engine is used. After completing the mission, the air vehicle is landed by a parachute and an air bag system at a commanded landing point with very high accuracy. The jam-resistant data link system uses a narrow-beam antenna inside the radome on top of the vertical fin.

The Forward Looking Infra-Red camera provides three fields of view and zoom function. Mounted on a tri-axis stabilization platform, it can be controlled by the ground operator or it can track targets automatically, always transmitting upright images to the ground station. During flight, the navigation system is updated by Rho/Theta using the digital data link or by correlation of the payload images with the digital map inside the Ground Control Station. GPS is available as an option.

The commonality of the BREVEL and the TAIFUN system is obvious. It comprises, in particular, the modular air frame design and construction, the FCC including software, but also the ground equipment as well as operational and logistic procedures.

Program status

The BREVEL is a joint German / French full scale development program which started at November 1992. The official first flight was on July 11, 1995.

2.3 Further Drone Applications

The following slides show examples of additional drone applications.

The "Mücke" Jamming Drone

The German and French forces have established a requirement for a drone which jammes the enemy VHF communication systems. STN ATLAS Elektronik has a solution for this demand, based on the reusable air vehicle. Mission preparation and mission sequence are very similar to a BREVEL or TAIFUN mission. Wind tunnel and EMC trials have been performed, to prepare a detailed system definition.

In a second stage, the MÜCKE will be equipped for jamming UHF communications, precise localization of radio stations and radar systems and for counter measures against point-to-point radio links.

For target localization, the drone has the advantage of short bearing ranges inside the scenario. Therefore the target localization is more precise than that achieved with stand-off systems.

Meteorological Data Collection

The Environmental UAV is a concept for using drones for measurement of meteorological data and atmospheric parameters inside the enemy airspace in various altitudes. The data will be transmitted to a ground station in real time. One advantage of precise wind data is the increase of hit accuracy of certain kinds of artillery ammunition, saving a lot of rounds.

Naval UAV

The NAVAL UAV is meant to provide over-the-horizon targeting and fire control. It shall be equipped with the TAIFUN seekerhead, using the automatic classification and radar imaging function for identification and localization of enemy vessels. The UAV is based on the TAIFUN cross wing drone. It is launched and controlled from the engaged vessel. The radar classification results and high resolution images will be transmitted to the control center of the operation ship by data link. Depending on the special operational requirements, it can be recovered by ship or operated as a fire and forget drone.

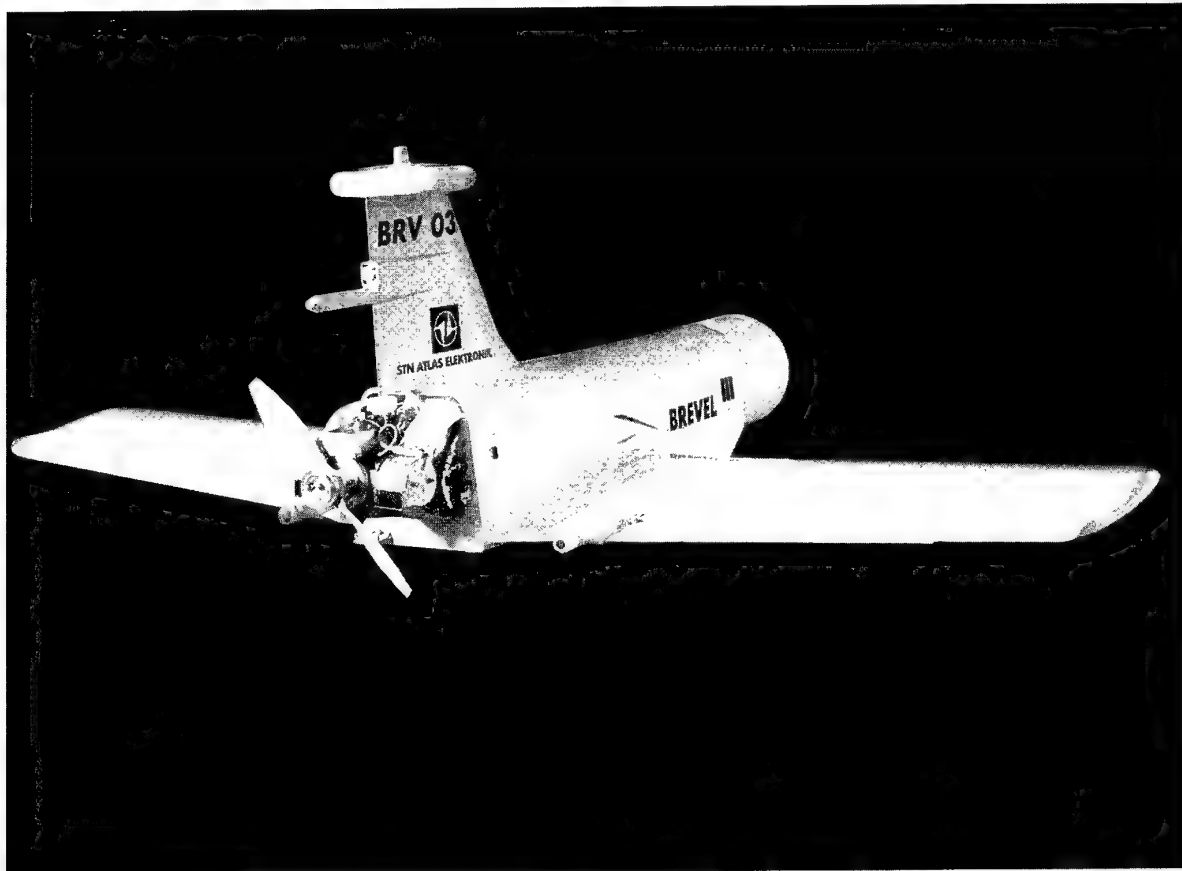
Close Range Mini Drone

The Close Range Mini Drone will reconnoitre tanks, armoured and other military vehicles in the close range. The drone system will be integrated in and operated from a light armoured vehicle.

In a first approach, the system requirements will be:

The take-off weight of the air vehicle should be less than 25 kg. A simple flight control system should allow to preprogram waypoints for the mission and also permit remote control by using the images of a commercial video camera for orientation. A simple data link should provide online image transmission to a display in the armoured vehicle. The flight endurance should be at least 30 minutes. After a short introduction, operation of the system should be possible by one soldier only.

The solution for the Close Range Mini Drone is a 2:3 scale model of the well-proven STN ATLAS "TUCAN" air vehicle. Flight trials in 1995 demonstrated that the small version had all the aerodynamic qualities of the 1:1 scale TUCAN. Even under rough weather conditions the smooth flight provided high-quality TV images with an unstabilized commercial camera. The drone is landed by a parachute.



BREVEL AIR VEHICLE

Enabling Technology for UAVs

Robert C. Michelson

*Principal Research Engineer
Georgia Tech Research Institute
Atlanta, Georgia 30332*

INTRODUCTION

Requirements for the performance of certain NATO missions in the 2015 - 2020 time frame have been examined. In addition, various unmanned aerial vehicle-borne sensor payloads have been identified which support the execution of these missions in an effective manner.¹ Present state-of-the-art sensors and air vehicle systems do not provide the performance necessary to prosecute these missions in light of the anticipated future civil and military environment. This paper presents a discussion of the under-girding technologies which will make the predicted unmanned aerial vehicle (UAV) performance possible. The description of these enabling technologies includes discussions concerning the present state of the art, their general applicability to a variety of UAV payloads, and the collateral technologies which will in turn facilitate the development of the chosen primary enabling technologies.

Though a number of enabling technologies have application to the various UAV missions, seven are recommended for near term investment. These are prioritized (in order of fundamental applicability and return on investment) as follows:

1. Photonics

Integrated optical systems and devices will essentially replace electrons with photons for many military applications. The next twenty-five years will see the emergence of photonic (light wave) systems which will be incorporated into optical sensors, communications links, information processing, and directed energy weapons.

2. Acoustic Charge Transport (ACT)

UAVs will be able to perform more tasks autonomously. To avoid high bandwidth data links, the data processing will need to be achieved on-board the UAV in real time. Surface Acoustic Wave (SAW) devices, charge-coupled devices (CCD), and ACT devices can perform complex signal processing on a single integrated device, but ACT devices will provide capabilities that are not possible with any current technology.

3. Full Spectrum, Ultra-Resolution Sensors

Many UAV missions will rely on remote sensors such as ultra-wideband radar, laser sounders, infrared sensors, and ultraviolet imagers. Improvements in the resolution and bandwidth for these sensor types will allow remote sensing missions to be carried out at greater stand-off ranges, or with increased information gathering capability. For example, focal plane arrays with 10^6 active elements and broad spectral coverage (typically 2 to 25 microns) will lead to surveillance systems having vastly increased resolution. Similarly, such advances in new semiconductor materials offer the potential for using significantly higher operating temperatures, thus reducing (or obviating) cryogenic cooling requirements.

4. Knowledge-Based Systems

UAVs of the 21st century will possess intelligence that enables them to "think" and react in ways that mimic the human decision-making process. These knowledge-based artificial intelligence systems, through the use of advanced component technologies such as photonics, will operate in real-time. In the year 2015, UAVs will be directed by human speech commands. Expert systems will allow the UAV to make on-the-spot decisions regarding the fulfillment of its mission and use reasoning to develop alternate courses of action. Not only will the UAV exhibit intelligence as a system, but the various payload components will themselves be able to draw conclusions about potential targets or the vehicle's environment through the use of data fusion and image recognition techniques. Finally, the air vehicle and sensors will be able to learn from past situations and automatically apply this experience to new scenarios. This will feature reliability afforded by fault tolerant, self-healing hardware and advanced introspective fault diagnosis.

5. Microelectromechanical Systems (MEMS)

MEMS combine mechanical structures and electronics on tiny silicon chips using semiconductor manufacturing methods such as sequential deposition, etching, and doping. MEMS technology offers three important assets. First, semiconductor processing allows smaller, lighter systems to be reengineered as retrofits in

¹ Simpson, R., Michelson, R., Fentem, P., et al, "Future Use of Unmanned Air Vehicle Systems in the Future Environment," NATO AGARD advisory report, Aerospace Applications Study (AAS)-36, AGARD-AR-307 Vols. 1 and 2, August 1994.

current applications. Second, since it is as easy to build millions of MEMS components as easily as it is to build one, the cost for subsystems will continue to drop just as it has for microelectronics. Finally, MEMS permit much closer integration of microelectronics with electromechanics through the use of identical materials and processes of fabrication.

6. Wafer-Scale Integration of Dissimilar Technologies

Wafer-scale "union" or "integration" refers to an emerging technology that will combine, on a single 3 by 8 inch sheet of material, signal generation, signal control, information processing, chemical and physical sensing, fluidic and mechanical actuation, as well as radiation generation and detection. Components of such combinations are now possible only on separate, isolated and mutually incompatible optical, magnetic, acoustic, or electronic substrates. Integration of UAV payload subsystems into single monolithic blocks will increase reliability while reducing size and weight, which translates into longer time on station at a lower cost.

7. Smart Skins

In traditional design, the skin of an air vehicle is a structural fabric which provides aerodynamic shape, strength and rigidity. When adding antennas and sensors to the air vehicles, holes are normally cut in the skin for installation, resulting in attendant structural, aerodynamic, thermal, and cost penalties. The concept of a smart skin is to embed the antennas, sensors, transmitters, receivers, signal and information processors, RF/ power/ electronic bus cables, and thermal controls within the skin during the design and construction of the air vehicle. Some structural surfaces could even be transparent to various RF, IR or optical wavelengths, and other surfaces be electronically reconfigurable (e.g., wing or rotor blade camber).

This paper does *not* provide recommendations for payload systems, but rather, for the *enabling technologies* which will lead to the payload system capabilities necessary to meet future NATO and private sector UAV mission requirements over the next two decades.

TECHNOLOGY FORECAST

The 1995 NATO handbook states that based on the security objectives and strategic principles of the new European environment, "the organization of the Allies' forces must be adapted to provide capabilities that can contribute to protecting peace, managing crises that affect the security of Alliance members, and preventing war, while retaining at all times the means to defend all Allied territory and to restore peace."²

To realize the objectives stated by NATO doctrine, the size, readiness, availability and deployment of the Alliance's military forces will have to reflect a strictly defensive mission and adapt to the new strategic environment and its arms control agreements, by reducing the overall size of the Allied forces, while not diminishing its readiness.

Unmanned aerial vehicles can play a major role in resolving the contradiction of a smaller force with the readiness of a larger one by supplanting many manned aircraft missions with less expensive and less labor-intensive unmanned ones. The logistics burden required to train and support a fighter pilot and his aircraft is enormous compared to that of an unmanned system which, for many missions, can supply the same function better and for less cost.

Beyond the future military missions for UAVs, there will be a growing commercial and law enforcement markets as well. NATO countries such as France, Portugal, Spain, Italy, and Iceland with large coastal regions will benefit from UAV operations in support of future monitoring, contraband interdiction, and fisheries. Other nations such as Turkey which border unstable neighbors like Iran and Syria will benefit particularly from the less expensive, but more comprehensive border monitoring that can be achieved with UAVs. Package delivery to remote sections of eastern Turkey or to snowbound reaches of Norway might emerge as profitable markets. The safe spraying of pesticides on German sugar beet crops are within the realm of possibility for commercial UAVs during peace time. Even nations with highly developed infrastructures such as the United States could benefit from more advanced and less expensive methods of traffic surveillance, utility inspection, and border patrol.

² Anon., "The Alliance's Strategic Concept," Agreed by the Heads of State and Government participating in the meeting of the North Atlantic Council in Rome on 7-8 November 1991, as found in Appendix IX, Paragraph 45 of the *NATO Handbook*, 1995.

In order for UAV systems to perform with sufficient accuracy, resolution, precision, and reliability to be effective against the projected NATO threat/mission scenario or to provide economically viable services to the private sector, certain underlying or "enabling" technologies will have to be developed or perfected. *Near term investment in enabling technologies is critical to the availability of future UAV systems in the 2015 - 2020 time frame.*

FUTURE CAPABILITIES AND TECHNOLOGIES

Many enabling technologies have application to the various future UAV missions. Some are implicit to all missions while others are more specific. For example, ultra-light high strength structures (composites), high temperature materials (ceramics), advanced propulsion systems, and of course room temperature superconductivity are all important technologies supporting the development of future UAVs. However, due to priorities based on fundamental development risk, centrality and criticality of the supporting technology to the majority of projected future missions, the list of enabling technologies recommended for near term investment has been limited to seven primary, and sometimes interrelated areas. The seven recommended areas for investment are (in order of ubiquity and return on investment): 1. *Photonics*, 2. *Acoustic Charge Transport*, 3. *Full Spectrum Ultra-Resolution Sensors*, 4. *Knowledge-Based Systems*, 5. *Microelectromechanical Systems*, 6. *Wafer-Scale Integration of Dissimilar Technologies*, and 7. *Smart Skins*.

These seven areas agree with recommendations made by the U.S. Air Force Forecast II technology study of the mid 1980's, having been updated during the AAS-36 NATO AGARD study initiated in November of 1991, and most recently in 1995 (this paper) to reflect advances in these technologies as they pertain to future UAV missions.

The following subsections describe these enabling technologies, demonstrate how they will be generally useful to a variety of UAV payloads, indicate the current state of the art, and identify other enabling technologies which will in turn facilitate the development of these seven primary areas.

PHOTONICS-BASED PAYLOAD CAPABILITY ENHANCEMENTS EXPECTED BY 2020

Integrated optical systems and devices will essentially replace electrons with photons in a large variety of military applications. The next 25 years will see the emergence of photonic systems that incorporate optical sensors, communications links, information processing, and weapons (directed energy). An entire future UAV system could operate principally in the domain of photons having minimal interaction with electronic devices.

The superiority of a photonic (light wave) communication system over an electronic system can be measured by information-carrying capacity (*four orders of magnitude greater for optical systems*); energy loss in signal transmission (*two orders of magnitude lower*); and error rate (*one order of magnitude lower*). The development of semiconductor lasers specifically designed for fiber optic systems promises even greater improvement in information-carrying capacity.

Photonic (optical) computing offers significant improvements in processing speed compared to electronic computing. This speed increase is due to the natural parallel architecture and large increases in throughput due to the high switching speeds of optical devices. Optical computer components need no physical connection: photons (light beams) replace the wiring. New distributed-processing architectures will also be possible by exploiting the no-wire advantage as well as continued improvement of fiber optics and lasers.

Photonic sensors, especially when used with active illuminators or adaptive optics, can provide high-resolution target recognition information that will be difficult to detect or jam. Numerous system concepts could provide enhanced information about potential targets based on a fusion of data from multiple sources (both active and passive). For example, a future tactical laser radar system composed of binary optical elements and a coherently phased array of laser diodes could provide simultaneous range, range/Doppler, passive infrared (IR) imagery, and visible imagery. Multispectral sensor data, coupled with an optical signal processor, could provide recognition of both stationary and fast-moving targets.

Future UAV-borne photonics systems will not be susceptible to electromagnetic interference or EMP damage. They will be radiation resistant and will have emanations that are difficult to detect and jam. Orders of magnitude improvements over electronics can be expected in communications, computing, and signal processing for advanced battle management and weapons systems. Photonic sensors will detect, recognize, and classify both mobile and stationary targets faster and with better resolution and greater precision than current lower frequency systems. Also, future UAVs using optical technology should benefit from the elimination of connections because they are a major source of failure in electrical systems.

Photonics is pervasive as an technology underlying UAV payloads—and to the extent that it is used within smart skins and structures—the UAV airframe itself. Because of the bandwidth, hardness, and reliability associated with optics, all UAV payload

systems can conceivably benefit from incorporation of (or total implementation with) photonic components. The range of potential applications for photonics includes sensors, communications, air vehicle guidance, and computing. The following specific applications are indicative of the potential uses for photonics throughout the UAV system:

Photonic Communications

1. Optical Secure Local Area Networks (*UAV as a low-altitude satellite for the fleet*)
2. Laser Communication (*secure extremely high-bandwidth air-to-space, air-to-air, or air-to-surface data links*)
3. C³I Applications
4. Optical Wave Guide
5. Over-the-Horizon Ultraviolet Communications

Photonic Sensors

1. Tactical Laser Radars (*target identification*)
2. Multispectral Imagery (*target identification under adverse conditions*)
3. Air Vehicle Monitoring/Sensing (*UAV self-awareness/feedback, health, status*)
4. Secure Beacon Identification Friend or Foe (*UAVIFF*)

Photonic Computing

1. Digital Optical Computer (*UAV flight control, on-board image processing, expert system*)
2. Artificial Intelligence (*intelligent real-time in-flight route planning*)
3. Wide Bandwidth Real-Time Spectrum Analysis (*target identification*)
4. Compact Real-Time SAR Processors
5. ECM/ESM Signal Processors

ACOUSTIC CHARGE TRANSPORT PAYLOAD CAPABILITY ENHANCEMENTS EXPECTED BY 2020

Key to the future of future UAVs will be the ability to contain significant on-board intelligence capable of real-time performance. By the year 2020, UAVs will be able to perform more tasks autonomously and will be able to assimilate more data based on higher resolution sensors, but in order to avoid high bandwidth data links, the manipulation of information will have to be done within the UAV, and done in real-time. Several technologies support this requirement, none-the-less of which is acoustic charge transport devices.

Acoustic Charge Transport (ACT) technology will be a major innovation in the area of signal processing. ACT devices promise high-bandwidth operation, with wide dynamic range and high-time bandwidth products, in very small packages with simple architecture.

These combinations of features will result in improved performance and lower cost for future signal processors.

Signal processing is essential to UAV communications (e.g. bandwidth compression, encryption, antijam capability), image processing (e.g. target recognition), and remote sensing (e.g. clutter rejection, low probability of intercept {covert interrogations}, performance enhancements {pulse compression}). ACT devices will allow capabilities that are not possible with any current technology. They will allow greater processing power in a smaller, lower power package than is possible with alternative technologies. Because of the monolithic nature of these devices, their reliability will be much greater than that of the circuit boards they replace. A side benefit will be the higher radiation resistance of GaAs material from which ACT devices are fabricated. ACT devices will process wider bandwidths with a greater dynamic range than is possible with any other technology. This capability is essential for wideband intercept systems.

There will be many applications for devices with the operating characteristics of ACT devices, especially UAV-borne imaging sensors due to the ability of ACT devices to meet the demands of focal plane imagers for high-speed, wide-dynamic-range image readout. The imaging application does not utilize the signal-processing power of ACT technology, but rather its raw speed and dynamic range as an analog shift register. These devices will also be capable of performing matched filtering for highly jam-resistant and low probability of intercept (LPI) communication systems. They will be capable of dehopping frequency-hopped, spread-spectrum communications systems. Very large time-bandwidth, fixed-tap devices will find application in compressive receivers for wide and signal intercept systems. The analog memory capability of the devices can be used to capture hostile radar pulses, remodulate them, and retransmit them for spoofing purposes.

One of the most promising applications of this technology is radar/ communication/ intercept, with front-end, high-speed, preprocessing data reduction and on-chip, high-speed, 400 mega sample/sec A/D capability. This capability will allow radio frequency (RF) or suitable intermediate frequency (IF) processing of signals with hundreds of MHz bandwidth received as analog or digital signals. The reduction of wide band input signals to low MHz or high KHz digital signals will allow cost-effective, microprocessor-based post processing.

The ultimate performance of ACT technology in UAV payloads will be a function of the processing architecture. The number of multiply-and-accumulate

operations per second, or MACs/s, represents *the* figure of merit for digital signal processors, or for any other digital computer, when processing signals. Currently the state of the art for real-time digitally-programmed transversal filters (PTF) is a signal correlation speed of 45 billion MACs/s (derived by multiplying the sampling rate of 358 MHz by the number (128) of delay taps used in Comlinear's hybrid IC PTF. The following table puts this performance in perspective by comparing a few other IC signal processors and computing machines which employ alternate technologies.

TABLE 1. PROCESSING POWER COMPARISON
FOR VARIOUS MACHINES³

Processor Approximate MACs/s

Comliner ACT hybrid IC	45 Billion
Connection Machine (mainframe)	5 Billion
Cray 2 (mainframe)	850 Million
High-speed digital FIR filter ICs	480 Million
Typical digital signal processor ICs	20 - 30 Million
Typical RISC IC processors	20 - 30 Million
i486 processor IC	0.5 Million

Theoretical analysis has been used to project the performance shown below for future devices. An analysis of the fundamental factors limiting current aperture indicates that sampling apertures on the order of 20 picoseconds are possible, but a conservative figure of 100 picoseconds was used to estimate the other parameters.

TABLE 2. PROJECTED ACT PERFORMANCE

Bandwidth	5 GHz
Sampling Rate	10 GHz (parallel-channel device)
Sampling Aperture	20 picoseconds
Transport Efficiency	0.99995
Dynamic Range	40 dB plus 6.5 log number of taps
No. of Taps	1,000

Multiplying the 10 GHz sampling rate by 1,000 taps produces an expected data retrieval rate of 10^{13} samples per second.

The monolithic integratability with GaAs ICs, speed, accuracy, versatility, radiation resistance, simplicity, and adaptability of the ACT device offer the potential for a magnitude of improvement in the performance of a wide variety of advanced systems. Systems benefitting from ACT device technology will include surveillance, identification, active stealth, imaging processing, artificial intelligence, as well as guidance and control.

Performance will be driven by future UAV system requirements, but the first demonstrations will probably be at the subsystem level. Representative subsystems are as follows:

Programmable Delay Line	Transformer
Variable Delay Line	Analog Memory
Multiplexers/Demultiplexers	Noise Whitener
Time Compressor/Expander	Burst Processor
Frequency Converter	A/D Converter
Adaptive Vector Processor	Synchronizer
Adaptive Beam Former	Synthesizer
Focal Plane Multiplexer	Track and Hold
Frequency Dehopper	Comb Filter
Laser/Radar Range-Sampler	Correlator

**FULL SPECTRUM ULTRARESOLUTION SENSORS
PAYLOAD CAPABILITY ENHANCEMENTS BY 2020**

The need for improved resolution, accuracy, coverage, and timeliness in remote sensing of targets, backgrounds, and the intervening environment pervades a wide range of current and future UAV systems and mission capabilities. Projected advances in electronics, information processing materials, and computer technology will make possible major improvements in performance of future sensors for future missions. Innovative new sensor designs are expected to emerge in radars, integrated infrared (IR) and ultraviolet (UV) focal plane arrays, cryogenic inertial sensors, LIDARs, and microwave sounders.

The cost-effective production of integrated infrared focal plane arrays with 10^3 to 10^6 active elements and broad spectral coverage (typically 2 to 25 microns) will lead to surveillance systems with vastly increased resolution; new semiconductor materials offer the potential of significantly higher operating temperatures thus reducing cryogenic cooling requirements. Compact, cryogenically cooled inertial measuring units will sense very accurately the linear and angular accelerations and gravity gradients experienced by an aerospace vehicle. New and improved sensors drawing on LIDAR and microwave approaches offer the opportunity to monitor the ocean environment with greatly enhanced coverage and resolution compared to current sensors. The development of digital RF memories, digital-beam-forming circuitry, and the adaptive electronic control of wide-band, arrays will enable the development of multistatic (from multiple UAV, ground-based, or ship platforms), simultaneous transmit and receive, and resource allocation radars capable of acquiring slowly moving surface and airborne targets with low-observable signatures.

The integration of active and passive sensors on a single platform would also have an important payoff for future UAV systems. Passive (e.g., non transmitting) sensors could be used where atmospheric

³ Goodenough, F., "IC Signal Processor Runs 45 Billion MACs/s," *Electronic Design*, July 23, 1992, page 54.

conditions permit. For military and law enforcement applications, these sensors would gather target data without betraying their presence through detectable transmissions. The active sensors would be used only when the atmospheric conditions made passive sensors unusable, or if some property possessed only by active sensors needed to be exploited.

As an example, advanced LIDAR sounding technology has good potential application to two areas:

- A surface-based LIDAR can make measurements of several atmospheric properties. In relatively clear areas it could also provide data on the troposphere, stratosphere, and mesosphere, and replace some meteorological balloons and rockets. At sea, it could detect chemical, biological, or radioactive agents.
- An airborne LIDAR could provide meteorological and atmospheric data for regions that are geographically or politically inaccessible.

Recent research aimed at development of imaging sensors operating in the ultraviolet (UV) wavelengths could have high payoff for both the military and commercial sectors. Not only can UV sensors be used to detect surface and airborne target emissions/reflections, but they can be used to image the electron density in the upper atmosphere and ionosphere. The electron density is important for communication or radar transmissions that are reflected from the ionosphere, as well as for transmissions that pass through the ionosphere. Areas of high electron densities disrupt these transmissions and a precise, real-time map of electron density could be employed to find the best available operating regions for over-the-horizon radars and high-frequency (HF) communications systems.

In general, UAV payload and avionics systems using ultrabandwidth radar, laser sounding, infrared sensors, ultraviolet imaging, and cryogenic inertial guidance all stand to benefit the most from full spectrum ultraresolution sensors.

CAPABILITY ENHANCEMENTS DUE TO INCORPORATION OF KNOWLEDGE-BASED SYSTEMS

Future UAVs of the 21st century will possess intelligence that enables them to "think" and react in ways that mimic the human decision-making process. This will be as a result of knowledge-based artificial intelligence systems which, through the use of advanced component technologies such as photonics, can operate in real time. In the year 2020, UAVs will

respond to human speech commands and may appear to a remote battle commander as a human-piloted reconnaissance aircraft. Expert systems will allow the UAV to make on-the-spot decisions regarding the fulfillment of its mission and use reasoning to develop alternate courses of action. Not only will the UAV exhibit intelligence as a system, but the various payload components will themselves be able to draw conclusions about potential targets through the use of data fusion and image understanding techniques. Finally, the air vehicle and sensors will be able to learn from past situations and apply this self-generated experience to new scenarios—doing all of this with the added reliability afforded by fault tolerant, self healing hardware and advanced introspective fault diagnosis.

It is difficult to summarize the effects of knowledge-based system technology on future UAVs since the spectrum of payloads and their capabilities is diverse. One expected result is a 50-percent reduction in the cost of payload systems when knowledge-based system technology is used in systems' acquisition, design, and fabrication. Maintenance costs, primarily manpower, should also be reduced by one-half. By improving the effectiveness of mission management and target acquisition, knowledge-based system technology could significantly reduce the number of future UAVs required to provide the equivalent of current capability. All of these effects together should provide twice the current effectiveness at somewhat less than current costs. Future military threats, however, can also be expected to increase in sophistication by the year 2020. It is probable that the net effect of the advantages of knowledge-based payload technology and enemy advances will be to maintain the current balance of capability.

Another benefit of knowledge-based system technology will be higher force readiness as a result of more advanced training and improved maintenance. The intelligent assistant for UAV system acquisition will also reduce acquisition. Advanced hardware and software technologies could thus be made available sooner. Intelligent assistants for embedded software development will shorten the development cycle, enhance maintenance and modification capabilities, and reduce costs.

The range of applicability of knowledge-based system to future UAV missions and payloads is almost as wide as the range of applicability of computers. Only in areas where specific algorithms are known to give a suitable (i.e., optimum) solution would knowledge-based system technology *not* normally apply. Even then, knowledge-based system technology might be used in some instances to reduce programming cost, execution time, computing costs, or

computer size/weight. The following list presents some major examples of potential future UAV applications grouped according to their relative development risks over the next twenty five years:

Low Risk:

- Knowledge-based systems for UAV maintenance
- Intelligent assistants for UAV block upgrade acquisition/design/fabrication
- More intelligent computer-aided training systems
- Much smarter built-in test.

Medium Risk:

- Tactical or logistics mission planners
- Autonomous target acquisition
- Intelligence data fusion
- Robust self-converting, antijamming sensors and data links
- Realistic future UAV air vehicle - mission simulation.

High Risk:

- Fully autonomous, real-time mission execution including in-flight replanning
- Intelligent assistance for embedded software development and support.

CAPABILITY ENHANCEMENTS EXPECTED THROUGH THE USE OF MICROELECTROMECHANICAL SYSTEMS

Microelectromechanical systems (MEMS) are small devices on the scale of a few millimeters or less. They are often made using variations on techniques used in fabricating electronics such as silicon etching to create high definition, very flat structures. However instead of semiconductor junctions, small motors, gears, and sensors are made. Other techniques such as deep X-ray (synchrotron) lithography, electric discharge machining, and acoustic laser etching are also employed to create three-dimensional structures.

Though a great deal of interest has been shown in MEMS, and strides are being made in basic research leading to laboratory demonstrations, these demonstrations are largely curiosities that have not been incorporated into fielded or even prototype systems. The MEMS field is still in its infancy. Little has been done at the systems level.

Table 3 lists some ongoing MEMS research directed toward six application areas of significance to UAVs.

TABLE 3. MEMS RESEARCH WITH APPLICATION TO UAVs.⁴

Application	Examples	MEMS Approaches
Accelerometers	Piezoresistive accelerometers (aircraft nav.)	Bulk micromachining, silicon mass, photolithography
Speed and position sensors	General Motors magnetoresistive sensors	Molecular beam epitaxy
Pressure transducer	Ford mass air-flow sensor, UM microflow device, gas, temperature, pressure flow sensors	Capacitive diaphragm, micromachining
Displacement and strain transducers	Rotary displacement transducer, uni-axial strain transducer, field-effect transistor detector array	Silicon bonding micropackaging
Electro-optical controls	AT&T fiber optic switching, camera autofocus motor	Metallization, etching, piezoelectric motors, SMA switches
Chemical and biological sensors	Sandia surface acoustic wave sensor (aircraft icing, chemical sensing), gas analyzer chip pump	Piezo quartz plane, capacitive pressure sensor

Miniature actuators are as important as sensors. New techniques and materials such as nitinol wire are being developed in this area also. In a recent Japanese concept, small wires of a shape-memory alloy act as latchable switches for handling power loads now switched by relays. The metal is deposited or drawn in a particular shape, then deformed cold into a another shape. When electrical currents heat the device above a transformation temperature, the metal remembers its original shape. It returns to the

⁴ Brendley, K., Steeb, R., "Military Applications of Microelectromechanical Systems," RAND Study MR-175-OSD/AF/A, Prepared for the Office of the Secretary of Defense, United States Air Force/United States Army, 1993 (from research concluded in December of 1991).

alternate shape when the temperature is lowered below the transformation temperature (for example, by lowering the heating current). Relays can be latched by separate ratchet wires that prevent the main switching wire from returning to its alternate shape. These actuators may be used in other configurations to control fluids (fuels), to lock or unlock mechanical motions (control surfaces), to open or close slits (circulation control airfoils), or to puncture membranes (bladder inflation).

Other MEMS implementations use silicon "flaps" that make surfaces rough on a microscopic level so as to trip boundary flow layers and set up or destroy turbulences upon command. This has application to UAV control when used en mass.

MEMS gyros combine multiple accelerometers to sense angular motion. These tiny gyros and accelerometers could be placed all over a UAV at structural members and within its aerodynamic shell (see "Smart Skins") to predict fatigue-induced failures. A significant problem to be overcome is that when devices grow very small, sensor output is very small, and any electronic noise will mask the output signal.

The Georgia Institute of Technology has produced a self-propelled planar variable reluctance magnetic micromotor with a micro machined nickel-iron rotor and a fully integrated stator, in which a new toroida-meander type integrated inductive component is used as the basis for stator flux generation.⁵ Such micromotors could ultimately be used to channel microwave energy like waveguide switches or sequentially present chemically-active substrates to the environment for air sampling.

Some have even proposed using MEMS devices as UAVs themselves. Tiny sensor chips that float on air currents and can control their decent direction could provide reconnaissance or threat system disruption if sprinkled from the air in large quantities.

The worldwide MEMS market is projected to double annually from a \$1B market in 1996 to about \$16B by the year 2000. Of this growth, seventy five percent will be divided almost equally between pressure sensing, inertial sensors, and optical switching, while the remaining 25% will relate to fluid regulation/control, mass data storage, and other applications.

ENHANCEMENTS EXPECTED BY 2020 DUE TO WAFER-SCALE INTEGRATION OF DISSIMILAR TECHNOLOGIES

Wafer-scale "union" or "integration" refers to an emerging technology that will combine, on a single 3-to-8-in sheet of material, signal generating, signal controlling, information processing, chemical and physical sensing, fluidic and mechanical actuating, radiation generating, and radiation detecting. Components of such combinations are now possible only on separate, isolated, and mutually incompatible optical, magnetic, acoustic, or electronic substrates. Integrating UAV payload subsystems into single monolithic blocks will increase reliability while reducing size and weight, thereby translating into longer time on station at a lower cost.

Current electronic materials and advanced solid-state electron device structures permit limited, but direct processing of radar and communication signals in digital or analog forms at near millimeter wave frequencies (15 to 30 GHz) without having to down-convert to intermediate frequencies. However, some critical high-bandwidth, high-throughput processes, such as phase shifting, time delaying, clocking filtering, signal isolation, and sensing, are more efficiently performed using specialized ferrite-based devices, charge-coupled device circuits, or optical and acoustic wave technologies. Unfortunately, these specialized processing devices involve currently incompatible manufacturing processes, or possess drastically different prime power requirements, thereby making them difficult to combine. Further problems will be caused by the hand-wired interconnects between the separate parts used in the system. A unified technology set incorporating several devices on one chip-to-wafer-sized unit could solve almost all of the problems discussed, simultaneously reducing manufacturing costs and assembly complexity.

Wafer-scale integration would develop techniques to integrate these diverse signal-handling requirements into monolithic structures. Accordingly, a set of compatible electronic materials and specialized fabrication processes would be developed. High-level integration of diverse technologies will provide effective, custom-built, adaptive circuits for new radar and communications payloads at a lower price and higher functional density than has been achieved to date. Compatibility with wideband optical and millimeter wave signal distribution links and flexible optical interconnects will permit effective use of these technologies and components in conformal antenna arrays and signal processing structures.

⁵ Brown, A., "Mems: Macro growth for micro systems," *Aerospace America*, a publication of the American Institute of Aeronautics and Astronautics, October 1994, pp 32 -37

The electron, optical, acoustic, and magnetic technologies currently emerging for use in future UAV payloads are largely isolated from one another. Integration of high-speed optical, magnetic, and electronic devices requires a common substrate (base material system) whose parameters and characteristics are tolerable to all devices. Devices and circuits must be fabricated using processes that do not interfere with one another, nor with the substrate integrity.

Various sensor devices have been fabricated on semiconductor substrates, allowing physical quantities to be detected and measured. Pressure, acceleration, impedance, moisture, strain, temperature, pH, chemical species, and orientation sensors are currently under investigation. The devices are constructed using techniques ranging from chemical micromachining to selective deposition and doping. When combined with microelectronic analog and digital processing and fiber optics signal busing, the detectors and sensors promise to revolutionize the capabilities of miniaturized UAV reconnaissance systems. Examples are temperature-compensated, digitally integrable accelerometers, aneroid barometer chips with pressure accuracy equivalent to less than a meter of altitude, and solid-state "noses" for identifying chemical warfare agents and ship exhaust vapors.

In summary, emerging materials, devices, processing methods, packaging, and cooling technologies support the development of devices that can be compatibly fabricated on a range of substrates without degradation due to the different processing and operating parameters of nearby devices. Such a technology should lead to enormous reductions in size and cost and large improvements in performance for a variety of sensors and controllers. Integrated analog, digital, acoustic, magnetic, electromagnetic, electro-optic, and mechanical circuitry would be beneficial to many future UAV payloads. Primary uses for wafer-scale integration will be in devices that have very high data throughput (analog-to-digital conversion, Fourier transform, and image processing), and where the volume is restricted (such as miniaturized sensors, guidance and control units, or miniature phased-array radar modules). Future material science advances and device structure inventions will continue to provide new opportunities for progress in this area.

CAPABILITY ENHANCEMENTS EXPECTED BY 2020 THROUGH THE USE OF SMART SKINS

Future ship-based UAVs, particularly those small coastal combatants used by many NATO countries, must be small in order to be launched, retrieved, and stored from their floating host. In order to carry out various missions, these same UAVs will have to be able to ferry various payloads aloft and maintain them

there for hours at a time. In the case of current turret-mounted FLIR and LLLTV payloads, the air vehicle attachment seems to be more of an afterthought than an engineered aerodynamic design. Protuberances such as FLIR turrets, antennas, and even control surfaces add to the aerodynamic drag of the air vehicle and tend to make its signature more detectable by threat sensor systems. The result of having a low level of payload-air frame integration is a physically larger air vehicle, less time on station (due to decreased flight efficiency—more drag), and impaired survivability.

In traditional designs, the skin of an air vehicle is a structural fabric to provide aerodynamic shape, strength, and rigidity. When antennas and sensors were added to the air vehicle, they were installed in holes cut in the skin. These installations have attendant structural, aerodynamic, thermal, and cost penalties. The concept of a smart skin is to imbed the antennas, sensors, transmitters, receivers, signal and information processors, RF cables, power cables, electronic control cables, and thermal controls in the skin during the design and construction of the air vehicle. Some structural surfaces should be transparent to various RF bands and/or have controllable properties for transmission and reception. The active and passive sensors would not necessarily be dedicated to any single communications, electronic warfare (EW), radar, identification friend or foe (IFF), or navigation system. A distribution of antennas or sensors might cover 75 percent of the air vehicle surface and provide aperture over a range of frequencies from several MHz to the optical.

Other payoffs provided by the extensive distribution of antennas around the air frame could be sensors that search a sphere around the air vehicle, therefore reducing the need for external pods. A grid of redundant power, signal, and electronic control cables could be embedded into the skin. This might be accomplished with fiber optic cables. The embedded fiber optic cable could offer the added function of measuring the temperature and stress on the skin panels. This information could be used for battle damage and failure assessment, to recognize that the air vehicle is approaching a structural limit, to record the structural history, and for nondestructive testing. The Smart Skin processing and associated logic would allow a control processor to assign resources to the various active and passive radiating systems very rapidly. If battle damage occurs, the processor could reassign the remaining resources on a logical, priority basis.

The Smart Skin concept could be extended to smart control surfaces. If various surfaces are damaged, the control processor could identify the

extent of damage and decide how to control the air vehicle with the remaining control surfaces and vectored engine thrust. Smart materials which can change shape, such as nitinol, can be used to modify the aerodynamics of a wing surface to modify lift, or might be modulated as part of a blown slot to effect circulation control and hence modify the attitude of the air vehicle without large moving "barn door" control surfaces.

Smart Skins technology complements fault-tolerant systems technology and should improve mission reliability and supportability of the systems to which it is applied.

The Smart Skins technology would increase air vehicle availability in two aspects. First, the concept of designing the antennas, sensors, and buses into the air vehicle would reduce the need for returning air vehicle to the modification line to have sensors and antennas installed as each new requirement appeared. Second, the concept of nondedicated antennas and sensors, in which resources are allocated by a central controller, would improve the reliability and sortie generation rate. Redundant sensors, reconfigurable antennas, and buses built into the air vehicle would allow it to continue to operate after failure or battle damage with only a slightly reduce capability.

Smart Skins technology can be applied to all future unmanned aerial vehicles. The application will require designing a complete capability from the start, with sensors, antennas, and buses integrated into the external skin structure. Examples of Smart Skin technology applied to future UAV missions by the year 2020 might include:

- Monolithic electronically agile (frequency, polarization, coding, etc.) radar
- 360° scanning conformal arrays
- Integrated wide band GPS, JTIDS, and IFF antennas
- Fiber optically-powered sensors and data busses integral to the air frame structure/skin
- Electronically variable transmission radome-windows for coboresighted RF/IR sensors
- Actuatorless airfoils that can change shape or lift/drag electronically
- Fault-tolerant control systems

CONCLUSIONS AND RECOMMENDATIONS

This paper has identified the NATO military and commercial requirements for the performance of certain UAV missions in the 2015 - 2020 time frame, and has established which sensor payloads will be required to support the execution of these missions in an effective manner. The present state of the art in sensor performance has been identified and the performance necessary to prosecute these missions in light of the future threat environment and civil markets has been predicted. A detailed discussion of the undergirding technologies which will make the predicted payload performance possible has been presented. The description of these enabling technologies includes discussions concerning the present state of the art, their general applicability to a variety of UAV payloads, and the collateral technologies which will in turn facilitate the development of the chosen primary enabling technologies.

Though a number of enabling technologies have application to various future UAV missions, seven are recommended for near term investment by NATO. These are prioritized (in order of general applicability and return on investment) as follows: 1. *Photonics*, 2. *Acoustic Charge Transport*, 3. *Full Spectrum, Ultra-Resolution Sensors*, 4. *Knowledge-Based Systems*, 5. *Microelectromechanical Systems*, 6. *Wafer-Scale Integration of Dissimilar Technologies*, and 7. *Smart Skins*

In conclusion, it is a recommendation that NATO countries pursue these seven technology areas by investing in their maturation today, in order to have the required future capability (circa 2015) which will allow the defined missions to be performed with a certain effectiveness. These investment recommendations are *not* for payload systems, but is for the *enabling technologies* which will lead to the capabilities necessary for feasible platforms and sensor/avionics payloads. The fallacy of the "non-developmental-item" strategies of the late 80's only guarantees that out-of-date technology will be fielded in the year 2000. Early investment in these seven enabling technologies will provide the incentive for the private sector to advance the areas critical to UAV systems growth so that affordable, capable UAV systems will available when they are needed twenty five years from now.

HIGH PERFORMANCE DATA LINK FOR UNMANNED AIR-VEHICLES

Wolfgang W. Rochus

Daimler-Benz Aerospace AG
Sensorsysteme - VS6V1
Wörthstr. 85
D-89070 Ulm

Dominique Garcia

MATRA CAP Systemes
3, avenue du Centre
B.P. 612
- Les Quadrants -
F-78056 St.Quentin en Yvelines Cédex

INTRODUCTION

As a result of various system studies and work on experimental and operational Data-Links for UAV and missile applications, **MATRA CAP SYSTEMES** of France and **Daimler-Benz Aerospace AG "SENSOR SYSTEMS GROUP"** of Germany are cooperating for the development of a high performance Data-Link for a franco-german UAV system.

The organization formed for the development of this Data-link comprises :

- a joint system engineering team for refinement of the overall data link design, definition of interface and specification of requirement to ground data terminal and air data terminal.
- Separate project teams in the two companies. One company responsible for ground station development, one company for development of airborne station.
Maximum commonality by using identical subcomponents in both stations as far as possible.
- Joint program direction comprising the program managers of both companies.

Based on the system work, which was done in the two companies in order to win that development contract and the knowledge of previous data links which are in development or production for missile systems, the subject of data links for UAV applications is presented here.

Starting from a discussion of general aspects for UAV data links and the trade-offs involved in

getting to an optimized response to the requirement a highly sophisticated data link is described, which facilitates accurate reconnaissance which may be used for target engagement by ground artillery based on data from the UAVs sensor.

1 Mission needs of Data-Links in Unmanned Air vehicles (UAVs) :

Unmanned air vehicles are qualified to perform a wide range of missions, some of which can be performed autonomously while others require a means of communication between the UAV and a ground station.

This communications means, called data-link, can either be a point-to-point line-of-sight data-link, which will facilitate tactical missions up to 100 or 150 km or the data-link between UAV and ground is maintained using relays like satellites or aircraft. In this case the capability to communicate can be over the horizon up to 500 km or more.

If the UAV is equipped with GPS using the (military) P/Y code, UAV position is available with very high accuracy. However, in conflict situations one is dependent on the operating authority of the GPS system, which can principally paralyse such a system by withholding the keys for the military code.

For this presentation only point-to-point data-links without GPS support are considered.

The following missions will either make a data-link highly desirable or even mandatory.

- Missions, where the flight-path of the UAV shall be influenced based on information, which becomes available only after UAV launch.

This requires a link from ground to the UAV to control the UAV, just like a model airplane.

This link requires a low capacity (data rate) only (typically some KB/second).

This link will also allow to control functions of the UAV payload like weapons release, activation of a jammer or activation of a recorder.

We call this type of link TELECOMMAND (TC).

- Missions, in which the behaviour or reaction of the UAV itself or its payload are important to be known in the ground station, require a data-link from the UAV to ground, through which status information from the UAV can be reported.

Also this link requires only a low capacity data-rate (typically some KB/second).

We call this type of link TELEMONITORING (TM).

- In reconnaissance missions, it is often necessary to have the data from sensors onboard the UAV available on the ground without delay. Depending on the type of sensor used (IR camera, IR line-scanner, synthetic aperture radar) the data rate will be between some hundred KB/second up to many tens of MB/second.

We call this type of link TELEVISION (TV).

In such a reconnaissance mission the position of the sensor image can be known with a CEP of some tens to some hundred meters by using civilian GPS or inertial navigation. The north orientation of the sensor image can only be derived from inertial data, however.

- For missions, where the information from the UAV sensor is used for targeting, i.e for the aiming of artillery or rockets, the position and orientation of the sensor image has to be known with higher precision than can be achieved by inertial sensors or GPS using the civilian code. In such cases the data-link may also be required to measure precisely the position of the UAV.

2. Data-Link Requirements for Reconnaissance and Targeting :

As shown above precision target information to be delivered by a UAV sensor for ground artillery or accurate reconnaissance leads to high requirements to the data-link, which can be summarized as follows.

- The on-board sensor of the UAV has to be controlled from a ground control station to optimize position and quality of the sensor image. Additionally mission-control of the UAV may be required. For this purpose a telecommand up link is required.

Through this link the relative bearing from ground-station to UAV may be sent to allow the pointing of directional antennas in the UAV as well as position updates.

- The status of UAV and on-board equipment has to be reported to the ground-station for mission control. UAV north orientation can also be reported to the ground station by this way.

Therefore a tele-monitoring downlink from the UAV to ground is required.

- The image from the UAV on-board sensor has to be transmitted to ground through a high data-rate channel for analysis.
- In order to precisely know the position of a target in the sensor image for engagement, the ground station has to measure the relative position of the UAV with high accuracy in bearing and range. This function should be integrated into the data-link function if possible.
- Due to the fact that a targeting system is used in a battlefield environment the data-link shall have the following additional features.
 - be stealthy i.e interception of the transmissions from airborne and ground station by enemy intelligence shall be very difficult or impossible.
 - be jam resistant, i.e in case of interception the Data-link design shall make it very difficult to be jammed effectively.

- be robust, i.e errors in communication resulting from jamming or other disturbances of the communications channel shall be corrected to the maximum feasible extent.

An example of such a UAV-System is shown in Fig. 1

3 - Trade-offs in Data-Link design

We intend to provide an analysis of the main problems concerning digital communication systems, so called "DATA LINKs" for the particular purpose of UAVs.

Throughout these topics, emphasis is placed on system goals and the need to trade off basic system parameters such as signal to noise ratio, probability of error and bandwidth.

Many complex trade-offs are involved in order to obtain an optimum performance and cost-effective solution. Key factors for data link design are the requirements concerning range, data rate and countermeasure environment, which have to be fulfilled under the constraints dictated by the air-vehicle, which are normally more stringent than the constraints for the Ground Data Terminal.

- Constraints for Air-Vehicle Integration

The air-vehicle imposes limitations to the airborne data link terminal in terms of :

- mass,
- size,
- power supply,
- thermal dissipation,
- antenna.

These limitations influence some key design features of the data link like :

- **Transmitter power** is limited by power-supply of the A/V, allowable thermal dissipation, mass and size.
- **Antenna type and gain** are limited by the antenna mass, size and position, which is allowed by the A/V under aerodynamic considerations.
- **Frequency band** has to be chosen based on the antenna size and transmitter-power, which allows to satisfy the link budget.

- Link Budget

The link budget is the output of the link analysis. It consists of the calculations and tabulation of the useful signal power and the interfering noise power available at the receiver. The link budget is a balance of gains and losses :

- **Gains :**

- * transmitter power (on board power is limited)
- * antenna gain (size is limited by UAV shape and aerodynamics)

- **Losses :**

- * propagation losses due to atmosphere attenuation and earth surface effects dependent with frequency band (UAV mission area)
- * engineering (implementation inside UAV).

⇒ The result of the link budget is the first step of the data link design.

It gives a fair estimation of the equipment that will be design to achieve the requirement, a good assessment of the margin of the system and confidence on the performance to be achieved.

- Link Design for Specified Quality (Modulation and coding)

Based on the link budget on one hand and on the quality of communication which is required, some trade-offs have to be done on the processing gain between base band modulation and coding.

⇒ The result of this analysis is to dimension the processing inside the equipment.

This drives particularly the computational load and the complexity of the processors in base band technology.

- Threats and Countermeasures

For the case of military applications, one of the specific constraint is to provide the quality required for the communication under threat, generally in the presence of hostile jammers, which represents also additional sources of noise in the link.

Electronic counter-counter measures are based on the characteristics of the jammers (power, bandwidth, time behaviour) and eliminate as much jammer power as possible by techniques on board the UAV and in the ground data terminal.

A number of counter-counter measures can be implemented in all the devices of the data-link in order to decrease the probability of interferences and, in case of interferences, to eliminate the effects on the quality of the link. Possibilities are :

- directional antennas,
- robustness of the modulation
- spread spectrum or frequency hopping
- forward error coding using convolutional codes.

4 - The Daimler-Benz Aerospace / MATRA CAP SYSTEMES solution :

4.1 General

Daimler-Benz Aerospace and MATRA CAP SYSTEMES are developing a flexible solution taking special concern of following severe requirements :

- high level of jamming protection associated to a very low level of detectability
- high accuracy of UAV localization in severe jamming conditions
- very severe environmental conditions of the battefield including NEMP (Nuclear Electromagnetic Pulse)
- large number of various operating modes and growth potential including jamming evaluation, highly safe peace time mode, possible guidance of two UAVs by a same ground station and a handover mode in addition to the basic modes.
- data transmission to the ground control station by means of optical links.

The very high degree of performance of our solution is achieved by means of specific techniques :

- combined Frequency Hopping (FHSS) and Direct Sequence Spread Spectrum (DSSS) modulation working above 10 GHz for three signals : Telecommand, Telemetry and Television.

- non coherent detection providing higher reliability, efficiency and robustness against spurious signals compared to straight forward designs based on carrier phase recovery.
- detecting and correcting codes (FEC) optimized on both random errors and message reconstruction.
- high speed synchronization process for shorter acquisition and reacquisition time due to specific Surface Acoustic Wave (SAW) matched filter.
- possibility of self adaptive level of transmitted power to minimize detectability and to take the most advantage of the transmitter power available on board.
- highly directional antennas with high gain, low side lobes and accurate motorization.
- design of the most complex functions at base-band level providing maximum flexibility for possible adjustments and future growth extension.
- calibration free ranging technique
- high ranging accuracy thanks to short time DSSS chip.
- unbiased monopulse processing for high azimuth localization accuracy under jamming conditions
- high dynamic range of the receiver associated with intelligent automatic gain control (AGC) strategy to cope with the high level of jamming signals.
- sophisticated and very accurate built in test (BIT) design to diagnose Line Replaceable Units (LRU) without any specific operational maintenance bench.
- high scale integration for devices (ASICs) offering the best compromise between :
 - volume/weight
 - power consumption/temperature
 - processing power/complexity
 - availability/reliability

The Ground Data Terminal (GDT) and Air Data Terminal (ADT) of the **Daimler-Benz Aerospace / MATRA CAP SYSTEMES** solution have been deeply analysed and implemented to take into account the following features:

- high modularity to satisfy the maintainability and also to facilitate the integration between antenna, microwave and base band technology.
- identical technology in the two equipments to harmonize the dual functions and also to simplify the spare parts.
- use of identical subunits in ADT and GDT wherever possible.
- use of solid state microwave power amplifiers
- NEMP hardening by means of a specially designed mechanical structure, state of the art electronic design, including suppression circuits and fibre-optic link to Ground Control Station.
- highly compact synthesizers.
- use of modular microchip thin films microwave circuits.
- use of chip carriers components on collaminated Printed Circuit Boards for signal processing circuit.
- Status monitoring

Sketches of ADT and GDT are provided in Figures 2 and 3.

4.2 AIR DATA TERMINAL

The Air Data Terminal (ADT) of the **Daimler-Benz Aerospace / MATRA CAP SYSTEMES** Data Link has been specifically designed taking into account the UAV constraints :

- **Aerodynamic** : the board antenna is installed in the tail fin of the UAV with minimum impact on the flight possibility of the UAV.
- **Weight** : the Air Data Terminal has a low weight impact from all the electronic devices embedded in the UAV.
- **Thermal** : the electronics are divided in two units :

- the Electronic Unit installed in the electronic room of the UAV.

- the Front-End (including power amplifier) installed between electronic room and board antenna inside the UAV.

This permits to split the thermal dissipation and to dispatch it in the UAV and also to offer possibility of growth potential. The Front-End and the antenna are the only frequency and transmitted-power sensitive components, and can be redesigned to suit the required transmitted power and/or frequency.

- **Accessibility :**

- Antenna mounting occurs from the tail-fin side

- Electronic Unit is installed on a trail in the electronic room

- Front-End has a small size and is easily accessible in the fuselage.

4.3 GROUND DATA TERMINAL

The Ground Data Terminal (GDT) of the **Daimler-Benz Aerospace / MATRA CAP SYSTEMES** Data Link has been specifically designed taking into account the ground constraints :

- The GDT combines features of a precision tracking radar (without the radar transmitter) with the primary Data-Link function. This way precise localization of the UAV is achieved.
- **Stabilization of the GDT** : due to high level of accuracy for localization of UAV position through the Data-Link, a very performant stabilization of the ground antenna is achieved.
- **Protection** : the GDT is designed to confirm with environmental constraints : NEMP, lightning, contamination without any damage.
- **Mechanical performances** : A sophisticated mechanical design has been chosen in order to handle the high performance antenna.
- Communication with a remote control center through a fibre-optic link.

5 - Potential for Evolution

Due to its modular design the **Daimler-Benz Aerospace / MATRA CAP SYSTEMES** data link described above allows to adapt one or a few subunits to changing requirements without affecting the remaining part of the design. For example the following modifications could be envisaged.

- Antenna (different beamwidth, frequency range)
- Antenna stabilization (different accuracy)
- Front End (different transmitter-power, frequency band)
- Electronic Unit (different interface to A/V or ground station).

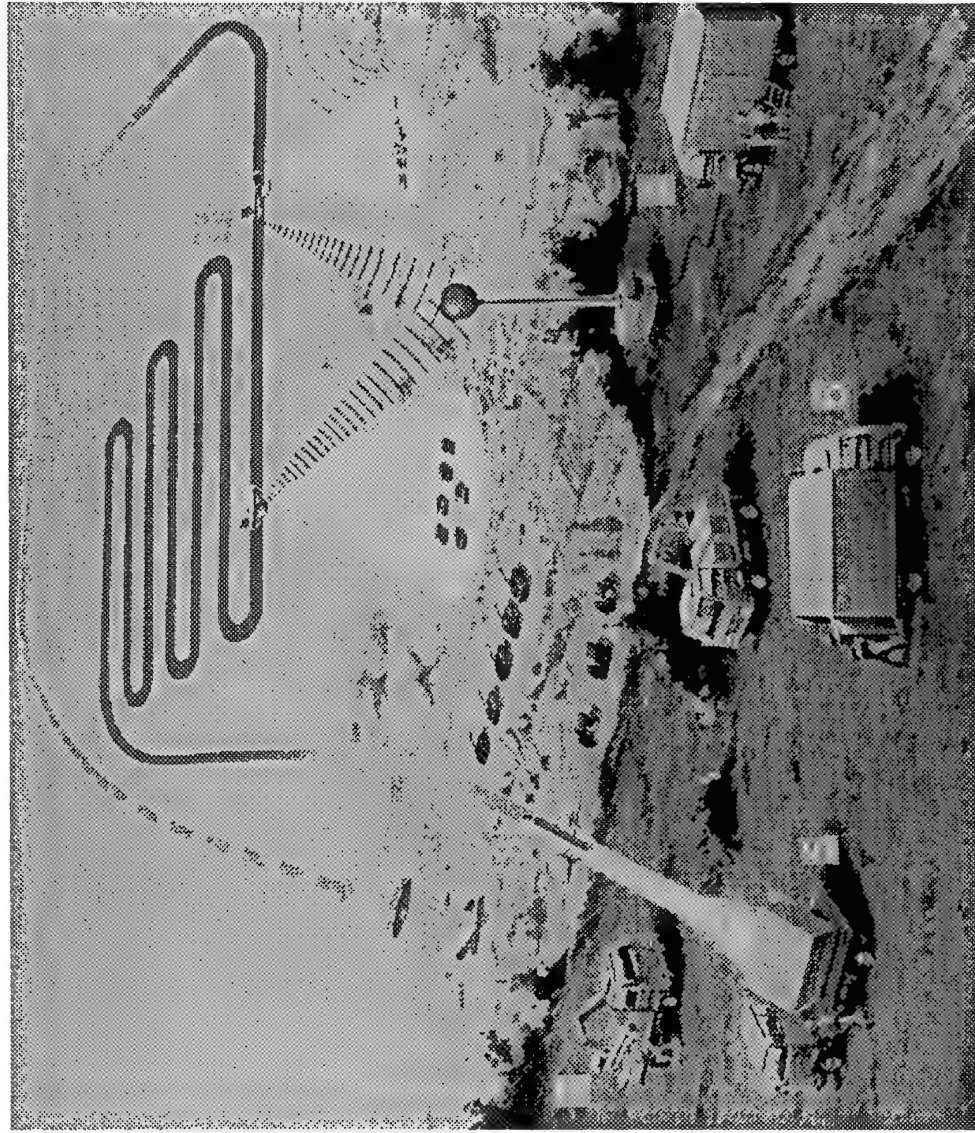
Also functions may be added (e.g. data compression) or deleted/simplified (e.g. A/V localization precision).

Such changes can be made without significant impact on the architecture of the design and with limited changes in software.

To summarize the design of the data link allows adaptation to a spectrum of requirements and has the potential to tailor its complexity to provide cost-effective solutions for requirements of extremely-high to medium sophistication.

- 1 Air Data Terminal**
- 2 Ground Data Terminal**
- 3 Unmanned Air-Vehicle**
- 4 Control Station**
- 5 Launching Vehicle**
- 6 Maintenance Vehicle**
- 7 Recovery Vehicle**

**Fig.1
RECONNAISSANCE
UAV SYSTEM**



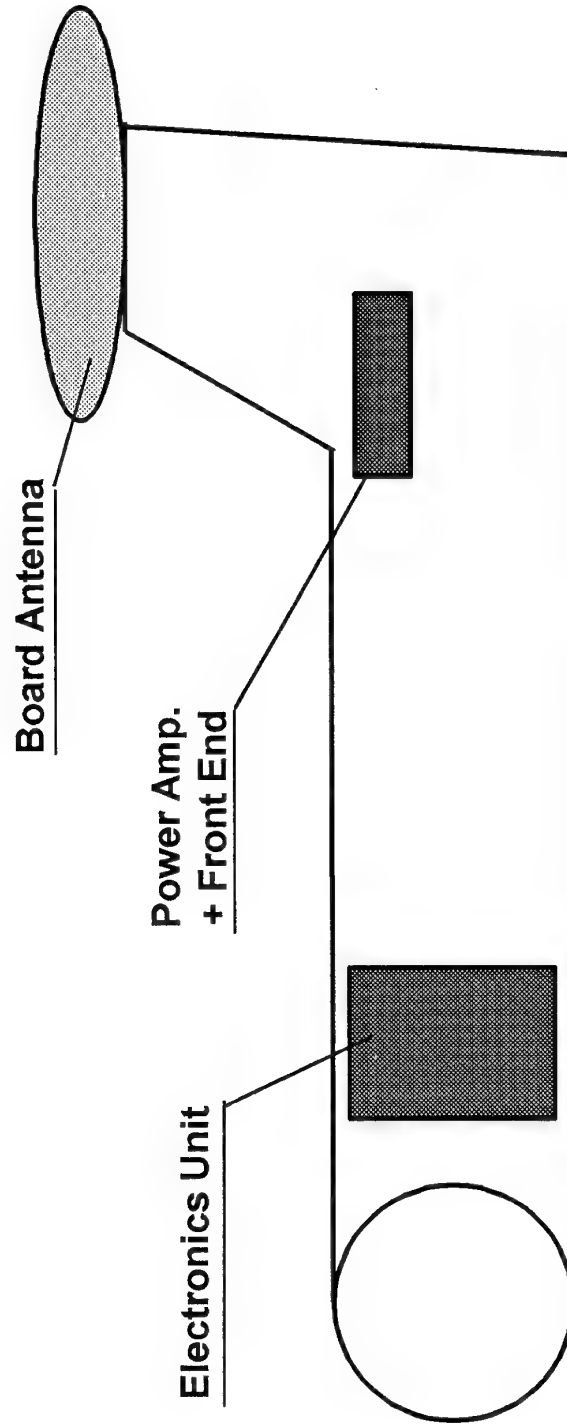


Fig. 2
AIR DATA TERMINAL

Modular Construction

allows adaption to

- Thermal and Space Constraints
 - Future Changes in Power/ Frequency
- gives optimum maintainability

Fig. 3
GROUND
DATA TERMINAL

combines

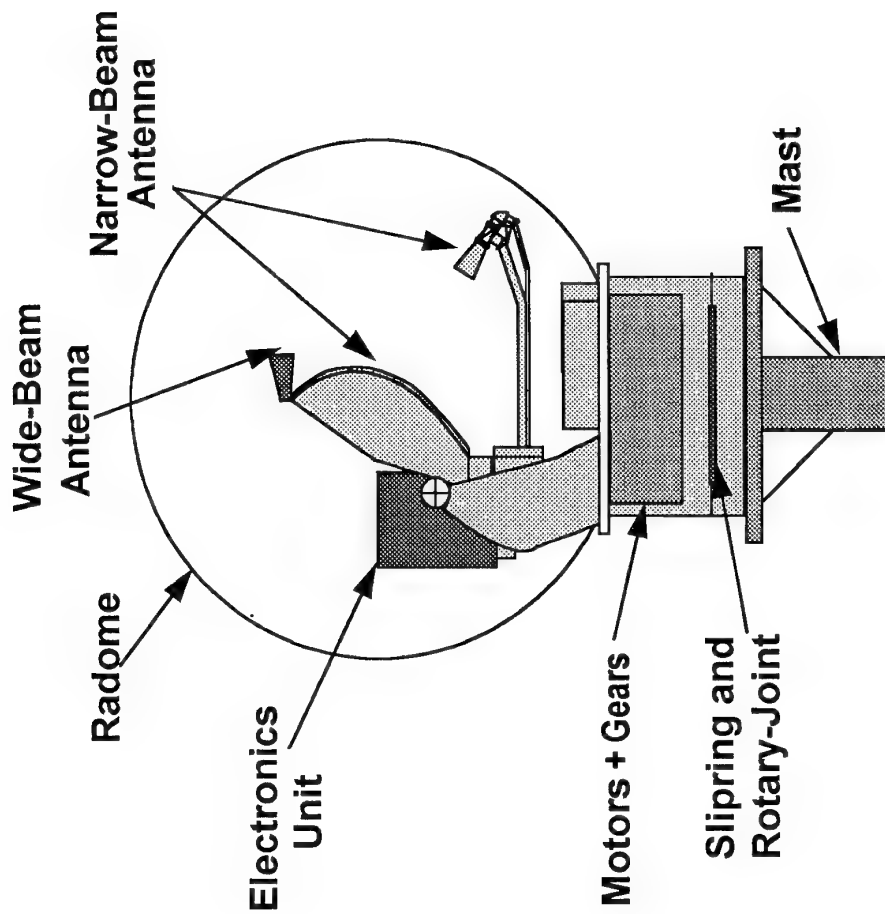
RADAR TECHNOLOGIES
for precision tracking
of air-vehicle

and

SIGNAL PROCESSING
TECHNOLOGIES
for error-free jam-resistant
communication

with

FIBER-OPTIC LINK TO
CONTROL STATION
for EMC and NEMP Protection



**UNMANNED TACTICAL AIRCRAFT
A LOCKHEED MARTIN PERSPECTIVE**

by

Armand J. Chaput, Timothy S. Albin, Douglas M. Hosmer, Stephen R. Weigel
Lockheed Martin Fort Worth
P.O. Box 748, Mail Zone 2646
Fort Worth, Texas 76101, USA

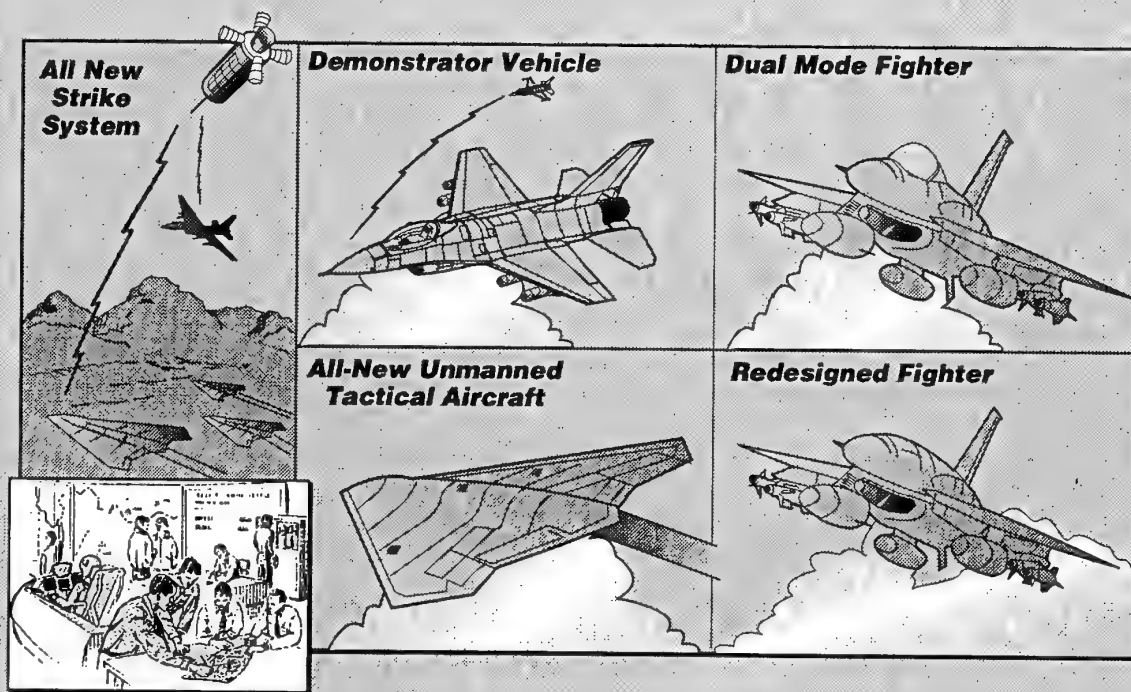
UNMANNED TACTICAL AIRCRAFT A Range of Concepts

V.G. #1

The Unmanned Tactical Aircraft Team at Lockheed Martin is pleased to present our views on the revolutionary potential of Unmanned Tactical Aircraft (UTA).

- A UTA, however, is more than an aircraft. It is a system. There is a broad range of potential UTA concepts ranging from straight-forward adaptations of existing platforms through all-new vehicles and systems of vehicles.
- In its simplest form, a UTA can be a "drone-like" demonstrator vehicle used to evaluate and flight demonstrate enabling technologies and/or concepts of operation.
- UTA can also be a modified version of an existing fighter that can operate in either manned or unmanned modes.
- A more capable UTA could be redesigned specifically for unmanned operations, allowing it to perform maneuvers that exceed manned fighter limits and factors of safety.
- In their most advanced form, UTAs will be initially designed for unmanned operation and will operate as an element of the future system of systems and be inherently compatible with the concept of Integrated Battlefield Management.
- UTAs have inherent cost advantages that can revolutionize current concepts of theater air combat and enable a new concept of a Mixed Force of manned and unmanned systems.
- While an early UTA operational capability can be adapted from existing manned assets, development of new UTA-specific technologies will be required to reap their full operational and cost potential.

Unmanned Tactical Aircraft – A Range of Concepts



UNMANNED TACTICAL AIRCRAFT Our Definition

V.G. #2.

Our definition of an Unmanned Tactical Aircraft platform is very similar to that of a manned fighter in that it has inherent multi-mission flexibility.

Unlike a manned fighter, however, it is not constrained by human physiological limits.

It can stay aloft for periods of time that exceed human endurance limits, will be able to maneuver beyond the limits of human consciousness, or it can be designed to have non-traditional front end shapes normally associated with manned fighters.

Overall, however, it will function as a part of the overall force structure and complement, not compete with, existing manned and unmanned systems.

Unmanned Tactical Aircraft – Our Definition

- **Unconstrained by Human Physiological Limitations**
- **Has TBD Levels of Manned Interaction at TBD Locations**
- **Has Primary Air-to-Ground Weapons Delivery Mission**
- **Has Flexibility to Perform Multiple Missions**
 - Strike
 - SEAD
 - BDA
 - Interdiction
 - TBM and Cruise Missile Defense
- **Is Responsive to Wide Range of Other Military Needs**
 - Instrument of National Policy
 - Deal with Political Irritants
- **Can Function as Autonomous or Fully Integrated Force Multiplier**
- **Complements Existing and Future Systems (Manned & Unmanned)**

Current

- Fills Force Structure “Void”
- Enhances (Vice Replaces) Fighters

Future

- Helps Optimize Manned/Unmanned Force Mix

UNMANNED TACTICAL AIRCRAFT Benefits

V.G. #3

In addition to the obvious operational benefits of a UTA in comparison to existing manned and unmanned systems as listed here, there are also significant potential cost savings that we will discuss in more detail later. These savings can be in the form of both reduced development and procurement as well as reduced operations & support costs.

UTA Benefits

- **Policy Level**
 - No Risk of Pilot Loss / Capture
- **Operational**
 - Reusable / Recallable / Retargetable Unmanned Strike
 - Not Limited by Physiological / Constraints
 - Enhances Existing Concepts of Manned & Unmanned Operations
 - Potential to Exploit New Tactical Operating Envelopes
 - Very High Altitude
 - Very Aggressive Maneuvers
- **Cost**
 - Significant Reduction in Development / Acquisition Cost
 - Initial Capability
 - End-of-Life Fighters
 - Off-Shelf Equipment
 - Later Capability (All-New)
 - Design for Combat Life Only
 - Significant Reduction in Operations and Support (O&S Cost)
 - Initial Capability
 - Reduced Requirement or Training / Proficiency Flying
 - Minimal Operations to Maintain Flyable Storage
 - Later Capability
 - Minimal Requirement for Training / Proficiency Flying
 - No Operations to Maintain Flyable Storage
 - Designed for Minimal Combat Maintenance

UNMANNED TACTICAL AIRCRAFT Phased Program Approach

V.G. #4

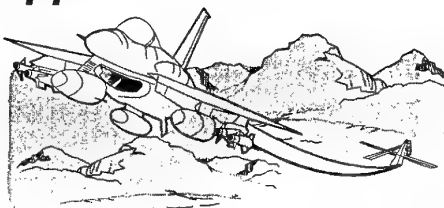
Our vision of a future UTA Program includes both technology and system (including non-technology) elements. We see a program that from the beginning has a low-cost demonstration platform capable of supporting both technology and operational concept objectives. This demonstration can be based on a contemporary manned fighter and retain manned pilot provisions to facilitate test and demonstration objectives at the lowest possible cost, risk and complexity. Based on an existing fighter with no new technology required, the cost of conversion to unmanned operation using existing drone or unmanned aerial vehicle (UAV) command and control systems should be minimal. This vehicle could also be the basis for an early operational capability that we believe could satisfy a number of currently identified Mission Area Plan (MAP) deficiencies.

A UTA demonstrator platform, and its early operational capability follow-on, will be an invaluable asset for development and demonstration of technologies and concepts of operation. The first missions we would expect assigned to UTAs are those that do not fall high on the manned mission desirability list (e.g., missions involving very long endurance or very high threat environments). Later we expect to see requirements for enhanced operational capabilities that go beyond the initial systems but may still be satisfied by modifications (albeit extensive) of existing airframe platforms. These enhanced capability UTA systems will meet a growing list of new operator requirements until all-new UTAs enter the force. Unlike their manned fighter-based predecessors, all new UTAs will have been designed from the start for their unique missions and will be the first of their type to take full advantage of the cost breaking new concepts of training and support that will enable them to meet combat demands with minimum strain on peacetime O&S budgets.

UTA – Phased Program Approach

Early Operational Capability

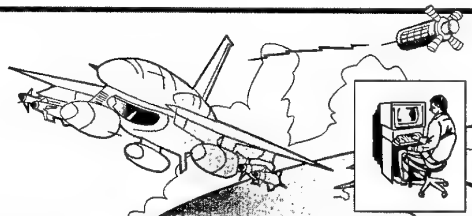
- Design Features**
- Minimum Modification of Existing Vehicle
- Capabilities**
- Autonomous Pre-Planned Mission
 - Reroutable/Retargetable/Recallable
 - Limited Auto Self Defense
 - Ops Concept & Technology Development



Technology Availability Date – Today

Interim Operational Capability

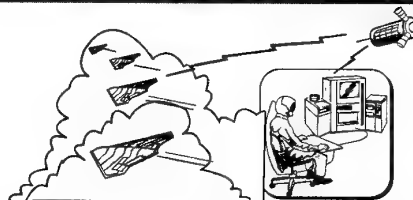
- Design Features**
- Redesign of Existing Vehicle
 - More Robust Communication Links
- Capabilities**
- On-Board "Intelligence" (PA Based)
 - Enhanced Situation Awareness
 - Expanded Man-In-Loop Involvement



Technology Availability Date – 1996

All New Platform Capability

- Design Features**
- All New Platform
 - All New Systems
- Capabilities**
- High Degree of Platform "Intelligence"
 - Full Up/Down Link SA Data
 - Virtual Pilot Operational Capability



Technology Availability Date – 1998

All New System Capability

- Features/Capabilities**
- Application Platform Capabilities/Technologies to Aid Ground Based Commander/Warfighters

Technology Availability Date – 2000 ?



LOCKHEED MARTIN PERSPECTIVE "Reuseables" vs "Expendables"

V.G. #5

Although Lockheed Martin's involvement in unmanned systems goes back many years, a 1993 internal study to reassess theater air combat needs and opportunities in the new defense environment established one of the compelling needs for UTA. Our study of recent conflicts clearly showed that National policy concerns had placed increasing demands on unmanned systems to achieve military objectives at minimal risk of pilot loss or capture. Despite their advantages, however, the cost of these systems relative to their effectiveness left much to be desired. Some of this is the result of conversion from nuclear to conventional warheads (e.g., Tomahawk) but fundamentally it is a characteristic of expendable systems.

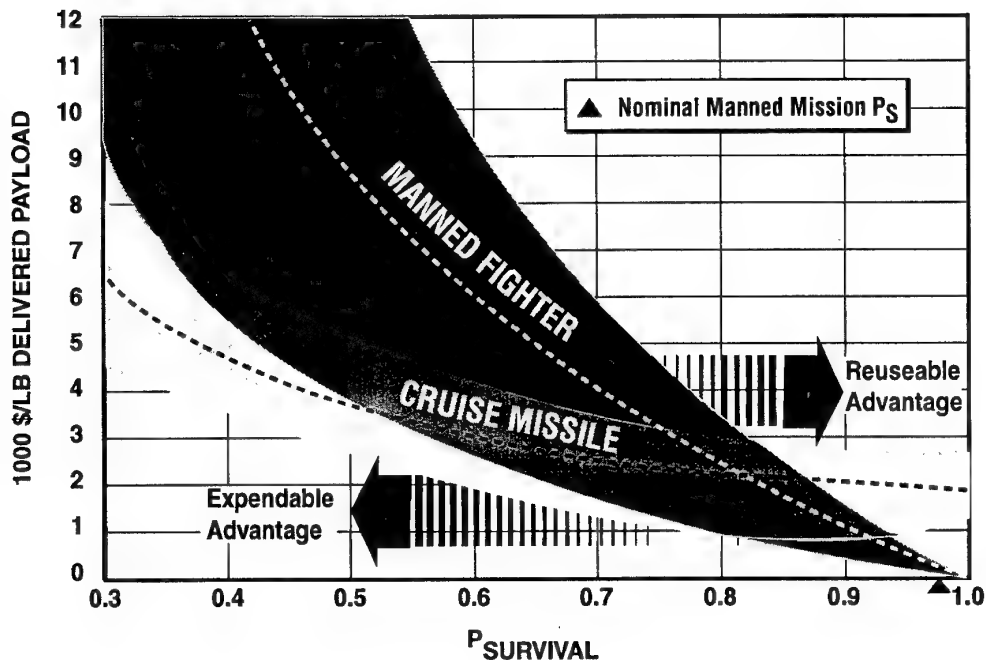
Using a typical cruise missile as an example, a \$1.4 million airframe and associated systems is thrown away every time it flies. When characterized in terms of cost per pound of payload, a cruise missile with a 1000 pound warhead performs its strike mission at a fly-away cost of \$1400 per pound of delivered payload (when operations and support costs are included the figure is higher). In comparison, a reusable manned fighter can deliver payloads at a cost per pound of payload an order of magnitude lower (even on a life cycle cost basis that includes pilot and training costs). However, a fighter's reusability advantage accrues only when its survivability is high enough that it can return to fight again another day.

For example, if a current production F-16C flew a one-way cruise missile type profile, its cost per pound of payload delivered would be very high. With a typical combat load (two 2000 lb MK-84s) at about 10 years into its 20-year lifetime, if it flew only one combat mission (one-way), it would be delivering payload at about \$8700 per pound. If it flew two missions (back-to-back), the average cost would drop by half. By the fifth mission its cost per pound of payload would be less than a cruise missile. By the 25th mission, the average cost per pound would be an order of magnitude lower. The data shown in the figure is based on this concept of amortized cost except it is expressed in terms of probability of loss instead of numbers of combat missions. The spread in the data reflects a life cycle range.

In comparison a cruise missile flies once and its cost does not amortize. However, when expressed in terms of probability of survival, a cost multiplier develops and generates a slope of the type shown.

One interesting characteristic of the data shown is the cost-effectiveness cross over point between reusable and non-reusable systems. Whether it is exactly 0.75 as shown, or simply in that range, it is significantly below the survivability levels where manned fighters operate. In today's battlefield environment, if projected survivability isn't on the order of 0.98 or better, manned assets don't fly. The targets are either assigned to unmanned assets or they don't get attacked until the survivability situation improves. A force of F-16C-like UTAs, however, could fly those missions and either significantly reduce the cost of the war or shorten its duration. Therefore, UTAs have a cost effectiveness "niche" that falls between cruise missiles and manned fighters.

Lockheed Martin Perspective – "Reuseables" vs "Expendables"



UNMANNED REUSABLE PLATFORM

Missile or Fighter?


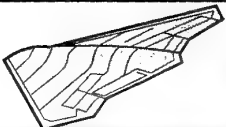

V.G. #6

The assessment of the need for a significant increase in unmanned strike system capability lead to the inevitable question about whether these new platforms should be considered missiles or airplanes. This chart shows why we concluded that they were more fighter-like (based on most of their system characteristics) except that, like missiles, UTAs can extend into combat arenas where man is the limiting factor. UTAs also have missile-like storage (wooden round) and training requirements which are key to their cost effectiveness during peacetime operations.

Our assessment of UTA employment during combat operations addressed the following questions:

- How might the UTA be used in today's Air Force?
- How does the UTA fit in the Air Force's Mission Area Plans?
- How might the UTA be used in today's combat scenarios?
- How might the UTA be used in future combat scenarios?

Unmanned Reusable Platform – Missile or Fighter?

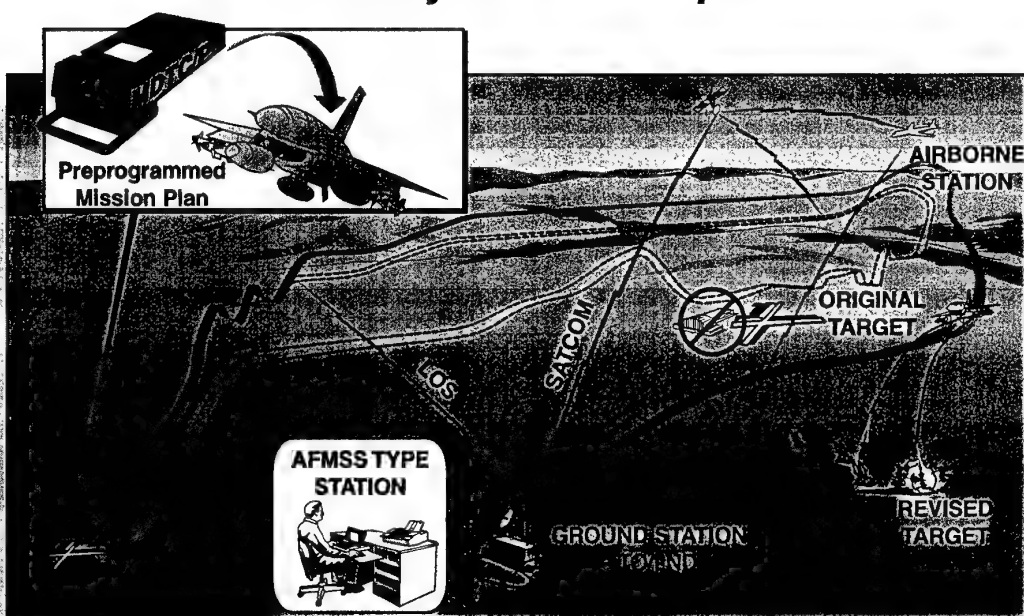
		
MISSILE	UNMANNED REUSABLE	FIGHTER
<ul style="list-style-type: none"> • Launch Only • One Way • Autonomous/Self-Contained • Not Reusable • "Wooden Round" Storage • Simulator for Proficiency • Limited Post-Launch Adaptability • Safe Passage Concept <ul style="list-style-type: none"> – Time Deconflicted • Position Reporting Not Required • Limited BDA • Range Limited to Fuel on Board, No Physiological Limits • No Mission Debrief • Limited Warhead Selection • Limited Fault Tolerance • Platform Consumed • Preplanned Fixed Targets • Limited Self Defense • Single Role 	<ul style="list-style-type: none"> • Launch and Recover • Two Way • Autonomous/Off Board Control • Reusable • "Wooden Round" Storage • Simulator for Proficiency • Adaptable to Post-Launch Tactical Changes • Safe Passage Concept <ul style="list-style-type: none"> – IFF – Position • Position Reporting Required • BDA Capability • Range Not Limited to Fuel on Board, No Physiological Limits • Mission Debrief • Unlimited Warhead Selection • Fault Tolerant to One or Two Levels • Weapons Consumed • Retargetable/Recallable/Retaskable • Countermeasures, A/A Missiles • Multi-Role 	<ul style="list-style-type: none"> • Launch and Recover • Two Way • On Board Control With Off Board Aids • Reusable • Not Stored • Proficiency Flying • Highly Adaptable to Tactical Situation Change • Safe Passage Concept <ul style="list-style-type: none"> – IFF – Position • Position Reporting Required • BDA Capability (Mission Not Popular) • Range Not Limited to Fuel on Board, Physiological Limits • Mission Debrief • Unlimited Warhead Selection • Very Fault Tolerant to Multiple Failures • Weapons Consumed • Retargetable/Recallable/Retaskable • Countermeasures, A/A Missiles • Multi-Role

UNMANNED TACTICAL AIRCRAFT System Concept

V.G. #7

UTA Operating Concepts. Different levels of UTA capability involve different levels of human interaction. At its simplest level, as shown here, UTA requires a human operator to plan the mission using an Air Force Mission Support System (AFMSS) system and to load the Data Transfer Cartridge (DTC). During mission execution new steerpoints or target coordinates can be datalinked over the Improved Data Modem (IDM) as required. More capable, advanced UTAs would employ the human operator as a strike coordinator. We envision a human sitting in front of a master control station into which correlated and filtered off-board intelligence as well as data from the strike package is integrated. The strike coordinator can then make decisions about mission routing and targeting as required, inputting to the flight through keyboard, touchpad, or light pen instructions. Operation of even more advanced UTAs would step into the virtual world and controllers/pilots would interact in the virtual world much as flight leads do today, except that one human could fly an entire strike package at once.

UTA System Concept



MINIMUM CAPABILITY SYSTEM

- | | |
|---|---|
| <ul style="list-style-type: none"> • QF Type TO/LND • Preprogrammed Mission <ul style="list-style-type: none"> - Route to TGT - Weapon Release Profile - Weapon Release - Target Area Exit Profile | <ul style="list-style-type: none"> <ul style="list-style-type: none"> - TGT Location - Steering to Release - BDA - RTB Profile • Ability to Upload New Coordinates <ul style="list-style-type: none"> - Steerpoints - Target - Landing Zone • Preprogrammed Maneuvers <ul style="list-style-type: none"> - Bingo/RTB - Etc. |
|---|---|

ADVANCED UTA SYSTEM CONCEPT

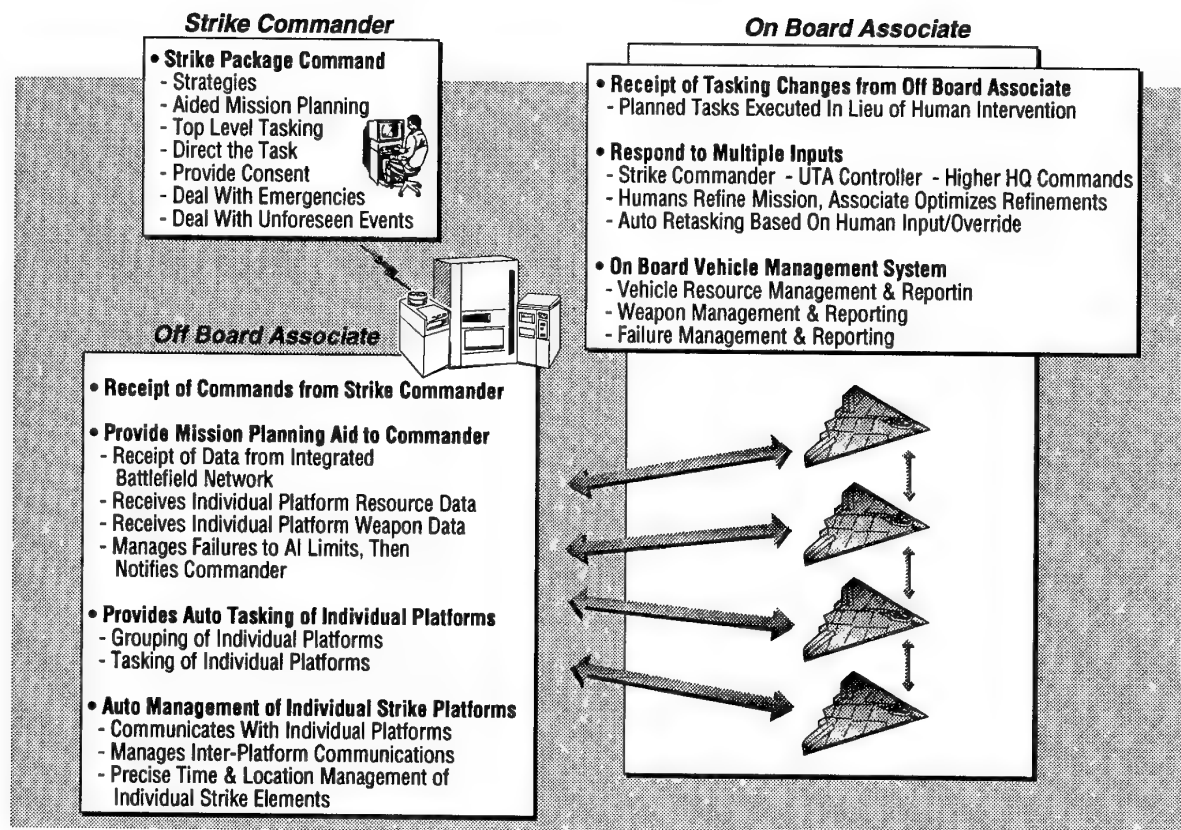
V.G. #8

As shown in the previous chart, in its most basic form, a UTA is controlled through a pre-defined mission plan and datalinked updates to that plan.

In a more advanced form, as shown in this chart, both the UTA operator and the UTA platform will be supported by off-board and on-board "associates." These "associates" are artificial intelligence systems that can interpret or predict events and/or function at a high level command mode. The technology to do both functions was developed in a previous ARPA program called Pilots Associate. When applied to UTA, these associate systems will provide the platform with intelligent options to deal with changes to the pre-planned tactical situation. The options can be presented to the ground operation for consent or invoked automatically as desired. The same technology will also reduce the workload for the operator as he or she manages multiple UTA assets.

Associate technologies that will be developed and integrated are categorized into situation assessment, integrated planning, and system status functions.

Advanced UTA System Concept

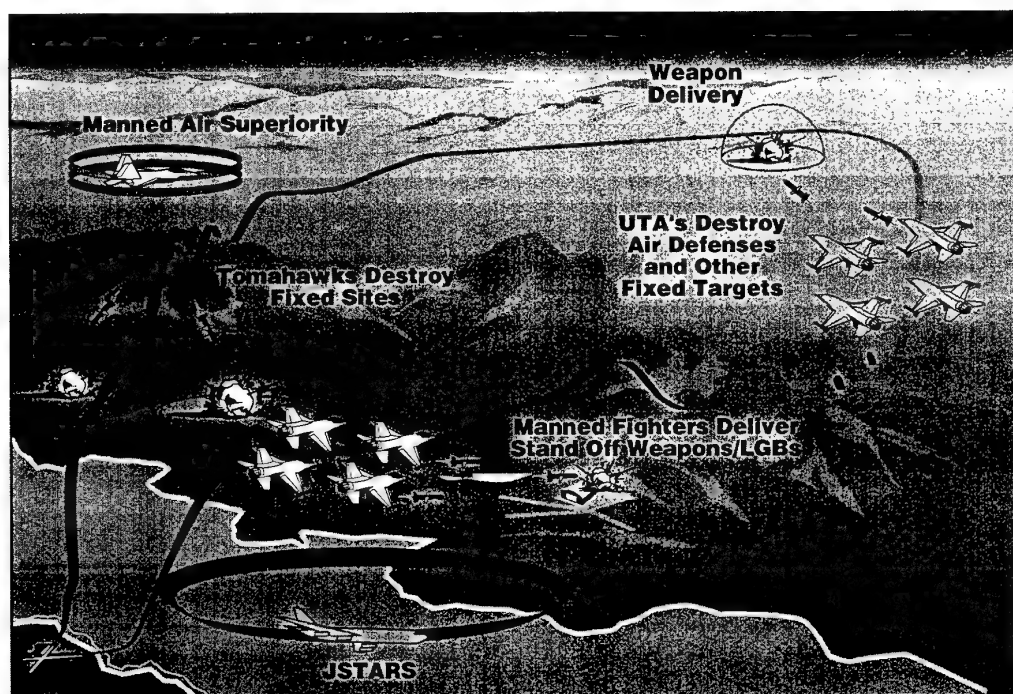


MANNED AND UNMANNED STRIKE PACKAGES One Example

V.G. #9

UTA Missions. Using a hypothetical example of a UTA in the U.S. Air Force, we believe a primary mission for the UTA would be to employ precision-guided weapons in integrated attacks against high and medium threat fixed targets. These missions would be performed in daylight hours and could be integrated with other unmanned vehicles such as the Tomahawk and TSSAM follow-on systems. Manned vehicles, such as F-16s and F-117s flying at night, could provide around the clock pressure on these highly defended targets. Manned air superiority fighters such as F-15s and F-22s would ensure air superiority for both manned and unmanned strike packages.

Manned and Unmanned Strike Packages – One Example



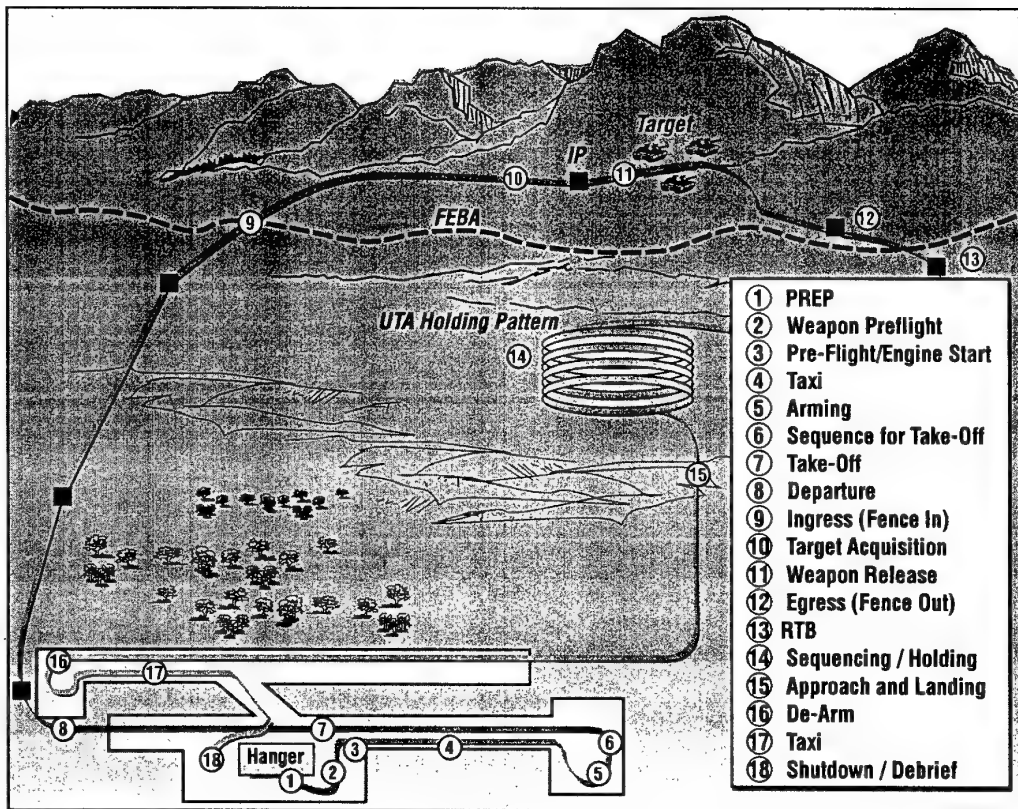
Force Mix Capitalizes on the Strengths of Each Vehicle Type

UNMANNED TACTICAL AIRCRAFT Reporting Requirements

Y.G. #10

Our assessment shows that one major difference between current unmanned vehicles such as cruise missiles and a UTA concept is reporting requirements. The UTA must report its position both inbound to the target and outbound from the target to established controlling agencies. These reports and unique flight paths dictated in the Air Tasking Order (ATO) are required to manager and monitor its mission and to confirm the UTA's friendly identity to our air defense network.

UTA Reporting Requirements



THE UTA AND TACTICAL AIRCRAFT MISSIONS

Y.G. #11

We examined Air Combat Command's Mission Area Plans to determine which missions could benefit most from tactical application of the UTA. Our assessment was designed to determine which high priority missions the UTA could effectively fulfill.

One of the most difficult missions for manned fighters is to attack high threat, high value targets on Suppression of Enemy Air Defenses (SEAD) missions. These, therefore, would be logical UTA missions.

Following the early SEAD missions, UTAs could then begin airfield attacks in earnest. Operating in daylight, with today's level of survivability, UTAs can attack and kill tactical threats around the airbase. Later waves of UTAs could attack the runways, fixed aircraft shelters, and airbase infrastructure.

We also see UTA performing a mission of great importance to the Army commander – interdiction of second echelon forces to the front. In effect, it provides the Army commander the equivalent of highly maneuverable long range artillery and firepower to slow and stop invading forces.

Theater missile defense missions could also use UTAs that endure for long periods, well beyond human limitations. When a missile launch is detected, national assets process launch warnings and pass location to controller aircraft or direct to the UTA. The UTA then picks up the missile early in the boost phase and destroys it with a high speed missile on on-board high-power laser. Similar approaches could be used for cruise missile defense.

Finally, the UTA can support the commander's requirement for Bomb Damage Assessment (BDA). Either as part of the last attack wave or as a dedicated mission, a UTA can come into the target area several minutes after the last bombs have fallen and collect BDA imagery of the designated targets. Radar or EO sensors can be used to collect views from several angles to provide sufficient detail for the commander to make decisions about retargeting these and other targets.

We do not, however, see UTAs being assigned the types of missions shown at the bottom of the chart. These are missions that we believe are best left to our manned fighter force to handle.

The UTA and Tactical Aircraft Missions

• Mission Tasking Probability for a UTA Squadron:

1. Electronic Combat/Lethal SEAD (Preemptive Destruction)

- Fixed Sites (EW/GCI)
- Strategic SAMs

2. Strategic Attack/Air Interdiction

- High Value Targets (Production Facilities, POL, etc)
- Airfield Attack

3. CAS/Interdiction

- 2nd Echelon Attack
- Under Control of JSTARS

4. Theatre Missile Defense

- Ballistic Missiles
- Cruise Missiles

5. Surveillance and Reconnaissance

- BDA

6. Counter Air – Air Superiority

7. Strategic Defense – Air Base Defense

8. Rescue

9. Traditional CAS – Troops in Contact

Highest
Probability of
ATO Tasking

Lowest
Probability

POTENTIAL NEW OPERATIONS CONCEPTS

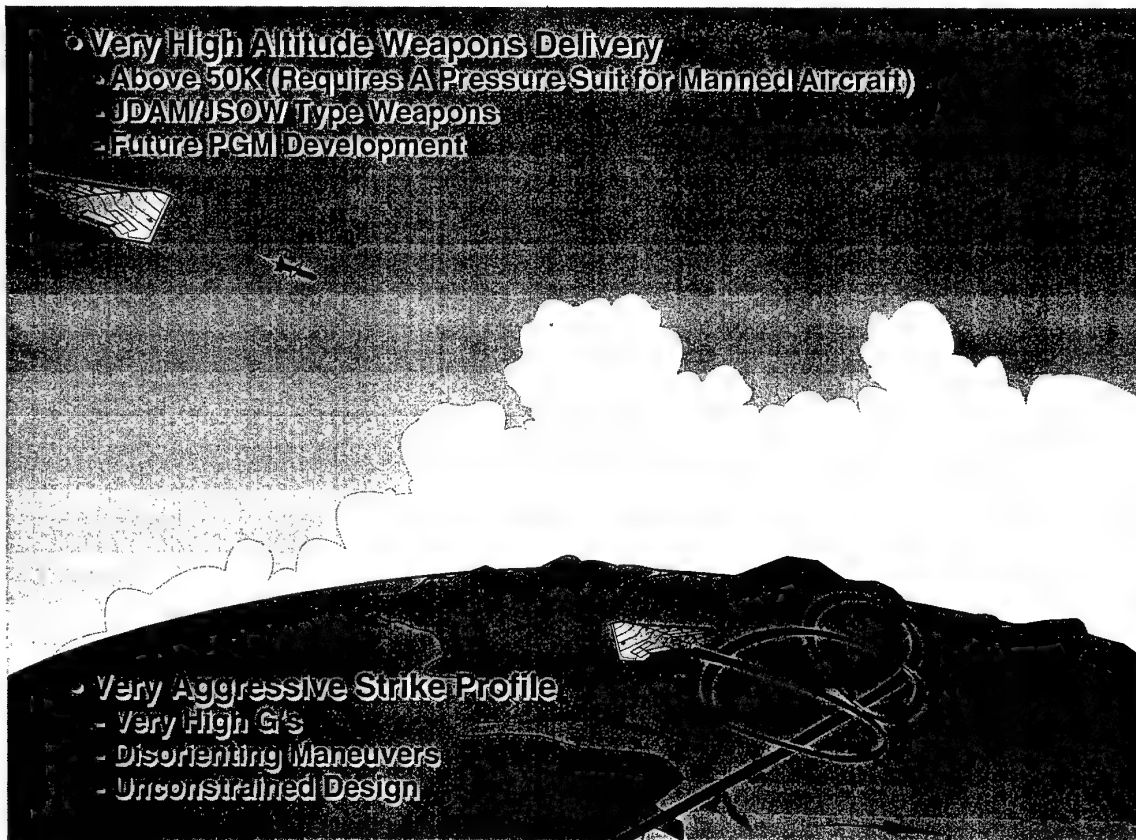
Y.G. #12

The discussions of a UTA in today's combat scenarios reflect classical combat missions flown by tactical aircraft in the past. Now, we will examine scenarios in which UTAs can provide a vital role not even envisioned in the Mission Area Plans.

We believe that there are two new applications where UTAs can provide tomorrow's battlefield commander with revolutionary strike capabilities. One involves strike from very high altitude. In addition to the inherent improvements in survivability associated with high altitudes, weapons would have impressive unpowered standoff ranges. In fact, the unpowered ranges could be equivalent to those currently associated with powered weapons.

The second potentially revolutionary application would be on conventional strike profiles, but with a vehicle capable of very aggressive maneuvering. It might be possible, for example, to design a UTA that can out maneuver surface-to-air and air-to-air missiles using a combination of very aggressive flight profiles and carefully timed defensive maneuvers.

Potential New Operations Concepts



A COST PERSPECTIVE

Y.G. #13

COST BENEFITS. Preliminary analysis of cost considerations associated in the design, operational and training concept inherent in UTA indicates they have potential to revolutionize the cost of strike warfare as we currently know it. The analysis shows that UTA operations and support (O&S) costs offer the greatest cost benefit compared to manned fighters. Contrary to the conventional wisdom, however, we have not identified major cost savings associated with simply removing man from the cockpit. Instead we conclude it will be a combination of effects to include how we build the vehicle, how we will store and maintain it, how we will operate and train with it, what it has to carry and the mission functions it has to perform that will bring about the revolutionary cost savings.

A Cost Perspective

- **UTA Has Potential to Drastically Reduce Cost of Strike**
 - **Compared to Manned Fighters/Bombers**
 - Huge Reduction in Life Cycle Cost Drivers
 - *Inherent in UTA Concept of Operation (& Training)*
 - **Compared to Unmanned Strike Systems**
 - Huge Cost Benefit Every Time Its Reused
- **Simply Removing Man from Vehicle Is Not Enough to Reap Cost Benefit**
 - **Manned Strike System Cost Driven by Functionality Requirements**
 - **Shedding Requirements Is What Sheds Cost**

COMPARISON OF ANNUAL OPERATIONS AND SUPPORT COSTS

V.G. #14

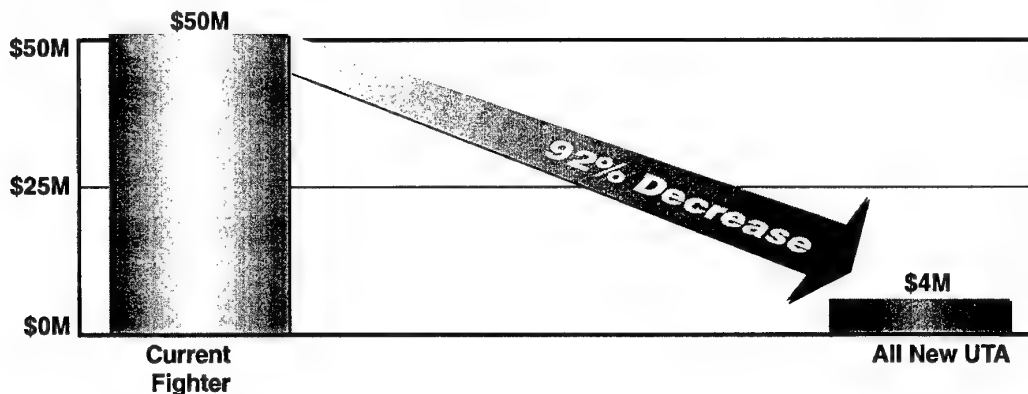
UTA Operations and Support (O&S) cost reductions result from the fact that, like most weapons, a UTA will probably be used in anger only a few weeks or months out of its entire life cycle. Most of its life after delivery will be spent "on the shelf", only to be periodically checked much like today's cruise missiles. A few UTAs will be used for routine maintenance training, launch and recovery operational proficiency, and used in combat exercises such as Red Flag and for tactics development and manned strike package integration training. The bulk of the "flying", however, could be done with simulators and return a significant cost savings to the user.

Our attempt to quantify UTA training and operations cost was based on a current fighter comparison. To maintain proficiency, all fighter pilots (and in some aircraft, their weapons systems operators) must fly regularly. Support of air crew training requirements, for example, puts 363 hours per year on a typical F-15E and 346 hours per year on an F-16C. During FY93 the F-15E fleet flew on the order of 70,000 flight hours to maintain proficiency while the F-16C fleet flew over 200,000 flight hours. Six hundred UTAs, on the other hand, could be built and prepositioned for rapid deployment to troubled spots around the world with perhaps only 30 being used at any one time for day-to-day operations at one existing base during peacetime. It is this mode of operation that has the potential for an order of magnitude decrease in operating costs compared to manned fighters.

Comparison of Annual Operations and Support Costs

Ground Rules

- 24 Aircraft/Unmanned Vehicles
- FY 1995
- O&S Costs Based on Air Force Instruction (AFI 65-503) Factors
- Personnel, Fuel, and Equipment Costs Included
- Simulator and Combat Deployment Augmentation Costs Included for UTA



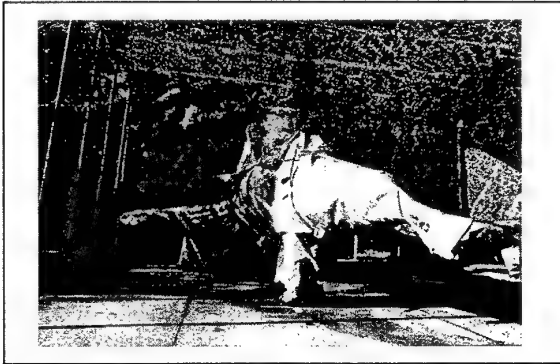
UTA CAN EXPLOIT MAJOR COST DRIVERS

Y.G. #15

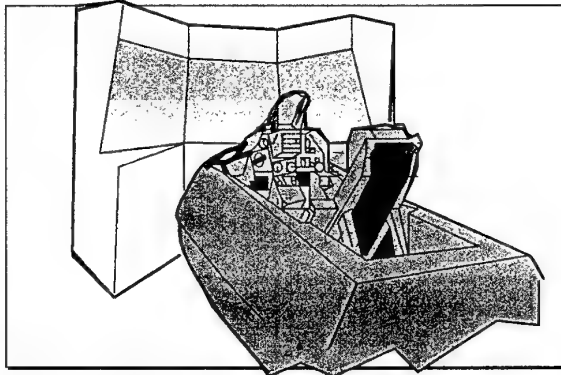
Reaping the full potential UTA cost advantage will not be realized until an all-new UTA is designed from the beginning for its unique mission and operations and training scenario. Therefore, despite the lower development and acquisition costs associated with converted fighters, by virtue of being based on existing designs, these early vehicles will not be fly-and-forget machines. All-new UTAs also could be designed for little or no unscheduled maintenance during combat deployments to further leverage the cost effectiveness of the force.

UTA Can Exploit Major Cost Drivers

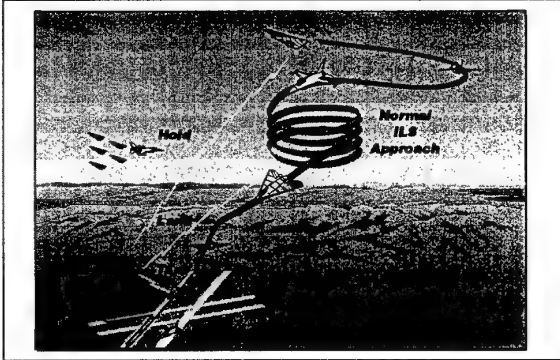
Minimum Non Combat Flight Ops



Simulator vs. Flying for Proficiency



Operations From Manned Base



Minimum Design Life

<i>Typical Fighter System</i>	<i>Current Fighter Design Life</i>	<i>UTA Life</i>
Airframe	8,000 Hrs	300-500 Hrs
Landing Gear	7,500 Cycles	300-500 Hrs
Radar	10,000 Hrs	300-500 Hrs
Environ. Control Sys	8,000 Hrs	300-500 Hrs
Engine Hot Section	4,000 Cycles	300-500 Hrs
Engine Cold Section	8,000 Cycles	300-500 Hrs

CONCLUDING REMARKS

V.G. #16

In conclusion, Lockheed Martin considers UTA to be a potentially revolutionary new tactical strike system that initially can benefit from many manned fighter capabilities, systems and technologies. In the end, however, a UTA will need to be designed and developed from the ground up to take advantage of its full range of revolutionary potential.

Concluding Remarks

UNMANNED TACTICAL AIRCRAFT

- UTA Can Enable Revolutionary New Tactics / Missions
- UTA Has Potentially Revolutionary Cost Benefits
- UTA Will Enable New Concept of Force Mix
- Early Operational Capability Can Be Adapted From Existing Manned Assets
- All-New UTA Required To Capture Full Operational and Cost Benefit
- F-16 Based Demonstrator Vehicle Can Cost Effectively Support Technology and Operational Objectives

An exploratory study of the human-machine interface for controlling Maritime Unmanned Air Vehicles

L. van Breda
TNO Human Factors Research Institute
P.O. Box 23
3769 ZG Soesterberg
The Netherlands
E-mail: vanBreda@tm.tno.nl

1. SUMMARY

Under contract by the Royal Netherlands Navy an exploratory study was conducted on the design of the user interface for Maritime Unmanned Air Vehicles (MUAVs) control. The goal of this study was to gain more insight into the various parameters that may influence system performance, given the present level of technology.

Two simulator experiments were conducted. Results of a first experiment made clear that the image transmission rate of the downlink is a critical factor. It appeared that with a single MUAV, only combined sensor and airframe control leads to an acceptable tracking performance, in particular at short observation distances. For low sensor image update frequencies (< 4 Hz), tracking becomes critical. Results of a second experiment revealed that the tracking performance in a MUAV supervisory control task is identical to the first experiment, even in high auditive/cognitive workload conditions. It is suggested to focus further research on ways to improve operator performance and awareness at low downlink transmission rates. This can be affected by integrating synthetic information on orientation and MUAV status into the sensor image.

2. INTRODUCTION

Maritime Unmanned Air Vehicles (MUAVs) are airframes with a payload that are launched and propelled through the air without an operator on board. Instead, these vehicles are remotely controlled by an operator who is situated in a base control station. The Royal Netherlands Navy (RNLN), as well as other participating countries in NATO PG/35 are interested in the development of these airframes, in particular for anti-surface-warfare purposes (1). This includes surface reconnaissance, surveillance and target acquisition (RSTA), as well as battle damage assessment (BDA). As MUAVs are not strictly autonomous, operators are closely involved, guiding the vehicles towards their targets while interpreting threat, tactical, and sensor information. Especially when tracking targets, the operator has to ensure that he is accurately following the target while envisioning an environment which is remotely obtained. As the sensor image has a limited resolution and field of view, and no vestibular feedback of the airframe behaviour is obtained, it is obvious that operator behaviour is crucial for effective MUAV operation. Therefore, the TNO Human Factors Research Institute was

asked to investigate the human-machine parameters of the MUAV user interface that affect operator performance.

In a first approach, a literature review (2) was performed, based on NATO launch, mission and recovery requirements (3), (4), (1), (5). It was concluded that the human-machine interface should be optimally designed for supervisory control (target acquisition phase) and tracking for RSTA/BDA. Requirements indicate that MUAVs should only be used under certain predetermined conditions. For instance, a certain predetermined observation distance to the target should be maintained in order to avoid early detection of the MUAV. Since target loss must be limited to a minimum, it is important to select the proper technology for the MUAV and carefully design the MUAV user interface. Eisen and Passenier (6) concluded that MUAV operators are involved in several functions during MUAV missions. Therefore various levels of information, such as target image, tracking, and overall MUAV system status information, need to be presented. Three levels of information can be distinguished:

- sensor information, providing a video image of the sensor area. This is the most local image of the MUAV system. Depending on the selection of the operator, either a wide field of view (FOV) image or a narrow FOV image may be displayed;
- tactical information, providing a spatial representation of the search area near the target. This is information regarding the process of the search, encompassing a sub-sector of the target search area, including the actual sensor footprint (actual covered surface search area) and possible area of target detection (cue);
- strategic information, providing spatial, operational and status information of the host ship, all involved MUAVs, friendly and enemy areas, and threat.

The experiments discussed in this paper cover all these levels of information. The first experiment is focused on the tracking task with a single MUAV, when mainly sensor and tactical levels of information are used. These levels are in particular relevant when the MUAV is in the final stage of approaching the target and following it afterwards. The principal goal is to control the MUAV and maintain a constant position and orientation relative to the target. Doing so, the operator is confronted with multiple degrees of freedom including altitude, horizontal position and yaw of the MUAV as well as pitch, yaw and FOV of the sensor system. These degrees of freedom affect the position of the sensor footprint,

determining its motion in addition to that of the MUAV. The goal of the experiment is to determine the extent to which the tracking performance is affected by basic system parameters. The second experiment concerns operator performance when dealing with so called multi-MUAV clusters, in which MUAVs are partly pre-programmed, partly manually controlled. The operator is involved in a supervisory control task: supervising sensor, tactical, strategic and MUAV status information, and simultaneously tracking targets manually. Under these operational circumstances operator workload may play an important role.

3. EXPERIMENT 1 "Single MUAV tracking"

The first experiment was undertaken to determine the extent to which the tracking performance is affected by basic system parameters such as *control input characteristics*, *observation distance* and *sensor image characteristics*. A MUAV workstation is a man-in-the-loop tracking system providing control input devices and visual feedback for the operator. The MUAV operator minimizes the deviation between the cross hair of the sensor image and the moving target. For accurate control, appropriate feedback is essential. Unfortunately, a MUAV has severe restrictions in minimum observation distance (forward distance to the target to be maintained, also called "standoff distance") and field of view (FOV) to be used for the sensor. Information concerning the target's future position may be derived from the perceived target position and orientation (perceptual anticipation) and from knowledge of the MUAV and target movement (cognitive anticipation). Since the primary mission of the MUAV system in the present study is RSTA, the a-priori information on MUAV and target characteristics is minimal. Therefore, with regard to target tracking, cognitive anticipation is hardly supported.

A MUAV operator has to perform a dual control task: tracking a moving target and simultaneously maintaining a constant observation distance, the so-called standoff distance. In this experiment, two types of control input devices are investigated, i.e. a separate control input device and a coupled control input device.

In the separate control mode, two independent joysticks are used, one for controlling the MUAV forward/backward acceleration and yaw rate, and one for controlling the pitch and yaw rate of the sensor. The operator is free to manipulate both sensor and MUAV airframe independently which allows the operator to observe a target from different viewing directions. However, these multiple degrees of freedom require the operator to make mental transformations between the desired footprint position and appropriate control actions. This may deteriorate the tracking performance.

In the coupled control mode, one single joystick controls the footprint (6). In this semi-automatic control mode, the control signal is interpreted by a control algorithm to maintain a constant standoff distance. If the target distance varies, the sensor footprint can be controlled in forward or backward direction by pushing or pulling the joystick. The corresponding platform motions are calculated to restabilize at the desired standoff distance. By moving the joystick sideward, the horizontal viewing angle is controlled by the yaw rate of the MUAV airframe.

Requirements indicate that small contacts should be detectable at 5000 m observation distance. For BDA, smaller observation distances will be necessary (e.g. 2000 m). The smaller

the observation distance, the better details of the target can be distinguished. However, the tracking accuracy may decrease because movements of nearby targets require the operator to make more control actions. In maritime and air situations visual estimation of the standoff distance is difficult under all circumstances, because visual distance cues are minimally available.

The quality of the image depends on the sensor characteristics. The resolution of the video system is 768×576 pixels. Since the operator is in the control loop, dynamic aspects of the sensor image may affect the operator's tracking performance. Therefore the sensor image should be real-time with a certain minimum update frequency.

The image is transmitted from the MUAV to the host ship by means of a datalink, the so-called downlink. The exact characteristics of this datalink, like transmission speed, are not available yet, as these depend on the technology used (5). Normal analogue transmission of the image results in update frequencies of 10-50 Hz. However, a digital datalink is the aim, resulting in image update frequencies varying from approximately 1-4 Hz (5). As analogue transmission technology is more sensitive to external disturbances, this will probably not be applied.

In summary, the MUAV operator minimizes deviations between the cross hair of the sensor image and the moving target. In the separate control mode, especially for small standoff distances, poor perceptual anticipation may produce relatively large errors in the estimated standoff distance, possibly in combination with disorientation with regard to the target position. To perform the dual control task more effectively, the coupled control mode combines sensor and airframe control, with corresponding control directions, thus reducing the number of degrees of freedom for control. Therefore, for this control mode a superior tracking performance is expected.

With regard to the sensor image update frequency, for both control modes, it can be expected that low update frequencies will deteriorate perceptual anticipation and therefore degrade the tracking accuracy.

3.1 Method

Subjects

Nine male subjects participated in the experiment. They were non-commissioned officers of the RNLN in active service and specialized in combat centre activities.

Task

For each subject, the first phase of a trial consisted of approaching a fast moving target ship in order to achieve a predetermined standoff distance (5000 m or 2000 m). During this approach phase, the sensor was zoomed out (46.7° FOV).

Once the desired standoff distance was reached, the subject had to zoom in on the target ship (3° FOV) and control the MUAV in order to maintain this distance. The other objective for this phase of a trial was to keep the cross hairs of the sensor image as accurately as possible on a special marker at the stern of the target ship (tracking phase).

In case of target loss, it was allowed to zoom out the image in order to retrace the target ship. Each trial was finished after four minutes of tracking.

Experimental design

Since the present study involved the limits of the human-machine system, the values of the independent variables were varied considerably:

- 1 Control mode:
separate control vs. coupled control
- 2 Standoff distance:
2000 m vs. 5000 m
- 3 Update frequency:
1 Hz, 4 Hz and 10 Hz.

These variables were independently combined within subjects in a balanced order. This made up a total of 12 conditions.

Instrumentation

The experiment was carried out on the MUAV simulator developed at the TNO Human Factors Research Institute. This simulator was based on a Silicon Graphics Iris 4D workstation for calculation of the position of the footprint and for generation and presentation of the tactical and sensor information. The subject was seated in a cubicle in which a monitor and control devices were installed. Control actions of the subject were fed into the Iris in which a mathematical model of the target ship behaviour and of the MUAV including sensor characteristics were implemented. In the separate control mode, a left-hand joystick was used to control pitch and viewing direction of the sensor, and a right-hand joystick to control speed and yaw rate of the MUAV. In the coupled control mode, only the right-hand joystick was used for combined sensor and MUAV motion control. Detailed information on simulator characteristics, MUAV and target behaviour are presented in the Appendix.

Procedure

Each subject participated one day, divided over two sessions in which one control mode was used. At the beginning of each session, the subject was trained for one hour, during which the controls and the information on the screen were explicated, then followed by a number of test trials were performed (four test trials of six minutes per control condition). The experimental trials were executed afterwards; each subject had to perform 12 blocks of 4 trials.

Dependent variables and analysis

The sample rate for collecting data of the state variables during the experimental trials was 4 Hz. For the data analysis the following dependent variables were calculated, representing the tracking accuracy of the operator:

- *target coverage*: percentage of time during which the target ship's stern observation marking was visible on the screen;
- *standoff error*: the difference between the predetermined standoff distance and the actual standoff distance of the MUAV, expressed in meters;
- *viewing error*: the total angular difference between the cross hair of the sensor image and the marking on the target ship, expressed in degrees.

The analysis concerned root mean square error (RMS error) of the variables, starting at the moment that the MUAV is within 1000 m. On these data, an analysis of variance (ANOVA), (7) was performed.

3.2 Results

Target coverage

Fig. 1 shows the target coverage, for both control conditions and three downlink conditions, averaged over the subjects.

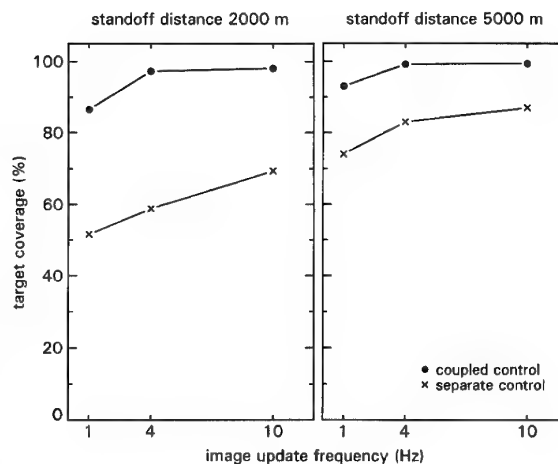


Fig. 1 Mean target coverage as a function of the sensor image update frequency and standoff distance, for two control conditions.

As can be seen in Fig. 1 the coupled joystick control resulted in an overall higher coverage percentage compared to separate joystick control. According to a 2 (Control input device) \times 2 (Standoff distance) \times 3 (Update frequency) ANOVA this effect was significant [$F(1,8)=81.2$; $p < 0.01$]. The significant interaction between control mode and standoff distance [$F(11,0)=1.8$; $p < 0.05$] revealed that the effect of control mode was largest in the 2000 m standoff distance condition. A Tukey test (7) revealed that there was no significant effect of standoff distance on the target coverage in the coupled control mode. The ANOVA also indicated that there was a significant effect of update frequency [$F(2,16)=14.3$; $p < 0.01$]; the target coverage was decreasing with lower update frequencies. The Tukey test also indicated that the 1 Hz condition significantly differed from the 4 Hz and 10 Hz condition (for both $p < 0.01$).

Standoff error

Fig. 2 shows the standoff error as affected by the update frequency of the sensor image, for both control conditions and three downlink conditions, averaged over the subject.

In Fig. 2 it can be seen that coupled joystick control resulted in substantially smaller standoff errors compared to separate joystick control. According to a 2 (Control input device) \times 2 (Standoff distance) \times 3 (Update frequency) ANOVA, this effect was significant [$F(1,8)=150.0$; $p < 0.01$]. The ANOVA also indicated that there was no significant effect of standoff distance, i.e. the standoff error was more or less constant over different standoff distances. The effect of update frequency was significant [$F(2,16)=6.9$; $p < 0.01$]. The Tukey test indicated that the 1 Hz condition significantly differed from the 4 Hz ($p < 0.05$) and 10 Hz ($p < 0.01$) condition. The standoff error was negligible in case the sensor update frequency was at least 4 Hz, in the coupled control mode.

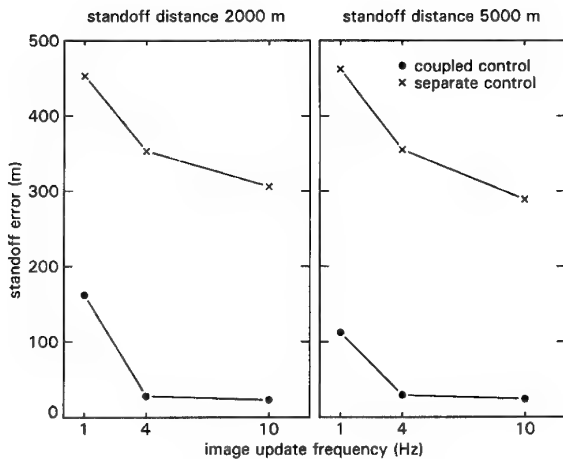


Fig. 2 Mean standoff error as a function of the sensor image update frequency and standoff distance, for two control conditions.

Viewing error

In Fig. 3 the sensor viewing error is presented, for both control conditions and three downlink conditions, averaged over the subjects.

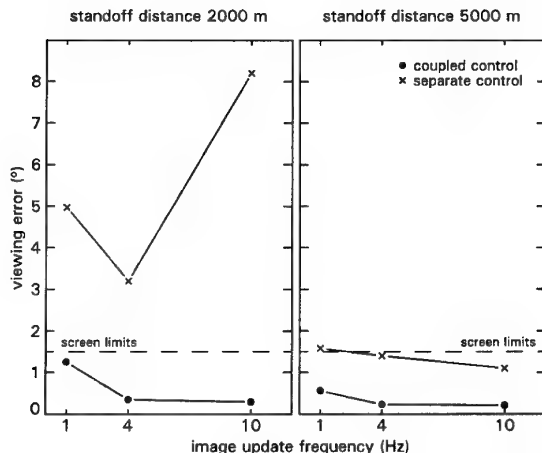


Fig. 3 Mean values of the sensor viewing error as a function of the sensor image update frequency and standoff distance, for two control conditions. The horizontal dashed line indicates the screen limits (distance from screen centre to screen-edges).

In Fig. 3 it can be seen that for all conditions the coupled control mode resulted in a smaller viewing error compared to the separate control mode. A 2 (Control input device) \times 2 (Standoff distance) \times 3 (Update frequency) ANOVA indicated that this effect was significant [$F(1,8)=21.0$; $p < 0.01$]. The results also showed that larger viewing errors occurred at smaller observation distances [$F(1,8)=9.4$; $p < 0.05$]. A significant interaction between control mode and standoff distance was found [$F(1,8)=7.5$; $p < 0.05$]. The

Tukey test indicated that there is no significant effect of standoff distance on the viewing error in the coupled control mode. In Fig. 3 the screen limits are shown, indicating the visibility criterion. For separate control, viewing errors at 2000 m standoff distance even exceeded the screen limits. No effect of downlink image update frequency on viewing error was found.

3.3 Discussion

The data clearly showed that the tracking performance was significantly better in case a single joystick control was used based on a coupled control algorithm. The coverage of the target was nearly 100% of the tracking time whereas the standoff distance error was negligible. As was expected, for this control mode tracking performance remained more or less constant for different standoff distances.

In the separate control mode, the target coverage had reduced considerably, in particular at short standoff distance (to about 60% of the tracking time for the 2000 m standoff distance condition). In this condition frequent target loss occurred. Observation of the subjects' tracking behaviour indicated that differences between sensor viewing direction and MUAV heading repeatedly remained unnoticed, possibly giving rise to disorientation.

For both control modes, the sensor image update frequency proved to be of crucial importance to the tracking performance. Especially in the 1 Hz condition, a significant performance degradation was found.

4. EXPERIMENT 2 "MUAV supervisory control"

Experiment 1 was focused on single MUAV operation. However, effective over-the-horizon MUAV missions will be based on a cluster of airframes. For example, one MUAV for tracking targets or for RSTA/BDA, two MUAVs as relay stations (the first is moving to the target area to take over the tracking job as soon as the actual tracking MUAV has to return to base for refuelling; the second is moving from the target area back to base to get refuelled), and one MUAV is being refuelled at the base. In such a MUAV configuration, only the tracking airframe is under direct control by an operator, whereas the other airframes are more or less autonomously flying from waypoint to waypoint, or waiting and hovering at predetermined positions, until action is needed. A global function description of a multi-MUAV mission contains the following main functions:

- **Track targets** Once the targeting MUAV is at a predetermined observation (standoff) distance, the operator uses the control input devices and visual feedback to minimize the deviation between the cross hair of the sensor image and the moving target.
- **Supervise** The MUAV operator has to supervise a multiple MUAV system, monitoring tactical mission information and control/status information to judge the state of the airframes. Therefore, the mission scenario should be considered as a procedure, supervised by the operator. He verifies the different system parameters and take the necessary corrective actions.
- **Communicate** The MUAV operator communicates with the Command. It is suggested that the operator has an open connection through the communication network using a headset, scanning messages that are assigned to him. It is essential that the operator recognizes these messages correctly and acts accordingly.

The RNLN is interested to know whether a single MUAV operator is able to perform multiple tasks in order to fulfil the functions described above. It seems logical to think that tasks, being performed simultaneously, affect each other (e.g. calculating and discussing). But it is also known that task combinations exist that can very well be performed in parallel (e.g. steering a car and discussing with someone, or listening to the radio). Therefore, multiple task performance should be investigated before a new system is developed. A model that can be used to evaluate human interface principles and to predict workload, is the multiple resource model developed by Wickens (8). This model is specific for multiple (continuous) task performance and distinguishes three resources (9):

- *modalities*; channels through which information is obtained (e.g. visual, verbal), or the way response is generated (e.g. verbal, manual);
- *stages of information processing*; perceive, central processing, respond;
- *coding*; the way information is being processed. This can be spatial (e.g. orientational tasks) or verbal (e.g. retaining names).

The model predicts that, when (independent) parallel tasks use the same resource (interfere), the task performance on each individual task will decrease. This will not happen when parallel tasks use different resources. For instance, verbal tasks can easily be combined with visual tasks; a task in an early phase of information processing (e.g. perceive, pattern recognition) can easily be combined with a task that generates a response (e.g. steering); a task that processes spatial information (e.g. interpreting radar information) can easily be combined with a verbal task (e.g. communicate).

To determine the effect of verbal/cognitive workload on tracking performance, an experiment was conducted. Subjects had to approach a moving target in an open sea scenario and follow this target at a predetermined standoff distance. In the experiment, a coupled control input device (10) was used, in which one single joystick controlled footprint and airframe (6). The control signal was interpreted by a control algorithm for maintaining a fixed standoff distance (2000 m). If the target distance varied, the sensor footprint could be manually controlled in forward or backward direction by pushing or pulling the joystick. The corresponding airframe motions were calculated and executed. By moving the joystick sideways, the horizontal viewing angle was controlled by the yaw rate of the MUAV airframe.

To vary the workload, a verbal/cognitive task had to be performed in addition to this visual-manual-spatial tracking task. This so called continuous memory task (CMT) (11) was presented to the subjects by means of a verbal display (headset) and was characterized by detecting certain target letters and mentally counting the frequency of their appearance. The task difficulty was varied by the number of target letters. The subjects were asked to perform the tracking task as accurately as possible, but to give the CMT the highest priority.

It should be noticed that the CMT only globally reflects the future MUAV operator task aspects when fulfilling the functions as described above. It is obvious that specific visual or manual (for instance emergency diagnosis and control tasks during erroneous MUAV functioning) could affect the operator task performance differently. This experiment is considered as a first test, so a normative approach was taken: the operator will not make procedural errors and no airframe malfunctioning will occur.

According to Experiment 1, the image update frequency of is one of the crucial factors to influence operator tracking performance. Therefore, both image update and CMT workload were varied in the experiment. With respect to the factor 'image update frequency', the sensor video image was supposed to be obtained through a digital datalink, resulting in image update frequencies varying from 1 to 10 Hz. For the factor 'cognitive workload', the difficulty of the CMT was varied at three levels: 'low', 'moderate' and 'high'.

In summary, the MUAV operator has to minimize deviations between the cross hair of the sensor image and the moving target. Based on the findings of Experiment 1, it can be expected that low sensor image update frequencies will deteriorate perceptual anticipation, causing relatively large viewing errors, and therefore decrease the operator tracking performance.

Wickens' multiple resource model predicts that the (visual/manual) spatial tracking task can well be combined with a verbal/cognitive task. Therefore, with regard to the verbal/cognitive workload introduced by the CMT, it can be expected that high workload will hardly influence the tracking task performance.

4.1 Method

Subjects

Ten male subjects participated in the experiment. These subjects were starting College students. Their age varied from 21 to 39 years (average 25.6 years).

Task

Each subject was sitting at a desk, providing a display and joystick for tracking targets, and a display and headset for the secondary CMT. The tracking task was conform Experiment 1: the subjects initially flew a MUAV at about 5000 m distance from a fast moving target ship. This target ship had to be approached until 2000 m standoff distance. During this approach, the sensor remained zoomed out (46.7° FOV). Once the desired standoff distance was obtained, the subject had to zoom in on the target ship (3° FOV) and track the target ship, which means to keep the cross hairs of the sensor image as accurately as possible on a special marker at the stern of the target ship (tracking phase). However, this target ship performed unexpected course changes. In case of target loss, it was allowed to zoom out and retrace the target ship.

At a certain moment, an additional task had to be performed. If so, a set of (two or four) target letters appeared on a screen and a button for acceptance had to be pushed, to start a continuous memory task (CMT). A series of 40 letters were presented in the subject's headset: one letter every 1.5 s. The subject had to press a 'recognition' button once, each time he recognized one of the target letters. Moreover, he had to push the 'recognition' button twice, each time any target letter was recognised for the third time. In case a double response was expected, the subject heard 'Correct' when giving a double response; the subject heard 'Wrong' once an omission was made or when the subject responded at the wrong moment. After the response (either 'Correct' or 'Wrong') the tally for the letter that was presented, was reset to zero. A CMT with two target letters was considered to be of 'moderate workload', a CMT with four target letters of 'high workload' (12), (13).

The subject was instructed to track the target ship as accurate as possible, using the coupled control system. Although, the secondary verbal/cognitive task had to be considered as the

highest priority task. Each trial was finished after four minutes of tracking. Then, the next trial would start.

Experimental design

The values of the independent variables were varied as follows:

- 1 Image update frequency (3 levels):
1 Hz, 4 Hz and 10 Hz.
- 2 Verbal/cognitive workload (3 levels):
low, moderate, high.

The variables were independently combined within subjects in a balanced order.

Instrumentation

The instrumentation of Experiment 2 was conform the instrumentation used in Experiment 1. However, for generation and presentation of the secondary CMT task, a Taskomat was used (14), consisting of a IBM PC with timer response and speech interface for stimulus generation and verbal presentation.

Procedure

The subjects came in pairs during one day. First, they were introduced to the MUAV simulator by the instructor, who explained the control input devices and the presented information on the screen. Then, a training session took place in which three tracking test trials (update frequency of 10, 4, 1 Hz, respectively) had to be performed. Finally, the subjects were trained to perform the CMT secondary task (moderate, high workload respectively), separately from, and simultaneously with the tracking task. The task performance was verified by the instructor.

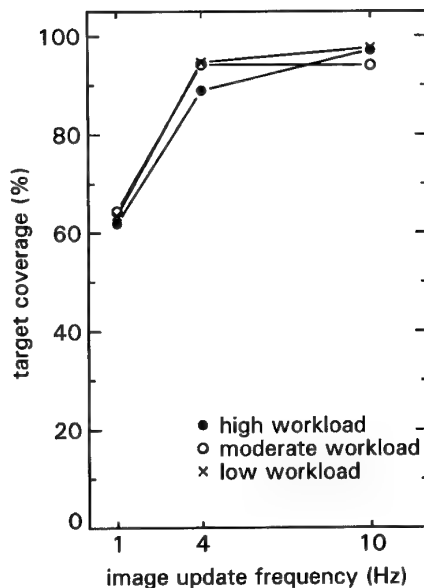


Fig. 4 Mean target coverage as a function of the sensor image update frequency and operator workload, averaged over the subjects.

During the actual experiment, each subject had to perform 6 blocks of 3 trials. When one subject was performing, the other was waiting and took over after each block. The in-

structor closely monitored the subject's task performance. In particular the CMT performance had to be monitored and kept at a maximum level.

Dependent variables and analysis

The dependent variables and the analysis was conform Experiment 1.

4.2 Results

Target coverage

Fig. 4 shows the target coverage, for the three image update and workload conditions, averaged over the subjects.

As can be seen in Fig. 4, the target coverage was decreasing with lower image update frequencies. This was nearly 100% at 10 Hz, and 95% or more at 4 Hz, but only about 60% at 1 Hz. According to a 3 (Update frequency) \times 3 (Workload) ANOVA this effect was significant [$F(2,18)=15.09$; $p < 0.01$]. However, the ANOVA did not show any effect of workload (CMT). A Tukey post-hoc test indicated that the 1 Hz condition significantly differed from the 4 and 10 Hz condition (for both $p < 0.01$).

Viewing error

In Fig. 5 the sensor viewing error is presented, for three image update and workload conditions, averaged over the subjects.

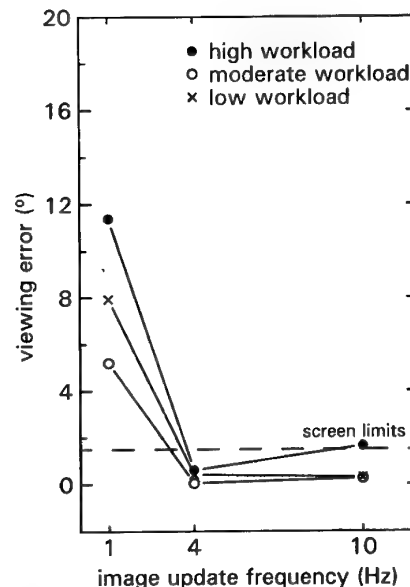


Fig. 5 Mean sensor viewing error as a function of the sensor image update frequency and operator workload, averaged over the subjects. The horizontal dashed line indicates the screen limits (distance from screen centre to screen-edges).

It can be seen that the viewing error was nearly negligible at image update frequencies of 4 Hz or more, and was increasing significantly at low update frequencies. However, according to a 3 (Update frequency) \times 3 (Workload) ANOVA this effect was hardly significant [$F(2,18)=3.36$; $p=0.05$].

In the figure, the screen limits are shown, indicating the visibility criterion of the tracking task. It can be seen that the viewing error only exceeded the screen limits at the lowest update frequency condition. This was also the only condition in which any effect of workload appeared. However, the ANOVA did not indicate any significance of this effect.

4.3 Discussion

As was expected, the experimental results showed a decrease of MUAV tracking performance with lower update frequencies of the sensor image. With 10 or 4 Hz, the coverage of the target remained at nearly 100% of the tracking time, but at 1 Hz this was only about 60%. This was caused by an increase of the viewing error, exceeding the field of view of the camera.

As was predicted by Wickens' multiple resource model, no significant decline in target coverage was found when the subjects performed the tracking task under moderate and high verbal/cognitive workload conditions. Only with 1 Hz update frequency the average viewing error increased. Hence, Wickens' predictions on task performance were not completely valid with regard to the most difficult tracking condition. Tracking with low update frequencies probably required more central (mental) processing concerning the target's behaviour. This interfered with the verbal/cognitive task.

Verification of the subjects' verbal/cognitive task performance pointed out that this task was properly executed; the target-letter hits, as well as the counted target-letter hits remained unchanged over the workload conditions.

5. GENERAL DISCUSSION

Two simulator experiments were conducted to investigate how effective operators can track fast moving targets with a MUAV system.

The first experiment was focused on single MUAV control conditions: subjects had to track a moving target while input device, standoff distance and sensor image update frequency were varied.

Results of the experiment show that no accurate tracking is possible with separate input devices for airframe and sensor control. In particular, at a small standoff distance frequent target loss occurs. For accurate tracking, a control input device based on a coupled control algorithm should be used. Only for this coupled control condition, the 4 Hz sensor image update frequency, as recommended (5), still leads to an acceptable tracking performance. For update frequencies less than 4 Hz, the results become more critical and therefore further research is only useful when details of the dynamic characteristics of the airframe and technical specification of the datalink are known.

The control algorithm used in the experiment is developed in this institute and is mainly based on setpoint control of sensor pitch and on forward/backward speed control of the airframe. A control algorithm for different MUAV viewing directions could enhance the observation possibilities. However, this is not within the scope of the study.

The second experiment was focused on multiple MUAV supervisory control conditions: subjects had to track a fast moving target with different image updates, and simultaneously perform an additional verbal/cognitive task under different workload conditions.

Results of the experiment show that moderate and even high workload conditions did not affect the mean target coverage of the sensor image. This remained at about 100% for update frequencies of 4 Hz and more, and at about 60% for 1 Hz update frequencies. However, in the latter condition, the tracking task became more discontinuous, decreasing operator's anticipation possibilities, and thereby demanding more central processing on the target's behaviour. This interfered with the cognitive task. As the subjects' verbal/cognitive task performance remained at a constant level, the viewing (tracking) error increased.

The fact that a significant tracking performance degradation was found at low image update frequencies, indicates that image update frequency is one of the crucial factors affecting operator performance. Many attempts are currently made to improve the MUAV downlink transmission bandwidth in order to increase information flow. However, high costs and technological limitations limit the progress in this field (5), (15). Since the decrease in operator performance is caused by lack of anticipation and orientation (10), it should be investigated whether provisions for enhanced visual information may be a more efficient way to improve operator performance. This should not only concern improvement of the sensor image characteristics, but also improvement of the operator's awareness by depicting additional graphics information onto the sensor image. For example, synthetic perspective graphics, creating a virtual landscape, as seen from the actual MUAV position, displayed at a high update rate (i.e. 60 Hz). It may be expected that such extra artificial information will improve the operator's anticipation and orientation and thereby enhancing the tracking performance.

REFERENCES

- 1 NATO Naval Armaments Group (PG-35) (1992). NATO staff requirement for a NATO maritime unmanned air vehicle system (Report AC/141(PG/35)D/8). Brussels.
- 2 Eisen, P.S. & Passenier, P.O. (1991a). Technology status of unmanned air vehicles (Report IZF 1991 A-31). Soesterberg, NL: TNO Institute for Perception.
- 3 LaMonica, G. (1988). RPV feasibility for small NATO ships (Report AC/141(SWG/11)D/6). Litchfield Park, AZ: Loral Defense Systems-Arizona.
- 4 NATO Naval Armaments Group (PG-35) (1990). NATO staff target for a NATO maritime unmanned air vehicle (UAV) system (Report AC/141-D/662). Brussels: Author.
- 5 Schwartz, M., Wallace, D., Libert, J.M., Tkacz, S., Solomon, D. (1992). UAV Imagery frame rate and resolution study (Report 02962). Silver Spring: Vitro Corporation.
- 6 Eisen, P.S. & Passenier, P.O. (1991b). An exploratory study of the human-machine interface for unmanned air vehicles (Report IZF 1991 A-43). Soesterberg, NL: TNO Institute for Perception.
- 7 Winer, B.J., Brown, D.R. & Michel, K.M. (1991). Statistical principles in experimental design, 3rd edition. New York: McGraw-Hill.
- 8 Wickens, C.D. (1984). Engineering psychology and human performance. Columbus, OH: Merrill.
- 9 Veltman, J.A. & Gaillard, A.W.K. (1993). Evaluation of subjective and psychological measurement techniques for pilot workload (Report IZF 1993 A-5). Soesterberg, NL: TNO Institute for Perception.

- 10 Breda, L. van & Passenier, P.O. (1993). An exploratory study of the human-machine interface for controlling a maritime unmanned air vehicles (Report IZF 1993 A-10). Soesterberg, NL: TNO Institute for Perception.
- 11 Boer, L.C. (1992). Taskomat: Betekenis van test scores (Report IZF 1992 A-29). Soesterberg, NL: TNO Institute for Perception.
- 12 Aasman, J., Mulder, G. & Mulder, J.M. (1987). Operator effort and the measurement of heart-rate variability. In: Human Factors, 1987, 29(2), p 161-170.
- 13 Veltman, J.A. (1991). Mental workload among pilots: theoretical background and literature review (Report IZF 1991 A-33). Soesterberg, NL: TNO Institute for Perception.
- 14 Spoelstra, P. (1993). Taskomat: Manual for usage, installation and system management (Report IZF 1993 A-15). Soesterberg, NL: TNO Institute for Perception.
- 15 NATO Naval Armaments Group (PG-35) (1993). Risk reduction plan for a NATO maritime unmanned air vehicle system (2nd Draft) (Working Paper AC/141 (PG/35) WP/31). Brussels.

APPENDIX: Simulation Parameters

Target area

- Surrounded by sea: a horizontal plane of infinite size and dark grey colour
- Sky: background of light bluish-grey
- Small area: an area of uncertainty (AOU) of 100 nm² provided by cue; circular in shape
- Large area: 1/3 of a sector, uncued. (A sector is defined as a 40° region, between 20 and 100 nm distance from ship; thus, 1/3 of a sector is approx. 1100 nm².)

Target

• class	frigate	
• length	100	m
• width	15	m
• height	4	m
• maximum speed	40	kts
• turning radius	400	m

Colour

- Dark grey hull, lighter grey deck.
- Colours approach that of sea, linearly in RGB (voltages of red, green, and blue electron guns of monitor), as distance from UAV increases (to simulate atmospheric effects on image). At 10 km distance, ship and sea colours are identical, simulating zero visibility.

Wake

- Light grey at ship; approaches colour of water at tail; visibility reduces with distance from UAV (in same manner as ship does).
- Width is roughly equal to width of ship.
- Length is a function of ship speed (it lasts for 20 s; maximum is 417 m).

Manoeuvring

The ship always moves at its maximum speed. Every 10 s, the ship has a 50% probability of turning in a random direction. Once a turn is initiated, the duration of the turn is randomly chosen between 0 s and 10 s. The intention is to

simulate a range between undisturbed straight navigation when the UAV is distant, and avoidance manoeuvres when the UAV is near. The latter assumes a worst-case scenario: the target pilot knows he is under scrutiny, and wishes to make his ship difficult to track.

MUAV motion

Horizontal translations

- maximum translational rate of ± 120 kts
- maximum yaw rate of ± 3 °/s
- acceleration control by longitudinal axis of position joystick or arrow keys (separate control only)
- rate of yaw control by lateral axis of position joystick or arrow keys
- first-order control system with 3-s time constant.

Vertical translations

- constant altitude 6561 ft

Sensor/Gimbal

Azimuth (Yaw)

- maximum rate of ± 30 °/s
- 360° range
- rate controlled by lateral axis of position joystick or arrow keys (separate control only)
- gain is proportional to FOV, allowing a constant sensitivity to input across all levels of zoom
- gain is proportional to *distance to footprint centre*, allowing a constant sensitivity to input across all distances.

Elevation (Pitch)

- maximum rate of ± 20 °/s
- range of 20° to -120°
- rate controlled by longitudinal axis of position joystick or arrow keys
- gain is proportional to FOV, allowing a constant sensitivity to input across all levels of zoom
- gain is proportional to *distance to footprint centre*, allowing a constant sensitivity to input across all distances.

Field of view

- maximum FOV of 46,7°
- minimum FOV of 3,0°
- FOV increase/decrease controlled by function keys.

Separate control

One input device controls UAV yaw laterally and UAV acceleration longitudinally. The other device controls pitch and yaw rates.

Coupled control

Single input device controls UAV yaw laterally and footprint speed longitudinally.

MULTIPLE UMA's IN-FLIGHT MANAGEMENT

Ing. Carlo SIARDI

METEOR C.A.E. S.p.A. - FINMECCANICA IRI GROUP

Via M. Stoppani, 21 - 34077 Ronchi dei Legionari (GO) ITALY

1. SUMMARY

Up to now significant effort has been posed in exploiting the basic UMA functionalities and operational growth potentials: almost all issues concerning single UMA employment are currently being addressed and solutions are due to come.

Instead, Multiple UMA's control and operational Management (MUM) is still an open issue which has to pass through accurate and comprehensive operational scenarios evaluation and thus ending up with proper requirement definition.

The present paper deals with this latter statement, also trying to outline potential problems which may arise operationally.

Among the many parameters involved, timing is going to be the key parameter to handle, in order to allow full UMA utilization within multiforces operations.

As far as multiple UMA's controlled by a single GCS are concerned, this issue can be translated in how accurately the time windows tied to each navigational waypoint are intercepted by the in-flight airvehicles. Therefore the question moves to which parameter must be controlled by the UMA Flight Management System and how is it influenced by the en-route wind.

Another intriguing subject is closely connected to the link band employed: provided satellite links represent a viable and effective solution, we hereon limit are discussion to conventional ground links.

In case of NATO standard J-Band link a narrow beam is necessary due to the band typical fading margin and energy losses. Since a GCS has to cope with several UMA's performing their missions, an accurate trade-off must be conducted to establish a proper balance between several basic parametric constraints, such as ground antenna beam width, spatial airvehicle navigational accuracy, Ground Data Terminal antenna stabilization, GCS Man Machine Interface and so on, in order to guarantee a reliable airvehicle acquisition for proper tracking and data gaining.

Morover, link loss and failures management during silent flight are going to be tough subjects to cope with, for they represent potential hazard within airspace control activities.

Last but not least is how to demonstrate the fulfillment of the requirements, keeping an eye on testing costs and risk reduction.

2. GLOSSARY

AGL	Above Ground Level
A/P	Auto Pilot
AV	Air Vehicle
ETA	Estimated Time of Arrival
ETD	Estimated Time of Departure
FLOT	Forward Line of Own Troops
GCS	Ground Control Station

GDT	Ground Data Terminal
GPS	Global Positioning System
GS	Ground Speed
IAS	Indicated Air Speed
mrad	Milliradians
MPC	Mission Planning Console
RMS	Root Mean Square
MEC	Mission Evaluation Center
MUM	Multiple UMA's Management
NATO	North Atlantic Treaty Organization
PCST	Programming and Control Station
RF	Radio Frequency
RGS	Remote Ground Station
TAS	True Air Speed
TGT	Target
UMA	UnManned Airvehicle
WP	Way Point

3. INTRODUCTION

Today's world crisis management under Unified Commands call for intimate coordination and, in particular, quick information availability at proper levels for timely situational decisions.

Recent operational use of UMA Systems emphasized the need for simultaneous airvehicles management as force-multiplier, thus endowing each UMA battery with improved flexibility, and dramatically expanding the range of missions which can be carried out at the same time and the area effectively surveilled by each GCS.

Even in limited conflict scenarios the resulting AirSpace Management now faces complex coordination among all forces employed and requires timing control and other novel capabilities by all in-flight airvehicles.

The present paper mainly focuses on Area Surveillance UMAs having the scope to keep significant portions of territory under constant round-the-clock control, which therefore implies the utilization of several UMAs operating at the same time in the same or adjacent areas in order to assure a proper data refreshment rate.

Generally speaking we distinguish between:

- **Multiple UMAs Discrete Management**, represented by most present-day tactical surveillance systems and characterized by a radius of action function of the link range capability.
- **Multiple UMAs Continuous Management**, being an extension of the previous case in that it employs a series of auxiliary ground stations disseminated along the territorial "belt" to be surveilled, provided the main operational and maintenance centers are located in a specific safe area well away from the front line.

On the other side, since Endurance UMAs perform very specific missions which usually do not require multiple airvehicle management, they are therefore not covered in this paper.

4. PRACTICAL CASES

4.1 MULTIPLE UMAs DISCRETE MANAGEMENT

Let's now review the typical case of a surveillance system which needs to operate several UMAs under the control of a single GCS, employing highly directional antennae for detection/jamming prevention either on GCS and airvehicle. In this case the MUM is conceived as discrete real time data collection from airborne airvehicles, each of them separately contacted by the GCS on a time schedule basis.

System Composition

Basically the System presents one or more AV Launchers, their number depending upon launch frequency and scenario, a GCS and a GDT.

Both the GCS and the AV have directional antennae with those on the AV aiming at the GCS throughout the mission.

The System Data Link guarantees bi-directional RF time-shared link between AV and GDT antenna, while digital modulation of the transmission data allows a high degree of link reliability.

Anti-jamming techniques (eg. spread-spectrum frequency hopping) are implemented to secure the communication channel.

Within such link architecture the GCS operates as the "slave" section with respect to the on-board equipment which actually activates the ground units for link set-up ("master").

System Operation

With reference to Fig.1 each GCS can have several UMAs simultaneously in flight with the radio-link connection possible one at a time.

Therefore it must be possible to shift from one AV to another with the remaining AVs performing their preprogrammed flight paths in silent mode, as illustrated in Fig.2. These passive AVs are remotely followed by the GCS via a simulation program, thus allowing the ground operator to monitor all AVs traces on a single screen, with their navigational accuracy function of enroute wind conditions.

Practically speaking, according to the rande-vous time schedule, the GDT directional antenna aims at a spatial window in wait for the arriving UMA. The specific mission code is then selected by the GCS for univocal connection with the incoming AV, in order to avoid any possible interference with other in-flight UMAs and prevent external insertions for data intercept.

The possibility to manage multiple AVs simultaneously is achieved through the following phases:

- Mission Programming
- Timing management by GCS Main Computer and Ground Link Equipment

The fundamental concept for the requirement fulfillment is the definition and allocation of the link activation timing for each AV.

Such sequence is prepared on the Mission Planning Console (MPC) with reference to the required flight plan, functionalities involved and AV performance.

Mission Programming

For each programmed flight leg it is defined the relevant percentage of leg coverage needed with the link; the choice to utilize the spatial percentage of activation instead of the temporal one is owed to the necessity to fully identify the geographical location where to activate the link.

The MPC will then translate such percentage in relative temporal basis thus obtaining a similar sequence based on time rather than on space.

The time to fly the leg is then defined on theoretical basis and it will be close to the actual figure, but not generally equal to, due to the obvious impossibility to foresee wind conditions along the route.

Fig. 3 gives an example of the concept.

All radio link activation/deactivation timing for each flight plan leg is then compared by the MPC with all other programmed flight plans temporal sequences.

MPC allows timely automatic warning if there is any mutual link required overlapping situation along the routes.

Corrective action is eventually taken by the operator in order to eliminate temporal incompatibilities.

Herebelow is described a synthetic example:

Link Compatibility Verification. With reference to Fig. 4, the picture shows a first MPC print-out of the link intervals share between four simultaneous UMAs missions with two error warnings (dotted line):

- flight plan 4, leg 1: link ON overlap with flight plan 2;
- flight plan 3, leg 3: link ON overlap with flight plan 1.

Following this error notice the operator can manage the link ON/OFF sequences of the various missions in order to assure correct link sharing.

In the conflicting case of simultaneous assigned target area overfly, an alternative re-routing will be necessary for one of them.

In this specific case a possible solution may be the layout in Fig. 5 showing no link overlap.

Once all temporal sequences are correctly defined and approved by the operator and are compatible with the requested target area coverage, they can then be passed to the Main GCS Computer together with the corresponding flight plans.

Such data is processed by the Main Computer which will enable the GDT to perform its tracking functions according to the various AVs flight plans.

In-Flight Timing Management

During the count-down procedure and upon reaching, say, T1=15 min. before ETD of the first flight plan, the Main Computer asks for the launch time confirmation, after which it automatically initializes the Station and starts the final count-down.

The GDT antenna is commanded to point the first link- ON WP some time in advance of the expected ETA.

The link will then be managed differently according to the leg having optional link or compulsory link, as reported by the flight plan.

If the expected AV has not appeared in the rendezvous window within a predefined amount of minutes, the GDT antenna automatically performs a dedicated research pattern in azimuth and elevation for positive AV acquisition. In case of definitely missed rendezvous the antenna is then directed towards the following WP as last effort for link activation with the same AV.

If again not so, or if the next scheduled link is due to be activated, the GDT antenna is commanded to point the next link-ON WP, belonging it to the same flight plan or to other AVs flight plans.

Critical Mission Parameters

As far as critical parameters are concerned, this system case represents the worst possible due to the utilization of a highly directional antenna beam imposed by operational factors, such as:

- frequency band sensitivity to fading;
- link range achievement;
- link protection.

The problem is confined to: **"how precise and timely is the rendezvous of our AV with the static ingress window viewed by the GDT antenna."** (see Fig. 6).

Geographical intercept is conditioned by the following:

AV parameters

- a) spatial navigation accuracy, needed anything better than 30 m. SEP, requiring improved Navigation Systems and static ports calibration, if employed;
- b) accurate route navigation flight laws, allowing contained transients during flight;

GDT parameters

- c) accurate geographical north antenna alignment, (within ± 10 mrad) and antenna mast stiffness;
- d) high antenna unit stabilization (50 mrad);
- e) ability to sustain ground winds up to 80 Km/h;
- f) ability to correct limited GDT attitude variations (eg. local terrain movements).

An example of GDT window intercept probability is illustrated in Figure 7.

The curves take into account an AV typical flying speed, on-board GPS (P-Code) navigational precision and the above mentioned critical parameters by applying the Errors Propagation Theory.

Once the AV intercepts the boundary of the GDT beam, mission code recognition and link synchronization take place in order to allow AV tracking. Therefore, beam amplitude vs. distance presents a set of minimum values below which AV illumination time results insufficient for positive synchronization.

Figure 8 gives an idea of the intercepted narrow beam amplitude as function of the relative intercept angle and distance.

Of course, at a given distance, small intercept angles and/or low ground speed will guarantee positive GDT antenna lock-on.

Window Intercept Timing gains particular importance when the UMA System operates within a varied mix of battlefield Systems coordinated by a higher level Air Space Management Center.

Under such circumstances the ideal solution for en-route UMAs is to control their Ground Speed (GS), which in reality presents a series of side-effects as reported herebelow.

In this case what affects the rendezvous timing is:

AV:

- a) wind components along the route (fig. 9)

- front winds force the AV to throttle-up in order to maintain the preset GS; if the encountered wind is strong (more than 35 KTS) it may become necessary to employ higher rated engines, but then we have to deal with the additional fuel consumption. Besides in this case it will be wise to adopt an auto overspeed sequence.
- tail winds may force the AV into an hazardous situation since the AV is going to throttle back in order to reduce the build-up of extra GS, thus lowering its actual IAS to dangerous levels. Therefore it becomes mandatory to implement an automatic pre-stall recovery sequence for adequate stall separation.

Of course if the AV is controlled in Indicated AirSpeed (IAS), either of the above mentioned problems fade away, but at the cost of limited operability within a Unified Forces AirSpace environment, due to the en-route winds-depending heavy delays or advances it may present.

- b) flight altitude (Fig.10)

- the higher the AV flies the less flexible its airspeed management becomes. Thus, at high altitudes the airvehicle has very limited flight speed range available (T_2) in order to counteract enroute winds for positive VG control, unless it employs supercharged engines and/or lift augmentation systems which effectively extend such airspeed envelope.

4.2 MULTIPLE UMAs CONTINUOUS MANAGEMENT

Continuous area surveillance in real time for civil and military applications is more and more requested where the geographic area is characterized by long extensions with limited depth.

According to this statement and to more or less recent theatre crisis, it is herebelow presented a conceptual system architecture for nearly constant real-time, long period surveillance of geographical areas having a marked preferential dimension, such as national borders, FLOT, IDZ, territorial waters, pipelines, roads, etc.

The length of the controlled "belt" virtually has no limit since the system modularity has the ability to guarantee the overall requested coverage.

System Composition

The system is composed by a series of stand-alone and portable ground stations, here called Remote Ground Stations (RGS), having the scope to passively monitor images and data coming from the UMAs on-board sensors and perform localization, provided the AV is within range.

If needed, such stations may functionally evolve towards AVs payload control to improve cueing.

Additional growing potential is achieved by enabling the stations to command UMAs route changes or partial flight plan reprogramming.

All meaningful data received via AV down-link is then transferred to the Mission Evaluation Centers (MEC) for processing and decision making.

Close to the launcher site is located the Programming and Control Station (PCS) which performs mission definition and programming, launches scheduling and general operational coordination.

AVs take-off or launch may either be possible through unprepared strips or launching station according to the scenario involved.

System Operation

The conceptual description refers to a typical military application (Beyond-FLOT Surveillance) with the understanding that all other mission types, including civil applications, fall within this case.

With reference to Fig 11, the area is surveilled from a stand-off AV position with the AVs themselves covering a common preprogrammed flight plan at two different altitudes (outbound and inbound).

The launching station is tasked to deliver the AVs according to a strict timeschedule in order to produce a constant cover of the area.

After launch each AV ingresses the assigned route and is progressively monitored in succession by all ground stations located along the FLOT.

The number of monitoring stations employed is function of the surveilled area extension, link range and stations location.

If the station has the payload control capability, in case of target of interest it will be possible to command Videotracking or Autotracking modes for further cueing.

Figure 12 illustrates the alternate pattern for deeper surveillance beyond the FLOT. Needless to say, AV route and flight altitude are function of link range, line-of-sight requirements for all stations and survivability.

Actual surveilled area dimensions and relative distance from the receiving stations substantially depend on:

- type and field of view of the sensor;
- link range

In the first case it depends on the chosen sensor, also function of the required resolution. For example a good compromise between area coverage and resolution for stand-off missions may be represented by SAR employment. For what concerns the video link it should be necessary to guarantee at least a 40 Km distance

coverage, either acting on bandwidth, irradiated powers or antenna gains. Taking into account the necessity to disseminate the video images generally along a perpendicular direction to the AV route, a solution may be represented by the utilization of AV on-board directional antennae facing laterally with a, say, 90 degrees radiation pattern and automatically switched left or right with reference to the FLOT position (see Fig.13).

Ground Stations are spaced in such a way as to guarantee full link range exploitation vs. reduced number of stations.

Figure 14 proposes a system architecture for MUM able to cope with consistent portions of territory to be surveilled (area sweeping).

According to this solution the area remains under almost constant watch with a definite minimum data refresh rate. AVs take-over scheduling for the single station becomes a smooth business provided that:

- AVs routes are accurately covered with reference to geographical fixes and timing with all criticalities mentioned in para 4.1; since the number of simultaneously airborne AVs is supposed to be consistent, timing management is again a major step to be solved through proper routes scaling, on-board computer wind management and accurate spatial navigation.
- AVs relative distances are readily achieved by strict launch sequences.
- no flight plan change occurs to any of the AVs unless all plans are contemporarily reprogrammed, which is a tough task to implement.

Of course under such architecture it is not convenient to perform additional cueing on detected targets by a single AV, since it would disrupt the overall sequence of stations take-over. Such task will then be transferred to MEC together with all target relevant data for further action.

Final Considerations

By the development of a series of simplified ground surveillance and control stations it is possible to offer an effective and almost continuous real-time Surveillance System, able to control long extensions of territory through the management of an array of UMAs simultaneously in flight.

The same System may accept an indefinite number of ground stations according to the area extension.

Data refreshment rate is function of the AV overfly period, and hence of the number of AVs employed.

Main advantage of this system architecture is its ability to conform to a wide range of missions both for civil and military applications.

The cost may also vary substantially with strict adherence to the user specific requirement, having the further advantage to furnish, as first step, basic systems in the "minimum operational capability" configuration, which can subsequently be improved according to a step-by-step plan due to its inherent modularity concept.

5. MUM QUALIFICATION

Let's now spend a few words on MUM System Qualification. Both cases (para 4.1 and 4.2) need to be field verified in the frame of System functions testing, and this must be carried out in the most realistic and less risky way possible.

The first major step is aimed at the single AV inflight behaviour verification: in eg., flight qualities and performances, A/P gains, flight and guidance laws must be satisfactorily tested within manual and automatic flight plans.

At this point a MUM system verification can be done on a basic configuration displaying two AV simultaneously in flight, with all other cases (three or more AVs) herein contained.

Now, since a direct verification of dual UMA's flight management is risky and costly, alternative solution is represented by the utilization of a manned airvehicle simulating the second flying UMA, in what we call Captive Flight.

Basically the manned airvehicle must:

- a) display flight performances comparable to those of the UMA. This is essential for realistic timing management and overall system verification, including navigational dynamics, target location and images operational evaluation;
- b) be certified to embark the complete UMA avionics and payload set. The light aircraft must therefore pass the Aviation Authority documentation, composition and functional examination, which requires a certain amount of time to be taken into account. The whole embarked UMA equipment must be totally independent from the aircraft systems apart from the common power source.
- c) present in the cockpit panel an auxiliary Flight Attitude Indicator whose tendency bars are directly commanded by the on-board UMA avionics set. Such device allows the pilot to follow the A/P pitch and roll indications during autonomous flight in order to cover the preprogrammed plan stored in the UMA computer.
- d) present in the cockpit area a monitor for direct cueing, in real time, of images taken by the sensor. Being such data extracted on-board, prior their processing for down link transmission, it is possible to assess the effective images resolution by comparing, post-flight, this recorded data with the same information as visualized and recorded on the Ground Station.

Figure 15 illustrates an example of dedicated manned airvehicle, as utilized by Meteor. The main adaption has been the fuselage structural modification in order to accommodate the stabilized platform and directional antennae.

The System test foresees the simultaneous flight of the two AVs according to preprogrammed routes.

Under such conditions the manned airvehicle will be seen from the GCS to behave just like an actual UMA.

Safety aspects are dealt with by assigning both the UMA and the light aircraft separate overfly areas and altitudes.

The pilot himself always maintains full control of his airvehicle throughout its visual flight.

An additional on-board operator assures nearly real time monitoring of the UMA equipment functionalities.

Scope of the test flight is checking the GDT ability to:

- aim at geographical windows in proper timing;
- lock on the incoming AV intercepting the window;
- track it along the link-on leg;
- receive AV telemetries and video images;
- transmit commands;
- perform localization.

In the meantime the UMA is checked for:

- navigational accuracy;
- flight laws adequacy;
- WP timing management.

The set-up of this Captive Flight activity covers almost all the functional system envelope and allows a brief follow-on flight campaign for actual MUM verification with a dual in-flight AVs test pattern.

6. MUM AIRSPACE MANAGEMENT

Multiple UMA operations require well coordinated and directed activities in order to minimize:

- potential flying hazard to friendly manned AVs;
- complex routes/timing rescheduling due to erratic UMAs;
- friendly fire.

In the near future the see-and-avoid concept, adopted by low-level flying manned aircraft in combat scenarios, will not be acceptable due to the increasing number of UMAs hanging around the battlefield.

Reliable IFF seems to be, at present, still the only effective means readily available which, coupled with stringent operating procedures, may introduce this UMAs integration in the tactical arena, thus ending their isolation in space and time as conceived up to now.

The responsibility for conducting safe multiple UMAs in operations is shared between the higher level AirSpace Management and the Surveillance Systems command posts communities, through specific mission programming and careful procedures adherence.

The easiest way is to allocate a UMAs airspace destined for multiple UMAs operation in terms of geographical area and assigned flight levels. For survivability reasons, in a war scenario all manned tactical traffic generally flows above 3000 m. or below 1000 m. AGL, thus leaving the needed altitude layer for unmanned operations.

At user level the required mission is defined in terms of UMAs routes, flight levels and area ingress/egress timings. Once cleared by the competing airspace control agency, which also assigns the proper Mission and IFF

coding, the flight plan gets listed on a Air Tasking Order by which all manned and unmanned missions are coordinated.

It becomes now necessary to identify all events able to influence smooth airspace control within such a complex environment which are:

a. Timing

Timing is critical for:

- ground launch window; in case of mislaunch a second AV should be ready for launch from a second station within a prefixed time tolerance.
- en-route tactically significant WPs intercept;
- time on station, to allow scheduled area ingresses by other warplanes.

Parameters influencing timing have already been dealt with in paragraph 4.1.

b. Navigational accuracy

It doesn't anymore pose a problem since many current navigation Systems are able to guarantee a fairly good accuracy in the order of 30 m. SEP or less, more than sufficient for area surveillance.

c. RPV System malfunction

Both the flying AV and the ground stations may sustain malfunctions which endanger mission prosecution and may spoil AirSpace coordination.

We can synthetically distinguish between:

AV:

- minor failure (mission is continued in degraded mode);
- mission equipment failure (mission is interrupted and the AV proceeds to an emergency recovery point in accordance to a preset procedure);
- major AV failure (if sustainable, the AV proceeds to the above mentioned emergency point, otherwise the autodestroy procedure is initiated);

GTD/GCS:

- ground stations temporary malfunctions (stations functionalities are restored after reinitialization process with possible partial mission achieved data loss);
- definitive link loss due to missed AV rendezvous or ground stations irreversible break-up (the AV performs approved link loss procedures which foresee AV reentry along preset WPs once a full link loss is detected).

d. Tactical scenario variation

Should any tactical plan change occur, all airborne manned and unmanned airvehicles must fit to the new scenario.

On the UMAs side of the matter, this may imply some reprogramming work to be performed, a notoriously tough task if the number of AVs is significant.

The cheapest solution, depending on available resources and if reprogramming is not possible, is to send-out new missions while terminating the existing ones through reentry procedure activation.

e. Environment

War Environment:

- down-link signal disturbances, which renders the mission impossible (mission termination by reentry);
- UMA is shot down (the problem for the airspace control center is to be sure that it is not anymore a flying object).

Atmospheric Environment:

- clouds covering the target (in case of electrooptical payload divert to alternate target or activate reentry);
- en-route icing conditions (in absence of de-icers, change flight level or activate reentry);
- strong winds aloft (if not manageable by the AV, activate reentry).

For what concerned **Interoperability**, it is well known that it will become fully effective if it is introduced according to the following steps:

1. at component level: eg. P/L package commonality between different UMA Systems;
2. at System Level: eg. the ability to operate other System's AVs and/or sensors package from any Ground Station;
3. at battlefield level: eg. the ability for the UMAs Systems to fit entirely within the Multinational C4I Systems architecture where all interfaces and data formats are codified and approved for operational use.

For the time being Interoperability is generally limited to the User exchanging in-flight AVs between front line Systems of the same type, with efforts starting now to achieve all three levels mentioned above.

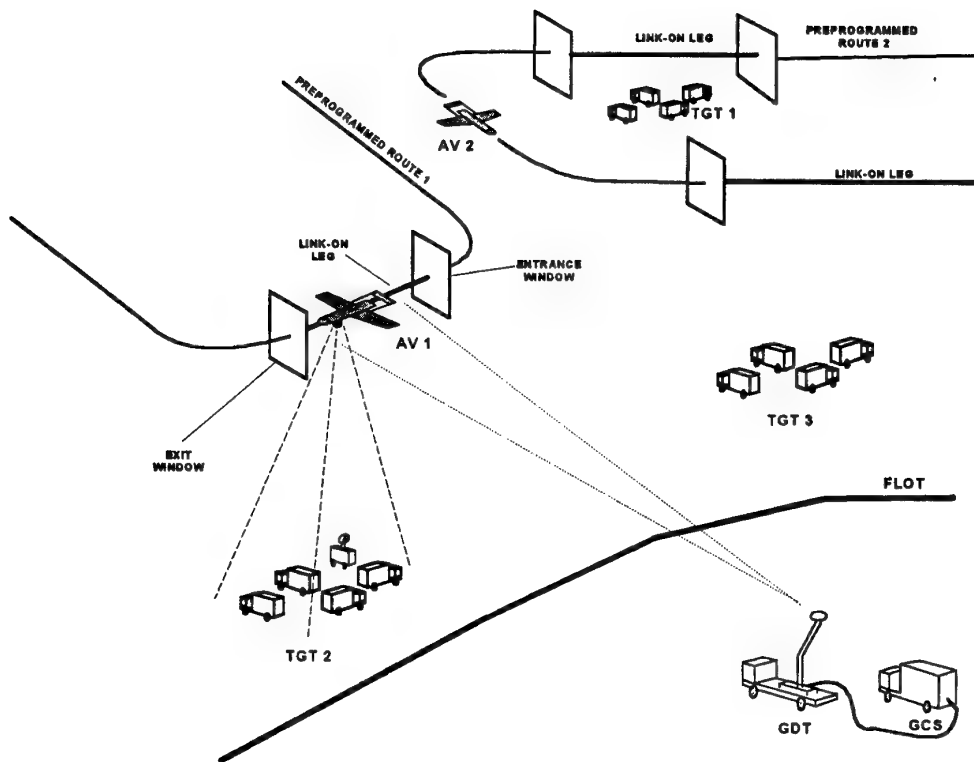


Fig. 1 - MULTIPLE UMA's DISCRETE MANAGEMENT

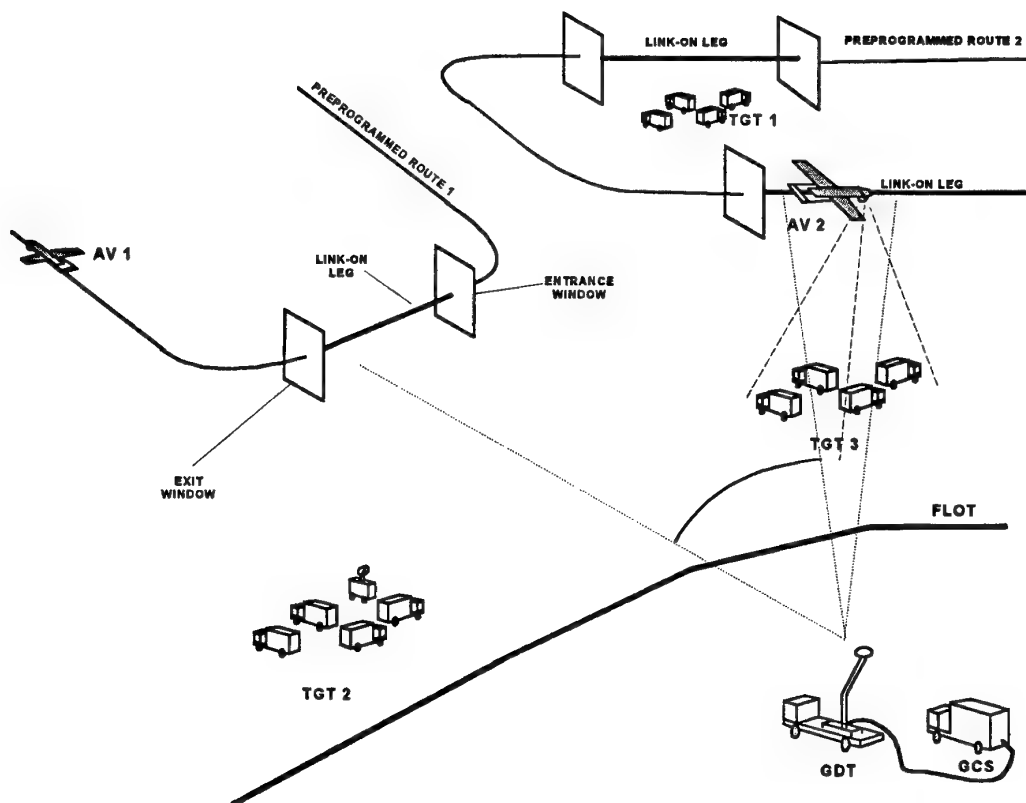


Fig. 2 - MULTIPLE UMA's DISCRETE MANAGEMENT

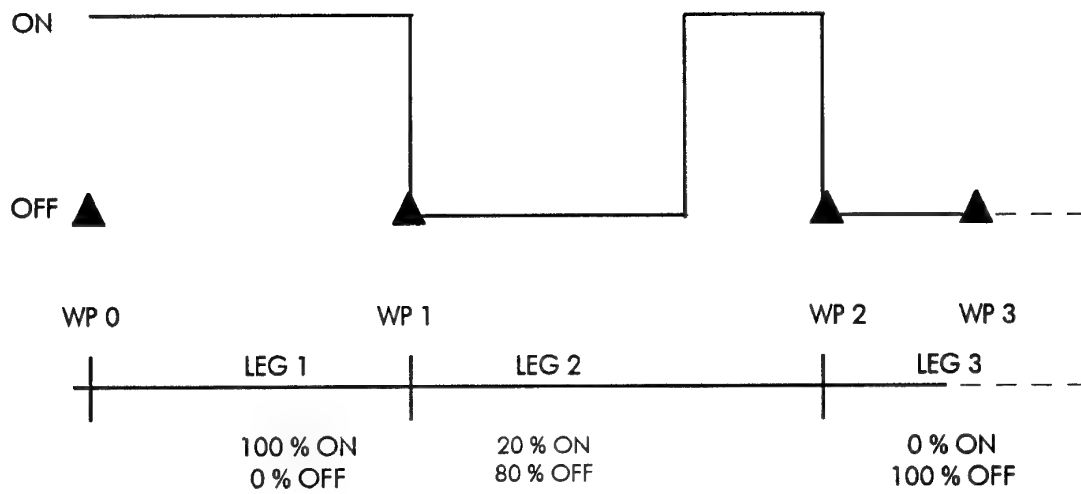


Fig. 3 - SINGLE MISSION LINK-ON PROGRAMMING

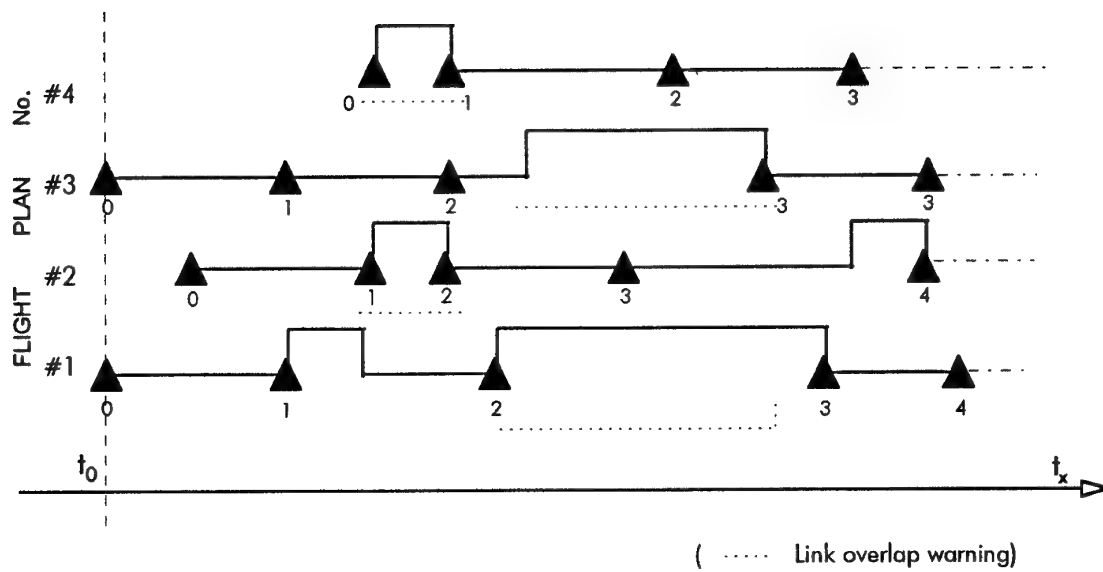


Fig. 4 - MULTI MISSION LINK PROGRAMMING

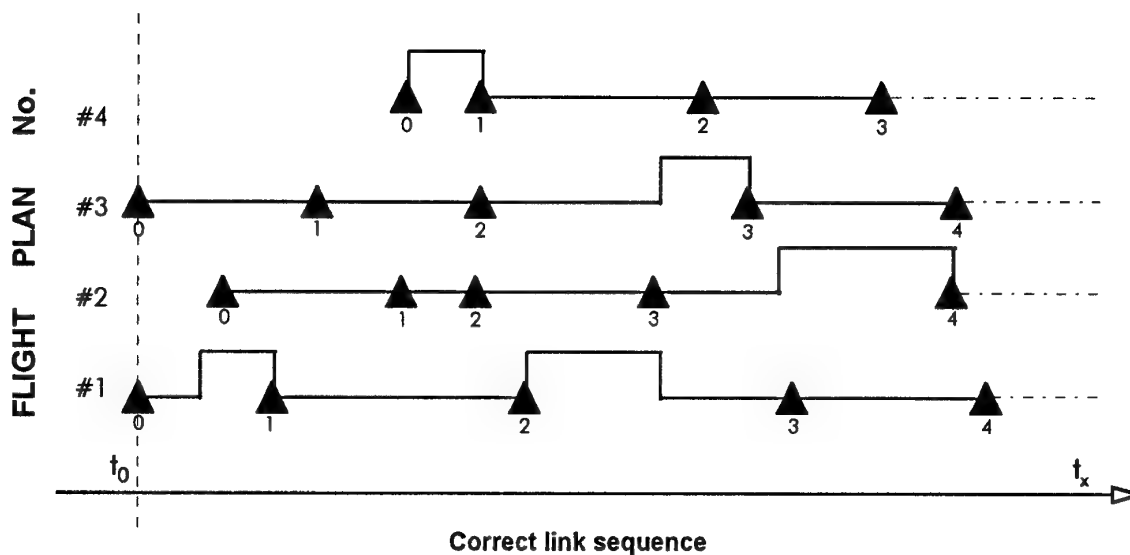


Fig. 5 - MULTI-MISSION LINK PROGRAMMING

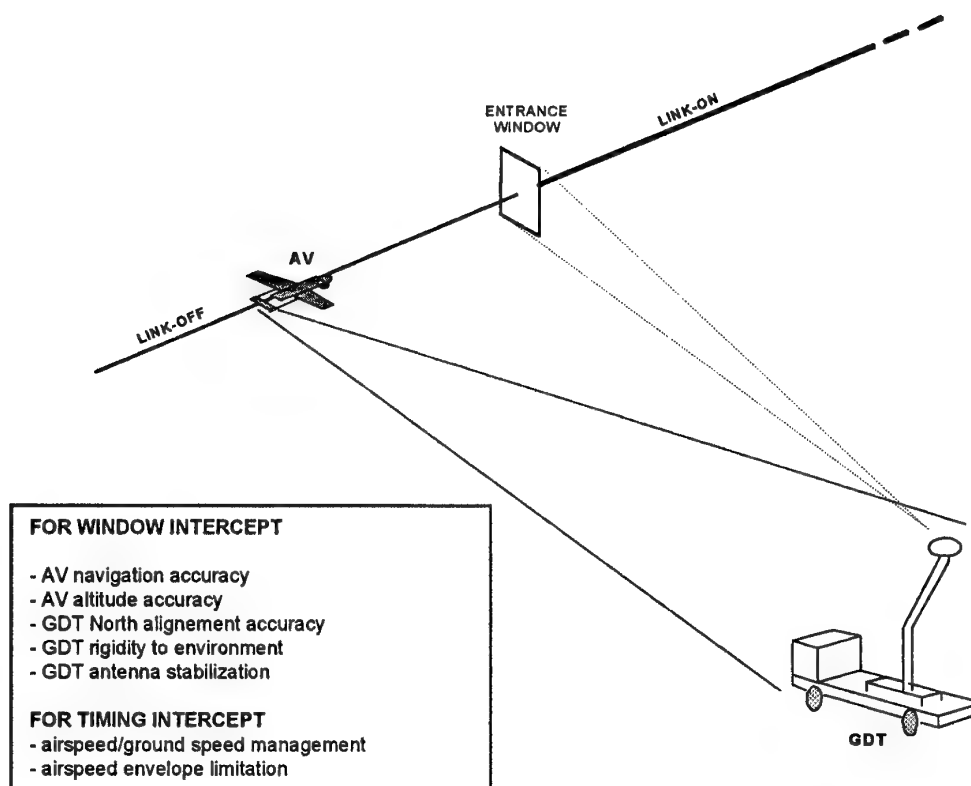


Fig. 6 - CRITICAL PARAMETERS FOR LINK WINDOW INTERCEPT

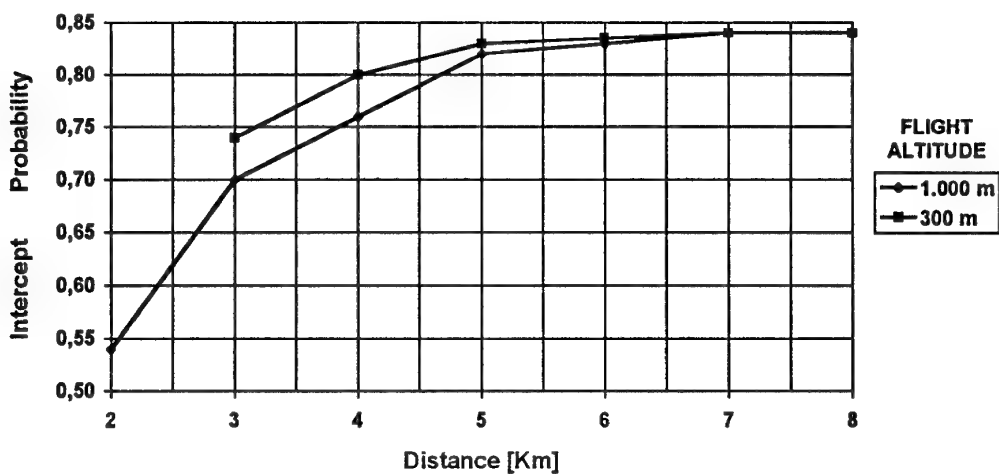


Fig. 7 - INTERCEPT PROBABILITY WITH ERRORS PROPAGATION THEORY

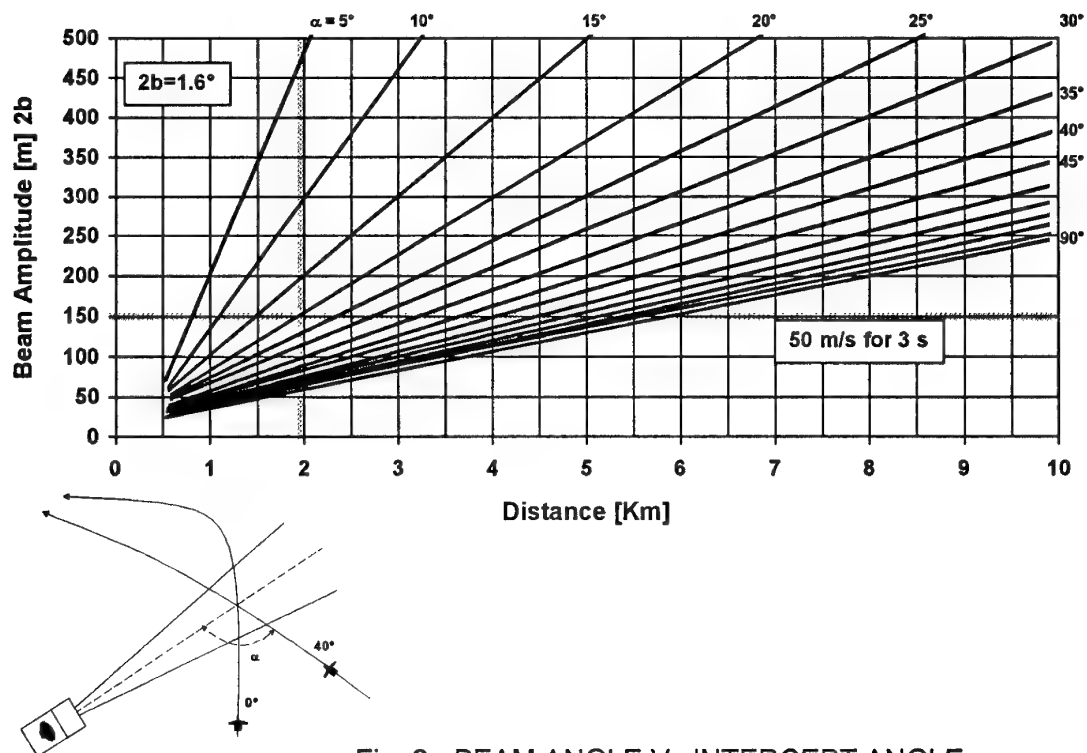


Fig. 8 - BEAM ANGLE Vs INTERCEPT ANGLE

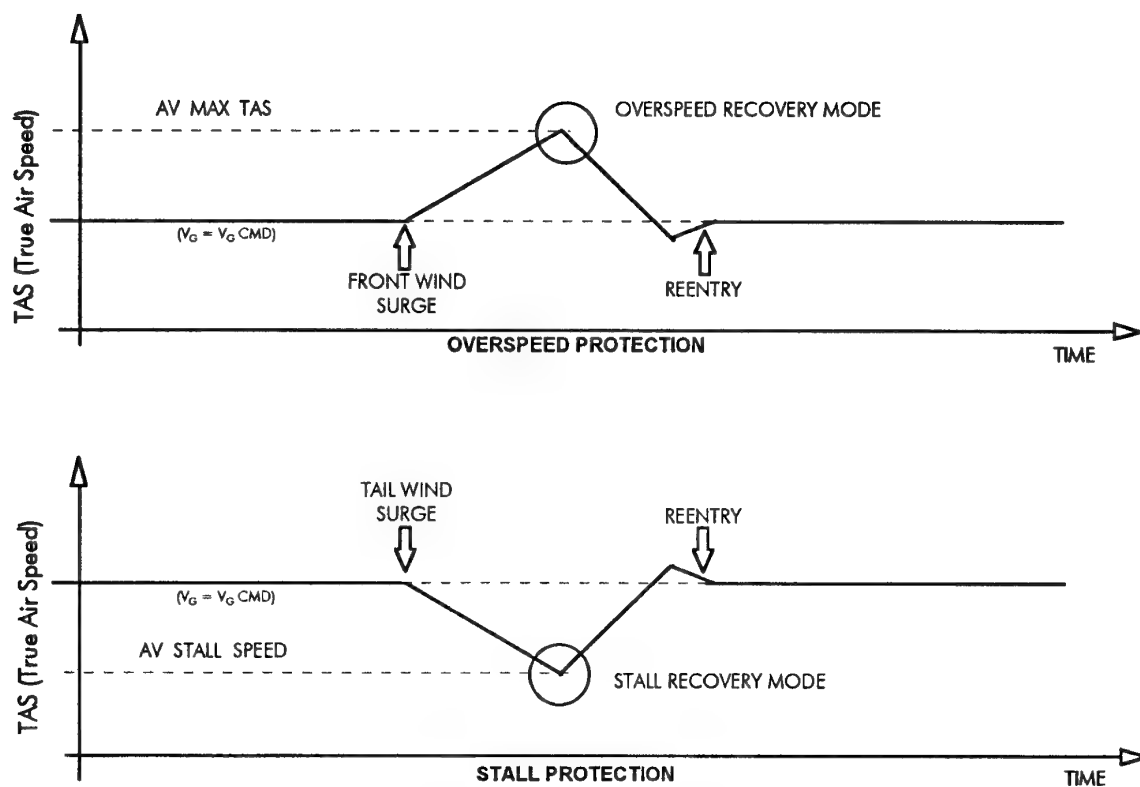


Fig. 9 - OVERSPEED AND STALL PROTECTION MODES

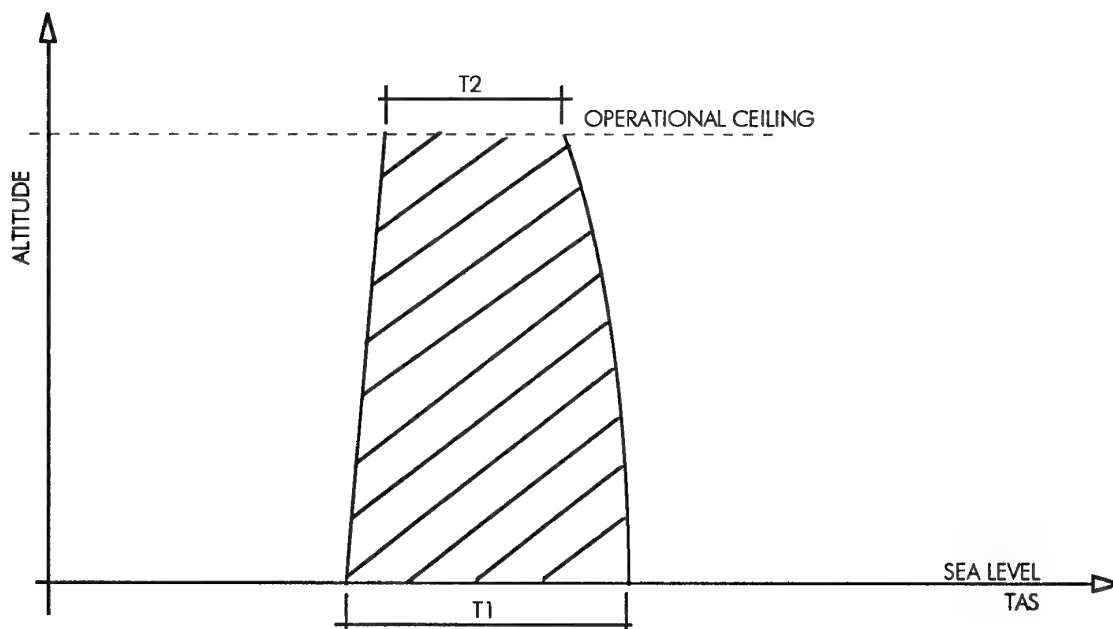


Fig. 10 - OPERATIVE AIRSPEED ENVELOPE Vs ALTITUDE

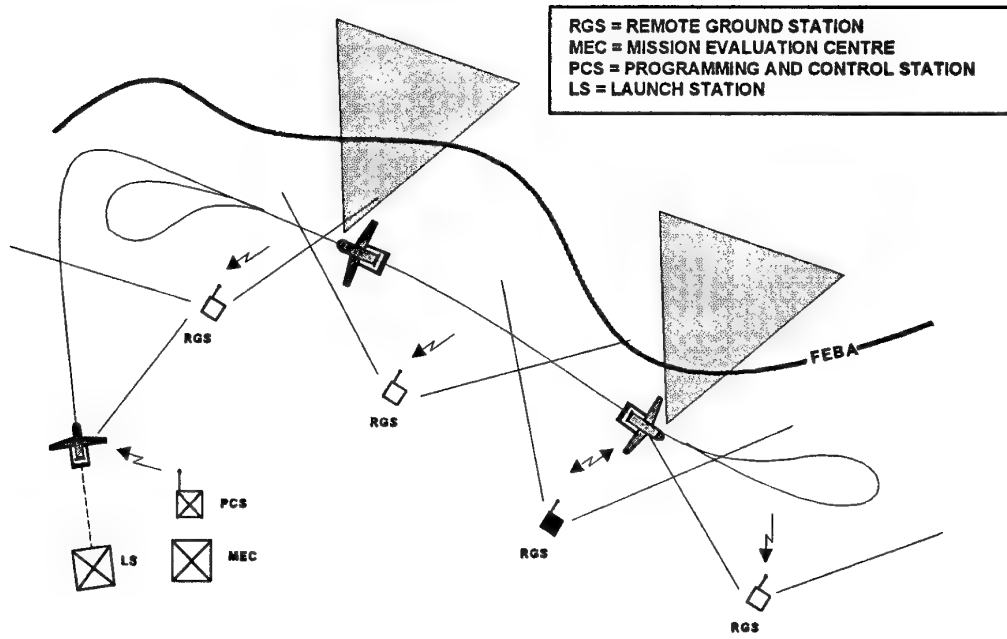


Fig. 11 - MULTIPLE UMA's CONTINUOUS MANAGEMNT - STAND OFF MODE

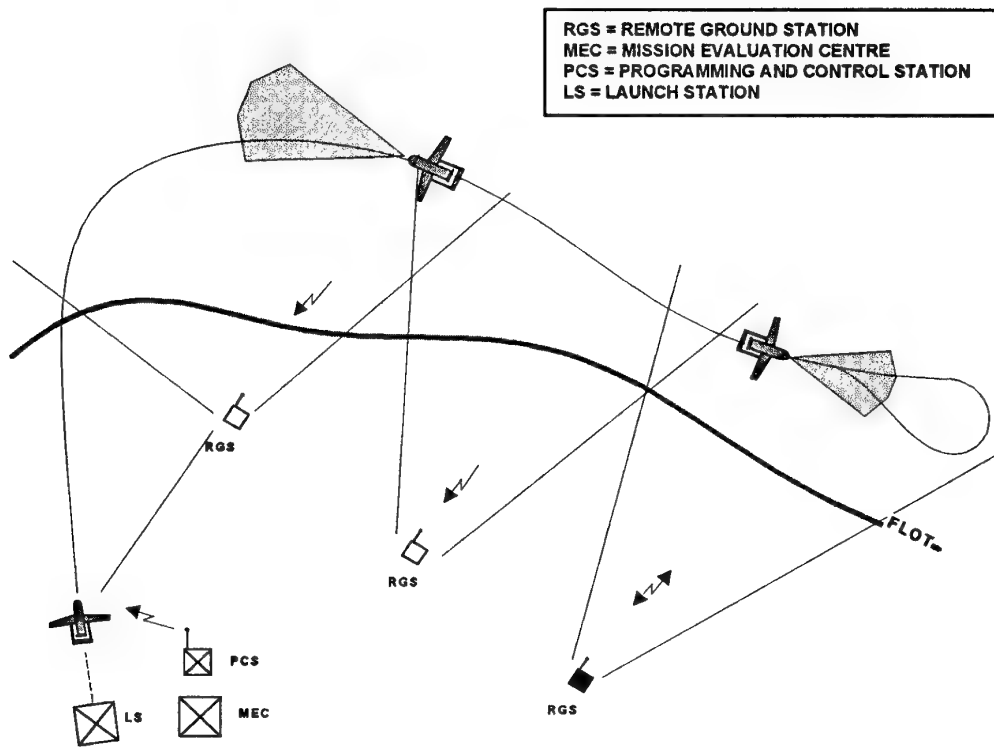


Fig. 12 - MULTIPLE UMA's CONTINUOUS MANAGEMNT - OVERFLY MODE

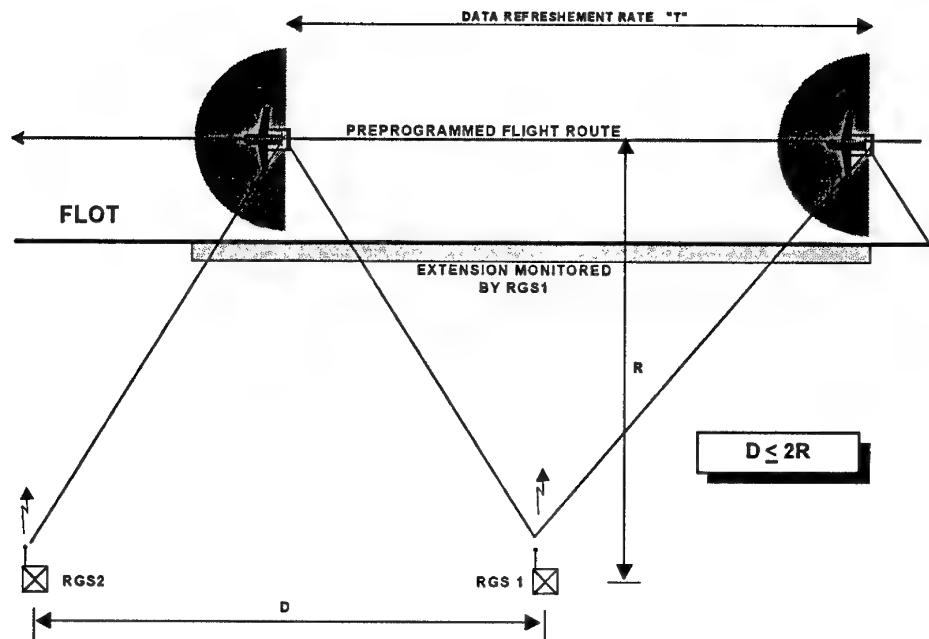


Fig. 13 - DATA REFRESHMENT SCHEMATICS

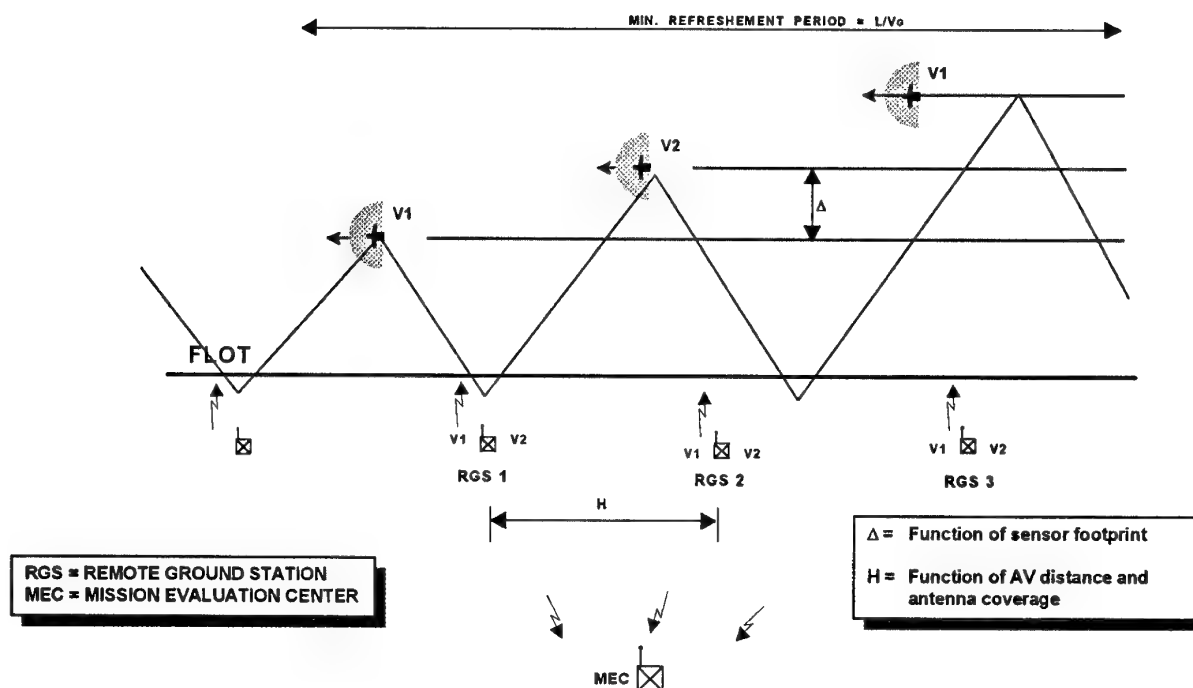


Fig. 14 - PERIODIC AREA SWEEPING

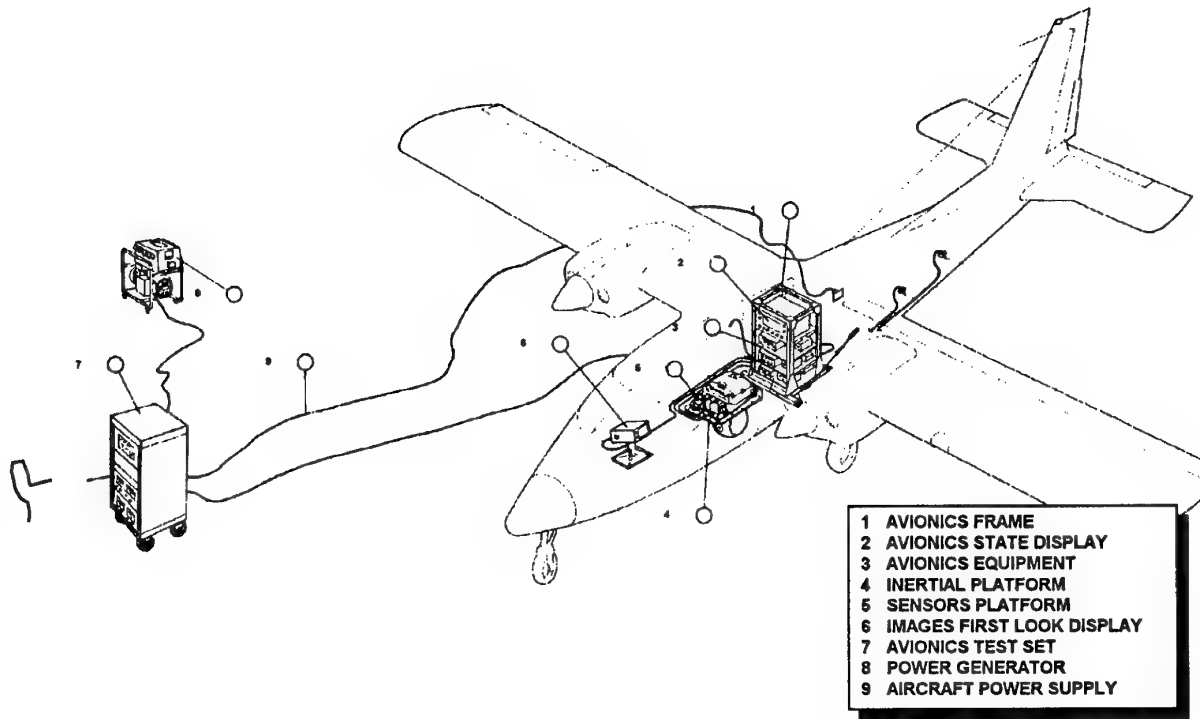


Fig. 15 - CAPTIVE FLIGHTS MANNED AIRCRAFT

ARMOR PROJECT - AUTONOMOUS FLIGHT CAPABILITY

P.Lourtie*, J.R.Azinheira*, J.P.Rente* and P.Felício#

*GCAR, DEM, Instituto Superior Técnico

Av. Rovisco Pais, 1096 LISBOA CODEX

#EST, Instituto Politécnico de Setúbal

R. do Vale de Chaves, Estefanilha, 2900 Setúbal

Portugal

1. Summary

Unmanned Aerial Vehicles have a definite potential for civilian observation and reconnaissance missions such as forest fire detection or coastal waters surveillance. For a decision to use such vehicles in significant numbers to be taken, once the adequate legal framework is defined, they must be easy to operate and low cost. The ARMOR project aims at developing such a vehicle. The ease of operation requires that the vehicle is sufficiently autonomous to perform most of the mission without the contribution of an experienced pilot. To achieve this degree of autonomy it must have a reliable Vehicle Management System (VMS) capable of dealing with both normal and anomalous situations. A structure for the VMS is presented and the work being done in fault detection is presented. The vehicle will have to be extensively tested, increasing progressively its complexity, starting with a simple guidance system and finishing with the full VMS. This means that the guidance system is one of the first to be developed. The work being done for this system is also presented. The guidance system has to be highly reliable but simple for low cost. For the types of operation envisaged, precision is not a very stringent requirement. As a whole, simplicity induces lower costs but also lower precision. One of the objectives of the work being done is to define the minimum amount of information on the flight path compatible with guidance system efficiency. Some of the results obtained so far are shown and discussed.

2. Introduction

The paper describes the work and options related to the Unmanned Aerial Vehicle being developed in project ARMOR, acronym for Robotized Aircraft for Observation and Reconnaissance Missions. The main objective of the ARMOR project is the design, construction and operation of an unmanned air vehicle for observation and reconnaissance missions. The typical applications envisaged for the vehicle are the early detection and report of forest fires, and the

surveillance of the national EEZ. This may allow a more regular and lower cost patrol of coastal waters, contributing to fisheries control and to prevent and detect smuggling, oil-spillage, etc. Military applications are also envisaged in a later stage [1].

This vehicle should be capable of autonomous flight, in the sense that a mission is loaded at the outset and the aircraft performs it until new instructions are received from the ground station. At all times, control may be regained by the ground station.

To achieve such a degree of autonomy, the vehicle must have the capacity for replanning the mission, if so instructed or if there is any external or internal event that requires it.

A general structure of a Vehicle Management System [2], accommodating for the different subsystems necessary to perform autonomous missions, has been defined. In this paper, emphasis is put on those subsystems that, at the moment, are the main object of the work of the Control and Robotics group of the ARMOR project: fault detection and guidance and control.

As the objective is to develop a low cost vehicle, an important trade off has to be reached between the degree of autonomy and the cost, and eventually weight, without sacrificing safety. Therefore, the on-board systems should be kept as simple as compatible with the desired autonomy features.

The implementation of the different subsystems will be done by steps and will undergo extensive testing: software simulation, hardware-in-the-loop testing and flight testing.

3. Vehicle Management System (VMS)

3.1 VMS Functions

In order to give the aeroplane the required degree of autonomy there is the need to provide it with special information acquisition, representation, and processing

capabilities. These are gathered under the name "Vehicle Management System" (VMS). The VMS functions are:

- To receive an initial plan of a mission;
- Command and monitor the execution of a mission;
- Monitor the state of the aeroplane and of its environment;
- Coordinate and monitor communications with the ground base;
- Decide and take adequate measures to deal with emergency or fault situations;
- Allow the operator on the ground to take control of the aeroplane;
- Register information and data of interest during the mission;
- Command the payload action and supervise all the systems inside the aeroplane.

3.2 VMS structure

Figure 1 shows a possible conceptual structure for the VMS. In the following a general discussion about each component of this structure is presented along with its relationship to the functions listed above. Note that the chosen structure is closely related to the VMS functions.

Two types of information processing systems inside the aeroplane are considered. Those which are internal to the VMS and the ones which are external to it. The chosen partition is shown in the figure. Its purpose is mainly to simplify the problem and to ease the management of the development teams. Outside the VMS we consider communications, navigation, sensors, auto-pilot and payload operation. These systems function as input and output information sources and destinations to the VMS shown in the centre.

3.3 VMS subsystems

Some of the VMS subsystems are described in the sequence.

3.3.1 External interface

The purpose of this interface is to allow the operators of the aeroplane to input mission data at the ground base before mission start. These include the mission plan, geographical data about the area where the mission is to be executed, etc. It also serves as a port for the output of reports at the end of a mission.

3.3.2 Mission management (MM)

This central part of the VMS is the one that integrates all the available data to decide about the continuation of the mission and to command the means that implement those decisions.

The type of missions to be accomplished by the aeroplane is an important aspect to be considered in the definition of this part of VMS. In an order of growing complexity we list the following mission types:

1. observation of fixed targets of known location
2. detection of fixed or slowly moving targets of unknown location
3. detection and recognition of fixed or slowly moving targets
4. detection, recognition and eventual following of mobile targets

To give the aeroplane the capability of executing these types of missions some essential features must be provided to the MM system:

- An "Executive command"
- A planning system.
- Availability and adequate representation of data and knowledge about the present situation.
- Adequate coordination of actions

Their complexity is conditioned by the type of missions to be accomplished and by the safety requirements for the aeroplane. The executive command must be able to command the execution of the current plan coordinating the trajectory and attitude of the aeroplane and the action of the observation systems. Also the control part of the MM must consider the outputs of monitoring and diagnosis, the navigation system, the sensors, and, in general, all the available information to decide if any emergency action or replanning is needed.

3.3.3 Monitoring and diagnosis (M&D)

During a mission the operationality of the aeroplane or the operational environment may change in ways that are important for the performance of the aeroplane or the observation systems inside it. The mission accomplishment or the safety of the aeroplane or the environment may be endangered. If it is possible to detect such changes in due time, their consequences may be avoided or minimised. The M&D system has the function of verifying the operational condition of the aeroplane and the state of its environment and, when adequate, to diagnose the causes of a detected problem. We note that the separation between the monitoring and the diagnosis is not always clear. When it is clear, there may be some advantage in separating the two functions. This is because diagnosis may not always be needed or as urgent as the taking of some corrective action.

The output of the M&D subsystem will be used, for example, by the mission management subsystem to:

- evaluate the feasibility of the actual mission plan in the present conditions,
- replan the mission

- change internal characteristics of controllers
- initiate emergency actions

3.3.4 Other components

Some of the VMS functions mentioned above were not directly associated to any of the components shown in the figure. These are the coordination of communications with the ground base, the various interfaces needed to the external systems. Adequate interfaces for information exchange between the VMS subsystems and between VMS and the external elements must be defined. Also the information representation inside the VMS must be carefully considered and defined. Aspects to be considered are the representation of each piece of information in ways that avoid repetition and ensure the coherence.

3.4 VMS Specification

The VMS will have to be able to give the aeroplane a reasonable degree of autonomy, allow it a good mission accomplishment level and satisfy the security constraints that will be imposed in the future to fly civilian missions. As such, its requirements and specifications must be carefully considered before any global successful implementation is to be tried.

Together with a detailed global and partial functional specification in a natural language we point towards the use of well structured real time system specification methodologies [3], [4] preferably integrated with the use of formal languages [5].

It is being considered to apply some techniques originally developed in the AI field to the functions of planning, guidance, monitoring and diagnosis in which they promise good results (see [6] and [7]). The integration of development techniques specific to this field like the "spiral development" with the specification techniques mentioned above will be considered.

Note that before such a detailed specification is feasible a lot of preliminary work has to be done.

4. Monitoring and Diagnosis (M&D)

There are several types of knowledge about one device that may be applied to its diagnostic [7]. By instance, they may be identified as relating to structure or connectivity, behaviour, function, and compiled knowledge. The latter is based on rules obtained from experience in previous diagnostics or from use of the other types of knowledge. Depending on the available types of knowledge, different methodologies may be used for diagnosis.

In a system like the M&D included in the VMS there is the need to include and integrate different types of methodologies.

Work has been done in the application of model based methods and of rule based methods of diagnosis to the ARMOR project VMS. We have chosen to describe here some efforts and results in the application of model based methods for diagnosis to the longitudinal behaviour of the vehicle. They are intended also to alert for the type of preliminary work that must be done before a VMS may be completely specified.

4.1 Model Based Sensor Failure Detection

The sensor failure detection system developed uses a state space model of the longitudinal dynamics of the aeroplane. Five sensors are considered measuring horizontal speed, vertical speed, pitch rate, pitch angle, and altitude. For failure detection we use the analytical redundancy [8] in the model. A battery of Kalman filters [9] and [10], is used to generate redundant estimates of the state vector. Each Kalman filter generates a subset of the states of the system using as input the input of the system and the output of one of the sensors. In this way a set of estimates of each measure is generated allowing for comparison. If the estimates generated from one of the sensors disagree in a significant manner from the rest of the signals, the sensor may be faulty. The fact that the system is subject to nonmeasured atmospheric turbulence and that the measurements are noisy makes it difficult to decide when the discrepancy is "significant".

Figure 2 shows the detection system structure. In the figure, the process is replaced by a process model subject to atmospheric turbulence disturbances and noise. The process model is a linearised five state model of the longitudinal dynamics of the aeroplane where the fifth state is the altitude and is obtained by integration of two other states [11] and [12].

$$\dot{x} = Ax + Bu \quad (\text{Eq. 1})$$

$$y = Cx \quad (\text{Eq. 2})$$

The five output signals correspond directly to the states (the output matrix is the identity matrix).

Five Kalman estimators were used, all of them derived from the system model. Each one uses the input to the model and the output from one of the sensors to generate a subset of the system states that depend on the observability of the system from the measured signal. Equation 3 represents the measurements and equations 4 to 8 represent the estimates based on measures 1 to 5 respectively:

$$y = [y_1 \ y_2 \ y_3 \ y_4 \ y_5]^T \quad (\text{Eq. 3})$$

$$\hat{y}_1 = [\hat{y}_{11} \ \hat{y}_{12} \ \hat{y}_{13} \ \hat{y}_{14}]^T \quad (\text{Eq. 4})$$

$$\hat{y}_2 = [\hat{y}_{21} \ \hat{y}_{22} \ \hat{y}_{23} \ \hat{y}_{24}]^T \quad (\text{Eq. 5})$$

$$\hat{y}_3 = [\hat{y}_{31} \ \hat{y}_{32} \ \hat{y}_{33} \ \hat{y}_{34}]^T \quad (\text{Eq. 6})$$

$$\hat{y}_4 = [\hat{y}_{41} \quad \hat{y}_{42} \quad \hat{y}_{43} \quad \hat{y}_{44}]^T \quad (\text{Eq. 7})$$

$$\hat{y}_5 = [y_{51} \quad y_{52} \quad y_{53} \quad y_{54} \quad y_{55}]^T \quad (\text{Eq. 8})$$

As the system output matrix is the identity matrix, the system outputs may be directly compared to the state estimates. Each basic fault indicator is a difference between an individual state estimate and its corresponding measured output. In the present case, due to state observability conditions, to turbulence and to the noise levels considered, only a few of the possible indicators are actually used. The basic indicators used are:

$$\begin{aligned} \Psi_{12} &= |\hat{y}_{12} - y_2| \\ \Psi_{31} &= |\hat{y}_{31} - y_1| \\ \Psi_{32} &= |\hat{y}_{32} - y_2| \\ \Psi_{34} &= |\hat{y}_{34} - y_4| \\ \Psi_{41} &= |\hat{y}_{41} - y_1| \\ \Psi_{42} &= |\hat{y}_{42} - y_2| \\ \Psi_{52} &= |\hat{y}_{52} - y_2| \end{aligned} \quad (\text{Eqs. 9})$$

To augment the detection scheme sensitivity and robustness, composite fault indicators are formed as products of basic indicators sensitive to faults in the same instrument.

$$\begin{aligned} \eta_1 &= \Psi_{12} \Psi_{31} \Psi_{41} \\ \eta_2 &= \Psi_{12} \Psi_{32} \Psi_{42} \\ \eta_3 &= \Psi_{31} \Psi_{32} \Psi_{34} \\ \eta_4 &= \Psi_{41} \Psi_{42} \\ \eta_5 &= \Psi_{52} \end{aligned} \quad (\text{Eqs. 10})$$

Each composite fault indicator is then normalised to unity by dividing it by its majorant in the case of normal functioning in project conditions. Each η_i serves the detection of faults in one instrument.

The decision logic compares each of the normalised composite fault indicators with a predefined value generating a logical signal meaning the presence or absence of faults in one instrument.

One sensor is declared faulty if and only if its corresponding logical signal indicates a fault and none of the others do.

4.2 Project conditions

The longitudinal model of the aeroplane was linearised around a straight horizontal flight condition at the constant speed of 15m/s and an altitude of around 700m.

The atmospheric turbulence considered in the project was modelled using the Dryden model by a linear filter with white noise input and transfer function [13]:

$$W_g(s) = \frac{\sigma_{w_g}}{\sqrt{\pi \frac{u_0}{L_w}}} \times \frac{1 + \sqrt{3} \frac{L_w}{u_0} s}{\left(1 + \frac{L_w}{u_0} s\right)^2} \quad (\text{Eq. 11})$$

where w_g is the air vertical speed. The effect of the horizontal component of the atmospheric turbulence was neglected because its influence in the aeroplane model states revealed to be about ten times less important than that of w_g . The effect of atmospheric turbulence in the pitch rate was modelled by [11]:

$$q_g = -\frac{\dot{w}_g}{u_0} \quad (\text{Eq. 12})$$

The magnitude of atmospheric turbulence considered in the project corresponds to a situation between cumulus clouds and storm.

The noise considered to affect each of the measures is white Gaussian noise of null mean. A fixed standard deviation was chosen for each measure. Their order of magnitude is between 0.2% and 0.5% of the range of measures.

4.3 Selection of detection levels

To select the decision value a trade off between the objectives of sensitivity and a low rate of false alarms must be made. In the present case the trade off was done by using a set of failures which were considered sufficiently small and levels of atmospheric turbulence and disturbing noise considered sufficiently high. If, in the presence of those noise and turbulence levels, the system could detect all the failures in the set it would be considered satisfactory.

A set of six situations is considered, the first one is the absence of faults. The other five are a small fault in one of the five sensors.

Considering that normal operating conditions are less severe than the chosen project conditions, majorants were found for each of the composite fault indicators η_i by simulation of the operation during a period of 300s. The selected detection levels must be higher than this majorants. This tries to satisfy a part of the robustness objective, avoiding false alarms.

Subsequently the detection levels are set to values that allow the scheme to detect all the five project faults and identify the sensor in which they occur. Adjustments may be made in subsequent tests if the values show any inadequacy.

All simulations were 300s long and the considered faults occurred 150s after the simulation start. The project fault consists in the maintenance of the instrument

measure at its expected mean value from the 150s to the end.

The chosen detection values are shown in table 1, where η_{in} is the i^{th} normalised composite fault indicator.

Table 1:

Fault indic.	Detection level
η_{1n}	5.0
η_{2n}	5.0
η_{3n}	1.5
η_{4n}	5.0
η_{5n}	1.2

4.4 Tests and Results

The performance of the sensor failure detection and identification scheme was tested using computer simulation models under MATLAB SIMULINK.

Typically, a sensor failure will have one of the following effects:

1. fixed value measure identical to one of the end-of-scale values;
2. fixed measure at any value;
3. measured value gradually deviating from the real value of the measured signal (drift);
4. change in the instrument gain;
5. randomly wrong measurements.

Three groups of tests were prepared, where the detection and identification of faults from items 1-2, 3 and 4-5 were tested.

4.4.1 First group of tests

In the first group of tests, we include the normal functioning situation and two sets of faults. The first set contains the five project faults, one in each sensor at second 150. In the second set, five similar faults were considered occurring at the instant 90s in the simulation.

In the normal functioning situation no false alarm occurred and in all the project situations the faults were correctly detected and identified.

For the faults occurring at time 90s, only those on sensors 2, 3 and 4 were correctly detected and identified. This is because the project faults are quite soft, corresponding to the maintenance of the measure at the value that the measured variable would have at the working point around which the simulation is being done. Such a fault is only detected when the disturbances are big enough, which was not the case at second 90.

4.4.2 Second group of tests

In this group we include two sets of tests where a linear drift is introduced starting at time 90s in one of the sensors. In the first set the drift causes a deviation of 1/4 of full-scale value after 100s. In the second set the deviation of the measure 100s after the drift start is 1/8 of full-scale value.

All faults in this group were correctly detected and identified, the faults in the second set taking a little longer than the faults in the first set.

As an example, we present graphically in figure 3 the results for the faults in sensor 2, in the first and second sets. These are respectively faults 12 and 17.

4.4.3 Third group of tests

In this group we include the detection of faults corresponding to the raise in the noise affecting one of the measures or to a change of gain on one of the instruments.

Although the augmented noise level was detected for some sensors, statistical indicators [14] would give better results.

The gain change in one of the instruments was correctly detected and identified for the various instruments.

As an example, we include the results of two tests in figure 4. Fault 23 is a 25% raise of the gain of instrument 1. Fault 24 is a 25% raise in the gain of instrument 3.

4.5 Conclusions

The proposed system for sensor fault detection and identification works within the project assumptions. These include that the system is in the operating point to which it was conceived. Future developments must include ways to cope for the nonlinearity of the aeroplane model.

The presented fault detection system is just a part of a wider monitoring and diagnosis system that will integrate other techniques and methods.

5. Guidance System

The guidance system is essential for the vehicle to be able to perform autonomous missions. It will have to be tested and operational before more advanced features of the VMS are flight tested.

It is an objective to keep it as simple and robust as possible, requiring the minimum amount of information for the definition of the flight path that is compatible with the performance required to execute the mission.

5.1 Route planning

The objective of route planning is to provide the guidance system with a well defined and executable flight path. The mission will begin by being described as a set of tasks, such as observation of a certain area, follow a given flight path, loiter above a given point, follow a moving object, etc. The mission tasks may be discrete, in the sense that between the different tasks there may be displacements that are not specifically defined at the beginning, as they are only required to take the vehicle from one point to the other. The tasks may not demand a well defined sequence or timing [15].

From this level of definition, given a set of constraints concerning time, available airspace, vehicle range, etc, a well defined sequence of activities, continuous in time, should be defined.

Finally, this sequence of activities must be translated into a flight path that is not only continuous in space and time, but also executable by the vehicle taking into account its capabilities, such as the rate of climb, the minimum turning radius, etc. The guidance system will then be provided with a flight path associated with additional information of speed and the control mode to be used.

The flight path is decomposed into a ground projection and altitude. For the project aircraft, the ground projection is considered to be defined as a sequence of path segments, each one consisting of a straight line or a circular arc segment.

In what follows only the ground projection or horizontal trajectory will be discussed.

The horizontal trajectory segments are defined using five variables:

- P_i - the coordinates of the initial waypoint of the path segment;
- P_f - the coordinates of the final waypoint of the path segment;
- r - the radius of the turning circle, the sign indicating direction of rotation and $r = 0$ indicating that it is a straight line;
- P_c - the coordinates of the centre of the circle;
- n - an integer containing information on the number of complete circles to perform before entering the next path segment.

In general, two sequential segments of the route make an angle at the waypoint common to them. Although the guidance system designed can cope with very important angles, as shown in the simulations below, limits to this angle or a blend segment will be introduced. The blending between two sequential segments is done at present by using the next flight path segment as reference when the distance to the next waypoint is less than a given value ϵ .

The work being done at present aims at testing the limits of the guidance system, so that the limits to flight path generation are established. Once these have been achieved, the automatic generation of the flight path from the sequence of activities may be developed.

5.2 Guidance controller

The guidance system will produce the references to the auto-pilot, given the errors between the reference flight path and the actual position (track distance error), on the one hand, and, on the other, between heading of the reference flight path segment and actual heading of aircraft (track heading error). For circular segments, a feedforward of the heading rate is also used.

For the aircraft being designed two different lateral auto-pilot modes are being considered, that differ in the turning attitude: roll control mode and side slip control mode. The first one, the roll control mode, will be the normal mode when there are no special requirements for the lateral attitude of the aircraft.

In side slip control mode the aircraft will perform turns with a minimum of roll angle and, therefore, may be used in observation tasks that would be perturbed by rolling movements and roll angles being applied to the pay-load.

5.3 Guidance controller design

Let us then consider the horizontal trajectory, without time constraints and let us assume that air speed is maintained constant.

The guidance controller will be designed to control and reduce the track distance between the defined trajectory and the actual position of the aircraft, issuing a correcting command for the auto-pilot lower level controller in terms of yaw rate demand as shown in figure 5.

The trajectory model used describes the response of the aircraft as a fourth order system and covers both the two segment types and the selected operational auto-pilot modes. The track distance (d) and track heading error (α) are estimated from the navigation output (GPS data) as compared to the flight path sequence, namely to the relevant segment followed at a given moment.

The trajectory error response to yaw demand may be approximated by a linear system and expressed using the state space formulation (Eq 1), where $x = [x_1 \ x_2 \ d \ \alpha]$ is the state vector, u is the yaw rate demand,

$$A = \begin{bmatrix} -2.24 & -2.56 & 0 & 0 \\ 1.00 & 0 & 0 & 0 \\ 0 & 0 & 0 & 17.0 \\ -3.84 & 2.56 & 0 & 0 \end{bmatrix} \quad \text{and} \quad B = \begin{bmatrix} 1 \\ 0 \\ 0 \\ 0 \end{bmatrix}$$

The controller design will obey to the typical robust objectives of a good tracking at low frequency and noise rejection at higher frequencies.

Obviously, the resulting controller has to be robust enough to tolerate:

1. the different characteristics of the two segment types,
2. the different response of the A/P modes and other structured model uncertainties over the whole flight envelope,
3. wind unmodelled disturbances, would it be a constant or a turbulent wind,
4. GPS specific awkward features, namely its poor instantaneous accuracy and its slow output rate
5. other model uncertainties, measurement and process noises

Furthermore, to avoid any extravagant and acrobatic command the yaw rate demand is limited to 45 deg/sec.

Finally, the guidance controller has to be implemented in the general purpose microprocessor to be used in the UAV, along with the navigation and track distance/heading error estimator. The estimation process is carried out with the GPS 1 Hz rate and the operations involved are time demanding. To reduce computer burden, the controller should be as low order as possible.

The guidance controller was designed using a H_∞ mixed sensitivity methodology [16], [17] and [18]. The design specifications are expressed in terms of weighting curves (W_1 , W_2 and W_3) to shape the sensitivity functions, respectively sensitivity S , actuator sensitivity R and complementary sensitivity T .

The weighting curves used are presented in figure 6.

The sensitivity function W_1 models the tracking specification and results in a low pass filter, with high gain at low frequencies and low gain, but impossibly zero, at high frequencies. The filter was chosen to be of second order to yield a high enough gain: final gain is above 120 dB.

The complementary sensitivity function weighting W_3 is a high pass filter and shapes the high frequencies for good robustness, along with the constraint derived from $S+T=I$.

The actuator sensitivity function weighting W_2 is a high pass filter (first order) which restrains demand amplitude at low frequencies (10 dB) and cuts high frequency demands.

The result is a system of seventh order shown in figure 7, with an adequate sensitivity curve (as shown in figure 8), in accordance with expectations.

5.4 Auto-pilot controller

The auto-pilot was also designed using a robust control methodology. This was assumed to be the best approach, considering the existing uncertainties due to:

- varying weight and mass distribution during long missions;
- low speed and significant gust influence on speed variations and attitude;
- low cost and, therefore, low precision instrumentation;
- non-linearities and coupling between lateral and longitudinal behaviour;
- relative poor precision of the GPS data;
- simplified controllers and low sampling rates.

The objectives of the auto-pilot (or inner loop) controller is to allow for a good heading rate tracking independently of the operational mode, either in a very precise and piecewise manner for observation purposes or in a more usual cruise flight, with endurance objectives.

For the fourth order lateral linear model these objectives are well expressed as a tracking and decoupling of side slip and roll.

Both modes guarantee a good heading rate response as shown in figure 9

5.5 Simulation

As a first test of the global solution, a software simulation of the guidance behaviour and flight path control was performed in MATLAB SIMULINK. Both controllers were introduced in discret form, with sample rates of 10 Hz and 5 Hz, respectively for the auto-pilot and the guidance controller.

GPS data, with a period of one second, were simulated through the addition of a noise component with approximated characteristics of actually received differential GPS data (10 m rms), a sample shown in figure 10.

The guidance behaviour was tested in the absence and in the presence of wind, with a constant wind of 5 m/s and a turbulent component of 3 m/s – to be compared with the model constant air speed used of 17 m/s.

Two trajectories are shown. The first one, in figure 11, corresponds to an observation mission and only involves straight line segments. The second, in figure 12, a stationary path (race course) for communications relay or a fixed point observation, includes straight lines and circular segments. The two control modes were considered for both trajectories.

Figure 11 demonstrates the stable behaviour of the guidance controller, independently of wind conditions and A/P modes.

The race course trajectories and track error (figure 12) show the influence of wind and of GPS inaccuracy.

5.6 Conclusions

A simple flight path definition and guidance method has been designed, aiming at the robustness of the system and particularly at:

- an easy route planning of a typical mission,
- a good behaviour with two different operational modes (or A/P controllers),
- stability in the presence of constant wind or turbulence.

The software simulations demonstrate a fair result in trajectory following, mostly dictated by the quality of GPS data.

Further simulations and tests are under preparation, to analyse and improve the system before entering the flight test phase.

6. Final remarks

The objective of the ARMOR project is to design a low cost, light UAV, capable of performing autonomous missions. It has to be kept simple, for low cost and low weight, but safe and reliable. Simplicity may also be an argument for reliability.

The vehicle is required to detect and react to occurring internal faults and the problem of obstacle avoidance, both static and dynamic, will have to be considered.

A general structure for a Vehicle Management System (VMS) has been proposed and the work on a Monitoring and Diagnosis System was presented. The results of the design of the guidance and auto-pilot systems was shown.

Extensive software, hardware in the loop and flight testing will be performed to develop the final system configuration. Flight tests will begin with a simple guidance configuration, increasing its complexity by progressively adding new VMS functions.

7. References

1. Brederode, V., "ARMOR - The Portuguese UAV Program", UV94, Paris, 1994
2. Felicio, P., "Sistema de Gestão Central de uma Aeronave Robotizada", Instituto Superior Técnico, Lisboa, MSc Thesis, 1995
3. Braek, R. and Haugen, O., "Engineering Real Time Systems", UK, Prentice Hall Ltd, 1993
4. Hatley, D.J. and Pirbhai, I.A., "Strategies for Real Time System Specification", New York, USA, Dorset House Publishing, 1987
5. Ince, D.C., "An Introduction to Discrete Mathematics, Formal Specification, and Z", Second Edition, Oxford University Press, 1992
6. AGARD Working Group 11, "Knowledge Based Guidance and Control Functions", AGARD AR 325, January 1995
7. Milne, R., "Strategies for Diagnosis", IEEE Transactions on Systems, Man and Cybernetics, Vol SMC-17 No 3, June 1987
8. Chow, E.Y. and Willsky, A.S., "Analytical Redundancy and the Design of Robust Failure Detection Systems", IEEE Transactions on Automatic Control, Vol AC-29 No 7, July 1984
9. Kalman, R.E., "A New Approach to Linear Filtering and Prediction Theory", Transactions ASME, Series D, 83, 1960, pp 35-45
10. Brawn, R.G. and Hwang, P.Y., "Introduction to Random Signal and Kalman Filtering", Second Edition, New York, USA, John Wiley & Sons Inc, 1992 (ISBN 0 471 55922 9)
11. Nelson, R.C., "Flight Stability and Automatic Control", USA, McGraw Hill Inc, 1989 (ISBN 0 07 046218 6)
12. Rente, J.P., "Modelação e Análise do Comportamento Dinâmico de duas Aeronaves Não Tripuladas", Instituto Superior Técnico, Lisboa, MSc Thesis, 1995
13. Lourtie, P., Rente, J.P. and Azinheira, J.R., "Análise do Comportamento e Controlo Longitudinal de uma Aeronave Não Tripulada", Controlo 94, Portugal, Vol 1, 1994, pp 17-24
14. Tzafestas, S.G. and Watanabe, K., "Failure Detection and Identification for Dynamic Systems, Statistical Approaches", New York, USA, Marcel Dekker Inc, 1993, pp 3-44 (ISBN 0 8247 8800 1)
15. Kolitz, S.E. and Beaton, R.M., "Overall System Concepts in Mission Planning", AGARD LS 192, October 1993, Paper 1
16. Doyle, J.C., Francis, B. and Tannenbaum, A., "Feedback Control Theory", New York, USA, Macmillan Publishing Company, 1992 (ISBN 0 02 330011 6)
17. Chiang, R.Y. and Safonov, M.G., "Robust Control Toolbox", The MathWorks Inc, 1988
18. Lourtie, P., Azinheira, J.R. and Rente, J.P., "Analysis and Simulation of the Longitudinal Control of an Unmanned Aerial Vehicle", IEE Colloquium on Control and Guidance of Remotely Operated Vehicles, London, June 1995, Paper 8

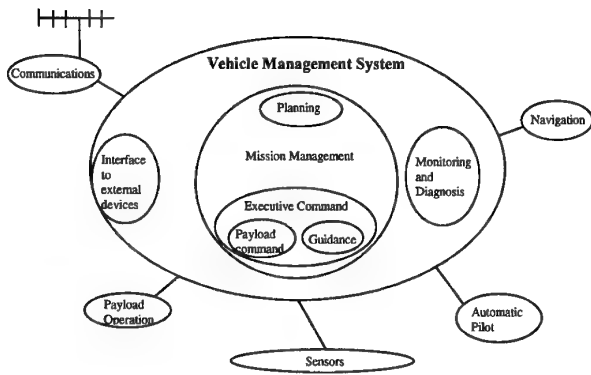


Figure 1

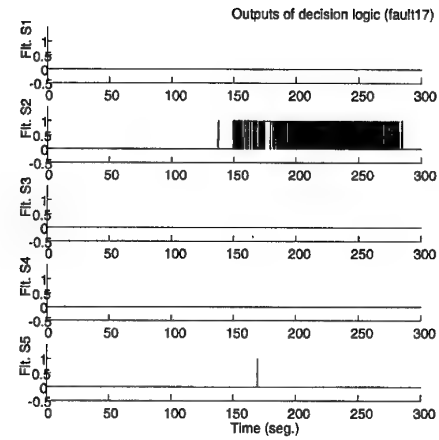


Figure 3b

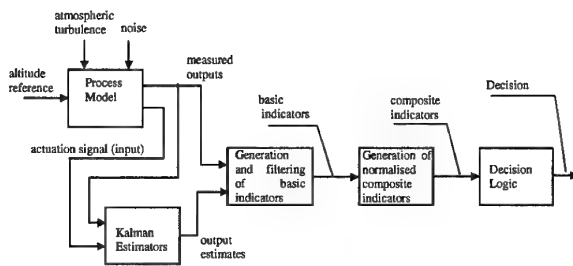


Figure 2

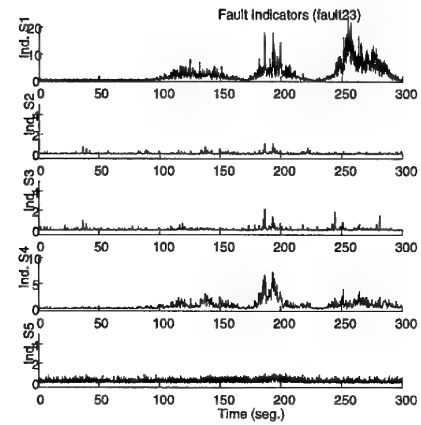


Figure 4a

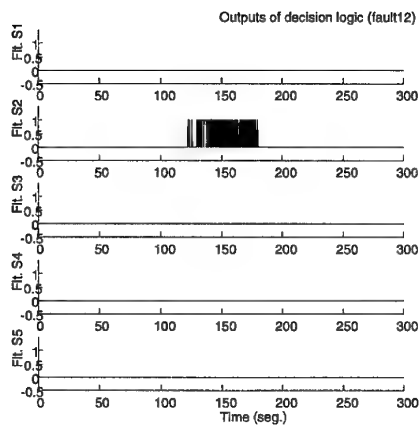


Figure 3a

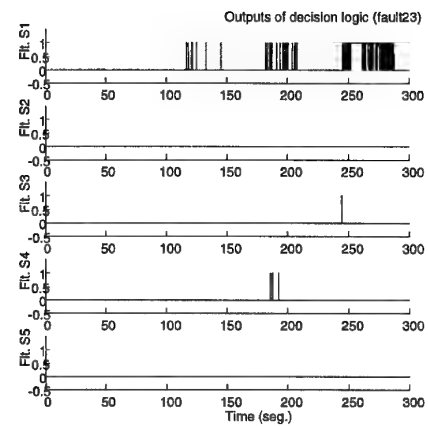


Figure 4b

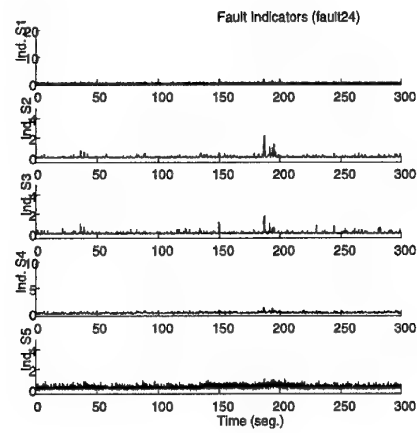


Figure 4c

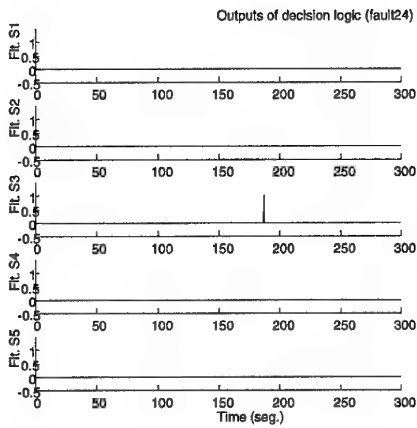


Figure 4d

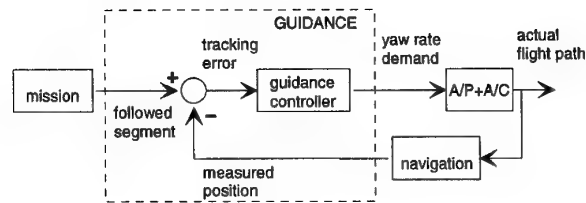


Figure 5

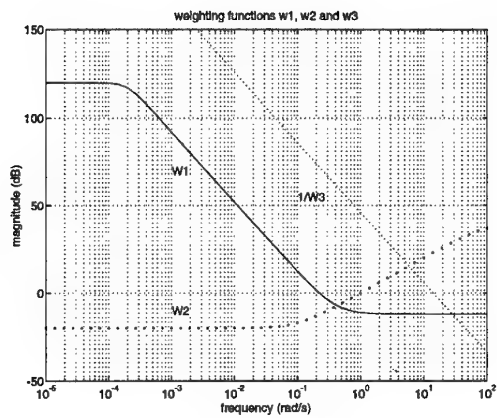


Figure 6

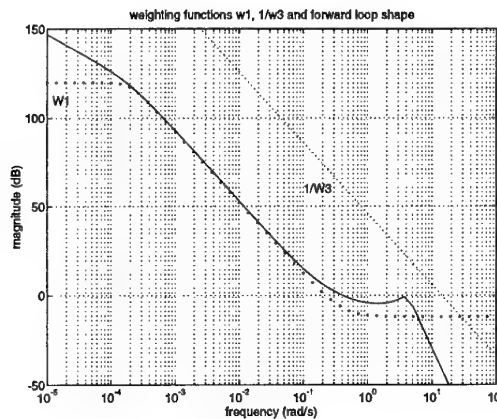


Figure 7

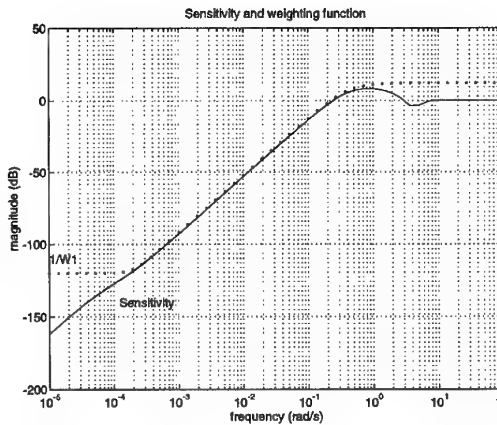


Figure 8

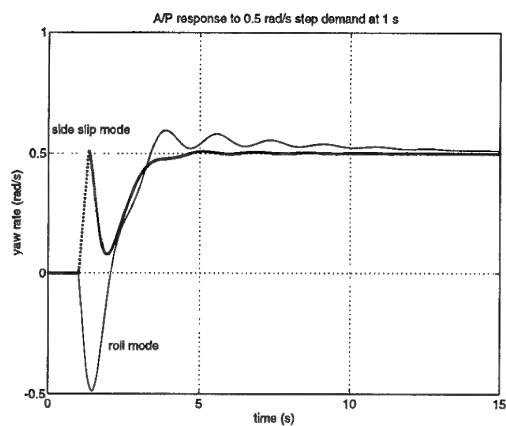


Figure 9

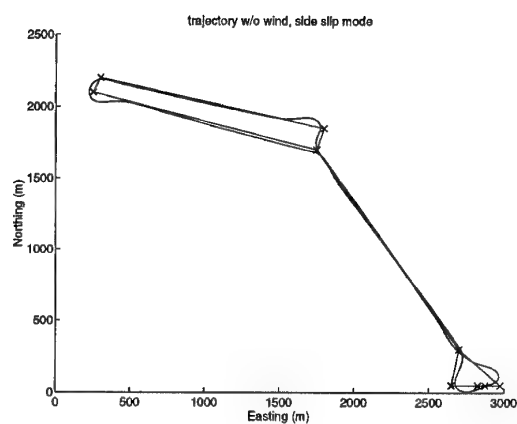


Figure 11b

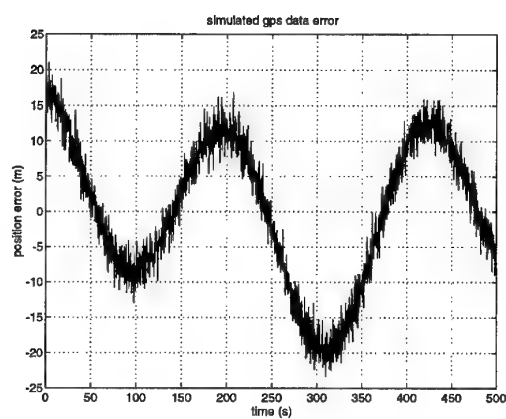


Figure 10

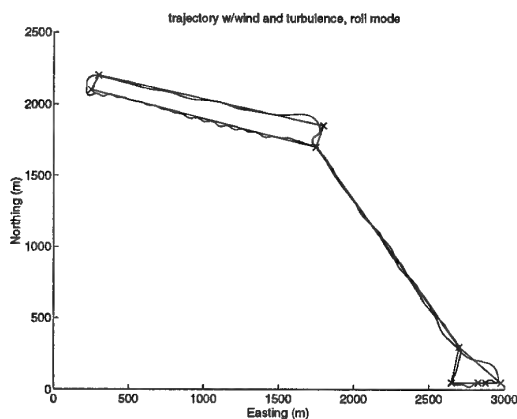


Figure 11c

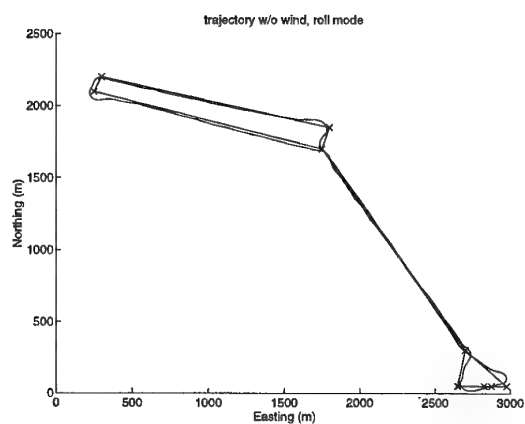


Figure 11a

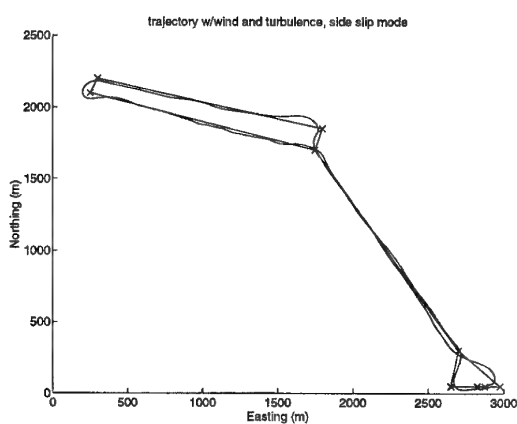


Figure 11d

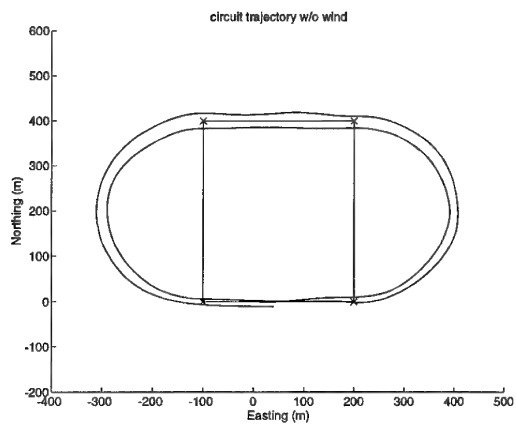


Figure 12a

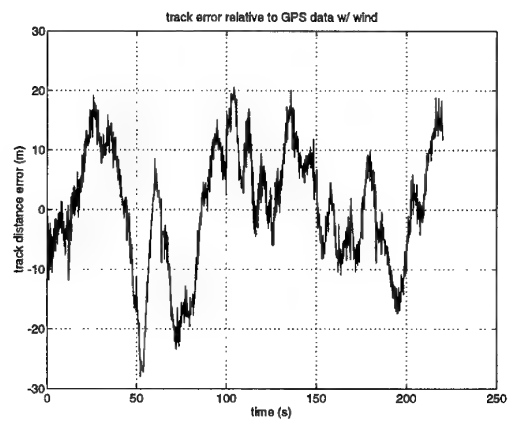


Figure 12d

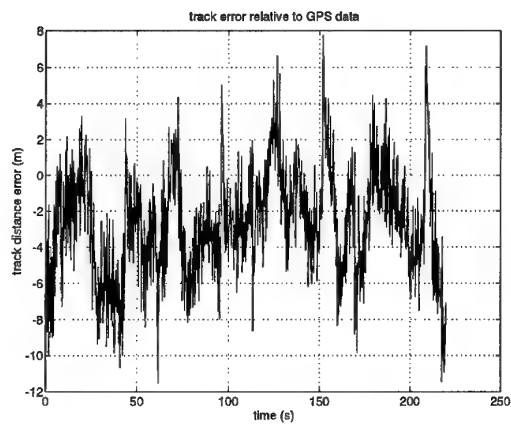


Figure 12b

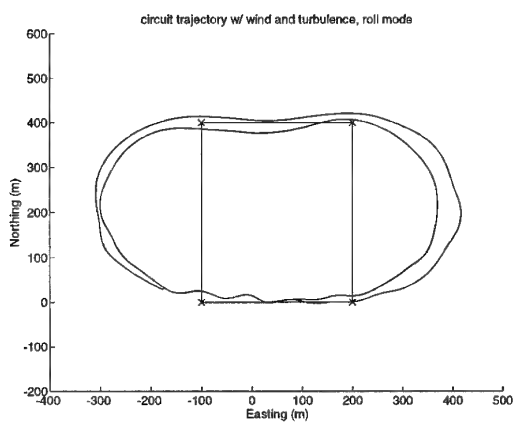


Figure 12c

The Marvel Maritime UAV *

Jean-Francois Pelous

Advanced Studies Division, Matra Defense, Velizy-Villacoublay, France

Jewel B. Barlow

Glenn L. Martin Wind Tunnel, University of Maryland, College Park, MD 20742-3215

1.0 Summary

In the first part, we review the essential requirements for a UAV system marine use. Then, we present some of the specific Freewing Tilt-Body MARVEL aerodynamic characteristics and a short description of the landing system equipment used during the ship deck approach.

2.0 Introduction

After having developed UAV programs for the Army, Matra Defense is currently interested in the possibility of putting a UAV system on board ships having a helicopter platform.

3.0 Maritime Requirements

UAVs, or more specifically heavier-than-air light craft with piston engines, are increasingly used in combat whether as a surveillance means or in electronic warfare.

The Navy has long been a high seas force capable of insuring the safety of maritime routes, of strategic importance for supplies and logistical support essential in case of generalized conflict. Since then, the Naval forces have seen their main action areas get closer to shore, whether to monitor maritime traffic (e.g. embargo on a country), to participate in the launch and/or recovery of troops, to share in protecting units in a context of intervention, insertion or to help friendly countries. These

international missions are made in addition to the still common missions of territorial waters surveillance and national interest protection. The naval units that are part of this deployment range from a carrier group down to a simple surface craft like a frigate or even a patrol boat. The first requirement in all these missions is surveillance of the space around the naval force. This surveillance may need to be made over a hundred kilometers with varying time on station requirements according to the mission, from a very short period for target recognition to a very long duration for the surveillance of hostile coasts. It is presently done with piloted aerial means, helicopter or aircraft. To use UAVs instead gives a continuity in the case of long duration missions and an increased safety in the case of recognition of potentially threatening targets. Independently from the mission itself, the UAV system must respond to constraints that are specific to a maritime use and that have to do with the aerial segment and the surface segment.

The surface segment includes two main elements: (i) the Mission Planning and Control Station (MPCS) in charge of mission planning, of flight follow up and control, of resource management, and of processing the mission results and (ii) the landing system intended to help the UAV approach and recovery of the aerial vehicle once it is on board the ship. The MPCS needs to be integrated or at least to interface with the command system of the ship so that it can track all data pertinent to the ship's environment (e.g. weather, tactical situation, approach paths) and to be able to give in return information related to the UAV flight profile so as to insure, for example, safe integration of the UAV in the local ATC system. The UAV arresting and capture gear must have minimal impact on the ship configuration. It should therefore be set up

* A French version of this paper follows at Section 24b.

and taken down easily and quickly. The aerial segment also includes special constraints for it to be used on a naval platform. The first constraint is the personnel that will implement the system. The personnel should not be specialized (for example no pilot). The qualifications of the pre-existing shipboard personnel should be sufficient for using, maintaining and repairing the system. Another constraint has to do with the ship and its route. It is out of the question to stop the ship for recovery operations. It is also out of the question to launch one or several rafts or to use a helicopter to lift a UAV that would have fallen at sea in a regular recovery scenario. The only routine concession possible would be a maneuver to position the ship in such a way as to insure the appropriate wind conditions for recovery.

All those requirements and constraints call for a UAV system:

- that can be integrated or interfaced with the existing systems on board a ship with the least modifications to its superstructures,
- that can fly quickly to the area of interest,
- that can stay there for a maximum period of several hours,
- and that can be recovered in an autonomous way on a naval platform.

The response of Matra Defense that will be explained in the rest of this document is based on the aerial platform MARVEL (designed by Freewing Aerial Robotics Corp.) with a landing system based on a laser technology. Payloads were not part of this study since a good number of them have been developed already for land based UAV systems.

4.0 Description of the Aerial Platform

The MARVEL drone includes two complementary innovations: the freewing and the tilt-body. The freewing means that the wing of the

UAV is linked to the fuselage in a manner that allows it to rotate freely around the pitch axis. The wing is therefore decoupled from the movements of the fuselage and positions itself in the relative wind like a weathervane. This makes it practically impossible for the wing to stall aerodynamically and it provides a strong decoupling between the response of the freewing and that of the body with regard to vertical aerodynamic turbulence and thereby reduces significantly the effect of turbulence on the body, giving an inherent stability to the payload. References 1 and 2 give some background on freewing aircraft for ultralight applications. Figures 1, 2, and 3 show the MARVEL configuration for cruise flight. Figure 4 shows a range of body tilt angles relative to the tail boom. Figure 5 shows an image of a wind tunnel model of the MARVEL in the University of Maryland's Glenn L. Martin Wind Tunnel. Characteristic data for the MARVEL is shown in Table 1.

TABLE 1. Characteristic Data of the MARVEL Vehicle

Total length, body tilt = 0	3.6 m
Total span	4.9 m
Body length	1.8 m
Maximum take off weight	177 kg
Power (Rotax 503)	50 hp
Maximum speed	80 m/s
Minimum landing speed	15 m/s
Endurance	4 hours +
Total Length, body tilt = 50	3.0m
Center body width	1.3 m
Empty weight	117 kg
Maximum body angle	55 degrees
Cruise speed	50 m/s
Minimum takeoff speed	11 m/s
Rate of climb	11.7 m/s
Ceiling	5000 m

The wing angle of attack with regard to the relative wind and thus the wing's lifting power is controlled by elevons on the trailing edge of the wing. Additional longitudinal control is provided by the throttle setting the propeller rotation rate and the angle of the body relative to the boom as indicated in Figure 4. Control in pitch is done by

setting the body angle relative to the boom and then making relative adjustments with the elevons and the throttle. The decoupling between wing and fuselage allows the fuselage to be at any angle without changing too much the wing lift values. The tilting of the body results in a vectoring of the propeller thrust which shares in the total lift of the aerial vehicle. This is what allows the share of the lift that is produced by the freewinging to be reduced and therefore to reduce the aerodynamic speed of the UAV down to approximately 12 to 15 meters per second. This same fact is what makes it possible to descend at steep slopes (beyond 45 degrees) and at a slow speed while keeping the platform perfectly under control.

The lateral control is achieved by differential deflections of the elevons on the wings. The vehicle is autostable in yaw and does not have a deflectable rudder control. The lateral dynamics are essentially the same as for fixed wing vehicles.

A prototype of the above description has had several dozen hours of flight time in the Mojave desert in California. Numerous wind tunnel tests have permitted refinement of the aerodynamic configuration of the MARVEL. Due to the fact that the propeller is in a tractor position, the air flow generated goes over the body and wing root. This generates strong nonlinearities which are increased by the high angles of attack that the body of the UAV can have in a tilted position. A brief description of some aerodynamic properties is provided here.

Figures 6, 7, and 8 show the lift coefficient variation with body angle of attack for boom angles of 0 degrees, 30 degrees, and 50 degrees respectively, all with a small fixed elevon angle, and with curves for three thrust coefficients. More details of the aerodynamic properties are given in Reference 3. It is instructive to consider the variation with thrust coefficient as well as with angle of attack. The equilibrium angle of flight will be approximately at an angle of attack equal to the boom angle. At the 0 degree boom angle the flight behaviour is somewhat like a conventional aircraft insofar as its response to a throttle change. Note that in this case the lift coefficient is not strongly coupled to the thrust coefficient. However, in the 30 degree and 50 degree cases the lift coefficient is a very strong function of the thrust coefficient

which is intuitively proper and reflects that the throttle is a powerful flight path control at high body angles.

An indication of elevon effectiveness is given by the data of Figure 9. This shows that the elevons give expected lift changes. Figure 10 shows the effect of elevons on pitching moment coefficient. Figure 11 shows an example of pitching moment variation with angle of attack and thrust coefficient for a boom angle of 30 degrees.

The piloting of the MARVEL UAV is not traditional due to the freewinging and the tilting of the body. There are four controls. These are: deflection of elevons in unison for wing lift control, deflection of the elevons differentially for roll control, engine speed control for setting thrust level, and body angle control to select the general flight regime. The elevon angle controls are the highest frequency controls followed by engine control at a somewhat slower rate, and finally the body angle is a very low rate control which may be considered as a trim control on a conventional aircraft.

5.0 Landing

Landing is the most delicate phase of the whole flight envelope for the UAV. Following its own means of navigations (GPS for example), the UAV gets to the entry point of the landing phase. The UAV is in tilt body position and has thus taken reduced its aerodynamic speed down to approximately 15 m/s. The UAV is then taken over by the landing system that will take it to the waiting area.

The landing system that we will describe is similar to an ILS system for civilian airports. An ideal approach axis is defined by the central axis of a laser beam encoded with space and time data (laser pattern). The encoding is made with an acousto-optical modulator (time domain) that will give pulsed trains and a mechanical rotating modulator (space domain) in the focal plane. Each point of the beam represents a point on the mechanical modulator. This beam includes a grid of 40 x 40 squares that has a distance code with regard to the center of the beam, with a resulting accuracy of less than one meter. The beam is generated by a laser source of 10.6 microns wavelength and a

power of less than 20 watts, assuring that the landing system is compatible with the use of the UAV. The beam is stabilized by a gyroscopic platform (stabilization is better than 0.6 mrad) and takes into account the motion of the ship.

So that it can decode the information received, the UAV has on board a detector and its associated electronics, the weight of which does not exceed 250 grams for a very small space requirement (a cylinder 40 mm in diameter and 100 mm long).

The guidance law has sensitivity inverse to the distance from the landing (from beam emission point). This law tends to cancel the distance variation, giving an acceleration proportional to the position deviation from beam center, and includes differential and integral terms so as to correct the errors due to angular speed and acceleration. Accelerations perpendicular to the beam axis are controlled by commands for acceleration sent to the UAV and then converted to control instructions for pitch and roll.

The beam will bring the UAV into a waiting area where it will stay until the ship movement gets relatively quiet. At that time the UAV receives the instruction to land and comes down on the ship deck. Arrest and capture gear prevents the UAV from moving. This device can be a metallic net stretched a few centimeters above the deck in which the landing gear of the UAV gets enmeshed.

6.0 Conclusions

In this system, the UAV prototype already exists and has flown several dozen hours. A scaled prototype of the landing system exists and its performance has been demonstrated. The development of the algorithms for guidance and control for the crucial phase of landing has started, and that of the arrest and capture system will start soon. The algorithms for control and guidance as well as the specifications for ILS-type equipment and servos will be available in 1996.

REFERENCES

1. Chen, W. & Barlow, J.B., "Stability, Control, and Gust Response Characteristics of an Ultralight Freewing Aircraft", AIAA-92-4342, Atmospheric Flight Mechanics Meeting, Hilton Head, SC, August 10-12, 1992.
2. Chen, W. & Barlow, J.B., "An Ultralight Freewing Aircraft Design Study", AIAA-92-4194, AIAA Aircraft Design System Meeting, Hilton Head, SC, August 24-26, 1992
3. Chen, W. & Barlow, J.B., "An Unmanned Tilt-body Freewing Vehicle Powered Wind Tunnel Test", AIAA-95-1902, 13th AIAA Applied Aerodynamics Conference, San Diego, CA, June 19-22, 1995

Figure 1. Top View of MARVEL

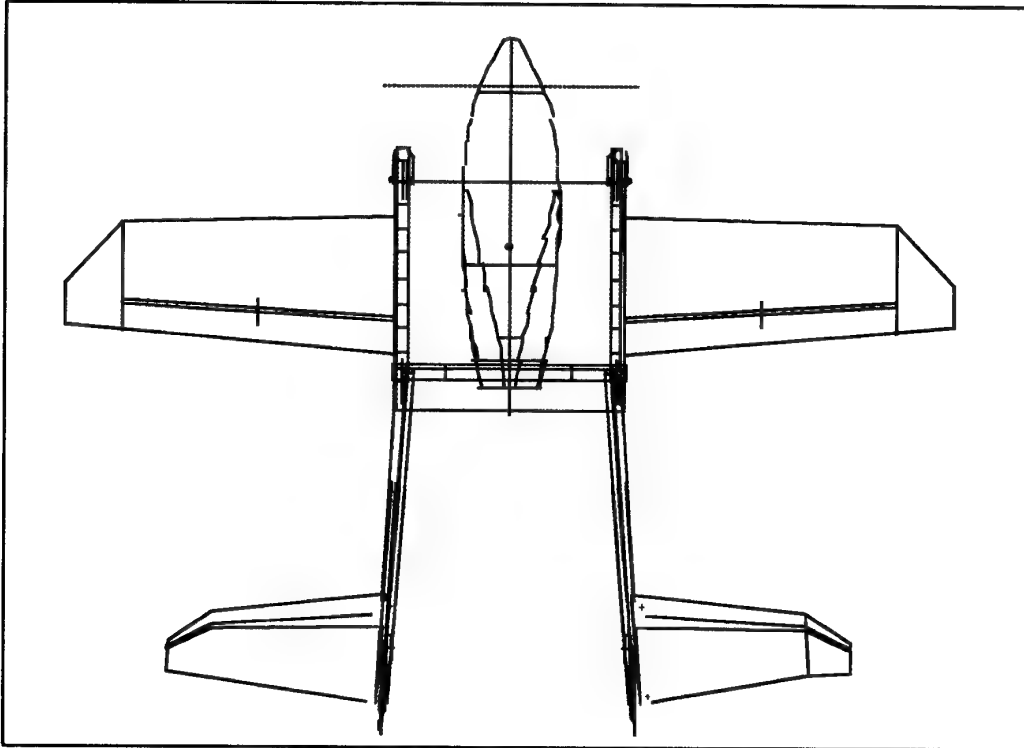


Figure 2. Front View of MARVEL

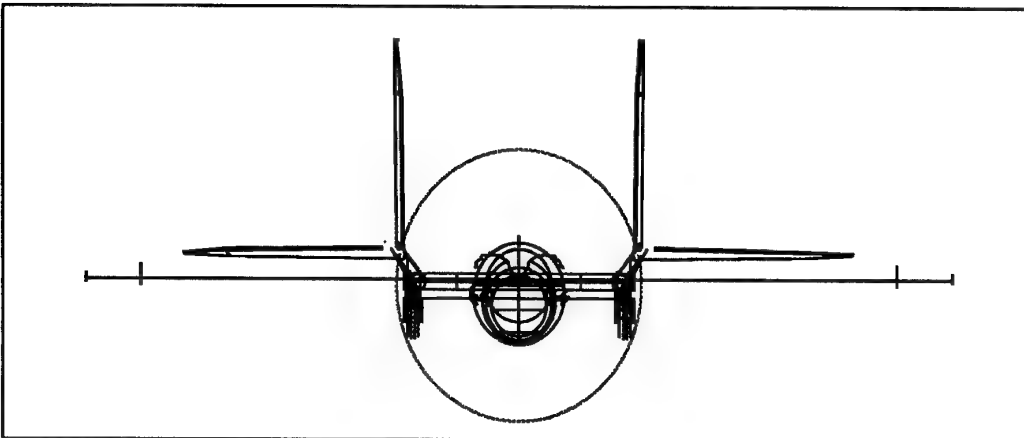


Figure 3. Side View of MARVEL

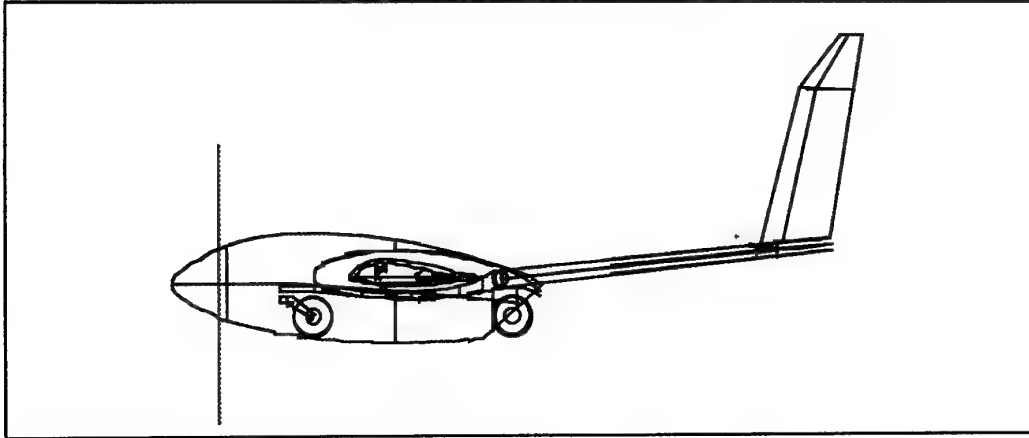


Figure 4. MARVEL at Several Body Angles

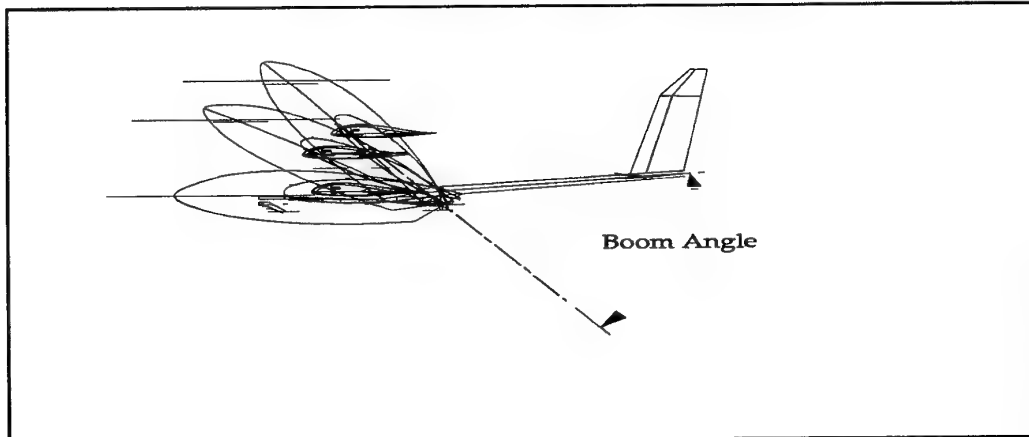


Figure 5. MARVEL Wind Tunnel Model

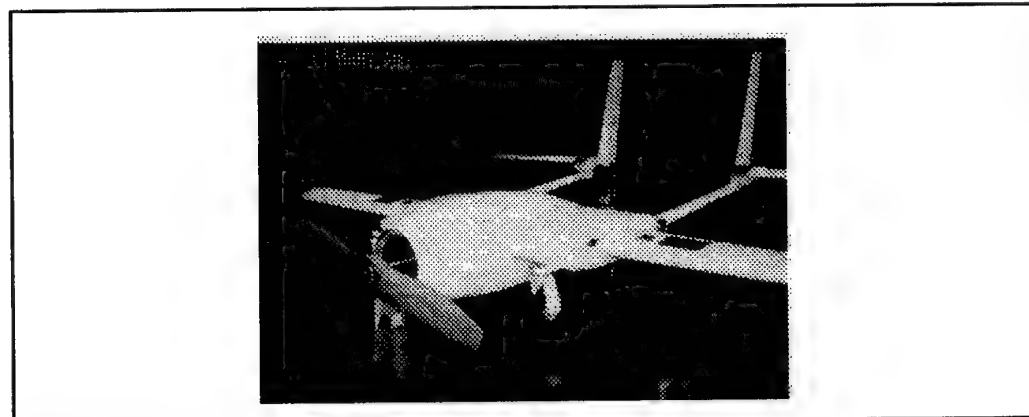


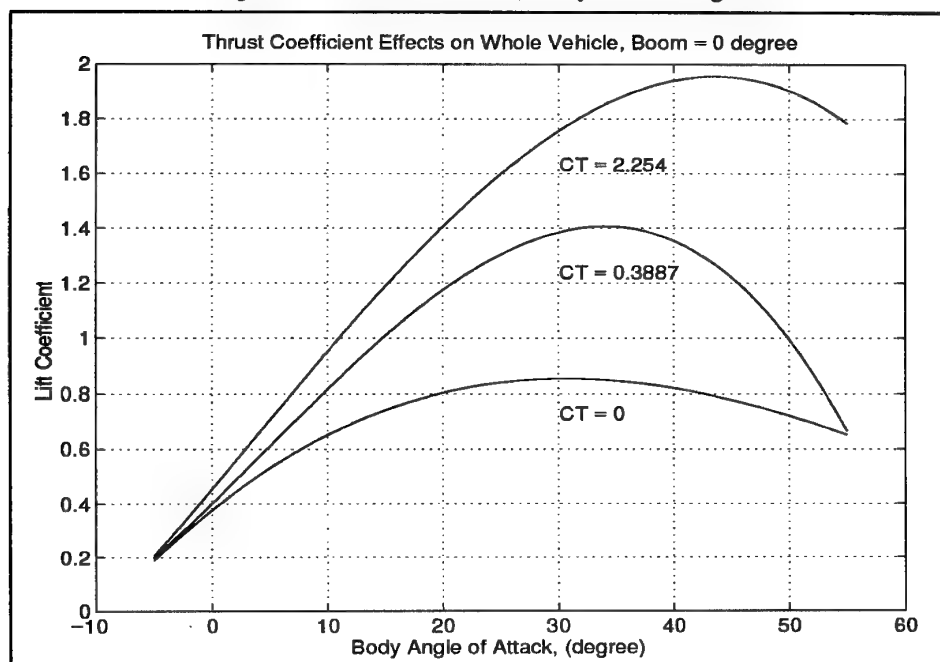
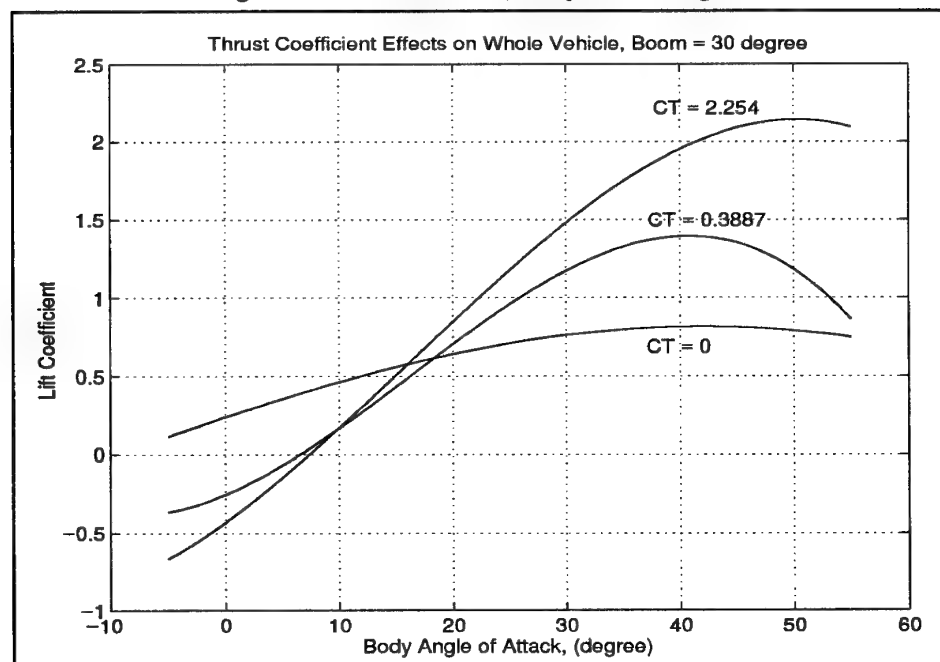
Figure 6. Lift Coefficient, Body-Boom Angle = 0**Figure 7. Lift Coefficient, Body-Boom Angle = 30**

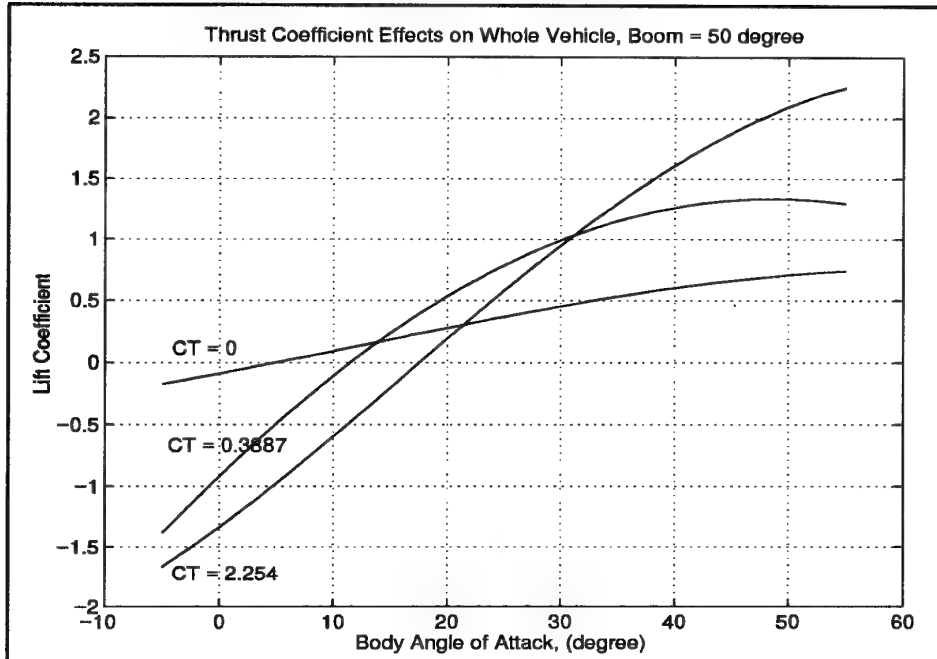
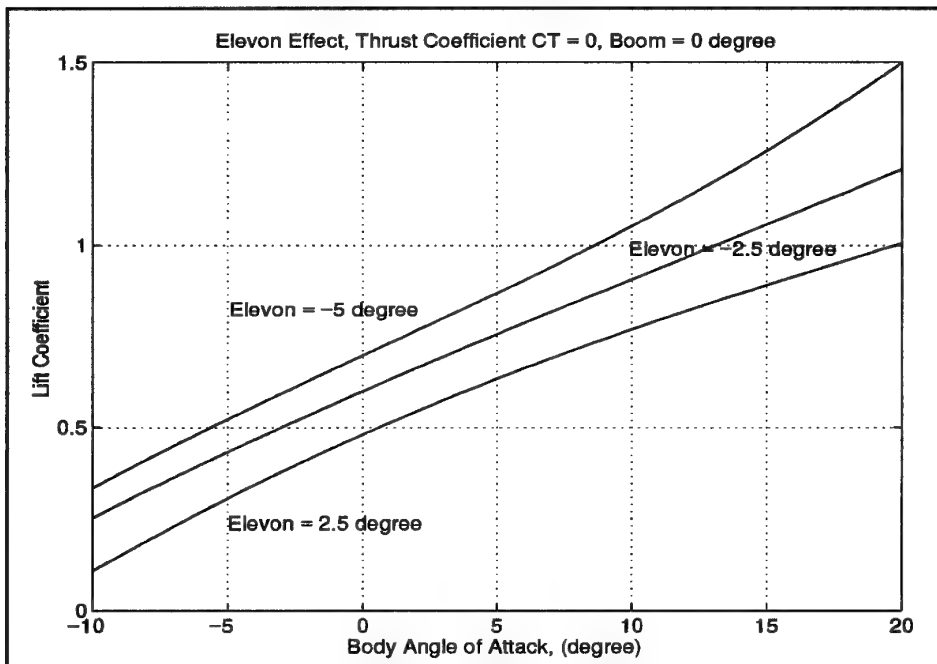
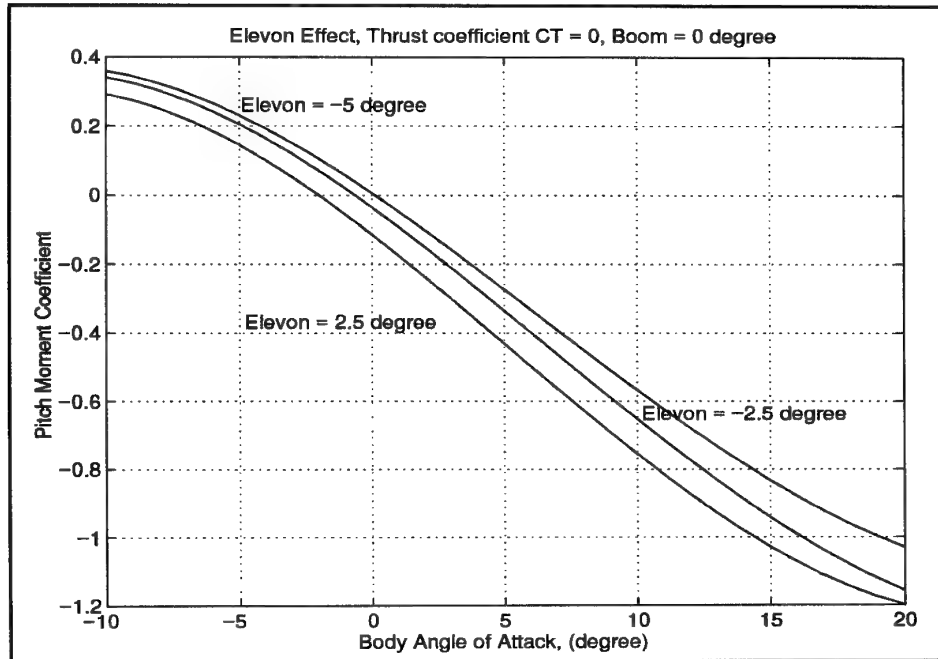
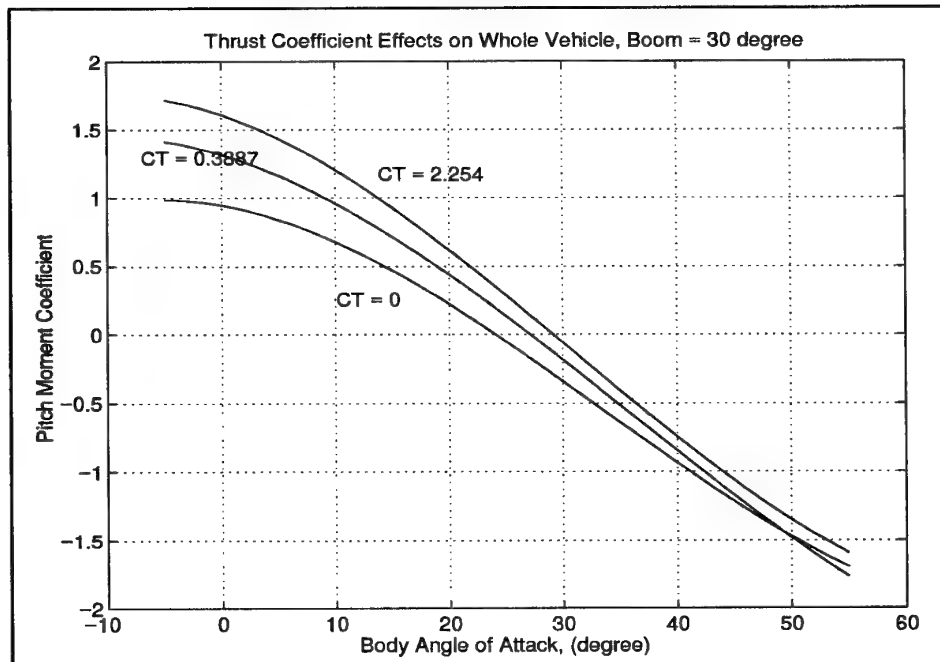
Figure 8. Lift Coefficient, Body-Boom Angle = 50**Figure 9. Elevon Effectiveness**

Figure 10. Elevon Effect on Moment**Figure 11. Thrust Effect on Moment**

Le système de drone marine MARVEL

Jean-François Pelous

Direction des Etudes Avancées, Matra Défense, Vélizy-Villacoublay, France

Jewel B. Barlow

Glenn L. Martin Wind Tunnel, University of Maryland, College Park, USA

0. RESUME

Après avoir cité les nécessités essentielles de l'utilisation marine d'un système de drone, il est présenté quelques caractéristiques aérodynamiques spécifiques de la configuration aile libre et corps basculant du MARVEL ainsi qu'une description succincte des équipements utilisés pendant l'approche du drone MARVEL.

1. INTRODUCTION

Les drones, ou plus exactement les aérodynes légers à moteur à pistons, prennent une part croissante dans le combat qu'ils agissent dans le domaine de la surveillance ou de la guerre électronique. Dans la lignée des programmes de drones développés pour l'Armée de Terre, MATRA DEFENSE s'intéresse aux possibilités d'implanter un système de drone à bord de navires disposant d'une plate-forme hélicoptère.

2. BESOINS DE LA MARINE

La Marine a longtemps constitué une force de haute mer apte à assurer la

sécurité des routes maritimes, stratégiques pour l'approvisionnement et le soutien logistique indispensables en cas de conflit de forte intensité. Depuis, les forces navales ont vu leur zone d'action principale se rapprocher des côtes, que ce soit pour surveiller le trafic maritime (embargo sur un pays), pour participer à la projection et/ou à la récupération de troupes, pour prendre part à la protection d'unités agissant dans un contexte d'intervention, d'interposition ou d'aide à des pays amis. Ces missions à caractère international sont effectuées en parallèle des missions toujours actuelles de surveillance des eaux territoriales et de participation à la protection des intérêts nationaux. Les unités navales concernées par ces déploiements vont du groupe aéronaval au simple bâtiment de surface de type frégate ou même, patrouilleur maritime. Le premier besoin dans toutes ces missions est la surveillance de l'espace autour de la force navale. Cette surveillance doit s'exercer à des distances dépassant la centaine de kilomètres avec des permanences sur site très différentes selon la mission : d'une durée courte pour une reconnaissance à coup sûr de cible à

une durée très longue pour la surveillance de côtes menaçantes. Elle est assurée actuellement par des moyens aériens pilotés, hélicoptère ou avion. L'utilisation de drones en leur lieu et place donne la permanence dans le cas des missions de longue durée et une plus grande sécurité dans le cas de la reconnaissance à coup sûr de cibles potentiellement menaçantes.

Indépendamment de la mission, le système de drone doit satisfaire des contraintes spécifiques d'une utilisation navale qui concernent le segment aérien et le segment de surface. Le segment de surface est composé de deux éléments principaux : (i) la station de programmation et contrôle du vol (PROCOVOL) chargée de la préparation de mission, du suivi et du contrôle du vol, de la gestion des ressources, de l'exploitation des éventuels résultats de la mission et (ii) le système de lancement et le système d'appontage chargé d'aider à l'approche du drone et de récupérer le vecteur aérien une fois celui-ci sur le navire.

La station PROCOVOL doit pouvoir s'intégrer ou tout le moins s'interfacer avec le système de commandement du navire afin de recevoir notamment les éléments de la situation environnant la plate-forme (météorologie, situation tactique, couloirs aériens) et de pouvoir fournir en retour des informations concernant le profil de vol du drone permettant, par exemple, sa prise en

compte dans une éventuelle régulation locale de la circulation aérienne. Le système d'appontage doit modifier de la manière la plus légère possible, la configuration initiale du navire. Son installation et son démontage doivent être faciles et rapides. Le segment aérien comporte aussi des contraintes d'utilisation particulières à un emploi sur une plate-forme navale. La première concerne le personnel qui mettra en œuvre le système. Il ne doit pas avoir besoin d'une spécialisation particulière (pas de pilote). Les qualifications existantes du personnel de bord doivent suffire pour l'utilisation, la maintenance et la réparation du système. Une autre concerne le navire et sa route. Il n'est pas question de stopper le bâtiment pour des opérations de récupération. Il n'est pas question non plus de mettre une ou plusieurs embarcations à la mer ou d'utiliser un hélicoptère avec treuillage pour ramener un drone tombé à la mer dans un scénario nominal de récupération. La seule concession possible serait une manœuvre pour positionner le navire dans une présentation assurant les conditions de vent appropriées à la récupération.

L'ensemble de ces besoins et de ces contraintes impose un système de drone :

- intégrable ou interfaçable avec les systèmes existants du navire en modifiant le moins possible les superstructures,
- rapide pour aller sur la zone

d'intérêt,

- susceptible de rester en place pendant une durée maximale de plusieurs heures,

- et surtout récupérable, de façon autonome, sur une plate-forme navale.

La réponse de MATRA-DEFENSE, exposée dans la suite du document, est basée sur le vecteur aérien MARVEL (conçu par la société Freewing Aerial Robotics) avec un système d'aide à l'approche fondé sur une technologie laser. La charge utile ne fait pas l'objet d'attention particulière, sachant que un bon nombre d'entre elles a déjà été développé pour les systèmes de drones terrestres.

3. DESCRIPTION DU VECTEUR AERIEN

Le drone MARVEL utilise deux innovations complémentaires : l'aile libre et le corps basculant. L'aile libre signifie que l'aile du drone est reliée au fuselage de manière à assurer sa libre rotation autour de l'axe de tangage. L'aile se trouve désolidarisée des mouvements du fuselage et se positionne dans le vent relatif comme une girouette. Ceci évite tout décrochage aérodynamique de sa part, assure un découplage fort entre la réponse de l'aile libre et celle du corps vis à vis des turbulences aérodynamiques verticales et permet une diminution importante de l'effet de turbulences sur le corps assurant

une stabilité naturelle à la charge utile. Les figures 1, 2 et 3 montrent le MARVEL en configuration de vol de croisière. La figure 4 illustre différentes inclinaisons du corps par rapport aux poutres de queue. La figure 5 est une photographie d'une maquette du MARVEL dans la soufflerie Glenn L. Martin de l'Université du Maryland.

Les caractéristiques techniques du MARVEL sont données ci-après :

Longueur totale corps horizontal: 3,6 m

Longueur totale corps basculé: 3,0 m

Envergure totale : 4,9 m

Largeur du corps : 1,3 m

Longueur du corps : 1,8 m

Masse (sans charge utile) : 117,0 kg

Masse maximale au décollage: 177,0 kg

Inclinaison maximale du corps : 55°

Puissance (ROTAX 503) : 50 cv

Vitesse de croisière : 50 m/s

Vitesse maximale : 80 m/s

Vitesse de décollage minimale: 11 m/s

Vitesse d'atterrissage minimale: 15 m/s

Vitesse ascensionnelle : 11,7 m/s

Endurance : > 4 h

Plafond d'utilisation : 5000 m

L'angle d'incidence de l'aile par rapport au vent relatif et par conséquent, la force de portance, est contrôlé par des élevons sur le bord de fuite. Un contrôle supplémentaire, en longitudinal, est obtenu par le régime moteur, régulant ainsi la vitesse de rotation de l'hélice et par

l'angle du corps par rapport aux poutres de queue comme le montre la figure 4. Cette désolidarisation entre l'aile et le fuselage autorise ce dernier à prendre une inclinaison quelconque sans trop perturber les effets de portance de l'aile. Ce basculement aboutit à une vectorisation de la traction de l'hélice qui participe à la portance globale du vecteur aérien. Cette contribution permet alors de réduire la part de la portance due à l'aile libre et ainsi de diminuer la vitesse aérodynamique du drone jusqu'à des valeurs de l'ordre de 12 à 15 m/s. Elle permet aussi d'effectuer des descentes avec une forte pente (supérieure à 45°) et à faible vitesse, tout en conservant un parfait contrôle du vecteur.

Le contrôle latéral est obtenu par un braquage différentiel des élevons des ailes. La cellule est autostable en lacet et ne possède pas de partie mobile sur la dérive. Le comportement dynamique en mode latéral est sensiblement identique à celui de vecteurs aériens conventionnels à voilure fixe.

Un prototype aux dimensions fournies ci-dessus, a effectué plusieurs dizaines d'heures de vol dans le désert de Mojave, en Californie. De nombreux essais en soufflerie ont permis de caractériser la configuration aérodynamique du MARVEL. A cause de la place de l'hélice en position tractrice, le flux d'air généré baigne le corps et

l'emplanture des ailes. Ce fait est générateur de fortes non-linéarités qui sont accrues par les forts angles d'incidence que peut avoir le corps du drone en position basculée.

Pour illustrer ces propos, les figures 6, 7 et 8 montrent la variation du coefficient de portance en fonction de l'angle d'incidence du corps pour des inclinaisons du corps par rapport aux poutres de queue de 0° , 30° et 50° , pour un même braquage des élevons et pour 3 coefficients de poussée. Il est intéressant d'étudier la variation du coefficient de portance aussi bien en fonction du coefficient de poussée qu'en fonction de l'angle d'incidence. Le vol équilibré se situe à un angle d'incidence voisin de l'inclinaison du corps. Avec un angle d'inclinaison de 0° , le comportement en vol est similaire à celui d'une cellule classique y compris la réponse à un changement de position du papillon des gaz. Il est à remarquer que dans ce cas, le coefficient de portance n'est pas fortement lié au coefficient de poussée. Par contre, dans des configurations à 30° et 50° d'inclinaison du corps, le coefficient de portance est fortement couplé au coefficient de poussée. Ce couplage, intuitivement correct est signe que le régime moteur est un moyen de contrôle efficace de la trajectoire pour des inclinaisons importantes du corps.

La figure 9 est un exemple de courbe d'efficacité des élevons qui montre qu'ils fournissent les variations de portance attendues. La figure 10 montre l'effet des élevons sur le coefficient de moment de tangage. La figure 11 est un exemple de variation du moment de tangage en fonction de l'incidence du corps pour 3 coefficients de poussée et une inclinaison du corps de 30° .

Le pilotage du drone MARVEL n'est pas classique du fait de l'aile libre et du corps basculant. Le pilotage agit sur 3 paramètres : (i) le braquage des élevons pour à la fois le contrôle de la portance des ailes et, en braquage différentiel, pour le roulis, (ii) le régime moteur pour la force de traction de l'hélice et (iii) l'inclinaison du corps pour choisir la phase de vol. Les ordres de braquage des élevons sont les ordres au temps de réponse le plus court, la commande moteur s'effectue à une fréquence plus basse et l'inclinaison du corps est à très basse fréquence, ce qui peut la faire assimiler à une commande de trim sur une cellule classique.

4. APPONTAGE

L'appontage est la phase la plus délicate de tout le vol du drone. Grâce à son moyen propre de navigation (GPS par exemple), le drone rejoint le point d'entrée de la phase d'approche. Le drone est en position corps incliné et a ainsi réduit sa vitesse aérodynamique horizontale jusqu'à

environ 15 m/s. Le drone est alors pris en charge par un système d'aide à l'approche qui va l'amener à une zone d'attente.

Le système d'aide à l'approche décrit ici s'apparente au système ILS des aéroports civils. Un axe de descente idéal est matérialisé par l'axe central d'un faisceau laser codé spatialement et temporellement (mire projetée). Le codage s'effectue au moyen d'un modulateur acousto-optique (pour l'aspect temporel) délivrant des trains d'impulsions et par un modulateur mécanique rotatif (pour l'aspect spatial) dans le plan focal de l'optique. Chaque point du faisceau est l'image d'un point sur le modulateur mécanique. Ce faisceau comporte une grille de 40×40 cases qui sont codées en distance par rapport au centre du faisceau donnant une précision sur la position inférieure au mètre.. Il est généré par une source laser de longueur d'onde 10,6 microns et de puissance inférieure à 20 watts assurant une disponibilité du système d'aide à l'approche compatible de l'emploi du drone. Le faisceau est stabilisé angulairement par une plate-forme gyroscopique (stabilisation meilleure que $0,6 \text{ mrad}$) et subit les effets de translation du centre de gravité du navire, principalement le pilonnement et l'embarquée.

Le drone, afin de décoder les informations reçues, dispose d'un détecteur embarqué et de son électronique associée dont la masse ne dépasse pas 250 g pour un encombrement très réduit (cylindre 40 mm de diamètre pour 100 mm de long).

La loi de guidage est une loi en alignement inverse (le drone se rapproche du point d'émission du faisceau). Cette loi tend à annuler l'écart métrique en lui associant une accélération proportionnelle à l'écart de position, à sa dérivée et à son intégrale de manière à corriger les erreurs dues à une vitesse angulaire et à une accélération angulaire de défilement. Les accélérations dans le plan perpendiculaire à l'axe du faisceau sont ensuite traduites en accélérations commandées au drone et enfin en ordres de pilotage sur les voies tangage et roulis.

Le faisceau amène le drone dans une zone d'attente dans laquelle il va rester jusqu'à ce que les mouvements du navire atteignent une zone de tranquillité relative. A cet instant, le drone reçoit l'ordre d'apponter et vient se plaquer sur le pont du navire. Un dispositif de fixation du drone l'empêche alors de bouger. Ce dispositif peut être un filet métallique tendu à quelques centimètres du pont dans lequel vient se prendre le train d'atterrissage du drone.

5. CONCLUSIONS

Dans ce système, le prototype du drone existe et a plusieurs dizaines d'heures de vol à son actif. Une maquette du système d'aide à l'approche existe et ses performances ont été démontrées. Le développement des algorithmes de guidage et de pilotage de la phase cruciale d'appontage a démarré et celui du système de maintien du drone après appontage va débuter sous peu. Les algorithmes de pilotage et de guidage ainsi que les spécifications des senseurs inertiels et des servomoteurs associés seront disponibles au cours de l'année 1996.

REFERENCES

1. **Chen W & Barlow J.B.**, "Stability, Control, and Gust Response Characteristics of an Ultralight Freewing Aircraft". AIAA-92-4342. Atmospheric Flight Mechanics Meeting, Hilton Head, SC, August 10-12, 1992.
2. **Chen W & Barlow J.B.**, "An Ultralight Freewing Aircraft Design Study". AIAA-92-4194, AIAA Aircraft Design System Meeting, Hilton Head, SC, August 10-12, 1992.
3. **Chen W & Barlow J.B.**, "An Unmanned Tilt-Body Freewing Vehicle Powered Wind Tunnel Test", AIAA-92-1902. 13th AIAA Applied Aerodynamics Conference, San Diego, CA, June 19-22, 1995.

Figure 1. Vue de Dessus du MARVEL

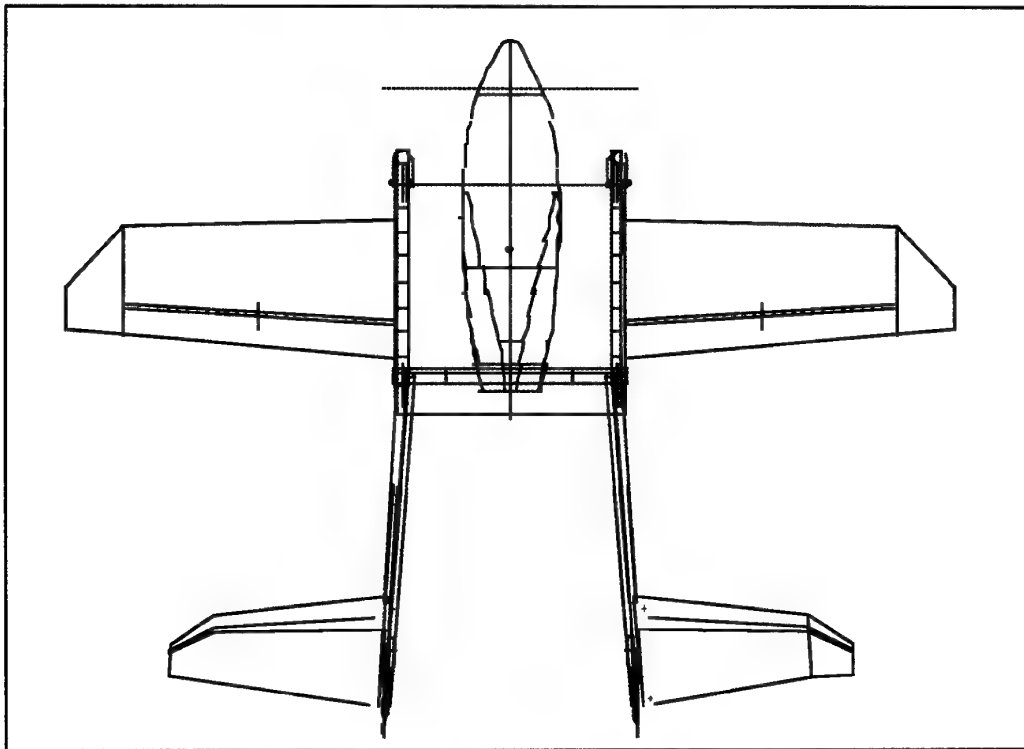


Figure 2. Vue de Face du MARVEL

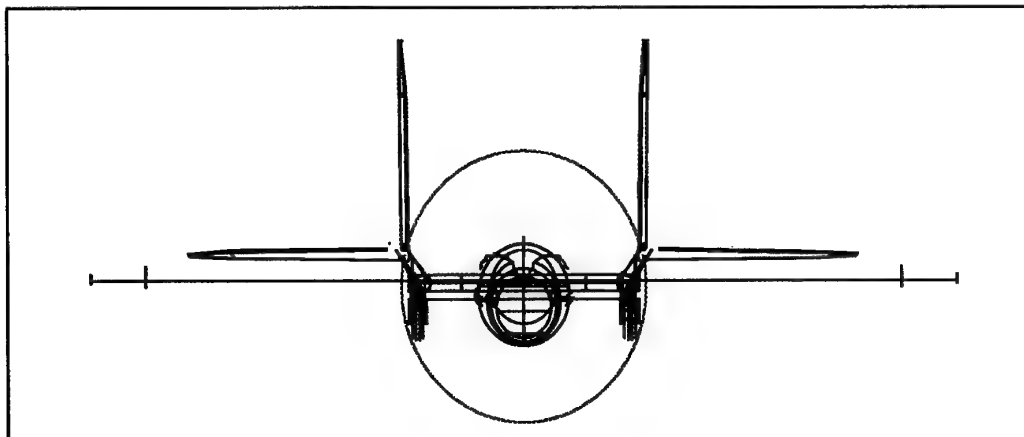


Figure 3. Vue de coté du MARVEL

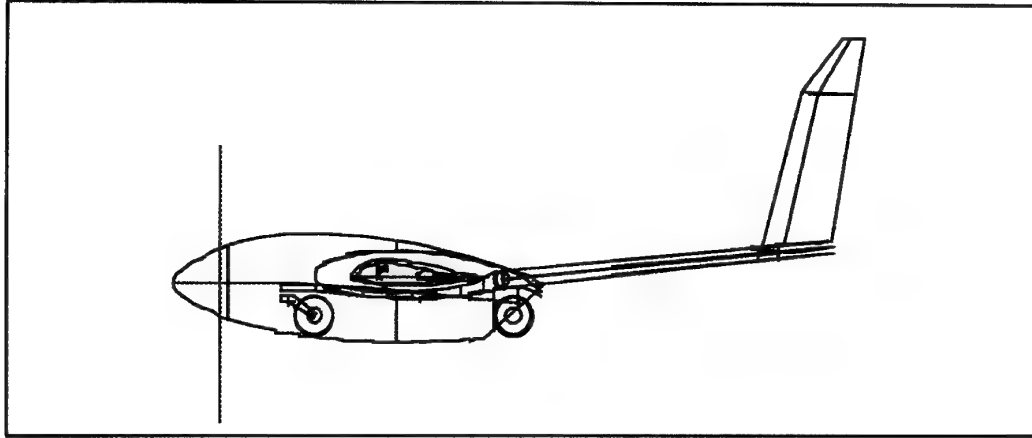


Figure 4. MARVEL Différents Angles d Inclinaison

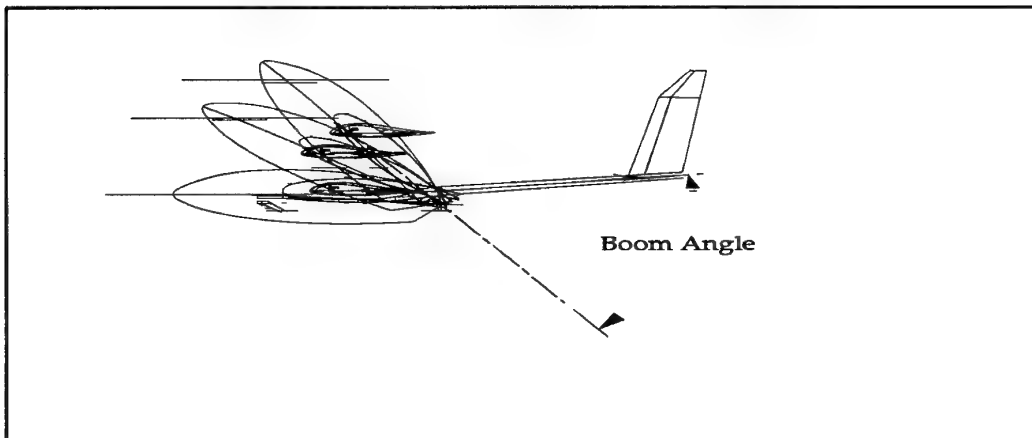


Figure 5. MARVEL Maquette de Soufflerie

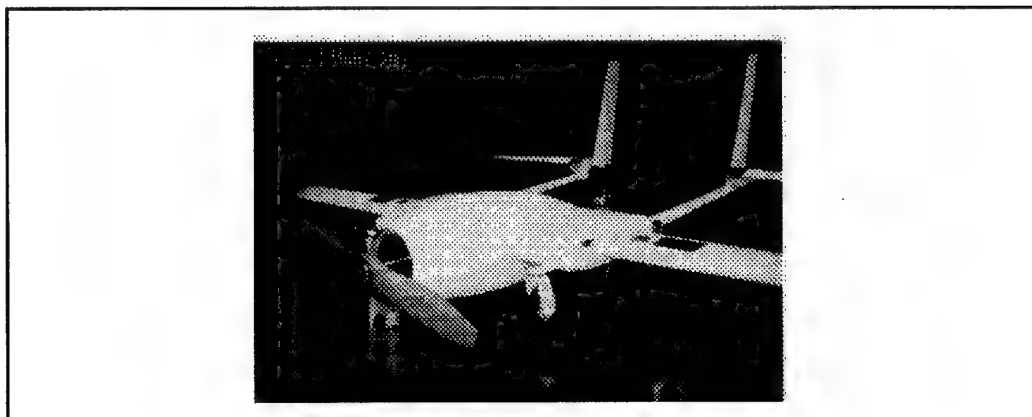


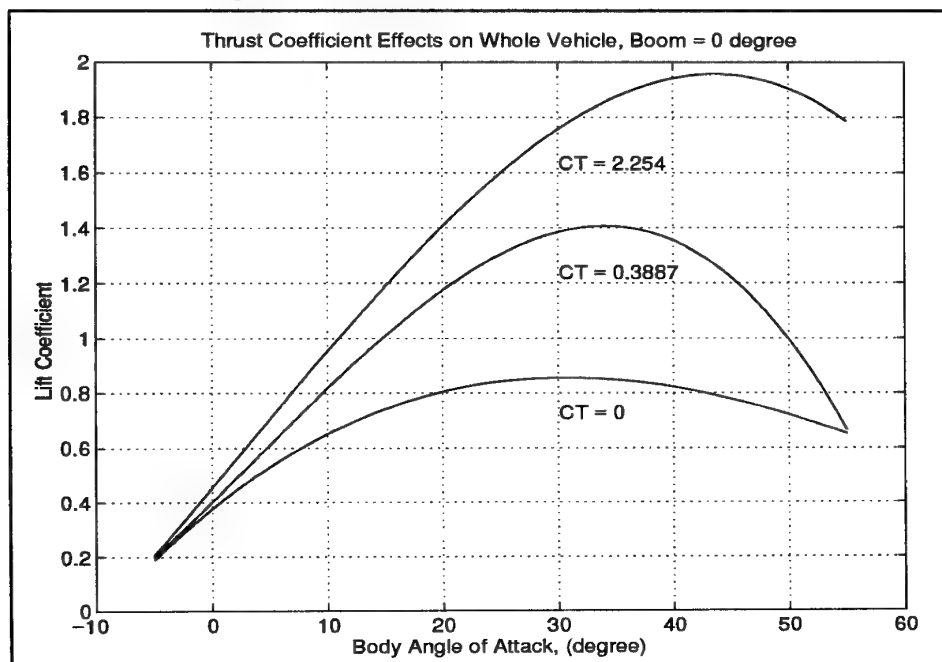
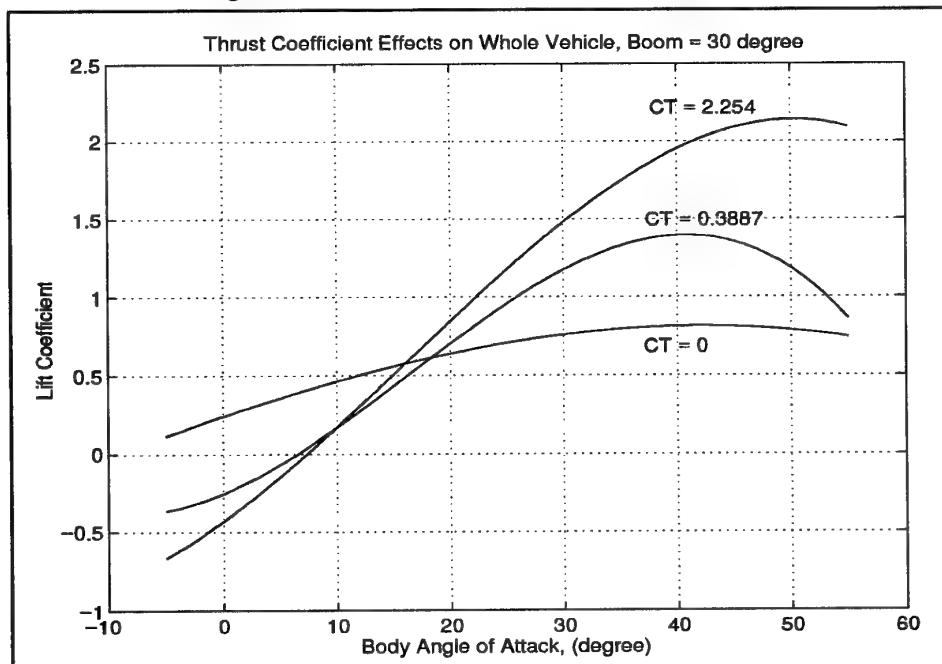
Figure 6. Coefficient de Portance, Inclinaison = 0**Figure 7. Coefficient de Portance, Inclinaison = 30**

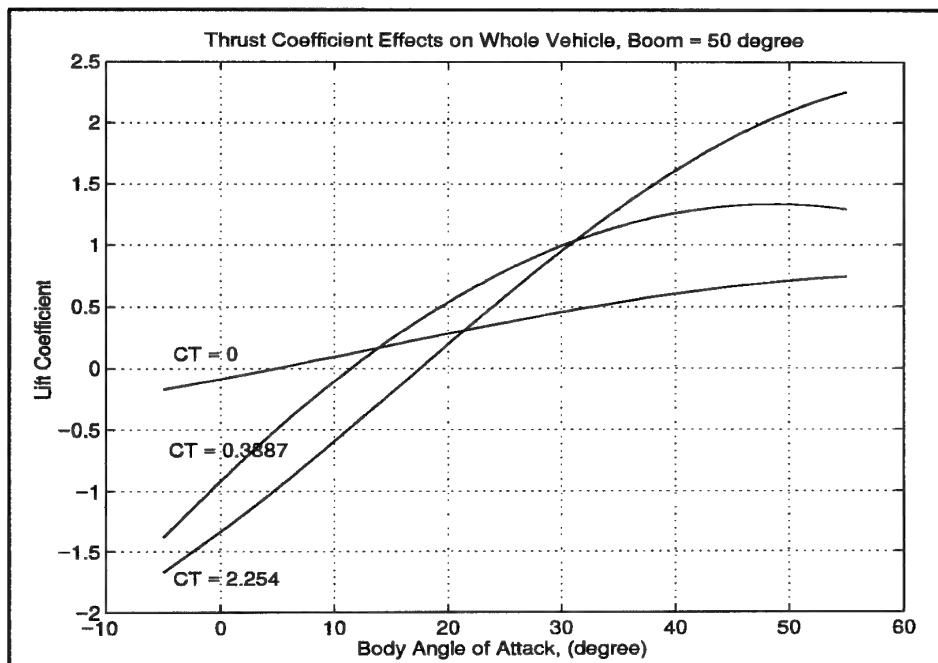
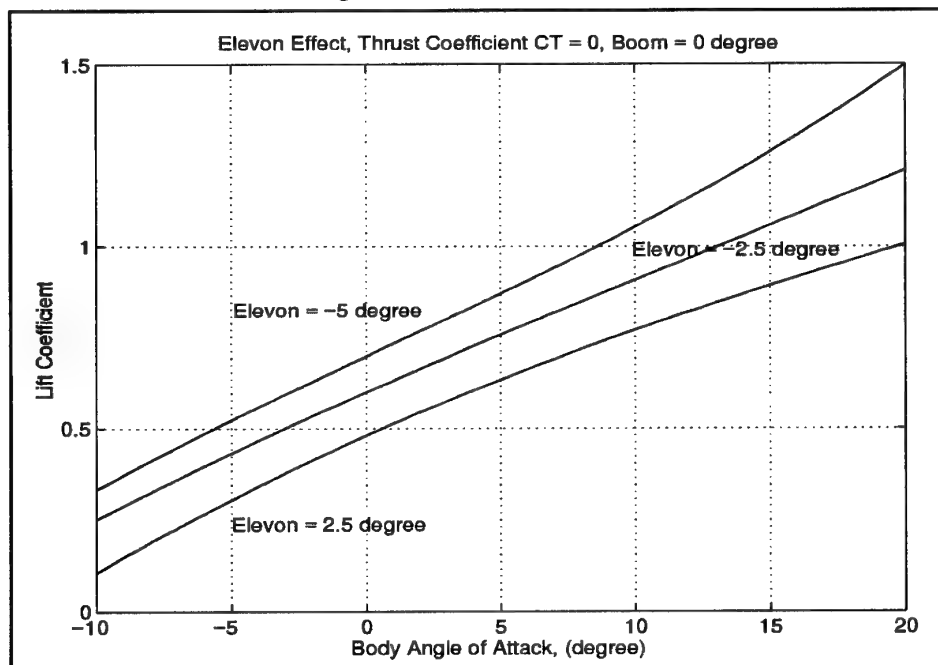
Figure 8. Coefficient de Portance, Inclinaison = 50**Figure 9. Efficacité des Elevons**

Figure 10. Effet des Elevons sur le Moment

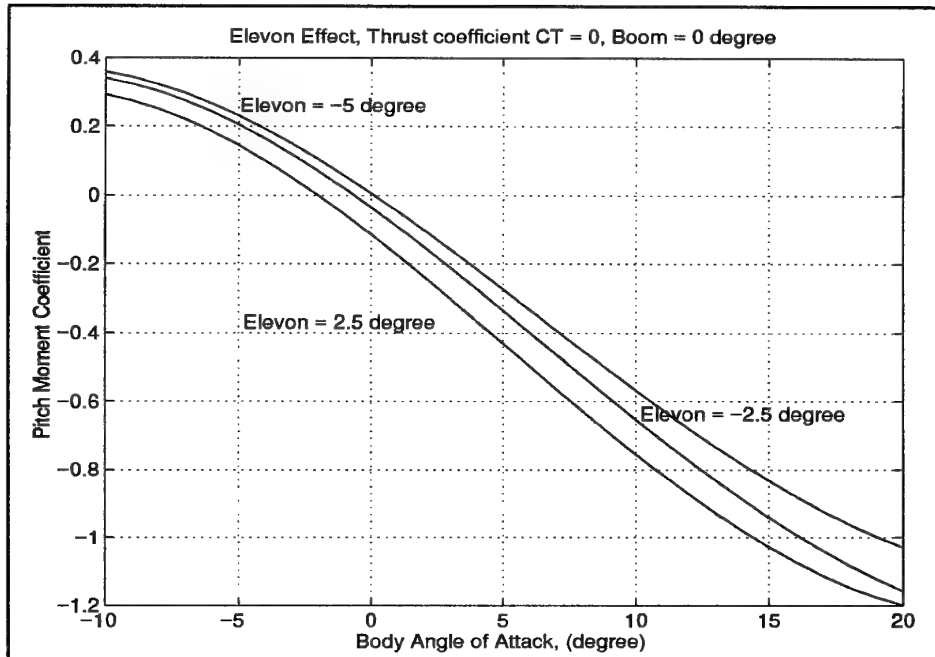
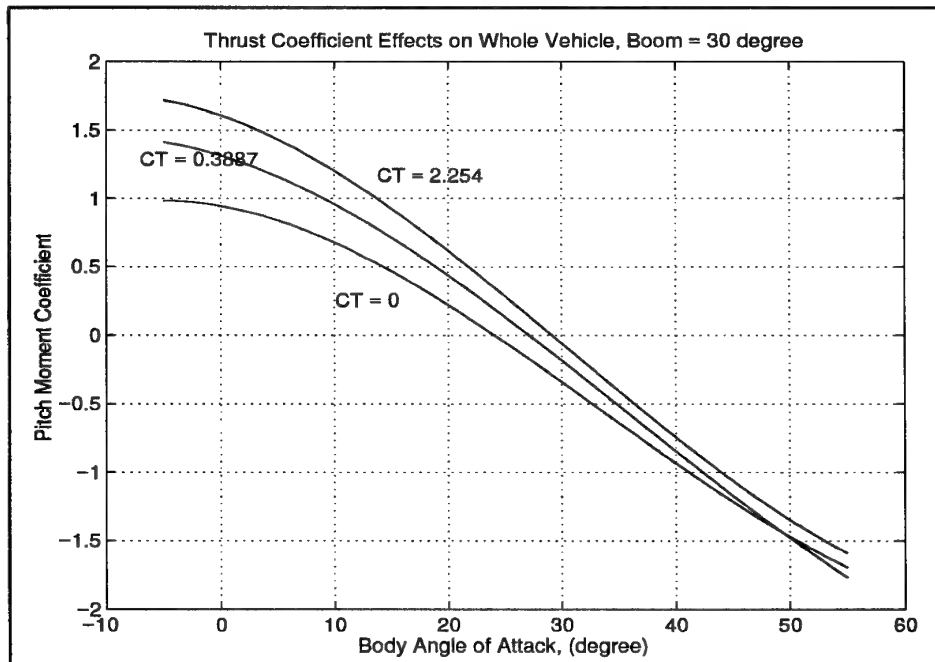


Figure 11. Effet de la Poussée sur le Moment



Conception et développement d'un système d'appontage maritime automatique d'un véhicule générique de type VTOL

Bernard de FERRIER

Chef de projet d'Interface dynamique aéronef-navire
Bombardier Inc., Canadair, Division systèmes de défense (Mirabel)
Montréal, Québec J7N 1H3, CANADA

Claude REBOULET

Responsable de recherches en Robotique
Département d'Études et de Recherches en Automatique
Centre d'Études et de Recherches de Toulouse (CERT-ONERA)
(BP 4025) 31033 Toulouse, FRANCE

Sommaire

Le bilan de l'évolution d'un système d'appontage automatique d'un véhicule télécommandé de type VTOL est ici présenté. Le modèle du véhicule-type est basé sur le CL227 de Canadair. Les résultats de tests sur le contrôle et la réponse du système sont présentés. La conception et l'agencement des composantes d'un système de capteurs sont analysés. L'approche qui décrit la position du véhicule est basée sur la décomposition du vecteur d'état en composantes observables et non-observables. Cette approche est validée par la simulation. Le modèle de simulation tient compte du véhicule aérien, du navire, du capteur et de l'environnement et est représenté par six degrés-de-liberté. Le modèle de capteur est basé sur des algorithmes du contrôle du véhicule et des mouvements du navire. Enfin, les profils de vols calculés par simulation sont également présentés.

Abstract

The evolution of an automated ship recovery system for a VTOL UAV is discussed. The generic UAV model is based on the Canadair CL227 VTOL UAV. Test results concentrating on system control and response are provided. A description of the data link software and hardware components is presented. The approach describing the location of the air vehicle is based on the decomposition of the state vector into observable and non-observable components. This approach is validated by simulation. The simulation model is based on a six degree-of-freedom representation of the air vehicle, the ship, the data link system and the environment. The data link/recovery system uses vehicle control and ship motion algorithms which close the loop between the air vehicle and ship. Finally, the flight profiles produced by simulation are also discussed.

Ferrier est diplômé de la Faculté des Études supérieures de l'École Polytechnique de Montréal.

1.0- Introduction

Le but de cet article est de présenter un résumé du programme expérimental établi entre la Société Bombardier, Inc. Canadair (CANADA), la Direction des Constructions navales (DCN) de la DGA (FRANCE) et la CERT (ONERA) qui a pour objet la conception d'un système d'appontage automatique pour un véhicule télécommandé du type VTOL.

La mise en place d'un appontage automatique nécessite la résolution d'un certain nombre de problèmes:

- tout d'abord celui de la localisation de l'engin par rapport au navire
- celui de la prédiction des mouvements du navire
- celui de la génération de la trajectoire d'appontage
- enfin celui du pilotage de l'engin sur la trajectoire

Le schéma montrant les principales composantes intervenant dans un système d'appontage automatique est présenté à la figure 1.

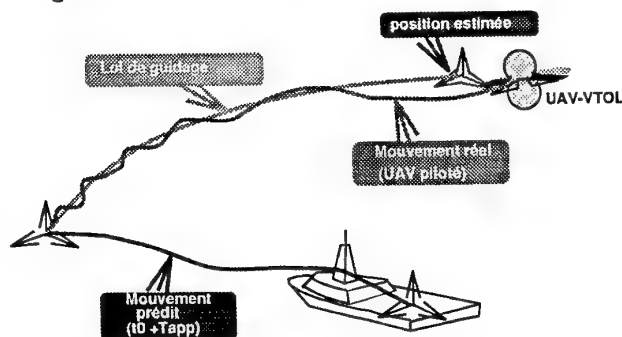


Figure 1- Problématique générale de l'appontage automatique

Chacun des problèmes contient ses propres difficultés, mais dans le cadre de cet article, c'est principalement du problème de la localisation dont il sera question. Ce problème est rendu relativement délicat en raison du contexte particulier de l'application maritime. En effet certains capteurs servant à la localisation sont situés sur le navire dont la position n'est pas parfaitement connue en raison des perturbations dues à la houle.

Le choix de la meilleure configuration des capteurs pour réaliser cette localisation est un problème qui mérite une attention particulière. On peut envisager l'utilisation de capteurs relativement coûteux fournissant une mesure de position du type radar c'est à dire possédant trois composantes (par exemple un angle de site de gisement ainsi que la distance), mais également l'utilisation de capteurs moins sophistiqués, fournissant une information incomplète de la position.

On sait dans ce cas que cet objectif n'est pas toujours atteignable. Si on considère à titre d'exemple le cas du suivi d'un UAV avec les seules mesures angulaires (angle de gisement et de site seulement), sa position devient inobservable lorsqu'il se déplace à une vitesse relative constante par rapport au navire. On sait en effet qu'une trajectoire homothétique conduira à la même série de mesures, donc à l'inobservabilité de sa position puisqu'on ne peut distinguer la trajectoire vraie de la trajectoire fausse.

Ce problème de l'observabilité de la position peut tout d'abord être résolu par une organisation adéquate des capteurs. On peut par exemple utiliser deux capteurs disposés en deux positions distinctes sur le pont du navire. L'intersection des deux rayons donne une mesure de position complète. L'inconvénient de cette technique vient du fait que lorsqu'on a plusieurs UAV à localiser simultanément, on est confronté au problème de la reconnaissance du même UAV par les deux capteurs. Une autre approche consiste à favoriser l'observabilité par l'adjonction d'autres types de mesures: par exemple des mesures par effet Doppler rendent le système complètement observable. Il existe bien sûr d'autres combinaisons de capteurs que nous ne passerons pas en revue ici. D'autre part, On peut également agir sur le scénario d'approche de l'UAV. Si nous reprenons le cas d'un capteur fournissant seulement deux informations angulaires, on peut rendre observable la position par une manoeuvre appropriée d'approche.

C'est dans ce cadre-là que se situent les résultats présentés ici. Les résultats couvrent

une étude préliminaire s'intéressant plus spécialement, à la reconstruction de la position à l'aide des seules mesures angulaires de site et de gisement d'un seul capteur. Le problème traité est celui de la fusion d'informations. Ceci consiste à combiner les informations angulaires avec les informations fournies par les centrales d'inertie du navire et de l'UAV, tout en s'assurant que le scénario envisagé garantisse l'observabilité de la trajectoire.

Il est connu que l'observabilité dépend des manoeuvres relatives de l'UAV par rapport au navire (une étude complète concernant le problème pourra être trouvée dans la référence [1]). Il est intéressant de voir quels sont les scénarii d'approche de l'UAV les plus favorables à l'observation de sa position. En fait la question sous-jacente est la suivante: est-ce que l'algorithme d'estimation de la position est suffisamment efficace pour converger rapidement? Ou bien en d'autres termes est-ce que, compte tenu des fréquences d'échantillonnage envisageables et des bruits sur les différents capteurs, le temps de recalage de la position est suffisamment court par rapport à de la durée d'une phase d'appontage?

En fait ce type de problème est relativement ancien et est similaire à celui que l'on rencontre dans les problèmes de navigation ou encore dans les problèmes de suivi de cibles. Plusieurs approches ont été utilisées pour résoudre ce problème. L'approche classique consiste à utiliser un filtre de Kalman étendu formulé en coordonnées cartésiennes. En effet les équations de mesures sont non linéaires et l'implantation d'un filtre de Kalman nécessite dans ce cas les dérivées partielles des mesures angulaires par rapport à x, y, z qui sont elles mêmes inconnues; l'incertitude sur les gains correspondant du filtre conduit alors parfois à des difficultés de convergence et même à des problèmes de stabilité. La fiabilité des résultats n'est donc pas toujours assurée avec cette approche.

Une solution bien connue qui régle généralement ce problème consiste à reformuler l'équation de mesures pour aboutir à un système d'équations pseudo-linéaires [2]. C'est cette approche qui, adaptée au cas tri-dimensionnel, a été utilisée lors de cette étude. Comme l'on sait également que ce type de méthode conduit généralement à des biais qui peuvent être importants, une attention toute particulière a été portée sur le choix des scénarii d'approche pour leur influence sur le biais d'estimation, car de l'ampleur du biais dépendra l'intérêt de cette approche.

1.1- Sommaire des composantes du système

Les composantes principales du système UAV (système d'engins de reconnaissance aérienne télécommandé) sont: véhicule du type VTOL (décollage et atterrissage vertical), système de capteur, de guidage et de communication, centre de contrôle d'opérations (centre de contrôle et de commandes), systèmes de manutention de véhicule et d'apportage automatique.

Véhicule aérien

Le modèle du véhicule utilisé est le CL227 qui est un véhicule à hélices contrarotatives et qui est construit de façon modulaire (voir la figure 2). Les modules principaux sont : le bloc de puissance (turbomoteur), le module d'hélices et le module de charge utile.

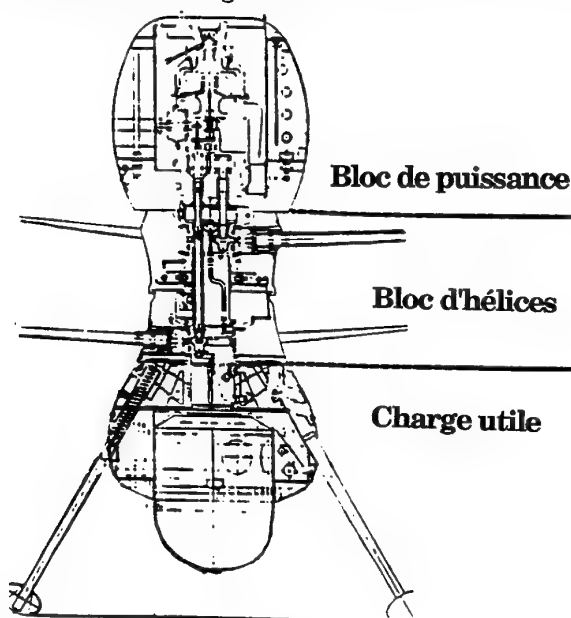


Figure 2- Modèle du CL-227

Le bloc de puissance est composé d'un turbomoteur (Turbine à gaz) intégré avec une boîte de vitesse différentielle qui est placée au milieu d'un réservoir de carburant de forme annulaire. Le réacteur est installé avec l'axe principal à la verticale. La manche d'entrée d'air est placée vers le bas et le canal d'éjection vers le haut du réacteur.

Le module d'hélices est composé de deux rotors contrarotatifs qui sont attachés aux plateaux oscillants et de timonerie associée. Les avionics et la soutenance des réacteurs sont intégrés dans la section inférieure du module. Les pales

et le train d'apportage sont également attachés à la section inférieure.

Finalement, les éléments du système de communication sont intégrés dans le module de charge utile. Le CL-227 peut transporter une grande diversité de capteurs dépendant de la mission en cours, comme, par exemple un détecteur infrarouge.

Système de communication

Le système de liaison de données (ou de communication) est composé d'un terminal de données à bord du véhicule (aéroporté), d'un terminal de données à bord du navire, d'un groupe d'antennes et d'une antenne de contrôle. Le terminal de données à bord du véhicule reçoit les commandes en provenance du centre de contrôle et commandes via des émissions RF (fréquences de radio). Les données télémétriques venant du véhicule sont transmises via la même liaison de données de fréquences de radio vers le centre de contrôle et de commande. L'organigramme de contrôle est présenté à la figure 3.

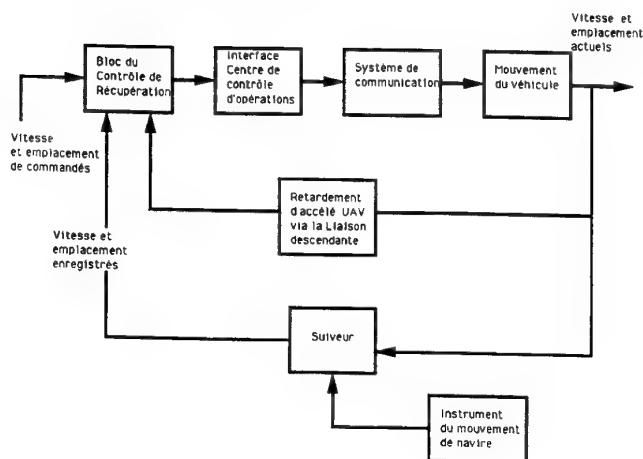


Figure 3 - Organigramme du système de contrôle

Les antennes sont séparées en fonction de la distance entre le véhicule et le navire. Un groupe d'antennes est utilisé lorsque le véhicule est en opération de vol de longue distance. Quand le véhicule est en approche finale l'antenne de précision de court rayon d'action est employée. Cette antenne est intégrée dans le système d'apportage automatique.

Centre d'opérations

Le centre d'opérations fournit en temps-réels les instructions au véhicule télécommandé et à la charge utile. Le centre d'opérations reçoit et traite les données, fournit la visualisation des résultats et enregistre les données provenant du véhicule aérien. Les données sont transmises par les communications RF (fréquences de radio). Le centre comprend les appareils nécessaires à la réception, l'interprétation et l'exploitation des systèmes du véhicule, et de la charge utile et des données de vols. Le centre d'opérations est l'interface homme-machine. La planification des missions est réalisée avant les vols. Les modifications des missions sont faites au centre d'opération pendant les vols.

Système d'appontage automatique

La figure 4 montre l'organigramme d'un système d'appontage automatique. Lorsque le véhicule est pris en charge par l'antenne de poursuite, le véhicule est contrôlé par l'ordinateur d'appontage automatique. Les composantes principales du programme sont: le programme de la compensation pour le mouvement du navire, les commandes de directive de pilotage dans les axes d'accélération du véhicule en X et en Y et le contrôle d'altitude du véhicule. La boucle est complétée par un programme qui définit la position du véhicule par rapport à la piste d'atterrissage située sur le navire. Ce programme de l'Indicateur des périodes d'appontage (IPA) est intégré dans l'ordinateur d'appontage automatique [3].

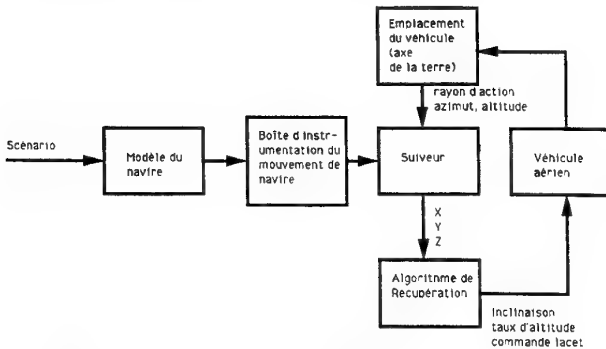


Figure 4 - Organigramme d'un système d'appontage automatique

L'objet de cette étude est de définir techniquement un concept de système d'appontage automatique pour un véhicule télécommandé du type VTOL et d'en évaluer les performances. Un des objectifs de la conception du système d'appontage automatique est la définition d'un système de suivi. La méthodologie pour la définition d'un système automatique est présentée dans la section suivante.

2.0- Formulation du problème

Considérons le schéma de la figure 5:

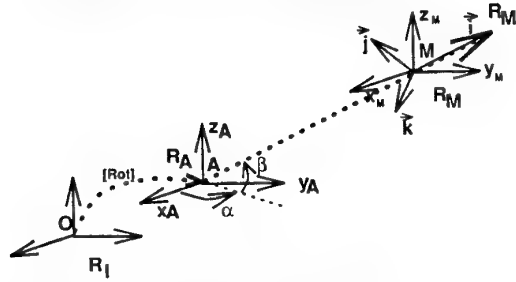


Figure 5- Formulation du problème

R_A représente un repère lié au navire.

R_M représente un repère lié à l'UAV.

R_I représente un repère inertiel.

Nous supposons que les centrales de navigation respectives de l'UAV et du navire fournissent les attitudes de chacun d'eux ainsi que leur accélération.

Équation d'état du système

Les mouvements de l'UAV et du navire peuvent être décrits par une équation d'état discrète qui résulte d'un développement limité de Taylor au deuxième ordre.

Soit pour l'UAV par exemple:

$$\vec{OM}(k+1) = \vec{OM}(k) + \vec{Ov}(k)dt + \frac{1}{2}\vec{O\gamma}(k)dt^2$$

où:

$$\vec{vM}(k) = \left(\frac{d}{dt}\right)_{/R_I} \vec{OM}(k)$$

est le vecteur vitesse de l'UAV, et:

$$\vec{\gamma M}(k) = \left(\frac{d}{dt}\right)^2_{/R_I} \vec{OM}(k)$$

est le vecteur accélération de l'UAV.

Nous avons également des équations du même type pour le navire. D'où l'équation d'état suivante:

$$X(k+1) = AX(k) + B\Sigma\gamma(k) + v \quad (1)$$

à condition de poser:

$$X = \left[\begin{matrix} A\vec{M} \\ \left(\frac{d}{dt}\right)_{/R_I} A\vec{M} \end{matrix} \right]_{/R_I}$$

$$\text{avec} \quad A = \begin{bmatrix} I & I \cdot dt \\ 0 & I \end{bmatrix} \quad \text{et} \quad B = \begin{bmatrix} I \cdot \frac{dt^2}{2} \\ I \cdot dt \end{bmatrix}$$

$$\Sigma\gamma(k) = \vec{\gamma M}(k) = \vec{\gamma A}(k)$$

où $\vec{\gamma}_M$, représente l'accélération de l'UAV, et $\vec{\gamma}_A$, représente l'accélération du navire, toutes deux fournies par les centrales inertielles de navigation.

Notons qu'en réalité l'accélération du point A résulte d'un calcul puisque la centrale de navigation inertielle du navire ne peut pas être au même point géométrique que le capteur c'est à dire le point A.

v représente le bruit sur les accéléromètres (avec Q comme matrice de covariance).

Équation de mesure

Considérons les vecteurs $\vec{i}, \vec{j}, \vec{k}$, (voir figure 5), ils constituent la base d'un trièdre orthonormé R'_M qui se déduit de R_A par une rotation d'angle α autour de l'axe z_A et par une rotation d'angle β autour de l'axe y_A . On remarque que l'axe x de ce repère est aligné avec l'axe de visée

du capteur, c'est à dire l'axe \vec{AM} .

Par définition nous avons:

$$\vec{j} \cdot \vec{AM} = 0 \quad (2)$$

$$\vec{k} \cdot \vec{AM} = 0 \quad (3)$$

Ces deux équations peuvent s'écrire matriciellement sous la forme:

$$H \cdot \vec{AM} / R_A = 0 \quad (4)$$

avec:

$$H = \begin{bmatrix} \vec{j}^T \\ \vec{k}^T \end{bmatrix} / R_A \quad (5)$$

Puisque:

$$\vec{AM} / R_A = [Rot]^{-1} \cdot \vec{AM} / R_I \quad (6)$$

$[Rot]$, étant la matrice de changement de base entre le repère inertiel et le repère lié au navire (fournie par la centrale de navigation inertielle du navire), on peut écrire:

$$\vec{AM} / R_A = [Rot]^{-1} \cdot 0 \cdot X \quad (7)$$

L'équation de mesure s'écrit donc:

$$H \cdot [Rot]^{-1} \cdot 0 \cdot X + w = 0 \quad (8)$$

On trouvera en annexe I le détail des calculs pour la matrice H .

Remarquons que H ne dépend que des mesures angulaires α et β (α et β , étant les mesures fournies par le capteur situé sur le navire avec ϵ comme bruit de mesure angulaire (R_ϵ étant la matrice de covariance associée)).

Il nous reste à en déduire la matrice de covariance R associée à w . Pour cela nous pouvons remarquer que l'équation de mesure résulte, comme nous venons de le voir, du

produit scalaire de deux vecteurs \vec{i} (ou \vec{j})

avec \vec{AM} . Il est facile d'en déduire que le bruit de mesure sera donc homogène au produit: $r \epsilon$, r étant la distance UAV-navire. On prendra donc comme matrice de covariance R , la matrice $r^2 R_\epsilon$.

Équation du filtre

Les équations (1) et (8) constituent le système d'équation d'état. Les équations permettant la reconstruction de la position de l'UAV sont celles d'un filtre classique de KALMAN. Elles sont données en annexe II.

2.1- Essais en simulation

Conditions des essais

Avant de présenter les résultats de simulation, nous allons tout d'abord décrire les conditions dans lesquelles sont effectuées ces essais.

Le navire est soumis à une houle relativement importante. Seuls les mouvements de pilonnement, de roulis et de lacet ont été introduits dans la simulation. Les valeurs numériques considérées sont les suivantes: soit:

0.88 ω^2 , pour le module de l'accélération linéaire de pilonnement,

0.17 ω^2 , pour l'accélération angulaire autour de l'axe de roulis,

0.05 ω^2 , pour l'accélération angulaire autour de l'axe lacet.

avec:

$$\omega = 0.089 \cdot 2 \cdot \pi \text{ rd/s}$$

L'intégration des équations de manière formelle fournit la position et l'orientation du navire au cours du temps, c'est-à-dire le repère R_A lié au navire et par conséquent de la matrice $[\text{Rot}]$ qui caractérise le changement de base du repère navire par rapport au repère inertiel. C'est dans ce repère que sont simulées les mesures angulaire α et β .

Par ailleurs on suppose que l'UAV se rapproche du navire en effectuant une trajectoire formée de demi-cercles (de rayon 50 m) à la vitesse de 5 m/s, comme schématisé sur la figure 6.

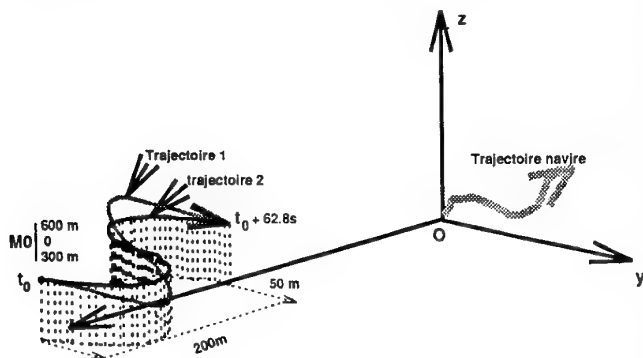


Figure 6 - Scénarii d'approche

Deux types de trajectoire ont été envisagées, la trajectoire 1 correspond à une approche selon une altitude variant de manière sinusoïdale, la trajectoire 2 correspond à une approche à altitude constante.

On suppose d'autre part que l'UAV à l'instant initial est situé en un point M_0 (600, 0, 300). En ce qui concerne l'erreur d'estimation initiale, on supposera que la position de l'UAV est située dans une sphère de 100m de rayon autour de la valeur réelle et que l'erreur sur le vecteur vitesse est contenue à l'intérieur d'une sphère de rayon 10 m/s.

L'écart type du bruit considéré pour la mesure d'accélération est: 10^{-5} m/s^2 .

L'écart type du bruit sur la mesure angulaire est: 0.5° .

La période d'échantillonnage choisie est de 40ms.

2.2- Commentaires sur les essais en simulation

Plusieurs essais effectués avec différentes valeurs de conditions initiales n'ont pas montré de différences notables sur le comportement du filtre. L'allure du transitoire diffère selon les valeurs initiales, mais dans tous les cas la convergence du filtre est tout à fait acceptable et est inférieure à 2% de la distance, lorsque l'UAV termine le deuxième demi-cercle de sa trajectoire, c'est à dire environ une minute après l'instant initial.

L'un des essais que nous avons effectué est présenté à la figure 7.

Cet essai a été effectué avec une trajectoire d'approche de type 1, mais nous avons effectué d'autres essais avec des trajectoires de type 2, c'est à dire à altitude constante. Ces approches conduisent généralement à une convergence sensiblement moins bonne (une dizaine de secondes supplémentaires sont nécessaires). L'utilisation de rayon de courbure plus important pour les trajectoires circulaires n'améliore pas l'observabilité, contrairement à ce qu'on aurait pu penser, et le temps de convergence est au contraire augmenté.

D'autres essais effectués en présence d'une houle plus faible, n'ont pas permis d'établir une conclusion définitive sur cet aspect. Il semblerait plutôt que la houle ait un effet favorable sur la convergence du filtre.

Nous avons également effectué des essais en considérant un biais constant sur la mesure d'accélération, simulant ainsi un décalage entre les informations de la centrale inertielle de navigation du navire et celle de l'UAV. Ce biais sur les capteurs accélérométriques qui se traduit par un bruit d'état à moyenne non nulle n'affecte pas la rapidité de convergence des algorithmes. En revanche l'estimé de la position est biaisé selon les composantes x et z. A titre indicatif une erreur de $5 \cdot 10^{-5} \text{ m/s}^2$ sur la mesures accélérométriques conduit à une erreur d'estimation d'environ 2% de la distance.

3.0- Conclusion

On sait que cette approche basée sur les pseudo-mesures résout généralement les problèmes de stabilité du filtre, mais en revanche conduit selon les scénarii à des biais qui peuvent être importants. Toutefois cette approche constituait pour nous une étape préliminaire et il était intéressant d'analyser l'importance de ces biais avant de songer à l'utilisation de techniques

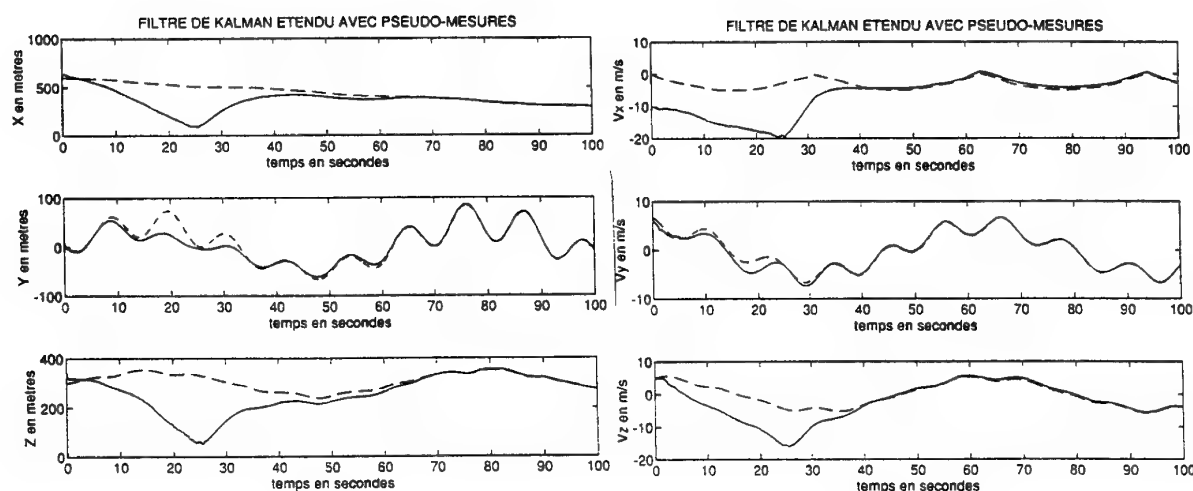


Figure 7 - Résultat d'essais en simulation

plus complexes réputées résoudre ce problème de biais (comme par exemple la méthode utilisant les coordonnées polaires modifiées, approche connue sous le nom de "modified polar coordinate"). Cette approche qui décompose le vecteur d'état en composantes observables et inobservables [4], est en effet connue pour éviter, non seulement les problèmes d'instabilité, grâce à un meilleur conditionnement de la matrice de covariance, mais également pour éliminer les biais.

Il est encore trop tôt pour conclure si l'approche que nous avons utilisée, basée nous le rappelons sur les pseudo-mesures, sera compatible avec l'application envisagée. Toutefois les résultats que nous avons obtenus, semblent déjà relativement satisfaisants et les biais que nous avons pu mettre en évidence sur certaines trajectoires d'approche sont assez faibles. L'étude qui va suivre et qui dépasse largement le cadre du seul problème de localisation, devrait nous permettre non seulement de tester d'autres scénarii d'approche, mais également de confirmer si la fonction de pilotage guidage de l'UAV, peut ou non tolérer ces biais et s'il y a lieu d'utiliser des techniques de filtrage plus sophistiquées.

4.0- Références

[1] Hammel, S.E., Aidala, V.J., "Observability Requirements for three-Dimensional Tracking via Angle Measurements". IEEE Trans. on Aerospace and Electronic Systems, AES-21, 200-207, March 1985.

[2] Aidala, V.J., "Kalman filter behavior in bearings-only tracking applications". IEEE Trans. on Aerospace and Electronic Systems, AES-15, 29-39, July 1982.

[3] Ferrier, B. & Semenza, J., "The Development, Simulation and Testing of the Landing Period Designator (LPD) Helicopter Recovery Aid", Proceedings of the American Helicopter Society, May 1994, Washington.

[4] Hoelzer, A.D., Johnson, G.W., and Cohen, A.O., "Modified polar coordinates-the key to well behaved bearings-only ranging", IBM Shipboard and Defense Systems, Manassas, VA, IBM Rep. 78-M19-0001A, Aug. 1978.

Remerciements

Les auteurs veulent remercier les services de Madame Sophie D. Radacovici (Institut de Recherches Cliniques de Montréal) et du Dr. René Kahawita (Ecole Polytechnique de Montréal).

Annexe I

Le repère R'_M se déduit de R_A par une rotation d'angle α autour de l'axe z_A et par une rotation d'angle $-\beta$ autour de l'axe y_A

La matrice de changement de base entre R_A et R'_M s'écrit donc:

$$R(\alpha, \beta) = R_{Z_A}(\alpha) \cdot R_{Y_A}(\beta)$$

$$R(\alpha, \beta) = \begin{bmatrix} \cos(\alpha)\cos(\beta) & -\sin(\alpha) & -\cos(\alpha)\sin(\beta) \\ \sin(\alpha)\cos(\beta) & \cos(\alpha) & -\sin(\alpha)\sin(\beta) \\ \sin(\beta) & 0 & \cos(\beta) \end{bmatrix}$$

On sait que cette matrice s'écrit aussi:

$$R(\alpha, \beta) = \begin{bmatrix} \vec{i} & \vec{j} & \vec{k} \end{bmatrix}_{/R_A}$$

D'où l'expression:

$$H = \begin{bmatrix} \begin{bmatrix} \vec{j} \end{bmatrix}^T \\ \begin{bmatrix} \vec{i} \end{bmatrix}^T \end{bmatrix}_{/R_A}$$

$$= \begin{bmatrix} \sin(\alpha) & -\cos(\alpha) & 0 \\ \cos(\alpha)\sin(\beta) & \sin(\alpha)\sin(\beta) & -\cos(\beta) \end{bmatrix}$$

Annexe II

Les équations utilisées sont celles d'un filtre classique de Kalman, rappelées ici:

$$X_{k+1/k} = A \cdot X_{k/k} + B \cdot \Sigma \gamma(k)$$

$$P_{k+1/k} = A \cdot P_{k/k} \cdot A^T + Q(k)$$

$$K(k+1) = P_{k+1/k} H^T(k+1) [H(k+1) \cdot P_{k+1/k} H^T(k+1) + R]^{-1}$$

$$X_{k+1/k+1} = X_{k+1/k} - K(k+1) H(k+1) X_{k+1/k}$$

$$P_{k+1/k+1} = [I - K(k+1) H(k+1)] \cdot P_{k+1/k}$$

TURKISH UNMANNED AIR VEHICLE DEVELOPMENTS

Ünver Kaynak
TUSAŞ Aerospace Industries (TAI) Inc.,
Design & Development Department
P.K. 16, Mamak, 06261 Ankara, TURKEY

1. FOREWORD

In parallel with the experimentation and acquisition of some state-of-the-art operational UAV systems for the military, in-country efforts were also initiated toward indigenous design and development of some UAV systems. Under government contracts, TAI has been involved in designing and developing of reconnaissance & surveillance UAV's as well as target drone prototypes. After demonstrating some Proof-of-Capability UAV and target drone prototypes, development of more advanced versions are being planned for the future.

2. INTRODUCTION

There is an increase on understanding of the benefits of using UAV's under certain scenarios. Acquisition of operational UAV's for the Turkish military, and lessons learned from recent conflicts in some troubled areas of the world (Ref. 1), give impetus to gaining some domestic expertise on the design and operation of drones. Under contract by the Undersecretariat of Defense Industries, TAI designed, developed and flight tested two line-of-sight UAV prototypes between 1990-1992. The intent was firstly to demonstrate TAI's design capabilities, and later, further develop the vehicles into mission capable vehicles by the addition of certain operational functions and mission payloads. The project was successfully completed with the delivery of the vehicles that had limited capabilities. TAI was responsible for the design and development of the airframe, systems integration, and ground and flight tests. Commercially available avionics systems were used in the ground control station and in the aircraft. The project enhanced the in-house knowledge base pertaining to unmanned air vehicles quite significantly, and encouraged the start of further activities that included target drones. Under the contract with MOD, TAI is currently developing a new target drone, TAI-UKHU, for use of the air defense units. In this paper, basically, TAI's efforts will be summarized which cover the UAV-X1 and the UKHU target drone.

3. TAI SHORT RANGE UAV : UAV-X1

TAI UAV-X1 is a short range, all-composite, double boom, pusher propeller, reconnaissance & surveillance drone that was indigenously designed and developed at TAI. The Ground Control Station subsystems and flight avionic systems were acquired from commercial vendors. The UAV-X1 has a steerable nose tri-cycle landing gear that was designed for conventional runway take-off and

landings. The vehicle has a nose video camera for observation missions that is also used as a visual aid for the internal pilot during take-off, final approach, and landing. There is a parachute system for emergency situations. During the development phase, handbook, as well as advanced theoretical methods were used for the design, and extensive ground and air tests were carried out that included wind-tunnel tests, structural and propulsion bench tests, surrogate airplane tests, and avionic bench tests. Since navigation capability was not installed yet, flight trials included only the line-of-sight tests within the airport traffic pattern. However, power and performance characteristics of the resulting drones still posed some interesting challenges for the crew during the flight trials.

3.1 System Description

TAI UAV-X1 system consists of two air vehicles, a ground control station including three omnidirectional antenna, and the ground support equipment (Fig. 1). Currently, crew of two which consists of one external and one internal pilot are required to operate the system. Each aircraft is equipped with a Digital Flight Control System (DFCS) which includes regular autopilot functions with optional GPS navigation function, emergency modes, and management of video and telemetry data. In the ground control station, there is a console that is comprised of a command panel for the internal pilot and a video monitor with telemetry data superimposed on it. The console also has two additional monitors showing digital telemetry data both in text and graphics format.

The air vehicles are all-composite, conventional pusher propeller, double-boom, two vertical tails and one horizontal tail, steerable nose tri-cycle landing gear configuration (Fig. 2). The air vehicles were designed for a short-range reconnaissance and surveillance missions with modest design goals as given in Table-I.

Table-I

Length	:	4.00 m.
Height	:	1.92 m.
Fuselage Width	:	0.40 m.
Wing Span	:	6.00 m.
Wing Chord	:	1.00 m.
Max T-O Weight	:	320 kg.
Payload Weight	:	45 kg.
Fuel Weight	:	50 kg.
Max. Cruise Speed	:	100 kt.

Stall Speed	:	42kt.
Max. Rate of Climb	:	360 m/min
Max. Range	:	741 nm.
Max. Endurance	:	7.5 hr.
T/O Distance	:	400 m.
Landing Distance	:	300 m.
Engine (Rotary)	:	42 hp
Propeller (3-blade)	:	1.40m. diam

In the flight control system, there are two flaperons for the roll control and high-lift requirements, one elevator for pitch control, and two rudders for the yaw control. FCS employs servos for the rudders, flaperons, elevator, throttle, steering and brakes. It was foreseen that in the initial phases of the developmental tests, the external pilot would fly the aircraft by visual contact, and the internal pilot would be the safety pilot monitoring the flight through the nose video camera, helping the external pilot in runway operations, particularly for aligning the vehicle during the final approach. In later phases, it was planned to use the internal pilot as the primary, while retaining the external pilot as the safety.

3.2 System Development

In the development phase, standard handbook, as well as advanced numerical and theoretical methods were used for the design, and extensive ground and air tests were carried out that included wind-tunnel tests, structural and propulsion bench tests, surrogate airplane tests, and avionic bench tests. CAD/CAM tools were used in the detailed design and production phase. A full scale actual and fully electronic "virtual" mock-ups (Fig. 3) were also prepared for systems lay-out planning and verification. In the following, some brief explanation of the kinds of methods and approaches that were taken in the air and ground systems development that cover the design, development, integration and ground and flight tests are explained.

Aerodynamic Design: Standard handbook type methods were used in the conceptual design phase. Later, the results were validated and further refined by using Computational Fluid Dynamics (CFD) tools along with graphics workstations for visualizing the results. A commercially available panel method (Ref. 2) was used to calculate the pressure and velocity field around the geometry. Figure 4 shows the surface pressure contours on the UAV-X1 as visualized in the graphics workstation. USAF DATCOM method (Ref. 3) was employed to study the stability and control characteristics of the aircraft, and to derive the hinge moments of the control surfaces. Based on the flight simulations with and without flaps, the hinge moments of each control surfaces were calculated from which the required servo powers, rates and deflections were derived. The aerodynamic coefficients and flow visualizations were obtained at wind-tunnel experiments that were

carried out at Middle East Technical University Low-Speed wind tunnel. Force and moment measurements were made using a mechanical balance, and flow visualizations were made using the tuft method. Also, propeller slip-stream effects were approximately simulated by means of an electrically driven powered model.

Structural Design: The UAV-X1 principally consists of four basic structures: Wing, Fuselage, Boom and Tails. The wing has two spars that are I-shaped and a channel beam, made of e-glass/epoxy laminates. Skin of the wing is composed of two layers of e-glass/epoxy laminates which cover the styrofoam wing profile. The fuselage skin is a sandwich structure of a grid score flexible foam between two layers of e-glass/epoxy laminates. There are four aluminum honeycomb bulkheads along the fuselage. Booms and tails are also made of the same composite material. The horizontal tail has two spars and vertical has one spar. The booms are composite laminates wrapped around a tapering rectangular cross-section styrofoam block.

Standard handbook methods were used in the conceptual design, and in-house developed and commercially available computerized design software were used for the preliminary sizing of the aircraft. Results were analyzed and verified by structural tests and advanced finite element simulations. The aircraft components were sized against +4.5/-1.5g loads. Starting from conceptual design to detailed design and production, computer aided design tools were utilized throughout the project. MSC/NASTRAN finite element software was used for the structural analysis (Ref. 4). Stress distributions and deflections of the wing, fuselage, tails, booms and the main landing gear strut were obtained. Figure 5 shows the stress distributions on the fuselage during flight. Structural tests were made to verify the calculations. The tests include material allowable tests like the tensile and shear testing of the composite laminates, adhesively bonded joint shear test and structural tests such as deflection test of the boom under tip loading, and wing test under distributed loading in which strains were measured at critical points.

Electronics Design: Use of commercially available electronic and avionic systems were preferred rather than a lengthy design & development process. For this reason, S-TEC Corporation of Texas and Aeromet Inc. of Oklahoma in U.S.A. were chosen as the main suppliers of the avionics and ground electronics systems. The S-TEC supplied nearly all the major avionic and control components including the Central Flight Guidance Computer (CFGC), i.e. the autopilot, and the sensors, servo actuators, and ground controller. The Aeromet Inc. supplied the on board real time video system, the data-link subsystem, some sensors, the Airborne Control System (ACS) and the rest of the ground control subsystems. Aeromet Inc. received the S-TEC developed equipment and added on their datalink, electrical

harness, video subsystem and ground control station equipment. Figure 6 shows the avionics architecture of the UAV-X1 including the ACS and CFGC. After accepting the systems at Aeromet by means of ground bench and surrogate aircraft tests, the harness design and manufacturing, system integration, ground bench tests and surrogate aircraft tests were done at TAI. In the following, the ground and airborne avionics systems will be described in more detail.

The Ground Control System: The GCS is a standalone workstation to manage all the data manipulation, total remote control, data storage, numerical and graphical display of all in-flight parameters and telemetered data. The GCS basically includes two computers; the ground control computer and the graphics computer, and three monitors. The ground control computer processes and sends the UAV control commands to the autopilot processor. Meanwhile, the telemetered information such as the speed, altitude, attitude and heading are displayed as superimposed on the nose video camera view in the pilot's monitor. The graphics computer processes and displays the telemetered data on two other monitors in text and graphics format. The telemetered data are the following: Altitude, IAS, Heading, Pitch/Roll/Yaw Attitudes, EGT, Engine RPM/Coolant Temp./Oil Level/Fuel Flow, Fuel Level, Chute Status, Battery Status, Alternator Status, Throttle Position, Rudder Position, Elevator Position, Flaperon Position. The GCS also includes the S-TEC ground controller, the data-link subsystem, the antennas, interface hardware, data storage medium, and power supply.

Airborne Avionics Systems: Airborne avionics and flight control systems consist of the Aeromet Airborne Control System (ACS), the S-TEC System-800 Central Flight Guidance Computer (CFGC), i.e. the autopilot, and all the necessary parts such as the sensors, servos, transducers, encoders, detectors, and transmitter/receivers. A fast scan real time video system is also included in the package with necessary support equipment. All the systems are powered by 24 to 28 VDC from the 28 VDC aircraft battery, or from the aircraft generator of 1.5 kW power.

The ACS is the integrating factor for all the subsystems on the aerial vehicle. Its minimal set of tasks includes providing an interface between all airborne subsystems, signal conditioning, error detection, in-flight telemetry, data routing, flight path and way-points storage and management, and analog/digital I/O operations. The ACS has a Motorola 68030 CPU module to exercise all the necessary functions over a VME bus, and connected to the CFGC and the VHF telemetry system through RS-232 serial ports (Fig. 6).

The S-TEC System 800 autopilot is a multiple mode autopilot system which can use inputs from an onboard pilot, can be controlled by remote command signals, or can be operated autonomously. The

System 800 is based around the CFGC that gets roll and pitch attitude information from the vertical gyro for inner loop stabilization, and steering information is derived from the directional gyro, navigation system or from remote control commands. The altitude encoder, altitude transducer and IAS transducer are used by the CFGC to determine the altitude, vertical speed and indicated air speed respectively. Normal autopilot operating modes include the altitude hold, heading hold, roll attitude hold and speed hold. In the stabilized mode, all commands to the autopilot are essentially attitude commands and the autopilot drives the roll and pitch servos to hold the aircraft at the commanded attitudes. In case of a link loss, there is an emergency mode that puts the vehicle into climbing and waiting mode after which an engine kill and parachute activation commands are executed if the link is not reestablished after a predetermined period of time, say 10 minutes. However, if the speed is less than 50 kts., it stops the engine and applies the brakes, because the aircraft is presumably not airborne in that speed. Also, the autopilot has a navigation system interface that uses most global type navigation systems including the GPS.

System Integration and Testing: The electronic equipment of the Aeromet Inc. and S-Tech Corp. were integrated in the Aeromet facilities. The bench test harness specifically built for the integration test was utilized to check functioning and integrity of all components. A common bench test procedure was developed between TAI and Aeromet, and modifications specified by TAI were applied. The electronic bench-test setup with the equipment was loaded into a manned aircraft owned by the Aeromet, and the on-board equipment was tested from the ground control station according to the radio range test procedures developed by the Aeromet. The test verified the predicted ranges for control up-down link, video downlink and back-up RC up-link. Later, the same tests were repeated at TAI using the TAI made harness in the bench and in a surrogate plane.

At Aeromet, pilot familiarization activities were also conducted using a manned aircraft that was equipped with a system that was highly similar to TAI's. This aircraft with the on-board safety pilot was flown by the TAI pilot both from the ground station and from outside using a hand-held RC radio. The autopilot functions and aircraft response were accustomed during the RC flight using an eye-contact with the plane in which case the TAI pilot acted as an external pilot. Alternatively, the plane was flown from the ground control station by the TAI pilot acting as the internal pilot using the video monitor that supplied the nose video camera view. Relative merits of each approach were assessed.

3.3 Flight Trials

Because of yet to be completed navigation capability, only line-of-sight flights were conducted in the airport traffic pattern. It was known that

conventional take-off and landing operations and low altitude flight of a relatively bigger size UAVs' flight testing might often times get rather complicated. During both the development and flight testing phases, significant changes were made to the aircraft which resulted in some overweight vehicles. Also, engine integration and performance goals were rather short which resulted in higher wing loadings and underpower configurations. Changed performance values added with a freshmen flight crew led into difficult test campaigns. Expert support was received from SADLER Aircraft Company of Arizona during all phases of the flight trials.

Three flight test campaigns such as the high speed taxi tests, crow-up tests and full circuit flight tests were conducted at remote flight test locations where the electromagnetic interference from other sources would be the lowest. In all these tests, the external pilot acted as the primary and the internal pilot acted as the back-up pilot, with the hope that the external pilot would become the primary when certain goals were achieved. This choice was dictated by the need to observe the aircraft motion very closely by using a chase car in which the driver and the pilot, observer-engineer and the video recording engineer were also present. Visual contact with the control surface motions and the total aircraft motions were found to be most useful especially for making autopilot gain adjustments. Hand-over procedures were developed and practiced between the primary and the back-up pilots in case of an emergency such as a link loss. The telemeter readings were communicated to the chase car crew by the back-up pilot. It turned out that this procedure had to be followed during the entire flight trials, and they were conducted in three stages: 1) High Speed Taxi Tests, 2) Crow-Hop Tests, and 3) the Traffic Pattern Flight.

1) In the high speed taxi tests, runway performance of the vehicles were measured such as the rotation speed and distance, engine performance, acceleration qualities, throttle and nose landing gear steering authority and response times, braking distance etc. Also, hand-over procedures between the pilots for the runway operations were practiced.

2) During the crow-hop tests, a sequence of high speed taxi, rotation, lift-off, low altitude level flight and landing in the short distance was practiced. This test helped the crew to better understand the aircraft runway performance, including the assessment of the maximum dynamic thrust available, take-off speed and rudder authority. However, one important element of these tests was to make the autopilot gain adjustments after visual contact with the aircraft response and its attitude against the given commands. The chase car technique in time got more difficult to execute, but was stuck with as being a useful method. During these tests, it was also understood that because of the insufficient power and thrust values, landing should be made with some open throttle which made the operation rather more difficult than with a conventional cut-off throttle.

This phase of the trials also helped to assess the landing gear performance and to modify it as necessary for this relatively overweight vehicle.

3) The full circuit pattern flight test was started after the assessment of the aircraft performance, mechanical modifications, autopilot adjustments and crew training. Again, the chase car was used, with a back-up pilot in the GCS and another back-up pilot flying in a chase plane in case the vehicle flies out of bounds. The chase car technique got truly difficult this time because of the fact that the air vehicle should at all times stay in a good visual range of the car and a good coordination between the pilot and driver was necessary. In this stage, after the take-off, the plane was followed up in the runway, and while the plane was making the downwind leg, the car was raced down in the taxiway back to the approach end of the runway. A left traffic pattern was used, so that the pilot visually followed the plane at all times to his right. During the final approach and landing phase, the chase car again raced up in the runway. It was originally planned that starting with the 2nd phase of the flight trials, i.e. during the crow-hops, the internal pilot would actually fly the aircraft. However, due to lack of time to repeat all the past tests with the external and internal pilots' role changed, and because the external pilot reached his peak time, the pilots' role change was not attempted. However, it was getting more clear that external pilot as the primary should be recommended early in the flight test program, but a gradual shift should be made to the internal pilot in time.

4. TAI TARGET DRONE : UKHU

After winning an MOD contract, TAI recently started indigenous design studies for a piston powered target drone prototype for use with the air defense units including air gunnery and missile units. The prototype called as the UKHU (which stands for a target drone in Turkish), is being designed for double use; as a target drone and as a close-range UAV with the addition of a payload. The prototype will be developed to demonstrate that it is a viable vehicle for simulating air attacks against air, sea and land forces. The body will be all composite, and will be usable in the naval environment also. The take-off will be from a catapult with a launch rail and the landing will be through a parachute. The first phase of the project only covers a flight within the visual range using an RC technique, and a simple auto stabilizer will be used to aid the operator when the plane is far away. The project includes the design and development of the catapult launcher and addition of some on-board mission equipment such as a radar reflector and a miss distance indicator (MDI). The drone will also tow a target banner. In the future, advanced capabilities will be added to the vehicles such as optical and radar tracking, surveillance camera, autopilot and navigation capabilities.

TAI-UKHU is an all-composite, pusher propeller vehicle with a cranked double delta wing and double vertical fins (Fig. 7). It has only elevons as control surfaces. The design studies of the TAI-UKHU were already concluded and these studies foreseen the following targets as given in Table-II.

Table-II

Length	:	2.50 m.
Height	:	0.88 m.
Fuselage Width	:	0.30 m.
Wing Span	:	2.84 m.
Max T-O Weight	:	80 kg.
Empty Weight	:	48 kg.
Max. Speed	:	180 kt.
Max. Rate of Climb	:	750 m/min
Max. Endurance	:	1.5 hr.
Engine	:	40+ hp
Propeller (2-blade)	:	0.6 m. diam

The project is now in the full scale development phase which will last for 11 months.

5. CONCLUSION

TAI has developed and flight tested, within the visual range, two short range unmanned air vehicle

prototypes. The complete system has now limited capabilities, but by the addition of mission equipment and navigation capabilities, operational systems could be obtained. However, rather than upgrading the present systems, plans are being made for developing an all new short range vehicle with advanced qualities for the future requirements. Furthermore, after the introduction of new target drones, versatile vehicles including close range UAVs can be developed if need arises. Finally, increased in-country capabilities in this area are being looked for in coming years.

References

- 1) Wagner, G., Rear Admiral, "US Experience with UAVs", UV94, Shepherd Conferences, Paris, France, 16-17 June 1994.
- 2) VSAERO Panel Method, COSMIC, Athens, GA 30602, USA.
- 3) USAF DATCOM, Wright-Patterson Air Force Base, Dayton, OH, U.S.A.
- 4) MSC/NASTRAN, Mac Neal-Schwendler Corporation, Los Angeles, CA, 90041-1777, USA.

FIGURES

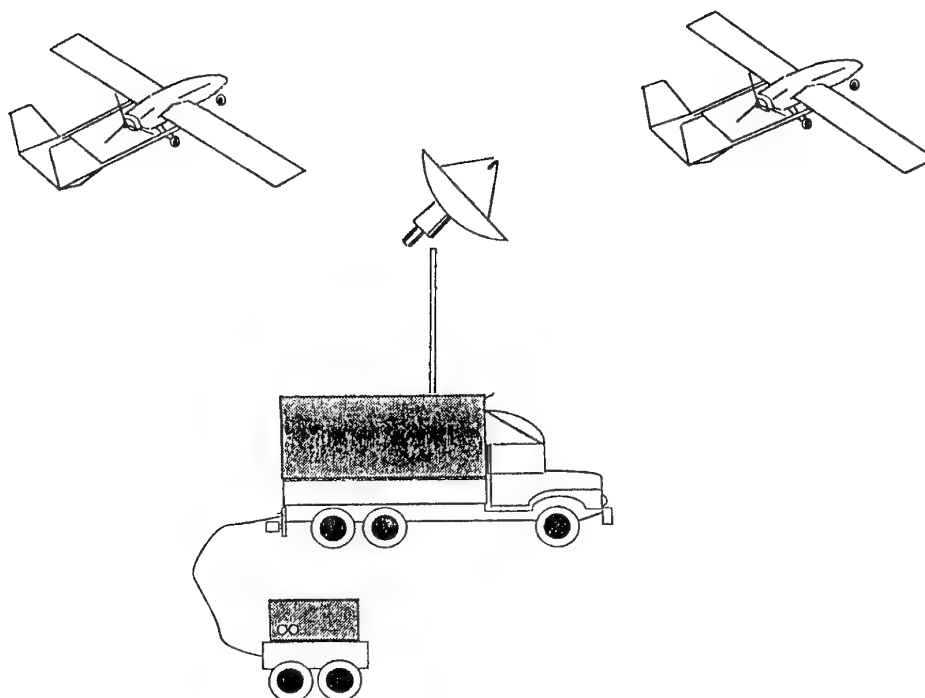


Fig. 1 TAI UAV-X1 system is composed of two air vehicles, a ground control station with antennas and the ground support equipment



Fig. 2 TAI UAV-X1 all-composite unmanned air vehicle

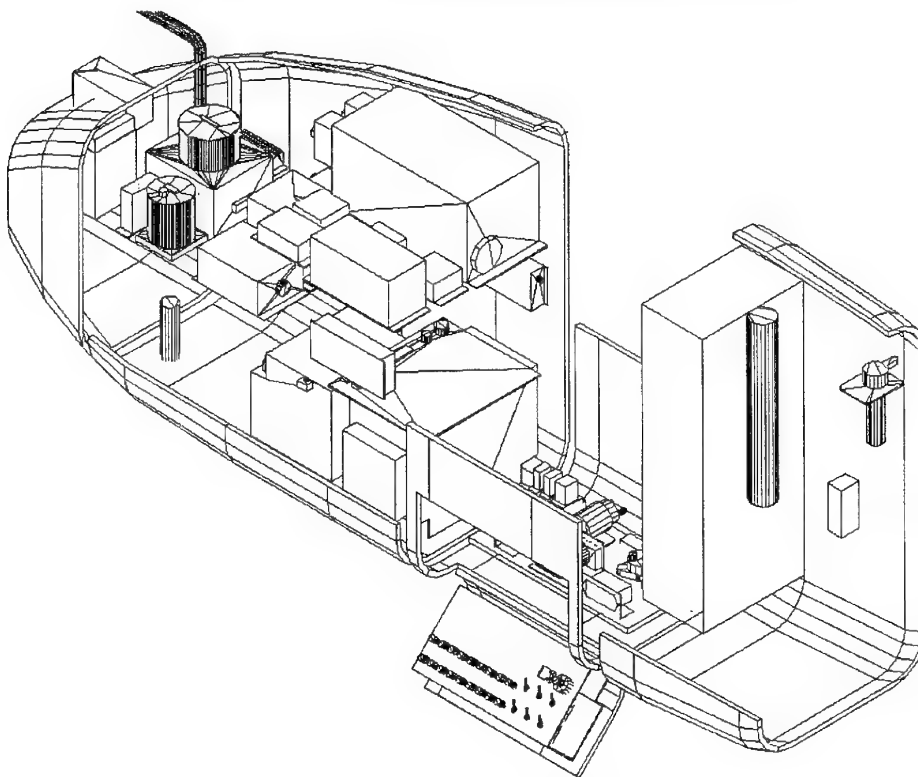


Fig. 3. Computerized mock-up of the airborne electronic units lay-out

PRESSURE COEFFICIENT
UAV-X1 WING/BODY/TAIL CONFIGURATION

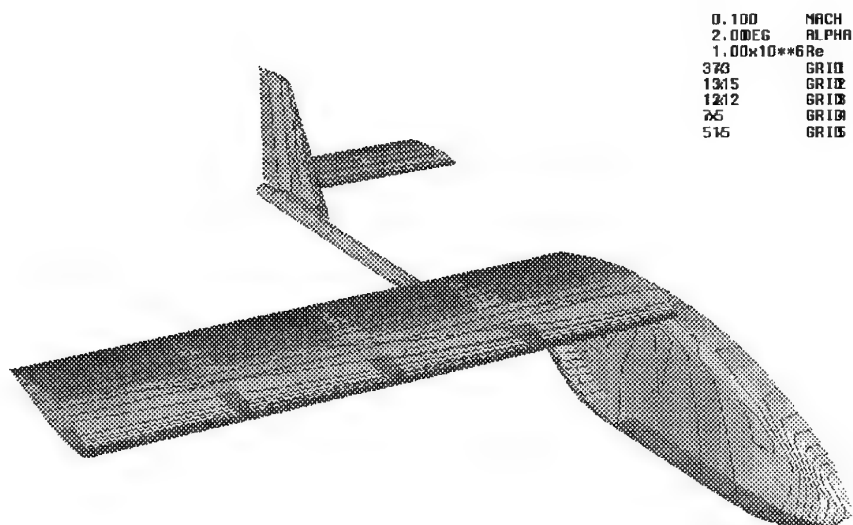


Fig.4 Pressure distributions on the UAV-X1 using the panel method

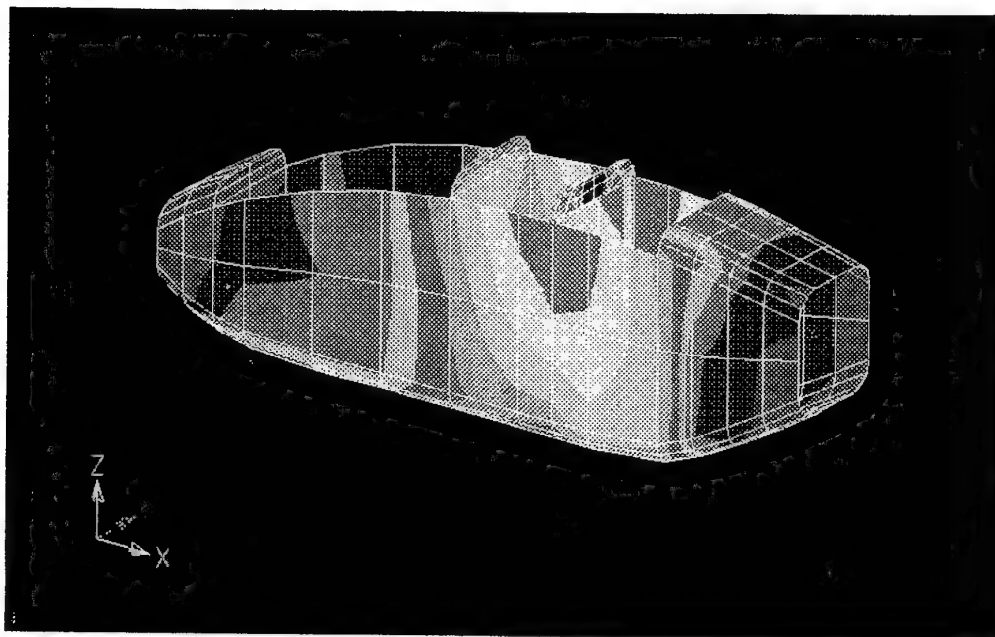


Fig. 5 Finite element calculation of stress distributions on the UAV-X1 fuselage

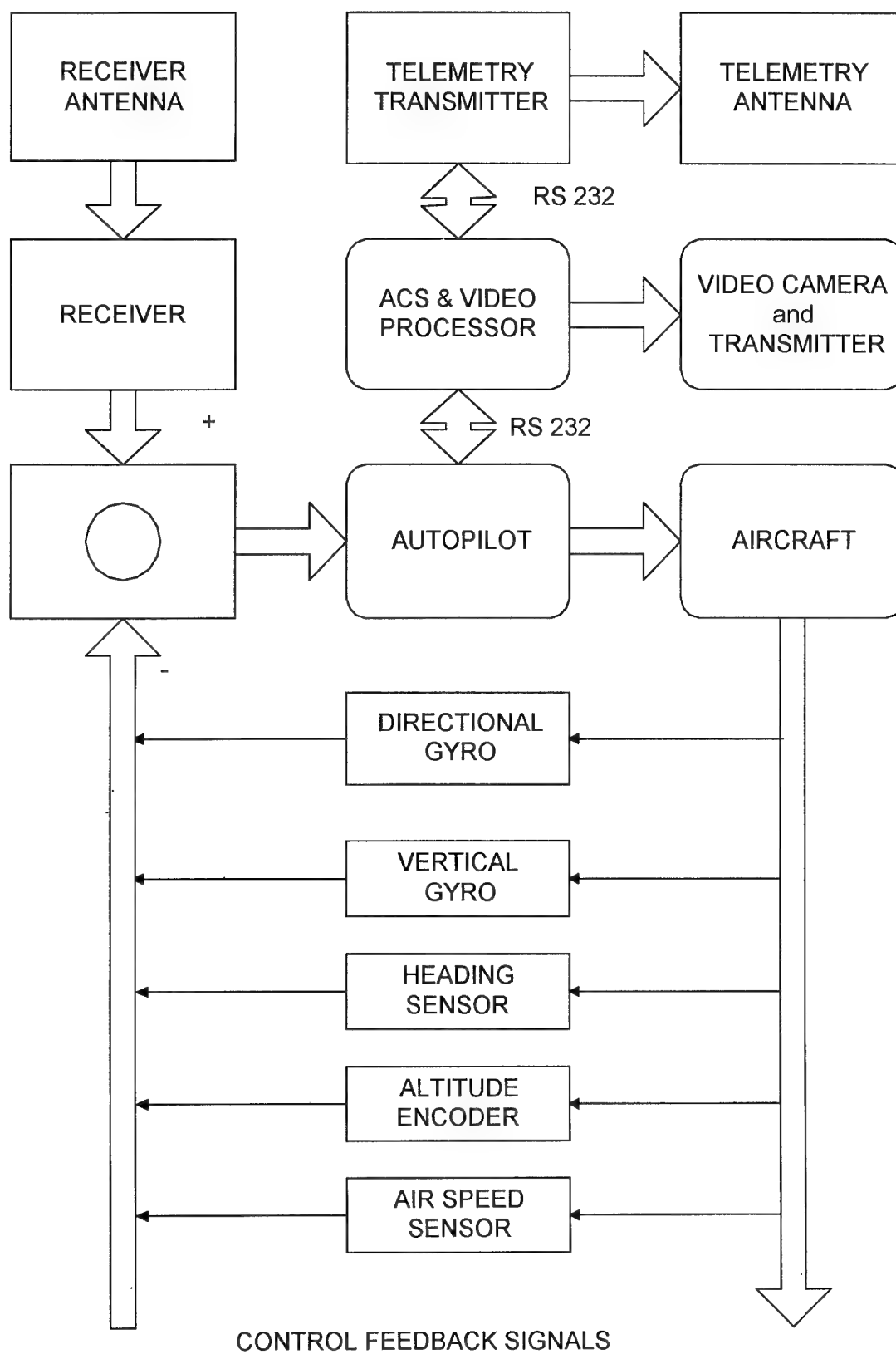


Fig. 6 Airborne electronics systems architecture of the UAV-X1

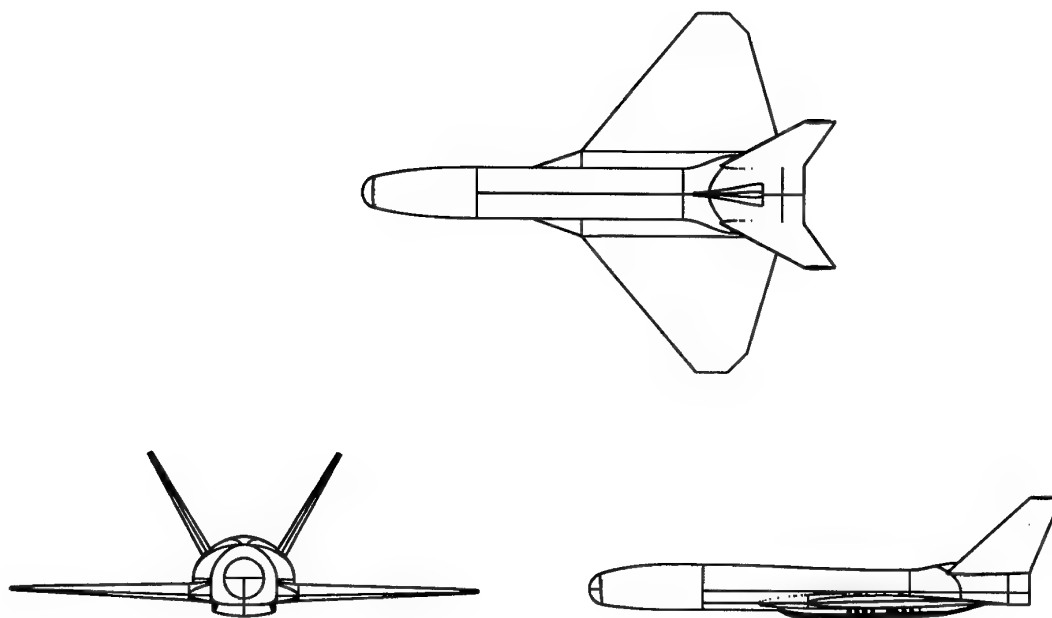


Fig. 7 TAI UKHU target drone

SYSTÈME D'ALERTE AUTONOME DÉPORTÉ CONTRE MISSILES ANTINAVIRES BASSE ET TRÈS BASSE ALTITUDE

S. FESLAND
P. NIGRON
THOMSON-CSF/DIVISION SYSTÈMES MISSILES
DT/SEPA/SDAE
9, rue des Mathurins, B.P. 150,
92223 Bagneux Cedex, France

1. RÉSUMÉ

Ce système s'inscrit dans le cadre d'un système d'alerte pour la Marine participant à la défense des bâtiments de surface contre les missiles anti-navires basse et très basse altitude.

Il s'appuie sur un concept original d'alerte précoce utilisant des UAV, Unmanned Aerial Vehicle, autonomes.

Une logique de commande de chaque UAV prenant en compte différentes contraintes (pas de collisions avec les autres UAV, déplacement du bâtiment porteur) est présentée. Elle utilise la théorie de la logique floue.

Une simulation informatique réalisée par THOMSON-CSF a permis d'obtenir des résultats prouvant qu'un tel concept est très prometteur. Ces résultats sont présentés et des variantes proposées.

2. INTRODUCTION

Le système d'alerte autonome déporté (SALAD) s'inscrit dans le cadre d'un système d'alerte pour la Marine participant à la défense des bâtiments de surface contre les missiles anti-navires basse et très basse altitude.

La détection de ces missiles par les moyens du bord ne peut être envisagée qu'à une distance maximale comprise entre 10 et 15 km. Les fortes contraintes d'environnement (horizon, clutter de mer, effet image, ...) rendent difficile une détection plus lointaine. Cette détection tardive limite le temps de réaction de la défense antiaérienne du bord et ampute d'autant la probabilité de survie des bâtiments.

L'alerte précoce doit donc être fournie par des moyens déportés voire externes au bâtiment. Les solutions actuellement opérationnelles dans les Marines sont constituées d'avions de guet avancés dont l'utilisation n'est envisageable que près des côtes amies ou par une force navale comportant un porte-avions.

La réflexion menée par THOMSON-CSF pour la Direction des Constructions Navales de l'administration française sur les possibilités d'intégration d'UAV, au sein d'une force navale a montré que le concept UAV peut être une solution pour doter nos frégates de cette capacité. L'étude a mis en avant également des contraintes d'utilisation:

- * pour assurer une couverture suffisante, le système doit comporter plusieurs UAV,
- * la plate-forme UAV doit être, indépendamment de la formule aérodynamique retenue, de très petite taille

afin de rendre possible son intégration dans un bâtiment de type frégate,

- * la mise en oeuvre ainsi que le contrôle du vol doivent être le plus automatisés possible.

Un système de contrôle des UAV, centralisé sur le bâtiment peut être envisagé. Les inconvénients d'un tel système résident dans la nécessité de disposer d'un moyen de contrôle de trajectoire depuis le bord du bâtiment chargé de la mise en oeuvre. Un système de plusieurs UAV en vol simultanés va s'avérer lourd à gérer: en particulier le contrôle des plans de vol pour éviter les collisions, ceci pendant le déploiement, le fonctionnement et la récupération des unités. Les trajectoires doivent intégrer des contraintes liées au besoin de continuité de la couverture d'alerte, au déplacement du bâtiment et donc de la zone à surveiller, aux différentes vitesses de vol des plates-formes... Le système doit prendre en compte les différences de performances des senseurs, ces différences pouvant être propres à chaque matériel (dispersion des caractéristiques des composants, dysfonctionnement d'un senseur, ...) ou induites par les conditions locales de fonctionnement (pluie, brouillage, ...).

Pour pallier à ces inconvénients, un concept UAV autonome a été imaginé. Chaque UAV doit, par ses propres moyens, contrôler sa trajectoire par rapport au bâtiment-porteur et aux autres plates-formes, tout en répondant aux exigences suivantes:

- * simplicité d'emploi et de mise en oeuvre,
 - * Robustesse face aux perturbations atmosphériques, aux dysfonctionnements des autres UAV, aux dispersions intrinsèques des composants et aux déplacements du bâtiment.
- L'action du bâtiment porteur se limite alors, par une unique commande adressée à l'ensemble des unités, à contrôler la distance qui le sépare du système d'alerte déporté.

On se propose d'organiser cette coopération en utilisant une des techniques d'intelligence artificielle: la commande floue. Cette technique est très adaptée à des systèmes non linéaires, à commande temporelle et dont un modèle est difficile, voire impossible à définir. Cette organisation permet d'optimiser le déploiement des UAV en environnement clair, brouillé, et dans des configurations comportant un ou plusieurs bâtiments en mouvement. Une simulation informatique réalisée par THOMSON-CSF et sur fonds propres a permis d'obtenir des résultats prouvant qu'un tel concept est très prometteur.

L'originalité du concept proposé repose sur trois points:

- * l'autonomie de chaque plate-forme volante par rapport aux autres, et la capacité d'autorégulation du

système d'alerte déporté ainsi constitué. Le bâtiment porteur gère globalement le système et non pas chaque unité,

- * le double emploi des équipements embarqués par l'UAV, limitant ainsi le besoin en charge utile de la plate-forme,

- * une commande interne de l'UAV utilisant la logique floue.

3. DESCRIPTION DU SYSTÈME

Le système SALAD est constitué de plusieurs plates-formes volantes porteuses de senseurs capables de détecter des missiles anti-navires évoluant à basse et très basse altitude.

Pour l'étude et la présentation du concept, la configuration retenue est constituée d'une ceinture d'UAV gravitant autour d'un bâtiment porteur. D'autres configurations sont envisageables et des exemples seront présentés à la fin de ce document.

Le concept permet une gestion simple de l'ensemble des trajectoires des UAV où un nombre a priori indéfini gravite autour du bâtiment.

Pour remplir cette mission, le bâtiment est équipé:

- * d'un émetteur hyperfréquence omnidirectionnel à onde continue et à fréquence commandable (E1),
- * d'un système de réception omnidirectionnel de message d'alerte (R1).

Les UAV sont, pour leur part, constitués:

- * d'une plate-forme volant à vitesse et altitude constantes pouvant effectuer des manoeuvres dans un plan horizontal, et asservie en altitude,
- * d'un senseur radar à couverture sectorielle capable de détecter la menace considérée, orienté dans l'axe de la plate-forme et pointé vers l'avant (E2),
- * d'un récepteur hyperfréquence dans la bande du radar, à couverture sectorielle, orienté dans l'axe de la plate-forme et pointé vers l'arrière, indiquant le niveau de signal reçu par rapport à un niveau de bruit et d'environnement (R2),
- * d'un récepteur hyperfréquence dans la bande de l'émetteur du bâtiment, à couverture sectorielle ou omnidirectionnelle, orienté horizontalement et perpendiculairement à l'axe de la plate-forme (i.e. dans la direction du bâtiment), indiquant la fréquence du signal reçu (R3),
- * d'un système d'émission de message d'alerte, à couverture sectorielle, orienté horizontalement et perpendiculairement à l'axe de la plate-forme (E3) (i.e. dans la direction du bâtiment),
- * d'un système de commande et contrôle des manoeuvres horizontales de la plate-forme, dont le principe est expliqué ci-dessous.

Le déploiement s'effectue par largage successif des UAV qui s'organisent de manière autonome en cercle autour du bâtiment comme nous le montre la figure 1.

Ainsi déployé, chaque UAV utilisera son senseur (E2) pour détecter la présence d'une menace. En cas de détection d'une cible, un signal d'alerte sera directement transmis au bâtiment au moyen du système (E3).

La récupération doit être effectuée par un moyen supplémentaire. Les UAV sont désactivés au fur et à mesure de leur récupération. Le rapprochement des UAV est alors commandé par le bâtiment, au moyen de l'émetteur (E1).

4. PRINCIPE DE FONCTIONNEMENT

Deux composantes régissent le comportement de la plate-forme volante:

- * la fréquence émise par l'émetteur (E1) du bâtiment qui détermine la distance entre l'UAV et le bâtiment (i.e. la trajectoire nominale de l'unité autour du bâtiment),

- * le niveau du signal reçu émis par l'ensemble des senseurs (E2) des autres UAV qui caractérise la position de l'UAV par rapport aux autres unités.

Pour cette configuration du système, deux conditions doivent être respectées:

- * les plates-formes sont mobiles en vol horizontal et défilent dans le même sens,

- * Chaque unité volante se déplace à vitesse constante.

Afin de respecter les exigences du système qui sont d'éviter d'une part des "trous" de surveillance dans la zone d'alerte (assurer la continuité de la couverture d'alerte) et d'autre part des collisions entre UAV, la commande à appliquer à l'unité doit satisfaire aux deux contraintes suivantes:

- * positionner l'UAV au plus près de la trajectoire circulaire nominale définie par le bâtiment via (E1),
- * assurer une répartition uniforme des UAV sur la trajectoire.

Dans la configuration envisagée, les UAV sont à voilure fixe, une seule commande est appliquée à la plate-forme portant sur l'accélération latérale, maintenant ainsi le module de la vitesse constant.

4.1 Positionnement de l'UAV sur la trajectoire nominale

Le positionnement de l'unité est réalisé de manière automatique par mesure de la fréquence émise par l'émetteur (E1) du bâtiment. Chaque unité compare alors la fréquence reçue par le récepteur (R3) à la fréquence de référence du système qui définit la trajectoire nominale sur laquelle doit graviter toutes plates-formes du système.

La commande alors générée visera à augmenter ou respectivement diminuer le rayon de courbure de l'unité si la fréquence reçue se trouve être supérieure respectivement inférieure à la fréquence de référence.

4.2 Positionnement de l'UAV par rapport aux autres plates-formes du système

Le positionnement de l'unité fait référence au niveau de signal reçu par le récepteur (R2), signal émis par l'ensemble des émetteurs (E2) des plates-formes du système.

L'action de l'unité consiste alors à éviter les autres plates-formes si un niveau trop important du signal reçu est constaté.

Le mécanisme d'évitement repose, comme précédemment, sur la capacité de l'unité à modifier son rayon de courbure par rapport à la trajectoire nominale du système.

En se rapprochant du bâtiment (i.e. en réduisant son rayon de courbure), l'unité possède alors une vitesse de rotation autour du bâtiment plus importante que les plates-formes qui le suivent, tout en gardant le module de sa vitesse constant.

Ceci a pour effet immédiat d'éloigner l'unité de celles qui la suivent et de diminuer ainsi le niveau du signal reçu par le récepteur (R2).

4.3 Exemple de fonctionnement

La figure 2 schématise les différents états d'un système constitué de 4 plates-formes volantes notées respectivement de UAV1 à UAV4, gravitant autour d'un bâtiment B1 immobile.

Quatre états sont décrits:

- 1) état collision: l'unité UAV1 se rapproche de l'UAV2 pour se positionner sur la trajectoire nominale du système,
- 2) état évitement: UAV2 réagit à la présence de UAV1 en diminuant son rayon de courbure par rapport à la trajectoire nominale,
- 3) état éloignement: UAV2 s'éloigne de l'UAV1 ayant une vitesse tangentielle supérieure.
- 4) état positionnement sur trajectoire nominale: l'UAV2 recherche à se positionner sur la trajectoire nominale définie par le bâtiment. Etant éloigné de l'UAV1, UAV2 n'est plus perturbé et peut donc retourner sur cette trajectoire, la distance entre UAV1 et UAV2 étant devenue suffisante.

Ces quatre états seront ainsi appliqués individuellement à l'ensemble des plates-formes qui gravitent autour du bâtiment. Ils seront répétés jusqu'à obtenir un niveau stable du système correspondant au cas où chaque unité se trouve à la fois à bonne distance des autres plates-formes et sur la trajectoire nominale établie par le bâtiment.

5. INTÉRÊT DU CONCEPT UTILISÉ

Par sa simplicité de fonctionnement, le système permet, sans contrôle supplémentaire et de manière automatique:

- * d'agir directement sur l'ensemble des plates-formes pour augmenter ou réduire la zone de surveillance du système global à partir de la fréquence de l'émetteur (E1) du bâtiment,
- * de maintenir en rotation autour du bâtiment en déplacement, toutes plates-formes volantes par décalage de la fréquence, induite de l'effet Doppler généré entre chaque unité et le bâtiment,
- * de compenser le brouillage et les pertes de transmission atmosphérique par un resserrement des plates-formes, maintenant ainsi les performances de détection et la capacité d'alerte,
- * d'éviter toute synchronisation des unités par le bâtiment: le déploiement ou la récupération d'unité peut être réalisé de manière indépendante sans gestion principale du bâtiment.

6. SIMULATION

Une simulation développée sur fonds propres par THOMSON-CSF a permis de valider les différents concepts proposés.

6.1 Description

Le système développé possède les fonctionnalités suivantes pour l'opérateur:

- * envoyer ou supprimer individuellement une plate-forme volante,
- * déplacer le bâtiment,
- * augmenter ou diminuer la fréquence émise par (E1).

La simulation modélise pour chaque unité:

- * le signal reçu par (R2) par un diagramme d'antenne simplifié,
- * la fréquence reçue par (R3),
- * le vol des unités à une vitesse constante,
- * une commande à appliquer (accélération latérale).

Le calcul de la commande à appliquer à l'unité est réalisé à partir de règles d'inférence et de prémisses incertaines ou imprécises. La technique de commande floue est ainsi utilisée.

Les paramètres d'entrée de la commande sont directement:

- * le niveau de signal reçu,
- * la fréquence émise par le bâtiment.

Des domaines d'application ont été définis pour chacune des variables d'entrée ainsi que pour la commande.

Ces domaines appliqués aux règles d'inférence régissent le comportement final de la plate-forme volante.

Ces ensembles sont subjectifs et ont été affinés en fonction:

- * de l'expertise demandée du système: réaction de l'unité face à la présence d'une plate-forme, capacité d'atteindre la trajectoire nominale plus ou moins rapide, ...
- * des caractéristiques techniques des systèmes embarqués dans l'unité: performance de l'émetteur, temps de réponse de la plate-forme, ...

Cependant, les deux règles suivantes ont été respectées:

- * trop peu de recouvrement tend à faire fonctionner le système comme un système à logique bivalente classique,
- * trop de recouvrement empêche le système de faire la distinction entre deux ensembles.

Un juste milieu dans le choix des domaines a été trouvé afin de permettre au système d'établir des solutions intermédiaires face à des situations antagonistes fortes, comme de vouloir:

- * réduire le rayon de courbure pour éviter toute collision,
- * augmenter le rayon de courbure pour se positionner sur la trajectoire nominale.

La simulation a permis de valider la définition de toutes les règles de décision décrite sous la forme:

SI antécédent, ALORS conséquent

Cet ensemble de règles a permis de passer des sous-ensembles flous d'entrée (présent dans l'antécédent de la règle) aux sous-ensembles flous de sortie (présents dans le conséquent).

La simulation propose seulement les opérateurs ET et NON pour la constitution des antécédents et conséquents. L'opérateur OU est sous-entendu, par réduction à une forme canonique, où l'emploi de plusieurs règles se rapportant au même ensemble flou de sortie est équivalent à l'utilisation de l'opérateur OU.

C'est ainsi qu'une dizaine de règles a été définie pour réguler notre système, nous en donnons ici quelques exemples:

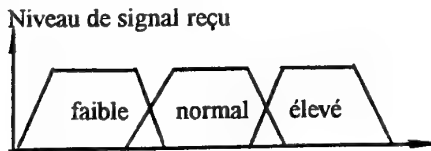
SI fréquence E1 EST en-éloignement,
ALORS commande EST à-gauche

SI niveau signal reçu EST élevé,

ALORS commande EST à-gauche

SI niveau signal reçu EST normal,
ALORS commande EST nulle

avec comme domaine:



6.2 Résultats

Quatre cas ont été traités à partir de la simulation, pour démontrer:

- * la faisabilité du système:
 - cas simple de 2 UAV mettant en avant les capacités d'anticollision du système, où une description du concept et l'évolution des paramètres de la commande floue sont réalisées,
 - cas de 6 UAV,
- * la robustesse du système face:
 - à une modification de la fréquence commandable,
 - aux déplacements du bâtiment-porteur.

La figure 3 représente différents états de la simulation, le système étant composé de deux UAV. La trajectoire nominale d'un UAV est présentée en figure 3.a. Une fois que l'UAV E1 est stabilisé, un deuxième UAV E2 est lancé (figure 3.b). La présence du deuxième UAV occasionne une gêne sur le premier, obligeant ce dernier à modifier sa trajectoire (figure 3.c). L'UAV E1 s'est suffisamment éloigné du deuxième pour se repositionner sur le rayon nominal défini par la fréquence émise par le bâtiment. Nous nous retrouvons alors dans un état stable du système (figure 3.d).

La figure 4 présente les différentes commandes appliquées en cours de simulation sur deux UAV. Sont présentés pour chaque unité, l'accélération latérale commandée (ACC), le niveau de signal reçu (NRE) et la fréquence commandable par le bâtiment (FRM). Au départ, chaque UAV perçoit une forte valeur de FRM, ce qui nécessite de commander à la plate-forme une forte accélération latérale. Le deuxième UAV est lancé quelques instants après. La présence pour la première unité d'une forte valeur pour NRE témoigne du risque de collision par la deuxième plate-forme. Les règles de commande floue déterminent alors une valeur d'accélération latérale plus faible, permettant de diminuer la valeur NRE du premier UAV. Les valeurs de FRM et NRE convergent ainsi progressivement vers la valeur nulle, signifiant la bonne position des plates-formes relative au bâtiment. Les accélérations latérales tendent de même vers une valeur stable, proche de -1: valeur nominale assurant le maintien des UAV autour du bâtiment.

La figure 5 présente la situation de la simulation, avec 6 UAV. Après la stabilisation des unités E1, E2, E3, 3 UAV (E4, E5, E6) ont été lancés du bâtiment. La figure 5.a présente la situation du système peu de temps après le lancement. Le système s'est stabilisé pour fournir au bâtiment une couverture fermée de la zone de surveillance comme le montre la figure 5.b.

La figure 6 présente la situation de la simulation après diminution de la fréquence émise par le bâtiment. Chaque UAV modifie sa trajectoire pour se positionner

progressivement sur le nouveau rayon de courbure déterminé par la fréquence du bâtiment.

Après stabilisation du système, la figure 7 présente la situation de la simulation après déplacement du bâtiment (a: vertical, b: horizontal). Chaque unité répercute les déplacements du bâtiment en adaptant sa trajectoire. Le système maintient ainsi la couverture globale de la zone de surveillance.

6.3 Limitations

L'exécution en simulation du système SALAD, à partir de la commande floue, a permis de faire les constatations suivantes:

- * il existe un rayon minimum fonction du nombre d'unités, afin de maintenir un système stable et à couverture homogène,
- * pour des besoins de continuité de la zone d'alerte lors du déplacement du bâtiment porteur, la vitesse de ce dernier doit être inférieure à une vitesse de l'ordre de deux fois la vitesse des plates-formes,
- * la stabilité du système est garantie si la dispersion des modules des vitesses des plates-formes n'est pas trop importante.

7. VARIANTES DU SYSTÈME

Le principe peut être généralisé à plusieurs bâtiments, chacun portant un émetteur à fréquence commandable. La figure 8 présente des déploiements à plusieurs bâtiments.

Ces configurations ne sont possibles que sur le respect de la règle suivante: le rayon de courbure reste supérieur à la distance maximale entre deux bâtiments adjacents. Le système permet le maintien de la zone de surveillance quelque soit la direction de déplacement des bâtiments (limité à la règle établie précédemment).

Nous pouvons également envisager un système d'alerte à plusieurs couches. Pour cela, il suffit de définir pour un même bâtiment différentes fréquences commandables pour chaque couche souhaitée. Les UAV des couches inférieures auront, en plus de leur fonction principale d'alerte, pour rôle de relais transmetteurs des signaux d'alerte provenant des couches supérieures.

D'autres variantes peuvent exister concernant les types d'émetteurs et de récepteurs utilisés (caméras infrarouge, lasers, ...) par les UAV ou le bâtiment.

Des plates-formes stationnaires à voilure tournante peuvent également être utilisées. Dans ce cas, les commandes ne sont plus des accélérations latérales mais des directions de déplacement. Le principe reste cependant le même: asservissement des positions relatives des plates-formes par mesure du niveau de signal venant des autres UAV et asservissement par rapport au bâtiment par mesure de la fréquence reçue. Ce concept demande néanmoins une mesure de la direction du bâtiment (par exemple, par goniométrie).

8. CONCLUSION

Pour une application Marine, le déploiement d'un système d'UAV tel que présenté dans cet article peut être une solution simple et efficace, pour pallier aux limitations physiques des systèmes de détection embarqués.

L'utilisation de la commande floue paraît être une méthode adaptée. Elle permet de démontrer rapidement

la faisabilité d'un tel système et le principe d'autonomie de chaque plate-forme.

La simplicité d'utilisation de SALAD, la richesse des configurations possibles prouve qu'un tel concept est prometteur. Et, couplé à des systèmes de défense antiaérienne, SALAD peut augmenter, dans des configurations critiques d'attaque (missile basse et très basse altitude, brouillage, ...), la survivabilité globale de la force navale qu'il accompagne.

Le dimensionnement opérationnel du système reste à étudier: combien d'UAV, à quelle distance du bâtiment est-il nécessaire de déployer les plates-formes pour obtenir une couverture optimale? Ceci ne peut être entrepris qu'à partir d'une définition des menaces envisagées, du besoin opérationnel du système et de la connaissance approfondie du matériel embarqué et de la plate-forme utilisée...

Des applications terrestres peuvent être envisagées et étendre ainsi le domaine d'action de ce système. Il peut être utilisé pour la détection de cibles (missile de croisière, intercepteurs) masquées par le relief, dans la défense aérienne d'un convoi militaire ou dans la lutte contre la drogue.

Une généralisation du concept peut déboucher sur un système de détection et d'interception de la menace. Chaque UAV serait alors porteur d'un senseur et d'une arme (missile, laser) ou de leurre. Il participerait de ce fait de manière active dans la défense antiaérienne d'un convoi ou d'un site.

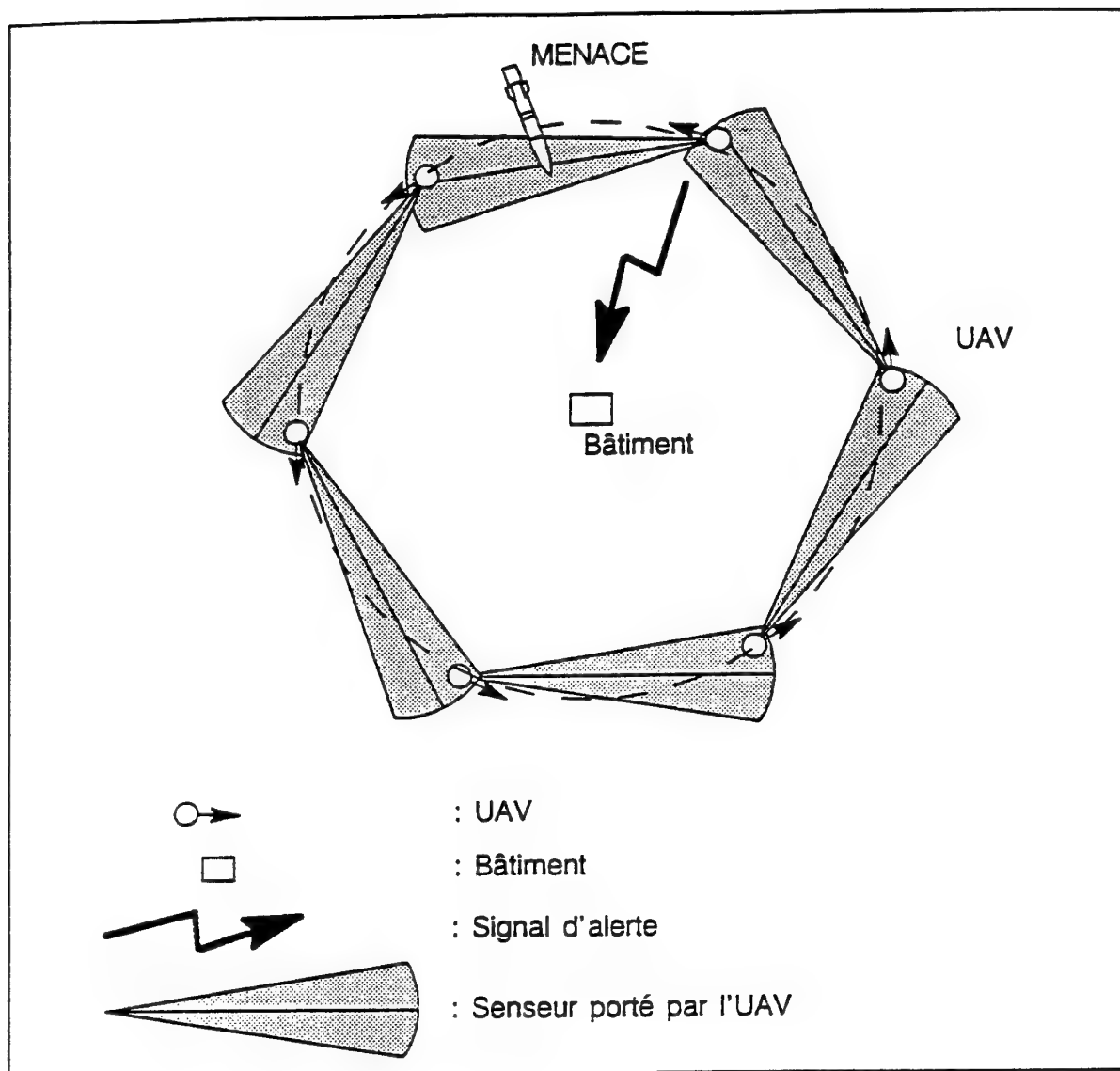


Figure 1: Dispositif du système d'alerte – configuration omnidirectionnelle

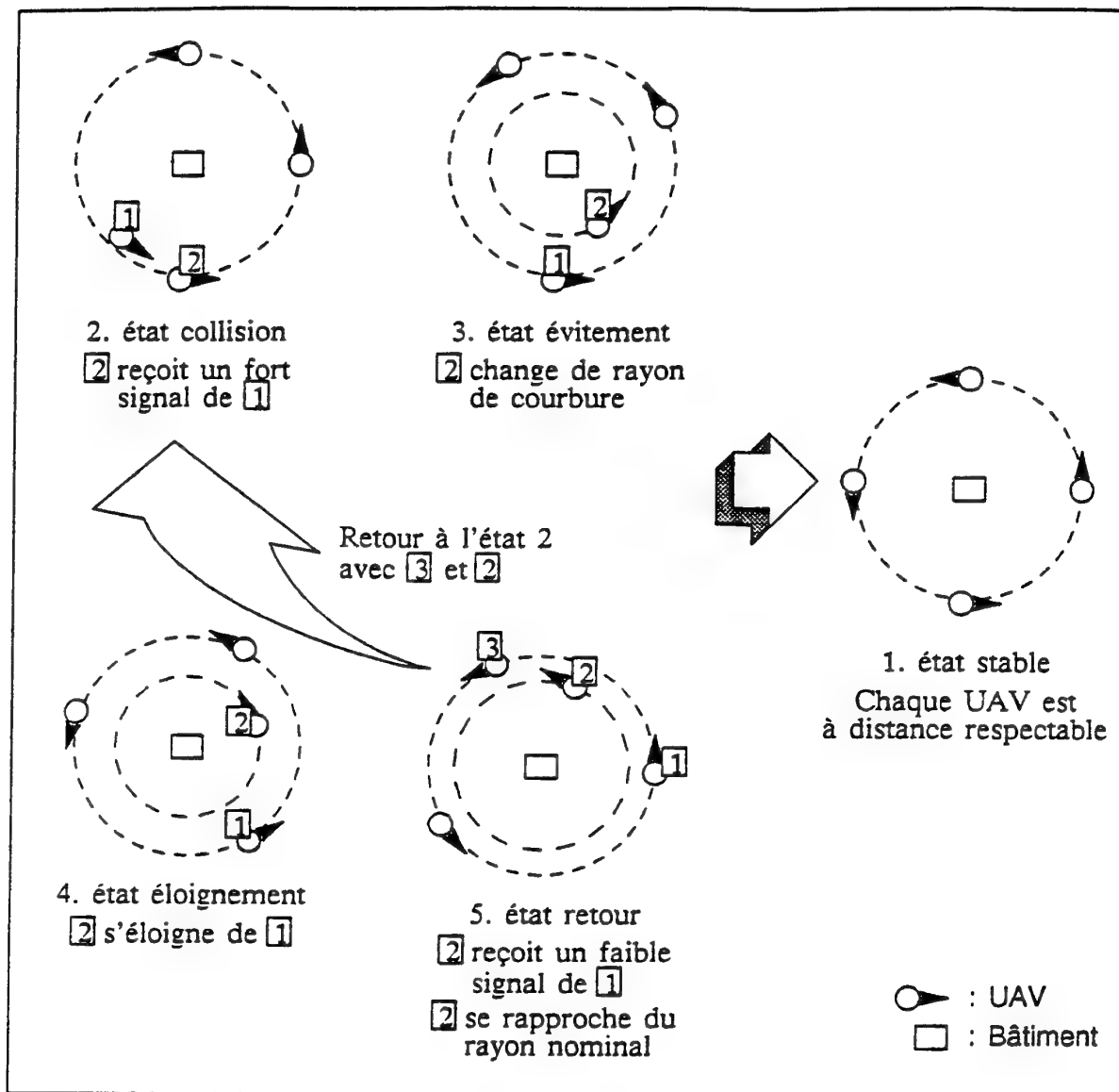


Figure 2: Différents comportements d'un UAV

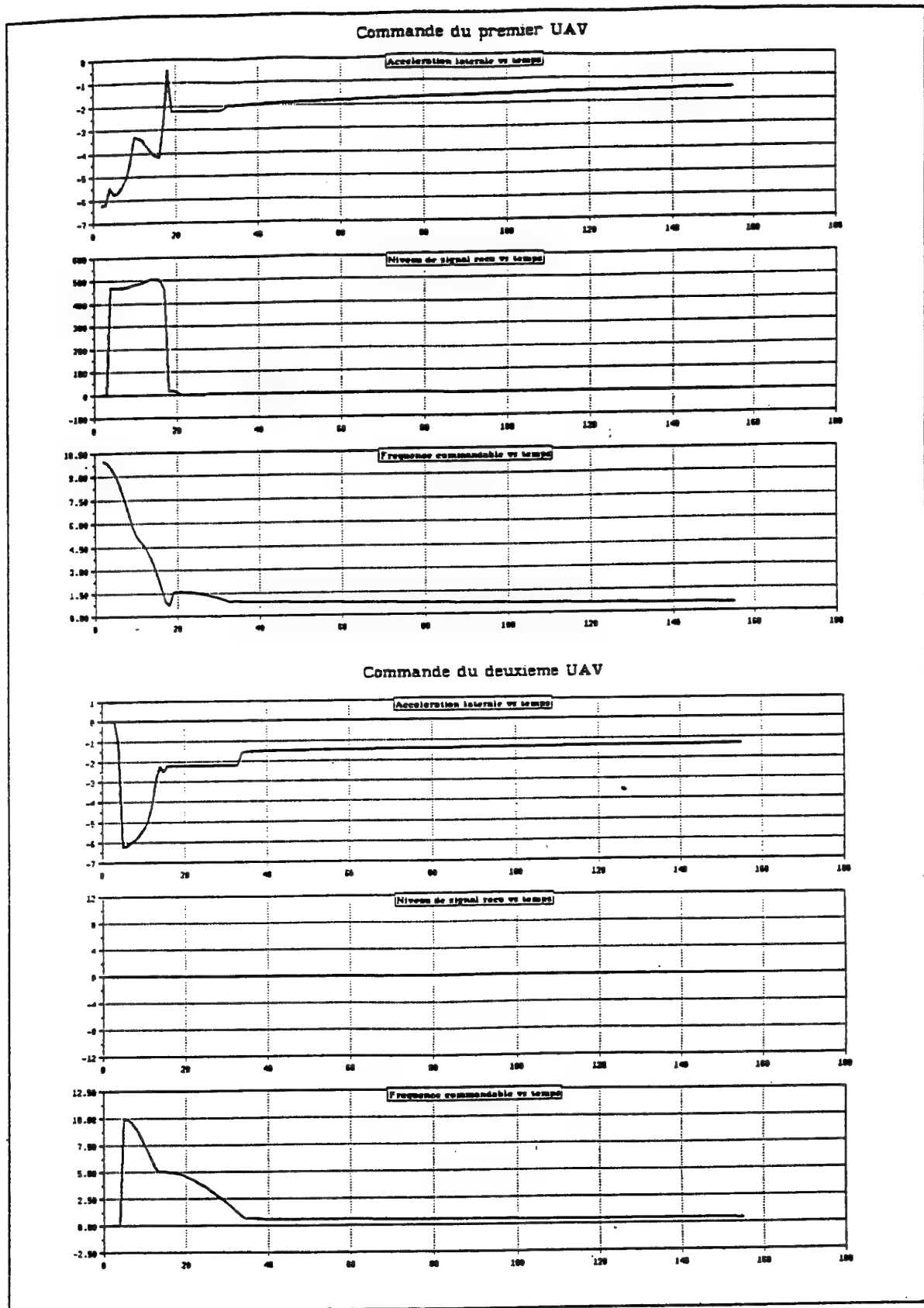


Figure 3: Résultats simulation 2 UAV

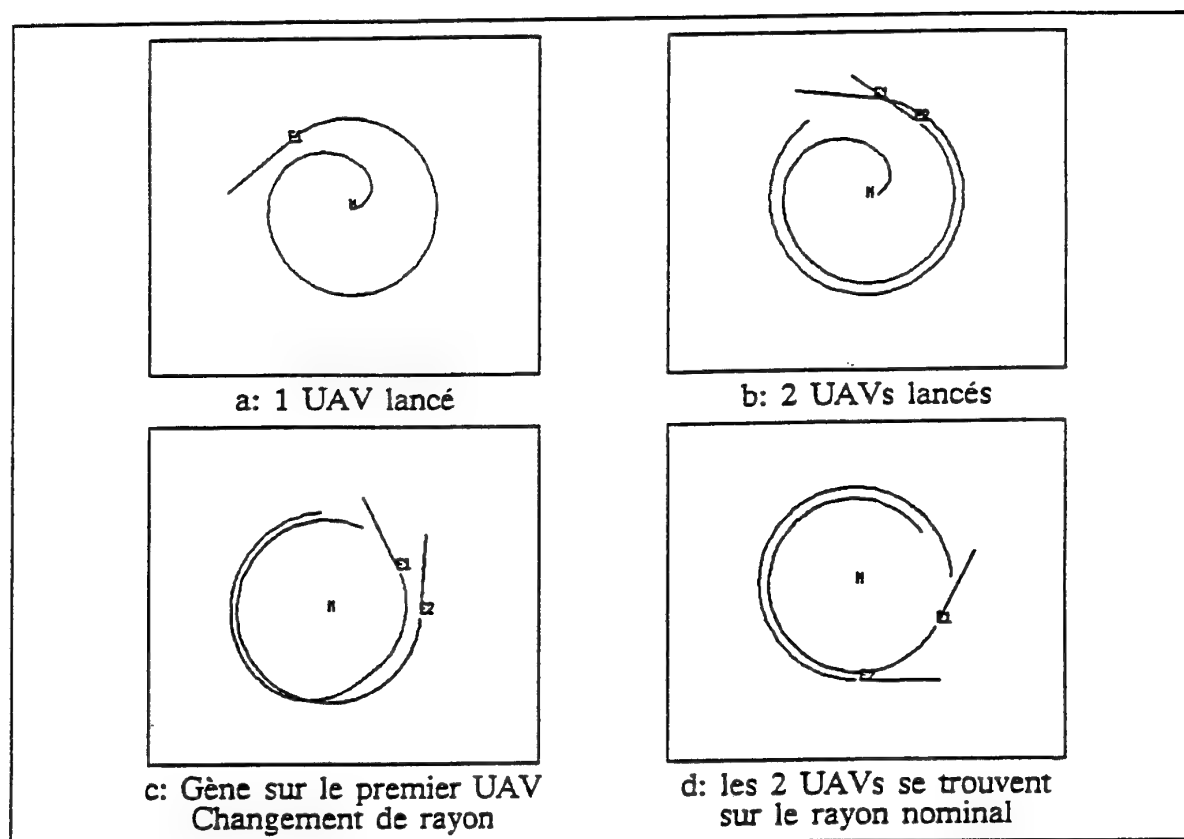


Figure 4: Résultats de simulation pour 2 UAV; commande floue

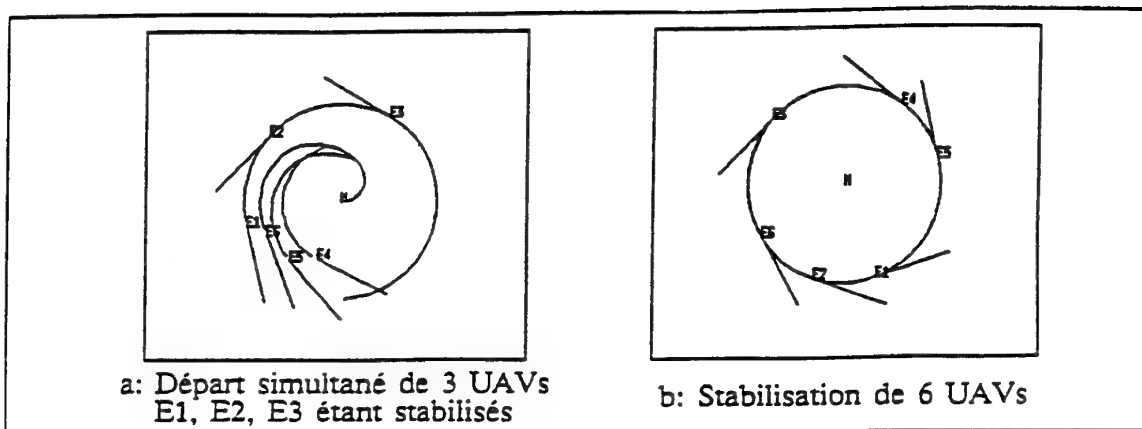


Figure 5: Résultats de simulation 6 UAV

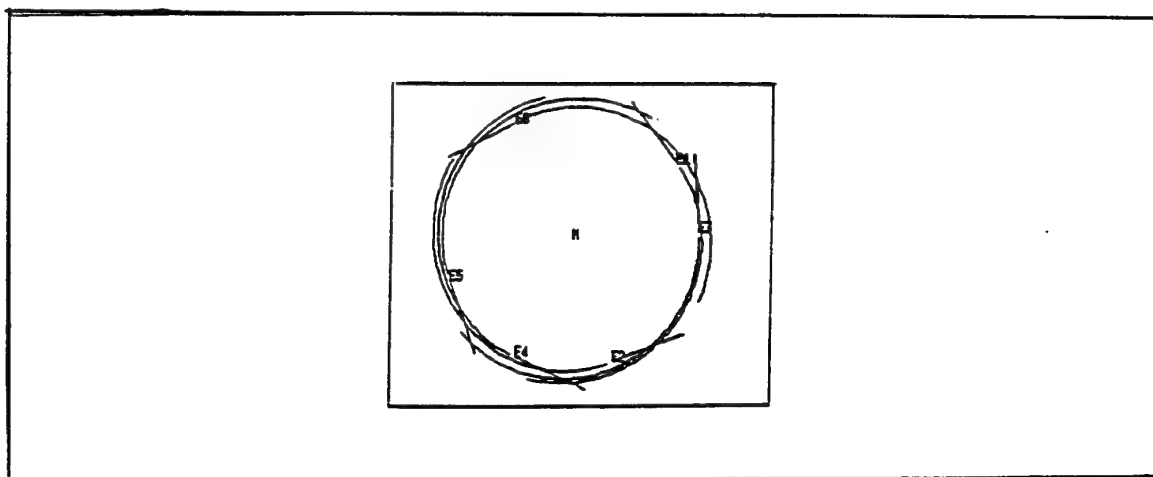


Figure 6: Diminution de la fréquence commandable

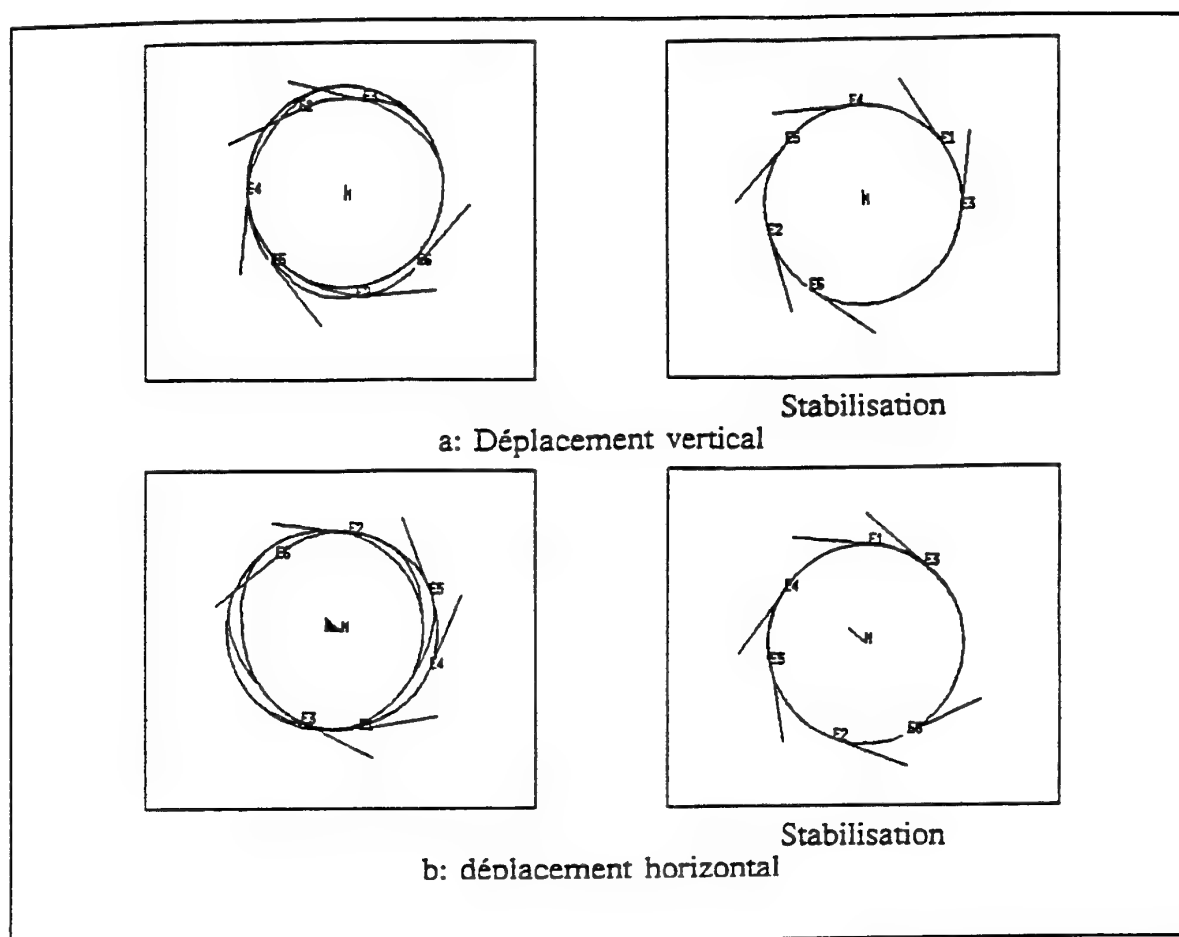


Figure 7: Déplacement du bâtiment

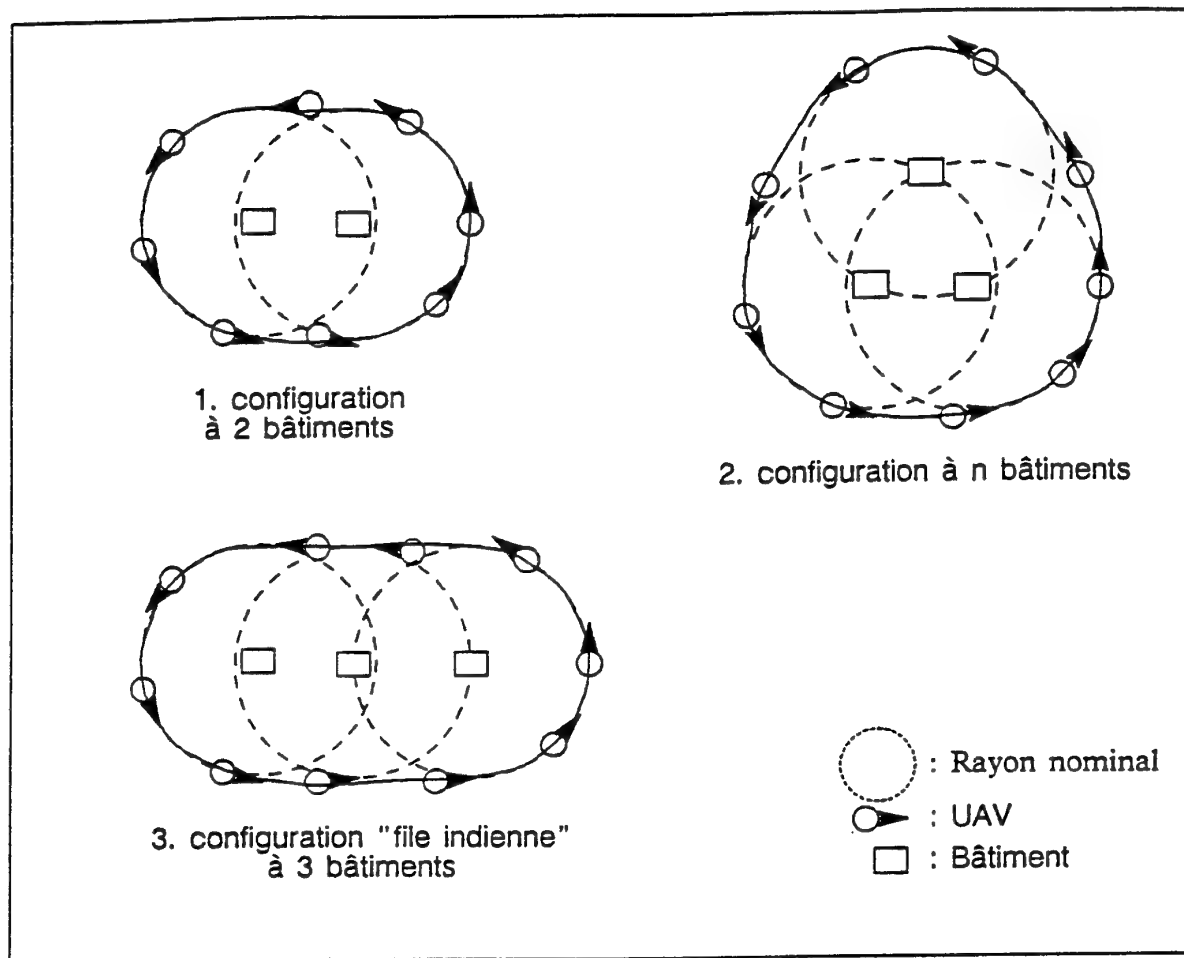


Figure 8: Configurations multi-batiments

THE PHOENIX TARGET ACQUISITION AND SURVEILLANCE SYSTEM

R.W. Dennis - General Manager

Flight Systems Group
Flight Systems Division
GEC-Marconi Avionics Ltd.
Airport Works
Rochester
Kent ME1 2XX
England

SUMMARY

Phoenix is the British Army's Battlefield Surveillance and Target Acquisition System in support of medium range artillery including MRLS. Unmanned Air Vehicles carrying Thermal Imaging sensors are controlled from a Ground Control Station (GCS) via a data link. This data link also sends real time thermal imagery to the GCS for analysis and fall of shot adjustment. Surveillance reports, target marks and fall-of-shot adjustments can be sent to the Fire Distribution Centre or direct to gun batteries via the Battlefield Artillery Target Engagement System (BATES).

This paper briefly describes the system, outlines a typical mission, covers the integration, testing and evaluation of the system.

OUTLINE OF PHOENIX SYSTEM

The system in Figure 1 comprises fixed wing Air Vehicles each carrying a roll stabilised pod in which a stabilised, steerable thermal imaging sensor is located. A secure two-way data link enables information to be relayed to and from the Ground Control Station via a Ground Data

Terminal (GDT). The Air Vehicle is launched hydraulically and recovered by parachute.

The GCS provides an environmentally controlled workspace for the crew who receive instructions from troop command, plan and implement the Air Vehicle mission, interpret the imagery and initiate fire orders or intelligence reports. Enclosed in an ISO shelter mounted on a 4 ton truck, this mobile control centre is provided with three workstations, each of which is a separate man/machine interface for the Mission Controller (MC), Air Vehicle Controller (AVC) and Image Analyst (IA).

A secure communications network provides for both voice and data exchange and a towed generator provides power to the GCS.

The GDT is trailer mounted. At the top of a hydraulically erected mast assembly is installed a narrow beam antenna on to which is fitted the transmitter/receiver unit.

Processing electronics are mounted on the trailer which is powered by a small, portable generator. The GDT is towed in a folded state by a Land Rover and the mast erected upon arrival at its pre-surveyed operational site which can be remote from the GCS by up to 1km.

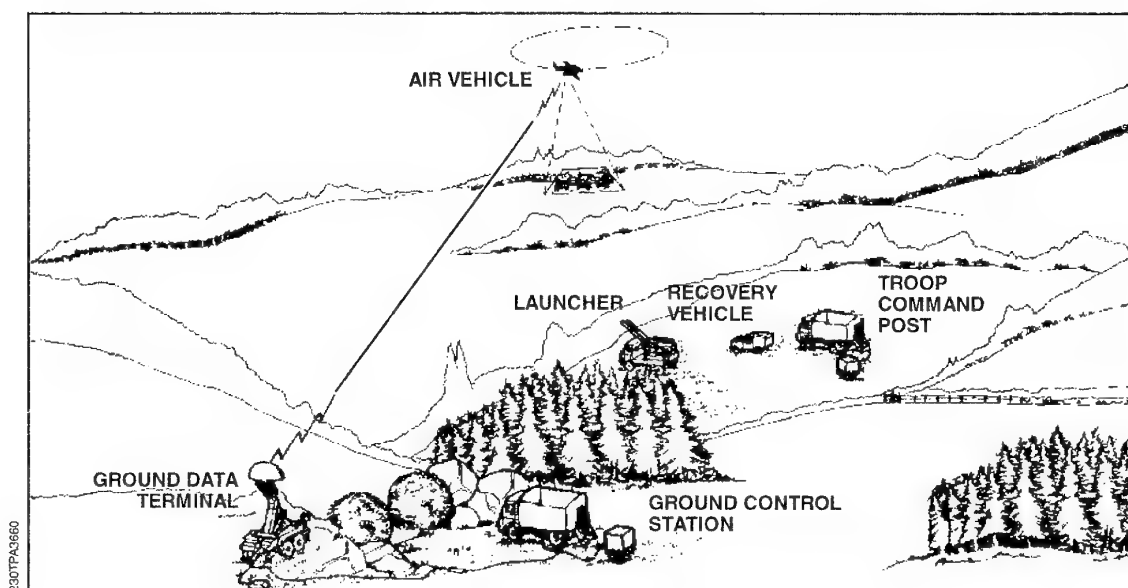


Figure 1 Key Elements of the Phoenix System

Paper presented at the FVP Specialists' Meetings on "Subsystem Integration for Tactical Missiles (SITM) and Design and Operation of Unmanned Air Vehicles (DOUAV)", held in Ankara, Turkey, from 9-12 October 1995, and published in CP-591.

The Air Vehicle systems include flight control and navigation, powerplant management and recovery system. In the Target Acquisition and Surveillance role, the payload pod, which is roll stabilised, carries a Thermal Imaging sensor mounted on a two axis gimbal. This enables it to be steered in both azimuth and elevation under control via the datalink from the GCS operator. Zoom and focus controls are also provided together with manual gain and offset controls which may be used in place of the automatic control system. The Thermal Imaging sensor extends the utilization of the system to greater than 95% due to its ability to detect targets, not only at night, but through poor ambient conditions such as battlefield smoke, heat haze, rain, mist or fog.

The launcher is an hydro/pneumatic catapult adapted to fit a standard flatbed truck thus providing full mobility. The launcher is provided with an Air Vehicle self-starter, hydraulic hoist and power pack to give a self-contained assembly. The launch rail is folded in transit and is deployed under hydraulic control. With an Air Vehicle mounted, the launcher may be manoeuvred from a hide to the launch point. It is operated by a two man crew.

Following parachute recovery the Air Vehicle is recovered by a two man crew in a Land Rover. Handling frames enable the Air Vehicle modules to be loaded into the recovery vehicle.

Logistic support at the operational level is provided by a Forward Maintenance Facility (FMF) which can be used to diagnose and repair faults in all areas of the system to replaceable module level. Within the FMF, electrical and mechanical work benches are provided whilst a penthouse provides an area for larger modules and for powerplant testing.

The Phoenix system provides a target acquisition, adjustment of fire and an intelligence capability at both Corps and Divisional level. To maximise the advantages of a real time system the Ground Control Station has three combat radios and a subscriber trunk access. Phoenix has been designed to be integrated into the British Battlefield Artillery Target Engagement System (BATES). This enables the Image Analyst to pass fire orders and corrections of fire directly to the gun battery or MLRS. These orders are passed over a data system via the combat net radio or trunk communications system and the message routing is automatically selected by the BATES computer.

OUTLINE OF A TYPICAL MISSION

Task Allocation

The Troop Command Post (TCP) is the centre for command and control of the Phoenix flight sections. Instructions for the Phoenix Troop arrive as tasking messages in the TCP where the Command Post Officer (CPO) uses his workstation software to assess the tasks and to decide which GCS is best able to undertake each task. The TCP issues deployment and tasking orders via a combat net radio to each GCS.

As tasks are completed, the responsible GCS sends a task complete message to the TCP and the CPO removes this task from his database.

GCS Architecture

The GCS is built around a MIL-STD-1553B data bus, the Phoenix Local Area Network (PLAN), which has three workstations each employing a 32-bit microprocessor, two Digital Colour Map Units (DCMU), a Frame Store Unit (FSU) and three Display Units (two colour and one monochrome) connected to it. This allows the operators to pass mission data around the GCS and to choose the video data to be displayed on their screens. The internal layout of the GCS is shown in Figure 2.



Figure 2 The Ground Control Station

Each of the colour displays are formatted as in Figure 3, the general area can be used to display digital maps at one of three scales or alternatively the thermal image. The Status area provides basic mission and task details together with key Air Vehicle parameters such as altitude and airspeed. The Dialogue area indicates the menu options available, these will change automatically dependant on the role of the workstation and the phase of the mission. The Operation Specific area provides the operator with data relevant to the current phase of the mission and responses to his commands.

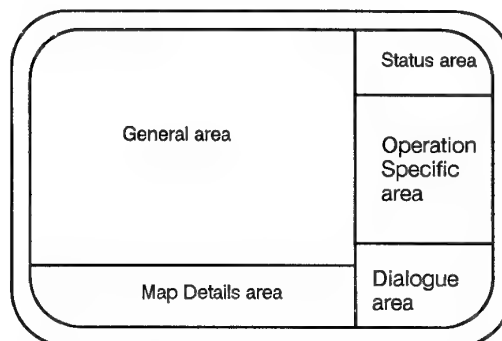


Figure 3 Phoenix Workstation Screen Layout

The Image Analyst's screen is monochrome to provide better resolution for the thermal image and is not sub-divided, the full screen being used for the image. Data such as target marks or the marking crosswire is overlaid directly onto the image but can be removed should the operator so wish.

Launch Planning

The Air Vehicle Controller (AVC) within the GCS is responsible for planning the launch and acquisition of the data link to the Air Vehicle. He inputs the data received from the Launch and Recovery Detachment of the launcher location and wind conditions and chooses the radial from the GDT on which the data link will be acquired. Using this data, the AVC software runs a simulation of the launch to determine the flight path of the Air Vehicle after launch and to calculate the data needed to acquire the chosen radial. This data is displayed numerically so that the AVC can relay a defined set of parameters to the Launch and Recovery Detachment prior to the launch.

The launch geometry is also displayed on a map background. (see Figure 4). When the section is ready, the Launch Controller launches the Air Vehicle, radioing the instant of launch to the AVC who starts the mission timing sequence, and for an autonomous launch sequence, commands the GDT to execute a search pattern. In the unlikely event that the data link acquisition fails, the Air Vehicle returns to the designated recovery zone and recovers. After launch and data link acquisition the Air Vehicle transits to the task area.

Mission Planning

Tasks are received into the Mission Controller (MC) workstation. The MC plans the sequence and timing of the various tasks forming the mission. As each task is allocated, the software calculates the time to execute all previous tasks, execute the allocated task and return to the recovery zone. As tasks are entered into the workstation they are displayed automatically against the selected map background (Figure 5). The software warns the MC if tasks cannot be completed by a specified time or if the mission duration exceeds the endurance of the Air Vehicle.

When all tasks are allocated, the MC may select an 'optimise' option that reorders the tasks to minimise the distance flown. Figure 6 shows the optimized mission plan shown previously in Figure 5. As new tasks are received from the Troop Command Post they may be allocated to the mission and the mission revalidated. The MC is responsible for initialising the task complete message that is sent to the CPO.

Transit Planning

The mission plan is passed from the Mission Controller over the Phoenix Local Area Network to the AVC workstation where the transit plan is prepared.

On receiving the mission plan, the AVC prepares the flight plan for the next task. The AVC can add waypoints to avoid air defended regions or to follow particular ground features, he can also define the speed and height of each transit. All timings and correction for wind are performed automatically. Figure 7 shows the detailed plan for the first transit shown in Figure 6.

Task Execution

During transit the Air Vehicle is commanded to fly from waypoint to waypoint with no direct operator involvement in flying the Air Vehicle. On task, the operator can command specific manoeuvres such as orbit, racetrack, figure of eight or area searches. For all manoeuvres, default conditions are supplied to allow rapid execution with minimal keystrokes.

Task execution benefits from co-operation between the AVC and the IA. The commands available to the IA allow the turret to be controlled directly from the joystick (manual control) or automatic modes, implemented in the Air Vehicle, to be engaged. These automatic modes provide:

- Fixed elevation and azimuth of the imager in space independent of the Air Vehicle motion
- Automatic steering in azimuth and elevation for searching
- Continuously updated pointing angles to keep the imager pointed at a designated ground location (ground point)
- Continuously updated pointing angles to keep the imager pointed at a moving ground location (fly the footprint).

The Image Analyst can vary the sensor magnification over the range x2.5 to x10 with the zoom control, select either white or black hot and by adjusting the offset and gain controls can override the automatic thermal sensitivity control when necessary. An image focus is also available.

Figure 8 shows a typical task display, the location of the Air Vehicle being shown by the circular icon and the footprint which the sensor can see on the ground by the trapezoid.

Figure 9 shows a typical thermal image display taken directly from the GCS screen which loses some quality. In this image white is hot.

The AVC signals task complete when appropriate and the system automatically sends a message to the MC.

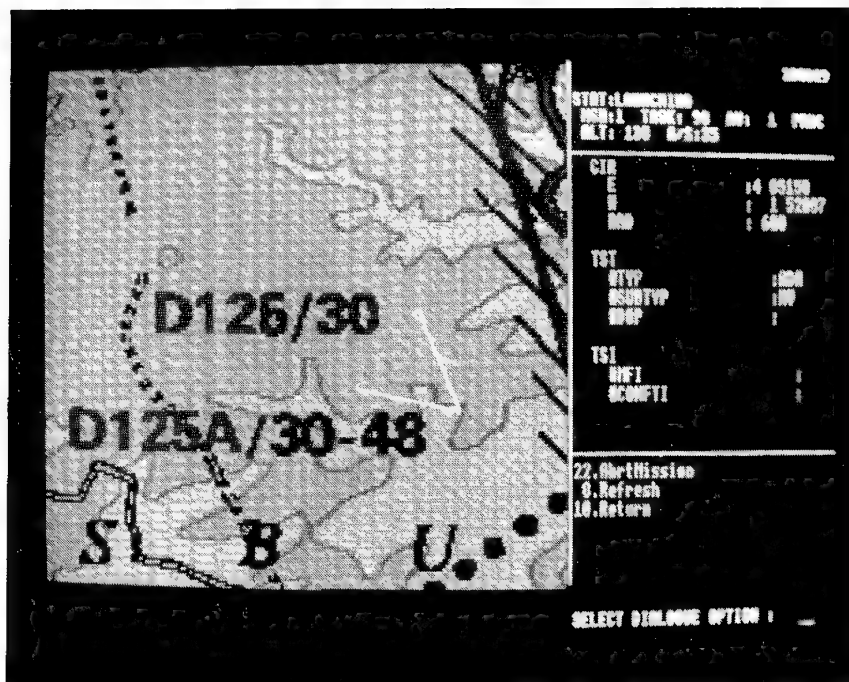


Figure 4 Launch Planning

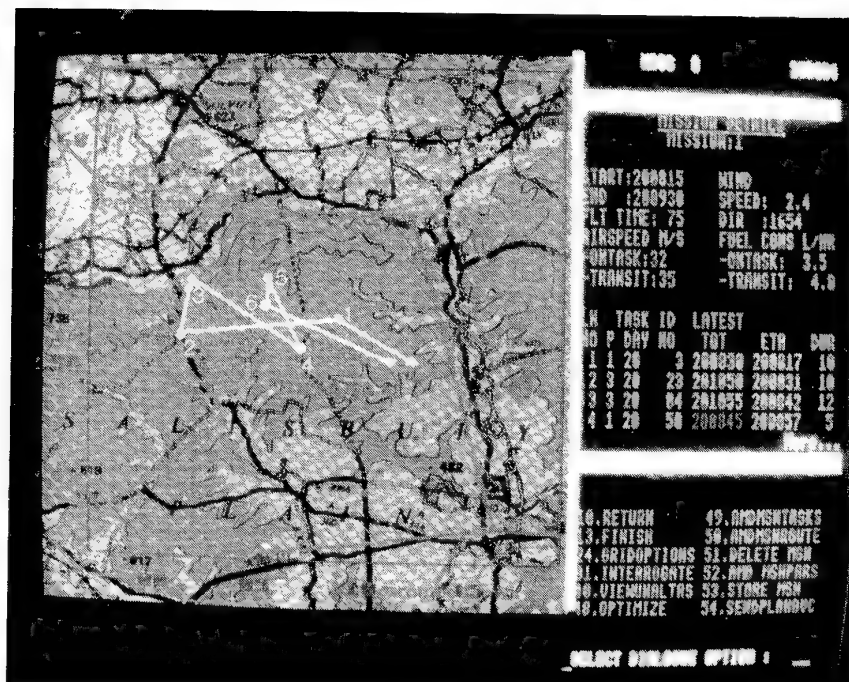


Figure 5 A Mission Plan

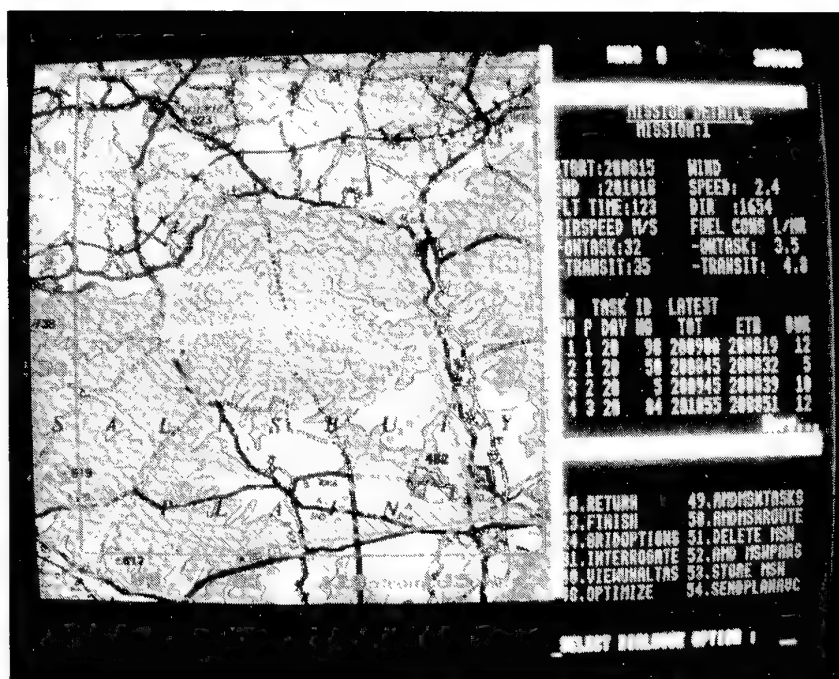


Figure 6 An Optimized Mission Plan

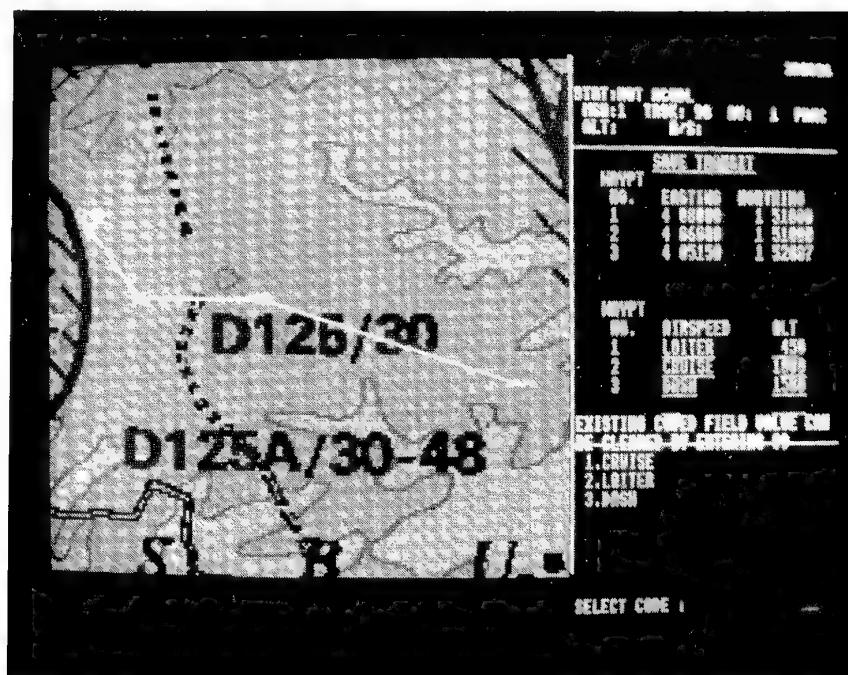


Figure 7 Transit Plan

Figure 9 Image Analyst Display

Reporting

Having placed the Air Vehicle in the task area and initiated a search with the imager, the IA is able to perform his primary role of detecting, recognising and reporting targets.

The target will most often be detected with the imager in wide field of view during a search. When the target is detected, the IA selects 'Hold' which initiates the ground point mode. In order to bring the target to the centre of his screen, he places the cross-wire over the target and presses 'Mark'. The imager then ground points at the target location. With the target at the screen centre, the IA will zoom in order to be able to recognise the target and will call up a report form on his screen. All system data (target location, grid zone, task number, target number, etc.) is input automatically and the IA has merely to select the target type, subtype and activity from coded lists.

One frame of imagery can be stored and it is also possible to mark and store 20 point targets for later display on the digital map to simplify the recognition and identification of enemy formations.

The adjustment of fire function is also simplified. The IA first marks the target with his crosswire and then the fall-of-shot. The correction is automatically computed and can be passed immediately to the guns via the BATES system.

Recovery

At any point in the mission, the AVC may redefine the recovery location to allow for a changing battlefield scenario. At the end of the mission, the AVC commands a return transit.

Recovery is then automatically controlled from the GCS via the data link which signals the parachute release at the correct time for an accurate recovery at the chosen location. Initially the Air Vehicle descends vertically following parachute deployment. The Air Vehicle is then turned into an inverted position in order to protect the thermal imager and the mission pod. On impact, a shock absorber reduces the landing loads and half the parachute lines are automatically released to avoid post recovery dragging. The recovery crew then dismantle the Air Vehicle and return it to the launcher for re-use.

Test and Evaluation

The objective of the test and evaluation phase was to demonstrate that the system functioned in accordance with the system design specification.

Tests and demonstrations were based on:

- System acceptance trials
- Design certification testing
- System modelling and performance analysis

Test and evaluation of the equipment took place at a number of different workcentres, subcontractor establishments and installations and the activities were co-ordinated throughout the programme to maintain confidence in the results of testing while ensuring that duplication of tests was minimised.

The performance of the system was validated by interpreting tests, analysis, simulations, environmental stress screening and rig tests as well as directly by means of flight tests. Integration of the results in terms of the predicted operational effectiveness of the system was harder to assess however, because most of the information that was gathered was statistical in nature or appropriate to ranges of operation which only partially simulate the extremes of the battlefield.

System Acceptance Trials

Progressive integration of the equipment, leading to design and performance confirmation was accomplished by the following test phases:

- Ground tests and trials
- Hardware design tests
- Software acceptance tests
- Reliability and maintainability assessments
- Signature measurement
- Automotive tests
- Flight tests.

Ground Tests

Ground tests included qualification tests, performance tests, deployment trials, an ease-of-maintenance assessment and data link tests.

A full programme of qualification testing to establish that the Phoenix system functions as required in the specified environmental conditions was completed.

As much testing as possible was performed at a high level of integration. For example the complete Air Vehicle and Launcher have been hot and cold tested as a single item. Similarly many of the environmental tests for the mission system were performed on a complete mission pod.

Deployment trials included mobility, handling and deployment time evaluation by the Phoenix military team with the complete system deployed in both day and night under realistic operational conditions. These trials included transit to the deployment site, operational preparation such as erecting the GDT, connecting and starting generators, deployment of cables, fitment of concealment sets, checkout using BIT and any alignment or initialisation required.

Hardware Design Tests

Hardware design tests included structural testing of the Air Vehicle, a 250 hours Air Vehicle endurance test and other tests needed to explore areas of performance which could not be adequately trialed.

A structural test rig was built by Flight Refuelling to test the following load cases:

- In-flight 3g symmetrical pullout
- Launch
- Recovery
- Handling loads

Limit, proof and ultimate loads were applied consecutively and relevant deflections were noted.

The 250 hours endurance rig test was designed in order to demonstrate the durability of the Air Vehicle and its systems in flight conditions. The rig comprised a support frame in which the Air Vehicle was suspended via elastic cords and an instrumentation facility which enabled the on-board systems to be monitored 'in flight' and also enabled BIT to be performed prior to and following each run. During simulated flights, the control surfaces were exercised by the Flight Control Computer under representative load conditions.

Temperatures were recorded at various sites using thermocouples. Powerplant performance was assessed via the on-board Engine Management System, recording critical parameters.

During the test, normal maintenance was performed at the required intervals, any failures being recorded and rectified prior to the test continuing.

The main findings were as follows:

- The durability of the UAV and its systems was confirmed
- The powerplant which was originally designed for a life of 150 hours completed the test
- The number of failures was below that expected, especially as the UAV was not provided with forced air such as would be normal in flight.

Software Testing

Software testing covered module level tests, subsystem functional tests and a complete system functional test.

Within the Phoenix system there is a wide range of software from embedded functions, such as the Flight Control and Navigation System, to the operational software in the TCP and GCS.

Embedded functions are implemented using Macro Assembler for efficiency. Operational software has been

constructed using MASCOT which employs the High Order Language CORAL 66. Processors have been standardised to either the Intel 8086 for embedded functions or the Intel 80386, 32 bit machine, for operational software. Program storage is effected in EPROM.

Host testing was performed using test harnesses running on Dec Vax computers.

Software host testing was conducted on each module prior to linking into a functional group of modules. The functional module group was then transferred onto the target when a functional test was completed.

For the flight control system the functional test was conducted using an in-line simulation. The Air Vehicle dynamics being simulated using a general purpose computer which was interfaced to the Flight Control Computer. Check traces were obtained over all phases of flight and compared with predicted results. Other elements of the system were functionally tested in a similar way.

Finally, before release to flight test, the complete system was checked on the system rig, where the Air Vehicle dynamics were simulated on a general purpose computer. Complete missions were run on the rig from mission planning to Air Vehicle control. The only feature which was not provided was representative thermal imagery. However, the imager was connected and its steering and control functions were checked out.

The output from the Simulation was recorded on an XY plotter which enabled the simulated UAV position and track to be monitored for comparison against the flight plan (Figure 10). A multi-channel recorder was used to monitor 'UAV' attitude, body rates, heading, height and airspeed which were also recorded for later analysis. Video recorders were used to record the mission and flight plan from the workstations.

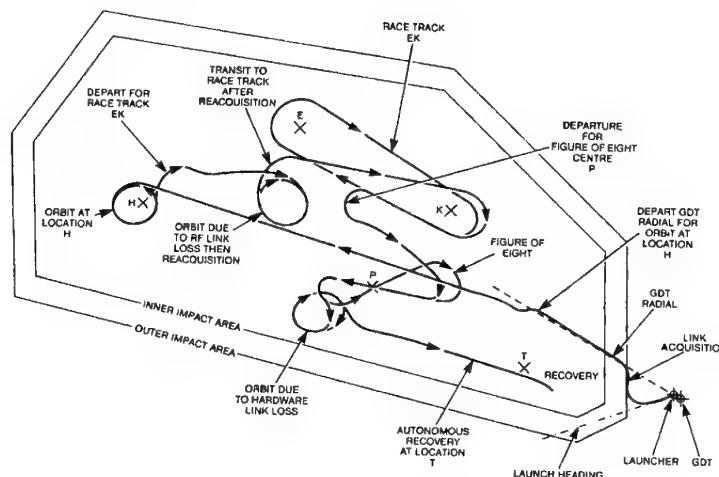


Figure 10 Trace from Systems Rig

Signature Measurement Tests

These comprised Radar Cross Section (RCS), Acoustic and Thermal signature measurements. RCS was measured over the lower hemisphere on a radar range, with in-flight measurements having also been made at representative look up angles.

Acoustic signature has been measured both on the ground and in-flight. Thermal signature has been measured using a radiometer operating in the 3-5 μ m band.

The classified nature of these tests precludes further discussion at an unclassified symposium.

Automotive Tests

Automotive tests have been performed on the Launcher, Ground Data Terminal, Recovery Vehicle, Ground Control Station/Troop Command Post, Forward Maintenance Facility and Launch Support Vehicles.



Figure 11 Automotive Tilt Test of Launcher

Automotive trials were performed at the UK Government test track at the Royal Armament Research Development Establishment (RARDE). Each vehicle, or in the case of the GDT, vehicle plus trailer, were weighed and then tilt tested to determine the point of tip-over. Following this, a track test was performed comprising a cross country section and a special surfaces section, such as cobblestones. All elements of the Phoenix system have satisfactorily completed their auto trials. Figure 11 shows the launcher undergoing the tilt section of the test.

Flight Tests

Trials of the data link and thermal imaging sensor have been conducted on a manned surrogate aircraft. The complete mission pod was mounted under the wing of a Britten-Norman Islander, using a pylon such that the pod could be roll stabilised as for the UAV. Within the fuselage, the Flight Control and Navigation System together with associated sensors were mounted such that pod stabilisation and antenna pointing were

representative of the Air Vehicle. The Islander was flown over representative Air Vehicle speeds and manoeuvres with instrumentation on board and at the GDT.

Performance at extremes of data link range were explored, together with thermal imager performance over a range of conditions including night flights. Image stability and quality were proven to be excellent and the data link performed beyond the required range. Data link performance in turning flight was difficult to assess as drop outs occurred due to fuselage and undercarriage screening. Full evaluation was deferred to UAV trials.

UAV flight trials included Air Vehicle performance measurement and assessments of autonomous navigation accuracy. Complete mission profiles were flown from the GCS via the data link including assessment of target marking accuracy and fall-of-shot correction using live firings. Recovery accuracy was also evaluated under a variety of wind conditions. UK range limitations provided some difficulties in assessing long range performance. In order to overcome this limitation the GCS and GDT were located at a site some distance away from the range, while the Air Vehicle was launched and flown over the limited range area. Tracking was provided by a calibrated tracking radar and kine theodolites with high speed cine cameras and video cameras recording launch and recovery operations.

System Modelling and Performance Analysis

Modelling was used to evaluate those areas of performance where it was not possible to measure performance under the full range of environmental conditions.

Principal areas were:

- UAV performance – where modelling was used to predict performance over the range of environment. Spot measurements from field trials supplement this analysis.
- Data Link – where bench test and modelling was used to predict performance over the required environment. Again field tests using both the Air Vehicle and a manned surrogate confirmed the analysis.
- Thermal Image performance where the Minimum Resolvable Temperature Difference (MRTD) was modelled over the environmental range. Measurements of parameters from environmental and bench measurements were fed into the model to enable an overall assessment of performance to be made.

System Acceptance Flight Tests

Five consecutive successful 'missions' were conducted in order to demonstrate the complete system under realistic operating conditions.

The following aspects were demonstrated:

- Tactical deployment
- Launch and control of the Air Vehicle
- Planning and amending missions
- Detection/recognition/identification and marking of targets

- Speed assessment of moving targets
- Observation and correction of fall-of-shot
- Recovery of the Air Vehicle
- Operation of autonomous modes such as 'fly the footprint' and 'ground port'
- Hand over of control between GCSs

In addition, degraded modes of operation were demonstrated viz:

- Loss of data link and autonomous Air Vehicle recovery
- Individual failures of AVC/MC/IS workstations
- Autonomous flight
- Loss of Digital Map facilities

During the acceptance flights certain performance parameters were measured to confirm earlier results, namely:

- Air Vehicle
 - maximum speed
 - climb and turn rates
 - crosswind launches
 - endurance
 - recovery accuracy
- Thermal Imager
 - detection and recognition ranges
 - target location marking accuracy
 - image stability
- Data link
 - maximum range
 - Air Vehicle location accuracy
- Deployment timings under day and night conditions

Acknowledgements

This work has been carried out with the support of the Procurement Executive of the Ministry of Defence.

Acknowledgement is also extended to the Defence Research Agency for the use of photographs and to all the Phoenix subcontractors.

**CRÉCERELLE : un système d'avion léger télépilote de nouvelle génération,
pour des missions de reconnaissance, de surveillance
et d'acquisition d'objectifs**

G. THIN et P. DURIEUX
SAGEM Le Ponant de Paris
27, rue Leblanc
75512 PARIS Cedex 15

RÉSUMÉ

Le système d'UAV de Reconnaissance, de Surveillance et d'Acquisition de cibles CRÉCERELLE conçu et réalisé par le Groupe SAGEM est en service opérationnel au sein du 7ème Régiment d'Artillerie. Par de nombreux aspects, ce système rompt avec les caractéristiques des systèmes antérieurs. Cette rupture est le résultat de nouvelles exigences opérationnelles et d'un nouveau contexte géopolitique qui ont conduit à réaliser un des premiers systèmes de reconnaissance robotisé basé sur des technologies récentes.

Le système CRÉCERELLE a été conçu comme étant en premier lieu une chaîne de recueil et de traitement de l'information schématiquement composée d'une entité centrale, -la station sol-associée à des capteurs de données et connectée avec les réseaux d'information et de renseignement du champ de bataille.

Cette chaîne, représentative des avancées technologiques réalisées sur CRÉCERELLE est décrite dans cet article.

On détaille aussi la méthodologie d'essais de validation de cette chaîne assurément nouvelle par rapport aux systèmes de première génération. S'appuyant sur de nombreux essais élémentaires et simulations, la validation de cette chaîne a pu être réalisée d'une manière exhaustive dans un délai court et avec un nombre d'essais en vol limité.

LISTE DES SYMBOLES

UAV	Unmanned Aerial Vehicle
VA	Véhicule Aérien
GCS	Ground Control Station

1- INTRODUCTION

CRÉCERELLE est un système d'UAV conçu au début des années 1990 pour répondre d'une part, aux menaces apparues après la rupture des équilibres géostratégiques établis au temps de la guerre froide et pour d'autre part s'adapter au nouveau contexte politico-économique.

En effet, depuis la chute du mur de Berlin, on assiste à la multiplication, en de nombreuses régions du globe, de zones de tensions et de conflits latents caractérisés par des évolutions rapides. Ceux-ci exigent des systèmes de reconnaissance et de surveillance flexibles, mobiles qui permettent à l'utilisateur final d'acquérir les informations dans un délai court.

Parallèlement à cette évolution, la situation économique internationale conduit la plupart des pays à réduire les crédits et investissements en matière d'armement.

Il est donc impératif de proposer des systèmes dont le coût global de possession est faible.

Enfin, la perte de vies humaines sur des théâtres extérieurs, est devenue intolérable aux yeux des opinions publiques occidentales.

Les avancées technologiques de ces dernières années en matière de miniaturisation de l'électronique et de puissance des calculateurs notamment, ont permis au Groupe SAGEM de réaliser un système d'UAV performant et répondant bien aux exigences précédentes, en privilégiant les aspects suivants :

- l'emploi de sous-ensembles à la pointe de la technologie, disponibles et qualifiés sur d'autres programmes,
- une conception compacte et modulaire,
- un haut niveau d'automatisation,
- une grande souplesse d'utilisation.

La première partie de cet article s'attachera à développer ces concepts.

La seconde partie sera consacrée à la description technique de la chaîne d'acquisition et de traitement d'image, illustrant la nature des avancées technologiques réalisées sur CRÉCERELLE.

Enfin, nous décrirons la méthodologie d'essais que SAGEM a retenu pour valider cette chaîne, sur la base de son expérience acquise dans le cadre de retrofit d'avion d'armes.

2- Description générale du système

Le coeur d'une section d'UAV CRÉCERELLE se compose

- d'un segment vol :
6 véhicules aériens (VA) incluant charge utile optronique nuit/jour (capteurs lignes infrarouge et visible) et équipement de transmission radio,

- d'un segment sol :
 - 1 véhicule station sol GCS (Ground Control Station) à partir de laquelle la mission est préparée, contrôlée, éventuellement reconfigurée, et où les images de l'ensemble des capteurs sont reçues en temps réel puis traitées,
 - 1 système de lancement mobile, associé à 1 véhicule de transport et de récupération des véhicules aériens qui remorque le système de lancement.

Le lancement du véhicule aérien s'effectue par catapultage, sa récupération s'effectue par parachute.

Pendant la phase de planification de la mission, le plan de vol est entré par l'opérateur sur un fond de carte digitale. Sa cohérence avec les contraintes tridimensionnelles du relief est ensuite vérifiée automatiquement, tant pour l'évitement de terrain que pour l'intervisibilité radio. Le plan de vol est ensuite téléchargé dans le véhicule aérien.

Après le lancement du V.A., le calculateur de bord contrôle le véhicule aérien tout au long de sa route pré-programmée et à l'intérieur de son domaine de vol avec des marges de sécurité pour garantir un vol sûr. Cette procédure automatique permet aux opérateurs de se concentrer sur les fonctions principales du système : le suivi de la mission d'observation et l'analyse des images reçues.

3- Caractéristiques opérationnelles

Mobilité stratégique

Le système CRÉCERELLE est transportable par avion de type C130 ou C160, sans montage ni démontage particulier, ce qui permet une projection rapide et aisée du système sur un théâtre d'opération extérieur.

Mobilité tactique

L'ensemble du système monté sur camion 4 x 4 léger permet au système d'être très mobile sur les champs d'opération. Ceci est déterminant étant donné que les conflits actuels sont caractérisés par des lignes de front et des concentrations d'objectifs diffus, en constante et rapide évolution.

Mise à disposition des informations

Les temps de déploiement très court (typiquement 2 heures) du système assure une disponibilité rapide des informations acquises par l'UAV. Le lancement et la récupération du véhicule aérien, s'effectuent sur des terrains ne nécessitant pas de préparation spécifique.

Pour les missions d'intelligence, le système peut couvrir 1 000 km² à 2 000 km² de terrain en un seul vol.

Les caractéristiques des cibles détectées sont transmises en temps réel sur les réseaux de données à destination du commandement ou de l'artillerie.

Les caractéristiques déterminantes qui permettent d'atteindre ces performances sont liées :

- à la compacité du système rendue possible par une forte miniaturisation de l'ensemble des équipements électroniques tant au sol que dans le véhicule aérien et par l'utilisation de matériaux alliant légèreté et résistance (matériaux composite de la structure du véhicule aérien par exemple) ;
- à une forte automatisation des fonctions conduisant à une équipe de mise en oeuvre de taille plus réduite que sur les systèmes antérieurs et à un accroissement de la sécurité des missions. De ce fait, la mise en oeuvre du système ne requiert pas de connaissance aéronautique spécifique ;
- à la simplicité d'utilisation et à la convivialité des interfaces opérateurs obtenues grâce au choix de stations de travail et d'outils graphiques de haute technologie.

Flexibilité et modularité

CRÉCERELLE au même titre que les autres systèmes de drone SAGEM est construit autour de sous-ensembles communs, et/ou standards généralement qualifiés et produits en série dans le cadre d'autres de ses programmes militaires (missiles, avions de combat, ...)

Outre l'avantage qui en découle sur le coût global d'acquisition par effet de série, cette caractéristique offre un intérêt opérationnel particulier puisqu'elle garantit la pérennité des équipements du système, l'adaptabilité du système à des missions différentes et un fort potentiel d'évolutivité suivant au plus près les évolutions technologiques (observation / guerre électronique ...)

CRÉCERELLE est donc un outil dynamique et efficace de recueil et de traitement de l'information au service du commandement tactique, doté d'un fort potentiel d'évolutivité.

4- Description fonctionnelle du système

Préparation de mission

Cette fonction consiste à élaborer le plan de vol sur la base des objectifs de mission fixés et de vérifier sa cohérence vis à vis du relief et des performances du porteur. Elle assure un niveau important de sécurité et de réussite de la mission avant le lancement même du véhicule aérien.

La préparation de mission est prise en charge par un des postes de la station sol. Celui-ci est directement issu des systèmes développés par SAGEM pour la préparation de mission des avions de combat. Il s'appuie sur une base de données géographique stockée sur CD-ROM permettant de disposer de fonds de cartes à différentes échelles ou d'images formées par les satellites d'observation ou les avions de reconnaissance. Cette base de données intègre des caractéristiques d'élévation de terrain. Ce poste contient en outre une base de données contenant les zones de menaces adverses à éviter, les amers remarquables du terrain survolé, les zones suspectes à observer, les sites propices au lancement et à la récupération de l'avion.

La mission est créée par simple entrée de points tournants sur la carte numérisée, le système vérifie automatiquement la conformité de la mission avec :

- les performances du véhicule aérien,
- l'élévation du terrain,
- l'intervisibilité radio entre le segment sol et le véhicule aérien,
- la portée et l'endurance maximum,
- les menaces ennemies.

Gestion du vol

Elle se décompose de la façon suivante :

- contrôle avant vol des sous-ensembles du système (station sol, liaison radio, véhicule aérien),
- initialisation du vol : téléchargement du vol et des informations d'initialisation,
- suivi du vol qui offre les possibilités suivantes :
 - lancement et atterrissage automatiques,
 - suivi de la progression du véhicule aérien sur fond cartographique,
 - accès aux informations tridimensionnelles disponibles en phase de préparation de mission,
 - affichage des paramètres avion et d'une vidéo panoramique de la zone survolée.
- gestion globale de la mission. Cette fonction s'appuie sur une navigation hybride GPS ou à

l'estime en mode secours et un positionnement des cibles réalisée par GPS différentiel.

Elle permet la replanification éventuelle du vol qui est réalisé d'une manière automatique à partir des informations issues de la préparation de mission avec des outils identiques à ceux utilisés avant vol.

L'opérateur chargé du suivi de mission peut en outre reprendre la main sur la procédure automatique de vol pour guider le véhicule aérien par des ordres de haut niveau (consigne de cap ou de taux de virage, altitude, vitesse air) sur des zones d'intérêt non connues initialement.

Enfin, la gestion de la sécurité de vol et d'éventuels incidents est réalisée d'une manière automatique sur la base de modes de reconfigurations pré-définis en fonction des types d'incidents.

- la gestion des équipements bord (gestion des senseurs optroniques et de la liaison de données radio).

Acquisition et traitement des images

La charge utile embarquée dans le véhicule aérien transmet au sol en temps réel un flot de données composite et cohérent contenant les informations suivantes :

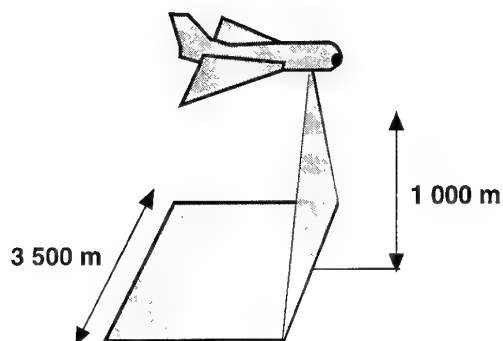
- signal de l'analyseur monoligne infrarouge (ventral),
- signal de l'analyseur monoligne CCD (ventral),
- paramètres de vol et de position du véhicule aérien,
- vidéo panoramique frontale.

Cette charge utile, dotée d'une capacité d'observation jour/nuit, permet de bénéficier de large champ de vue (90° à 120°) et donc de balayer des surfaces de terrains très importantes tout en conservant une bonne résolution d'image.

La stabilisation des capteurs, c'est à dire la compensation des mouvements résiduels de l'avion n'est pas réalisée mécaniquement mais au sol par logiciel en utilisant des informations de vitesses angulaires et d'attitude mesurées à bord.

Cette solution technique permet d'obtenir une robustesse et une fiabilité meilleure, ainsi qu'un coût de charge utile d'observation plus faible que celui des systèmes gyrostabilisés mécaniquement de performance équivalente.

Cette orientation technologique peut être comparée à celle des systèmes de navigation inertielle (centrale à cardans / centrale à composants liés).



Chaque pixel d'image transmis est géoréférencé.

Les données sont traitées en temps réel dans la station sol : les images ventrales reçues défilent sur un premier écran. Lorsqu'une zone d'intérêt ou un objet est détectée, l'image est transférée sur le poste d'analyse et d'exploitation d'image avec toutes les informations de géoréférencement.

Sur cette deuxième station, un opérateur interprète dispose d'outils de traitement des images, de corrélation image / carte, de positionnement précis des cibles identifiées (plusieurs systèmes géodésiques de référence peuvent être utilisés).

Les données relatives aux cibles sont ensuite transmises sur le réseau PR4G vers l'utilisateur final (groupe d'artillerie, C3I, ...). Les images qui ont été traitées sont transférées sur cartouches magnétiques pour une éventuelle post-exploitation.

Une dizaine de secondes séparent le survol d'une cible de la disponibilité de ses caractéristiques pour une frappe d'artillerie, avec la pleine résolution et toutes les performances de localisation.

La précision de positionnement est bien supérieure à celle du tir d'artillerie, elle ne dépend pas de la distance entre le segment sol et le véhicule aérien.

Rejeu et formation

- Post exploitation des images

Les images traitées pendant un vol peuvent être revisualisées après le vol et subir de nouveaux traitements ou être utilisées pour localiser de nouvelles cibles.

- Rejeu de mission

L'ensemble de la mission est enregistrée sur cassettes vidéo. Elle peut être rejouée comme lors du vol en offrant les mêmes fonctionnalités de visualisation / sélection / traitement d'images.

- Formation

Le rejeu de mission permet de simuler l'ensemble des fonctionnalités liées à la chaîne image. Il peut s'effectuer sans matériel spécifique dans la station sol ou dans une configuration installée en laboratoire ou salle de formation.

5- Description détaillée du système d'acquisition et de traitement d'image

5.1- Organisation générale

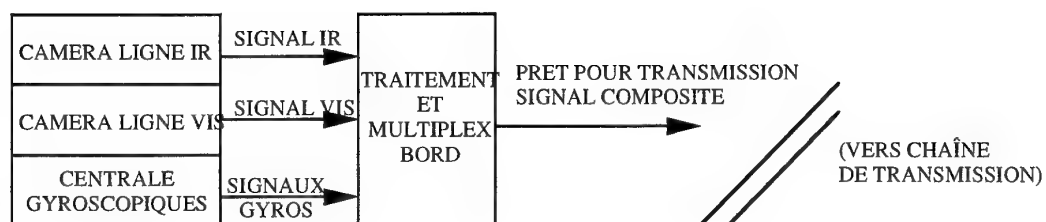
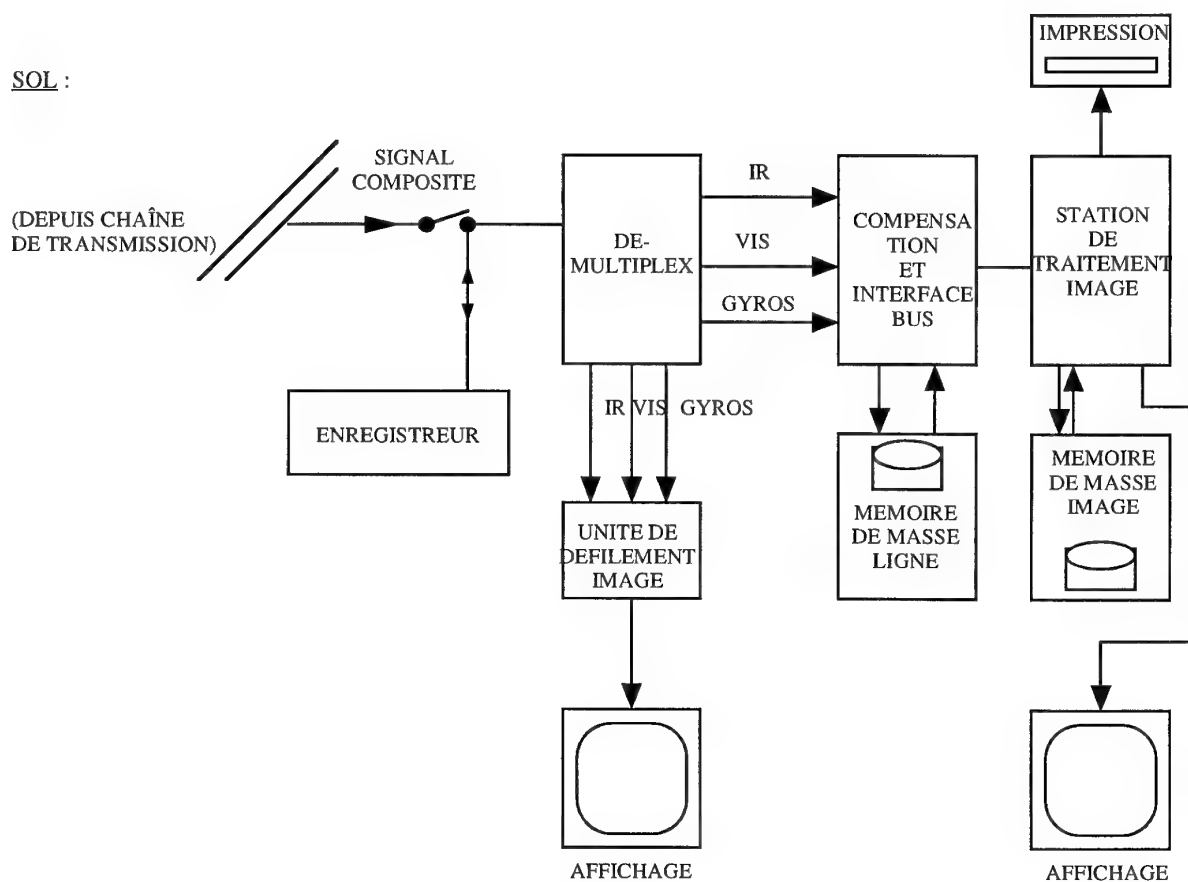
Les principales chaînes fonctionnelles sont :

- la chaîne de commande et de surveillance générale incluant la station de travail du pilote, son écran, son pupitre de commande, et les équipements du véhicule aérien (capteurs, avionique, servo-gouvernes),
- la chaîne de transmission, incluant tous les équipements R F sol et bord et leurs antennes, plus le système de poursuite automatique,
- la chaîne d'acquisition des images incluant les caméras, les équipements de traitement du signal bord et sol, et la station de travail d'affichage et de traitement des images au sol.

Nous décrivons ci-après la chaîne d'acquisition et de traitement de l'image.

5.2- Synoptique

Le synoptique général de la chaîne d'acquisition et de traitement de l'image est le suivant :

BORDSOL :

5.3- Section bord

La section bord a trois fonctions principales :

- acquisition initiale des lignes (infrarouges et visibles),
- l'acquisition des données inertielles pour la compensation des images,
- le traitement des lignes pour leur transmission.

5.3.1- Acquisition

L'acquisition est confiée aux deux caméras lignes :

- pour l'infrarouge : le cyclope 2000, analyseur monoligne infrarouge (miroir tournant, détecteur intégré réfrigéré),
- pour le visible : une caméra ligne CCD (4 096 pixels, avec contrôle automatique de gain).

Chaque caméra délivre des signaux analogiques de type vidéo à un rythme constant ; chaque ligne est marquée par un signal de synchronisation.

Les deux caméras sont montées de façon liées dans la structure de la charge utile, et donc dans le véhicule aérien. Ceci implique que les mouvements résiduels de roulis et de tangage doivent être compensés de façon à éviter les déformations de l'image dues aux mouvements du véhicule aérien en vol.

La compensation est effectuée au sol à partir des données inertielles mesurées à bord.

Cette disposition a l'avantage d'éviter l'installation de dispositifs de compensation mécanique à bord, qui sont délicats de conception et de réalisation et coûteux ; ils conduisent à augmenter le nombre de pièces et de composants mécaniques à bord, rendant le mécanisme plus lourd et plus fragile, notamment lors des récupérations par parachute.

Un capteur gyrométrique mesure les vitesses angulaires de roulis et de tangage, pendant qu'un capteur de champ magnétique mesure les variations de cap.

5.3.2- Traitement des lignes

Le signal analogique venant des caméras et du capteur gyrométrique est numérisé et subit ensuite plusieurs traitements de façon à être mis en forme pour transmission : compression, datation, multiplexage des trois sources de signal (IR, visible, mesures inertielles).

Enfin, une trame composite est élaborée et envoyée aux émetteurs ; le rythme de ces trames est fixé à 300 Hz.

Les trames image contiennent toutes les informations infrarouge et visible, plus toutes les informations de base nécessaires à la compensation au sol.

5.4- Segment sol

5.4.1- Enregistrement et rejeu

Immédiatement après réception RF, les trames image composites sont envoyées vers un enregistreur en parallèle du reste de la chaîne. Pendant le rejeu, le segment sol de la chaîne image reçoit ces informations depuis l'enregistreur au lieu du récepteur. Cette fonctionnalité permet d'expertiser des vols en temps différé ou de transformer la station sol en un simulateur d'entraînement pour les opérateurs.

5.4.2- Démultiplexage

Un équipement sol démultiplexe les trames composites afin de restituer les trois sources séparément : IR, visible et données inertielles plus datation.

5.4.3- Image défilante

Les trois sources sont envoyées vers une unité qui élabore l'image défilante en affichant les lignes les unes après les autres sur un écran. L'infrarouge et le visible sont tous deux disponibles et peuvent être permutés instantanément sur l'écran.

5.4.4- Calculs de compensation et gestion mémoire

Les trois sources sont envoyées vers une autre unité qui accomplit la compensation numérique fine, stocke en temps réel les lignes numérisées sur disque dur, et gère les transferts d'images sur le bus VME.

L'opérateur qui observe l'image défilante peut sélectionner des zones d'intérêt. Les lignes correspondantes sont alors marquées sur le disque et transférées sur demande vers la station de traitement des images.

La compensation numérique des mouvements résiduels offre une très grande souplesse associée à une optimisation du temps de calcul. Les défauts compensés sont : les décalages latéraux liés à la dérive et au roulis, les aberrations longitudinales liées aux mouvements de tangage, les superpositions de lignes liées au rapport vitesse sur altitude, et enfin les défauts d'uniformité des pixels de la caméra ligne visible.

5.4.5- Traitement des images

La station de traitement des images reconstitue alors la pleine image compensée (infrarouge et visible en parallèle) à partir des lignes reçues, et effectue la localisation géographique fine sur l'ensemble de l'image, en utilisant les informations GPS associées aux lignes, et traitées par la chaîne de télécommande et télémesure.

L'image est alors disponible pour tout traitement, annotation, localisation, corrélation avec la carte, etc...

Enfin, elle peut être envoyée vers une unité de stockage des images traitées en vue de travaux ultérieurs, ou bien vers une imprimante couleur de haute résolution. Elle peut aussi être écrite sur bande magnétique pour traitement sur une autre station en dehors du système.

6- Méthodologie des essais système de la chaîne image

6.1- Généralités

Les essais de la chaîne image effectués au niveau système ont consisté en :

- essais en vol des équipements spécifiques et des sous-systèmes,
- intégration au sol de la chaîne image,
- essais en vol de la chaîne image intégrée dans le système complet.

Ce chapitre va décrire cette troisième catégorie de test, sa méthodologie et son organisation.

6.2- Aperçu de l'enchaînement des essais système de la chaîne image

Au cours de la série d'essais en vol du programme CRÉCERELLE, une séquence particulière fut consacrée à l'intégration en vol et à l'évaluation exhaustive de la chaîne image. En effet, ses performances sont intimement liées aux autres fonctions du système notamment pour la qualité d'image (les senseurs sont liés à la structure de l'avion et ne sont pas stabilisés mécaniquement) et la précision de localisation de cibles (qui dépend de performances du système de navigation).

Les essais système en vol de la chaîne image ont débuté à partir du moment où l'ensemble de la chaîne a été réuni : segment bord et segment sol. Ils se sont déroulés sur une période de 5 mois.

Le nombre limité de vols système nécessaires aux essais de la chaîne image est la conséquence des caractéristiques de la conception et de l'étude de CRÉCERELLE :

- a) utilisation généralisée de senseurs d'équipements et de sous-systèmes existant et ayant volé sur d'autres systèmes, associés à du matériel informatique standard ; tous les équipements étaient déjà validés au début du programme.
- b) importance donnée aux phases d'intégration au sol des chaînes, impliquant des simulateurs

(simulateur de vol de l'avion et simulateur d'image déformée).

- c) recours à de nombreux vols de tests partiels avant les vols systèmes.

La forte modularité du système a permis d'intégrer la chaîne image avec les autres principales fonctions séparément ; Pour cette raison, le calendrier des essais fut divisé en trois phases :

- 1) les essais initiaux de la chaîne d'acquisition image et son intégration avec la chaîne transmission,
- 2) les essais d'intégration de la chaîne image avec la chaîne de commande du véhicule aérien (guidage, navigation, initialisation et interruption du vol),
- 3) capacité globale de mission, vis à vis des performances opérationnelles de la chaîne image.

Cet ensemble de tests fut entièrement exécuté par les personnels industriels du Groupe SAGEM. Ces tests ont été suivis d'un stage d'entraînement en vol des utilisateurs militaires, et par une évaluation complète du système effectuée par le client. Ces deux dernières phases ne sont pas décrites ici.

6.3- Essais initiaux de la chaîne d'acquisition d'image

L'ensemble de la chaîne fut testée au banc et ensuite au sol avec l'avion réel et à travers les transmissions radio réelles. Ceci a permis de vérifier toutes les fonctions. Mais les performances en terme de qualité d'images ont été attestées en vol. En effet :

- a) l'utilisation d'analyseur monoligne nécessite un mouvement de la caméra par rapport au sol,
- b) la focale utilisée nécessite d'être à une distance du sol d'au moins 10 à 20 mètres,
- c) la performance de compensation d'image doit être évaluée sur des schémas de terrain réel.

Au cours des vols consacrés aux essais image, le guidage n'était volontairement pas actif. L'avion était commandé par son autopilote de base, qui maintient une altitude, une vitesse et un angle de roulis directement commandé depuis le sol. Ceci permettait de vérifier les interactions entre la chaîne image et le pilotage de base du Véhicule Aérien. La performance de l'image et de la localisation fut examinée dans les conditions suivantes :

- basse et moyenne, puis haute altitude,
- basse à haute vitesse,
- différents types de météo et d'ensoleillement,
- distance VA-Station Sol variant de 0 à 60 km.

6.4- Essais d'intégration chaîne image / chaîne de commande

Les performances de guidage et la navigation ont été testés en profondeur au banc, en utilisant un banc d'intégration complet de l'avionique couplé à un simulateur de vol du véhicule aérien à 6 degrés de liberté. Le simulateur a la capacité de prendre en compte le vent, les rafales, et tout un ensemble de défauts et d'erreurs des capteurs. Il fut couplé à la vraie station sol pour la planification des missions simulées, et la surveillance des vols simulés. Les mesures de performance de guidage ont constitué des points d'entrée pour les simulations de déformation d'images.

Lors des vols de cette phase, les performances de navigation (calcul de position) et de guidage (erreur par rapport à la route désirée au sol) furent mesurées par le biais des images reçues : l'objectif étant de s'assurer qu'un objectif donné sur la carte pouvait être survolé de façon suffisamment précise pour être placé au centre ou sur les bords de l'image.

6.5- Performances globales

Leurs buts essentiels étaient d'évaluer :

- la résolution selon l'altitude,
- les erreurs de localisation dans diverses situations (coin d'images, ...) et selon l'altitude.

Des vols ont été effectués à des altitudes comprises entre 300 et 3 500 m au dessus de véhicules et d'hommes placés en différents endroits ; des points de référence géodésique ont aussi été désignés pour évaluer la localisation.

Ces tests ont aussi été conduits avec un planning limité, à évaluer les capacités opérationnelles.

6.6- Conclusions sur les essais systèmes de la chaîne image

L'intégration, la mise au point et l'évaluation des performances de la chaîne image ont été réalisés dans un délai court avec un nombre limité d'essais en vol, malgré l'imbrication forte de cette chaîne aux autres chaînes fonctionnelles du système et le haut niveau de performances et de sécurité recherchés.

Ceci a été rendu possible par :

- le recours à des outils de simulation évolués permettant d'évaluer les performances du système d'une façon exhaustive et notamment aux limites sans avoir à mettre en oeuvre le système complet,
- une méthodologie d'essais en vol progressive s'appuyant sur la forte modularité matérielle et fonctionnelle des chaînes et confirmant au fur et à mesure les résultats de simulation.

Cette méthodologie rigoureuse est dérivée de celle que SAGEM a utilisée pour le retrofit d'avions depuis de nombreuses années. Elle s'oppose à celles utilisées sur les systèmes d'UAV de première génération où le nombre d'heures de vol accumulé par le système était le seul témoin du niveau de validation, et qui conduisait à des systèmes insuffisamment validés ou au contraire, onéreux et rapidement dépassés technologiquement compte tenu du temps nécessaire à l'obtention d'un niveau de validation satisfaisant.

7- CONCLUSION

Cette présentation s'est attachée à démontrer notamment à travers l'exemple de sa chaîne image, les innovations du système d'UAV CRÉCERELLE en matière :

- d'utilisation opérationnelle,
- de conception,
- de technologie,
- et de méthodologie d'essais.

Ces innovations sont déterminantes pour répondre aux caractéristiques du marché d'UAV tactiques où les exigences de performance, de flexibilité, de sécurité de planning et de coût sont de plus en plus fortes.

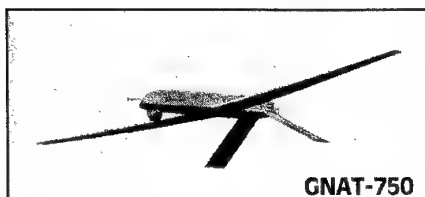
A ce titre, CRÉCERELLE peut être considéré comme un des premiers système de seconde génération.

PREDATOR — Medium Altitude Endurance

by

Larry Ernst
General Atomics
10130 Sorrento Valley Road
San Diego, CA 92121, USA

MEETING TOMORROW'S SURVEILLANCE CHALLENGES TODAY . . . WITH A FULL SPECTRUM OF STATE-OF-THE-ART UAVs



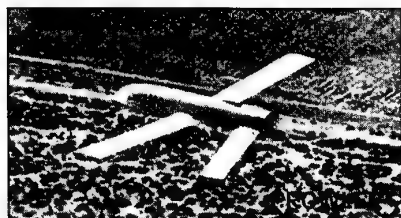
GNAT-750

Tier I Tactical Endurance UAV

- Long Endurance
- Proven Performance
- Deployed with U.S. Government and Overseas
- EO/IR Payload
- Multi-Frequency Data Link

Tier II Medium Altitude Endurance UAV

- Expanded EO/IR Payload
- SAR All-weather Capability
- Satellite Control
- GPS and INS
- Over 24 hours on Station at 500 nm
- Under Contract with U.S. Government

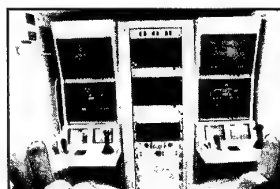


Joint Tactical UAV Maneuver Variant

- Close Range
- Demonstrated Capability
- EO/IR Payload
- Line-of-Sight Data Link and Autonomous Flight
- Met or Exceeded Performance Requirements

State-of-the-Art Common Ground Control Station

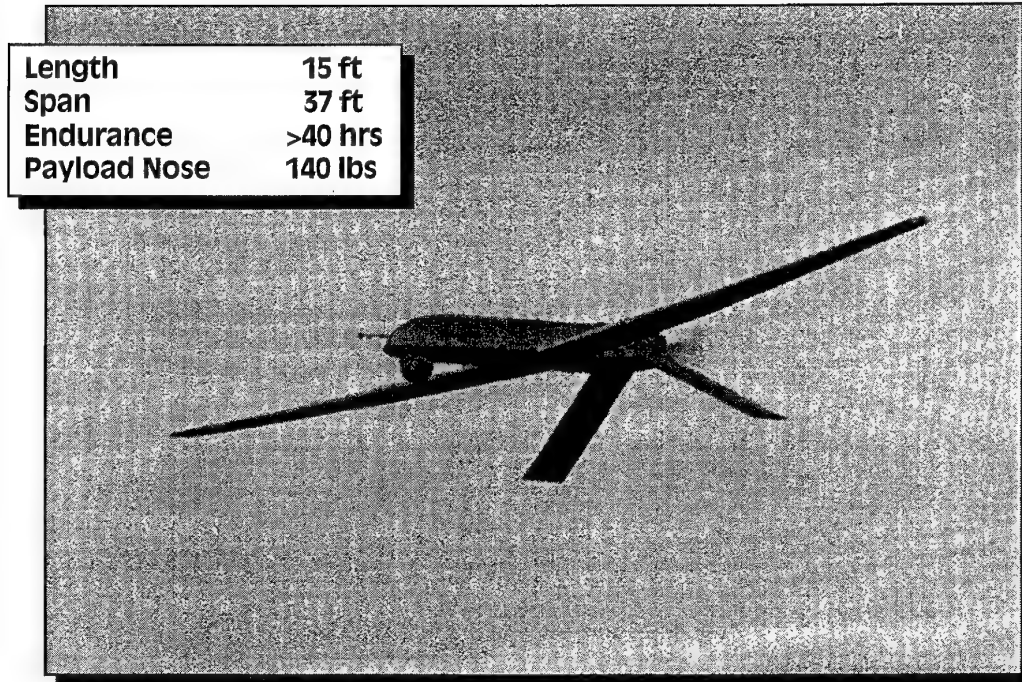
- Multi-UAV control
- Multi-payload control
- Software programmable
- Advanced mission planning
- Cockpit-like human factors



Reliable • Proven • Deployed

GNAT-750

UNMANNED SURVEILLANCE AIRCRAFT

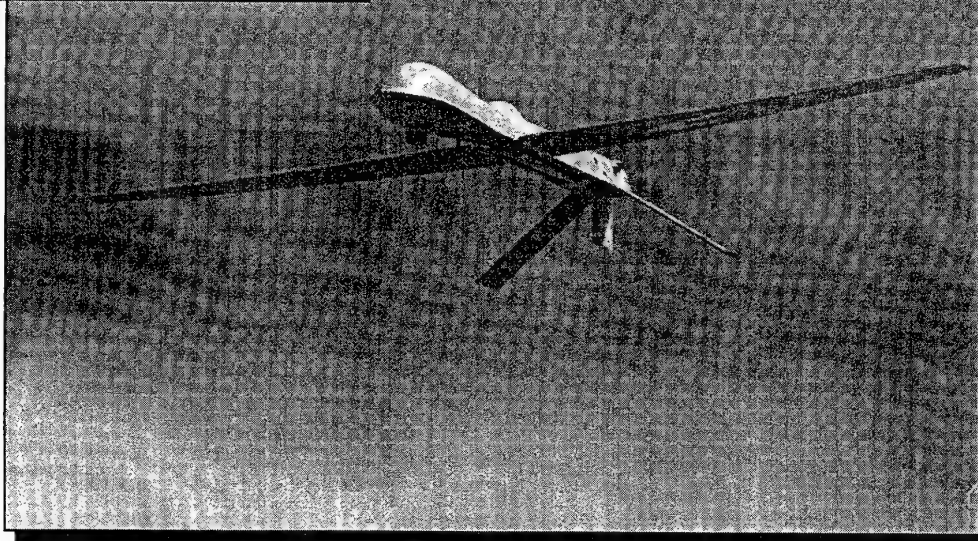


GNAT-750

- **COMBAT PROVEN**
 - OVER 1200 FLIGHT HOURS FLOWN
 - DEPLOYED TO 13 SITES WORLDWIDE
 - THREE COMBAT DEPLOYMENTS
- **OPERATIONAL WITH TURKISH FORCES**
 - DEPLOYED TO FIVE SITES
 - » TRAINING INTEGRATION IN SIVAS
 - » PILOTS FULLY QUALIFIED
 - » PAYLOAD OPERATION FULLY QUALIFIED
 - » TURKISH MAINTENANCE
 - » DAILY TRAINING FLIGHTS

PREDATOR

Length	27 ft
Wing Span	48.7 ft
Payload	450 lbs
T/O Weight	2080 lbs



MAE OPERATIONAL REQUIREMENTS

- **MISSION**
 - 24 HOURS ON STATION AT 500 NM
 - 450 LBS OF PAYLOAD
 - CLIMB TO 25,000 FT AFTER TAKE-OFF
- **PAYLOAD**
 - STABILIZED GIMBAL
 - » 2 DAY TV
 - » 1 FLIR
- **SAR**
- **DATA LINK**
 - UHF & KU BAND SATELLITE LINK
 - C BAND LOS LINK
- **GROUND CONTROL STATION**
 - AIR VEHICLE CONTROL
 - MISSION PLANNING
 - INTELLIGENCE EXPLOITATION

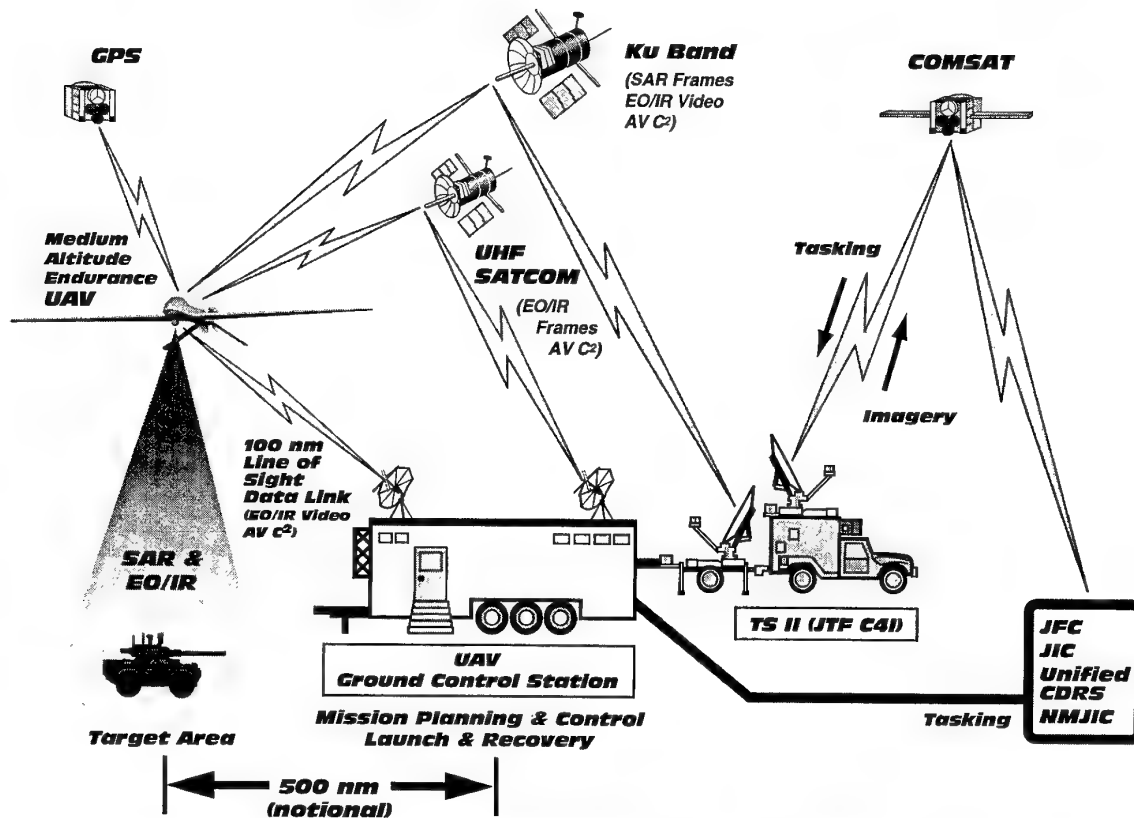
MAE UAV MISSION REQUIREMENTS

- QUICK RESPONSE WORLD WIDE
- AIR TRANSPORTABLE
- RAPID SETUP
- OPERATIONAL COMMANDER TASKING
- PRE PROGRAM MISSION BEFORE LAUNCH
- LAUNCH UNDER LOS CONTROL
- HAND OFF TO SATELLITE CONTROL
- AUTONOMOUS NAVIGATION AND TARGET SEARCH
- 24 HOURS ON STATION AT 500 NM
- MONITOR VEHICLE STATUS AND SENSORS NEAR-REAL-TIME
- UPLINK MISSION PLAN CHANGE DATA
- CONTROL HANDOFF OF RELIEF UAV

USAF 11th RECOGNIZANCE SQUADRON



MEDIUM ALTITUDE ENDURANCE UAV Concept of Operations

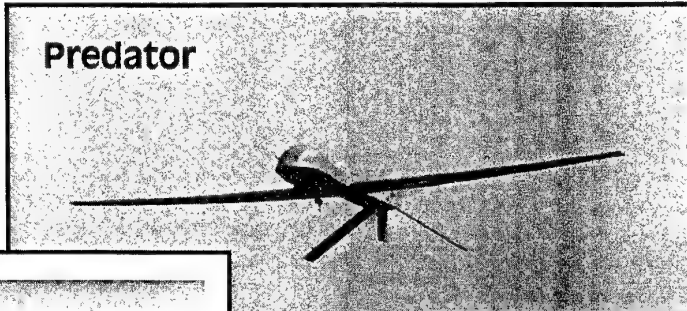


PILOT AND PAYLOAD OPERATOR STATIONS

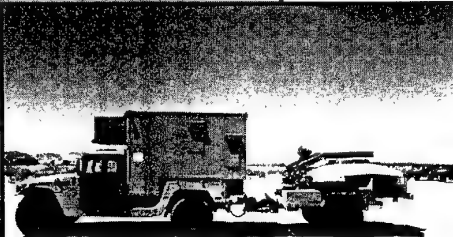
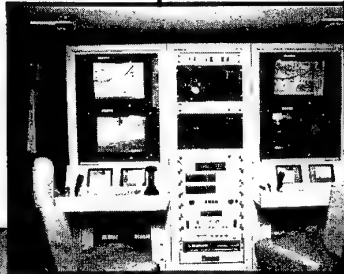


PREDATOR MEDIUM ALTITUDE ENDURANCE SYSTEM

Predator



Ground
Support
Equipment



Trojan Spirit (JTF C4I)



Ground Control Station

Global Surveillance Now A Reality

General Atomics Aeronautical Systems, Inc. • 10130 Sorrento Valley Road • San Diego, CA 92121 • (619) 455-2810

EO/IR PAYLOAD

- VERSATRON MODEL 18
- ZOOM AND SPOTTER DAYLIGHT TV
- MITSUBISHI 3-5 MICRON FLIR
- 14" DIAMETER GIMBAL
- RS-422 INTERFACE
- 4 AXIS GYRO STABILIZED
- FIELD OF REGARD:
 - 360° CONTINUOUS AZIMUTH
 - +30° TO -120° ELEVATION PLUS STOW POSITION
- <20 μ RAD LINE OF SIGHT STABILITY ON GNAT 750
- >1.5 RAD/S SLEW RATE, >5 RAD/S² ACCELERATION
- LASER TRACKER OPTION

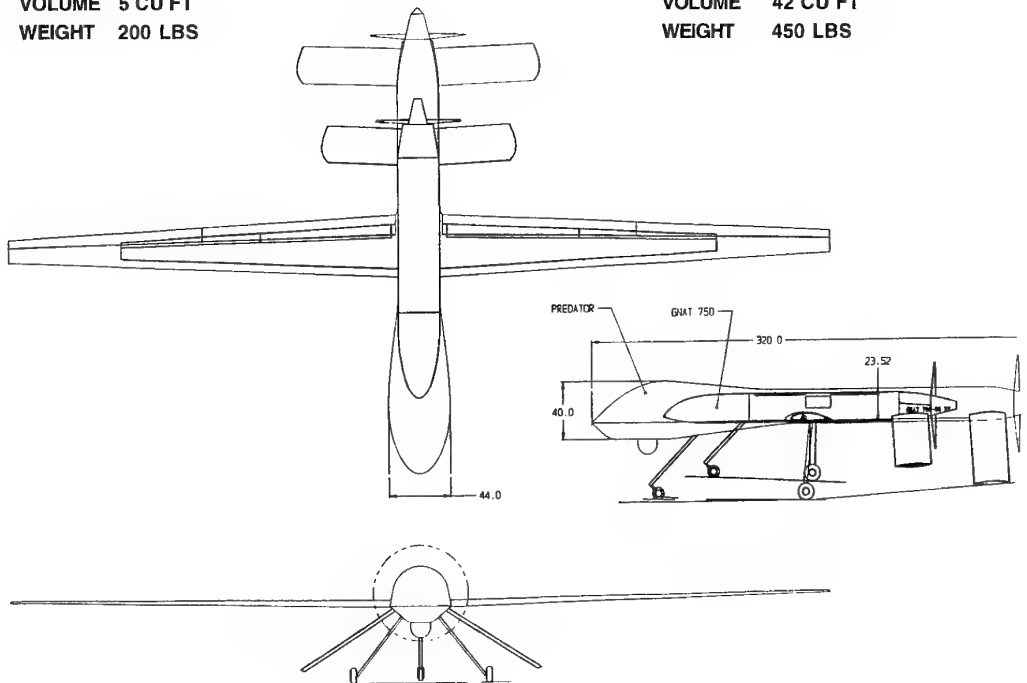
SAR RADAR

- WESTINGHOUSE KU BAND SAR
- 1 FT RESOLUTION
- 4 - 11.2 KM RANGE
- 800M SWATH WIDTH
- GROWTH
 - MTI
 - SAR SPOTLIGHT

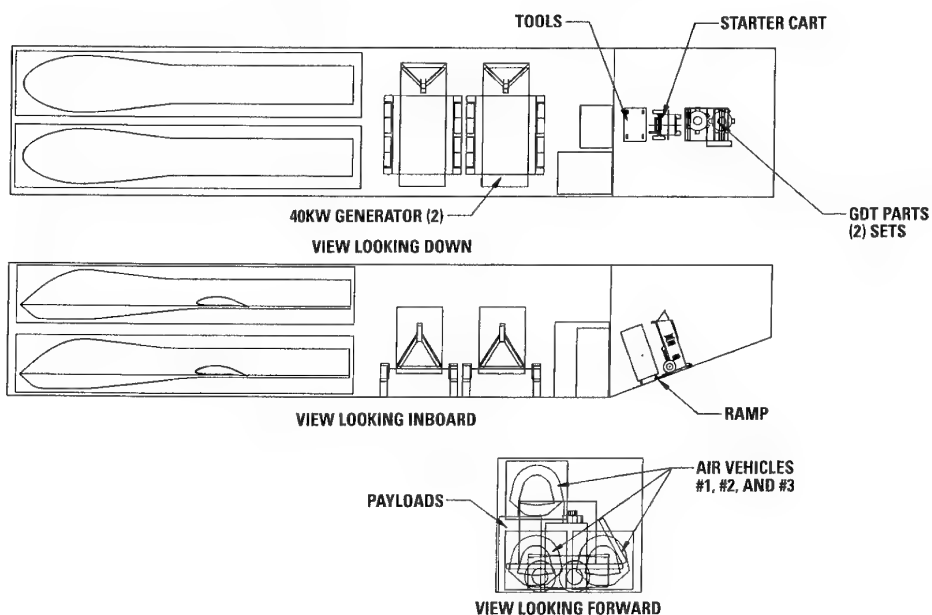
GNAT 750-45 / PREDATOR COMPARISON

PAYLOAD
VOLUME 5 CU FT
WEIGHT 200 LBS

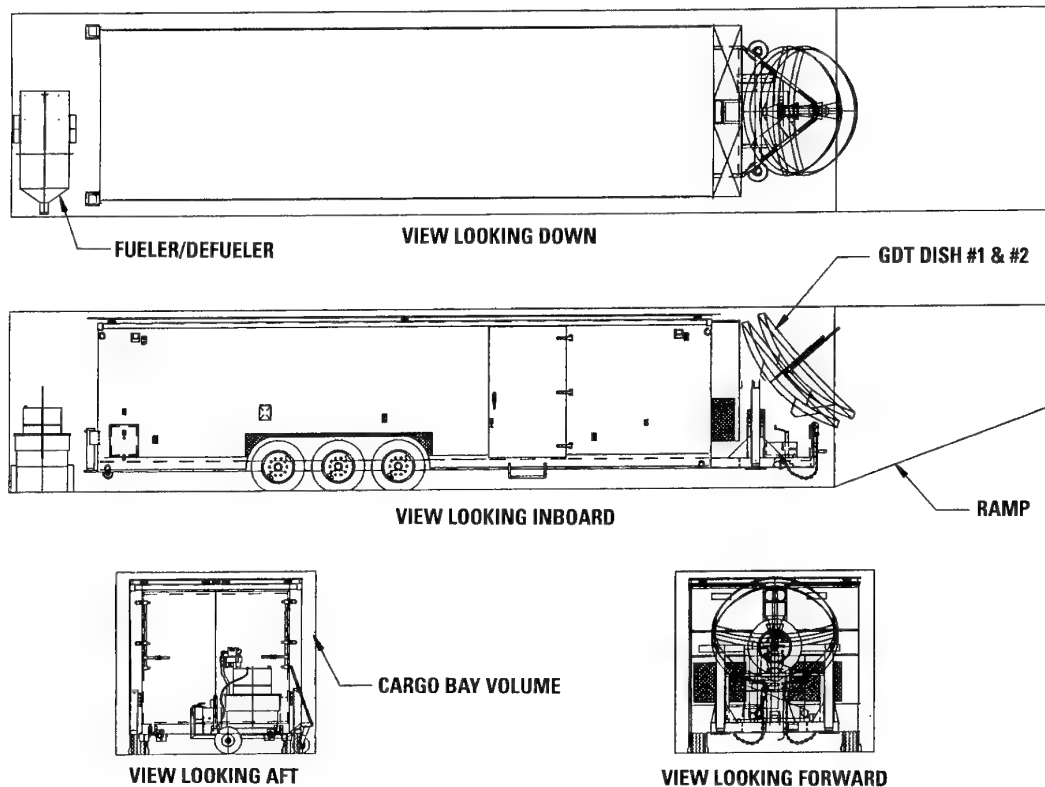
PAYLOAD
VOLUME 42 CU FT
WEIGHT 450 LBS



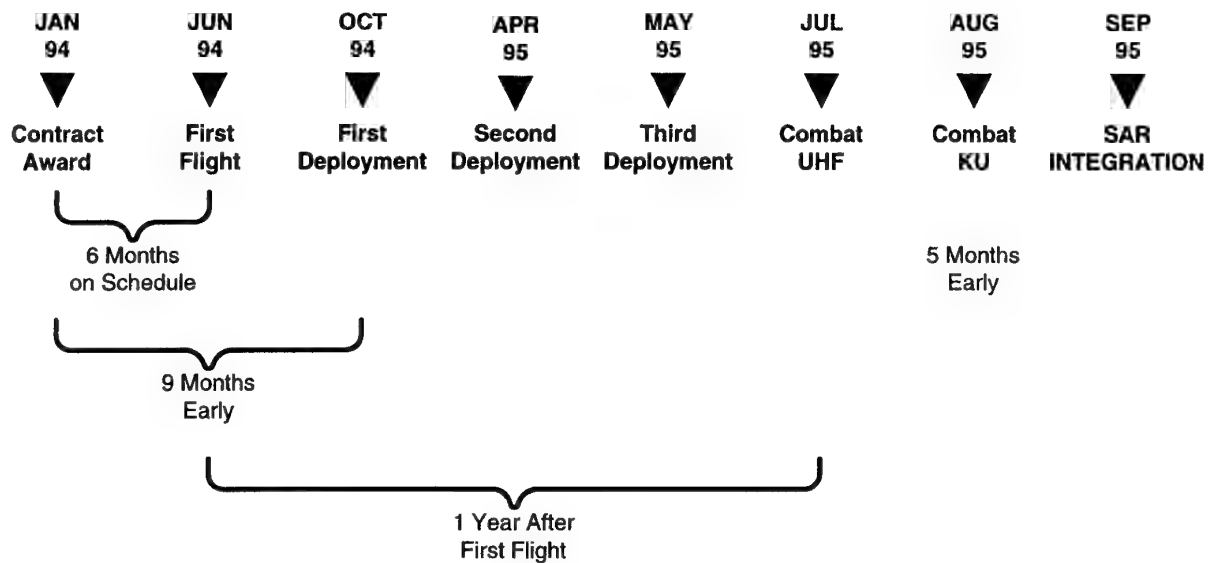
PREDATOR, GSE LOADOUT C-130 CARGO BAY



PREDATOR GCS LOADOUT C-130 CARGO BAY



SCHEDULE (MONTHS AFTER CONTRACT AWARD)



TIER II

- **CONTRACT AWARD - JANUARY 1994**
- **FIRST FLIGHT - JULY 1994**
 - **LESS THAN 6 MONTHS AFTER CONTRACT AWARD**
- **DEPLOYED TO FT. HUACHUCA - OCTOBER 1994**
 - **LESS THAN 9 MONTHS AFTER CONTRACT AWARD**
 - **OPERATED AND MAINTAINED BY SOLDIERS, SAILORS AND AIRMEN**
- **DEPLOYED TO FORT SUMNER, NEW MEXICO FOR ROVING SANDS '95**
- **DEPLOYED TO KEY WEST, FLORIDA FOR SPECIAL OPS SUPPORT**
- **OVERSEAS DEPLOYMENT JULY 1995**

ACHIEVEMENTS SINCE CONTRACT AWARD

- **SIGNIFICANT FLIGHT HOURS FLOWN**
- **SYSTEM DEPLOYED TO FT. HUACHUCA AND IN EXERCISE SUPPORT**
 - **NEAR DAILY FLIGHT OPS ROUTINE**
 - **5 CONTRACTOR TECHNICIANS**
 - **PAYLOAD VIDEO ROUTINELY PASSED THROUGH TROJAN SPIRIT NATIONWIDE**
 - **ROUTINE OPERATIONS IN LANDING PATTERN WITH OTHER FIXED WING AIRCRAFT**
- **40+ HOUR FLIGHT**
 - **ALL SYSTEMS FMC ON LANDING**
 - **JOINT USA, USN, USAF CREW**
- **AIRCRAFT & PAYLOAD CONTROL DEMONSTRATED OVER THE HORIZON VIA SATELLITE**
 - **UHF AND KU BAND SATELLITE CONNECTIVITY DEMONSTRATED**
 - **AIRCRAFT OVER EL MIRAGE CONTROLLED FROM SAN DIEGO**
 - **AIRCRAFT CONTROLLED OVER BOSNIA FROM ALBANIA**

ACHIEVEMENTS SINCE CONTRACT AWARD (CONTD.)

- **DEPLOYED TO KEYWEST IN SUPPORT OF SOCOM EXERCISE**
 - ROUTINE OPERATIONS WITH MIAMI CENTER
 - ROUTINE OPERATIONS IN LANDING PATTERN WITH OTHER FIXED WING AIRCRAFT
 - TACAN APPROACHES THROUGH AN OVERCAST SEQUENCED WITH CIVIL AIR TRAFFIC
- **DEPLOYED TO FORT SUMNER IN SUPPORT OF CENTRAL COMMAND EXERCISE ROVING SANDS/OPTIC COBRA**
 - ROUTINE OPERATIONS IN CONTROLLED AIRSPACE
 - SIGNIFICANT CAPABILITY TO LOCATE SCUD MISSILES
- **MILITARY USERS DEPLOYED TO SUPPORT BOSINA OPERATIONS**
 - OPERATING OUT OF ALBANIA AND SUPPORTING OPERATIONS OVER 260 NM AWAY IN BOSINA
 - ROUTINE LINE OF SIGHT DATA LINK OPERATIONS TO 150 NM
 - ROUTINE NEAR REAL TIME OVER THE HORIZON SURVEILLANCE USING SATELLITE DATA LINKS

ROVING SANDS

OPERATIONAL

- **THREE PREDATORS DEPLOYED**
 - 1 GCS
- **TRI SERVICE SUPPORT AND OPERATION**
- **FULL INTEGRATION WITH MANNED TACTICAL AIRCRAFT**
- **OPERATED CONTINUOUSLY IN CONTROLLED & UNCONTROLLED AIRSPACE**
 - FAA ACCEPTANCE
 - INCLUDING "A" AIRSPACE
- **NEAR CONTINUOUS REAL TIME VIDEO AND STILLS TO EXERCISE COMMANDERS 200 MILES AWAY**
- **PREDATOR PROVIDED 85% OF ALL EXERCISE IMAGERY**
 - WHICH INCLUDED NATIONAL ASSETS
- **ALL SCUD DETECTIONS MADE BY PREDATOR**
- **REPORTED AS "STAR OF THE EXERCISE"**

ROVING SANDS (CONTINUED)

MAINTENANCE/LOGISTICS

- **FLEW 25 FLIGHTS IN 26 EXERCISE DAYS**
 - 173 FLIGHT HOURS
- **TOTAL MAINTENANCE PERFORMANCE**
 - **AIRCRAFT**
 - SCHEDULED 30 HOURS
 - UNSCHEDULED 70 HOURS
 - **GCS 0 HOURS**
- **MAINTENANCE MANHOURS PER FLIGHT HOUR**
 - SCHEDULED 10 MINUTES
 - UNSCHEDULED 23 MINUTES
- **NO AIRCRAFT OUT OF FLIGHT STATUS OVER 1 DAY**

ROVING SANDS EXERCISE

- **WORD FROM CENTCOM AT EL PASO IS:**
 - “...EVERY SINGLE CONFIRMED SCUD KILL IN THIS EXERCISE WAS DIRECTLY ATTRIBUTED TO PREDATOR...”
- **85% OF ALL THE EXERCISE IMAGERY IN DISTRIBUTION WAS PROVIDED BY PREDATOR, ALTHOUGH THE EXERCISE ALSO INCLUDED A LARGE NUMBER OF NATIONAL LEVEL ASSETS.**
- **AS OF 7 MAY 1995, TWENTY FIVE FLIGHTS WERE FLOWN IN TWENTY SIX DAYS INCLUDING A PILOT TRAINING FLIGHT ON A SCHEDULED DAY OFF.**
- **FLIGHT HOURS TOTAL 173.3**
- **DID NOT LOSE A SINGLE MISSION DUE TO MAINTENANCE / AIRCRAFT**

KEY WEST

- OPERATED FROM NAS KEY WEST
- SPECIAL OPS SUPPORT
- OPERATIONS IN CONTROLLED & UNCONTROLLED AIRSPACE
 - WITH MILITARY & CIVIL AIRCRAFT
- FLEW ACTUAL IFR TACAN APPROACHES
 - SEQUENCED WITH MANNED AIRCRAFT
- UHF TRAINING
 - LIMITED SATELLITE ACCESS

OVERSEAS DEPLOYMENT

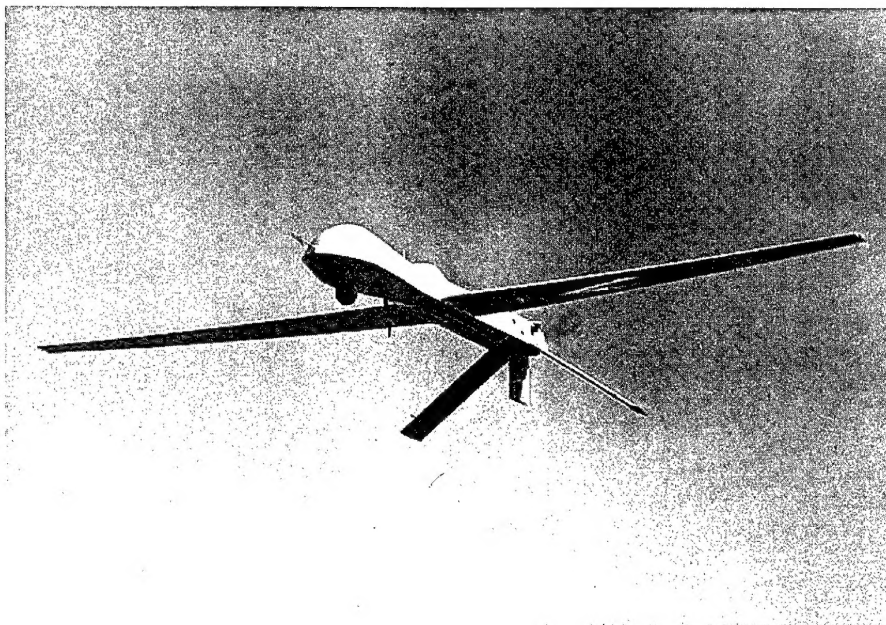
- DEPLOYED TO ALBANIA JULY 7, 1995
 - THREE AIRCRAFT AND A GCS
- ROUTINE OPERATIONS BEYOND 250 NM
- ALMOST DAILY MISSION SUPPORT
 - 20 HOUR MISSIONS THE NORM
 - 100% MISSION AVAILABILITY
- DIRECT LINK TO 150 NM
- UHF CONNECTIVITY DEMONSTRATED
- ROUTINE KU BAND OVER THE HORIZON OPERATIONS
 - DEPLOYED 5 MONTHS EARLY
 - REAL TIME SURVEILLANCE BEYOND 250 NM
- SUPPORT FOR TACTICAL COMMANDERS AFLOAT AND ASHORE
 - DIRECT SUPPORT TO AIR COMPONENT COMMANDER
 - PRESTRIKE PLANNING
 - REAL TIME BDA ASSESSMENT
 - PREDATOR NOW AN INTEGRAL PLAYER IN ALL AIR OPERATIONS
 - » ADM. SMITH, GEN. MOORHEAD, GEN. RYAN

PREDATOR SUMMARY

- MAE PROVIDES OPERATIONAL COMMANDERS:
 - TARGETING QUALITY INTELLIGENCE
 - DAY OR NIGHT
 - ALL WEATHER
 - NEAR-REAL-TIME
 - 24 HOURS PER DAY
 - ON MOVEABLE / RELOCATEABLE TARGETS

The Preferred System

- State-of-the-art Technology
- Creative, Dedicated People
- Unique Mission Responsive Flexibility
- A No-nonsense Approach to Tactical Surveillance
- A Winning Combination



REPORT DOCUMENTATION PAGE

Recipient's Reference	2. Originator's Reference AGARD-CP-591	3. Further Reference ISBN 92-836-0033-9	4. Security Classification of Document UNCLASSIFIED/ UNLIMITED												
5. Originator Advisory Group for Aerospace Research and Development North Atlantic Treaty Organization 7 rue Ancelle, 92200 Neuilly-sur-Seine, France															
6. Title Subsystem Integration for Tactical Missiles (SITM) and Design and Operation of Unmanned Air Vehicles (DOUAV)															
7. Presented at/sponsored by The Flight Vehicle Integration Panel Specialists' Meetings held in Ankara, Turkey, 9-12 October 1995															
8. Author(s)/Editor(s) Multiple			9. Date November 1996												
10. Author's/Editor's Address Multiple			11. Pages 356												
12. Distribution Statement There are no restrictions on the distribution of this document. Information about the availability of this and other AGARD unclassified publications is given on the back cover.															
13. Keywords/Descriptors <table style="width: 100%; margin-top: 10px;"> <tr> <td style="width: 50%;">Missiles</td> <td style="width: 50%;">Integrated systems</td> </tr> <tr> <td>UAV (Unmanned Aerial Vehicle)</td> <td>Missile guidance</td> </tr> <tr> <td>Reconnaissance drone aircraft</td> <td>Flight tests</td> </tr> <tr> <td>Remotely piloted vehicles</td> <td>Design</td> </tr> <tr> <td>Target acquisition</td> <td>Payloads</td> </tr> <tr> <td>Systems engineering</td> <td>Tactical operations</td> </tr> </table>				Missiles	Integrated systems	UAV (Unmanned Aerial Vehicle)	Missile guidance	Reconnaissance drone aircraft	Flight tests	Remotely piloted vehicles	Design	Target acquisition	Payloads	Systems engineering	Tactical operations
Missiles	Integrated systems														
UAV (Unmanned Aerial Vehicle)	Missile guidance														
Reconnaissance drone aircraft	Flight tests														
Remotely piloted vehicles	Design														
Target acquisition	Payloads														
Systems engineering	Tactical operations														
14. Abstract <p style="margin-top: 10px;">This conference proceedings contains papers presented at two specialists' meetings held in Ankara, Turkey in October of 1995. The meetings were, "Subsystem Integration for Tactical Missiles" and "Design and Operation of Unmanned Air Vehicles". In the field of subsystem integration for tactical missiles, papers focused on successful examples of integrating advanced sensors, guidance control systems, and navigation systems. An additional session focused on methods for testing missiles, including lessons learned from Norway's testing of the Penguin Mk2. The meeting on UAVs focused on design issues, payloads and their associated technologies, and operational issues. Specific systems described included: the French Self Contained Early Warning System against anti-ship missiles; the Phoenix; Boeing's heliwing; the Crecelle, and the US Navy's Tilt Rotor UAV demonstrator.</p> <p>Two keynote speeches introduced both meetings, clearly establishing the importance of the topics.</p> <p>Copies of papers presented at the Flight Vehicle Integration Panel Specialists' Meetings held in Ankara, Turkey, 9-12 October 1995.</p>															

Aucun stock de publications n'a existé à AGARD. A partir de 1993, AGARD détiendra un stock limité des publications associées aux cycles de conférences et cours spéciaux ainsi que les AGARDographies et les rapports des groupes de travail, organisés et publiés à partir de 1993 inclus. Les demandes de renseignements doivent être adressées à AGARD par lettre ou par fax à l'adresse indiquée ci-dessus. *Veillez ne pas téléphoner.* La diffusion initiale de toutes les publications de l'AGARD est effectuée auprès des pays membres de l'OTAN par l'intermédiaire des centres de distribution nationaux indiqués ci-dessous. Des exemplaires supplémentaires peuvent parfois être obtenus auprès de ces centres (à l'exception des Etats-Unis). Si vous souhaitez recevoir toutes les publications de l'AGARD, ou simplement celles qui concernent certains Panels, vous pouvez demander à être inclu sur la liste d'envoi de l'un de ces centres. Les publications de l'AGARD sont en vente auprès des agences indiquées ci-dessous, sous forme de photocopie ou de microfiche.

CENTRES DE DIFFUSION NATIONAUX

ALLEMAGNE

Fachinformationszentrum Karlsruhe
D-76344 Eggenstein-Leopoldshafen 2

BELGIQUE

Coordonnateur AGARD-VSL
Etat-major de la Force aérienne
Quartier Reine Elisabeth
Rue d'Evere, 1140 Bruxelles

CANADA

Directeur, Services d'information scientifique
Ministère de la Défense nationale
Ottawa, Ontario K1A 0K2

DANEMARK

Danish Defence Research Establishment
Ryvangs Allé 1
P.O. Box 2715
DK-2100 Copenhagen Ø

ESPAGNE

INTA (AGARD Publications)
Carretera de Torrejón a Ajalvir, Pk.4
28850 Torrejón de Ardoz - Madrid

ETATS-UNIS

NASA Goddard Space Flight Center
Code 230
Greenbelt, Maryland 20771

FRANCE

O.N.E.R.A. (Direction)
29, Avenue de la Division Leclerc
92322 Châtillon Cedex

GRECE

Hellenic Air Force
Air War College
Scientific and Technical Library
Dekelia Air Force Base
Dekelia, Athens TGA 1010

ISLANDE

Director of Aviation
c/o Flugrad
Reykjavik

ITALIE

Aeronautica Militare
Ufficio del Delegato Nazionale all'AGARD
Aeroporto Pratica di Mare
00040 Pomezia (Roma)

LUXEMBOURG

Voir Belgique

NORVEGE

Norwegian Defence Research Establishment
Attn: Biblioteket
P.O. Box 25
N-2007 Kjeller

PAYS-BAS

Netherlands Delegation to AGARD
National Aerospace Laboratory NLR
P.O. Box 90502
1006 BM Amsterdam

PORTUGAL

Estado Maior da Força Aérea
SDFA - Centro de Documentação
Alfragide
2700 Amadora

ROYAUME-UNI

Defence Research Information Centre
Kentigern House
65 Brown Street
Glasgow G2 8EX

TURQUIE

Millî Savunma Başkanlığı (MSB)
ARGE Dairesi Başkanlığı (MSB)
06650 Bakanlıklar-Ankara

Le centre de distribution national des Etats-Unis ne détient PAS de stocks des publications de l'AGARD.

D'éventuelles demandes de photocopies doivent être formulées directement auprès du NASA Center for AeroSpace Information (CASI) à l'adresse ci-dessous. Toute notification de changement d'adresse doit être fait également auprès de CASI.

AGENCES DE VENTE

NASA Center for AeroSpace Information
(CASI)
800 Elkridge Landing Road
Linthicum Heights, MD 21090-2934
Etats-Unis

The British Library
Document Supply Division
Boston Spa, Wetherby
West Yorkshire LS23 7BQ
Royaume-Uni

Les demandes de microfiches ou de photocopies de documents AGARD (y compris les demandes faites auprès du CASI) doivent comporter la dénomination AGARD, ainsi que le numéro de série d'AGARD (par exemple AGARD-AG-315). Des informations analogues, telles que le titre et la date de publication sont souhaitables. Veuillez noter qu'il y a lieu de spécifier AGARD-R-nnn et AGARD-AR-nnn lors de la commande des rapports AGARD et des rapports consultatifs AGARD respectivement. Des références bibliographiques complètes ainsi que des résumés des publications AGARD figurent dans les journaux suivants:

Scientific and Technical Aerospace Reports (STAR)
publié par la NASA Scientific and Technical
Information Division
NASA Langley Research Center
Hampton, Virginia 23681-0001
Etats-Unis

Government Reports Announcements and Index (GRA&I)
publié par le National Technical Information Service
Springfield
Virginia 22161
Etats-Unis
(accessible également en mode interactif dans la base de
données bibliographiques en ligne du NTIS, et sur CD-ROM)



AGARD holds limited quantities of the publications that accompanied Lecture Series and Special Courses held in 1993 or later, and of AGARDographs and Working Group reports published from 1993 onward. For details, write or send a telefax to the address given above. *Please do not telephone.*

AGARD does not hold stocks of publications that accompanied earlier Lecture Series or Courses or of any other publications. Initial distribution of all AGARD publications is made to NATO nations through the National Distribution Centres listed below. Further copies are sometimes available from these centres (except in the United States). If you have a need to receive all AGARD publications, or just those relating to one or more specific AGARD Panels, they may be willing to include you (or your organisation) on their distribution list. AGARD publications may be purchased from the Sales Agencies listed below, in photocopy or microfiche form.

NATIONAL DISTRIBUTION CENTRES

BELGIUM

Coordonnateur AGARD — VSL
Etat-major de la Force aérienne
Quartier Reine Elisabeth
Rue d'Evere, 1140 Bruxelles

CANADA

Director Scientific Information Services
Dept of National Defence
Ottawa, Ontario K1A 0K2

DENMARK

Danish Defence Research Establishment
Ryvangs Allé 1
P.O. Box 2715
DK-2100 Copenhagen Ø

FRANCE

O.N.E.R.A. (Direction)
29 Avenue de la Division Leclerc
92322 Châtillon Cedex

GERMANY

Fachinformationszentrum Karlsruhe
D-76344 Eggenstein-Leopoldshafen 2

GREECE

Hellenic Air Force
Air War College
Scientific and Technical Library
Dekelia Air Force Base
Dekelia, Athens TGA 1010

ICELAND

Director of Aviation
c/o Flugrad
Reykjavik

ITALY

Aeronautica Militare
Ufficio del Delegato Nazionale all'AGARD
Aeroporto Pratica di Mare
00040 Pomezia (Roma)

LUXEMBOURG

See Belgium

NETHERLANDS

Netherlands Delegation to AGARD
National Aerospace Laboratory, NLR
P.O. Box 90502
1006 BM Amsterdam

NORWAY

Norwegian Defence Research Establishment
Attn: Biblioteket
P.O. Box 25
N-2007 Kjeller

PORTUGAL

Estado Maior da Força Aérea
SDFA - Centro de Documentação
Alfragide
2700 Amadora

SPAIN

INTA (AGARD Publications)
Carretera de Torrejón a Ajalvir, Pk.4
28850 Torrejón de Ardoz - Madrid

TURKEY

Millî Savunma Başkanlığı (MSB)
ARGE Dairesi Başkanlığı (MSB)
06650 Bakanlıklar-Ankara

UNITED KINGDOM

Defence Research Information Centre
Kentigern House
65 Brown Street
Glasgow G2 8EX

UNITED STATES

NASA Goddard Space Flight Center
Code 230
Greenbelt, Maryland 20771

The United States National Distribution Centre does NOT hold stocks of AGARD publications.

Applications for copies should be made direct to the NASA Center for AeroSpace Information (CASI) at the address below.

Change of address requests should also go to CASI.

SALES AGENCIES

NASA Center for AeroSpace Information
(CASI)
800 Elkridge Landing Road
Linthicum Heights, MD 21090-2934
United States

The British Library
Document Supply Centre
Boston Spa, Wetherby
West Yorkshire LS23 7BQ
United Kingdom

Requests for microfiches or photocopies of AGARD documents (including requests to CASI) should include the word 'AGARD' and the AGARD serial number (for example AGARD-AG-315). Collateral information such as title and publication date is desirable. Note that AGARD Reports and Advisory Reports should be specified as AGARD-R-nnn and AGARD-AR-nnn, respectively. Full bibliographical references and abstracts of AGARD publications are given in the following journals:

Scientific and Technical Aerospace Reports (STAR)
published by NASA Scientific and Technical
Information Division
NASA Langley Research Center
Hampton, Virginia 23681-0001
United States

Government Reports Announcements and Index (GRA&I)
published by the National Technical Information Service
Springfield
Virginia 22161
United States
(also available online in the NTIS Bibliographic
Database or on CD-ROM)

